A STUDY OF VISCOELASTIC MAGNETIC ABRASIVE FINISHING PROCESS

A Thesis Submitted in the partial fulfillment of the requirement for the
Doctor of Philosophy
in
the Department of
MECHANICAL ENGINEERING
Submitted
By

KROVVIDI SRINIVAS
Roll Number:2K11/PHD/ME/12
Under the Supervision of
Prof. QASIM MURTAZA **Prof. A K Agrawal**

Department of Mechanical, Production& Industrial Engg. and Automobile Engg.
Delhi Technological University,
Shahbad Daulatpur, Main Bawana Road
Delhi-110042, India

CERTIFICATE

This is to certify that the work embodied in this thesis entitled, "***A study of Viscoelastic Magnetic Abrasive Finishing process*"** being submitted by **Krovvidi Srinivas (Roll No-2k11/Ph. D/ME/12)** for the award of Doctor of Philosophy Degree (Ph. D) in Mechanical Engineering at Delhi Technological University, Delhi is an authentic work carried out by him under our guidance and supervision.

It is further certified that the work is based on original research and the matter embodied in this thesis has not been submitted to any other university/institute for award of any degree to the best of our knowledge and belief.

Dr. Qasim Murtaza
Professor,
Dept. of Mechanical Engg.

Dr. A K Agrawal
Professor,
Dept. of Mechanical Engg.

ACKNOWLEDGEMENT

Firstly, I would like to express my gratitude to my Supervisors Prof. Qasim Murtaza and Prof. A K Agrawal for their pertinent support of my Ph.D study and related research, for their patience, motivation and immense knowledge. Their valuable guidance and mentorship helped me in all the time of research and thesis writing.

Beside my supervisors, I would like to thank Prof. R S Mishra, DRC Chairman, Department of Mechanical Engineering for his valuable suggestions and encouragement. I am extremely thankful to Prof. Vipin, Head of the Department, Department of Mechanical Engineering for his constant encouragement. Prof. Samsher is a source of motivation to me in handling both my academic work and research work.

I am extremely thankful to Sh. Lakhanji, Sh. Roshan Kumar, Sh. Sunilji and Sh. Rajesh Bhora who spared their valuable time in the toughest Covid time. Without their help, I would not have even ventured to perform the experiments in the lab.

I always got constant encouragement from Prof. Ranganath M S, Prof. Rajiv Chaudhary, Prof. R C Singh for their motivation during my testing time. I am extremely thankful to Mr. Anant Bhardwaj, Ph.D scholar, Delhi Technological University for his cooperation in performing the modelling work.

I am indebted to my father Late Mr.Satyanarayana Murthy who left us very recently and mother Mrs. Subhadra for their encouragement. I am extremely thankful to my wife Mrs. Satya and son Sai Sridatta for creating amicable environment at the domestic front such that I would be able to concentrate on my work. I also express my sincere thanks to my brother, sister in law, sister and brother in law for their constant encouragement.

Finally, I express my sincere thanks to Prof. N S Raghava and Dr. Jayasimhadri. M for their cooperation and encouragement.

KROVVIDI SRINIVAS

PREFACE

In this thesis titled "Study of Viscoelastic Magnetic Abrasive Finishing Process" the problem of sedimentation of the mixture of Carbonyl Iron Particle (CIP) and abrasive particles in the absence of Magnetic field has been addressed by preparing Viscoelastic medium, which retains Viscoelastic properties in the absence of Magnetic field. Both internal and external finishing has been carried out and the wear of the external finished surfaces has been studied.

Chapter 1 Begins with the discussion about different manufacturing processes adopted in the industry and then discusses about the importance of Nonconventional machining processes. Different types of abrasives, their properties are discussed. A discussion is made about different types of commercially available magnets their application is discussed. A detailed discussion about different types of Magnetic field assisted finishing processes, their applicability, achievable surface finish is discussed.

Chapter 2 is about the literature review done quiet exhaustively. Contemporary work done in different Magnetic force assisted finishing process is discussed. Research gap from the literature survey is found and analysed. Viscoelastic Magnetic abrasive finishing process as a solution to the short coming in the research work done earlier is discussed. Research objectives and research methodology are being discussed.

Chapter 3 Different Viscoelastic media has been studied and most suitable Viscoelastic media for present research work has been prepared and their viscosity is found by experiment and the results have been analysed.

Chapter 4 A brief discussion is made about the design of experiments and different optimization techniques presently used.

Chapter 5 Simulation and Modelling has been done with ANSYS MAXWELL ANOSOFT 16 (student version) for finding the best geometry of the Permanent Magnets that produce Maximum Flux density, followed by this the flux densities produced by the Permanent Magnets used for Internal and External finishing for different working gaps is simulated.

Chapter 6 In this chapter a detailed discussion is made about the Test rig used for Internal finishing of the splined shaft. An Aluminium fixture is designed and fabricated for the internal finishing process. Step by step Assembly of different components of the fixture has been discussed. Flow parameters have been simulated for 10MPa, 15 MPa and 20 MPa. Experiment

has been performed based on L27 Orthogonal Array of Design of Experiments. The results have been critically analysed and optimisation has been done for Maximum material removal using Taguchi's Optimisation Technique.

Chapter 7 . In this chapter the detailed description of the test rig has been made**.** Three material; Steel, Brass and Aluminium have been finished with Viscoelastic Magnetic Abrasive Medium. Orthogonal Array of Design of experiments has been adopted for finishing operation. Results have been analysed for change in surface roughness and the metal removal. Optimisation has been done for metal removal using Taguchi's linear regression Model. Minitab 17 is used for getting the output of results.

Chapter 8 . Dry sliding wear test has been performed on the External finished specimen. Experiment has been performed on "Reciprocating Tribometer". Both the rough and finished specimen have been tested for Minimum wear condition. The wear behaviour has been analysed for the rough specimen and the finished specimen. Optimisation of the process parameters has been done using Taguchi's linear regression Model. Minitab 17 is used for getting the output of results.

Chapter 9: In this chapter Conclusions and future scope of research has been discussed.

10: The list of research papers referred has been mentioned.

11. Publications

ACRONYMS

AFM	Abrasive Flow Machining
AJM	Abrasive Jet Machining
AMN	Abrasive Mesh Number
ANN	Artificial Neural Network
CIP	Carbonyl Iron Powder
EP	Extrusion Pressure
FT	Finishing Time
MAF	Magnetic Abrasive Machining
MFD	Magnetic Flux Density
MGOe	Mega Gauss Oersteds
MPa	Mega Pascal
mPa-s	Mille Pascal Second
MRAFF	Magneto Rheological Abrasive Flow Finishing
MRF	Magneto Rheological Finishing
MTRS	Magnetic Tool Rotational Speed
NOC	No of Cycles
RSOW	Rotational Speed of Workpiece
T	Tesla
VEMAF	Viscoelastic Magnetic Abrasive Finishing

ABSTRACT

Magnetic field Assisted surface finishing concept started during 1940s in the USA, subsequently different countries started working in this field and developed processes like Magnetic Abrasive finishing, Magnetic flow finishing, Magnetorheological finishing process, Magnetorheological abrasive flow finishing process. Dr.W.Li[2013] developed Viscoelastic Magnetic Abrasive finishing process. In the present thesis Entitled "A Study of Viscoelastic Magnetic Abrasive Finishing Process" an investigation has been made about the finishing of Complex Internal surfaces and external surfaces.

First two chapters are Introduction and the Literature review. In the third chapter, Viscoelastic Magnetic Abrasive medium has been prepared with Silicone oil, Transformer oil and AP3 Grease. These Media have been tested for their Viscosity by Rheometer. Based on the results obtained, Viscoelastic Medium to be used for internal finishing of the Spline shaft and external plane surfaces has been decided.

In the fourth chapter different Optimisation techniques presently adopted has been briefly discussed. In the Fifth Chapter, Modelling and Simulation of the Permanent magnets with same material, same volume and different geometries has been done. Based on the results obtained, it has been observed that Fan Magnet and Arc Magnet are found to give better Magnetic flux density for the same working gap. A segmental arc Magnet, normally used for Power generation by Wind turbine has been used for creating Magnetic flux density for finishing of the internal surface of the Spline shaft. Magnetic Flux density of the spline shaft for three different levels has been simulated. Based on the simulated results, the median value has been taken as the Magnetic flux density for finishing operation.

Abrasive Flow Machine in the Advanced Manufacturing lab is used for finishing of the internal splines. An Aluminium fixture has been designed and

fabricated for accommodating the Segmental Magnet, which encompasses the spline shaft. The rotary motion is provided to the spline shaft with set of gears and the Viscoelastic Magnetic Abrasive medium gets reciprocating motion due to the controlling motion. Medium makes motion inside the spline shaft due to the difference of pressure. Six process parameters have been considered and experiments have been performed based on the L27 Orthogonal array of Design of experiments of Taguchi. Nine specimen have been prepared and have been subjected to Finishing process based on Design of experiments. In first cycle Magnetic flux density of Level 1 is considered and all the nine specimen have been finished under this flux density. In second cycle these nine specimen have been subjected to finishing operation based on the Magnetic flux density Level 2. The last cycle of finishing has been performed with Magnetic Flux densities of Level-3. After every cycle each specimen is thoroughly cleaned and greasiness has been removed. Surface roughness and the mass of the specimen before and after each cycle for all the nine specimens has been measured. Optimisation for the maximum material removal has been done with Taguchi's Linear regression model using MiniTab 17 software. Results have been critically examined.

In the Seventh chapter, finishing of Brass, Steel and Aluminium Specimens has been carried out. Test rig for this is the CNC Drilling and Tapping Machine centre available in Metal cutting lab of Delhi technological university. A mild steel based Magnetic finishing tool has been designed and fabricated, which accommodates the N52 cylindrical permanent magnet. Magnetic tool that has been fixed to the spindle of the test rig rotates and the Viscoelastic Magnetic abrasive medium attached to the powerful magnet finishes the top surface of the specimen during the rotary motion and feed motion of the spindle. In total six process parameters have been considered for external finishing of the specimen made of all the three material. Experiments have been performed based on Taguchi's L27 Orthogonal Array of Design. Only Nine specimen have been considered for finishing operation

and each specimen is subjected to three cycles. First cycle of experiments for all the nine specimens is based on 2 mm working gap, second cycle with 1.5 mm gap and the third cycle is with 1 mm gap. After every cycle the specimen have been thoroughly cleaned and greasiness has been removed. Surface roughness, Mass of the specimen before and after each cycle has been noted and tabulated. Optimisation has been done for Maximum metal removal by Taguchi's linear regression model using Minitab 17. Results have been critically examined. Residual stresses of each specimen before the start of the first cycle has been measured and the values of the residual stresses has been measured after finishing the third cycle and comparison shows that the specimens are subjected to compressive stresses.

Sliding wear test has been performed on the specimen finished with VEMAF process. Specimen with best surface finish have been selected from all the three materials and cut into size as per the requirement. Eighteen Cylindrical specimens each for Brass, Al6351T6 and Mild steel have been prepared, which are having surface roughness value of the order 0.09 μm ±10%. Three process parameters; Load, Time and Frequency have been considered for wear test. L9 Orthogonal Array of design of Taguchi has been selected for performing the wear test. Rough surfaces are the rear surface of the finished surfaces and these rough surfaces have been subjected to Wear test. The initial and final masses have been noted for the specimen, the difference of which gives the wear for the rough side of the specimen. After completing the wear test on all the rough surfaces, same procedure is adopted for the finished surfaces also. The same procedure has been adopted for all the three materials. Results have been analysed and Optimisation has been done with Minitab 17 based on Taguchi's linear regression model. Significance of process parameters, their ranking has been tabulated.

CONTENTS

CHAPTER.1 INTRODUCTION

In this chapter, a brief discussion about different Non-Conventional machining processes presently used in the industry has been made, followed by this discussion of Different Types of Magnetic field-assisted abrasive finishing processes presently adopted in the industry for the finishing of the surfaces at Nano-level has been done. Viscoelastic Magnetic abrasive finishing [VEMAF] process, process parameters in VEMAF, Mechanism of finishing during VEMAF process has been discussed in brief.

1.1.Background: Manufacturing is the process of obtaining the required geometry and dimensions from the raw material as per the requirements of the design. Though the concept of manufacturing started from the stone age, when Homo Sapiens Sapien started preparing crude tools, the revolution in Manufacturing started with the beginning of the Industrial Revolution in London. The rapid growth of the Mechanical Engineering Manufacturing processes attributes to the discovery of purification methods of different metals from their ore. Initial manufacturing processes were aimed at the preparation of weapons for Warfare and the transportation equipment. After the Industrial Revolution in Britain, different types of Manufacturing machines have been discovered, due to which Mechanical Manufacturing processes became multidimensional.

Broadly Manufacturing processes could be classified into two groups, they are:

i. Primary Manufacturing: Provides only basic size and shape as per the design requirements, Powder metallurgy, forming, and Casting fall under this category.

ii. Secondary Manufacturing: In this, the dimensional accuracy and the better surface finish are the primary concern apart from maintaining the shape and Size. This could be achieved by removing the material in the form of chips under controlled conditions by skilled technicians.

Material removal processes can be divided further into two groups and they are "Conventional Machining and Non-Conventional Machining processes".

In the conventional Machining process, the required shape, size, and surface finish are obtained by removing the material in the form of chips. So the energy expended is purely Mechanical energy and a hard tool bit will remove the material from a relatively lesser hard workpiece surface. Turning, milling, drilling, shaping, boring are some of the examples. However, the limitation of Conventional Machining includes the inability to generate Complex surfaces, the Surface finish of Nano-meter size, and very hard materials like Ceramic materials.

1.2. Non- Conventional Machining Process: The most important drawback of the Conventional Machining process is the inability to machine the very hard Workpiece material, which has been addressed by Non- Conventional Machining process. In this process, Mechanical Energy, Electrical Energy, and Electro-Chemical energy are used for removing the material from the workpiece for getting the desired shape and size. Third-dimensional components with Complex shapes, miniature sizes that cannot be processed/finished economically and rapidly by traditional machining/finishing processes will be efficiently finished by adopting Non- Conventional Machining process.

In the present scenario, the quality of the product is assessed by its aesthetic appearance, surface finish, and expected life. The non-Conventional machining process is the right choice to tackle these problems. Though Buffing and lapping have been in use as surface finishing processes, the main disadvantage associated with these processes is Uneconomical and the time taken for generating a finely finished surface is more.

Fig.1.1 below shows the Machining accuracy obtained by different manufacturing processes that are in use since 1940. It may be observed that in the same class of Machining the surface finishing or Machining accuracy improved considerably in subsequent years starting from the year 1940 to the year 2000. The primary reason could be due to entry of Computers in the Manufacturing industry. Other factors contributing are improved design and better expertise in operating these machines

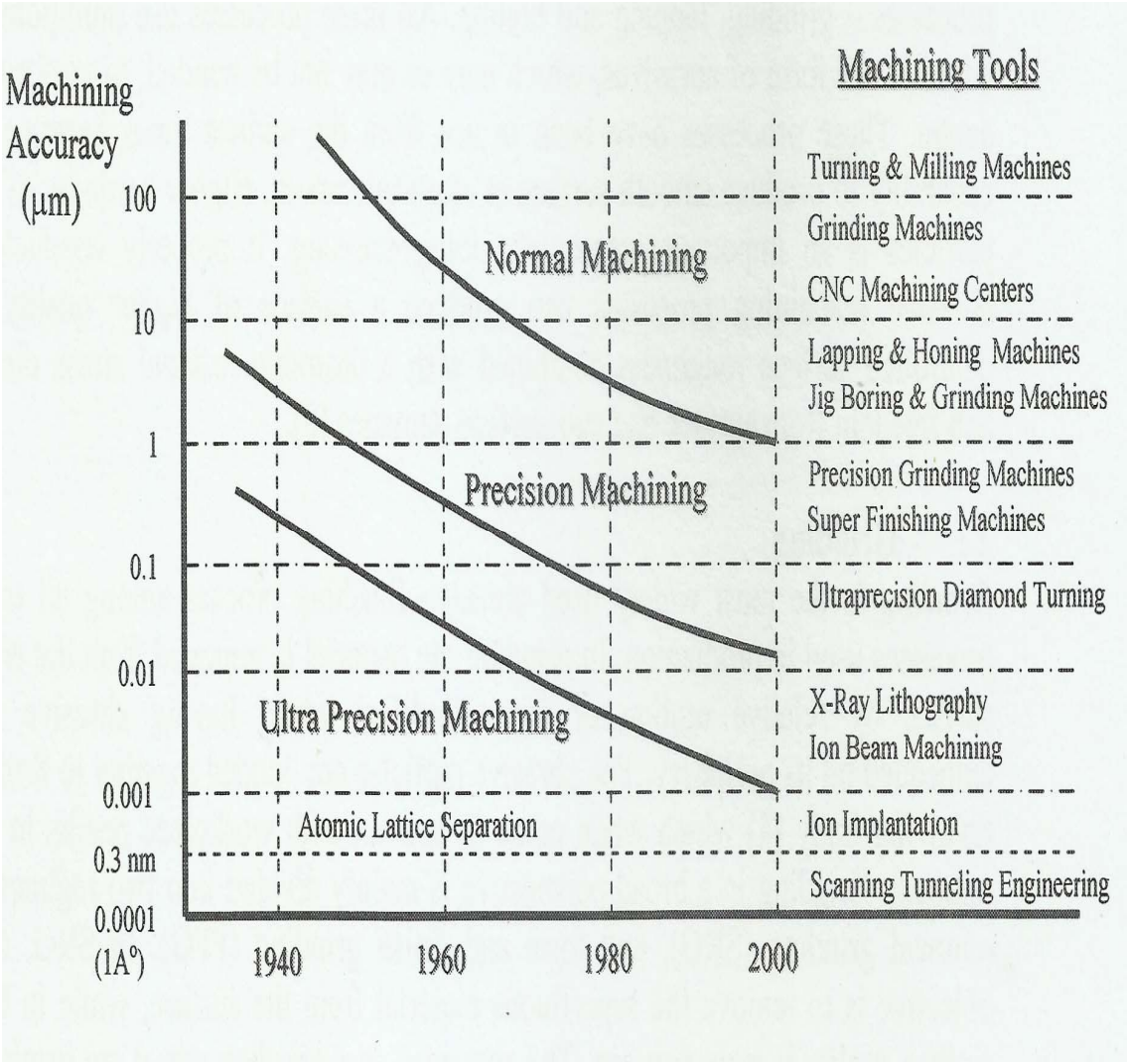

Fig.1.1 Evolution of machining Courtesy: Dr.Komanduri

Though Ultra-precision Machining gives a better surface finish, the cost involved is very high and it cannot be adopted for manufacturing components that are to be used for the general purpose at a lower cost.

1.2.1 Classification of Non- Conventional Machining process:

Non- Conventional machining process, which is getting prominence from the latter half of the 20th Century onwards could be classified based on the type of energy used. The following table gives a clear picture of different types of Non - Conventional Machining processes presently adopted in the industry.

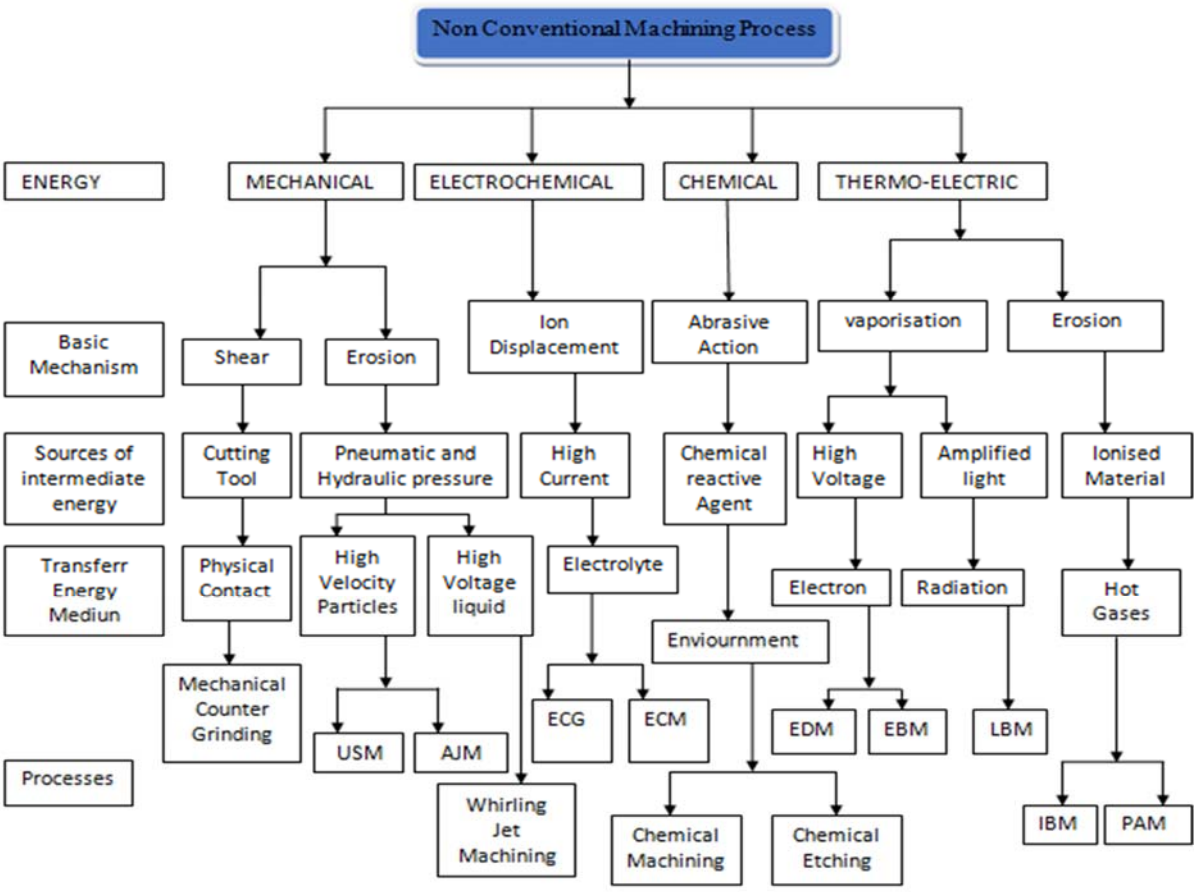

Fig. 2. Classification of Non- Conventional Machining Process

The classification of Non- Conventional Machining process is primarily based on the energy that is utilized Viz, Mechanical, Electrical, Electrochemical, Chemical, and Thermo-electric. The next method of classification is based on a basic mechanism that involves shear, Erosion, Ion displacement, abrasive action, Vaporisation, and Erosion. The next classification of the Non-Conventional Machining process is the source of intermediate energy which involves cutting tools, Pneumatic and Hydraulic pressure, high current, Chemical reactive agent, high voltage, amplified light, and ionized material. The next classification is the Transfer energy medium, which involves physical contact, high-velocity particles, high voltage liquid, electrolyte, electron, radiation, hot gases. Considering the above parameters, Non-Conventional Machining processes presently in use are Mechanical Counter Grinding, USM, AJM, Whirling Jet Machining, ECG, ECM Chemical machining, Chemical etching, EDM, EBM , LBM ,IBM and PAM are the examples of Non- Conventional machining process.

There is one more Non- Conventional Machining process, which could not get its place in the above Classification, and more prominent is the ***Magnetic Field Assisted finishing process***.

1.3. Magnetic Field Assisted Finishing process: Initially developed as a machining process known as Magnetic abrasive finishing (MAF), in the United States of America in the early 1930s, however, the first patent was obtained in 1940. This paved the way for conducting University-level research from the earlier part of the 1960s then technically advanced countries like the USSR, Bulgaria, Germany, Poland along with the Universities in the United States of America. began in the 1960s. However, the practical application could materialize from the 1980s onwards. The development of the semiconductor industry, aerospace industry, and optics industries have brought continuous up-gradation of the manufacturing industry for obtaining better methods for achieving high form accuracy as well as better surface integrity.

In Magnetic field-assisted process, Electromagnets or Permanent Magnets are used for generating Magnetic field and when the mixture of Ferrous particles and abrasive particle mixture mixed thoroughly passes through the magnetic field makes the Ferrous particles to form a chain-like structure and hence push the abrasives.

1.3.1. Classification of Magnetic Field Assisted Finishing Process:

Magnetic Field Assisted Finishing Process would be classified broadly as

i.Magnetic Abrasive Finishing (MAF)

ii. Magnetorheological Finishing (MRF)

iii. Magneto-Rheological Abrasive Flow finishing (MRAFF)

iv. Viscoelastic Magnetic Abrasive Finishing process (VMAF)

1.3.1.1 Magnetic Abrasive Finishing (MAF):

Magnetic abrasive finishing is an external surface finishing technique, whereby the external surfaces are finished by placing the mixture of Carbonyl Iron Particle(CIP) and the abrasive between the Magnet and the surface to be finished. Under the Magnetic field, a flexible brush comprising of CIP and the abrasives are formed. Due to Magnetic flux lines passing through the Flexible brush, Carbonyl Iron particles re-orient themselves in the form of a chain and the abrasive particles in the mixture will be projected to the surface to be finished. In the case of

finishing external cylindrical surfaces as shown in Fig.1.3 (35) below, due to the rotary motion of the magnet and the translator motion of the flexible brush, the finishing operation would be completed.

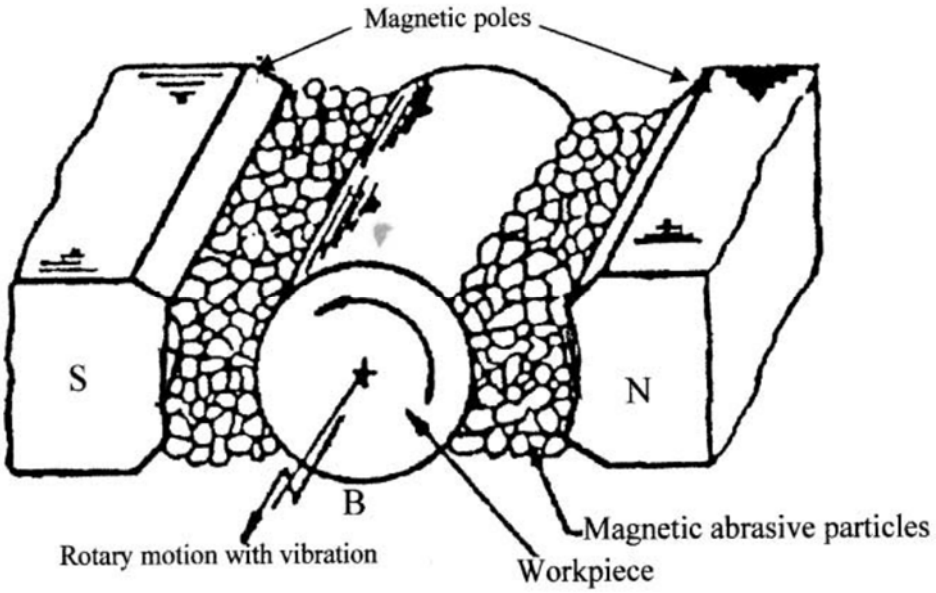

Fig.1.3 External Finishing of Cylindrical Surfaces [35]

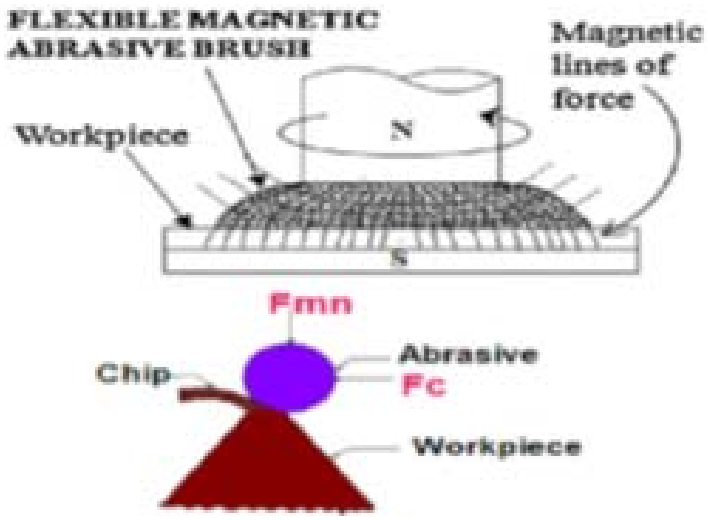

Fig.1. 4 External Finishing of Plane Surfaces [82]

In the case of external finishing of the flat surfaces, shown in Fig 1.4 above (82), the flexible brush forms between the rotating magnet and the flat surface to be finished. The rotary and translator motion of the Magnet will perform the finishing operation of the flat surface.

1.3.1.2. Magnetorheological Finishing (MRF):

Magnetorheological finishing is mostly used in the finishing of lenses used in the Optical industry. Fig. 1.5 (82) below represents the Magnetorheological finishing process adopted for finishing the Optical surface. A slurry comprising of Carbonyl Iron particles, abrasive particles, and carrier fluid will be pumped through the Nozzle in the space between the optical lens to be finished and the Electromagnet at the inlet. Carbonyl Iron Particles in the slurry after entering into the gap between the lens and the electromagnet form a chain and hence project the abrasive particles on the surface to be finished. The slurry will be sucked at the outlet and made to pass through the conditioner of MR Fluid and the cycle continues. The main advantage of this process is there will not be sub-surface damage.

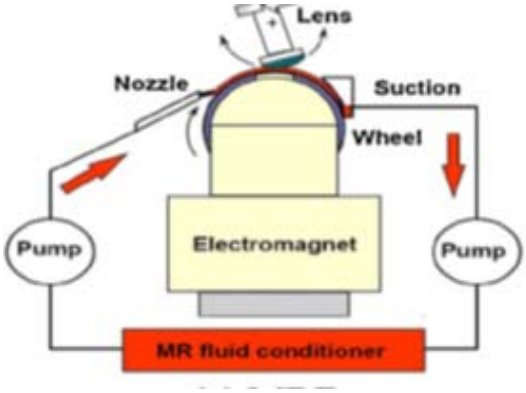

Fig.1.5 Magnetorheological finishing (MRF) process [82]

1.3.1.3. Magneto-Rheological Abrasive Flow finishing (MRAFF):

Magnetorheological abrasive flow finishing is adopted for finishing the internal surfaces of both Ferrous and Non-Ferrous Material. In this type of Finishing process, the medium prepared with a carrier fluid, abrasive particles, and CIP is made to flow through the internal surface to be finished. Fig1.6 (82) below represents the Magnetorheological Abrasive Flow finishing process. The formation of the CIP chain takes place under the influence of

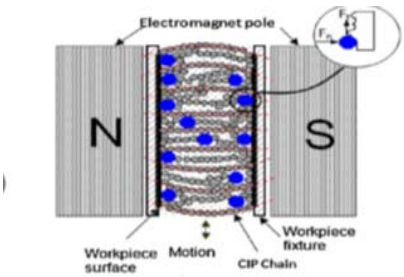

Fig.1.6 Magneto-Rheological Abrasive Flow finishing (MRAFF)[84]

Magnetic field and also the medium starts acting as a Viscoelastic Medium due to Rheological effect. The formation of the chain throws the abrasive particles onto the internal surface to be finished. Due to the rotary and reciprocating motion of the Magnetorheological medium, the peaks of the surface will be sheared and the surface. the finish is obtained which is of the order of a few Nano-meters.

Magnetic Float Polishing (MFP) and Ball End Magnetorheological Finishing Process (BEMRF) are two other Magnetic field-assisted finishing processes, which have specific application and do not fall under the General classification of the Magnetic Field Assisted Finishing Process.

1.3.1.4. Viscoelastic Magnetic Abrasive Finishing Process:

The concept of Viscoelastic Magnetic Abrasive finishing(VEMAF) was brought forward by ***Wenhui Li et al.*** in 2013(98). In the VEMAF process, the main advantage is that the medium comprising the Carbonyl Iron Particles(CIP), Abrasives, the semi-solid medium continues its Viscoelastic property in absence of the Magnetic field. The main drawback with earlier Magnetic Assisted Finishing processes is the sedimentation of the CIP in absence of the Magnetic field, which has been addressed by the VEMAF Process. Since the Viscosity continues throughout the travel of the Viscoelastic Medium during finishing operation, the sedimentation of CIP will not take place.

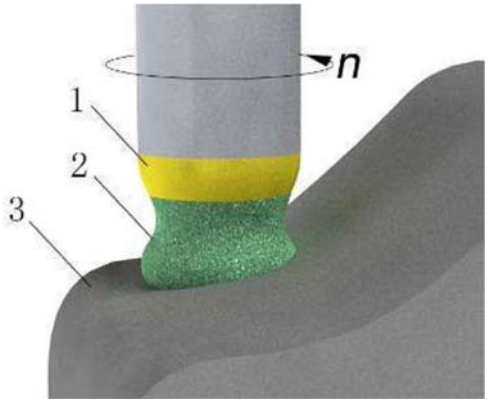

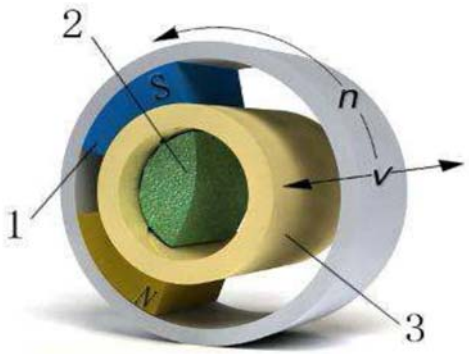

1. Magnetic Tool 2. Viscoelastic Medium 3. Workpiece

Fig.1.7. VEMAF of External Surface[98] **Fig.1.8. VEMAF of Internal Surface[98]**

Fig.1.7 above shows the Viscoelastic Magnetic Abrasive Tool (98), which is used for finishing both the Internal surfaces and External Surfaces. This comprises CIP, abrasive

particles, and a special matrix prepared, which continues its Viscoelastic operation throughout the cycle of operation of finishing. The matrix due to its flexibility and ability to retain CIP and abrasive particles in the proper position will be able to finish both the internal and external surfaces efficiently.Fig.1.9 below shows the schematic diagram of the VEMAF Tool.

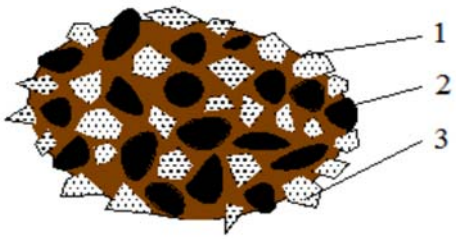

1.Matrix 2. Carbonyl Iron Particle 3. Abrasive

Fig.1.9 Viscoelastic Magnetic Abrasive Tool [98]

1.4. Mechanism of Viscoelastic Magnetic Abrasive Finishing Process:

The finishing process involved in the Viscoelastic Magnetic Abrasive Finishing process could be assumed to have two different mechanisms (98). They are

i. Micro Grinding and Sliding.
ii. Micro Rolling and sliding.

1.4.1 Micro Grinding and Sliding mechanism:

The first Mechanism that can be applied for the finishing process of the Viscoelastic Magnetic Abrasive Finishing Process is by Micro Grinding and Sliding. Fig.1.10 (98) below shows the schematic representation of the finishing process under Micro Grinding and Sliding Operation. The chain formation CIP that takes place due to Magnetic flux lines traps

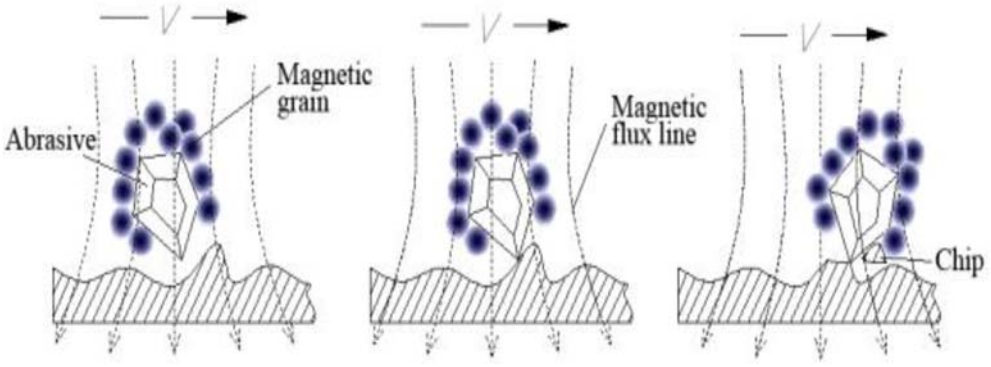

Fig 1.10 Micro Grinding and Sliding Mechanism for VEMAF[98]

the abrasive particles and due to the normal force created due to flux density and centrifugal

force acting on the Viscoelastic Magnetic Abrasive brush the peaks on the surface will be sheared as the brush slides over the workpiece surface. In this case, forces incur due to Gravity has been neglected.

1.4.2 Micro Rolling and sliding:

The second mechanism that can be applied to the Viscoelastic Magnetic Abrasive Finishing is Micro Rolling and Sliding, in which the abrasive grains trapped between the Carbonyl Iron Particles (CIP) will perform the finishing Operation by rolling and sliding shown in

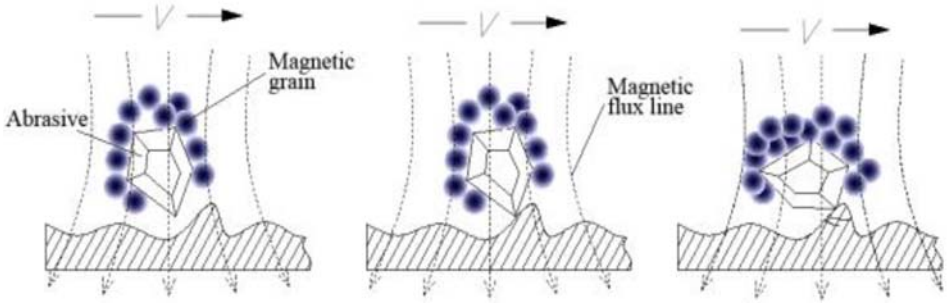

Fig1.11 Micro Rolling and Sliding Mechanism for VEMAF

Fig 1.11. Due to the rolling and sliding of the abrasive, it will get both rotational Kinetic energy and Translational Kinetic energy, which will shear the peaks of the surface of the workpiece. If the energy of the abrasive is not sufficient elastic deformation takes place and in successive cycles, the crack propagation along the peaks takes place and hence the shearing in the form of a Microchip takes place.

1.5 **Parameters influencing Viscoelastic Magnetic Abrasive Finishing Process :**

Viscoelastic Magnetic Abrasive Finishing is an extension of Magnetic Field Assisted Finishing Process, So most of the parameters that are considered to be prominent for Magnetic Field Assisted Finishing (76, 82, 97, 98, 102,103,106,107, 108, 112,114,119, 124, 125, 126, 131, 132) are also prominent in VEMAF process. Important parameters are as enlisted below.

i. Flux Density
ii. Abrasive Size and Shape
iii. Type of Carbonyl Iron Particle
iv. Relative Size of CIP and Abrasive Particle
v. The concentration of CIP and Abrasive.
vi. Material hardness
vii. Working gap.

viii. No of Cycles.

1.5.1.Flux density: One of the most important parameters in any Magnetic abrasive finishing is the Flux density. Magnetic flux lines will arrange the Carbonyl Iron Particles (CIP) in the form of a chain. The Normal force acting on the surface of the workpiece due to a Magnetic Flux density (B)(65) is given by

$$F_N = B^2(1-1/\mu_m)/2\mu_O \quad (65)$$

Where F_N = Normal force generated by the Magnetic field

B = Flux density

μ_O = Permeability in vacuum

μ_m = Relative permeability of the brush

From the above equation for the Normal force, it may be realized that $F_N \alpha B^2$, Normal force is more important for maintaining the CIP columnar chain and is proportional to the square of the flux density assuming that other parameters are constant.

Fig.1.12 (69) below shows the Magnetic flux distribution of External surfaces by adopting the Magnetic Field Assisted Finishing process. The circuit of the flux lines gets completed, once the flux lines enter into south pole starting from the North pole. The orientation of the CIP chain will be distributed along the flux lines and the abrasives will be pushed towards the surface to be finished.

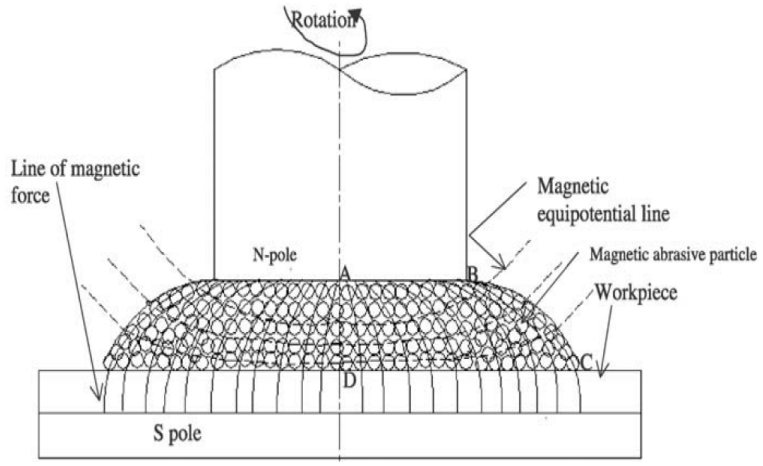

Fig.1.12 Schematic representation of Magnetic Abrasive Finishing set up[69]

There are two types of Magnetic flux generators used in the Magnetic field-assisted abrasive finishing process. They are

1.5.1.1.Electromagnet: In this, a copper coil is wound over a soft iron core and the magnetic flux density is produced due to the passage of the AC Power. The flux density depends on the number of turns of the coil and the Magnitude of the Current(I). Fig.1.13 [70] is

the schematic representation of an Electromagnet.

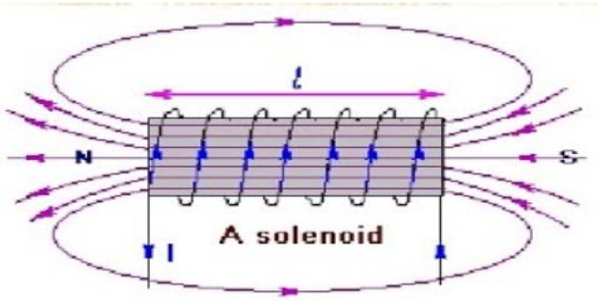

Fig.1.13 Electromagnet Flux Generator [70]

1.5.1.2.Permanent Magnet: Flux density due to permanent magnet depends upon the type of material used, the shape of the magnet, and the Volume of the Magnet.

1.5.1.3.Type of Material used: The following material is used in industry for making permanent magnets.

TABLE.1.1 Magnetic Properties of Commercially Available Permanent Magnets

Type of Material	Chemical Composition	Total no of Grades	Magnetic Coerciveness range B_r (mT)	Maximum energy range (kJ/m^3)
Alnico Magnets	Aluminum, Titanium, Nickel, Iron, Cobalt, and Copper	15	720-1350	10.7- 59.7
Ceramic Magnets	Barium/Strontium and Fe_2O_3	8	230-410	8.35 – 31.20
Rare-Earth Magnets	Cobalt, Praseodymium, Cerium, Neodymium or a combination	31	830-1410	130-400
Iron- Chromium-Cobalt Magnets	Iron, Chromium and Cobalt	07	880-1400	8.0- 41.80

Courtesy: Magnetic Materials Producers Association data

The choice of material is always based on the Magnetic Coerciveness and the Maximum energy/m^3, based on the data available, rare earth magnets give better flux density. In Magnetic Assisted Abrasive finishing processes, Neodymium magnets are preferred.

1.5.1.4. The shape of the Magnet: Flux density depends upon the geometry of the Magnets used. Figures. Fig.1.14 to Fig. 1.21 below are the shapes of the commercially available Neodymium magnets. However, Arc and Fan magnets are found to give better Magnetic Flux Density for the given volume as per the data available from the simulation work done in this thesis.

Fig.1.14. Disc Magnet

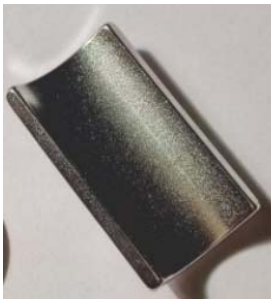

Fig.1.15. Arc Magnet

Fig.1.16. Ring Magnet

Fig.1.17. Fan Magnet

Fig.1.18. Cube Magnet

Fig.1.19 Block Magnet

Fig.1.20 Cylindrical Magnet

Fig.1.21. Spherical Magnets

[courtesy: Patel Magnets, Vadodara]

1.5.2. Abrasive size and Shape: While preparing the abrasives, the manufacturer does not have any control over the shape of the abrasives, however for most of the experimental analysis the

abrasive shape is assumed to be either Spherical or Wedge-shaped. The spherical shape does not give much plowing of the workpiece surfaces and plastic deformation and shearing in successive cycles is the main reason for removing the microchips from the surface. Wedge shape abrasives will have the advantage of plowing into more depth of the workpiece surface and hence material removal is higher.

Abrasives Normally used in the Nonconventional machining process will have the Grit size from 200 to 1200. The higher the Grit size, the finer will be the abrasive size.

The following table gives the idea about the Grit size and application in the manufacturing process.

TABLE. 1.2 Application of Abrasives in Manufacturing

S.NO	GRIT NUMBER	GRIT TYPE	APPLICATION
1.	40-80	COARSE	MATERIAL REMOVAL
2.	100-150	MEDIUM	LEVELLING
3.	180-500	FINE	FINISHING
4.	600-1500	MICRO	FINE SANDING

Present research work comes under finishing and Micro finishing (Fine Sanding) as per the table and the Grit size is between 180-1500. A smaller grit number indicates the coarse abrasive and material removal will be higher for smaller Grit size abrasives but they produce a relatively rough surface. A larger Grit number indicates Finer abrasives and the material removal will be lesser but produce a fine surface.

Most commonly used abrasives for the Non-Conventional Machining process, where the chips are removed by Mechanical energy have been enlisted in Table.2. In the present research work, Silicon carbide has been used for finishing.

Table.1.3 Properties of Most Commonly used Abrasives

ABRASIVES	DENSITY(gm/cc)	HARDNESS (Mohs)	HARDNESS (Knoop)
Diamond	3.52	10	700

Boron Oxide	2.52	9.30	3200
Silicon carbide (SiC)	3.22	9.20	2500
Aluminum Oxide (Al_2O_3)	3.98	9.00	2150
Chromium Oxide (CrO_2)	5.21	8.5	1800
Zirconium Oxide (ZrO_2)	5.85	8	1200
Silicon Oxide (SiO_2)	-	7	820
Cerium Oxide (CeO_2)	7.13	6.0	-
Iron oxide (Fe_2O_3)	5.24	6.0	-
Yttrium oxide (Y_2O_3)	5.01	5.5	700
Copper oxide	6.32	3.5	225
Molybdenum oxide	4.59	1.5	-

1.5.3. Grade of Carbonyl Iron Particle: Another important parameter that contributes to the finishing of the surfaces using the Viscoelastic Magnetic abrasive finishing process is the Grade of Carbonyl particle used. Table.4 below gives the details of the application, Grades, and the Iron percentage in the commercially available Carbonyl Iron Powders.

Table. 1.4 Composition & Application of Carbonyl Iron Powders

S.NO	Application	Grades	Iron%	Carbon %	*d_{50} value in Microns
1	Electronic components	CIP EM, CIP SQ, CIP SQ-1, CIP SW-S, CIP SP-1, CIP EW	97-99.5	0.03-0.9	3.0 - 10
2	Microwave absorption	CIP EW, CIP ER, CIP ES, CIP EW-1	97-97.4	0.90 -1.1	3.0-4.5

3	Metal Injection molding	CIP OM, CIP OS, CIP CC	97.5-99.5	0.05- 0.9	3.4 - 5.3
4	Powder metallurgy	CIP CS, CIP CM, CIP CN	99.5	0.3	7.0-9.5
5	Diamond	CIP SM, CIP EN	97.5-99	0.10-0.90	

*d_{50} Indicates that at least 50% of the abrasives will be having a size in the range mentioned. Recommended Carbonyl Iron powder type for Magnetic Assisted abrasive finishing process is CIP CS, which has Ferrous content up to 99.5% and the d_{50} size is 7.0-9.5 microns.

Courtesy: BASF The Chemical company data

1.5.4 Relative Size of CIP and Abrasive Particle:

Both Carbonyl Iron particles and Abrasive Particles are assumed to have a spherical shape. Based on the experimental results of *Jae—Seob Kwak et al.* (91), it has been observed that for the best surface finish the ratio of diameters of CIP to Abrasive particles is 4:1. Figure.1.22 below describes probable ratios of CIP and Abrasives.

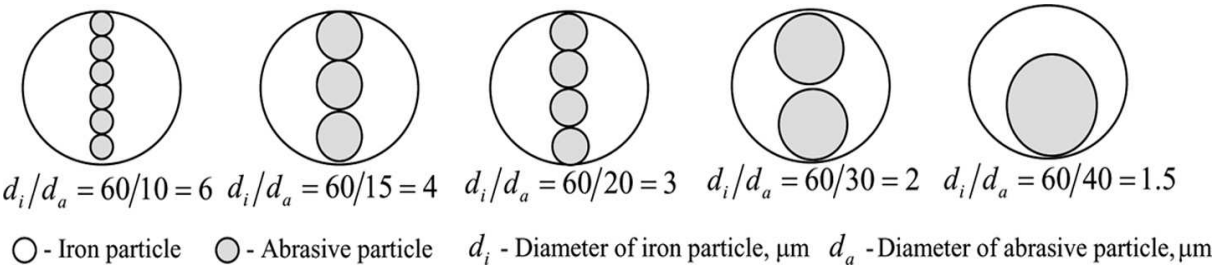

Fig.1.22. Different combinations for Abrasive and Magnetic particles

However, as per the literature survey, Jae-Kwak et al. (91) claim of the ratio of sizes 4:1 is more prominent for bonded abrasives, which are prepared by the Sintering process. In the present thesis, Unbonded abrasives are used.

1.5.5 Concentration of CIP and Abrasives: Concentration decides the number of abrasive particles available for micromachining and the Carbonyl Iron Particles available for making the chain in presence of the Magnetic field. A higher magnitude of the CIP will give better chain formation and more number of chains in a given volume but the number of Abrasive particles available for finishing will reduce considerably (71,92). If the magnitude of Abrasive particles increases the formation of a stable chain will become difficult and machining can't be done. During the literature survey, it has been observed that both volume concentration and the mass concentration has been adopted by the researchers. In the present thesis, a mass ratio of

1:3 for CIP and Abrasives has been adopted. Since the density of the CIP is 7.2 g/cc and abrasive particles are 2.6 g/cc. the approximate ratio of 0.92 is obtained by volume.

1.5.6 Hardness of the material: Surface roughness obtainable depends upon the hardness of the workpiece material. In the present thesis abrasive selected is Silicon Carbide and the material finished are Mild steel, Brass (45), and Aluminium. The hardness of the Mild steel is the highest and the Aluminium is the lowest. The hardness of all these materials is lesser than SiC. However, if the material is too soft then during the finishing operation, the abrasives will penetrate beyond the bottom of the valley and hence a new rough surface is obtained. So, for very soft and ductile material the finishing will not be good as compared to the material with moderate hardness and ductility. If the workpiece material is very hard it is difficult to remove the microchips from the surface and Viscoelastic Magnetic abrasive finishing is not suitable.

1.5.7 Working Gap: The working gap is the gap between the Magnetic tool and the surface to be finished in the VEMAF process for external finishing operation. For internal finishing operation, it is the gap between the inner surface of the Magnet and the Outer surface of the Hollow piece. This gap is occupied by the Viscoelastic abrasive medium in the VEMAF process. Flux density increases with the decrease in the Working gap. In the modeling chapter, a detailed analysis has been made. The higher the flux density means, the higher would be the Normal Force (F_N).

1.5.8 No of Cycles: One to and fro motion of the medium cylinder completes a cycle and each cycle comprises two strokes**.**No of cycles decides the material removal and the surface finish. However, from the literature and the experimental investigation of the present thesis it has been observed that When Unbonded abrasives are used in Magnetic Field Assisted abrasive finishing process, after completing a certain no of cycles, the abrasives start filling the Valleys and further material removal is not possible, this is especially prominent for Non-ferrous metals.

1.6. Viscoelastic Magnetic Abrasive Medium: A Viscoelastic abrasive Medium specially prepared for the experimentation of the present thesis. The medium comprises a Viscoelastic medium and a Magnetic abrasive medium. Viscoelastic medium prepared has got two components. The first one is the Viscous component made of Silicon oil or the Transformer oil as the base oil and when boric acid is added to Silicon oil cross-linking of the polymer takes place, which makes this more viscous. The elastic component is due to the sophication of Aluminium stearate. When these two or mixed Viscoelastic medium is obtained.

Now the Viscoelastic medium and the Magnetic Abrasive medium are mixed thoroughly to get the Viscoelastic Abrasive Medium, which retains its Viscoelasticity in presence of the Magnetic field and hence, sedimentation of the CIP will not take place. The detailed discussion about the preparation and the Experimental results of Viscosity of different media has been discussed in a different Chapter.

1.7. Simulation and Modelling of Permanent Magnets for Flux density: As mentioned in article 1.5 above, Flux density is one of the important parameters in Viscoelastic Magnetic Abrasive Finishing is the flux density, in the earlier research work on Magnetic Assisted Abrasive finishing has been found by Finite Element Analysis[63, In the present research work, ANSYS MAXWELL ANOSOFT 16 student version is used and the modeling of different geometries and orientation for a multi-pole system for Internal finishing and the Flux density for different gaps for external finishing of Steel, Bras, and Aluminium has been done.

Also, flow parameters have been modeled for internal finishing for three-level extrusion pressure.

1.8. Motivation of the present research: Magnetic field Assisted Abrasive finishing, which started in the 1940s has seen much development in the 21st Century. However, it is felt that there is an immediate need for a system where the Complex surfaces, both internal and external may be finished up to a few Nano-meters roughness. Knee prosthetic presently is being finished by using lapping and Honing. The present Thesis, which is done on Three material for external finishing may be applied for finishing any Complex shapes like Knee Prosthetics and other Complex shapes with the help of advanced CNC machines.

SUMMARY

a. Viscoelastic Magnetic Abrasive Finishing is a new method first introduced by W.H.Li is an extension to Magnetic Abrasive finishing, where the medium used is having the Viscoelastic property throughout the operation domain and hence Complex shapes could be finished.

b. The problem of sedimentation will be addressed by the Viscoelastic medium

c. Flux density is the most important parameter for finishing in the VEMAF process and other important process parameters include Abrasive size, Relative size of CIP and abrasive, Working Gap, etc.

d. The problem of settlement of the abrasives and CIP in the valleys during the machining will not be there due to the viscoelastic medium.

CHAPTER 2. LITERATURE REVIEW

In this chapter, a brief discussion about different research papers reviewed during the present thesis has been discussed. Literature Survey Covers Four different areas. Firstly, a literature review of the Viscoelastic medium has been discussed. Secondly, the finishing of internal surfaces by using the Magnetic Abrasive Finishing process has been discussed, followed by the Finishing of external surfaces by using Magnetic abrasive finishing has been discussed, and finally about the wear of material has been discussed. Research gap found based on the literature review, Objective of present research and the Research Methodology has been mentioned at the end of the Chapter.

2.1 Literature Review of Viscoelastic Medium:

B. Metzner et al. (1968) discussed elaborately the Viscoelastic behavior of the material. It had been observed that the Viscoelastic material possesses superior rheology characteristics when compared with the Newtonian fluids. The deformation rate always depends upon the Deborah number(N_{Deb}), which is a dimensionless number and is the ratio of Relaxation time to the time interval of deformation. The higher values show that the material is elastic in nature and the value less than "1" indicates Viscous flow.

H Schiessel et al (1995) had discussed the most commonly used Viscoelastic models. They correlated the Physical models of Viscoelasticity with fractional calculus. Viscoelastic models are between pure solid elastic model and pure viscous flow model. Viscoelastic model is between these two models and hence treated as a fractional model. Four types of Viscoelastic models had been discussed. The Maxwell model comprises a Spring and a dashpot in series, Kelvin- Voigt model has the spring and the dashpot in series which constitutes a fractional model which is a Viscoelastic model, Third model discussed had been Zener model in which a parallel spring is added to the Maxwell model, which also constitutes a Viscoelastic model and the fourth model Poynting-Thomson model in which a series spring is added to the Kelvin model. All these models had been analyzed and it is observed that these models are deterministic.

Mark R Jolly et al (1996) discussed the properties of Magneto mechanical chains that are arranged in a parallel position. Proposed a model that examines the behavior of the MR material. At the magnetic saturation point, non-linear behavior had been observed for the MR elastomers. For the pure iron experimental data states that the Magnetic saturation would have arrived at 2.1 Magnetorheological properties of the medium comprising of 10%, 20% and 30%

volume of Carbonyl particles had been tested and found that for 30% volume CIP the Magnetic saturation would have arrived at 0.63 T. MR fluids exhibit elastic behavior during the pre-yielding and they exhibit elastic behavior at post yielding zone. There will not be any change in the viscoelastic property by increasing the CIPs from 30% to 40%.

B. J. de Gans et al (1999) made an investigation of linear viscoelastic behavior of the Magnetorheological fluid medium made of colloidal Silicon particles which are in a spherical shape and the Carbonyl Iron particles(CIPs), with the help of a Magnetorheometer. The investigation suggests that the Elastic modulus (Storage modulus) is higher than the Viscous modulus (Loss modulus) when experimented against different Magnetic field strengths. Further, it had been observed that the elastic modulus does not depend much on the frequency, however, its magnitude had a linear relationship with volume fraction.

Byung Doo Chin et al.(2001) experimented with finding the Rheological response of MR fluids and their dispersion stability by using Carbonyl Iron Particles, Magnetite, and Silicone oil. The Yield stress of the MR medium is found to be proportional to $H_o^{1.5}$, where H_o is the External Magnetic field strength. Further, it had been observed that the Yield strength is proportional to the volume fraction of the particle concentration at a lower volume and would be having higher values as the concentration of the particles increase. The stability of the MR fluid medium would increase by adding the thickening agents like Cobalt, Ferrous oxide, and Chromium. These thickening agents reduce rapid sedimentation. Increased Magnetic field also brought an increase in the Yield Stress of the MR fluid medium.

Pardeep Kumar et al. (2004) performed the mathematical model for finding the effect of Magnetic field on wavenumber range. Planes of instability between two Newtonian fluids had been considered for the study and found that the fluids which were not stable in the absence of magnetic field were found to give stability under variable magnetic field.

Jerome Claracq et al (2004) studied the behavior of some of the MR fluids under the influence of the external magnetic field, as the fluid medium passes through the Magnetic flux-region, a rheological effect had been observed, which depends on the percentage of the Ferrous particles, Magnitude of the Magnetic flux density and the viscosity of the base fluid. Due to the effect of peeling of the ferrous particles, which will be having the structure of an onion, magnetic saturation takes place. The Recovery modulus is essentially due to the long chains made of the Ferrous particles and the Loss modulus is due to the flow of the broken chains. Rheological

properties have been observed, when the percentage of Ferrous particles by volume is as low as 5%.

Haobo Cheng et al. (2008) in their experimental work on Nano finishing of the Optical mirror using Magnetic assisted fluid finishing could reduce the roughness of the K9 mirror from 1.52 nm to 0.47 nm. For getting effective Rheological effect, Carbonyl Iron Particles had been treated. The percentage of CIP by volume is 33.84% and CeO_2 6% had been used in preparing the medium along with the Silicone oil and additive. The rheological fluid has shown an increase in Viscosity with the increase in the Voltage.

Haining An et al. (2010) had experimentally investigated the Viscoelastic Properties of the Magnetorheological gels which are highly swollen gels. In their experimentation, three different samples have been considered. All the samples are prepared with the Carbonyl particles having a disk-like structure. The first sample had been tested for its rheological behavior under Zero magnetic field strength (Isotropic. The second sample had the Magnetic field parallel to the gel surface and the third sample had the magnetic field perpendicular to the Gel surface. It had been found that in the third sample the Storage modulus got increased by 60 times in the orientation where the Magnetic field and the particle string are in phase and perpendicular to the shear direction. The behavior of the MR gels had been observed to be between MR elastomers and MR fluids.

D. N. Chirikov et al.(2010) Proposed a statistical model for finding the Macroscopic Viscoelastic behavior of Ferrofluids. They dealt with the Nonlinear Viscoelastic phenomenon. The viscoelastic phenomenon could be found by the evaluation of the aggregates which are Heterogeneous in Ferrofluids.

Bong Jun Park et al. (2010) discussed the preparation of Magnetorheological fluids based on different types of Ferrous particles like Carbonyl Iron particles, Magnetite, Magnetite based composite materials, Carbonyl particles, and Multiwalled Carbon Nanotubes. When these materials are used in preparing the MR fluids and subjected to a very low Magnetic field a linear relationship between Yield stress and the Magnetic field strength H has been observed. At the intermediate stage, the Yield stress is proportional to $H^{1.5,}$ and at the Nonlinear region, Yield strength is found to be proportional to H^2. Increased dispersion stability has been observed by adding Silica and Carbon Nanotubes.

Ji Eun Kim et al.(2011) experimented on a Magnetorheological fluid prepared with CIP, Polyisobutylene, and Polybutene. Storage modulus, Recovery modulus, and other Viscoelastic

properties had been studied using a Rheometer. Four stages of field strength had been considered from Zero field strength to a maximum field strength of 314 kA/m for finding the Recovery modulus and Loss modulus. The results showed that the Shear modulus is the best for 342 kA/m and the Loss modulus also gave a better result at 342 kA/m.

Min Su Kim et al. (2012) Examined the dispersion properties of Magnetorheological fluids prepared from Carbonyl Iron particles and a polymeric solution. Emphasis had been made on the rheological properties and the density of the medium prepared. The magnetization of the medium increased with Magnetic field strength and found a saturated Magnetisation value of 190 emu/g at a field strength of 7 koe. Shear stress increased in proportion to the field strength. At higher field strengths MR fluids started to exhibit Bingham fluid behavior.

J. P. Segovia-Guti_errez et al. (2012) studied the gelation regime in Magnetorheological fluids. Increase in Magnetic particle concentration by volume percentage had increased magnetic rheological properties and suddenly the values increase once the critical values achieved. Formation of the gel took place for Carbonyl iron particle percent of 10% and field strength of 10 kA/m. There will not be an appreciable increase in Storage modulus, once the volume percentage of the Carbonyl Iron Particles reach approximately 20% by volume for all the Magnetic field strengths.

Song Li et al. (2013) found the theoretical values of the shear stress under different Magnetic field strengths of Magnetorheological grease by using a computer model using Simulink and compared these values with the experimental data. Electrostatic properties had been considered for the simulation. Under Zero Magnetic field strength analysis had been made for the variation of the Shear stress concerning particle size, Shear stress with field strength. It had been observed that the value of the Shear strength was coinciding with the experimental values for the lower density of the Ferromagnetic particles in the MR Grease. When the density of the Ferromagnetic particles increased the Shear strength values are lower than the experimental values.

Miao Yu et al. (2014) prepared a Magnetorheological gel comprising of Carbonyl Iron particles in a dispersed state in Polyurethane gel and found the resistance values against different Magnetic field strengths for different Carbonyl iron particle concentration by weight. Experimental results showed that the concentration of CIP had a greater role in the resistance and by controlling the Magnetic field strength the resistance values could be altered. The CIP

composition of 70% by weight, when subjected to 0.1T had a resistance value of 7.56 MΩ and its value got reduced to 2.4 MΩ when the Magnetic field strength increased to 1 T.

Bablu Mordina et al.(2014) Investigated the Magnetorheological properties of the medium prepared from Polydimethylsiloxane and $FeCo_3$ Nanocomposite. Solution casting technique had been used for preparing the samples having the composition of $FeCo_3$ weight percentage of 5%, 10%, and 20%. Both Isotropic and Anisotropic samples had been prepared and tested for the Rheological properties. It had been observed that Anisotropic medium got a Higher amount of Magnetisation saturation when measured parallel to the plane of the particles compared to the values obtained when the measurement had been made perpendicular to the plane of the particles. Isotropic medium on the other hand exhibited better Magneto rheological properties both absolute and relative for all the values of the concentration of $FeCo_3$ under study.

Vyacheslav S et al. (2014) Synthesis of Magnetorheological elastomers(MRE) had been done on the medium made of Silicone oil and Carbonyl Iron Particles (CIPs). When the Magnetic field had been applied on a plane perpendicular to the shear plane it had been observed that bot Recovery modulus and loss modulus are dependent on the shear strain. An increase in flux density would increase the strain dependence of the moduli. Temperatures in the range of -40^{O} C to 300^{O} C would give stable Magnetorheological properties.

Shreedhar Kolekar et al. (2014) investigated the Rheological properties of the Three samples made of Silicone oil as the carrier fluid, Carbonyl iron particles having the composition of 22%, 30%, and 40% by weight for the Sample A, Sample C, and Sample B respectively along with Lithium Grease as additive. Plate and Cone type Rheometer had been used for measuring the rheological characteristics of the three samples. The Viscosity vs Shear rate showed that sample A and Sample C are having a linear relationship and a reduced value of Viscosity with increased shear strain had been observed. Sample B is having a nonlinear relationship. For all three samples, strain amplitudes between 0.001% to 10% were considered and the result shows that Elastic modulus(G^{I}), Loss modulus (G^{II}), and loss factor are sensitive to the applied strain. A considerable increase in the Storage modulus with the increase in the Magnetic field strength had been observed.

Seung Hyuk Kwon et al. (2015) experimented on the Magnetorheological grease prepared with Carbonyl Iron Particles and Halloysite Nanoparticles using rotary Rheometer under different magnetic field strengths. Experimental investigation under five levels of a magnetic field

having pure CIP and CIP with Halloysite Nanoparticles had shown that the shear viscosity had a proportional relationship with Magnetic field strength. Constant shear stress values for the entire set of shear strains had been observed and this would be due to the well-established chain structure formed by the CIP. The addition of Halloysite Nanoparticles had reduced the sedimentation considerably.

Dongdong Wang et al. (2015) performed the experiments for finding out the Magnetic saturation phenomenon on the Magnetorheological fluids prepared with Carbonyl Iron Particles, Fe_3o_4, Sodium Dodecyl Benzene Sulfonate, and Oleic acid. For finding. Ethyl alcohol and nanoparticles had been added for reducing the sedimentation problem. Yield stress increases with an increase in volume fractions up to 45%. Between 45% to 55% an erratic increase in yield stress had been observed due to the formation of columnar structure. High and stable Yield stress had been observed.

Vikram G. Kamble et al. (2015) Experimented with finding the Magnetorheological properties of two different samples. The first sample had Castor oil as the carrier oil and CIP and Lithium grease had been added. The second sample has Honge oil as the carrier oil and Carbonyl iron particles and Lithium grease had been added. The following rheological properties had been observed when tested with Cup and Bob type Rheometer. The sedimentation ratio for both the samples got stabilized at 200 hours. For the Castor oil medium, the shear stress increased with Shear strain whereas in the Honge oil medium, the shear stress increased with shear strain and there was a sudden drop in shear stress at the strain rates between 5-7% and from there the shear stress increased with Shear strain. For both, the samples Dynamic viscosity reduced with an increase in shear strain and both attained the minimum values of shear stress at shear strain values of 21. Storage and loss modulus showed decreased values with an increase in shear strain, however, Honge oil medium showed a decrease in these values at relatively lesser shear strain compared to Castor oil medium.

Shih-Hsien Chou et al. (2016) Proposed a Novel gel for finishing the Mild steel rods using the Magnetic Abrasive Finishing technique. Bean Gel prepared for this purpose will hold the Ferrous particles and the Magnetic Abrasive Finishing (MAF) process, under centrifugal forces would not be drifted away from the working space. Out of the three gels used for the experimentation, Bean gel had 1.2 Pa-S, Silicone Gel I 120 Pa-S, and Silicone Gel II 500 Pa-s, and Bean Gel gave a better surface finish. Surface roughness values with the bean gel as Medium under a finishing time of 5 minutes improved from 0.65 μm to 0.09 μm. The novel

method known as Magnetic Finishing with Gel Flow Abrasive(MFGA) produced a better surface finish which is three times better than that obtained by Magnetic Abrasive Finishing (MAF) without Gel as the medium.

Wei Gao et al. (2017) experimented with finding the Magnetorheological properties of the composite medium made of Polydimethylsiloxane, Carbonyl Iron Particles, and Cobalt. Experimental results showed that there had been a considerable increase in thermal stability, loss factor, Saturation values of the relaxation modulus and loss modulus, Ultimate stress with an increase in the mass percentage of Cobalt particles. There was a decrease in the Variation of the Coercive field with an increase in mass percentage Cobalt in the composite medium.

Kashif Ali Abroa et al. (2018) performed the mathematical analysis of the influence of the Magnetic field on Viscoelastic fluid using the Mathematical Transformation Technique. Mathematical solutions had been obtained for the behavior in presence of a Magnetic field and absence of a magnetic field. It was observed that the velocity field thickens and shear stress scatters with an increase in viscosity. The velocity of flow of the medium and shear stress is inversely proportional to the magnetic field.

N. Mohamad et al. (2018) Investigated the Magnetorheological effects of the media prepared with Plate shaped Carbonyl Iron Particles and Spherical Carbonyl Iron Particles. Three samples each having the CIPs weight percent of 30, 50, and 70 prepared and their rheological characteristics under eight different Magnetic field strengths starting from 0T to 0.7T in steps of 0.1T under continuous mode and Oscillatory mode had been investigated. It had been observed that for both the types of samples apparent viscosity and Storage modulus strongly depend on the Magnetic field strength. Shear stress vs Shear strain curve plotted shows that for MRG 70 (70% weight fraction) Shear stress initially falls as the shear strain increased then continuously increases with increase in shear strain for a field strength of 0.7 T. Both Storage modulus and Loss modulus increase with the increase in flux density.

Shuhei Sasaki et al. (2018) had performed the experiments to find the Storage modulus values for both Un cross-linked and Cross-linked elastomers. Under zero magnetic field, the Storage modulus was found to be scattered and upon application of the Magnetic field sudden increase in the storage, modulus had been observed for Uncross linked elastomer. Cross-linked elastomers also exhibited a similar result as shown by the Un cross-linked elastomers.

Siti Aishah Abdul Aziz et al. (2019) studied the changes in Viscoelastic properties and Electrical resistance properties of three samples prepared. The first sample prepared without

Mg and the remaining two with Nano-sized Ni- Mg Cobalt Ferrite particles. The samples comprising the Ni-Mg Cobalt Ferrite particle exhibited 43% raise in the storage modulus when compared with the sample prepared without these nano-sized particles. The magnetization curve for all these samples was similar. Electric resistance had a sharp fall for the Nanoparticle samples.

Huixing Wang et al. (2019) found the values of Normal force of the Viscoelastic medium prepared from Lithium based grease under different Magnetic field strengths. Percentage of Carbonyl Iron particles in three media prepared were having a weight percentage of 30, 50, and 70 respectively. Normal stress exhibited higher values at higher flux density and the Normal stress value decreases at 25% strain and remains constant for different Magnetic field strengths. Normal stress gets decreased with the increase in Shear stress.

Irfan Bahiuddin et al.(2019) predicted the Magnetorheological properties of MR Grease using a backpropagation artificial neural network. Five samples having a percentage weight of 10, 30, 50, 70, 80 Carbonyl Iron Particles had been added to the commercial grease NLG 3. Simulated results showed that the higher shear stress for higher flux density. Both the experimental and simulated values of Yield stresses showed that the Yield stress values were higher for the sample with higher weight % of CIP at higher Magnetic flux density.

Tiger Hu Sun et al. (2019) in their experiment with Magnetorheological grease prepared by them found the rheological properties. In total five types of grease prepared by them having a different composition of Carbonyl iron particles. It had been found that the Viscosity got increased with the increase in flux density. However, the Viscosity for the grease with 5% volume of CIP has shown an appreciable increase in Viscosity with an increase in the flux density. As the volume fraction of the CIP increased, the increase in Viscosity with flux density is gradually started reducing. Shear stress also got increased with the increase in flux density.

Huixing Wang et al.(2019) investigated the Quasi-Static Rheological properties of the Lithium-based Rheological medium having different carbonyl iron particle proportion by weight. Three samples having the CIP proportion by weight of 30%, 50%, and 70% had been chosen for the experimentation. Shear stress is the highest for the Magnetorheological Grease with a 70% CIP proportion. Shear stress increases sharply up to 20% of strain under zero flux density, then the Shear stress remains constant and the medium with the higher value of CIP got higher shear stress. At a higher magnetic field, the material behaves like a solid. Yield stress for all three samples.

Norzilawati Mohamad et al. (2019) investigated the Rheological properties of Bidisperse Magneto-Rheological Grease, having Carbonyl Iron Particles having spherical and plate-like geometry. Five different samples, each with a different weight percentage had been chosen to prepare Magnetic Rheological Grease. Transient response of the MR Grease having CIP with Bidisperse geometry and Mono-Geometry under a stepwise increase in the Magnetic flux density had been investigated. The behavior of MRG1 & MRG5 is similar under an increase in Magnetic field, whereas the behavior of MRG 2, MRG 3, and MRG 4 exhibited similar behavior under increasing magnetic field. The viscosity of MRG 2, MRG 3, and MRG 4 started to show a steep rise approximately at 0.6 T. The alignment of Spherical CIP can be easily disrupted compared to Carbonyl Iron Particles with plate-like Geometry.

Kejie Wang et al. (2019) Prepared Magneto-Rheological Grease having Aluminium Stearate as the thickener and the effect of Silicone Oil Viscosity, the Weight proportion of Carbonyl Iron Particle and size of the Carbonyl Iron Particle on Dynamic Yield stress had been investigated. The medium prepared had been treated as Bingham fluid. As per the Optimisation done with Analysis of Variance (ANOVA), the Dynamic Yield stress produced by the MR Grease depends on CIP weight fraction from 0.65 to 0.75 and Silicone Oil Viscosity 50 m^2-s to 1000 m^2-s. Experimental data for Shear stress and Shear strain mostly coincides with the Viscoplastic Bingham fluid model. The highest value of the Yield stress obtained was found to be at 65.96 kPa.

2.2 . Literature Review of Internal Finishing by MAF Process:

Takeo Shinmura et al (1995) proposed a mixed type of Magnetic abrasive comprising of White Alumina abrasive sintered with Ferrous particles for obtaining internal fine finishing of the internal surface of Stainless Steel Tube and Clean Gas Bomb. For a given mass of the ferrous particles, Magnetic field strength for Ferrous particles with different sizes is approximately similar. The field strength of Ferrous particles is five times that of mixed abrasive. Internal finishing with mixed abrasives gave roughness values up to 0.2μm

Jeong Du Kim et al (1996) calculated the magnetic force at static state and intermediate state by using the finite element method for three-step mode and six-step mode and found that the field strength of three-step mode gives better results than the six-step methods.

Jeong Du-Kim et al. (1997) found experimentally that smaller velocities of the jet of the fluid medium will allow the abrasives to move nearer to the internal surfaces to be machined and the size of the magnetic abrasive has no role in deciding the path of the abrasive motion. Maximum

material removal is obtained at an intermediate impact angle of 30^0 and the metal removal reduces considerably with an increase in the impact angle. At zero degree impact, angle metal removal is also found though does not give optimum value.

Hitomi Yamaguchi et al. (1999) proposed a semisolid abrasive finishing tool that gave better surface finish as the semi-solid abrasive penetrates through both the peaks and valleys due to which it gives better material removal and surface finish. In their research and development, for removing the lesser amount of material, a fixed tool known as Magnetic Jig has been proposed

Hitomi Yamaguchi et al. (2000), in their study, found that the distribution of the magnetic field decides the finishing conditions in the Magnetic abrasive flow finishing process. They considered two geometries of permanent magnets and calculated the field strength, one is straight pair of magnets and the other set is tapered pair of magnets.

Sehijpal Singh et al. (2002) Material removal is proportional to the flux density, higher magnetic flux and lower medium flow give higher metal removal and lower ΔR_a. A medium flow rate does not have a significant effect on MR and ΔR_a in the presence of a magnetic field. Hitomi Yamaguchi et al. (2004) found that the composition of the carbonyl particle, size of the abrasive, and the quantity of the lubricant employed will decide the surface finish of the workpiece and also observed that the material removal takes place from the peaks only. The residual stresses before finishing were compressive, which became tensile after the finishing operation. However, the effect shown is marginal.

Sunil Jha et al.(2004) in their experiment on finishing of internal surfaces concluded that for better surface finish the size of the Carbonyl Iron Particle should be higher than the size of the abrasive since the chains formed by the smaller Carbonyl Iron Particles is weaker.

Debin Wang et al (2004) adopted a poll rotating mechanism with permanent magnets. They observed that the finishing under distilled water gives a better finish than the dry finishing condition. Chemical action between Cr_2O_3 and Si_3N_4 will give mechanochemical finishing.

Y.Wang et al(2004) based on their experiment with permanent magnets found that single magnet, double magnets with 90^0 and 180^0, due to the distribution of their magnetic field could not give a smooth flow of the abrasives and Jumbling of the abrasives takes place, which in turn does not give a better surface finish. For obtaining smooth surface finish using four magnets, it is preferred to have the orientation as N-S-S-N as this orientation gives better

surface finish and the orientation N-S-N-S does not give the movement of the abrasives. They also found that an increase in magnetic flux density from 0.1 T to 0.3 T increased the surface finish. Bigger abrasives give a rough surface finish and leave deep scratches, whereas smaller grains give a better surface finish in a given finishing time.

Yan Wang et al. (2005) found that the configuration of the abrasive particles and magnetic force acting on the ferrous particles depends upon the magnetic field distribution, Maximum material removal is obtainable for an optimum abrasive size only, and below that the metal removal reduces. Metal removal is proportional to rotational speed, however at higher rotational speeds frictional force dominates the magnetic force, hence the permanent magnets with better field strength are recommended. For machining of the Brass alloy TiC/Fe (35%) by weight is preferred. For most other materials Al_2O_3/Fe (20%) is preferred.

Sunil Jha et al , (2006) proposed that in the Magnetorheological abrasive flow finishing process the metal removal is proportional to the Magnetic field strength and also a continuous increase in Magnetic field strength will not give a proportional increase in Metal removal since the abrading forces depend on the size of the abrasive finish and also initial R_a value.

Amit M. Wani et al. (2007) verified his mathematical modeling by considering the Static Magnetic Potential analysis and verified with the experimental outcome and found that first, the diameter of the magnetic polishing brush has to be decided, and then the size of the abrasive has to be decided. A comparison has been made between the abrasive flow machining without and with the Magnetic abrasive and it is observed that for a given material removal lesser no of cycles are needed for Magnetic abrasive flow finishing when compared with abrasive flow finishing.

Hitomi Yamaguchi et al. (2007) performed the internal finishing operation of the Capillary tube made of SU304 Austenitic Stainless steel having a diameter of 800 μm with mixed abrasives comprising of Al_2O_3 and Ferrous particles. For obtaining better Magnetic flux density pole tip has been tapered, which correspondingly increases Magnetic force. Unstable behavior of the mixed abrasives inside the capillary tube has been observed in the zone away from the pole tip. For effective finishing of the capillary tubes which are rotating at very high speeds of the order 30000 rpm, support at 3 points has been suggested. [105d]

Manas Das et al. (2008) in their investigation for the Magnetorheological abrasive finishing process assumed the Length to radius value of the Capillary tube to be approximately equal to 60 and with this assumption the medium hence prepared will exhibit Viscoplastic behavior. The CIP and abrasive combination are treated as half Body-centered cubic structure. The chain formed is along the magnetic lines and when the resultant force due to the extrusion pressure and the magnetic field exceeds the Yield strength of the specimen material the finishing takes place. However, initially rapid improvement in the R_a has been found due to the removal of the loose particles in the initial stage and plowing takes place.

K. Handa et al (2008) has experimented with the finishing of the plane surfaces using a composite powder comprising of the Iron particles and diamond powder. He observed the removal of diamond particles trapped between the Carbonyl Iron Particles (CIP). This problem could be addressed by adopting a plasma pray system, whereby the thermal diffusion of diamond particles and CIP will take place, which gives spherical abrasives of 10 μm diameter and these particles could be efficiently used for the internal finishing of Capillary tubes.

M.Ravisankar et al. (2010) described finishing of Metal Matrix composites by rotating abrasive flow finishing, calculated the helix angle for the path traversed by the abrasives, the total path traveled gets increased and hence a single abrasive will travel more distance than an abrasive, which travels in a straight path. Smoother surfaces gives higher hardness as the available valleys are lesser and hence such surface offers more resistance to penetration. Three modes of micro-cutting have been proposed. When the cutting force is lesser than the yield stress of the work-piece material, the abrasives will rotate, Cutting force is higher than the resistance force by the work-piece, the material will be removed in the form of fragmented chips and brittle fracture is observed.

Hitomi Yamaguchi et al. (2010) while performing the internal finishing of the Nonferromagnetic elbow-shaped hollow pipe, in their study, observed that the material at the elbow section is having a ferrite structure and the other straight portions Martensitic structure is existing. At the elbow section, where a larger radius of curvature is smaller finishing force is required for given material removal, and for the lesser radius of curvature of the elbow section, larger finishing forces are needed.

Junmokang et al (2012) single and multiple point arrangement for the finishing of the inner surface. For ferromagnetic tubes the magnetic abrasives supplied would not be distributed

uniformly as they follow the magnetic lines of force, so a multiple pole system is proposed for proper finishing. In some zones, the frictional force is more than the magnetic force and in ferromagnetic tubes, the accumulation of the abrasive particles takes place.to counteract this problem shorter magnetic regions have been proposed.

Junmokang et al. (2012) experimentally found the material removal and surface finish for internal surfaces of the capillary tubes with single and multiple pole systems at very high speeds. The experimental result revealed that when magnetic abrasive internal finishing took place at higher speeds, the amount of material removed at 20 minutes is more than two times higher than the material removed after 10 minutes. When the specimen is rotated at 20000 Rpm, it has been observed that the material removal is increasing but the surface finish goes down, this is due to an increase in the centrifugal forces, which will indent the surface.

Zhen Hog You et al. (2017) performed the polishing of the internal surface of a curved pipe. For finding the trajectory of the machining path Centreline reconstruction method has been adopted. At the inner surface of the elbow pipe, due to smaller grinding pressure, Magnetic abrasive Particles tend to adhere to the internal surface, so poor metal removal and surface finish, this is due to the lesser amount of the flux density at this zone to counteract this issue Spherical magnets have been proposed.

Valens Nteziyaremyea et al. (2017) performed both the internal and external finishing by using the magnetic abrasive finishing technique simultaneously using a pair of permanent magnets. It is observed that when the Magnets are placed at 90^0 with each other the amount of Magnetic force is higher than when they are placed at 180^0. As the magnetic force is proportional to H.gradH, where H is the field intensity and grad H is the gradient of the field intensity and H.gradH is higher for 90^0 compared to 180^0. Surface finish at this orientation of the magnetic field is far better for the inner surface compared to the outer surface. For getting a uniform high surface finish the inner surface is loaded with magnetic abrasive and the outer surface is loaded with diamond abrasives with rubber magnet or magnetic slurry is preferred.

H. Yamaguchi et al performed the internal finishing of the large size bent hollow tubes made of SUS316 and SUS304. The large size tubes selected for the study are made by cold drawing and high-frequency induction bending. These large pipes must have a better surface to resist contamination due to the flow of fluids due to chemical action. Internal surface finishing by magnetic abrasive finishing will be carried by the rotary and translator movement of the

magnetic abrasive brush inside the tube along with the external rotation and curvilinear motion of the permanent magnet tip. Cold drawn tubes will achieve the required internal surface finish of the order of 0.03 μm with the iron particles of size 330 μm and magnetic abrasives of 80 μm, on the other hand for the finishing of the internal surface of the pipes made by high-frequency induction bending, two-stage finishing is proposed. Initially, rough machining takes place by using the Iron particles of 1680 μm and magnetic abrasives of size 80 μm, followed by finishing with iron particles of 510 μm and magnetic abrasives of 80 μm.

Talwinder Singh Bedi et al. (2018) performed internal finishing of Ferromagnetic cylinder by introducing an Electromagnetic tool, which rotates and reciprocates inside the hollow cylinder such that the maximum flux density is on the surface of the Electromagnetic tool, due to which the ferrous particles will be sticking to the surface of the tool and the abrasive particles are projected to the inner surface of the Ferromagnetic cylinder. As per their observation, if the maximum flux density is on the inner surface of the Ferromagnetic surface, the iron particles will stick to the surface and hence the finishing can't be done. Two geometries one an I section and the other a T section have been prepared for making the Electromagnetic tool. Flux density has been obtained by using the Maxwell Ansoft V13(Student) version and based on the simulation, it is also found that the geometry with T shape is giving better result and in this case, the peaks have been sheared and the surface finish obtained is of the order of 120 nm.

Sahil Kajal et al. (2019) performed the Nano finishing of the rifle barrel, where a surface finish up to 150 nm is achieved. A special finishing tool is prepared for finishing the barrel, which has an internal diameter of 0.32 inches. The tool comprises of a steel rod having button magnets attached to its surface. CIP 40% by volume and the abrasives 23% by volume and lubricant have been used for the finishing purpose. The tool prepared reciprocates and rotates inside the barrel, this gives the required surface finish at optimum values. An increase in the rotational speed of the tool increases the centrifugal forces, which in turn reduces the stability of the brush.

2.3 Literature review of External finishing by MAF process.

Kuppusamy (1979) in his experimental verification of magnetic field effect on electrolytic grinding found that Material removal rate proportionally increases with increase in Magnetic field, similarly, Faraday's efficiency proportionally increases or decreases with increase or decrease in Magnetic field strength. He observed that there exists an inverse relationship between the magnetic field and the Surface energy.

T. Shinmura et al. (1990) in their experimental study observed that the magnetic forces are proportional to the Volume of the magnetic abrasive, however, the magnitude of the finishing pressure has no bearing on the abrasive particle size. Factors contributing to good surface finish finer mesh number of the abrasive particle is preferred. However, the material removal will not be appreciable. A finer finish of the order of 0.04 μm could be obtained, when CI particles are coated with diamond powder.

Jeong – Du Kim et al. (1995) performed the simulation for the Magnetic abrasive finishing process and found that the Magnetic flux density is proportional to the air gap, and the Cross-section area of the air gap does not influence the magnitude of flux density. MRR is not in proportional relation to the time of finish. An increase in Machining Pressure would be observed after a sluggish start as the flux density increases

Jeong – Du Kim et al(1997) performed Magneto Electrolytic abrasive polishing by adopting permanent magnets of 0.06T capacity, Electrolyte forms a Viscoelastic sheet on the surface. The higher Speed of the tool does not give a better surface finish. Initial higher flux density gives a better surface finish.

Shaohui Yin et al. (2004) in their experimental work on vertical vibration-assisted magnetic abrasive finishing for Magnesium alloys found that the finishing of the Magnesium alloy could be done with a lesser amount of time when compared to the non-vibrating Magnetic abrasive finishing method. Around 20% reduction in time is found while performing the deburring process. It has been observed that by adopting this method complex 3D geometries could be finished efficiently with a lesser amount of time.

Shaohui Yin et al.(2004) had performed magnetic abrasive finishing for SU304 stainless steel by adopting 3 modes of vibration, along with horizontal "X" direction(mode), Vertical "Z"

direction (mode), and “ZX” direction (mode) and found that Stock removal and surface finish were higher in the vibration of the abrasive brush along Z direction followed by ZX direction, followed by X-direction. Compared to the Non-vibrating mode, Vibration modes had given better stock removal and surface finish. In X-direction vibration and ZX direction finishing was due to cross-cutting. ZX mode had given a better surface finish with the highest finishing efficiency compared to the Z mode which gave some rough surface also.

Dhirendra K Singh et al. (2004) found that Maximum flux density for an electric magnet would be found at a distance away from the center for all the voltage steps under consideration and the flux density increases with the increase in voltage. Unbounded abrasive particles having 75% CIP, 22% SiC, and 3% lubricant by weight have been used in the experiment and optimization has been done by using the TAGUCHI method. It has been found that the reduction in surface roughness depends on the voltage (in electromagnets) and the gap between the surface to be finished and the magnetic brush, for better surface finish, the significance of the Size of the abrasives and the rotational speed is of little effect.

S.C. Jayswal et al. (2005) have done the theoretical investigation of the Magnetic abrasive finishing process. It has been observed by them that Magnetic abrasive flexible brush acts as the brush made of the composite material having nonlinear material properties. Magnetic forces have been determined by using the Finite Element Method and found that the Normal Magnetic force is the highest approximately near the edges of the Magnetic brush.

Dhirendra K. Singh et al. (2005) in their experimental study observed that the strength of the Magnetic abrasive brush increases with an increase in the current and the depth of penetration of the abrasive particles depends on the amount of current supplied. It has been observed that the finishing of the workpiece is due to scratching and or Micro cutting. Flux density increases from the center of the magnetic abrasive brush and reaches the maximum value at a particular distance and maintains this value for some distance from the center and subsequently decreases. The finer the size of the abrasive, the better would be the surface finish.

N. Umehara et al. (2006) suggested a new method for polishing for the finishing of Silicon nitride balls. In this the finishing operation is by Magnetic float polishing followed by Chemo Mechanical Polishing. A water-based medium is prepared, which will work effectively in both MFP and CMP processes. Metal removal rate increases with an increase in polishing load and abrasive concentration. Maximum MRR is obtained at 20% concentration. The material

removal rate increased by 48% as the speed got increased from 300 rpm to 400 rpm, however, MRR reduces by 13% when the speed increased from 400 rpm to 550 rpm.

Xiaozuoyi (2006) conducted experiments by adopting Unbounded magnetic abrasives as the polishing brush. Steel particles and Iron particles have been mixed separately with the abrasives of size 5.5 μm along with the lubricant. The best result in terms of metal removal and surface finish is obtained when the iron grit by weight is 80%.

S.L.Ko et al. (2007) experimented with micro deburring of the Fe-Ni alloys by using the MAF method. Higher productivity and better surface finish could be attained by adopting an oscillatory motion to the table, which increases the self-sharpening characteristic of the abrasive powder and hence better surface finish is obtained. Further, it is observed that the finishing in the increasing order is dry finishing, intermittent coolant supply, and the continuous supply of the coolant at the surface finishing zone.

Ching-Tien Lin et al.(2007) performed two-stage finishing comprising of rough finishing followed by fine finishing. When the working gap is 1.5 mm it had been observed that a very stiff polishing brush got generated and the surface finish obtained is very rough when compared to the working gap of 2.5 mm, which was the calculated optimum value using the TAGUCHI optimization technique. The lower feed rate gave a better surface finish and the optimum value obtained was 10m/min. Smaller quantities of abrasives give better surface finish, however, very few quantities of abrasive gives insufficient cutting edges, and hence finishing can't be performed.

Berhanu Girma et al. (2007) conducted experiments for finishing the cylindrical as well as Plane surfaces using Magnetic abrasive finishing processes. For optimization of process parameters, they adopted response surface methodology. The better Surface finish had been obtained with an increase in the size of the abrasive particles for finishing the plane surfaces, whereas the surface finish of cylindrical surfaces got reduced. For both the external and internal finishing higher surface finish got achieved, when the size ratio is around 1.5 to 2.0. With lower spindle speeds, magnetic abrasive particles remove the peaks of both flat and cylindrical surfaces efficiently, on the other hand, higher speeds gave rough finishing. Increased current input, increased feed rate resulted in better surface finish and better metal removal is obtained with the reduction in size ratio.

Yan-Cherng Lin et al. (2008) suggested a novel method of surface finishing method whereby they discovered a hybridized method comprising EDM and MAF. The accumulation of the

debris is the main problem with EDM, which had been reduced by using the Hybridised method. The hybridized method gave more number of waveforms than the conventional EDM, reduction in the problem of the debris, increase in Metal removal rate up to three times the conventional EDM had been attained in this process and also Electrode wear rate got reduced considerably upon increasing the pulse duration

S. O. Kim et al. (2008) performed the finishing operation of a flat surface made of AZ31 Magnesium alloy using Magnetic abrasive polishing technique. For increasing the Magnetic flux density for Nonmagnetic Magnesium alloy workpiece, a permanent NdFeB magnet had been kept on the opposite side of the inductor. Verified results with and without Permanent magnet had been observed and found that with the Permanent magnet the flux density got increased and also the metal removal rate and the surface finish had been better. TAGUCHI optimization technique suggests that the increase in rotational speed increases the metal removal

A.C.Wang et al.(2009) have studied the finishing of the Tool steel material (SKD 11) by adopting a novel method known as "Magnetic finishing with Gel abrasive" . In their work they found that the Silicone gel mixed with SiC and Steel grit gave better surface finishing and the surface finishing of the order 0.038 μm is obtained under the magnetic field due to rotation and vibration of the workpiece.

Bongsu Jung et al. (2009) in their experimental study on finishing of the hard material. Two methods have been investigated for increasing the metal removal and surface finish. The rotational speed of the tool and the minimum gap between the tool and the workpiece are two process variables considered during the study. For a given gap, it had been observed that the better surface finish and material removal rate could be obtained at the higher rotational speed of the tool. However, when the working gap is increased up to 5mm, it is observed that there won't be appreciable variation in the material removal rate.

Yan-Cherng Lin et al. (2009) had discussed Magnetic force-assisted Electrical Discharge Machining and optimization of process parameters using the Taguchi method. Clearing of the debris due to the EDM process is faster in the Magnetic force assisted finishing process. Material removal is approximately three times by using the magnetic force in the EDM process. The peak current has a significant effect on the material removal and the surface roughness. Optimized values obtained are 5A peak value current, 1.2A auxiliary current with 200V no-load voltage, and 460 μs pulse duration.

V.K. Jain et al. (2010) suggested a Hybrid method comprising the characteristics of both Chemical polishing and Magnetic abrasive finishing known as Chemo Mechanical Magnetorheological finishing for Silicon substrates up to Nano-metric level. Design Expert 7.0 had been used for finding the optimum values. It had been observed that the increase in the working gap between the tool and the workpiece than the optimum value gives insufficient indentation force and hence a lesser amount of material removal and poor surface finish. The decrease in the working gap would not allow a sufficient amount of abrasives for removing the material from the workpiece surface.

H. Yamaguchi et al.(2010) had discussed the processing principle of finishing of Silicon Curvilinear micropore structure, finer finishing of the micropore would enable better X-ray focusing of the mirrors used in satellites. They could achieve mass to the area of the order up to 1000 by using Magnetic abrasive finishing process. Higher magnetic field strength would result in a better surface finish. Bigger abrasive grains gave deep cut and better surface finish when they passed through the micropore and surface finish up to 4 nm had been attained.

A. Sadiq et al. (2010) have studied about Magnetic Rheological Abrasive Honing process of ferrous material specimen comprising of Mild steel of AISI 1020 category(Magnetic) and Stainless steel of SS 316L (Nonmagnetic). The medium used comprising of Green Sic 25% by volume, Carbonyl Iron particles of 30% volume and nonferrous metals and found that the surface finishing does not increase continuously with increase in flux density and Saturation of the finishing fluid takes place. It had been observed that as the flux density increased beyond 0.5T, the CIP particles stick to the Mild steel specimen and further surface finishing was not possible on the other hand for the SS specimen inconsistent surface roughness variations had been observed with the increase in flux density. Surface roughness reduces up to 0.2T, increases from 0.2T to 0.4T, and then surface roughness decreases from 0.4T to 0.6T. For obtaining an optimum surface finish they suggested a novel method in which the non-magnetic specimen had been placed in the opposite direction and the magnetic specimen had been inserted in the remaining slots. By this method, the flux density around the SS specimen got increased and for a field strength of 0.65T, surface finish improvement is of the order of 43%.

Rahul S. Mulik et al.(2010) in their experimental study on Ultrasonic assisted magnetic abrasive finishing found that the flux density increases from the center of the magnetic pole towards outer pole direction till it reaches optimum value for all the ranges of voltages, however after obtaining the peak value, the flux density starts falling towards the outer tip of the pole.

Cutting torque and Normal force increase linearly for all the voltages under consideration. Percentage change in surface roughness is better for the 90V, which was the highest voltage under consideration for a given rotary speed of approximately 240 Rpm of the magnet. Subsequently, a fall in the percentage of change in surface roughness had been observed at higher speeds. By adopting the hybrid method comprising of Ultrasonic and Magnetic Abrasive Finishing using Unbonded abrasives, the antifriction bearing made of steel material having hardness up to 730 HV had been finished under lower Normal forces and cutting torques and the mechanism responsible for finishing had been microchipping and Nano-scratching. The hardness of the finished surface would increase up to 960 HV.

Rahul S. Mulik et al.(2011) performed the finishing of AISI 52100 Steel using Ultrasonic assisted Magnetic abrasive finishing. It had been observed that the flux density increases with the increase in the applied voltage to the electromagnet. Flux density at the center of the electromagnet is minimum and increases in the outward direction and attains maximum value at a particular point and from there the flux density falls. Due to Ultrasonic vibration, the finishing torque gets increased, which increases the material removal and a better surface finish had been attained. In a finishing time of 80 sec, it had been observed that Ultrasonic assisted Magnetic abrasive finishing gives a better surface finish when compared to Magnetic abrasive finishing. Percentage change in surface roughness was inversely proportional to the rotational speed of the magnet. Percentage change in roughness was the highest for SiC abrasive with 25% by weight for all the mesh sizes.

Ajay Sidpara et al. (2011) in their experimental work found the optimum value of the Net force for different working gaps and abrasive concentrations. In their observation based on the experimental data, found that both the Normal Force and the Tangential force decrease with the increase in Working gap. The tangential force would increase with the increase in the rotating speed of the specimen up to 300 rpm but starts reducing subsequently, whereas Normal force increases continuously with the increase in the rotating speed of the specimen. The net force increases continuously up to the volumetric concentration of the abrasives up to 3.5%. Based on the experiment and ANOVA, it is found that flux density, working gap, and the concentration of the Carbonyl iron particles are having contributed to better surface finishing whereas the wheel speed is less significant.

H. Yamaguchi et al.(2011) proposed a novel system in which by partial heat treatment magnetic and non-magnetic zones had been created due to which the flux density variation had

been observed. Two tool tip systems 18-8-9 and 9-8-18 had been adopted for getting simultaneous finishing of multiple sections. Tooltip 18-8-9 system gives a better surface finish compared to Tooltip system 9-8-18.

Ajay Sidpara et al. (2012) proposed a theoretical model for the Magnetorheological based finishing process and verified with the experimental results. For finishing theory of rolling principle had been proposed and studied. Theoretical values of Tangential and Normal forces were found to be in good agreement with the experimental values. Both the Normal force and the Tangential force increase with the increase in the percentage of Carbonyl Iron particle by volume, similarly the values of Normal and Tangential forces also increase with the increase in the volume percentage of abrasive particles up to 3.5% and from there, these forces would show a reduction in their magnitude. An increase in the working gap reduces the Normal and Tangential forces.

Jae-Seob KWAK (2012) had developed a mathematical model for improvement of the surface finish by adopting Magnetic abrasive polishing. He used Electromagnet as well as Permanent magnet in the proposed method. He observed that at the center of the polishing tool the flux density is relatively lesser and increases symmetrically on either side from the center of the magnets for a working gap of 2mm. He adopted diamond powder of size 3 μm and 100 μm ferrous particle size for magnetic abrasive finishing and found that for a speed of 9m/min and for finishing time of 20 min sharp decrease in surface roughness and further extending the finishing time did not give any appreciable reduction in surface finish, from 50 min to 60 min there is almost no observable surface finishing. The optimization done through the TAGUCHI method gives utmost importance to the flux density and optimum finishing is obtainable at 1500 rpm, 82 mT, 1.5 amp current, and the working gap of 1.5 mm.

Ajay Sidpara et al. (2012) performed the finishing operation of Silicone single crystal by using Magnetorheological abrasive finishing process by using permanent magnets of type Nd-Fe 48 category. It had been observed that under lower CIP concentration by volume, metal removal rate and surface finish is lower due to weak formation of the chains under an external magnetic field, however, Higher CIP concentration by volume, gave better Metal removal rate and Surface finish. At lower abrasive concentration better surface finish and lower metal removal rate had been observed, this is because at lower abrasive concentration the abrasives would be trapped between the CIP chain. The higher concentration of abrasive particles would weaken the chain. Cerium oxide that had been used as the abrasive would react with the Silicone

material chemically and hence increase the metal removal rate also. Optimized values obtained for the finishing of the Single Crystal Silicone specimen were Rotational speed of the specimen as 298.36 revolutions per minute, CIP concentration as 39.58%, and abrasive concentration as 5%.

Hitomi Yamaguchi et al. (2012) discussed the surface finishing of the tool inserts by using 5 axis machining center. The finishing medium comprises Steel grit of size 700 μm, iron particle up to a size of 105 μm, diamond paste with size 1 μm, and soluble type fluid. The Magnetic abrasive finishing operation performed on the tool insert could give surface roughness of the order of 25 nm on the tool flank and 50 nm on the tool rake.

Jisheng Pana et al.(2012) had discussed the computer-simulated abrasive kinematic models. Better polishing quality had been observed in uncertain polishing compared to eccentric polishing. Better Polishing quality could be obtained when the speeds of the workpiece and the polishing tool were in the opposite direction. Experiments conducted based on the modeling had shown a decrease in surface finishing from 72.89 nm to 1.9 nm.

Anant Kumar Singh et al. (2013) had developed a mathematical model known as the Ball End Magnetorheological Finishing Process for measuring magnetic normal forces and compared it with experimental results. The experimental values are nearly in agreement with the mathematical modeling. For a given working gap variation in Magnetic Normal force is proportional to the variation in flux density. Better material removal and improvement in the surface finish could be obtained with higher magnetic flux density and a lesser gap as the penetrating force on the abrasive would be more.

K.B. Judal et al.(2013) had developed the hybrid process comprising Magnetic abrasive finishing and Electrochemical milling process for finishing Magnetic Stainless Steel AISI 420. Simulation had been made for the process and experimental validation had been done. The passive layer formed on the workpiece due to the Electrochemical milling operation had been removed by the Magnetic abrasive finishing. Experimental values of Flux densities developed at different input currents had been lesser than the simulated values. Both simulation and experimental data showed that there would be an improvement in the surface finish with the increase in Electrolytic current under ECM had been observed for both the simulation and experimentation at the workpiece speed of 710 Rpm, on the other hand, reduction in surface roughness had been observed with the increase in electromagnetic current up to 1.5 A and there will not be any change in the surface roughness between 1.5 A to 2.0 A and further increase in

Electromagnet current lead to increase in surface roughness for both simulation and experimentation at the workpiece speed of 710 Rpm.

Prateek Kala et al. (2013) had performed the finishing of Copper alloy by Ultrasonic assisted Magnetic abrasive finishing process and compared the percentage change in the surface finish with the Magnetic abrasive finishing and optimized values had been found by applying Taguchi method. It had been observed that when the finer abrasive particles were used, the percentage change in surface roughness got reduced, this was due to the disruption in the continuity of the CIP chain. For the same input parameters Ultrasonic assisted Magnetic abrasive finishing found to give a better surface finish compared to Magnetic abrasive finishing, this was due to the reason that ultrasonic pulse traveling through the magnetic brush would increase the collision of the abrasive particles, which in turn would remove more number of peaks.

Ajay Sidpara et al.(2013) had analyzed the significance of the process parameter in finishing the three-dimensional free form surface both experimentally and theoretically. Experimental data reveal that the force components Tangential Force (F_T), Axial Force (F_A), and Normal Force (F_N) are higher at the angle of curvature of 5^o at 1000 Rpm and feed of 4mm/min. All the three force components F_T, F_A, and F_N increased up to 100 rpm, and then they started to reduce. Theoretical values of all the three force components were lesser than the experimental values. It had been observed that the Tangential Force (F_T) is more significant out of all the process parameters.

H. Suzuki et al.(2014) performed fine finishing of Synthetic silica lens used as Diffractive Optical Element in space application by adopting Magnetic abrasive polishing process. For a circular lens they observed that surface roughness got reduced for all the radius steps under consideration up to 10 minutes and subsequently there was no effect due to Magnetic abrasive polishing process.

G.Y. Liu et al. (2014) performed the finishing of Al 6061 workpiece, which is a soft nonferromagnetic material by adopting a Hybrid process comprising of Electrochemical machining process and Magnetic abrasive finishing process known as Electrochemical Magnetic abrasive finishing process. In their experiment they found that the flux density increases in the outward direction when measured from the center and after reaching the optimum value it starts decreasing towards the edge of the electromagnet. First, the Electrochemical machining with a working gap of 1 mm had been formed followed by magnetic abrasive finishing. The minimum surface roughness(R_a) 0.2 μm had been obtained

after polishing for 10 minutes, subsequent continuation of the EMAF process increases the surface roughness(R_a) value. However, material removal would increase with increasing the time of finishing. Similarly, the surface roughness(R_a) will be minimum when the rotational speed of the tool was 1200 rpm, further an increase in rotational speed would reduce the surface roughness(R_a).

Prateek Kala et al. (2014) had found the most significant process parameters by using the TAGUCHI technique based on the experimental data available. Four Permanent magnets arranged on a circular path on an Aluminium disk of diameter 50 mm for providing necessary Magnetic force for finishing paramagnetic copper alloy workpiece. It had been observed that the maximum flux density was recorded at a distance of 25 mm from the center of the disk. Average Normal force decreases linearly with the increase in the working gap for both the upper disc and lower disc. The average normal force also reduces linearly with an increase in the abrasive by weight percentage and rotational speed increase would also reduce the Normal force. Variation in rotational speed is not significant for the Normal force. A higher working gap for both the upper and lower disc would reduce the magnitude of finishing torque.

T.C. Kanish et al. (2014) discussed the optimization of process parameters involved in finishing the SS316L material by Magnetic abrasive finishing process. A Fuzzy model had been developed considering three new process parameters other than used for ANOVA. The most significant process parameter was found to be Voltage. The surface finish would be better, with the voltage of 20 volts, the rotational speed of the brush 540 rpm, and a working gap of 1.5 mm. The fuzzy model had a close relationship with the experimental values up to 7.16%.

Hitomi Yamaguchi et al.(2014) had performed the finishing operation of the Titanium alloy cutting tool used in high-speed machining by adopting a Magnetic abrasive finishing process. The composition of the abrasive brush is more critical in the Magnetic abrasive finishing operation. For getting efficient finishing operation, a mixed size of iron particles had been proposed. The Magnetic brush comprising of different sizes of the iron particles would generate more magnetic force and efficient finishing of the coated Titanium alloy would take place with minimum material removal. Tool bit life got increase by 150% and improvement in tribological properties had been observed.

Prateek Kala et al. (2015) performed the Magnetic abrasive finishing on Copper alloy workpiece and Stainless Steel workpiece and compared the finishing characteristics. For copper alloy Percentage change in Average surface roughness (R_a) increases linearly from

1mm working gap to 2 mm working gap and then decreases. Percentage change in Average surface roughness (R_a) increases with increase in abrasive quantity by weight percentage up to 25 % from there it starts decreasing, similarly finer mesh size, lesser feed, and higher rotational speed increased the Percentage change in Average surface roughness (R_a). For stainless steel continuous reduction in Percentage change in Average surface roughness (R_a) with increasing the working gap. Percentage change in Average surface roughness (R_a) got improved for Copper alloy up to 30% of the weight of the abrasive and up to 22.5% of the weight of the abrasive. Up to 300 rpm of the percentage change in average surface finish had been increasing for copper and, whereas up to 500 rpm the percentage change in average surface finish got increased and a further increase in rpm had reduced this value. As per the simulation, Placement of the magnetic pole at 180^o phase difference would give more flux density.

K. Saraswathamma et al. (2015) in their experimental study for the finishing of the Silicon wafers adopted the novel finishing process known as Ball End Magnetorheological finishing process. The medium made of Deionised water, Cerium oxide and Carbonyl particles had been used for finishing Silicon wafers. ANOVA had been adopted for studying the process parameters. Higher values of current would give better Magnetic field strength, which increases Magnetic force due to which the surface roughness would decrease. Reduction in the working gap would reduce the surface roughness of the finished part and the working gap was the more critical parameter under the BEMR process.

Nitesh Sihag et al. (2015) Performed the finishing operation of the Tungsten workpiece by adopting a Hybridised finishing process comprising of Chemical Mechanical polishing and Magnetic abrasive finishing. The etching agent used was H_2O_2, which removes the surface layer of the Tungsten workpiece followed by the Magnetic abrasive finishing. Experimentation had been designed based on Taguchi L_9 Orthogonal array and the data obtained had been analyzed by applying Analysis of Variance Technique. Four process parameters; Percentage of abrasive weight, working gap, the rotational speed of the magnetic disk, and concentration of the etching agent had been considered. The result showed that the most significant process parameter had been the rotational speed and the least significant process parameter was the concentration of H_2O_2. Tally surf measurement of the workpiece surface before and after finishing operation showed that the ratio of the height of the peak to the valley in the finished surface was 1/5 times that of the values measured for the unfinished workpiece.

Satish Kumar et al. (2015) had proposed a novel method for finishing a complex free form three-dimensional surface using a rotational Magnetorheological abrasive flow finishing process. The workpiece was similar to the Knee joint made of Stainless Steel material. Four faces had been considered for the study and eight cycles of experiments had been conducted with, four different mesh sizes, five different extrusion pressures, five different finishing times, and five angles of impinging of the abrasive particles with the surface had been considered. The best surface finish had been obtained on all four faces under consideration with the mesh size of 2000. Optimum values of process parameters were the extrusion pressure of 15 Mpa, 228 minutes of operation, 1600 cycles for getting the best surface finish 35 nm.

Zsolt Kovacs et al. (2016) had performed the finishing operation of a cylindrical workpiece made of C 45 Normalised steel. Magnetic abrasive polishing and Magnetic abrasive burnishing had been performed on the Cylindrical specimen. Results obtained show that the combination of Magnetic Roller burnishing and Magnetic polishing could give the best surface finish when compared with Pure Magnetic polishing or pure Magnetic burnishing operation, the best possible surface finish was 0.21 μm.

Junji Murata et al. (2016) performed the polishing of specimens made of Soda-lime glass with low-cost core-shell abrasive particles made of CeO_3 – Fe_3O_4. In the absence of the magnetic field, these Core-Shell particles gave inferior surface finish. When the Magnetic field is applied to these particles, they exhibited better surface finishing characteristics compared to many conventional abrasives.

Yuyue Wang et al. (2016) had proposed a new method of magnetic abrasive finishing known as Dual Rotation Magnetorheological finishing. Studied the surface texture of both Magnetorheological finishing and Dual Rotation Magnetorheological finishing. Magnetorheological finishing had two types of textures namely Raster path and Spiral path texture and both these textures were directional and had uniform grove angle, whereas the Dual Rotation Magnetorheological finishing, did not exhibit any directional texture and uniform distribution of grove angle.

Mehrdad Vahdati et al. (2016) had performed the concave surface of Aluminium alloy with a Magnetic Abrasive finishing process. Hemispherical shape magnetic tooltip had been used for finishing operation. Both electromagnet and Permanent magnet had been used as the tooltip. For electromagnet, hemisphere having a purity of iron up to 99.8% was used as the tooltip and Permanent Magnetic Hemisphere made of N 35 had been used as a tooltip. The simulation

results obtained by using the Finite element Maxwell showed that the flux density was the highest at the center for both types of hemispherical magnets, however spherical permanent magnet had given the higher value of flux density at the center when compared to the hemispherical electromagnet. As the gap between the concave surface and the hemispherical magnet got increased, surface roughness after Magnetic abrasive finishing operation was higher compared to the lesser working gap when the other process parameters are kept constant. Higher feed rate gave better surface finish up to 40 mm/min and from there surface roughness (R_a) got increased. Percentage change in surface finish increased with the increase in the cutting speed and had the maximum value when the cutting speed was 1600 rpm, subsequent increase in cutting speed had reduced the percentage change in surface roughness. Surface roughness got reduced to 0.2 μm from 1.3 μm.

Nitesh Sihag et al. (2017) had proposed Chemo Ultrasonic Assisted Magnetic Abrasive Finishing (CUMAF) process a novel surface finishing process for finishing the Tungsten substrate. In this process, an oxide layer was formed on the surface of the Tungsten specimen due to the Chemical reaction with H_2O_2. The Ultrasonic vibration would make the abrasive cutting edges to collide with the peaks of the surface and shear of the peaks which were already subjected to oxidation. By using Ultrasonic vibration, the surface finish got an improvement up to 21.9 %. The most significant process parameter was the working gap followed by the concentration of H_2O_2.

Rui Wang et al.(2017) had performed the finishing operation of AISI 304 bars by adopting an Ultra-high-speed Magnetic abrasive finishing process where the rotational speed of the workpiece up to 80000 rpm had been considered. AISI 304 bars are very difficult to cut due to their higher hardness. The simultaneous rotary motion of the workpiece and linear motion of the permanent magnets had been adopted during the finishing operation. Two different geometries of the magnets, one with a sharp edge and the other with a flat surface had been used for analysis. The data obtained from the experiment had been analyzed with ANOVA. AISI 304 round bars had got surface finish up to 0.03 μm by adopting sharp magnet, with 80000 rotational speed of the workpiece by adopting diamond abrasive having an average diameter of 0.5μm and finishing time of 60 seconds and vibrational frequency of 10 Hz with the injection of Neon gas. For finishing the workpiece having micro- diameter process parameters remain the same as adopted for AISI 304 round bar but the finishing time required was 120 seconds.

Prateek Kala et al. (2017) had developed a new method for surface finishing of Paramagnetic materials known as Double Disk Magnetic abrasive finishing (DDMAF). A mathematical model had been created and had been verified with the experimental results. Two discs each having four magnets were adopted during the finishing process. One disk is kept above the Paramagnetic workpiece and the other below the paramagnetic workpiece. Both the normal force and the tangential force on the iron particle were found to be higher for a 1 mm gap and these values got reduced with the increase in the working gap. The angle of inclination of the Flexible Magnetic Abrasive Brush increases with the increase in the rotational speed of the disk up to 400 rpm attains a maximum value of 10^{o} and then falls with a subsequent increase in the rotational speed. An increase in the percentage of abrasive particles by weight would decrease the percentage change in surface roughness.

Vipin C. Shukla et al.(2017) performed the ultrasonic Assisted Magnetic abrasive finishing process on the workpiece made of SS 304 material. Modeling of the normal forces and finishing torques had been done and the results had been verified with the experimental values. The penetration of the magnetic abrasive depends upon the Magnetic field strength. When the indentation is made beyond the critical depth then it had been considered as plowing effect and above the critical depth, the mechanism of removal was due to shearing operation. A higher value of the current (1.2 A) had given a higher value of Normal force (F_y) and finishing torque (T_f). When the input current was 1.2 A, the magnitude of Normal force in modeling and experimentation had a difference of 10.45% and finishing torque had a difference of 9.43%. These values at 0.9 A input current were lesser.

Saraswathamma. K et al. (2017) experimentally studied the rheological behavior of Magnetorheological polishing(MRP) fluid while polishing the workpiece made of Silicon material. The characteristics of the MRP fluid mainly depend upon the characteristics of the constituents viz abrasive size, percentage of the abrasive by volume, Type Carbonyl iron particles, percentage of Carbonyl particles by volume, carrier fluid. Flow characteristics of MR fluid had been analyzed treating the MR fluid to be Bingham plastic fluid, Herschel-Bulkley fluid, and Casson's fluid. Yield stress proportionally increased with the increase in current for CS grade Carbonyl Iron Particle. Value of Shear viscosity for the magnetorheological medium comprising HS grade Carbonyl particle with Rhodite abrasive found to be zero for the input current ranging from 1 A to 5 A. Shear-thinning was more prominent for CIP coated with SiO_2.

Hitomi Yamaguchi et al. (2017)performed Sanding, Magnetic abrasive polishing, and Magnetic abrasive burnishing as the post-processing techniques for getting a better surface finish on a workpiece made of SS 316L material, which got its geometry by selective laser melting process. In sequence, sanding, Magnetic abrasive polishing, and Magnetic abrasive burnishing had been performed on the workpiece. The best surface finish had been observed when the burnishing time was 1 hour, an increase in the burnishing resulted in a rough surface.

Patrick Munyensanga et al. (2018) reviewed the applicability of the Magnetic abrasive finishing (MAF) process for finer finishing of the external spherical surfaces of the Stainless steel balls used in ball bearings. Different process parameters in the MAF process had been reviewed. For a given finishing time, an Iron particle with a mean diameter of 330 μm found to give a better surface finish compared to 75 μm and 1680 μm size iron particles. Higher voltage, lesser working gap, a higher rotational speed of the specimen would result in a better surface finish.

Jiang Guo et al.(2017) performed the finishing operation on the mold inserts that are used in Microfluidics in the sequence of operations. The mold insert understudy had a curved geometry. The initial geometry of the mold insert was obtained by CNC milling operation. Subsequently, Magnetic abrasive finishing (MAF) operation had been adopted for final finishing. MAF process removes burrs and scratches on the mold tool insert. Simulation work done for finding the material removal characteristics on the mold insert showed that the height of the microstructure of the mold insert was lesser when the abrasive flow was parallel to the surface. Micro-hardness, residual stresses, and coefficient of friction on the surface after the MAF process got reduced when compared with these values recorded after precision milling operation.

Anwesa Barman et al. (2017) performed the finishing of a Titanium workpiece that had a flat geometry. Adopted permanent Magnets of N48 grade and simulation had been done using Ansys Maxwell software to find the flux density of three different cylindrical magnets having diameters 5 mm, 10 mm and 15 mm. Simulation results showed that the magnet with a 10 mm diameter could be preferred for Magnetic abrasive finishing operation. The height of the magnet concerning the surface to be machined had no significance on the flux density. The simulation result showed that the maximum flux density was obtained at the center of the magnet for the first and fourth configurations of the permanent magnets. The fourth

configuration that gave 0.4T on the surface of the workpiece had been used and surface roughness of 10 nm could be achieved from an initial roughness of 180 nm.

Prateek Kala et al. (2017) studied the force signature of machining of Paramagnetic thin workpiece by using single and double disk magnetic abrasive finishing process. For the same working gaps of 2.5 mm and 2.0 mm and the time duration considered, the single disk magnetic abrasive finishing had a higher value of normal force during the time the working gap was 2.0 mm and the maximum normal force had been 20 N, on the other hand, the double-disk magnetic abrasive finishing had the highest value of normal force to be around 32 N. Both the normal force and the tangential force got increased with a reduction in the working gap.

Zafar Alam et al. (2017) had performed the modeling of surface roughness of ferromagnetic workpiece using Ball End Magnetorheological finishing process. Flux density followed a sine wave and had the maximum value at the center of the tool. Magnetic abrasive chain formed considered to follow BCC structure with the abrasive particle occupying the center. Flux density increase had increased the yield stress of the Magnetorheological polishing fluid. The variation between the modeled value of surface roughness and the experimental value of surface roughness was between 7.23% to 31.19%.

Kanish T C et al. (2017) had investigated the process parameters that affect the Normal force and Tangential force in the Magnetic field-assisted abrasive finishing process. The experiment had been conducted based on Taguchi L_{27}. Process parameters considered include the working gap, abrasive dimensions, abrasive concentration, rotational speed, the external voltage to the electromagnet. As per ANOVA analysis suggests the most significant parameters were External voltage and working gap and the maximum Tangential force of 14.16 N and Normal force of 33.92 N were obtained at an external voltage 22V, working gap 1.5 mm, a grit size of the abrasive 1200 at a rotational speed of 540 rpm.

Aviral Misra et al. (2017) had developed a model for predicting the surface roughness attainable under the Ultrasonic assisted magnetic abrasive finishing process and verified with experimental data obtained. Instantaneous surface roughness values recorded at different time intervals for a cycle time of 120 seconds for initial surface roughness of 0.3088 μm, Voltage of 80V, the working gap of 1.5 mm, a rotational speed of 300 rpm, the amplitude of ultrasonic vibration 8 μm at 20 kHz were almost same for experimental data and the modeling data. Considering a cycle time of 120 seconds and for the same process parameters, the Instantaneous surface roughness value got increased with the increase in the voltage applied to the

electromagnet. Percentage change in surface roughness got increased linearly with the increase in the amplitude of the vibration. Percentage change in surface roughness got reduced with the increase in the hardness of the material.

Lida Heng et al. (2017) reviewed the development of the Magnetic abrasive finishing process, discussed the suitability of different types of Magnetic abrasive finishing processes for different types of material. The most critical parameters suggested include the size of the Iron particle, size of the abrasive particle, rotational speed, working gap, Magnetic flux density, percentage of the abrasive, and percentage of the iron particle by weight.

Pei-Yeing Wu et al. (2018) had experimentally found the effect of size of the abrasive on the MRR and surface finish while finishing a SS workpiece prepared by selective laser melting. For 30 finishing passes under consideration, G14 steel grit had removed more material compared to steel grit G25. Material removal by conventional abrasive was higher than the Magnetic abrasive for the 200 finishing passes under consideration. Brush made of large particles behaved as a rigid tool and remove the peaks of the surface on the other hand smaller abrasive particles that produced flexible magnetic abrasive brush had removed the material along the surface of the workpiece.

Sachindra J et al. had finished an aluminium circular rod made of Al 6061 by using the Magnetic Abrasive Finishing process. Three mixture ratios by weight for the iron particles and abrasive particles were considered during the experiment. L9 orthogonal had been selected for studying the surface roughness obtained. The optimum values obtained were: the mixture ratio 3:2, a rotational speed of the workpiece 300 rpm and the time of finishing 2 minutes, and a working gap of 1 mm. With these optimum values, the surface finish had an improvement between 29.9% to 71.21%.

Yuewu Gao et al. (2018) performed the finishing of two paramagnetic workpieces made of copper alloy and SS316 by a Magnetic Abrasive Finishing process. The atomized type of abrasive powder had been used for the finishing process. Percentage change in surface roughness continuously decreased for SS316 with the increase in the working gap. For the copper alloy, the percentage change in surface finish continuously increased up to a gap of 2 mm and then the value started to decrease. Similarly, feed rate (mm/min) showed that the increased feed rate had decreased the percentage change in the surface finish for SS316. For copper alloy percentage change in surface finish increases continuously up to a feed rate of 10 mm/min and then the fall in percentage change in the surface finish could be observed.

Rajneesh Kumar Singha et al. (2018) reviewed the Magnetic abrasive finishing process considering different geometries viz external cylindrical finishing, internal cylindrical finishing, plane finishing, and 3D profile finishing. Suggested different types of Magnetic abrasive finishing processes for different types of materials. The most significant process parameters suggested were the magnetic flux density and the working gap.

D. Sai Chaitanya Kishore et al. (2019) had optimized the process parameters of surface finishing of Al6061 a Paramagnetic material. Experimentation had been designed based on the TAGUCHI method and process parameters had been analyzed for their significance. The size of the abrasive is larger than the size of the Carbonyl iron particle. The most significant process parameter was the applied voltage for electromagnet, which had a value of 24 V, followed by a working gap which had a value of 1.25 mm and the third significant process parameter was the rotational speed of the magnetic brush which had an optimum value of 240 rpm.

Huijun Xie et al. (2019) had found the effect of the alternating magnetic field in Magnetic abrasive finishing and found that for a given time of the magnetic field considered, the magnetic force would act twice the time consideration of the magnetic field. Both the change in the finishing force and the magnetic force would lag the applied alternate magnetic field. Experimental data showed that the magnitude of the finishing force was proportional to the size of the magnetic particle, nevertheless, the frequency of the magnetic field was not having any influence on the finishing force. Very fine finishing of Al5052 had been observed and the surface finish got increased to 3 nm from 318 nm.

Henan Liu et al. (2019) performed the surface finishing operation of the irregular-shaped complex component with a radius less than 3 mm by using a small end permanent magnetic polishing head. Material removal rate (MRR) gradually increased from finishing angle of 50^{O} to 55^{O}, MRR increased sharply from 55^{O} to 60^{O} and attains the maximum value at 65 ^{O} from there the MRR drops till the recorded value pf finishing angle 80^{O}. Flux density was higher at a distance of 0.45 mm from the internal finishing surface and at 0.75 mm from the external surface. Surface roughness(R_a) had increased from 0.0538 μm to 0.0107 μm.

Jiong Zhang et al. (2019) performed the surface finishing of the specimen made of Selective laser melting process with Magnetic Abrasive Finishing process. Five samples made of different slope angles had been selected for the study. The initial roughness of the selected samples got the surface roughness increased till 60^{O} slope angle and then got decreased. For a polishing time of 75 minutes, the specimen with 0^{O} slope angle had more metal removal. The

theoretical study showed that the 0^O slope angle had minimum surface roughness (R_a) and maximum for 90^O slope angle, whereas the experimental result showed that the surface roughness was minimum for 90^O slope angle specimen.

Meng Nie et al.(2019) developed the mathematical model for the distribution of the magnetic flux density and the orientation of the magnets. The comparison made between the permanent magnets with different radii, magnets with higher radius gave better surface finish and surface finish decreased with a reduction in the diameter of the magnet, whereas the flatness was better for the magnet with a smaller diameter. When the same no of magnets was considered, hexagonal cross arrangement produced a higher amount of flux density.

Mohammad Mosavat et al. (2019) had simulated the finishing of the Monocrystalline silicon wafers with a Magnetic abrasive finishing process by using Smoothed Particle Hydrodynamic (SPH) model, a meshless model, and verified the simulated results with experimental data. The simulated version showed higher values of change in the surface roughness compared to the experimental values, however, both simulated and experimental values showed that the change in surface roughness increases with the increase in abrasive size. Both simulated and experimental values showed that the change in surface roughness decreases with an increase in the working gap. The slope between the increase in material removal with the increase in abrasive size had been steeper for simulation compared to the experimental value. The simulated result showed a higher value of material removal for increased rotational speed compared to the experimental values. The best possible reduction in the surface finish was 0.65 μm and material removal was 39.09 mg.

Ravi Datt Yadav et al. (2019) performed the finishing of the spur gear with the Magnetorheological gear profile finishing process(MRGPF). An increase in the working gap between the finishing tool and the gear profile reduces the flux density. Flux density measured along the flank line on either side of the profile line showed that the flux density maintained symmetry on either side of the profile line, but the maximum flux density was towards the right side of the profile line. Surface finish improvement from an initial value of 0. 242 μm to 0.0253 μm and surface texture improvement had been observed with this method.

Jiang Guo et al. (2020) Performed the polishing of rectangular micro features with Vibration assisted magnetic abrasive polishing method, an experimental as well as analytical analysis had been done. Contact forces get reduced with the increase in the working gap. A higher surface

finish had been observed with a reduction in abrasive replacement interval. With the increase in polishing time better, the surface finish could be achieved.

Jiabao Liu et al. (2020) had experimentally and analytically established the importance of pressure in the Metal removal of Magnetorheological abrasive finishing for the Optics. Both the analytical and experimental values showed that the Normalised volumetric material removal rate was inversely proportional to the immersion depth per mm. Both the simulated and experimental results showed that the Normalised volumetric removal rate increases with an increase in the viscosity of the Magnetorheological fluid. Normalized peak removal increases with the increase in rotational speed. Accurate values of Material removal could be obtained by considering the pressure in addition to the shear stress.

2.4. Literature review of Dry sliding wear:

A. Rac [1985] Studied the dry wear through the dry sliding condition of grey cast iron (containing flakes and nodular graphite), using the pin on disc machining. the investigation of the experiment aimed to determine the influence of working conditions on the wear rate and also to find the speed and load condition which is subjected to low wear. The researchers concluded that the wear characteristic was found the same for both flakes and nodular graphite cast iron for the dry sliding test. The second observation was that the wear rate initially diminishes with the increasing sliding speed and then the wear rate started again. The wear resistance of flake graphite cast iron is lower than the nodular at a speed greater than 4 m/s and if the speed is lower, then the wear resistance of nodular cast iron is more, The researcher also characterized the region of lower wear in the paper.

Komvopoolus et al. [1986] observed and studied the plowing friction in both the lubricated and sliding wear test. The researchers experimented with pure aluminum, OFHC copper, pure titanium, logs steels, and chromium. The researchers concluded that both dry and lubricated sliding test showed the plowing mechanism. The relation was obtained between the coefficient of the friction due to plowing, the sharpness of the asperities, and the interfacial friction by the slip line model. The next observation was that slip line analysis showed the plastic deformation of the asperity and the plowed surface was proposed.

Hokkirigawa and Kato [1987] dated five kinds of wearing Steel and took a flat specimen of the steel. The researcher used a single point test with the hemispherical. The temperature of the steel was eight sixty degrees Celsius, 200 degree Celsius 350 degree Celsius five hundred

degrees Celsius, and 750 degrees Celsius (650 HV, 560 HV, 380 HV, and 280 HV) respectively. After carrying out the following experiment the researcher concluded that when the degree of penetration increases the wear mode changes from plowing to wedge forming mode and wedge forming mode to cutting mode. The second observation was that the Everest surveyor was found to be a function of the degree of penetration and the hardness of the specimen. This world two important functions. The next observation was the transition between the Ploughing mode and wedge forming mode which was independent of hardness. And this degree of penetration was inversely proportional to the hardness.

Lim et al. [1989] experimented to explore the wear characteristic of the steel using dry sliding of the steel and commented on the variation of the friction by friction regime map. The researchers observed that with a sliding speed of less than 1 m/sec, the condition of the surface influences the coefficient of friction. With velocity greater than 1m/s, the coefficient of friction depends on the pressure and the sliding velocity and not on the surface. It was also an interesting fact that a layer of the molten materials forms on the surface of the steels when the load and speed are high and this results in a lower value of the coefficient of frictions.

Joyee et al. [1993] studied the closed 3 body abrasive wear process. The researchers studied the elastohydrodynamic lubrication rig and studied the deformation and frictional analysis of the debris obtained from the brittle and ductile material. The researchers bused the ball on a disc machine for the experiment of the dry sliding test. The researchers used abrasive diamond for the experiment and observed some points. Firstly the particle was embedded in the softer surfaces and on the hard surfaces, these diamond particles made stretches on those surfaces. The next point of observation was that the mass of worn surfaces is proportional to abrasive concentration. Also the worn surfaces are proportional to sliding distance. Also, the point of the observation was that the smaller particle tumbled over the contact, and plowing was observed by the larger particles. As the particle size increases, the wear rate increase. The researchers also made a model of the abrasive process and were compared it with the experimental data.

Terrace et al. [1994] studied the wear characteristic of grey cast iron which was used to study the cylindrical liner. The researchers studied various mechanism which may influence the wear characteristic of the material like (truncation, adhesion, delamination, and plowing). The researchers explored the parameters like the relationship between the measurement of

friction and wear load number of cycles. also, it was observed that the load is the most sensitive factor for friction and wear.

Wang et al. [1995] studied the wear characteristic of steel 1080 by SEM and TEM and by wear testing of worm plastics. The experiment resolved 3 wear zone mechanisms which were mainly dependent on three parameters like the condition of the testing microstructure of the steel and sliding speed. The researcher studied the following points by which they stated, as the load or the sliding speed increases, three-zone of wear which are mild wear by oxidation, Severe wear by adhesion and declamation, and the melting wear appeared in succession with normal load for steel 1080. The second point of observation is that the wear characteristic is general for the general microstructure of steel, for the severe wear, wear volume varies with the microstructure also. The order of increasing wear resistance was of the order of spherical carbide, Martensite, Binate, and laminar Pearlite. It is also observed that the wear surface contains a laminated structure.

Kato et al.[1996] studied 3D model of the asperity present in the WC- alloy whose composition was 88% W, 6% Cobalt, and HRC 90.5. The experiments were conducted to confirm the same. The researchers observed the dihedral angle of 0- 180 and the attack angle of 90^{o}. The observation of the researchers was the increase in attack angle increases Wear rate in proportion.

Koji Kato et al. [1997] represented his views on the abrasive wear mode, wear-resistance, and its rate of wear and also talk about the plastic deformation and fracture. He stated that the wear rate depends upon the sliding speed. Also, all 4 types of wear were observed in the experiment which is adhesive, fatigue, corrosive, abrasive wear mode. Also, the macrostructure of alloy and its influence on wear was studied.

K H Zum Gahr et al. studied [1998] metallic and ceramic surfaces and justified the fact that abrasive wear is caused by sliding of hard particles on the softer surface and also resistance against abrasive wear is a function of hardness. The researchers also commented that different wear models are due to the interaction of different surfaces, resulting in different wear rates.

Wang et al. [1999] studied 52100 and 1080 steel and observed its surface from the SEM test. The researchers concluded that there are three ways for characterizing the wear they are mild wear characterized by oxidation, Severe characterized by adhesion, and when the speed and

load increase it causes the melting wear.

Sudhakar et al.[2000] studied the wear behavior of two composite materials made by powder metallurgy technique having the different proportion of Nickel(2% and 1%) and Carbon (0.46% and 2%). The alloys were heat tempered, such that hardness attained a maximum value of 90HRB. They observed during their experimentation that wear rate initially decreased than remain constant with the sliding distance. Researchers used many mechanical techniques such as optical microscopy and SEM to observe micro plowing and formation of surface platelets on the surface and proposed the wear modes on the surface.

Straffelini Molinari studied [2001] the wear mechanism of PM material compared with the wrought iron. The author studied Ashby's map and observed the dry sliding wear and concluded that the sliding wear of PM material is similar to the wrought iron. The Researchers found that porosity in the surface deeply affects the wear rate and treatment with steam may influence the wear resistance of PM materials.

Sehijpal Singh et al. [2002] studied the mechanism of material removal and wear behavior in magnetically assisted AFM and concluded that magnetic field has a strong effect on material removal and surface finish.

Gvan et al. [2004] studied the wear behavior of Fe – 28 Al and Fe -28 Al-10T alloy and concluded that wear rate depends on the dynamic mechanical property of the surface rather than the static one. also, delamination and peeling off was the mechanism of the wear of the surface. The researchers also computed the value of the coefficient of friction through the experiment.

Straffelini et al. [2005] studied the tribological characteristic of the copper alloy with the beryllium against AlSi M2 steel and commented about the mechanism of wear in the alloy and explained the result in form of tribological terms.

Wan et al. [2006] studied carbon fabric reinforced epoxy resin and commented about its tribological characteristic after an experiment against MM200 tester with a load of 50, 150, and 250N. The Researcher observed the following point firstly, the influence parameter for wear rate was velocity, load, and sliding distance. Secondly micro and specific wear rates change considerably during the experiment. The researchers observed that the specific wear rate increases with the product of load and velocity also SEM was used for debris analysis and wear mechanism.

Sing et al. [2007] studied the wear mechanism of Cu–15Ni -8Sn bronze alloy which was rubbed against stainless steel of 440C. The Researchers used X-ray diffraction, SEM, TEM energy deprive spectroscopy (EDS) and revealed the formation of a subsurface crack in the interface between the deformed surface layer and the adjacent layer to it. The researchers also studied the microstructural after the wear and gave its explanation.

Basavarajappa et al [2007] studied Aluminium MMC with reinforced graphite particles. The dry sliding test was performed and the observation was done to investigate the influence of the parameter like sliding velocity, sliding distance on wear rate. For this purpose Taguchi method of optimization and orthogonal array technique was used to find the result.

An et al. [2008] studied the cast mechanism alloy Mg–Zn_1Y_2 and AZ91 by the pin-on-disc mechanism. The coefficient of friction and wear rate were measured. The load range applied on the pin on the disc machine was 20 to 380 Newton and 20 - 240 Newton. And the sliding velocity of .785m/sec. X-ray diffraction, scanning electron microscopy was used to examine the worn surfaces. The researchers observed all 5 types of wear mode that is abrasion, oxidation, delamination, melting, and thermal softening. He also used surface temperature analysis to analyze the surface temperature and thermal stability of alloy.

Gaard et al. [2008] Studied Steel sheet material wear. The researchers tested carbon steel sheet for the strength was comparatively low with dry sliding test initially adhesive wear was there And also it was revealed that the adhesion of steel is much more than that of carbide. As the material transfer proceed a thin layer of tool material occurs on the tool surface. There was an initiation of local micro scratching of sheet surface Due to the formation of a lump of sheet material list of factors affecting the adhesion of sheet were Distribution of carbide size of carbide and amount of carbide. Lastly, the researchers concluded that it is easy to remove clean the surface of powdered metallurgy maid services due to higher and properly distributed homogeneous finer carbide particles.

Todor Sheiretov et al. [2008] observed that the wear depends on the contact pressure and the loading history. Proposed a new concept about the fracture of the subsurface.

A. Gaard et al. [2009] in their investigation on Sheet metal found that at higher loads material lumps form and low adhesive wear is observed at the initial cycles of sliding.

G.B. Veeresh Kumar et al. [2012] in their investigation observed that Al 6061 composite with SiC as reinforcement exhibits better wear resistance than without SiC as the reinforcement agent.

S. Sivakumar et al. [2014] in their experimental investigation on Al- Garnet composites found that during the initial stages the wear between the contact surfaces is treated as two bodywear, which transforms into three bodywear at higher speeds.

Pushkar Jha et al. [2017] in their experiment for finding the wear of Cu4Ni alloy and composites found that the wear increases with the load. The presence of TiC gives a higher value of the Coefficient of friction.

2.5. Research Gap:

- **The finishing of Para and diamagnetic material is in the primitive stage.**
- **Modeling and simulation of Magnetic flux densities for the complex shapes like internal gears, Cams, internal splines have not yet been done.**
- **Modeling and simulation of flux density of the commercially available permanent magnets are yet to be done.**
- **Machining of the complex shapes using Magnetic Force Assisted finishing process is yet to be done.**
- **Wear behavior of different grades of the softness of the workpiece after Magnetic field-assisted finishing is to be done extensively**

2.6.The objective of Present research:

- **Design and development of Viscoelastic Magnetic abrasive finishing(VEMAF) process for the finishing of complex geometries. An attempt will be made to finish the complex geometry workpieces such that the surface roughness obtained will be of the order of a few Nano-meters.**
- **Comparative study of various Viscoelastic abrasive media prepared for their Viscosity.**
- **Modeling of Commercially Available Magnets for Magnetic field strengths to get the optimum values.**
- **Finding the Metal removal (∆m) and Change in Surface Roughness (∆Ra) of the components finished through VEMAF.**
- **Optimizing the process parameters.**
- **To study the wear behavior of Brass, Steel, and Aluminium workpieces finished**

by VEMAF process.

2.7.Research Methodology:

i. **Design and Development of VMAF setup for fine finishing of workpiece.**
ii. **Mixing of different polymers with magnetic particles and abrasives for getting an optimum abrasive medium.**
iii. **Finding the Viscosity of the VEMAF medium prepared using the Rheometer.**
iv. **Finding the flow parameters of Viscoelastic Magnetic abrasive Medium with ANSYS FLUENT15.**
v. **ANSYS MAXWELL ANOSOFT 16 is used for finding the flux densities of the permanent magnets to be used in the experiments**
vi. **Finishing of both internal and external surfaces using VEMAF medium and finding the surface roughness and the metal removal.**
vii. **Finding the relative importance of process parameters using Minitab Software 17 and Optimizing these parameters.**
viii. **Analyzing the wear behavior of the external workpieces finished during VMAF with Tribometer**

CHAPTER.3: PREPARATION & TESTING OF VISCOELASTIC MAGNETIC ABRASIVE MEDIUM

In this chapter, a brief discussion will be made about the linear Viscoelastic Models. Subsequently, the preparation of Viscoelastic Magnetic abrasive Medium preparation will be discussed. In total 7 Viscoelastic Magnetic Abrasive Media have been prepared and their Viscosity has been tested using Modular Compact Rheometer (MCR 102). The Results have been Tabulated and the graphs have been shown for the shear stress vs shear strain and shear stress vs Viscosity. Based on this a suitable Viscoelastic Magnetic Abrasive Medium has been proposed for the internal finishing of the Complex surface and the external surfaces.

3.1. Introduction to Viscoelasticity: In the present research, the abrasive medium prepared is known as Viscoelastic Magnetic Abrasive Medium, specially prepared for performing both internal and external finishing of a metallic specimen. The main problem found during the literature review is that the medium used for Magnetic abrasive finishing experiences Sedimentation of the heavier particles. In the Magnetic Assisted finishing process, the density of the Carbonyl Iron particle is higher compared to the Abrasives used. As the CIP particle settles down before and after the exposure to the magnetic field it becomes difficult to form the CIP chain under the Magnetic field. So, a Viscoelastic medium that addresses the sedimentation is prepared and experiments have been performed for finding the viscosity, before choosing a suitable medium.

3.2. Viscoelasticity and Rheology: Materials with Viscoelastic properties exhibit both Viscous behavior and Elastic behavior (1, 2). Most of the material exhibits Viscoelasticity both Natural and artificial. However, the dominance of Viscosity or Elasticity depends upon the individual material prepared and the operating conditions. All the Rheological material will exhibit Viscoelastic property (3),. When a material is under Static loading the Elastic behavior dominates, whereas the Viscous behavior is dominant with the Dynamic loading.

3.3. Linear Viscoelastic Models: Viscoelastic behavior may be modeled as a system comprising of a Spring, which is elastic, and a dashpot, which exhibits viscous characteristics. There are two types of Linear Viscoelastic Models (2). They are

i. Voigt Model

ii. Maxwell Model

3.3.1. Voigt Model: This model is also known as "Kelvin body", which comprises of a dashpot and a spring arranged in parallel. This model is generally adopted for Viscoelastic solid systems.

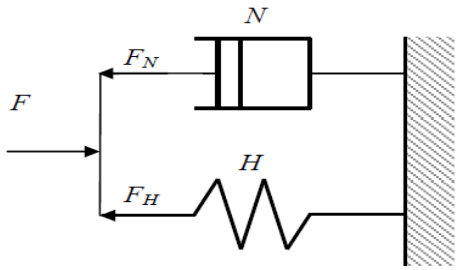

Fig.3.1. Voigt Model [Courtesy: Stanislav Doubal]

The net force acting on the system, neglecting the Inertial effect, $\boldsymbol{F = F_N + F_H}$

$$\boldsymbol{HL + N.\frac{dL}{dt}}$$

Where H is the Hook's Coefficient also known as Static Coefficient.

L is the deformation.

N is the Newtonian Coefficient.

3.3.2. Maxwell Model: Maxwell model (2) is adopted for Viscoelastic fluids. In this model, the dashpot and the Spring are connected in series.

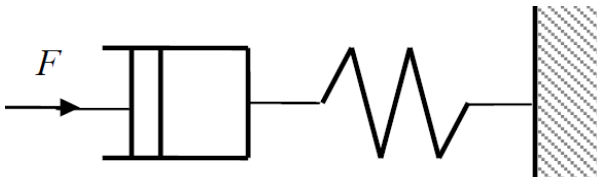

Fig.3.2. Maxwell Model [Courtesy: Stanislav Doubal]

In Maxwell model, $F = F_H = F_N$,

And the net elongation (L) = $L_H + L_N$

Where L_H is the elongation due to Spring

L_N is the elongation due to Viscous Dashpot.

All the Rheological systems are considered to be the systems comprising of Spring, dashpot, and mass, and they are treated as lumped systems comprising of these small units, and the lumps are distributed throughout the domain of the Rheological systems under consideration. However, the real Viscoelastic systems are the continuous systems comprising of Elastic components, Viscous components, and Inertial components.

3.4. Viscosity measurement: Basically, the Viscosity and Rheology measurement could be done by three different equipment, each one of these equipment has got a specific purpose and would be used depending upon the type of loading. The types of equipment used for measuring Viscosity/Rheology are:

1. Rotational Viscometer: Used for Steady loading condition. The probes used for this purpose are Cylindrical, Flat plate having Circular cross-section, and Conic section. For measuring the fluids with Very high viscosity usually, the flat plate Viscometer is preferred.

2. Oscillatory Rheometer (Viscometer): Used for finding the viscosity, when the force associated with is Oscillatory or bending force.

3. Transient Condition Rheology tester: This equipment is the advanced version of the Steady State Viscometer, in which the variation in the deformation of the specimen with time under impulsive loading would be measured.

In the present research work, Modular Compact Rheometer (MCR 102), a Rotational Viscometer is used for finding the Viscosity of the Viscoelastic Magnetic Abrasive Finishing Medium specially prepared.

3.5 Experimental set up: Fig.3.3 shows the Modular Compact Rheometer (MCR 102), a product of Antonpar is used for finding the Viscosity of the Samples prepared. Important parts of MCR has been shown in Fig3.4 below

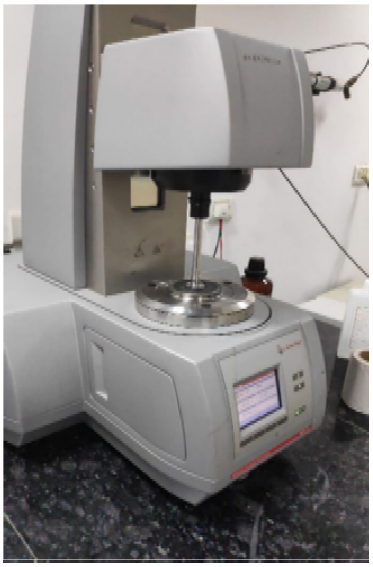

Fig. 3.3. Modular Compact Rheometer [MCR 102] Anton Par

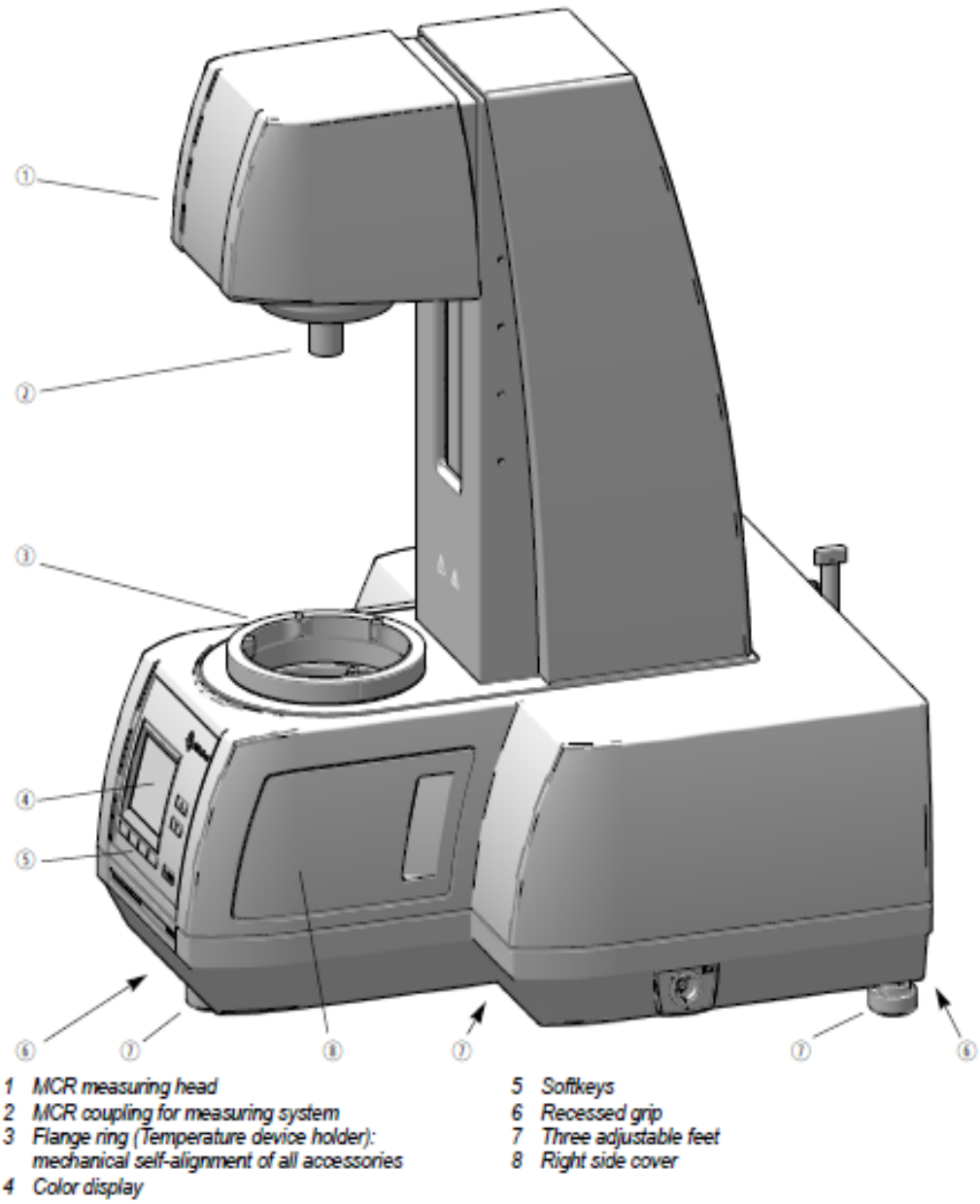

Fig.3.4. Modular Compact Rheometer parts [MCR 102]

i. Measuring Head: Holds the rotating probe known as PP 50 measuring system.

ii. MICR coupling: A part used for holding the rotating probe.

iii. Flange ring: Holds the Temperature device holder.

iv. Color display: Displays the temperature, position in mm, Normal force, and status.

v. Soft keys: Used for initiating different operations of the instrument.

vi. Adjustable feet: For making the platform plane.

Other important information of the MCR 102 is as mentioned below:

a. Weight : 42 kg

b. Size : Width 444 mm, Height 678 mm, thickness 586mm.

c. Operating Temperature: 15ºC to 35ºC, preferred temperature 23ºC ± 3ºC

d. Actuating system: Pneumatic system

e. Maximum Rpm: 3000

f. Software used: RheoCompass

Fig.3.5 to Fig. 3.7 shows three different types of measuring probes used for finding the Viscosity.

Plate-Plate Filling shown in Fig. 3.5 is normally used for Very High Viscous fluids, subjected to High shear stress range, the sample size is normally very small.

Cone-plate filling shown in Fig.3.6 is used for testing small samples subjected to Constant Shear rate within the entire gap.

Concentric Cylinder filling shown in Fig. 3.7 is used for measurements, where side leakage is a primary concern, and for large size volumes.

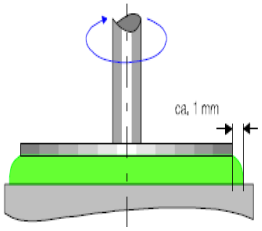

Fig.3.5 Plate-Plate Filling

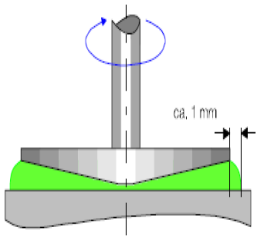

Fig.3.6 Cone - Plate Filling

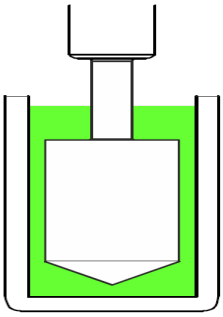

Fig.3.7. Concentric Cylinder Filling

. ***Courtesy: Anton Par Manual, DTU Chemistry lab***

In the present research work, the Viscosity of the specimen is found by using Plate- Plate Filling and Plate- Cone filling system only.

3.6. Viscoelastic Magnetic Abrasive Medium preparation: In the present work Seven samples have been prepared and their Viscosity has been measured using MCR 102. Initially, the Viscosity of the Rheological fluids used in preparing the samples has been measured (4, 12, 19, 20) and based on the experimental results, the base fluid for preparing the Viscoelastic Magnetic abrasive finishing (VEMAF) Medium has been decided. Subsequently, the addition of required ingredients has been taken place, Which produced the required Viscoelastic medium. By adding the mixture of Carbonyl Iron Particle (CIP) of CS grade and the Silicon Carbide abrasive in predefined proportion with the Viscoelastic Medium (22)the required Viscoelastic Magnetic abrasive Medium has been prepared. Three types of Viscous fluids and AP3 grease have been considered for preparing the samples, they are :

i. Transformer oil (white)

ii. Transformer oil (Red)

i. Silicone oil
ii. AP3 Grease

While, performing the viscosity measurement experiment for the base fluids mentioned at i to iii above, Plate-Plate filling type probe has been used and the AP3 Grease Cone- Plate filling type probe has been used. The sample has been placed below the probe, which is initially compressed and then the probe starts rotating (10, 11), which in turn induces shear stress and shear strain on the sample. The quantity of the sample depends upon the gap between the probe and the platform. The experimental results have been shown below.

3.6.1. Viscosity Measurement of Transformer Oil (White):

Table 3.1 Experimental results for Viscosity of Transformer oil (White)

Point No.	Shear Rate	Shear Stress	Viscosity	Temperature	Torque	Status
	[1/s]	[Pa]	[mPa·s]	[°C]	[mN·m]	
1	0.1	0.001228	12.283	28.58	2.31E-05	Dy_auto
2	0.126	0.001751	13.916	28.58	3.30E-05	Dy_auto
3	0.158	0.003454	21.795	28.58	6.51E-05	Dy_auto
4	0.2	0.004974	24.927	28.58	9.38E-05	Dy_auto
5	0.251	0.004101	16.327	28.58	7.73E-05	Dy_auto
6	0.316	0.003238	10.24	28.58	6.10E-05	Dy_auto

7	0.398	0.005018	12.605	28.58	9.46E-05	Dy_auto
8	0.501	0.010327	20.604	28.58	0.000195	Dy_auto
9	0.631	0.00974	15.436	28.58	0.000184	Dy_auto
10	0.794	0.012685	15.97	28.58	0.000239	Dy_auto
11	***1***	***0.012183***	***12.183***	***28.58***	***0.00023***	***Dy_auto***
12	1.26	0.017855	14.183	28.58	0.000337	Dy_auto
13	1.58	0.01792	11.307	28.58	0.000338	Dy_auto
14	2	0.022282	11.168	28.58	0.00042	Dy_auto
15	2.51	0.027659	11.011	28.58	0.000521	Dy_auto
16	3.16	0.03391	10.723	28.58	0.000639	Dy_auto
17	3.98	0.043894	11.026	28.58	0.000827	Dy_auto
18	5.01	0.054054	10.785	28.58	0.001019	Dy_auto
19	6.31	0.067098	10.634	28.58	0.001265	Dy_auto
20	7.94	0.085127	10.717	28.58	0.001605	Dy_auto
21	10	0.10763	10.763	28.59	0.002029	Dy_auto
22	12.6	0.13485	10.712	28.59	0.002542	Dy_auto
23	15.8	0.16967	10.706	28.59	0.003198	Dy_auto
24	20	0.21295	10.673	28.58	0.004014	Dy_auto
25	25.1	0.26583	10.583	28.59	0.005011	Dy_auto
26	31.6	0.33158	10.485	28.59	0.00625	Dy_auto
27	39.8	0.41582	10.445	28.58	0.007838	Dy_auto
28	50.1	0.51932	10.362	28.58	0.009789	Dy_auto
29	63.1	0.65093	10.317	28.58	0.01227	Dy_auto
30	79.4	0.8137	10.244	28.58	0.015338	Dy_auto
31	100	1.024	10.24	28.58	0.019301	Dy_auto
32	126	1.2906	10.252	28.58	0.024328	Dy_auto
33	158	1.6196	10.219	28.58	0.030529	Dy_auto
34	200	2.0357	10.202	28.58	0.038371	Dy_auto
35	251	2.5763	10.257	28.58	0.048563	Dy_auto
36	316	3.2438	10.258	28.58	0.061143	Dy_auto
37	398	4.1065	10.315	28.58	0.077405	Dy_auto
38	501	5.2121	10.399	28.58	0.098245	Dy_auto

39	631	6.6092	10.475	28.58	0.12458	Dy_auto
40	794	8.5046	10.706	28.58	0.16031	Dy_auto
41	1.00E+03	11.132	11.132	28.58	0.20984	Dy_auto

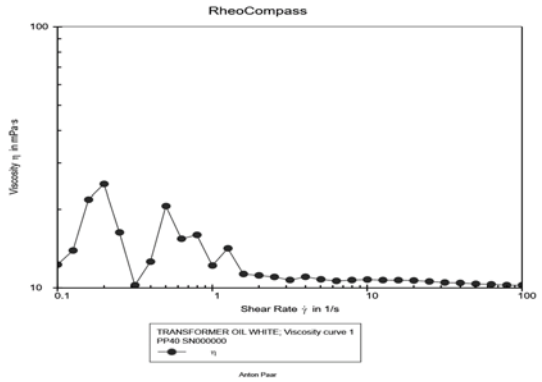

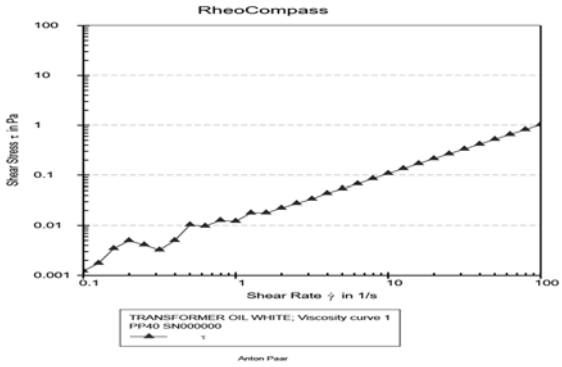

Graph.3.1. Viscosity Vs Shear rate (white) **Graph.3.2 Shear Stress vs Shear Rate**

3.6.2. Viscosity Measurement of Transformer Oil (RED):

Table 3.2 Experimental results for Viscosity of Transformer oil (Red)

Point No.	Shear Rate	Shear Stress	Viscosity	Temperature	Torque	Status
	[1/s]	[Pa]	[mPa·s]	[°C]	[mN·m]	
1	0.1	0.006164	61.663	28.89	0.000116	Dy_auto
2	0.126	0.006425	51.043	28.88	0.000121	Dy_auto
3	0.158	0.007847	49.52	28.88	0.000148	Dy_auto
4	0.199	0.010316	51.711	28.88	0.000194	Dy_auto
5	0.251	0.008533	33.97	28.88	0.000161	Dy_auto
6	0.316	0.006391	20.211	28.88	0.00012	Dy_auto
7	0.398	0.007868	19.764	28.88	0.000148	Dy_auto
8	0.501	0.009765	19.484	28.88	0.000184	Dy_auto
9	0.631	0.010046	15.922	28.88	0.000189	Dy_auto
10	0.794	0.015581	19.615	28.87	0.000294	Dy_auto
11	***1***	***0.020466***	***20.466***	***28.87***	***0.000386***	***Dy_auto***
12	1.26	0.025267	20.07	28.87	0.000476	Dy_auto
13	1.58	0.028031	17.686	28.87	0.000528	Dy_auto

14	2	0.033808	16.944	28.87	0.000637	Dy_auto
15	2.51	0.042763	17.024	28.86	0.000806	Dy_auto
16	3.16	0.052155	16.493	28.86	0.000983	Dy_auto
17	3.98	0.065535	16.462	28.86	0.001235	Dy_auto
18	5.01	0.082389	16.439	28.86	0.001553	Dy_auto
19	6.31	0.10303	16.329	28.86	0.001942	Dy_auto
20	7.94	0.12846	16.172	28.85	0.002421	Dy_auto
21	10	0.1611	16.11	28.85	0.003037	Dy_auto
22	12.6	0.20118	15.98	28.85	0.003792	Dy_auto
23	15.8	0.252	15.9	28.84	0.00475	Dy_auto
24	20	0.31573	15.824	28.84	0.005951	Dy_auto
25	25.1	0.39688	15.8	28.84	0.007481	Dy_auto
26	31.6	0.49769	15.738	28.84	0.009381	Dy_auto
27	39.8	0.62515	15.703	28.83	0.011784	Dy_auto
28	50.1	0.78866	15.736	28.83	0.014866	Dy_auto
29	63.1	0.99015	15.693	28.83	0.018664	Dy_auto
30	79.4	1.2475	15.706	28.82	0.023516	Dy_auto
31	100	1.5672	15.672	28.82	0.029541	Dy_auto
32	126	1.9766	15.701	28.82	0.037259	Dy_auto
33	158	2.4861	15.686	28.82	0.046861	Dy_auto
34	200	3.1347	15.711	28.82	0.059088	Dy_auto
35	251	3.9384	15.679	28.81	0.074237	Dy_auto
36	316	4.9745	15.731	28.81	0.093767	Dy_auto
37	398	6.2665	15.741	28.81	0.11812	Dy_auto
38	501	7.9	15.762	28.8	0.14891	Dy_auto
39	631	9.9987	15.847	28.8	0.18847	Dy_auto
40	794	12.7	15.989	28.8	0.2394	Dy_auto
41	1.00E+03	16.189	16.188	28.79	0.30515	Dy_auto

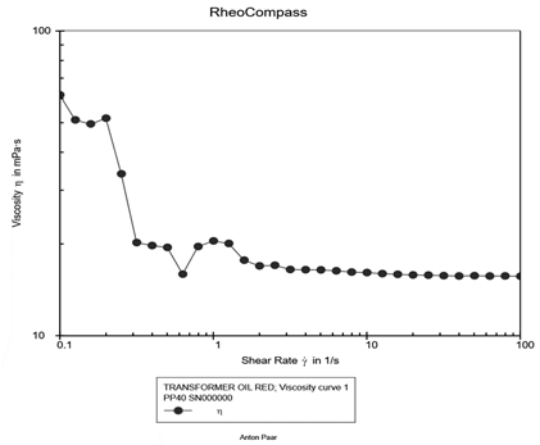

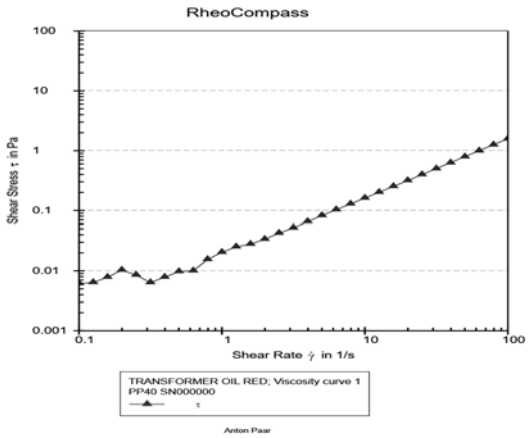

Graph.3.3. Viscosity Vs Shear rate (Red) **Graph.3.4. Shear Stress vs Shear Rate (Red)**

TRANSFORMER OIL (RED)

3.6.3. Viscosity Measurement of Silicone Oil:

Table 3.3 Experimental results for Viscosity of Silicone Oil

Point No.	Shear Rate	Shear Stress	Viscosity	Temperature	Torque	Status
	[1/s]	[Pa]	[mPa·s]	[°C]	[mN·m]	
1	0.1	0.022616	226.22	28.71	0.000426	Dy_auto
2	0.126	0.026813	213.03	28.71	0.000505	Dy_auto
3	0.158	0.034698	218.94	28.71	0.000654	Dy_auto
4	0.2	0.046505	233.09	28.72	0.000877	Dy_auto
5	0.251	0.062807	250.05	28.72	0.001184	Dy_auto
6	0.316	0.078689	248.83	28.72	0.001483	Dy_auto
7	0.398	0.098443	247.29	28.72	0.001856	Dy_auto
8	0.501	0.1232	245.81	28.72	0.002322	Dy_auto
9	0.631	0.15001	237.74	28.72	0.002828	Dy_auto
10	0.794	0.18839	237.17	28.72	0.003551	Dy_auto
11	***1***	***0.2362***	***236.2***	***28.72***	***0.004452***	***Dy_auto***
12	1.26	0.29154	231.58	28.72	0.005495	Dy_auto
13	1.58	0.36731	231.76	28.72	0.006924	Dy_auto
14	2	0.46124	231.17	28.72	0.008694	Dy_auto
15	2.51	0.58332	232.22	28.72	0.010995	Dy_auto

16	3.16	0.73428	232.2	28.72	0.013841	Dy_auto
17	3.98	0.91922	230.9	28.72	0.017327	Dy_auto
18	5.01	1.1525	229.95	28.72	0.021724	Dy_auto
19	6.31	1.4553	230.65	28.71	0.027431	Dy_auto
20	7.94	1.8201	229.14	28.71	0.034308	Dy_auto
21	10	2.291	229.11	28.71	0.043185	Dy_auto
22	12.6	2.8842	229.1	28.71	0.054365	Dy_auto
23	15.8	3.6278	228.9	28.71	0.068382	Dy_auto
24	20	4.5694	229.01	28.71	0.086131	Dy_auto
25	25.1	5.7539	229.07	28.71	0.10846	Dy_auto
26	31.6	7.2438	229.07	28.71	0.13654	Dy_auto
27	39.8	9.1202	229.09	28.71	0.17191	Dy_auto
28	50.1	11.48	229.06	28.71	0.21639	Dy_auto
29	63.1	14.454	229.09	28.71	0.27246	Dy_auto
30	79.4	18.193	229.03	28.71	0.34292	Dy_auto
31	100	22.905	229.05	28.71	0.43174	Dy_auto
32	126	28.829	229	28.71	0.54342	Dy_auto
33	158	36.275	228.88	28.7	0.68377	Dy_auto
34	200	45.621	228.65	28.7	0.85993	Dy_auto
35	251	57.361	228.36	28.7	1.0812	Dy_auto
36	316	72.041	227.81	28.7	1.3579	Dy_auto
37	398	90.385	227.04	28.71	1.7037	Dy_auto
38	501	113.2	225.86	28.71	2.1337	Dy_auto
39	631	141.31	223.96	28.71	2.6637	Dy_auto
40	794	164.25	206.78	28.72	3.0961	Dy_auto
41	1.00E+03	89.501	89.5	28.73	1.687	Dy_auto

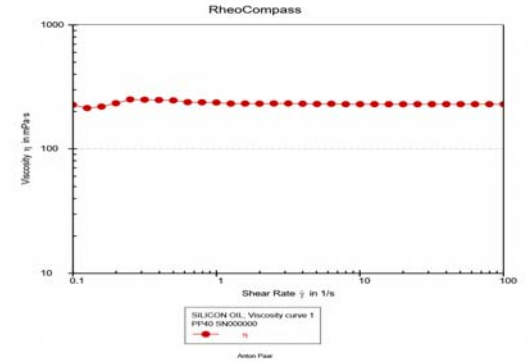

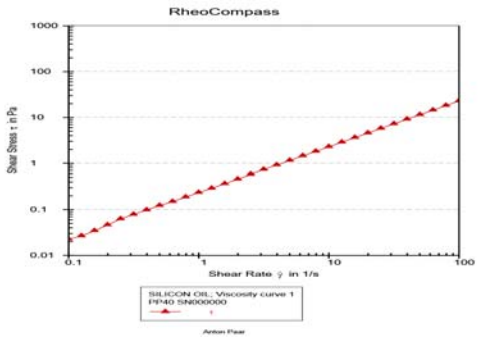

Graph.3.5. Viscosity Vs Shear rate (Silicone oil) Graph.3.6. Shear Stress vs Shear Rate (Silicone oil)

From the tabulated data and the Graphs for Viscosity vs Shear strain and Shear Stress vs Shear Strain for White Transformer oil it may be noted that after initial disturbance, Viscosity is almost constant and obtained an average value of 12.183 mPa-s and the Shear stress vs Shear strain is maintaining a constant slope from point 11 in the table.

From the tabulated data and the Graphs for Viscosity vs Shear strain and Shear Stress vs Shear Strain for Red Transformer oil, it may be noted that Viscosity drops to a lower value for a strain rate of 1.2 after that Viscosity is almost constant and obtained an average value of 20.466 mPa-s and the Shear stress vs Shear strain is maintaining a constant slope from the point 11in the table.

From the tabulated data for Silicone oil, it may be noted that the Viscosity of the Silicone oil is almost constant within the experimental range and has a magnitude of 236.2 mPa-s. Also, the Shear Stress-Shear Strain curve is almost linear.

Based on the results obtained above, Silicone oil and the Red transformer oil have been chosen as the base Rheological fluids for making the Viscoelastic Magnetic Abrasive medium.

3.6.4. Preparation of Silicone oil-based VEMAF Medium:

The preparation has got the following steps.

a. **Preparation of Polymer:** Mixing of 1000 ml Silicone oil with 50 grams of Boric acid thoroughly and heating from room temperature up to 60° C makes the required polymer which would be white in color. Here, Cross-linking of the chained structure of Silicone oil with Boric acid takes place. A schematic representation of Crosslinking(27,36,37) is shown in Fig. 3.8 below. Subsequently, Lewis acid 10 grams has been added at 40° C of

temperature, followed

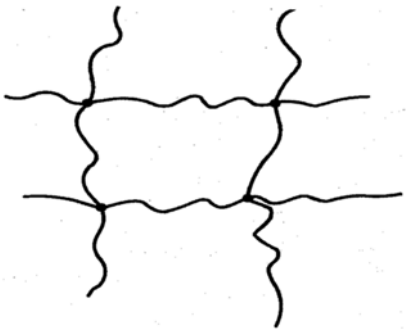

Fig.3.8 Cross-Linking of Polymer **Fig.3.9. Polymer**

by addition of ammonium Carbonate and heating up to boiling temperature along with continuous stirring brings the final stage to the polymer, which is having pale yellow color shown in Fig.3.9 above. Cooling takes place in the open atmosphere. Polymer hence prepared will behave as a Viscous medium in the Viscoelastic Magnetic Abrasive Finishing Medium and has a marginal reduction in Viscosity compared to the Silicon oil, which is shown in Fig. 3.15 below. The Polymer has a Viscosity of 231.43 mPa.

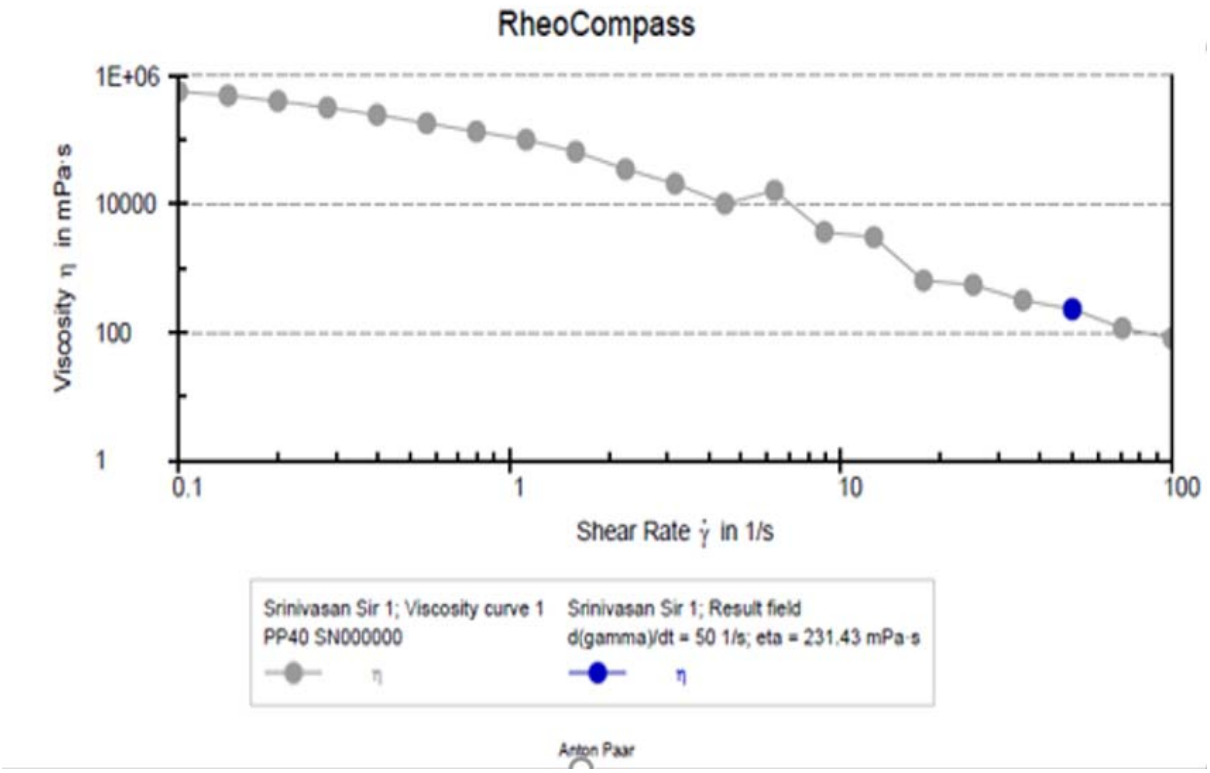

Graph.3.7. Viscosity vs Shear rate of Polymer

a. Preparation of Gel: The Gel is prepared with the Chemical reaction(9, 14, 16, 25) of the Hydrocarbon oil and Aluminium Stearate. For this 500 ml of the Hydrocarbon oil and

25 grams of Aluminium Stearate is mixed thoroughly and heated up to 120^{O} C. The product hence obtained is called as the Gel having red color and has very high Viscosity. The experimental result of the Viscosity experiment of the Hydrocarbon oil is shown below.

3.6.5. Viscosity Measurement of Hydrocarbon Oil:

Table 3.4. Experimental results for Viscosity of Hydrocarbon oil

Point No.	Shear Rate	Shear Stress	Viscosity	Temperature	Torque	Status
	[1/s]	[Pa]	[mPa·s]	[°C]	[mN·m]	
1	0.1	0.030749	307.57	28.42	0.00058	Dy_auto
2	0.126	0.035967	285.76	28.42	0.000678	Dy_auto
3	0.158	0.041956	264.73	28.42	0.000791	Dy_auto
4	0.2	0.04978	249.51	28.42	0.000938	Dy_auto
5	0.251	0.061151	243.45	28.42	0.001153	Dy_auto
6	0.316	0.078275	247.52	28.41	0.001476	Dy_auto
7	0.398	0.10024	251.79	28.41	0.001889	Dy_auto
8	0.501	0.12396	247.33	28.41	0.002337	Dy_auto
9	0.631	0.16082	254.88	28.41	0.003031	Dy_auto
10	0.794	0.19707	248.1	28.41	0.003715	Dy_auto
11	***1***	***0.24732***	***247.32***	***28.41***	***0.004662***	***Dy_auto***
12	1.26	0.31095	247	28.41	0.005861	Dy_auto
13	1.58	0.39361	248.35	28.41	0.007419	Dy_auto
14	2	0.49163	246.4	28.42	0.009267	Dy_auto
15	2.51	0.61897	246.42	28.42	0.011667	Dy_auto
16	3.16	0.7808	246.91	28.42	0.014718	Dy_auto
17	3.98	0.98041	246.27	28.42	0.01848	Dy_auto
18	5.01	1.232	245.82	28.42	0.023223	Dy_auto
19	6.31	1.5499	245.64	28.43	0.029215	Dy_auto
20	7.94	1.95	245.49	28.43	0.036756	Dy_auto
21	10	2.4521	245.21	28.43	0.046221	Dy_auto
22	12.6	3.0855	245.09	28.44	0.05816	Dy_auto
23	15.8	3.882	244.94	28.44	0.073174	Dy_auto
24	20	4.8833	244.74	28.45	0.092047	Dy_auto

25	25.1	6.142	244.52	28.45	0.11577	Dy_auto
26	31.6	7.728	244.38	28.45	0.14567	Dy_auto
27	39.8	9.7208	244.18	28.46	0.18323	Dy_auto
28	50.1	12.228	243.98	28.46	0.23049	Dy_auto
29	63.1	15.382	243.78	28.47	0.28994	Dy_auto
30	79.4	19.348	243.58	28.48	0.36471	Dy_auto
31	100	24.335	243.35	28.48	0.45871	Dy_auto
32	126	30.601	243.08	28.49	0.57682	Dy_auto
33	158	38.489	242.85	28.49	0.72549	Dy_auto
34	200	48.4	242.57	28.5	0.91232	Dy_auto
35	251	60.835	242.19	28.51	1.1467	Dy_auto
36	316	76.432	241.7	28.52	1.4407	Dy_auto
37	398	95.927	240.95	28.53	1.8082	Dy_auto
38	501	120.23	239.88	28.54	2.2662	Dy_auto
39	631	150.38	238.34	28.55	2.8347	Dy_auto
40	794	187.51	236.06	28.57	3.5345	Dy_auto
41	1.00E+03	232.99	232.99	28.59	4.3918	Dy_auto

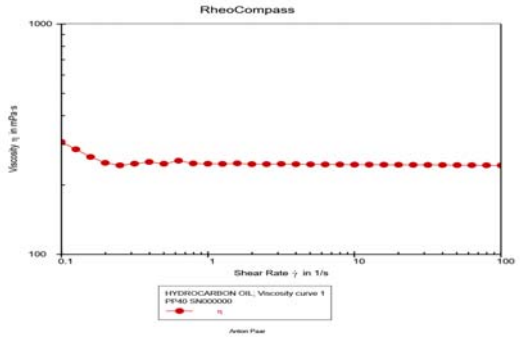

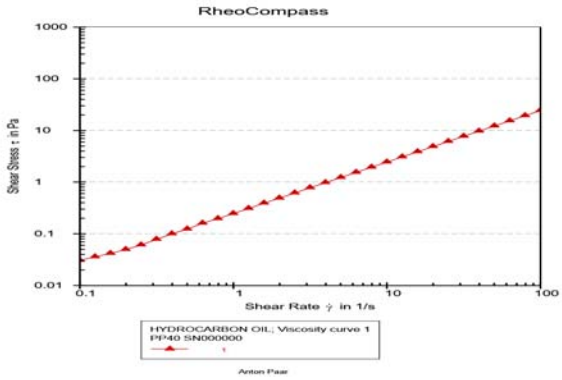

Graph.3.8. Viscosity vs Shear rate[Hydrocarbon oil] **Graph.3.9 Shear Stress vs Shear Rate**

The viscosity of the Gel is found experimentally and the graphical representation of Viscosity vs Shear strain has been shown below in Fig. 3.18. The Viscosity is 13589 mPa-s. A gel is assumed to be a Semi-solid (38) elastic member.

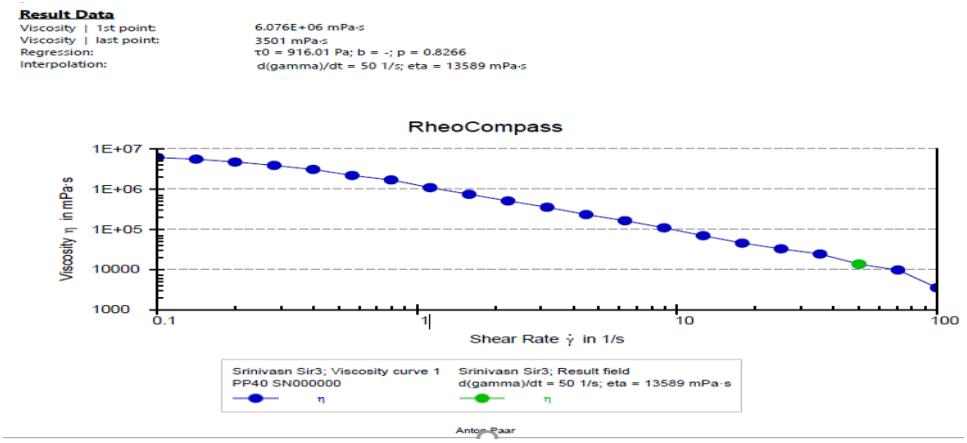

Graph.3.10. Viscosity vs Shear rate of Gel

Fig.3.10. Gel

b. Mixing of Carbonyl Iron Particle and Silicon Carbide:

Carbonyls Iron Particles (CIP) of CS grade and Silicon Carbide(SiC) of Abrasive Mesh Number 320, 400, 600, and 800 have been used for preparing the mixture. The density of CIP is approximately 7.2 grams per cm^3 and the Sic powder from manufacturers' catalog has a density of 2.6 grams per cm^3. Carbonyl particles and Silicon Carbide have been taken in a ratio of 3:1 by weight. Separately, the mixture has been prepared for each abrasive size. Ball mill has been used for thorough mixing of CIP and the abrasive powders.

The table below shows the Abrasive Mesh Number (AMN) and the average size of the abrasive particle of the Abrasives used in the present work

3.6.6. Abrasive Mesh Number and the Mean diameter of the Abrasive: Abrasive Mesh number and the Mean diameter of the Sic abrasive has been shown in the table below.

Table.3.5. Abrasive Mesh Number and Mean Diameter table.

ABRASIVE MESH NUMBER(AMN)	MEAN DIAMETER IN MICRONS

320	36
400	23
600	16
800	12

c. Final mixing: Here, the polymer and the Gel have been mixed in the ratio of 8:1 by weight thoroughly by Gel mixing machine. Now the Polymer-Gel medium hence prepared is mixed with CIP- Abrasive mixture in a ratio of 2:1 by weight and finally the viscosity of the Viscoelastic Magnetic Abrasive medium has been found. This medium is used for the internal finishing of the Spline shafts. The results have been shown below.

3.6.7. Viscoelastic Magnetic Abrasive Medium (sample 3): Viscosity 954.06 mpa-s.:

The results of Viscosity have been shown in Table 3.5 below.

Table 3.6. Experimental results for Viscoelastic Magnetic Abrasive medium [sample3]

Point No.	Shear Rate	Shear Stress	Viscosity	Temperature	Torque	Status
	[1/s]	[Pa]	[mPa·s]	[°C]	[mN·m]	
1	0.1	1.9369	1.94E+04	27.07	0.00797	Dy_auto
2	0.126	2.4185	1.92E+04	27.07	0.00995	Dy_auto
3	0.158	2.3979	1.51E+04	27.07	0.00981	Dy_auto
4	0.2	2.2599	1.13E+04	27.07	0.00937	Dy_auto
5	0.251	2.0606	8.20E+03	27.07	0.00854	Dy_auto
6	0.316	1.849	5.85E+03	27.07	0.00766	Dy_auto
7	0.398	1.7228	4.33E+03	27.08	0.00713	Dy_auto
8	0.501	1.5846	3.16E+03	27.08	0.00654	Dy_auto
9	0.631	1.4275	2.26E+03	27.08	0.0059	Dy_auto
10	0.794	1.1525	1.45E+03	27.08	0.00474	Dy_auto
11	***1***	***0.9540***	***9.54E+02***	***27.08***	***0.0039***	***Dy_auto***
12	1.26	0.8464	6.72E+02	27.09	0.00353	Dy_auto
13	1.58	0.7180	4.53E+02	27.09	0.00292	Dy_auto
14	2	0.6245	3.13E+02	27.09	0.00272	Dy_auto
15	2.51	0.5847	2.33E+02	27.09	0.00246	Dy_auto

16	3.16	0.5203	1.65E+02	27.09	0.00217	Dy_auto
17	3.98	0.4827	1.21E+02	27.10	0.00208	Dy_auto
18	5.01	0.444	0.8861	27.10	0.00186	Dy_auto
19	6.31	0.4327	0.6858	27.10	0.00178	Dy_auto
20	7.94	0.4124	0.5192	27.10	0.00171	Dy_auto
21	10	0.3920	0.3920	27.10	0.00161	Dy_auto
22	12.6	0.415	0.3294	27.11	0.00106	Dy_auto
23	15.8	0.4164	0.2627	27.11	1.7132	Dy_auto
24	20	0.41412	0.20756	27.11	0.00170	Dy_auto
25	25.1	0.2603	0.1036	27.11	0.00107	Dy_auto
26	31.6	0.1970	0.6227	27.11	0.00810	Dy_auto
27	39.8	0.1770	0.4447	27.11	0.00728	Dy_auto
28	50.1	0.1820	0.3628	27.11	0.00748	Dy_auto
29	63.1	0.1870	0.2964	27.11	0.00769	Dy_auto
30	79.4	0.172	0.2151	27.11	0.00703	Dy_auto
31	100	0.1560	0.1557	27.12	0.00641	Dy_auto
32	126	157.28	1249.4	27.12	0.00647	Dy_auto
33	158	142.78	900.87	27.12	0.00587	Dy_auto
34	200	104.51	523.79	27.12	0.00429	Dy_auto
35	251	73.555	292.82	27.12	0.00302	Dy_auto
36	316	48.78	154.26	27.12	0.00201	Dy_auto
37	398	57.586	144.65	27.12	0.00237	Dy_auto
38	501	16.786	33.493	27.13	0.00069	Dy_auto
39	631	16.754	26.554	27.13	0.00068	Dy_auto
40	794	21.052	26.503	27.13	0.00086	Dy_auto
41	1.00E+03	17.351	17.351	27.13	0.00071	Dy_auto

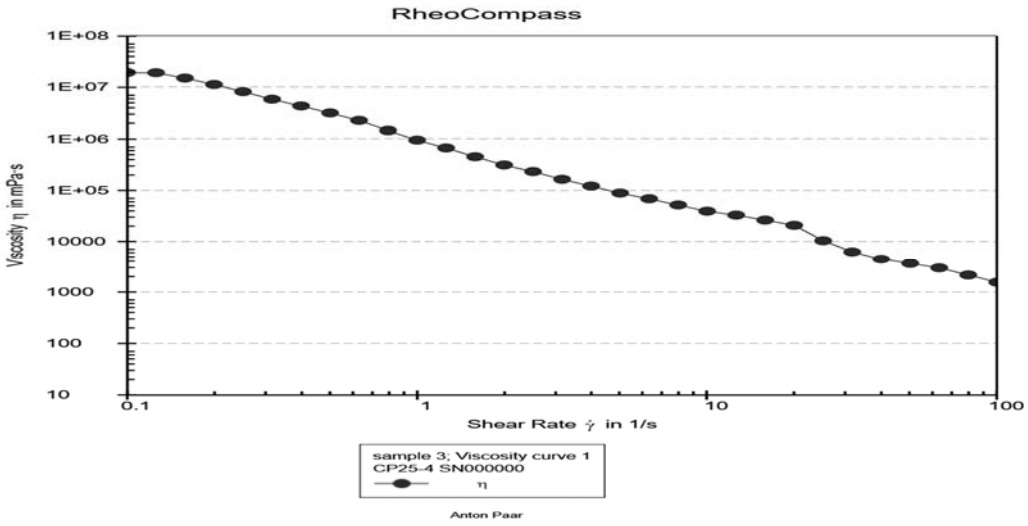

Graph.3.11. Viscosity vs Shear Strain VEMAF Medium [Sample 3]

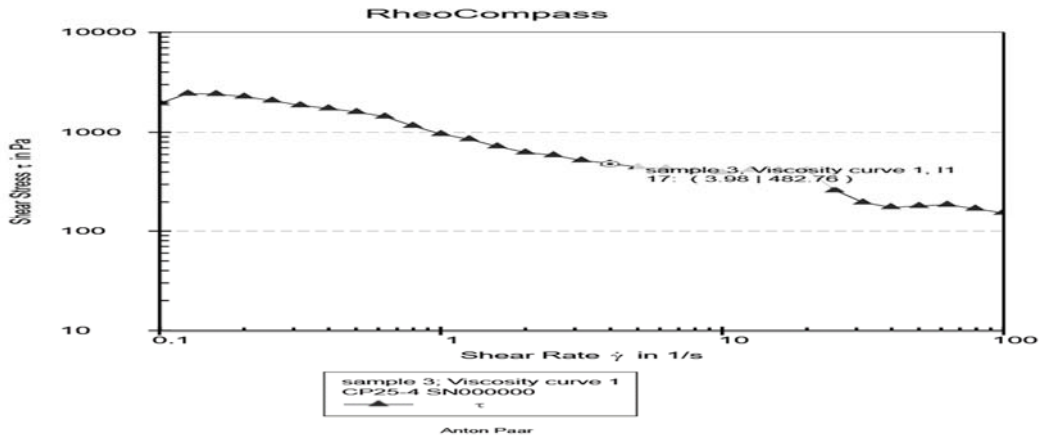

Graph.3.12. Shear Stress vs Shear Strain VEMAF Medium [Sample 3]

It has been observed that the Viscosity variation based on the abrasive size is marginal.

Fig. 3.11. Silicone Oil-based Viscoelastic Magnetic Abrasive Medium

3.6.8. Preparation of Transformer oil (Red) based Viscoelastic Magnetic Abrasive Medium:

The following steps are followed in sequence for making the Viscoelastic Magnetic abrasive Medium.

i. 1000 ml Red transformer oil is heated till the moisture is removed.

ii. 500 ml Transformer oil is heated up to 50° C and 50 grams of ***Sodium Stearate*** is added and thoroughly stirred till a thorough mixing takes place. This will make the medium-thick compared to its initial condition. Further heating up to around 150° C will saponify the mixture and it becomes further thick. Water content left is removed. This makes the semi-solid, which acts as an elastic body.

iii. The remaining 500 ml transformer oil is heated up to 40° C and Simultaneously 50 ml boric acid solution and 50 ml Sodium hydroxide solution are added and thoroughly stirred. This converts the transformer oil to highly viscous. Viscous oil

iv. Both the saponified semi-solid and the viscous transformer oil have been mixed thoroughly at 50° C and stirred for 60 minutes. The antioxidant solution of 1% concentration is added. This gives Viscoelastic medium.

v. Now the Carbonyl Iron Particle and SiC mixture in 3:1 ratio by weight have been mixed thoroughly in Ball mill.

vi. Now the Viscoelastic medium and the CIP and SiC powder in 1:3 ratio by weight have been mixed and thorough stirring takes place by the Chemical stirrer. This makes the Viscoelastic Magnetic Abrasive Medium.

The Viscosity has been measured for this medium.

3.6.8.1 Viscoelastic Magnetic Abrasive Medium sample 1 Transformer Oil Based: Viscosity 2926.2 mPa-s.

Table 3.7. Experimental results for Viscoelastic Magnetic Abrasive medium [sample1]

Point No.	Shear Rate	Shear Stress	Viscosity	Temperature	Torque	Status
	[1/s]	[Pa]	[mPa·s]	[°C]	[mN·m]	
1	0.1	452.31	4.52E+06	27.31	1.8609	Dy_auto
2	0.126	622.91	4.95E+06	27.32	2.5628	Dy_auto
3	0.158	799	5.04E+06	27.32	3.2873	Dy_auto
4	0.2	956.05	4.79E+06	27.33	3.9334	Dy_auto

5	0.251	1141.1	4.54E+06	27.34	4.6948	Dy_auto
6	0.316	1360.7	4.30E+06	27.34	5.5981	Dy_auto
7	0.398	1612.5	4.05E+06	27.35	6.6343	Dy_auto
8	0.501	1889.3	3.77E+06	27.36	7.7731	Dy_auto
9	0.631	2209.1	3.50E+06	27.36	9.0886	Dy_auto
10	0.794	2551.9	3.21E+06	27.37	10.499	Dy_auto
11	***1***	***2926.2***	***2.93E+06***	***27.37***	***12.039***	***Dy_auto***
12	1.26	3356.2	2.67E+06	27.38	13.808	Dy_auto
13	1.58	3815.4	2.41E+06	27.38	15.698	Dy_auto
14	2	4314.7	2.16E+06	27.39	17.752	Dy_auto
15	2.51	4827.2	1.92E+06	27.39	19.86	Dy_auto
16	3.16	5397.7	1.71E+06	27.4	22.208	Dy_auto
17	3.98	5933.7	1.49E+06	27.4	24.413	Dy_auto
18	5.01	6401.6	1.28E+06	27.4	26.338	Dy_auto
19	6.31	6917	1.10E+06	27.41	28.458	Dy_auto
20	7.94	7364.5	9.27E+05	27.41	30.299	Dy_auto
21	10	7695.6	7.70E+05	27.42	31.661	Dy_auto
22	12.6	7990	6.35E+05	27.42	32.873	Dy_auto
23	15.8	8162.2	5.15E+05	27.43	33.581	Dy_auto
24	20	7796	3.91E+05	27.43	32.075	Dy_auto
25	25.1	7739.7	3.08E+05	27.44	31.843	Dy_auto
26	31.6	8014	2.53E+05	27.45	32.971	Dy_auto
27	39.8	8950.2	2.25E+05	27.45	36.823	Dy_auto
28	50.1	9609.3	1.92E+05	27.46	39.535	Dy_auto
29	63.1	10228	1.62E+05	27.47	42.082	Dy_auto
30	79.4	10877	1.37E+05	27.49	44.749	Dy_auto
31	100	11929	1.19E+05	27.51	49.079	Dy_auto
32	126	11018	87513	27.54	45.329	Dy_auto
33	158	10793	68098	27.57	44.403	Dy_auto
34	200	10219	51210	27.6	42.043	Dy_auto
35	251	6684.7	26613	27.63	27.502	Dy_auto
36	316	5420.7	17138	27.66	22.302	Dy_auto

37	398	3329.4	8363	27.68	13.698	Dy_auto
38	501	10341	20643	27.7	42.544	Dy_auto
39	631	11605	18392	27.83	47.745	Dy_auto
40	794	12870	16201	27.99	52.951	Dy_auto
41	1.00E+03	10726	10726	28.17	44.128	Dy_auto

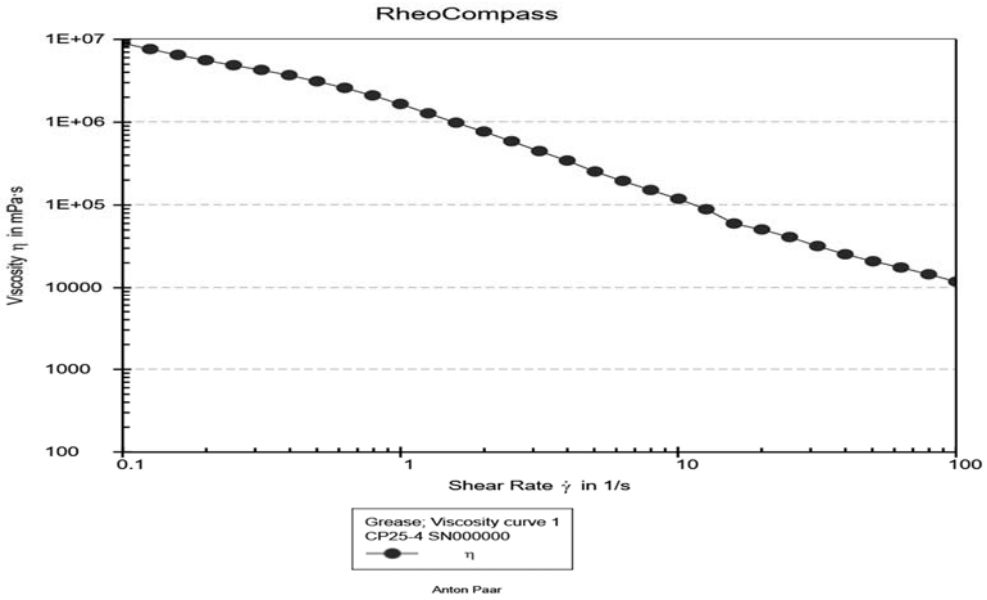

Graph.3.13. Viscosity vs Shear Strain [Sample 1]

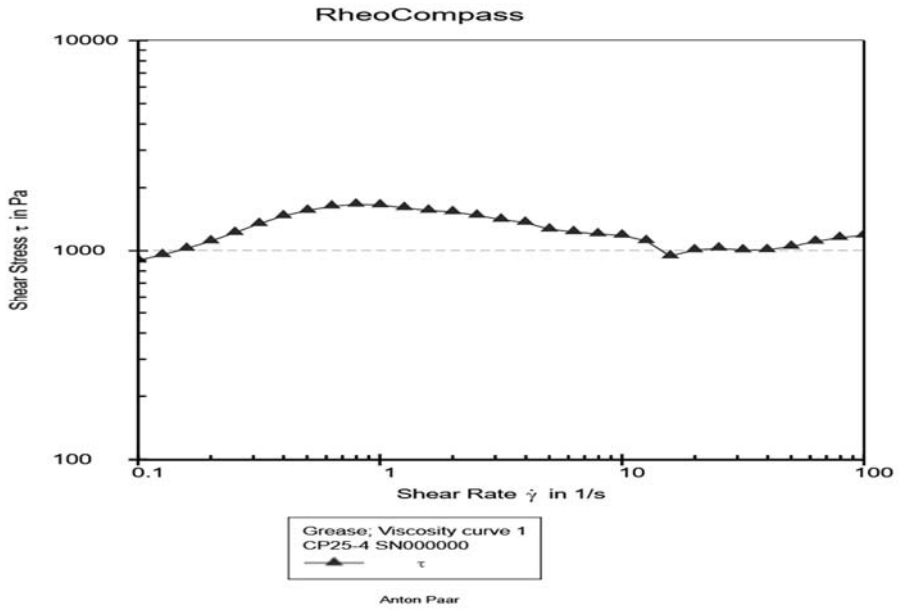

Graph.3.14. Shear Stress vs Shear Strain [Sample 1]

Fig.3.12. Transformer oil-based Viscoelastic Magnetic Abrasive Medium

The Viscoelastic Magnetic Abrasive Medium prepared based on Transformer oil(Red color) is having a Viscosity of 2926.2 mPa-s (Milli Pascal-Second). This lies in the Viscosity of Semisolids. Also, Shear-thinning is observed as there is a decrease in Viscosity with Shear strain shown in Graph.3.14

3.6.9. Preparation of Viscoelastic Magnetic abrasive Medium based on AP3 Grease:

In this, the mixture of Carbonyl Iron Particle and Silicone Carbide abrasive mixture has been added to the AP3 grease and a semi-solid is prepared. The Viscosity of each sample is found. The viscosity of Grease has been found and the results have been shown below.Graph.3.15 and Graph.3.16 show the relation between Viscosity Versus Shear strain and Shear stress versus Shear Strain.

Table 3.8. Experimental results for Viscosity of AP3 Grease

Point No.	Shear Rate	Shear Stress	Viscosity	Temperature	Torque	Status
	[1/s]	[Pa]	[mPa·s]	[°C]	[mN·m]	
1	0.1	901.25	9.01E+06	29.19	3.708	Dy_auto
2	0.126	957.46	7.61E+06	29.19	3.9392	Dy_auto
3	0.158	1025.2	6.47E+06	29.18	4.218	Dy_auto
4	0.2	1113	5.58E+06	29.18	4.579	Dy_auto
5	0.251	1221.1	4.86E+06	29.18	5.024	Dy_auto
6	0.316	1347.4	4.26E+06	29.18	5.5434	Dy_auto
7	0.398	1467.5	3.69E+06	29.17	6.0375	Dy_auto
8	0.501	1558.1	3.11E+06	29.17	6.4102	Dy_auto
9	0.631	1632.4	2.59E+06	29.17	6.716	Dy_auto

10	0.794	1666.4	2.10E+06	29.17	6.8559	Dy_auto
11	***1***	***1654.3***	***1.65E+06***	***29.16***	***6.8063***	***Dy_auto***
12	1.26	1605.4	1.28E+06	29.16	6.605	Dy_auto
13	1.58	1558.8	9.84E+05	29.16	6.4135	Dy_auto
14	2	1534.7	7.69E+05	29.15	6.3141	Dy_auto
15	2.51	1476.5	5.88E+05	29.15	6.0747	Dy_auto
16	3.16	1412	4.47E+05	29.15	5.8095	Dy_auto
17	3.98	1365.6	3.43E+05	29.15	5.6185	Dy_auto
18	5.01	1267.7	2.53E+05	29.14	5.2156	Dy_auto
19	6.31	1231.7	1.95E+05	29.14	5.0677	Dy_auto
20	7.94	1203.5	1.52E+05	29.14	4.9515	Dy_auto
21	10	1186.3	1.19E+05	29.13	4.8807	Dy_auto
22	12.6	1116.2	88660	29.13	4.5921	Dy_auto
23	15.8	945.04	59631	29.12	3.8881	Dy_auto
24	20	1009.4	50594	29.12	4.1531	Dy_auto
25	25.1	1029.2	40974	29.12	4.2344	Dy_auto
26	31.6	1008.4	31888	29.11	4.1487	Dy_auto
27	39.8	1010.9	25393	29.11	4.1591	Dy_auto
28	50.1	1048.4	20919	29.1	4.3135	Dy_auto
29	63.1	1108.7	17572	29.1	4.5613	Dy_auto
30	79.4	1155.8	14551	29.1	4.7554	Dy_auto
31	100	1187.3	11873	29.1	4.8849	Dy_auto
32	126	1252.2	9946.4	29.1	5.1516	Dy_auto
33	158	1263.2	7970.3	29.1	5.1971	Dy_auto
34	200	1357.9	6805.8	29.1	5.5868	Dy_auto
35	251	1419.9	5652.7	29.1	5.8417	Dy_auto
36	316	1500	4743.6	29.1	6.1715	Dy_auto
37	398	1163.5	2922.6	29.11	4.7868	Dy_auto
38	501	1730.9	3453.8	29.12	7.1215	Dy_auto
39	631	1045.5	1657.1	29.13	4.3016	Dy_auto
40	794	596.01	750.35	29.14	2.4521	Dy_auto
41	1.00E+03	581.67	581.67	29.14	2.3931	Dy_auto

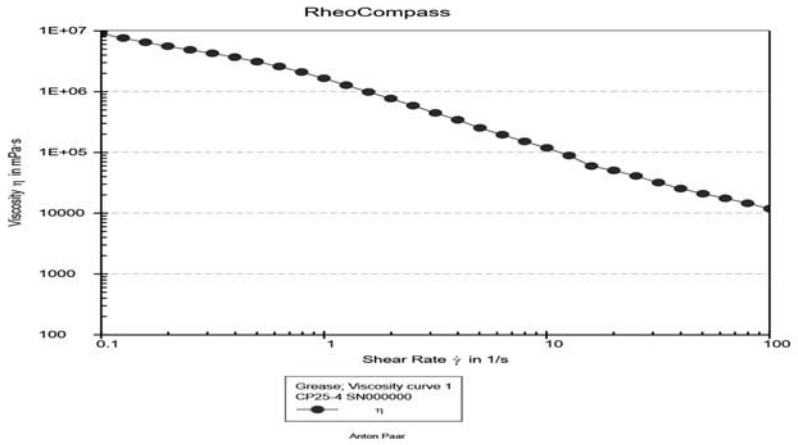

Graph.3.15.Viscosity vs Shear Strain AP3 Grease

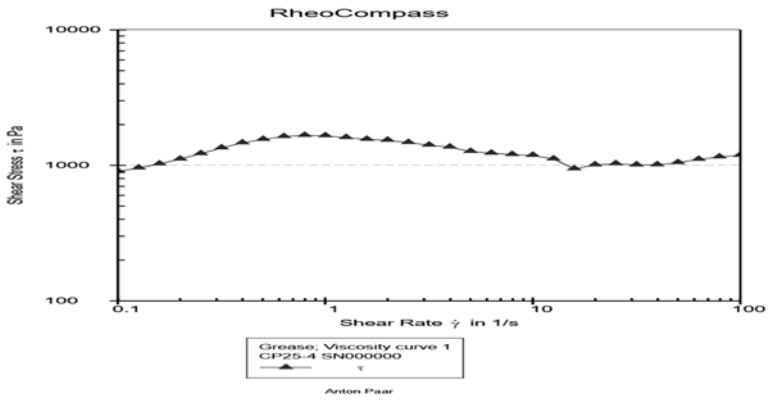

Graph.3.16. Shear Stress vs Shear Strain AP3 Grease

3.6.9.1. AP3 Grease based Viscoelastic Magnetic abrasive Medium lab Sample 5:

In this sample, 30 grams of AP3 Grease and 10 grams of CIP and SiC mixture is thoroughly stirred and the sample has been tested for Viscosity using MCR 102. Viscosity obtained is 1640mPa-s.The results are given below. Graph.3.17 and Graph.3.18 show the relation between Viscosity Versus Shear strain and Shear stress versus Shear Strain.

Table.3.9. Experimental results for Viscosity Sample 5: Viscosity 1640 mPa-s.

Point No.	Shear Rate	Shear Stress	Viscosity	Temperature	Torque	Status
	[1/s]	[Pa]	[mPa·s]	[°C]	[mN·m]	
1	0.1	1195.2	1.20E+07	26.97	4.9174	Dy_auto
2	0.126	1334.1	1.06E+07	26.97	5.4886	Dy_auto
3	0.158	1444.4	9.11E+06	26.98	5.9425	Dy_auto

4	0.2	1534.4	7.69E+06	26.98	6.3128	Dy_auto
5	0.251	1604.5	6.39E+06	26.99	6.6014	Dy_auto
6	0.316	1648.7	5.21E+06	27	6.7832	Dy_auto
7	0.398	1664.6	4.18E+06	27	6.8485	Dy_auto
8	0.501	1666.1	3.32E+06	27	6.8545	Dy_auto
9	0.631	1665.1	2.64E+06	27.01	6.8506	Dy_auto
10	0.794	1654.2	2.08E+06	27.02	6.8058	Dy_auto
11	***1***	***1640***	***1.64E+06***	***27.02***	***6.7473***	***Dy_auto***
12	1.26	1617.3	1.28E+06	27.03	6.6537	Dy_auto
13	1.58	1605.2	1.01E+06	27.03	6.6044	Dy_auto
14	2	1621.1	8.13E+05	27.04	6.6697	Dy_auto
15	2.51	1553.6	6.19E+05	27.04	6.3919	Dy_auto
16	3.16	1524.3	4.82E+05	27.05	6.2713	Dy_auto
17	3.98	1542.6	3.88E+05	27.05	6.3468	Dy_auto
18	5.01	1531.1	3.06E+05	27.05	6.2995	Dy_auto
19	6.31	1515.8	2.40E+05	27.06	6.2365	Dy_auto
20	7.94	1610.9	2.03E+05	27.06	6.6274	Dy_auto
21	10	1550.9	1.55E+05	27.07	6.3808	Dy_auto
22	12.6	1531.4	1.22E+05	27.07	6.3003	Dy_auto
23	15.8	1492.2	94153	27.07	6.1393	Dy_auto
24	20	1488.5	74601	27.08	6.1239	Dy_auto
25	25.1	1550.1	61713	27.08	6.3777	Dy_auto
26	31.6	1586.1	50159	27.09	6.5258	Dy_auto
27	39.8	1681.9	42249	27.09	6.9199	Dy_auto
28	50.1	1639.2	32706	27.09	6.744	Dy_auto
29	63.1	1258.3	19943	27.1	5.177	Dy_auto
30	79.4	1280.5	16121	27.1	5.2682	Dy_auto
31	100	1138.2	11382	27.1	4.6828	Dy_auto
32	126	1202	9547.7	27.11	4.9451	Dy_auto
33	158	1297.5	8186.9	27.12	5.3384	Dy_auto
34	200	1352.6	6779.2	27.12	5.565	Dy_auto
35	251	1425.3	5674.2	27.13	5.8639	Dy_auto

36	316	1334.8	4221.1	27.14	5.4917	Dy_auto
37	398	1377.6	3460.4	27.15	5.6678	Dy_auto
38	501	1409.2	2811.9	27.17	5.7979	Dy_auto
39	631	1978.3	3135.3	27.19	8.1392	Dy_auto
40	794	943.87	1188.2	27.22	3.8833	Dy_auto
41	1.00E+03	750.09	750.09	27.23	3.086	Dy_auto

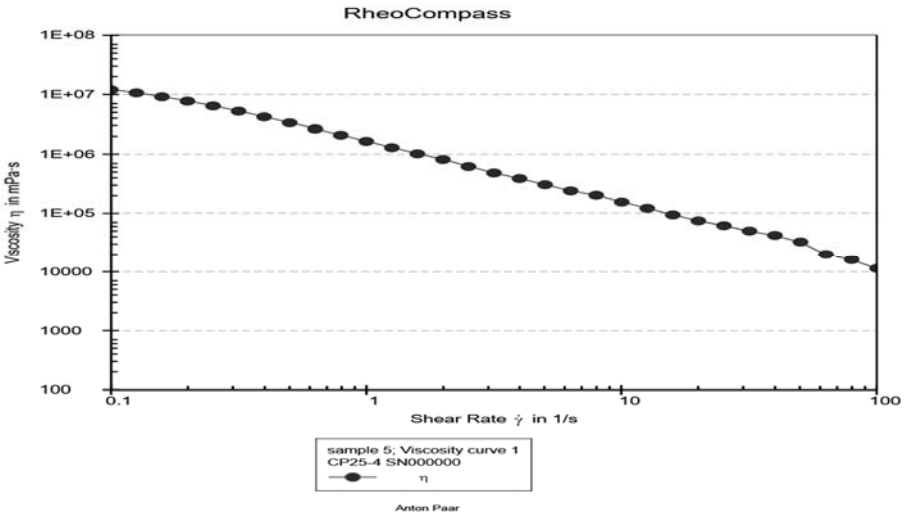

Graph.3.17 Viscosity vs Shear Strain [sample5]

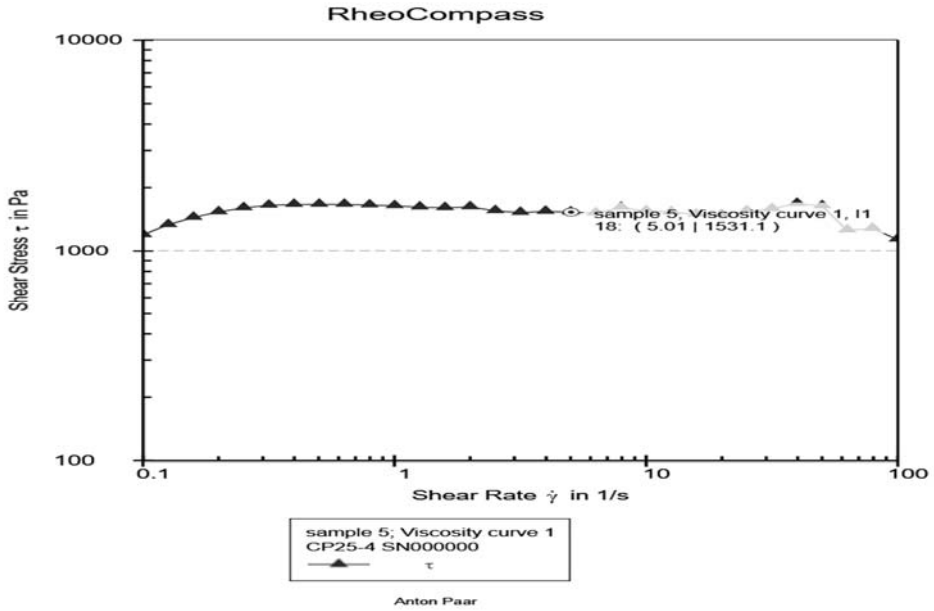

Graph.3.18. Shear Stress vs Shear Strain [Sample 5]

3.6.9.2. AP3 Grease based Viscoelastic Magnetic abrasive Medium lab Sample 6:

In this sample 30 grams of AP3 grease and 15 grams of CIP- SiC mixture is thoroughly mixed and the sample has been tested for Viscosity**. Graph.3.19 and Graph.3.20** show the relation between Viscosity Versus Shear strain and Shear stress versus Shear Strain.

Table.3.10. Experimental results for Viscosity Sample 6: Viscosity 1666.7mPa-s.

Point No.	Shear Rate	Shear Stress	Viscosity	Temperature	Torque	Status
	[1/s]	[Pa]	[mPa·s]	[°C]	[mN·m]	
1	0.1	1101.6	1.10E+07	26.95	4.5321	Dy_auto
2	0.126	1219.2	9.68E+06	26.95	5.0162	Dy_auto
3	0.158	1329.7	8.39E+06	26.95	5.4708	Dy_auto
4	0.2	1436.7	7.20E+06	26.96	5.9107	Dy_auto
5	0.251	1536.3	6.12E+06	26.96	6.3205	Dy_auto
6	0.316	1623.4	5.13E+06	26.96	6.6789	Dy_auto
7	0.398	1668.5	4.19E+06	26.96	6.8646	Dy_auto
8	0.501	1670.4	3.33E+06	26.96	6.8726	Dy_auto
9	0.631	1666.6	2.64E+06	26.96	6.8568	Dy_auto
10	0.794	1670.6	2.10E+06	26.96	6.8733	Dy_auto
11	***1***	***1666.7***	***1.67E+06***	***26.96***	***6.8572***	***Dy_auto***
12	1.26	1661.5	1.32E+06	26.97	6.8359	Dy_auto
13	1.58	1635.9	1.03E+06	26.97	6.7306	Dy_auto
14	2	1612.3	8.08E+05	26.97	6.6335	Dy_auto
15	2.51	1589.2	6.33E+05	26.97	6.5381	Dy_auto
16	3.16	1580.5	5.00E+05	26.97	6.5026	Dy_auto
17	3.98	1590.3	3.99E+05	26.97	6.543	Dy_auto
18	5.01	1604.3	3.20E+05	26.97	6.6006	Dy_auto
19	6.31	1579.7	2.50E+05	26.97	6.4992	Dy_auto
20	7.94	1582.9	1.99E+05	26.97	6.5124	Dy_auto
21	10	1508.9	1.51E+05	26.97	6.2079	Dy_auto
22	12.6	1377.6	1.09E+05	26.97	5.6678	Dy_auto
23	15.8	1194.3	75360	26.97	4.9137	Dy_auto
24	20	1193.4	59811	26.97	4.9098	Dy_auto
25	25.1	1151.4	45838	26.97	4.7371	Dy_auto
26	31.6	1032.8	32660	26.98	4.2492	Dy_auto
27	39.8	1193.6	29982	26.98	4.9107	Dy_auto

28	50.1	1282.7	25594	26.98	5.2775	Dy_auto
29	63.1	1346.2	21336	26.98	5.5387	Dy_auto
30	79.4	1429.8	18001	26.98	5.8826	Dy_auto
31	100	1488.3	14883	26.99	6.1232	Dy_auto
32	126	1578.3	12537	26.99	6.4933	Dy_auto
33	158	1129.2	7125	26.99	4.6458	Dy_auto
34	200	1113.6	5581.3	26.99	4.5816	Dy_auto
35	251	1130	4498.8	27	4.6492	Dy_auto
36	316	1144	3617.7	27.01	4.7068	Dy_auto
37	398	1208.9	3036.6	27.02	4.9736	Dy_auto
38	501	1248.5	2491.1	27.03	5.1365	Dy_auto
39	631	1950.6	3091.6	27.05	8.0253	Dy_auto
40	794	874.03	1100.4	27.06	3.596	Dy_auto
41	1.00E+03	504.43	504.43	27.07	2.0753	Dy_auto

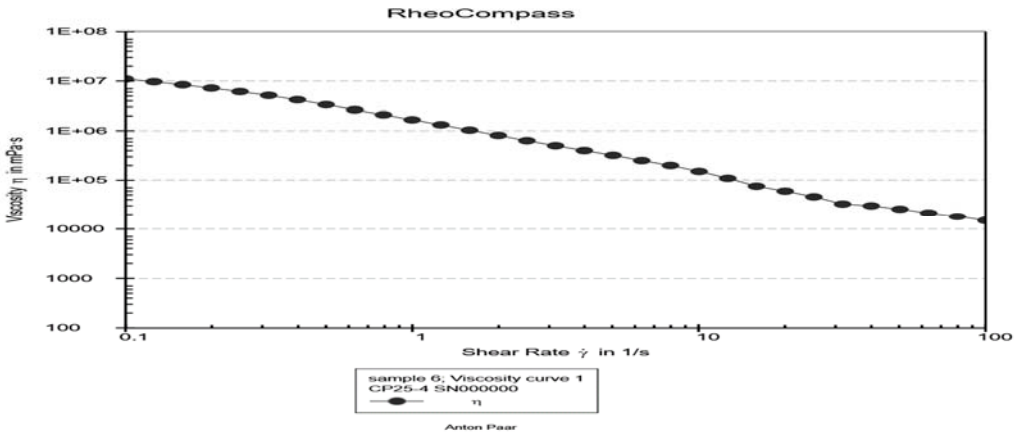

Graph.3.19. Viscosity vs Shear Strain [Sample 6]

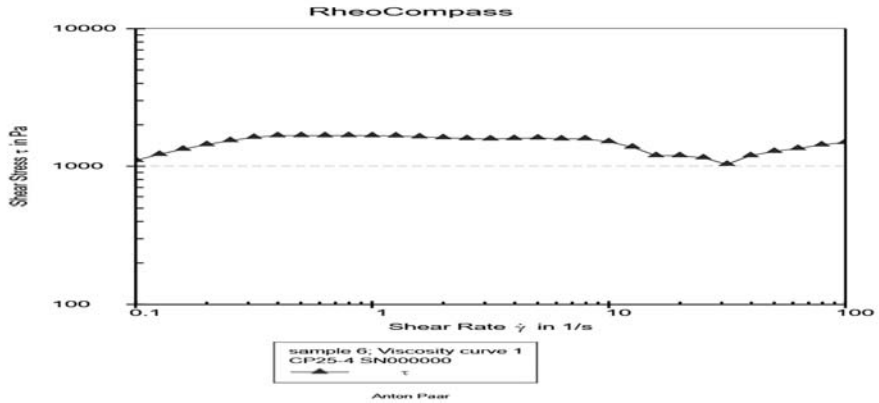

Graph.3.20. Shear Stress vs Shear Strain [Sample 6]

3.6.9.3. AP3 Grease based Viscoelastic Magnetic abrasive Medium lab Sample 7:

In this sample 30 grams of AP3 grease and 20 grams of CIP- SiC mixture is thoroughly mixed and the sample has been tested for Viscosity. Graph..3.21 and Graph.3.22 respectively show the relation between Viscosity Versus Shear strain and Shear stress versus Shear Strain.

Table.3.11. Experimental results for Viscosity Sample 7: Viscosity 1782.3mPa-s.

Point No.	Shear Rate	Shear Stress	Viscosity	Temperature	Torque	Status
	[1/s]	[Pa]	[mPa·s]	[°C]	[mN·m]	
1	0.1	1324.4	1.32E+07	26.79	5.4491	Dy_auto
2	0.126	1438	1.14E+07	26.79	5.9164	Dy_auto
3	0.158	1513.8	9.55E+06	26.8	6.228	Dy_auto
4	0.2	1588.3	7.96E+06	26.8	6.5347	Dy_auto
5	0.251	1660.2	6.61E+06	26.8	6.8306	Dy_auto
6	0.316	1726	5.46E+06	26.8	7.1011	Dy_auto
7	0.398	1772.8	4.45E+06	26.81	7.2936	Dy_auto
8	0.501	1818.9	3.63E+06	26.81	7.4834	Dy_auto
9	0.631	1827.6	2.90E+06	26.82	7.5191	Dy_auto
10	0.794	1811	2.28E+06	26.82	7.4508	Dy_auto
11	***1***	***1782.3***	***1.78E+06***	***26.83***	***7.3327***	***Dy_auto***
12	1.26	1757.7	1.40E+06	26.83	7.2317	Dy_auto
13	1.58	1739.9	1.10E+06	26.84	7.1583	Dy_auto
14	2	1702.8	8.53E+05	26.84	7.0055	Dy_auto
15	2.51	1661.3	6.61E+05	26.85	6.8348	Dy_auto
16	3.16	1587	5.02E+05	26.85	6.5293	Dy_auto
17	3.98	1589.9	3.99E+05	26.86	6.5411	Dy_auto
18	5.01	1538	3.07E+05	26.86	6.3277	Dy_auto
19	6.31	1592.7	2.52E+05	26.87	6.5529	Dy_auto
20	7.94	1563.2	1.97E+05	26.88	6.4312	Dy_auto
21	10	1599.8	1.60E+05	26.88	6.582	Dy_auto
22	12.6	1654.1	1.31E+05	26.89	6.8055	Dy_auto
23	15.8	1649.1	1.04E+05	26.9	6.7846	Dy_auto
24	20	1635.2	81954	26.91	6.7274	Dy_auto

25	25.1	1395.3	55547	26.91	5.7406	Dy_auto
26	31.6	1350.4	42705	26.92	5.556	Dy_auto
27	39.8	1045.1	26253	26.93	4.2999	Dy_auto
28	50.1	1283.1	25601	26.94	5.2788	Dy_auto
29	63.1	1321.1	20938	26.95	5.4352	Dy_auto
30	79.4	1385.7	17446	26.96	5.7013	Dy_auto
31	100	1434.9	14349	26.97	5.9033	Dy_auto
32	126	1500.1	11916	26.98	6.172	Dy_auto
33	158	1554.1	9805.9	27	6.394	Dy_auto
34	200	1641.1	8225.1	27.01	6.7518	Dy_auto
35	251	1458.2	5805.1	27.03	5.9996	Dy_auto
36	316	1281.5	4052.4	27.05	5.2722	Dy_auto
37	398	1392	3496.6	27.07	5.7272	Dy_auto
38	501	1476.2	2945.5	27.09	6.0735	Dy_auto
39	631	1606.9	2546.8	27.12	6.6113	Dy_auto
40	794	1701.2	2141.7	27.16	6.999	Dy_auto
41	1.00E+03	1278.9	1278.9	27.2	5.2618	Dy_auto

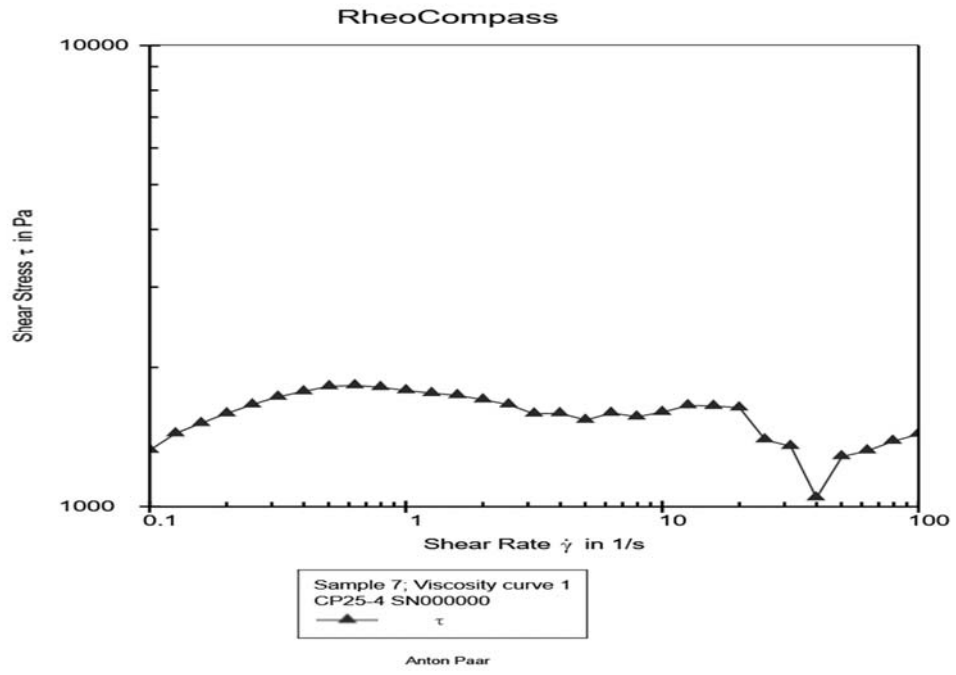

Graph.3.21 Shear Stress vs Shear Strain [Sample 7]

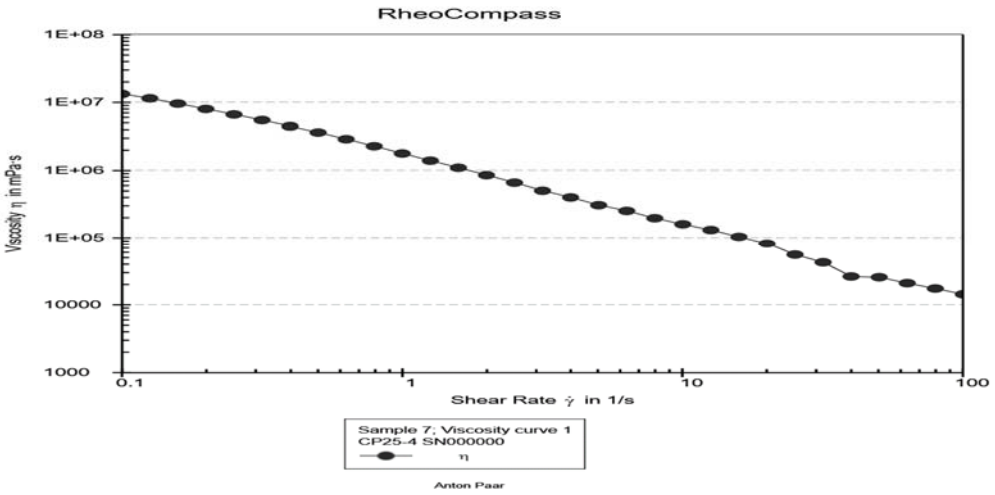

Graph.3.22. Viscosity vs Shear rate [Sample 7]

3.6.9.4. AP3 Grease based Viscoelastic Magnetic abrasive Medium lab Sample 8:

In this sample 30 grams of AP3 grease and 30 grams of CIP- SiC mixture is thoroughly mixed and the sample has been tested for Viscosity. Graph.3.23 and Graph.3.24 respectively show the relation between Viscosity Versus Shear strain and Shear stress versus Shear Strain.

Table.3.12. Experimental results for Viscosity Sample 8: Viscosity 1782.3mPa-s.

Point No.	Shear Rate	Shear Stress	Viscosity	Temperature	Torque	Status
	[1/s]	[Pa]	[mPa·s]	[°C]	[mN·m]	
1	0.1	1238.1	1.24E+07	27.15	5.0939	Dy_auto
2	0.126	1355.5	1.08E+07	27.17	5.5767	Dy_auto
3	0.158	1472.5	9.29E+06	27.18	6.0582	Dy_auto
4	0.2	1585.7	7.95E+06	27.19	6.5239	Dy_auto
5	0.251	1686	6.71E+06	27.21	6.9364	Dy_auto
6	0.316	1791.5	5.67E+06	27.22	7.3705	Dy_auto
7	0.398	1887.8	4.74E+06	27.23	7.767	Dy_auto
8	0.501	1956.9	3.90E+06	27.25	8.0512	Dy_auto
9	0.631	1968.3	3.12E+06	27.26	8.0979	Dy_auto
10	0.794	1960.9	2.47E+06	27.27	8.0676	Dy_auto
11	***1***	***1959.4***	***1.96E+06***	***27.28***	***8.0613***	***Dy_auto***
12	1.26	1931.2	1.53E+06	27.3	7.9453	Dy_auto
13	1.58	1882.1	1.19E+06	27.31	7.7434	Dy_auto
14	2	1823.3	9.14E+05	27.32	7.5013	Dy_auto

15	2.51	1820.3	7.25E+05	27.34	7.4891	Dy_auto
16	3.16	1828.8	5.78E+05	27.35	7.5243	Dy_auto
17	3.98	1855.9	4.66E+05	27.37	7.6357	Dy_auto
18	5.01	1871.4	3.73E+05	27.38	7.6994	Dy_auto
19	6.31	1913.2	3.03E+05	27.39	7.8713	Dy_auto
20	7.94	1941.1	2.44E+05	27.41	7.9859	Dy_auto
21	10	1993.4	1.99E+05	27.42	8.2012	Dy_auto
22	12.6	2023.1	1.61E+05	27.44	8.3235	Dy_auto
23	15.8	2054.1	1.30E+05	27.46	8.4512	Dy_auto
24	20	2084.9	1.05E+05	27.47	8.578	Dy_auto
25	25.1	2103.7	83750	27.49	8.655	Dy_auto
26	31.6	2155.4	68162	27.5	8.8679	Dy_auto
27	39.8	2167.4	54444	27.52	8.9174	Dy_auto
28	50.1	2141.4	42728	27.54	8.8103	Dy_auto
29	63.1	2117	33553	27.56	8.7099	Dy_auto
30	79.4	2199.2	27687	27.58	9.0482	Dy_auto
31	100	2078.9	20789	27.59	8.553	Dy_auto
32	126	2149.7	17076	27.62	8.8445	Dy_auto
33	158	2217	13988	27.64	9.1212	Dy_auto
34	200	2357.4	11815	27.66	9.699	Dy_auto
35	251	2107.6	8390.4	27.69	8.6711	Dy_auto
36	316	2044.1	6464.2	27.72	8.41	Dy_auto
37	398	1960	4923.3	27.75	8.0639	Dy_auto
38	501	1638.8	3270	27.79	6.7425	Dy_auto
39	631	1572.2	2491.7	27.82	6.4684	Dy_auto
40	794	1277.8	1608.5	27.87	5.2573	Dy_auto
41	1.00E+03	873.55	873.49	27.9	3.594	Dy_auto

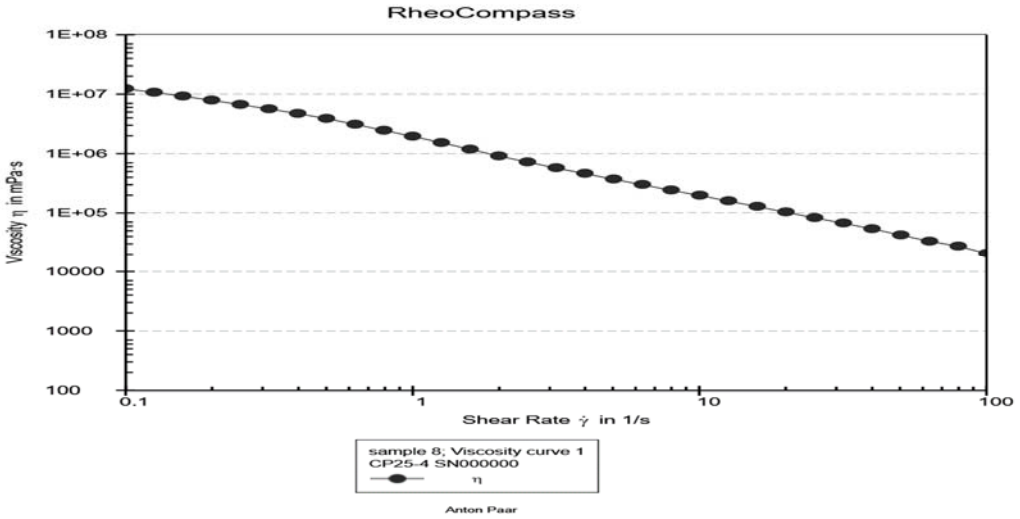

Graph.3.23. Viscosity vs Shear Strain [Sample 8]

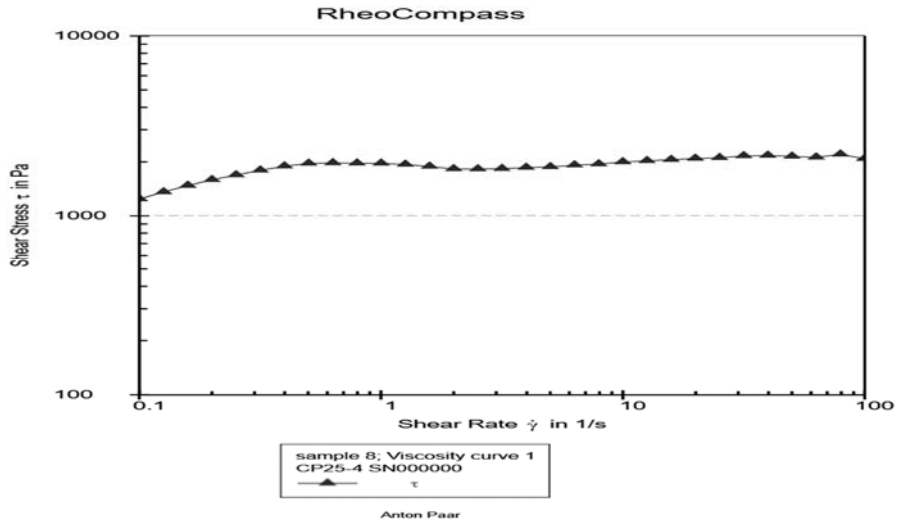

Graph.3.24. Shear Stress vs Shear Strain [sample8]

3.6.10 Experimental Investigation of the Viscosity of the Silicone oil-based Viscoelastic Magnetic Abrasive medium 30 days old:

An experimental investigation has been made to find the Viscosity of Silicone oil-based Viscoelastic Magnetic Abrasive medium which is 30 days old and the results have been as mentioned below. Graph.3.25 and Graph.3.26 show the relation between Viscosity Versus Shear strain and Shear stress versus Shear Strain.

Table.3.13. Experimental results for Viscosity of 30 days old Silicone-based VEMAF medium: Viscosity 5688 Pa-s

Point No.	Shear Rate	Shear Stress	Viscosity	Temperature	Torque	Status
	[1/s]	[Pa]	[mPa·s]	[°C]	[mN·m]	
1	0.1	2674.1	2.67E+07	27.46	11.002	Dy_auto
2	0.126	4374.6	3.47E+07	27.46	17.998	Dy_auto
3	0.158	5116.9	3.23E+07	27.45	21.052	Dy_auto
4	0.2	5216.3	2.61E+07	27.45	21.461	Dy_auto
5	0.251	5146.4	2.05E+07	27.45	21.173	Dy_auto
6	0.316	5095.7	1.61E+07	27.45	20.965	Dy_auto
7	0.398	5078.8	1.28E+07	27.45	20.895	Dy_auto
8	0.501	5135.4	1.02E+07	27.44	21.128	Dy_auto
9	0.631	5261.3	8.34E+06	27.45	21.646	Dy_auto
10	0.794	5446	6.86E+06	27.44	22.406	Dy_auto
11	***1***	***5688***	***5.69E+06***	***27.44***	***23.402***	***Dy_auto***
12	1.26	5992.2	4.76E+06	27.44	24.653	Dy_auto
13	1.58	6373.6	4.02E+06	27.44	26.223	Dy_auto
14	2	6838.3	3.43E+06	27.44	28.134	Dy_auto
15	2.51	7175.9	2.86E+06	27.44	29.523	Dy_auto
16	3.16	7340.6	2.32E+06	27.44	30.201	Dy_auto
17	3.98	7286.5	1.83E+06	27.44	29.978	Dy_auto
18	5.01	6817.6	1.36E+06	27.44	28.049	Dy_auto
19	6.31	5755.3	9.12E+05	27.44	23.679	Dy_auto
20	7.94	4214	5.31E+05	27.44	17.337	Dy_auto
21	10	3230.4	3.23E+05	27.44	13.29	Dy_auto
22	12.6	1272	1.01E+05	27.44	5.2335	Dy_auto
23	15.9	474.03	29907	27.44	1.9503	Dy_auto
24	20	67.23	3369.7	27.44	0.2766	Dy_auto
25	25.1	32.71	1302.4	27.44	0.13458	Dy_auto
26	31.6	20.78	657.15	27.44	0.085495	Dy_auto
27	39.8	19.303	484.89	27.44	0.079419	Dy_auto
28	50.1	14.296	285.26	27.44	0.058818	Dy_auto
29	63.1	13.218	209.5	27.44	0.054382	Dy_auto
30	79.4	6.7229	84.636	27.43	0.027659	Dy_auto

31	100	6.2149	62.15	27.43	0.02557	Dy_auto
32	126	5.6752	45.08	27.43	0.023349	Dy_auto
33	158	5.7526	36.297	27.43	0.023668	Dy_auto
34	200	5.8598	29.369	27.43	0.024109	Dy_auto
35	251	5.952	23.695	27.43	0.024488	Dy_auto
36	316	6.0375	19.092	27.43	0.02484	Dy_auto
37	398	6.2116	15.603	27.43	0.025556	Dy_auto
38	501	7.0105	13.988	27.42	0.028843	Dy_auto
39	631	7.8486	12.439	27.42	0.032291	Dy_auto
40	794	8.1758	10.293	27.42	0.033637	Dy_auto
41	1.00E+03	8.304	8.304	27.42	0.034165	Dy_auto

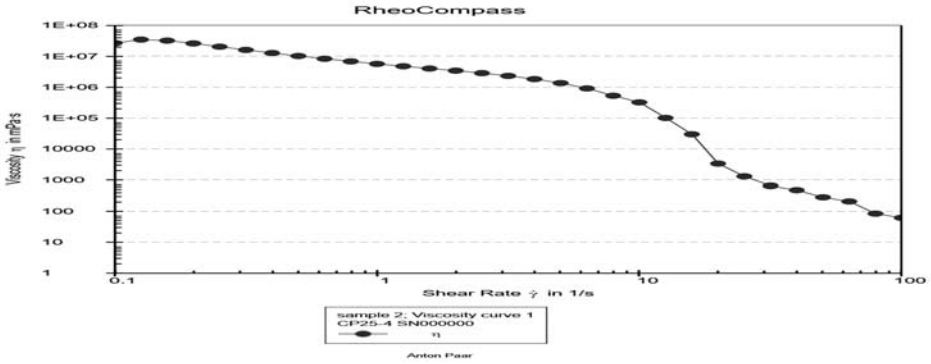

Graph. 3.25. Viscosity vs Shear Strain 30 days old VEMAF medium

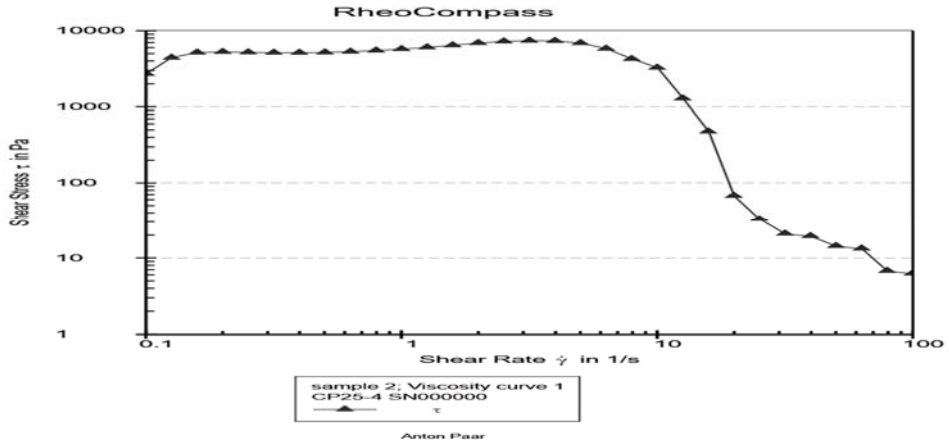

Graph.3.26. Shear Stress vs Shear Strain 30 days old VEMAF medium

SUMMARY

1. A total of six Viscoelastic Magnetic abrasive media have been prepared and their Viscosity has been tested.
2. The viscosity of the AP3 Grease-based Viscoelastic Magnetic Abrasive Media has shown an increase in the Viscosity with the increase in the proportion of CIP-Abrasive powder. However, with the increased temperatures during the finishing operations, there is a higher chance of reduction in the Viscosity.
3. White transformer oil could not be used due to its instability during the initial period of loading.
4. Silicone oil based Viscoelastic Magnetic Abrasive Medium is preferred for internal finishing as the primary requirement there is flowability.
5. The viscosity of the Silicone oil has drastically increased from 954.06 mPa-s to 5688 mPa-s in 30 days from the date of preparation and at this higher viscosity, this medium can’t be used for finishing operation.

CHAPTER 4. OPTIMISATION TECHNIQUES

In this chapter, a brief discussion will be made about the Design of Experiments. The design of experiments guides the researcher to plan his/her experimental sequence logically. In this chapter, a brief discussion is made about Taguchi's design of experiments. Subsequently, a discussion is made about some of the Optimisation Techniques under practice. The importance of Analysis of Variance has been discussed.

4.1 Introduction:

Design of Experiments abbreviated as DOE is a tool that guides the researcher to plan his experiments logically based on Statistical Techniques, Sir. R.A Fischer is the pioneer of Design of Experiments, Who used his technique for getting optimum yield for the Agriculture land. Based on Fischer's model, there exists a relation amongst the experiments actually to be performed (K), Number of levels considered for each factor (M) under consideration, and Total no of factors (p), for full factorial design, which is given by

$K = M^p$,

For example in the present research work, no levels considered are 3, Total no of factors is 6. Based on the above relation, the no of experiments actually to be performed is 3^6, which is 729. As the number of levels and factors increases, the total no of experiments would increase substantially. This in turn increases the overall cost of the product, as a final decision could be taken only after getting the results from all such experiments.

Genichi Taguchi, an electrical Engineer, and researcher from Japan have suggested a very Robust Design of the experimental model, which is believed to the best tool for Optimization. The other optimization techniques considered by most of the researchers for optimization include Generic Algorithms and Artificial Neural network and Response Surface Methodology (RSM)

4.2 TAGUCHI METHOD: The main aim of the Taguchi method is the reduction in variation of the procedures by adopting appropriate Design of Experiments and hence producing the desired product, with increased quality at the economic price to the manufacturer. Taguchi developed this method while working on the variation of the data. For any statistical data, Mean and Variance are the most important factors, which affect the process and these factors decide

how much efficient and adaptable, the process is. So, the Design of Experiments developed by Taguchi targets the mean and the variance of the process and their effect on process parameters. Orthogonal arrays are used to organize the parameters that affect the process and the levels at which they are expected to be varied. One of the noteworthy features of the Taguchi method is that it takes pairs of a different combination of factors for testing that gives the optimal value of factors with appropriate magnitude at least amount of time. The Taguchi method is generally used when the variables are three to fifty, with interactions between these variables and out of which very few numbers of variables have a significant contribution.

4.2.1Taguchi Method Designs of Experiments

The Sequence of steps in the Taguchi Method are as mentioned below:

1. The first step is the selection of the process objective, which is the requisite target for the measurement of the performance. In the present research work attainment of least surface roughness is the objective.

2. Second step is determining the Parameters and Number of levels of these parameters, which would considerably affect the Process. Different values may be assigned to a particular parameter that determines each level of a chosen parameter. Six parameters having three levels have been considered in the present work.

3. Third step is the creation of Orthogonal arrays for parameter design, which must include the details of a particular experiment containing number as well as the conditions. The number of parameters and levels of variation of these parameters is an important factor while selecting Orthogonal Arrays.

4. Fourth step is experimenting indicated on the Orthogonal Array and measuring the performance. In the present work $L_{27,}$ the Orthogonal array system has been adopted.

5. Data analysis is done to get the requisite results.

Most of the Optimisation work done by different researchers in Nano finishing is based on Taguchi Method only.

4.3 ANOVA

Analysis of Variance abbreviated as ANOVA is an established Statistical tool used for data analysis and data processing application. Almost all the emerging and modern statistical techniques are based on the ANOVA results, which is further associated with Hypothesis

testing. Before going for further discussion about the ANOVA technique, we need to know that what is variance. Variance term was first coined by Ronald fisher in 1918. In very simple words the variance is defined as the spread of the center quantity or in the statistical term, it is defined as the squared deviation or the square of the distance of the defined variable (Random Variable) from the mean of the statistical data. So in simple words, it measures the spread of a set of numbers compared to their average values.

In Mathematical term the variance is represented as :

$$\textbf{Variance}(s^2) = \frac{\Sigma(x-\overline{x})^2}{N-1}$$

that is the variance is defined as the ratio between the algebraic sum of the squared value of the difference between present value and the mean of the values under consideration and the N-1, where N stands for the number of values or observations under consideration. During research work, a bulk amount of data has to be analyzed before making any interpretation about a particular process. The bulk data that is to be studied or analyzed is called Population. ANOVA is used for comparing the magnitude of variation among the groups with the magnitude of variation within the groups. ANOVA is used in Hypothesis testing. In the hypothesis testing, we compare the center tendency of two populations. if the two values are equal we say that the hypothesis is not rejected otherwise the hypothesis is rejected. So Hypothesis testing is the precursor of the ANOVA. Also, the variance calculation is an essential component for the descriptive statistic, goodness of fit, Monte Carlo sampling, and the Analysis of variance. Further, there are two types of ANOVA techniques widely in use. They are One Way ANOVA and Two-way ANOVA.

The most important feature of One-way ANOVA is that only one Independent variable is considered for analysis, whereas for Two-way ANOVA two independent variables are considered. The common feature for these two types is that means of three or more groups are being considered for analysis one-way ANOVA in which the mean of the two populations is compared using the F- test. similarly, the t-test is also used in the analysis of the variance. F test is often used for the model whose population is fitted according to the least square method or in other words, we could say that it is a test in which the test statistic under null hypothesis has F distribution. George W Snedecor was the person who coined the term of F test. some of the application where this test is used involves the hypotheses where normal distribution is used for population and have an equal standard deviation in that

situation F test is used. in the second situation where the population is fitted with the regression model, the F test is an important tool for the ANOVA

When handling the bulk data during research work, manual calculation of the variation and Standard deviation consumes a lot of time. So, for getting accurate results with very little time, researchers are depending on the latest software. One such software adopted in the present research work is Minitab. The main objective is to calculate the central tendencies from the population under consideration. New methods have been developed for calculating the analysis of variance. the theorem states that the average of samples of a random variable with finite mean and variance is a random variable and further if the number of samples increases, its distribution would converge to the normal distribution.

4.4 MINITAB 17 SOFTWARE: Minitab software is the lifeline in the field of statistical analysis, where large statistical computation and analysis have to be done accurately with a lesser amount of time. The software finds its key role in performing Taguchi analysis. The sequence of Operational steps while using the Taguchi technique are as mentioned below:

The first step in the analysis of Taguchi is framing the requisite table for the operation which can be done by selecting the ***stat*** from the title bar and then selecting Taguchi from the drop-down table. Minitab Software has a wide range of operations that can be selected like the computation of basic statistics, techniques like power and sample sizing, Equivalence test and non-parametric computation may be done.

The Minitab software ***stat*** drop-down menu provides the options like table creation, time series analysis, Control charts both for the parameters and the attributes. Moreover, the software has a good range of capabilities for solving the data related to the ANOVA, Regression, and reliability.

The next part of the mini tab software is to present the calculation result which can be effectively prevented by the graph. the software provides a wide variety of graphs which are the Scatter plot, Matrix Plot, Bubble Plot, and marginal plot. The mini tab software has a wide range of inbuilt tools like Histogram, Dot plot, Stem and leaf, Profitability Plot. Apart from that various tools which are statistically linked like the Empirical CFD Plot and the probability distribution Plot are also available for use. Graphs like Box plot, interval plot, Individual value plots, and line plots are important tools for the presentation of the comparison of the statistical data. The software has a wide range of other creative tools such as Bar charts, Pie charts, etc. Minitab also provides an interactive tool such as the Time

series plot, Area graph where the results of the computation are presented in form of the graph. The other tools which have a wide application are the Counter Plot, 3-D Scatter Plot, and the 3-D Surface Plot. The software provides easy access to distributions, correlations, outliers, and missing values. Apart from that, the other important tests include t-test, proportions test, normality test, chi-square test, and non-parametric tests. The software can move the files into various formats like TIF, EMF, GIF, BMP, PNG, and JPEG. The unique features of the software are that it provides the linkage between the other software like Excel or Microsoft Access. one-click sort, stack, transpose, and merging of worksheets are easily available for the computation of work. The software is equipped with Time Series and Forecasting, Gage studies, Arbitrary censoring (left, right, or interval censoring), and Warranty Analysis and Repairable Systems Analysis. so with the help of Minitab ANOVA and the Taguchi L27, an Orthogonal array may be selected and used for the computation of the value of the optimal parameter for the computation of the results of the experiment. most of the features are inbuilt in the system and the software gets better calculation and computation techniques with every upgrade. the other best part of the software is that it is compatible with both the 32 and the 64-bit system and links easily with the MS office of any version.

4.5 RSM TECHNIQUES

Response surface Methodology abbreviated as RSM technique is widely used in the research work of Mechanical Engineering for optimization of the statistical results, where the response of interest is affected by various variables and thus the response optimization is the main objective of this method. The parameters, that are affected by the process or the parameters that are targeted are called the Dependent Variables. The responses are called the Dependent Parameters. The sequence of steps involved in the RSM technique is as mentioned below.

1. The first step is identifying the problem that is to be optimized.
2. The second step is the determination of the dependent variables, which are called the Response Parameters.
3. The third step is the determination of the independent extraction variables which are called the factors.
4. The Fourth is deciding on the factor level which may be called the screening of the experiment.
5. The Fifth step in the surface response methodology comprises the selection of proper design in which a design is selected from BBD, CCD, and CCRD, etc.

6. The Sixth step of the surface response methodology is the running experiment.
7. The Seventh step successful running of the experiment next step is the Evaluation of the model. (In this step the ANOVA test to check the fitness of the model is done).
8. The eighth step in the surface response methodology is the optimization of the model.
9. The ninth step is the validation of the model. There are different ways to validate the model and some of them are the Chi-square test, Student t-test, and the experimental error rates. So RSM emerged as an efficient tool when two energy systems are taken into consideration.

4.6. ARTIFICIAL NEURAL NETWORKS

ANN stands for Artificial Neural Network, which is abbreviated as ANN is the most advanced method of Optimisation technique, mostly used by the electronics engineers and computer science engineers. ANN is a mathematical tool that functions in the same way as the human brain functions while processing the data. The human brain is having the capability to adapt to the environment, create new solutions, self-learning, etc. More or less present-day ANN is capable of performing all these things like the Human brain. Beginning of the development of ANN started way back in 1943, is an offspring of Neural network started its journey in 1943 when McCulloh and Pitts developed a model based on their understanding of the brain function.

ANN a relation between the input and the output variable is achieved and a structure is developed through which we can observe the relation between the functions and can get the relevant output. In this technique, the computation is done similarly as done in the Neural Network (NN).

The definition of the neural network in simple words is "the ability to learn, to memorize and to generalize, prompted research in algorithmic modeling of biological neural systems. There is the general classification of the Artificial neural network is Single-layer Artificial Neural Network, the example of this type of Neural Network is called the Hopfield Neural Network. The next type of Neural Network is the Multilayer Feed Neural Network. This type of ANN is used for the backpropagation application also. Multilayer Neural Network is also used in the functional link as well as the Neural Network used in the product unit network is also multilayer neural network system. The next type of Neural Network system is the Temporal Neural Network. An example of this type of Neural Network System is the Elman and Jordan simple recurrent networks. The other example of this type of neuron system

is the Time Delay Neural Network. The next category in this issue is the self-organizing Neuron Network. An example of such a network is the Kohonen, which has self-organizing features.

Different architectures allow for the generation of functions of different complexity and power. There are three major types of architecture in the artificial neuron network which are firstly the feed-forward network. The second type of network is the feedback network and the third one is the lateral network. ANN for the present work is shown in Figure 4.1 below.

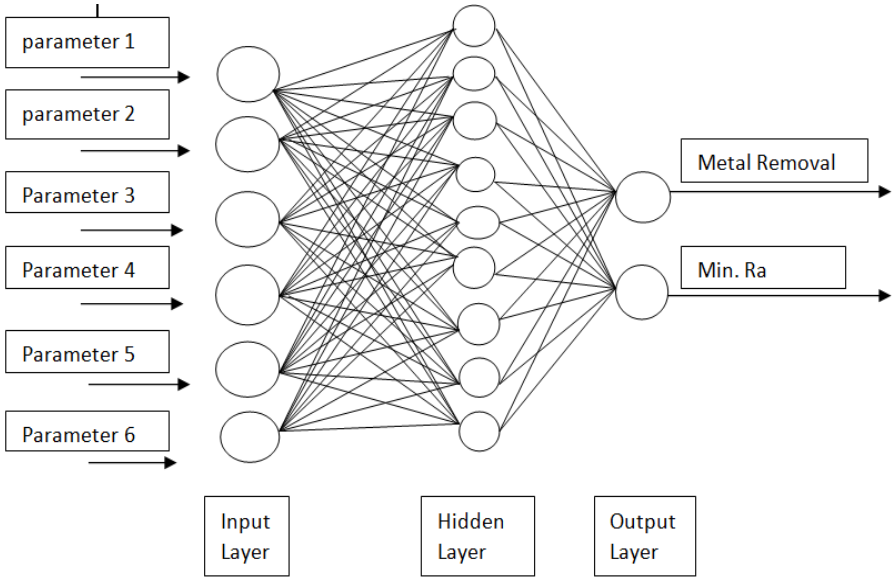

Fig.4.1 Ray diagram of Artificial Neural Network.

Some of the applications of ANN are mentioned below.

1. Pattern matching in which an adequate pattern is matched or made relating the input variables or parameters.
2. Pattern completion is used to complete the missing input variable in the pattern or the input parameters.
3. Artificial Neural Network is used for optimization, in which ANN is used to compute the most appropriate value from the given formulated problem.
4. ANN is used to control the process by taking adequate action in the input parameters based on optimal results.
5. ANN is used for time series modeling of the functional approximation. This functional approximation aims to achieve the relationship between the input and the output variables by constructing an appropriate structure between the two and linking the

variables between various steps. The last step in the computation is the step relating to the data mining, which aims for resolving the hidden step in the former process and to compute the hidden layer in the structure or the relation between the input and the output relationship between the parameters.

6. Artificial Neural Networks are used as the universal approximation to compute the relationship between the input and the output parameters and thus the Artificial Neural Network uses approximation and the non-linear function to compute the parameters and the structure relating the input and the output parameters.

CHAPTER 5. SIMULATION AND MODELING IN VEMAF PROCESS

In this chapter modeling and Simulation of Flux densities for internal surface finishing as well as external surface finishing has been done using ANSYS MAXWELL ANOSOFT 16 Student version. Simulation has been done for Permanent magnets, which are used to generate required flux density for the finishing of both Internal and External surfaces. Four types of Commercially available magnets each with a different shape have been considered for modeling flux densities for internal finishing. Modeling and Simulation of Flux densities of three different working gaps for Steel, aluminum, and Brass have been considered. Flow parameters have been found for internal finishing using ANSYS FLUENT 15.

5.1. Introduction to Modelling of Flux densities: Flux density is the most important parameter in all Magnetic Field Assisted finishing process. For maintaining the Carbonyl Iron particle (CIP) chain, sufficient Flux density is needed. The CIP chains formed would throw the abrasive particles towards the surface to be finished. Magnetic flux density(MFD) depends on the magnitude of current and Number of coils (7, 26, 33) in Electromagnets and for the Permanent magnets, it depends on the grade, Volume, and shape. Earlier researchers determined the Flux density of the magnets with the help of Finite Element Analysis (40), which is time-consuming, and also the verification of the accuracy of such calculation is a difficult task. In the present research work, ANSYS MAXWELL ANOSOFT 16 is used to find the Flux density distribution of the commercially available magnets.

5.2. Important features of ANSYS Maxwell Anosoft 16: ANSYS Maxwell is simulation software, which is used in the analysis of permanent magnets and electromagnets for their magnetic field intensity, distribution of the magnetic field pattern, and Energy distribution pattern. This software is used for designing Actuators, Electric motors, transformers, and other electrochemical and electromagnetic devices. The software also finds its application in the field of low-frequency electromagnetic field simulators. However, the Simulation could be done for Permanent Magnets made of Neodymium, Iron, and Boron (NdFeB) material of grade 35. Designated as N35. Other grades available for research work are N38, N42, N52, etc. 38, 40, 52 indicate Mega Gauss Oersteds (MGOe), which is the measure of the strength of the Magnet. The strength of the magnet increases from N35 to N52 in

ascending order. Magnetic Characteristics of the Commercially available Magnets are shown in Table 5.1 below.

Table 5.1. Magnetic Characteristics of Sintered NdFeB magnets

Magnetic Characteristics of Sintered NdFeB

Properties / Grade	Max Energy Product (BH)max KJ/m³(MGOe)	Remanence Br mT(KGs)	Coercive Force Hcb KA/m (KOe)	Intrinsic Coercive Force Hci KA/m(KOe)	Temp Coefficient αBr %/°C	Temp Coefficient βHci %/°C	Curie Temp Tc °C	Max Working Temp Tw °C
N35	263-287(33-36)	1170-1220(11.7-12.2)	≥868(≥10.9)	≥955(≥12)	-0.12	-0.6	310	≤80
N38	287-310(36-39)	1220-1250(12.2-12.5)	≥899(≥11.3)	≥955(≥12)	-0.12	-0.6	310	≤80
N40	302-326(38-41)	1250-1280(12.5-12.8)	≥907(≥11.4)	≥955(≥12)	-0.12	-0.6	310	≤80
N42	318-342(40-43)	1280-1320(12.8-13.2)	≥915(≥11.5)	≥955(≥12)	-0.12	-0.6	310	≤80
N45	342-366(43-46)	1320-1380(13.2-13.8)	≥923(≥11.6)	≥955(≥12)	-0.12	-0.6	310	≤80
N48	366-390(46-49)	1380-1420(13.8-14.2)	≥923(≥11,6)	≥876(≥11)	-0.12	-0.6	310	≤80
N50	382-406(48-51)	1400-1450(14.0-14.5)	≥796(≥10.0)	≥876(≥11)	-0.11	-0.85	320	≤60
N52	398-422(50-53)	1430-1480(14.3-14.8)	≥796(≥10,0)	≥876(≥11)	-0.11	-0.85	320	≤60

Courtesy: First 4 Magnets.

5.3. The methodology adopted for Simulation and Modeling: In the present Simulation and Modeling for the Magnetic Flux density, the first step is the preparation of the 3D model of the Workpiece and the Magnet respectively by using CREO 3.0 software. The second step involves the exportation of IGES files of these 3D models prepared in CREO 3.0 to ANOSOFT 16. The third step is the selection of other required input parameters from the ANOSOFT 16 for obtaining the desired results. Only N35 Permanent magnets have been considered for the simulation, due to the limitation of the software.

During the simulation with ANSYS MAXWELL, ANOSOFT, VERSION 16, the Shape of the mesh element has been assumed to be Hexagonal and the size of each element is 3 $X10^3$. After several trials, it is concluded that the result obtained is independent of the mesh size.

5.4. Modelling and Simulation of Flux densities of Permanent Magnets: In the present modeling and Simulation of Permanent magnets of grade N35, only Fan shape, Arc shape, Ring

shape, and Block shape are considered for simulation work. The workpiece material is Aluminium. The volume of the magnets is almost the same for all these Magnets. A sequence of steps involved in Simulation is discussed in section 5.3 above. The material of the specimen used for the initial simulation work of Internal finishing is Aluminium. Initial simulation is used for finding the most suitable geometry of the magnets. The Centre angle of the Arc Magnet is shown in Fig.5.1. The working gap is the distance between the Magnet surface and the workpiece surface.

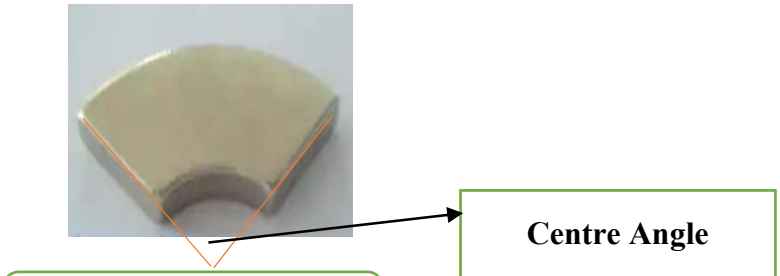

Fig.5.1.Arc Magnet

5.4.1 Modelling of a Single Fan-shaped N35 magnet with 90º Centre angle: A single Fan-shaped Magnets with a center angle of 90º having an inner diameter of the magnetic pole as 32 mm and the outer diameter of the magnetic pole as 126 mm. The workpiece material is Aluminium with an inner diameter of 25 mm and outer diameter of 30 mm and height of 30 mm. Fig.5.2 shows the Flux density distribution on the workpiece. The maximum value of Flux density is 0.5994T. The red area in the simulation shows the area of the maximum flux density. The working gap of 1 mm is maintained for this simulation.

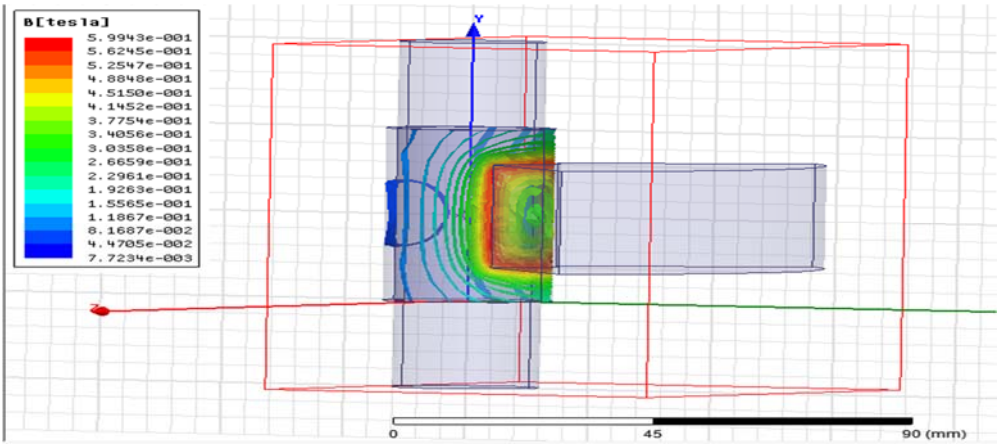

Fig. 5.2 A Single Fan-shaped Magnets with 90º Centre Angle

5.4.2 Modelling of Two Fan-shaped N35 magnets with 90° Centre angle and 90° angle:

Two magnets are taken with a center angle of 90° and an angle between the central lines of the magnets as 90°. The inner diameter of the magnetic pole is 32 mm and the outer diameter of the magnetic pole is 126 mm. The workpiece is Aluminium with an inner diameter of 25 mm and an outer diameter of 30 mm, with a height of 30 mm. A working gap of 1mm is maintained for this simulation. The maximum value of flux density is 0.67658 T. The red area in the simulation shows the area of the maximum flux density as shown in Fig. 5.3 below.

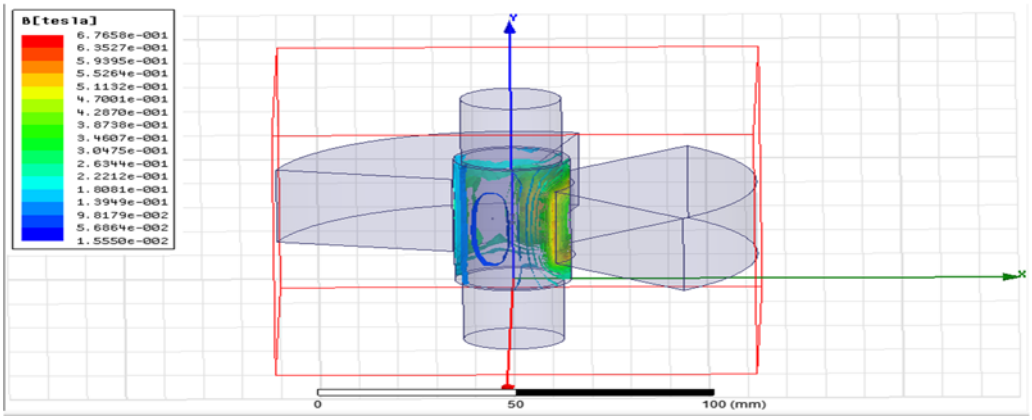

Fig. 5. 3 Fan-shaped Magnets with 90° Centre Angle and 90° angular pitch

5.4.3 Modelling of Two Fan-shaped magnets with 90° Centre angle and 180° angle: Two Fan-shaped magnets, with an inner diameter of the magnetic pole as 32 mm, the outer diameter of the magnetic pole as 126 mm, and the thickness of the pole as 30 mm are used for Modelling. The material of the specimen Aluminium with an inner diameter of 25 mm and an outer diameter of 30 mm and has a height of 30 mm. Fan magnets are kept at 180° and a working gap of 1 mm is maintained. The simulated results are shown in Figure 5.4, the maximum value of Flux density is 0.6205T, shown in red color.

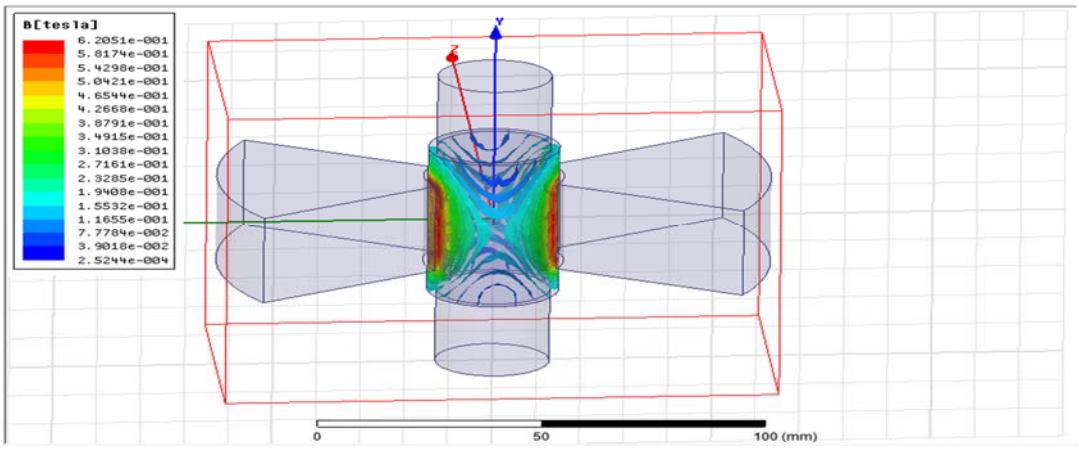

Fig.5.4.Two Fan-shaped magnets with 90° with 180° angle

5.4.4 Modelling of Two Fan-shaped magnets with 90° Centre angle and 120° angle:

Two Fan-shaped magnets, with the inner diameter of each pole as 32 mm, an outer diameter of the magnetic pole as 126 mm, and the thickness of the pole as 30 mm are used for Modelling. The material of the specimen Aluminium with an inner diameter of 25 mm and an outer diameter of 30 mm and has a height of 30 mm. Fan magnets are kept at 120°. The angle between the central axis of the magnets is also known as the Pole angle. The simulated results are shown in Figure 5.5, the maximum value of Flux density is 0.67658T, shown in red color.

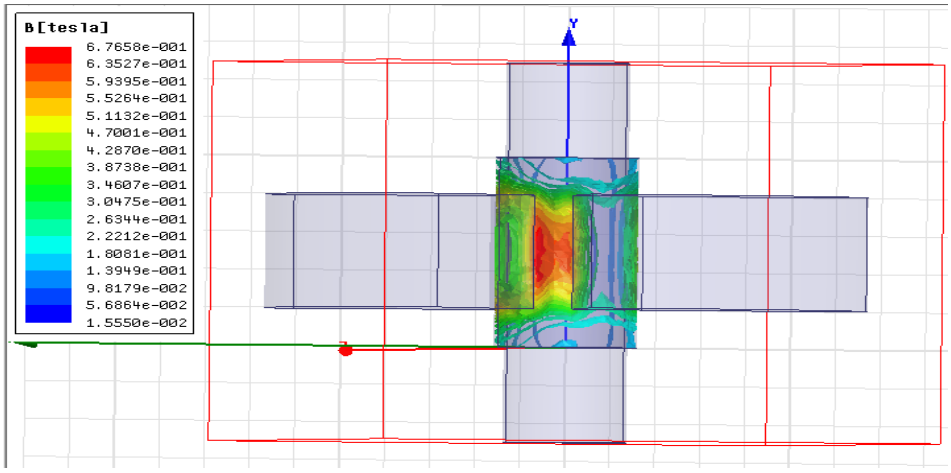

Figure 5.5 Two Fan 90° Centre angle with 120° pole angle

5.4.5 Modelling of Three Fan-shaped magnets with 90° Centre angle and 120° angle:

Three Fan-shaped magnets, with the inner diameter of each magnetic pole as 32 mm, an outer diameter of each magnetic pole as 126 mm, and the thickness of the pole as 30 mm and center angle 90° are used for Modelling. The aluminum specimen has an inner diameter of 25 mm and an outer diameter of 30 mm and has a height of 30 mm. Fan magnets are kept at 120° and a working gap of 1 mm is considered. The simulated results are shown in Figure 5.6, the maximum value of Flux density is 0.6134 T.

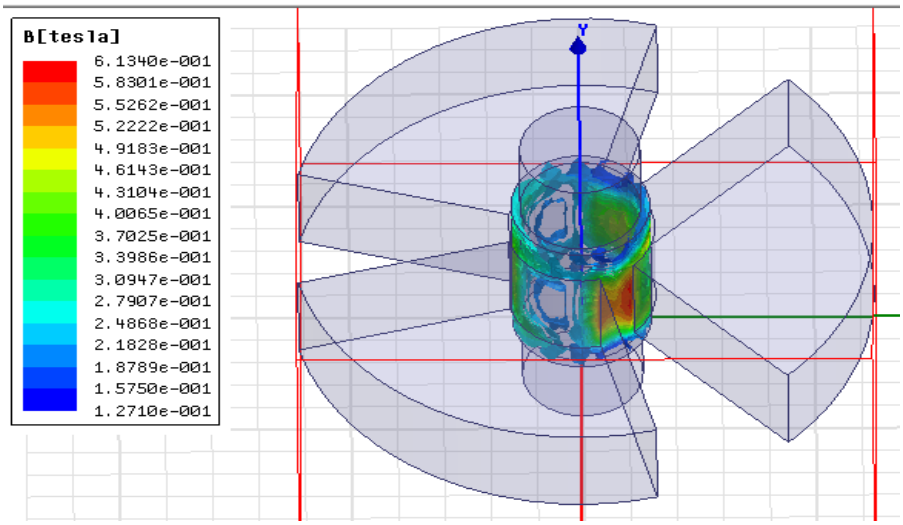

Fig. 5.6 Three Magnets with 90° Centre angle with 120° pole angle

5.4.6 Modelling of Single Fan-shaped magnet with 60° Centre angle:

The simulation is performed using a single fan-shaped magnet with a center angle of 60° having an inner diameter of a magnetic pole of 32 mm and the outer diameter of the magnetic pole 126 mm and a height of 30 mm. Material of the specimen Aluminium with an inner diameter of 25 mm and outer diameter 30 mm and has a height of 30 mm. The maximum value of the magnetic field came out to be 0.4852 T for a working gap of 1 mm. The red area in the simulation shows the area of the maximum magnetic Flux density. Flux distribution is shown in Fig 5.7 below.

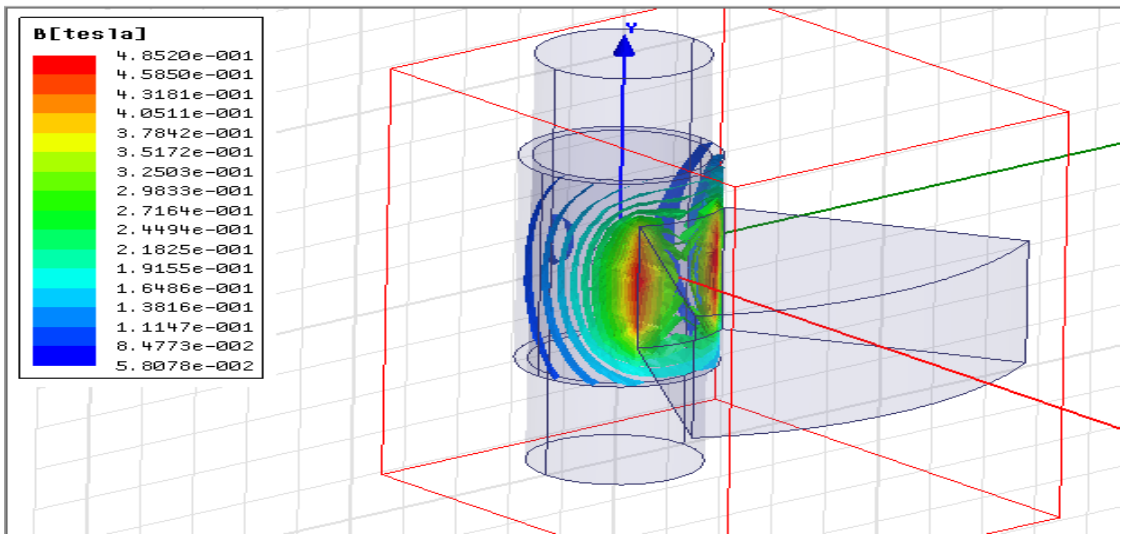

Fig. 5.7. Single Magnet with 60° Centre angle

5.4.7 Modelling of Two Fan-shaped magnets with 60º Centre angle and 60º Angle. : Two Fan-shaped magnets having a center angle of 60º, with the inner diameter of the magnetic pole as 32 mm, the outer diameter of the magnetic pole as 126 mm, and the thickness of the pole as 30 mm are used for Modelling. The material of the specimen Aluminium with an inner diameter of 25 mm and the outer diameter of 30 mm and has a height of 30 mm. Fan magnets are kept at 60 degrees and the simulated results are shown in Figure 5.8, the maximum value of magnetic Flux density is 0.5958T for a working gap of 1 mm.

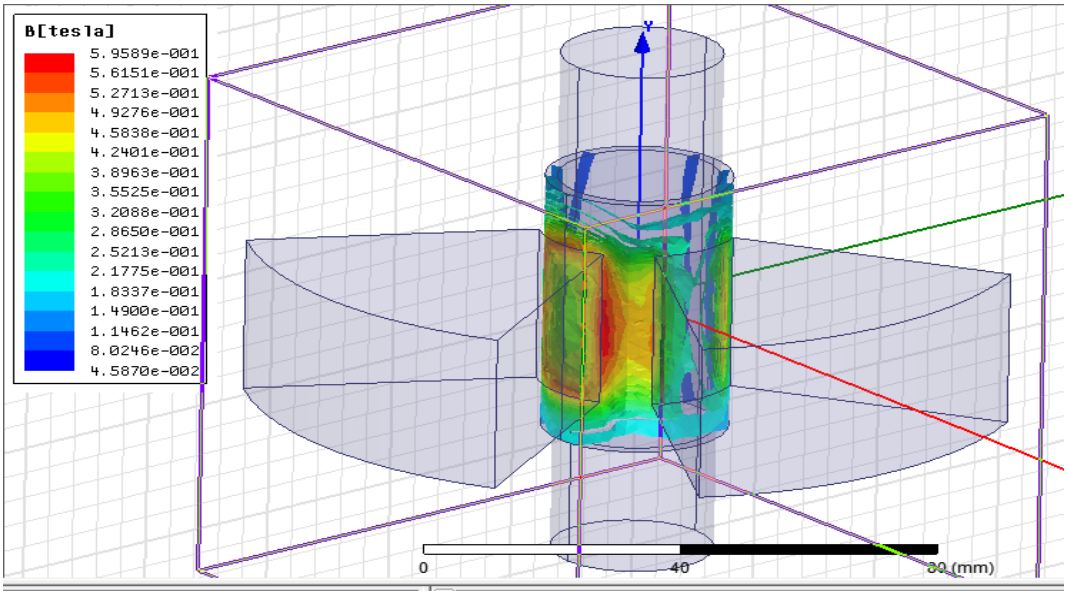

Fig.5. 8 Two Magnets with 60º Centre angle with 60º pole angle

5.4.8 Modelling of Two Fan-shaped magnets with 60º Centre angle and 90º angle: Two Fan-shaped magnets having center angle 60º, with an inner diameter of the magnetic pole as 32 mm, the outer diameter of the magnetic pole as 126 mm and the thickness of the pole as 30 mm are used for Modelling. The material of the specimen Aluminium with an inner diameter of 25 mm and outer diameter of 30 mm and has a height of 30 mm. Fan magnets are kept at 90 degrees and the simulated results are shown in Figure 5.9, the maximum value of Flux density is 0.5958T for a working gap of 1mm.

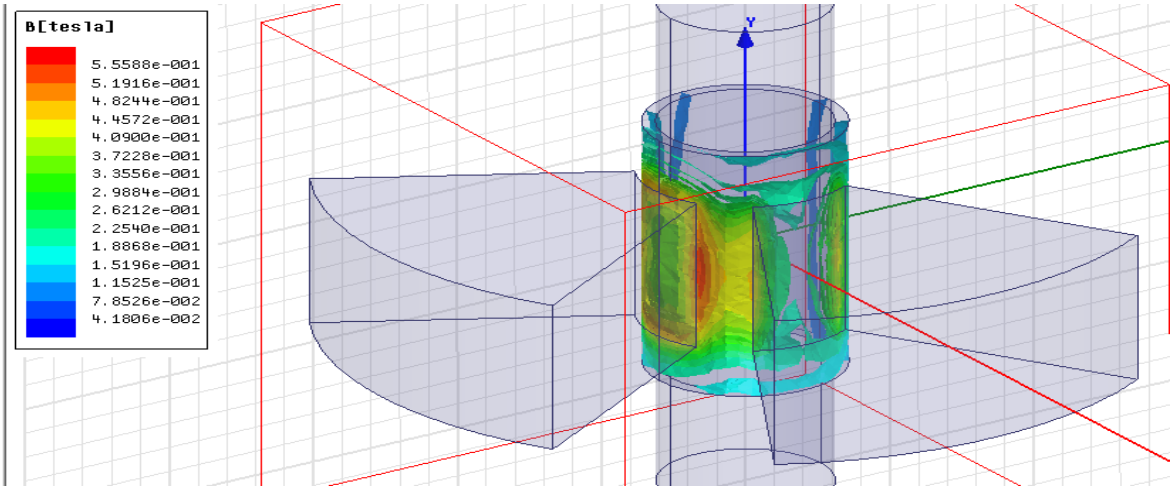

Fig. 5.9.Two Magnets with 60° Centre angle with 90° pole angle

5.4.9 Modelling of Three Fan-shaped magnets with 60° Centre angle and 60° angle:

Three Fan-shaped magnets having a center angle of 60°, with the inner diameter of the magnetic pole as 32 mm, the outer diameter of the magnetic pole as 126 mm, and the thickness of the pole as 30 mm are used for Modelling. The specimen is a hollow tube, made of Aluminium with an inner diameter of 25 mm and the outer diameter of 30 mm and has a height of 30 mm. Fan magnets are kept at 60° and the simulated results are shown in Figure 5.10, the maximum value of magnetic Flux density is 0.56 T for a working gap of 1 mm shown in red color.

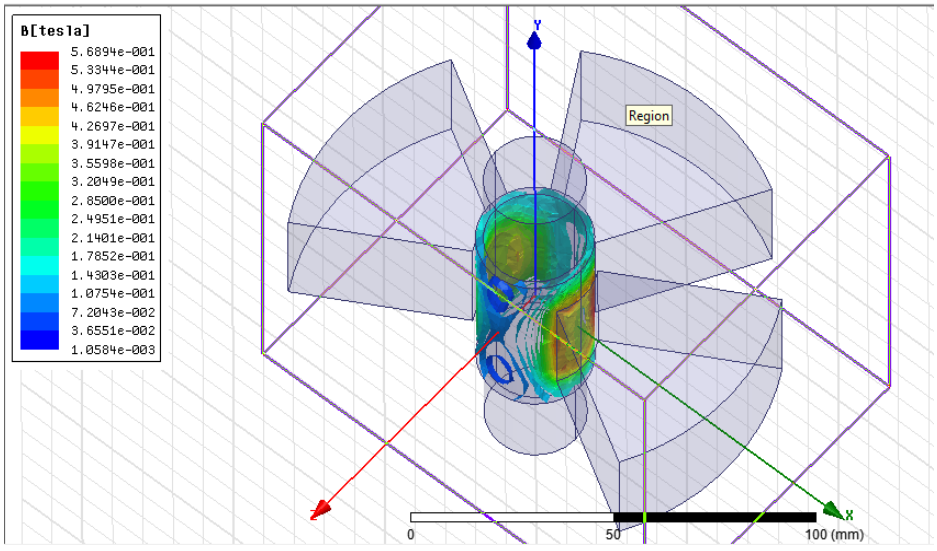

Figure 5.10 Three Magnets with 60° Centre angle with 60° Pole angle

5.4.10 Modelling of Four Fan-shaped magnets with 60° Centre angle and 90° Pole angle:

Four Fan-shaped magnets having a center angle of 60°, with the inner diameter of the magnetic pole as 32 mm, the outer diameter of the magnetic pole as 126 mm, and the thickness of the pole as 30 mm are used for Modelling. The specimen is a hollow Aluminium tube with an inner diameter of 25 mm, an outer diameter of 30 mm, and a height of 30 mm. Fan magnets are kept at 90° and the simulated results are shown in Figure 5.11, the maximum magnitude of Flux density is 0.5115 T for a working gap of 1 mm.

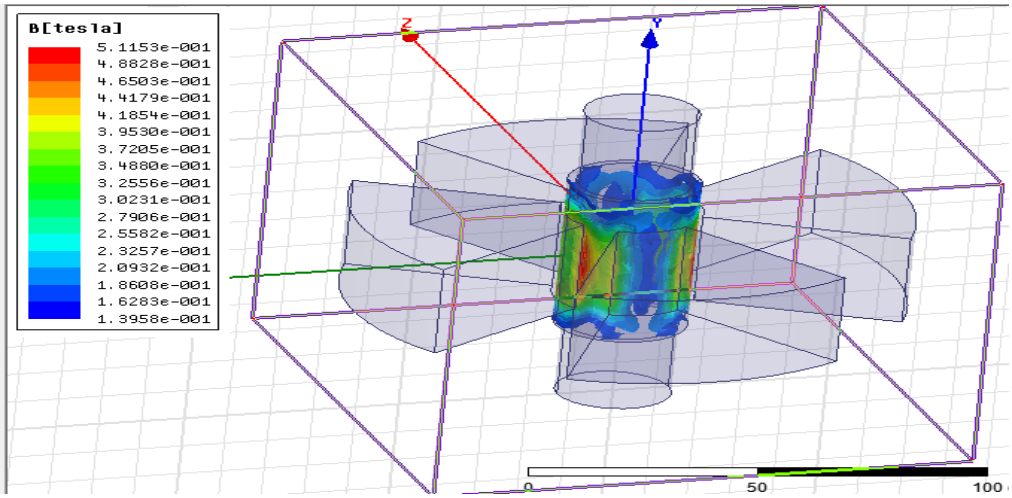

Figure 5.11 Four Magnets with 60° Centre angle with 90° Pole angle

5.4.11 Modelling of Arc shaped Magnets: The next Simulation is done on the Arc shaped magnet and hollow Mild Steel Specimen. Commercially available Arc Magnets procured for the research purpose have an outer radius of 15.8 mm, an inner radius of 12.8 mm, length of outer arc as 24.8 mm, and the height as 41 mm. In our simulation work with one, two, and four Arc magnets, it has been observed that two Arc magnets placed at 180° apart are producing the Maximum value of Magnetic Flux density on Mild steel hollow cylindrical tube with 25 mm outer radius, 20 mm inner radius and height of 40 mm is 0.7725T as shown in red color in Fig. 5.12. A working gap of 1 mm is maintained during the simulation.

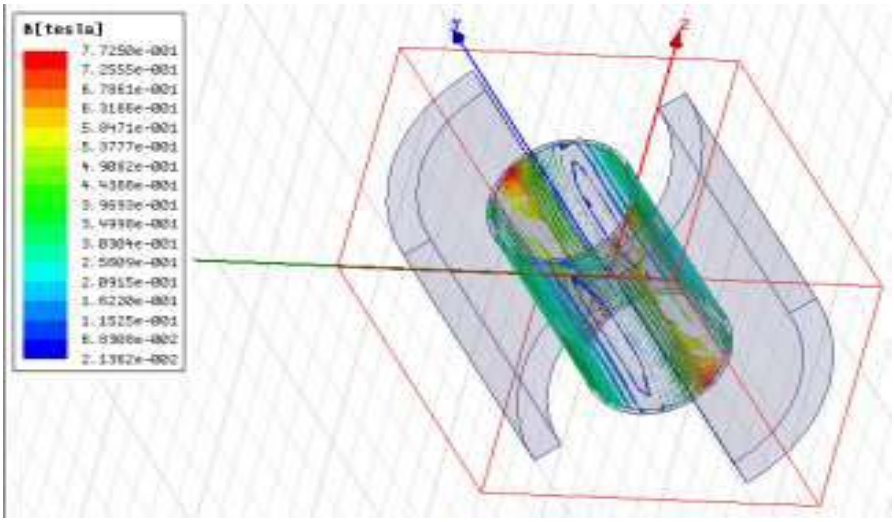

Fig. 5.12. Magnetic Field Intensity for arc Shaped Permanent Magnet

5.4.12 Modelling of Ring-shaped Magnets: Next simulation is done for the Ring magnet, Which is commercially available. Two ring magnets have been placed at an angle of 180^{o} on Opposite sides of the MS specimen. The dimensions of the specimen are height 30 mm, Inner diameter 20 mm, and outer diameter 25 mm. The dimensions of the magnet are 28 mm outer diameter, 10 mm inner diameter, and 12.5 mm thickness. A Working gap of 1 mm is maintained between the specimen and the workpiece outer surface. Maximum flux density is shown in red color in Fig.5.13 below.

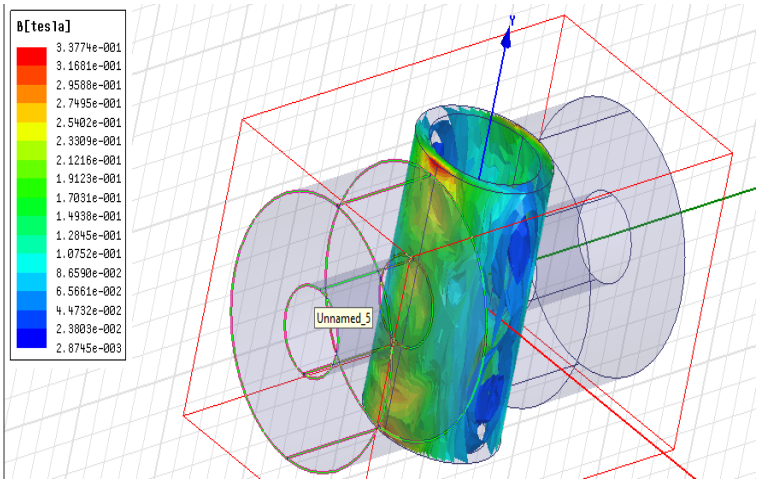

Figure 5.13 Magnetic Field Intensity for Ring-Shaped Permanent Magnet

5.4.13 Modelling of Block shaped Magnets: Next type of Magnet under consideration is the block type of Magnet having dimensions 12 mm X9 mmX6 mm. Steel specimen with an external radius of 15 mm, internal radius of 12.5 mm. the distance between the magnet surface

and the specimen is 1mm. The flux density distribution obtained has been shown in Figure.5.14. Maximum Flux density, which is uniform is 0.07889 T for a working gap of 1mm.

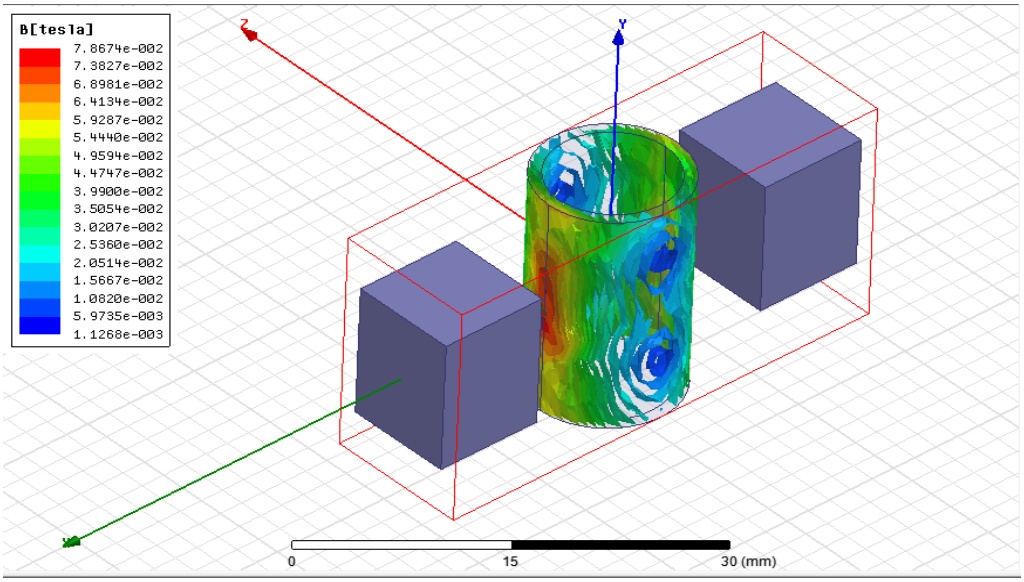

Figure 5.14 Magnetic Field Intensity for Block Shaped Permanent Magnet

Based on the Simulation work shown above, it may be concluded that the best geometry preferred for Magnetic field-assisted finishing of internal surfaces is Fan Magnet, which has given reasonably higher values for Aluminium specimen. The next preferred geometry is arc Magnet, which is simulated on Mild steel. The permeability of steel is 100 times the permeability of Aluminium. However due to the limitations of space and availability, in the present research work, Arc Magnets also known as the segmental magnets have been chosen for the Internal surface finishing of the Mild steel spline shaft. Further, the N42 Magnets are used in the present research work for finishing the internal surface of the Spline shaft and the simulation has been shown in the subsequent articles.

5.5. Simulation and Modelling for Flux densities of Internal spline shaft:

In the present research work titled "A study of Viscoelastic Magnetic abrasive finishing Process," one of the experimental works performed is Finishing of internal the surfaces of the spline shaft. For this, a special Permanent Magnet, used in Wind Turbine Power plants has been procured and used for producing Magnetic Flux densities. The NdFeB magnet procured is of the grade N42. Which has eight arc magnets of each segment having a Central angle of 45^{o}, an Outer radius of 18 mm, an inner radius of 14 mm, and a height of 20 mm is used for finishing the spline shaft that has an outer diameter of 20 mm. Since the Modelling for Anosoft 16 could be done for N35 magnets only and the Magnets used are N42 grade, which would give flux densities up to 1.1 times higher based on the inference made from Table 5.1, the Flux

densities obtained based on simulation could be accepted without any hesitation. Fig 5.15 shows the image of the Magnet used for the finishing of internal surfaces of the Spline shaft. Further, Simulation and Modelling has been done for finding out the flow parameters using ANSYS Fluent.

5. 15 Segmental Arc Magnet

5.5.1 solid work Modelling of Internal Spline shaft: In the present research work internal finishing of an Internal spline shaft made of Mild steel has taken place. The dimensions of the spline shaft have been shown in Fig 5.16 below.

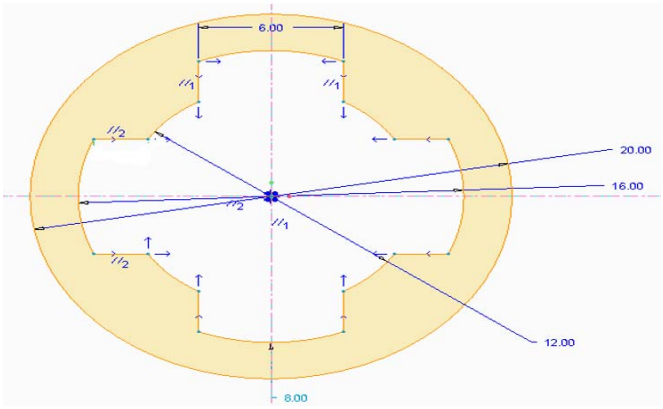

Fig.5.16. Internal Spline Shaft

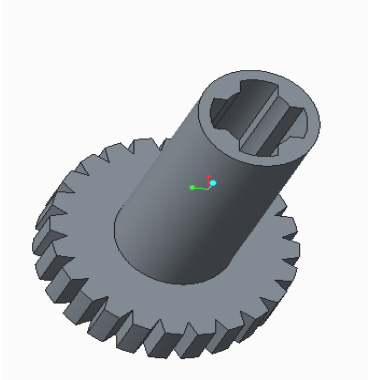

Fig.5.17 Solid Model of Spline shaft

Fig. 5.17 above, shows the Solid Model of the Spline shaft. This model is made on CREO 3.0 Software.

5.5.2 Modelling and Simulation of Flux densities for Internal Surface finishing of Splines:

Flux density simulation has been done using the Anosoft XVI student version. In total 3 levels have been considered. In level, I two segmental magnets having a 180^{o} angle, in level II four segmental magnets having 90^{o} angle and in level III all eight segmental magnets have been considered for simulation. The gap between the inner surface of the magnet and the outer surface of the spline shaft is 4mm.

5.5.2.1 Modelling of Flux densities for Two Arc Magnets at 180^{o} angle:

Magnetic Flux density distribution of Two arc magnets considered in present research work has been shown in Fig.5.18. The maximum flux density obtained is 1.035 T, which is on the surface of the Mild steel specimen exactly below the inner surface of the Magnet. The maximum flux distribution is shown in red color and spreads throughout the outer surface of the spline exactly facing the inner surface of the arc magnet.

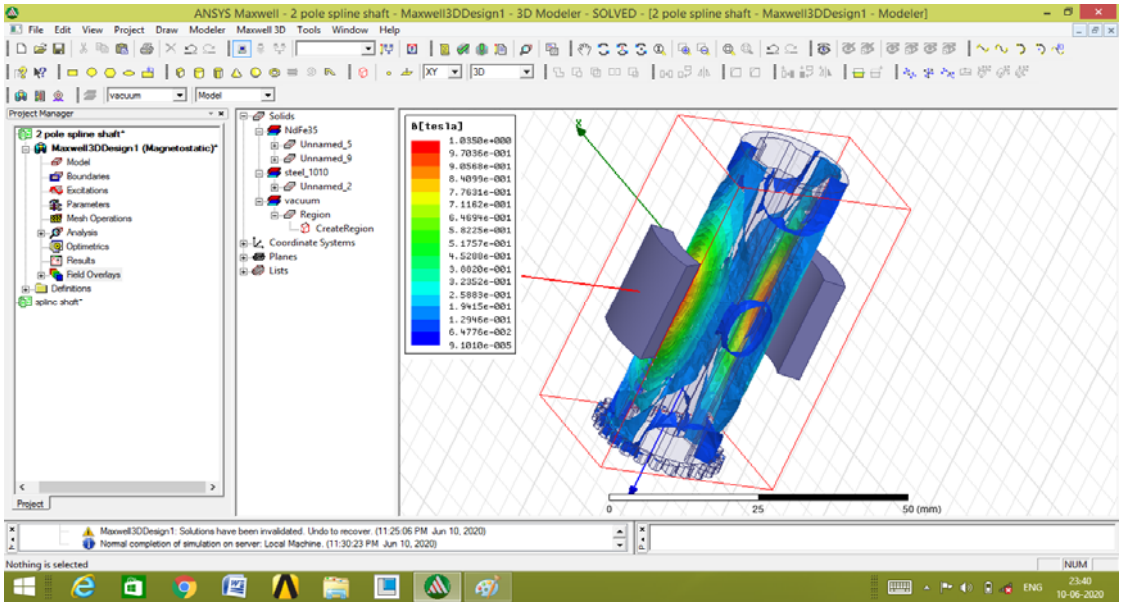

Fig. 5.18 Flux Distribution of ARC Magnet – Level I

5.5.2.2 Modelling of Flux densities for Four Arc Magnets at 90^{o} angle:

Magnetic Flux density distribution of Four arc magnets considered in the present research work has been shown in Fig.5.19. The maximum flux density obtained is 1. 518 T, which is on the surface of the Mild steel specimen exactly below the inner surface of the Magnets.

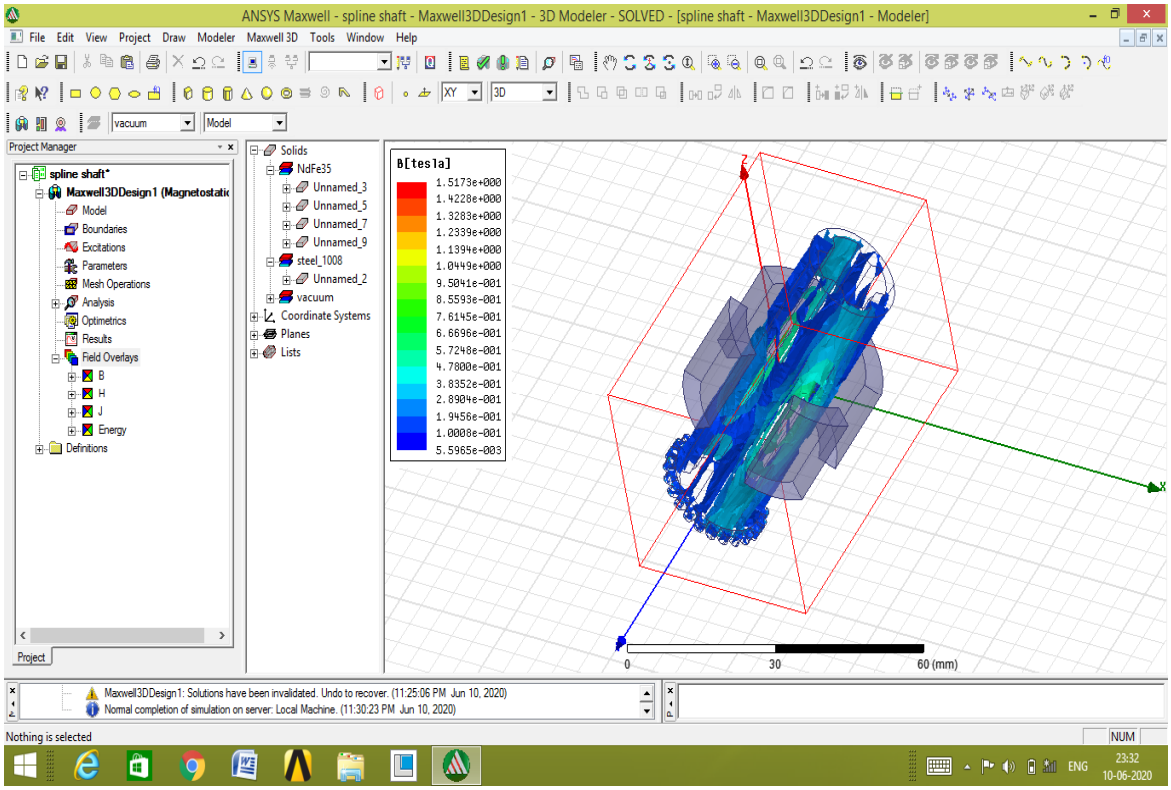

Fig. 5.19 Flux Distribution of ARC Magnet – Level II

5.5.2.3 Modelling of Flux densities for Eight Arc Magnets :

Fig. 5.20 below shows the eight arc Magnets surrounding the Spline shaft. The maximum flux density obtained is 1.599 T, however, most of the Flux distribution is having a flux density of the order of 1.20 T a mixed color representation of Green, yellow and brown colors.

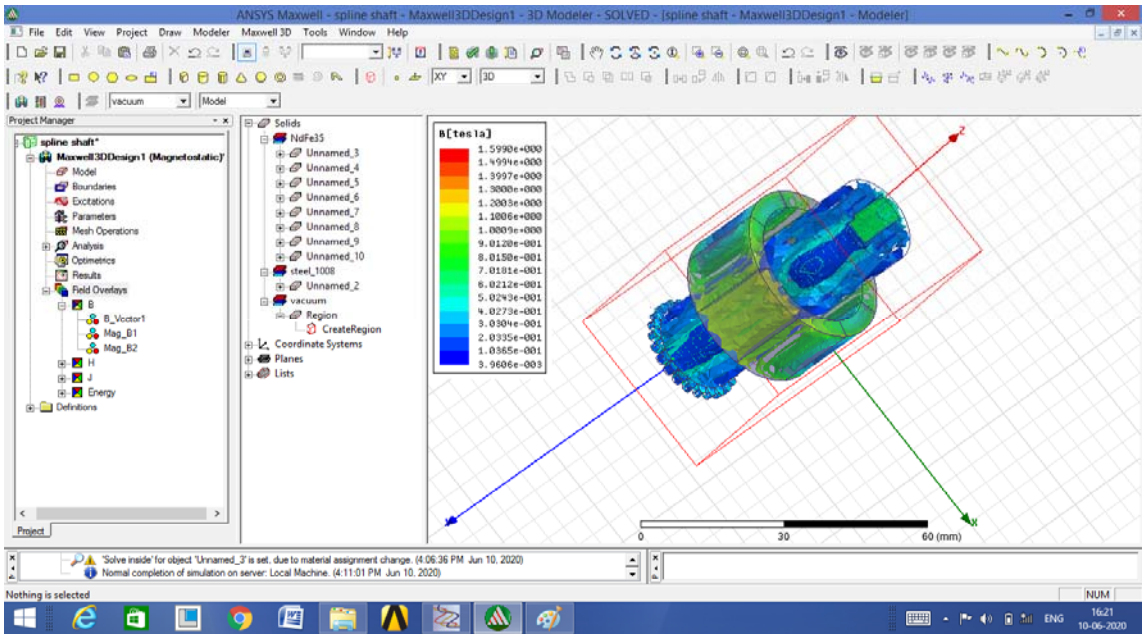

Fig. 5.20 Flux Distribution of ARC Magnet – Level III

Obtainable Magnetic flux densities for N42 magnets are 1.2 times the values of flux densities obtained for Level I, Level II, and Level III of the above three simulations.

5.6. Modelling and Simulation for Flux densities of External surface finishing:

In the present research work, external surfaces have been finished using Viscoelastic Magnetic Abrasive Medium. Aluminum (Al 6351 T6), Brass, and Steel specimen having similar dimensions have been finished by this process. The working gap is the gap between the face of the Magnet and the surface to be machined. In the present work for all three specimen Steel, Aluminium, and Brass working gaps of 2 mm, 1.5 mm and 1 mm has been maintained, accordingly, the Magnetic flux distribution varies. The front view and Top View of the surface to be finished have been shown in Fig.5.21 and Fig.5.22 respectively. Neodymium, Iron, and Boron based Permanent Magnet of the category N52 has been used for external finishing. The diameter of the N52 Magnet is 20 mm and the Height 20 mm. However, the limitation of the Anosoft 16 is that it can simulate N35 Grade Magnets only, which is having lesser strength than N52.

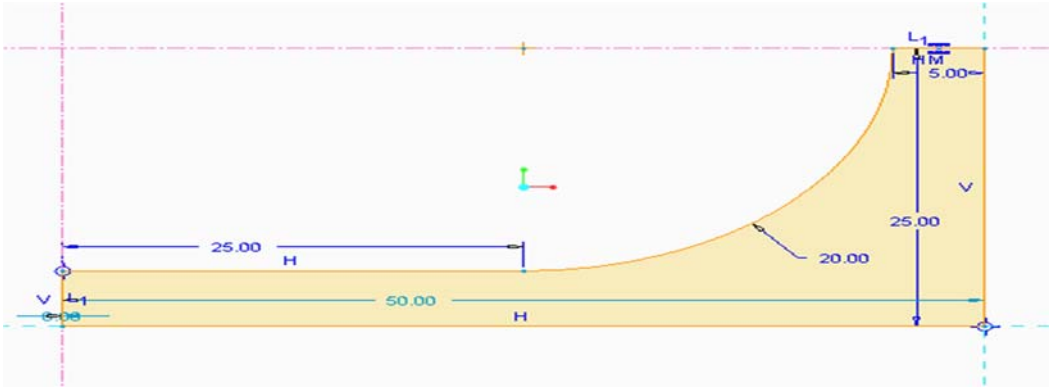

Fig. 5.21 Front view of the External Specimen to be finished by VEMAF

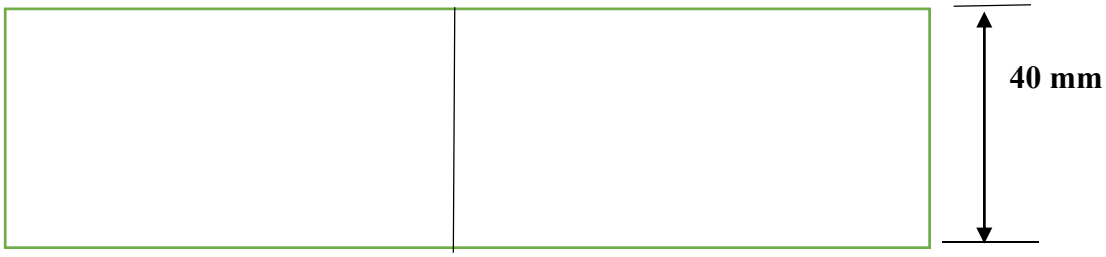

Fig. 5.22. Top view of the External Specimen to be finished by VEMAF

5.6.1 Simulation of the Flux density distribution of Steel Specimen:

Distribution of the Flux densities has been shown for the Steel for three working gaps. The gaps considered here are 2 mm, 1.5 mm, and 1 mm.

5.6.1.1 Simulation of flux density of Steel specimen with 2mm gap:

Fig.5.23 below shows the distribution of Magnetic Flux density on steel specimen for a working gap of 2 mm. The maximum Flux density on the specimen is 0.7200 T, which is just below the center of the Magnet. Flux density is decreasing on the corresponding points on the specimen, from the point below the center of the magnet towards the circumference of the Magnet.

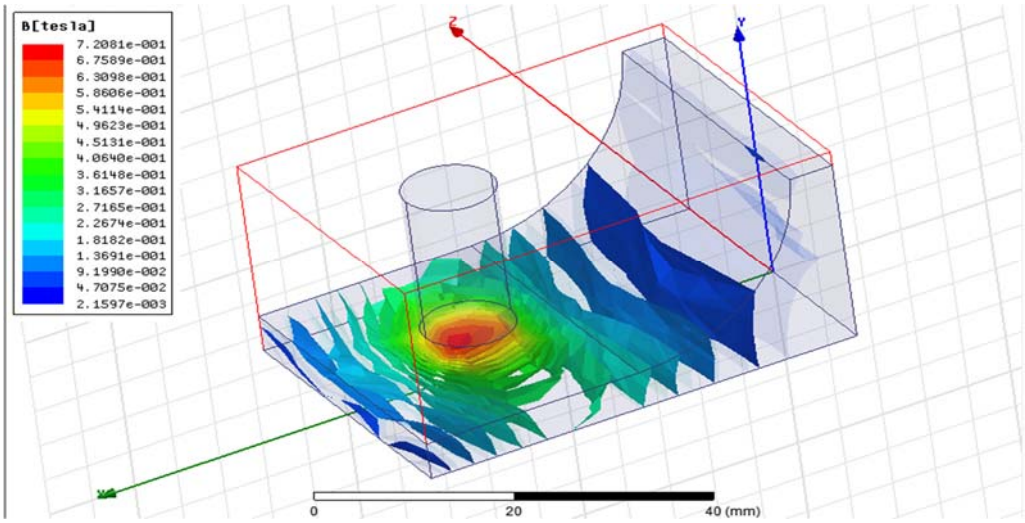

Fig. 5.23 Flux density distribution of Steel specimen 2 mm Gap

5.6.1.2 Simulation of flux density of Steel specimen with 1.5mm gap:

Fig.5.24 below shows the distribution of Magnetic Flux density on Steel specimen for a working gap of 1.5 mm. The maximum Flux density on the specimen is 0.8134 T, which is just below the center of the Magnet. Flux density is decreasing on the corresponding points on the specimen, from the point below the center of the magnet towards the circumference of the Magnet.

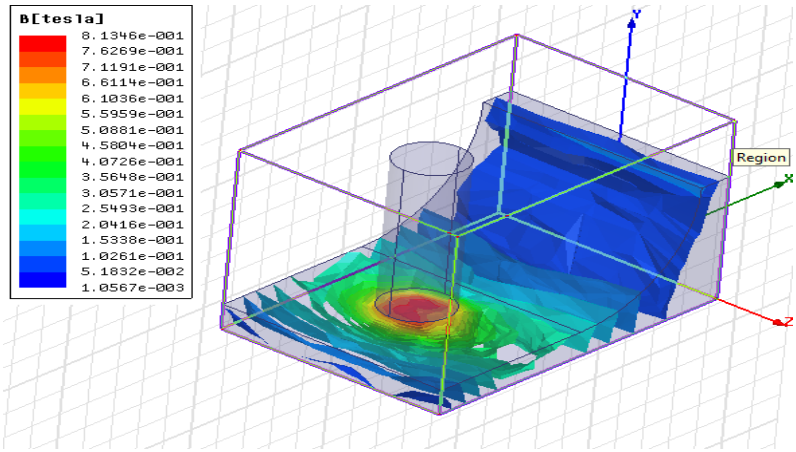

Fig. 5.24 Flux distribution Steel specimen 1.5 mm Gap

5.6.1.3 Simulation of flux density of Steel specimen with 1 mm gap:

Fig.5.25 below shows the distribution of Magnetic Flux density on Steel specimen for a working gap of 1 mm. The maximum Flux density on the specimen is 0.8875 T, which is almost constant on the surface of the specimen that is below the face of the Magnet.

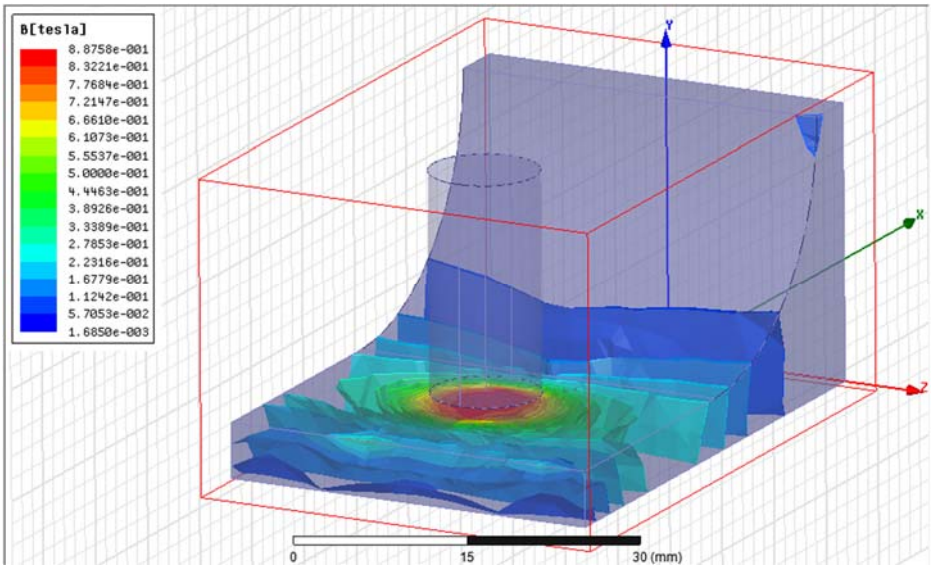

Fig. 5.25 Flux distribution Steel specimen 1 mm Gap

5.6.2 Simulation for Flux density distribution of Aluminium Specimen:

Distribution of the Flux densities has been shown for the Aluminium specimen for three working gaps. The gaps considered here are 2 mm, 1.5 mm, and 1 mm.

5.6.2.1 Simulation of Flux density of Aluminium specimen with 2 mm gap:

Fig.5.26 below shows the distribution of Magnetic Flux density distribution on Aluminium specimen for a working gap of 2mm. The maximum Flux density on the specimen is 0.2408 T, which is just below the center of the Magnet. Flux density is decreasing on the corresponding points on the specimen, from the point below the center of the magnet towards the circumference of the Magnet.

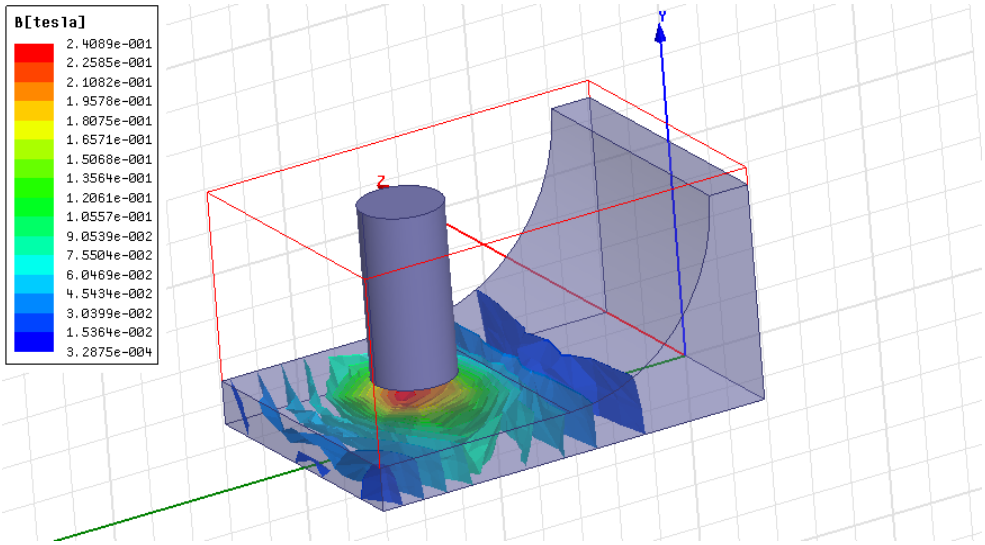

Fig. 5.26 Flux density distribution of Aluminium specimen 2 mm Gap

5.6.2.2 Simulation of Flux density of Aluminium specimen with 1.5 mm gap:

Fig.5.27 below shows the distribution of Magnetic Flux density on Aluminium Specimen with a working gap of 1.5 mm. The maximum Flux density on the specimen is 0.2858 T, which is just below the center of the Magnet. Flux density is decreasing on the corresponding points on the specimen, from the point below the center of the magnet towards the circumference of the Magnet.

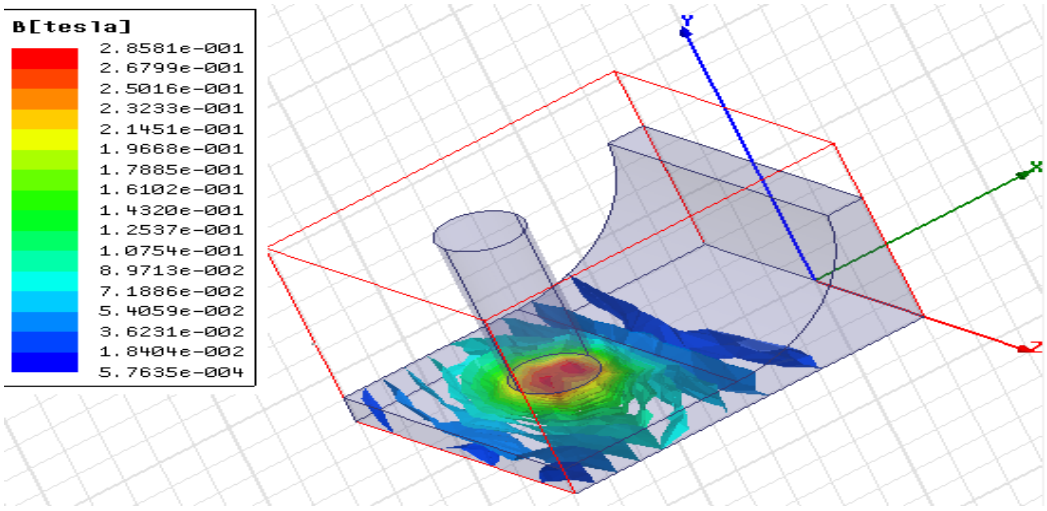

Fig. 5.27 Flux density distribution of Aluminium specimen 1.5 mm Gap

5.6.2.3 Simulation of Flux density of Aluminium specimen with 1 mm gap:

Fig.5.28 below shows the distribution of Magnetic Flux density distribution on Aluminium specimen with 1 mm gap. The maximum Flux density on the specimen is 0.3204 T, which is almost constant on the surface of the specimen that is below the face of the Magnet.

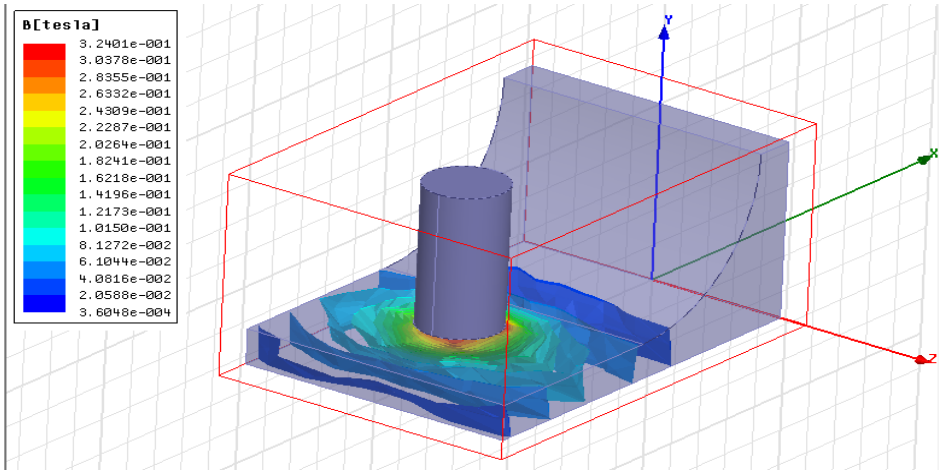

Fig. 5.28 Flux density distribution of Aluminium specimen 1 mm Gap

5.6.3 Simulation for Flux density distribution of Brass Specimen:

Distribution of the Flux densities has been shown for the Brass specimen for three working gaps. The gaps considered here are 2 mm, 1.5 mm, and 1 mm.

5.6.3.1 Simulation of Flux density of Brass specimen with 2 mm gap:

Fig.5.29 below shows the distribution of Magnetic Flux density distribution on Brass specimen for 2mm working gap. The maximum Flux density on the specimen is 0.2400 T, which is just below the center of the Magnet. Flux density is decreasing on the corresponding points on the specimen, from the point below the center of the magnet towards the circumference of the Magnet.

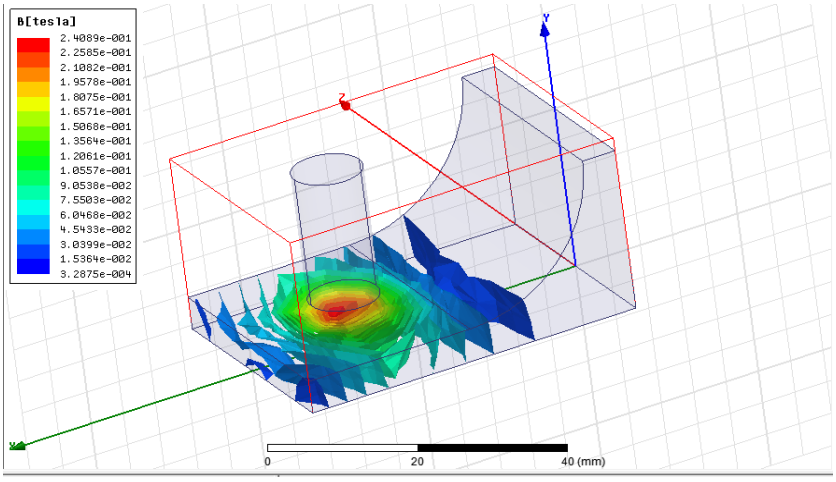

Fig. 5.29.Flux density distribution of Brass specimen 2 mm Gap

5.6.3.2 Simulation of Flux density of Brass specimen with 1.5 mm gap:

Fig.5.30 below shows the distribution of Magnetic Flux density on Brass specimen for a working gap of 1.5 mm. Flux density on the specimen has got a maximum value of 0.2858 T, which is just below the center point on the face of the Magnet. Flux density is decreasing on

the corresponding points on the specimen, from the point below the center of the magnet towards the circumference of the Magnet**.**

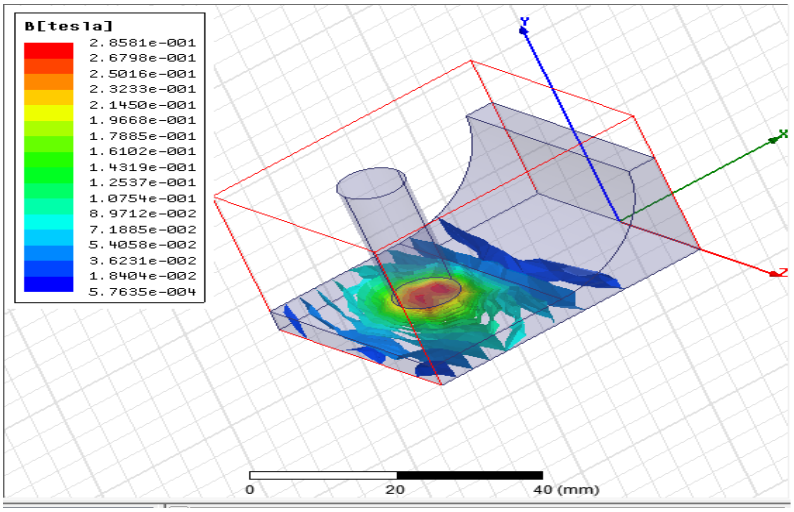

Fig. 5.30 Flux density distribution of Brass specimen 1.5 mm Gap

5.6.3.3 Simulation of Flux density of Brass specimen with 1 mm gap:

Fig.5.31 below shows the distribution of Magnetic Flux density on Brass specimen with a working gap of 1mm. The maximum magnitude of Flux density on the Brass specimen is 0.3240 T, located from the edge towards the center. However, the flux density at the corresponding points below the geometric center of the Magnet is less than 0.3204 T.

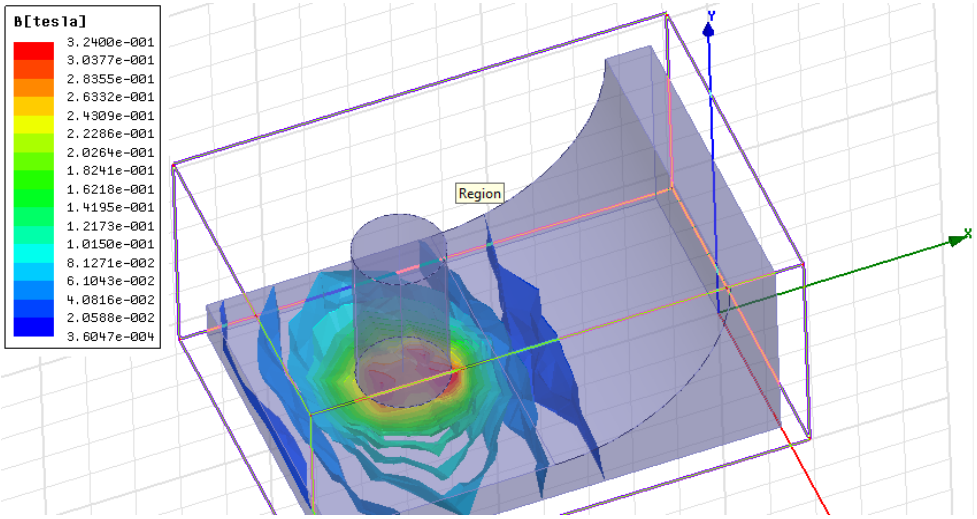

Fig. 5.31 Flux density distribution of Brass specimen 1 mm Gap

SUMMARY

1. **Out of four magnets, Arc magnet, Fan magnet, Ring magnet, and arc magnet having same volume and working gap, it is observed that Fan Magnet produces more flux density under similar conditions compared to other three magnets. The next geometry under consideration is Arc magnet or Segmental magnet followed by ring magnet and the least preferred magnet is the Block magnet.**
2. **Based on the above results N42 Segmental arc magnets having an Outer diameter of 36 mm, Inner diameter of 28 mm, a height of 20 mm, and Arc angle of 45^{o} have been procured for the present research work and Simulation has been done for two magnets, four magnets and eight magnets and the flux densities are of the order 1.035 T, 1.519 T, and 1.599 T respectively.**
3. **The actual values obtained are 1.2 times the simulated values as the ANSYS MAXWELL Version 16 can simulate only N35 magnets and N42 magnets are 20% stronger than the N35 magnets.**
4. **For external finishing N52 magnet with 20 mm diameter and 20 mm height has been used which is 1.49 times more powerful than N35 magnets.**
5. **For all the three materials, Aluminium, Brass, and mild steel specimen a working gap of 2 mm, 1.5 mm 1nd 1 mm is considered and it is found that the lesser the working gap higher would be the flux density.**
6. **For all the material and the working gaps, it has been observed that the maximum flux density is just below the magnet itself.**
7. **Flux density produced for Aluminium and Brass is almost the same for all the working gaps under consideration.**

CHAPTER 6. INTERNAL FINISHING OF SPLINE SHAFTS

In this chapter, a detailed description of the test rig used for Internal surface finishing of the Spline shaft has been made., followed by this a brief analysis is made about the flux densities obtained due to the Simulation and Modelling of Segmental arc magnets, which has been carried out in Chapter 5. A brief discussion about the Modelling and Simulation of flow parameters for three different Extrusion Pressures of the Viscoelastic Magnetic abrasive medium that flows through the Spline shaft has been made. The experiment has been performed based on Taguchi's Orthogonal Array of design. Experimental results have been discussed and Optimisation for the Maximum material removal has been done.

6.1 Introduction: Finishing of the internal surfaces is one of the challenging tasks and most of the research work done is confined to the finishing of hollow circular shapes of a different material (36,37,38,40, 41,42, 44, 46, 47,49). In the present work finishing off the Spline shaft made of Mild steel has been performed using Viscoelastic Magnetic Abrasive Medium. A fixture is specially designed and fabricated, which accommodates the segmental magnet made of NdFeb42, which is used for generating Electrical power for Wind Turbines. The fixture is placed between the upper and lower cylindrical platforms of an Abrasive Flow Machine, that support the upper and lower cylinders. Viscoelastic Magnetic abrasive medium is loaded in the hollow space of the Medium cylinder. The medium passes through the internal surface of the spline shaft which will perform the finishing of the internal surface. A detailed description of the various components of the test rig used is discussed below.

6.2 Description of the test rig:

The Test rig used for experimenting comprises the following components.

1. Abrasive Flow Machine
2. Rotational motion Mechanism
3. Aluminum fixture for VEMAF process
4. Viscoelastic Magnetic Abrasive Medium

6.2.1 Description of the Abrasive Flow machine: Abrasive Flow Machine (AFM) located in the Advanced Manufacturing lab of the Delhi Technological University, Delhi is used for performing the Internal finishing of the Spline shaft. Fig 6.1 below shows the images of the AFM, the brief description of the components are mentioned below.

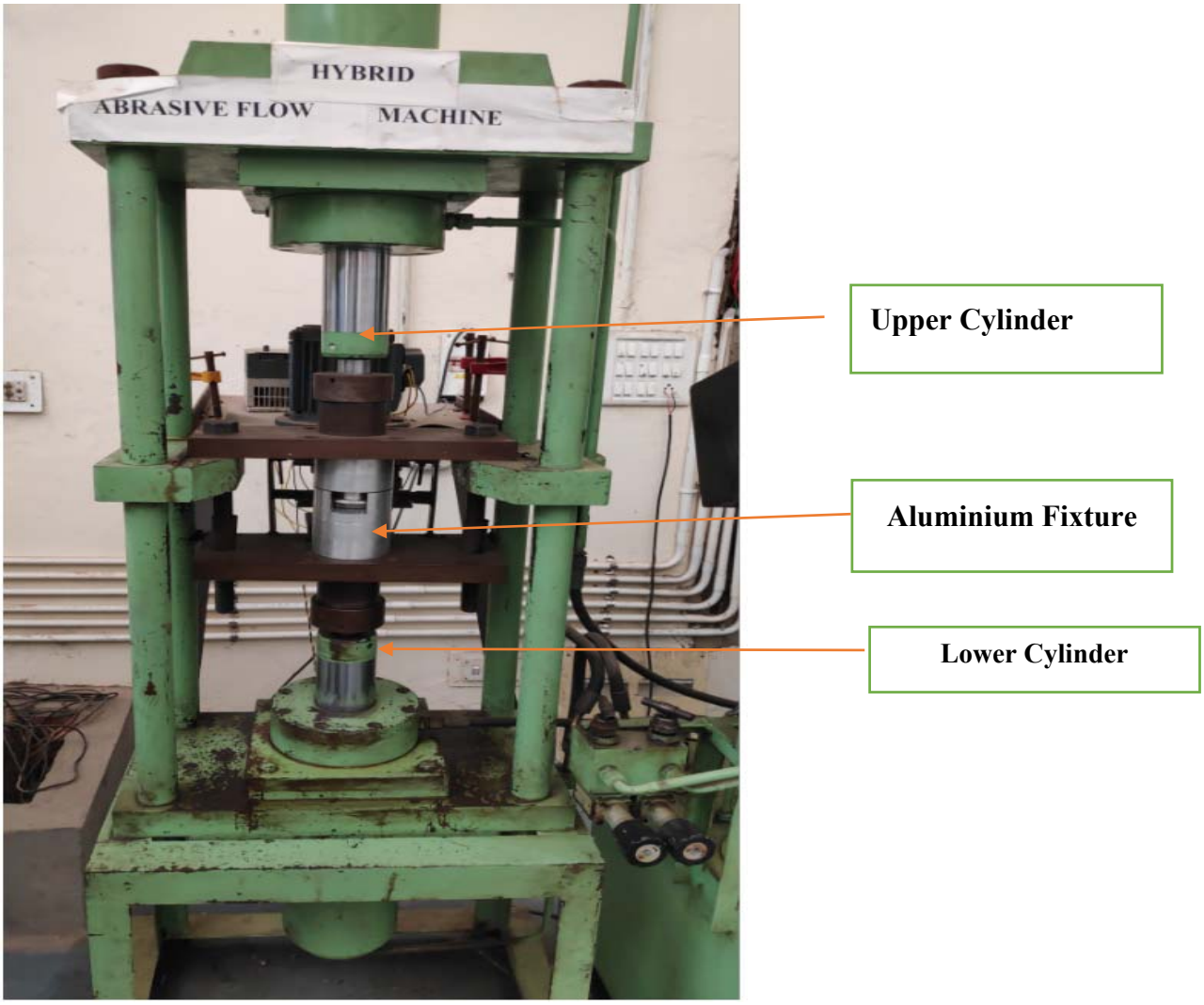

Fig.6.1 Experimental setup for VEMAF process of Spline shaft

6.2.1.1 Hydraulic Power pack: Hydraulic power pack is designed to give upward and downward motion to the Pistons located in the Hydraulic cylinder. Important elements in the Hydraulic power pack are:

6.2.1.2 Hydraulic Circuit: This permits the flow of the oil from the Oil sump to flow in a specific direction.

6.2.1.3 Hydraulic Cylinder: Two cylinders in Vertical position having a phase difference of 180^{o} have been placed co-axially. The piston in the Hydraulic cylinder gets upward and downward motion due to the pressure difference. The hydraulic cylinder here acts like a Mechanical actuator by driving the piston in one direction at a time. Bore and stroke of the

Hydraulic cylinder are respectively 130 mm and 96 mm. Fig.6.2 below shows the image of the Hydraulic Cylinder.

Fig.6.2 Hydraulic Cylinder

6.2.1.4 Hydraulic Power Pack: Hydraulic Pressure generating system called as Hydraulic Power Pack is shown in Fig. 6.3 Hydraulic Power pack comprising of a Hydraulic pump, Hydraulic filter, Oil sump, and the metallic pipes. The Maximum Capacity of Pressure generation by this system is 25 MPa.

6.2.1.5 Direction Control Mechanism: Direction of flow of the Viscoelastic Magnetic Abrasive Medium is obtained by operating the levers shown in Fig.6.4 below. The left side lever is used for controlling the motion of the lower cylinder and the right side lever controls the motion of the Upper cylinder which in turn moves the medium up and down respectively.

Fig.6.3 Hydraulic Power Pack

Fig.6.4 Direction Control Mechanism

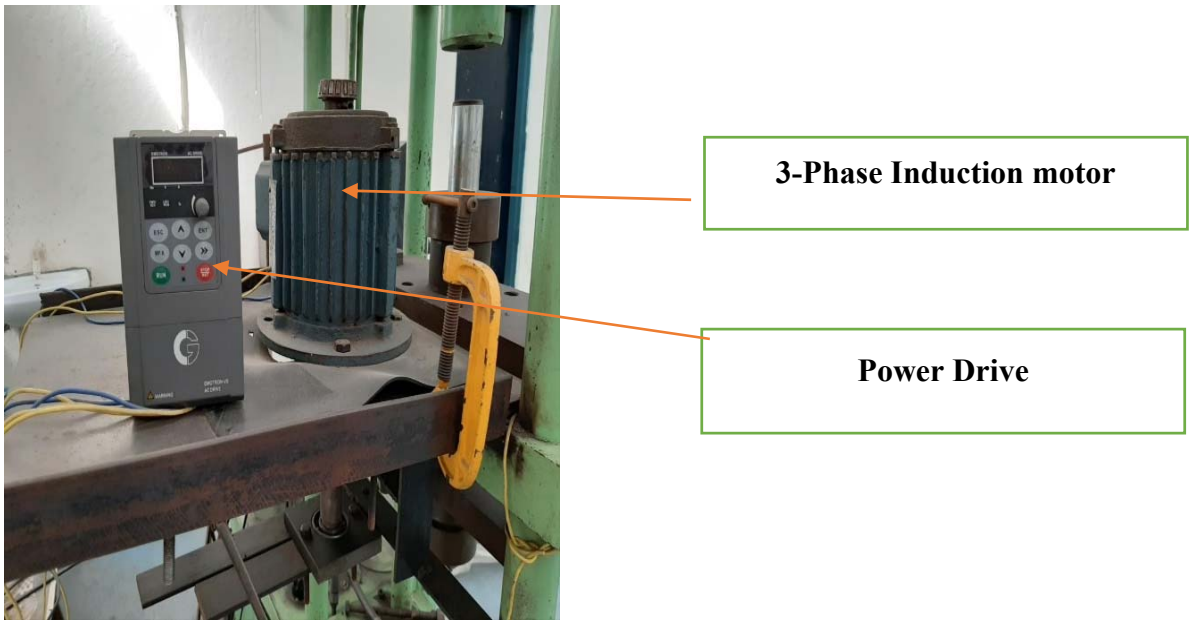

Fig. 6.5 Rotational Motion Mechanism

6.2.2 Rotational Motion Mechanism: This comprises a Three Phase Induction motor having a rated power of 1hp and rotational speed of 900 rpm. The speed of the Induction motor is controlled by the power drive. Power drive operates at an AC voltage range of 200V to 240V with a capacity of 1 HP. The rotational motion mechanism is shown in Fig.6.5 above.

6.2.2.1 Gear train: A gear train is used for obtaining the required rotational speed to the workpiece. Present gear train comprises of the gears with 2 mm module. Out of the four gears used for obtaining the rotational speed of the workpiece, the first Gear with 44 teeth is mounted on the induction motor, which meshes with an intermediate gear having 58 teeth and located on a bracket attached to the frame of the AFM. Fig 6.6 below shows the first two gears having 44 teeth and 58 teeth respectively. Intermediate gear meshes with the pinion mounted on the central portion of the fixture having 18 teeth. This pinion with 18 teeth meshes with the workpiece gear, which is mounted on the spline shaft. Fig.6.7 shows the pinion and gear mounted on the Central portion of the Aluminium fixture.

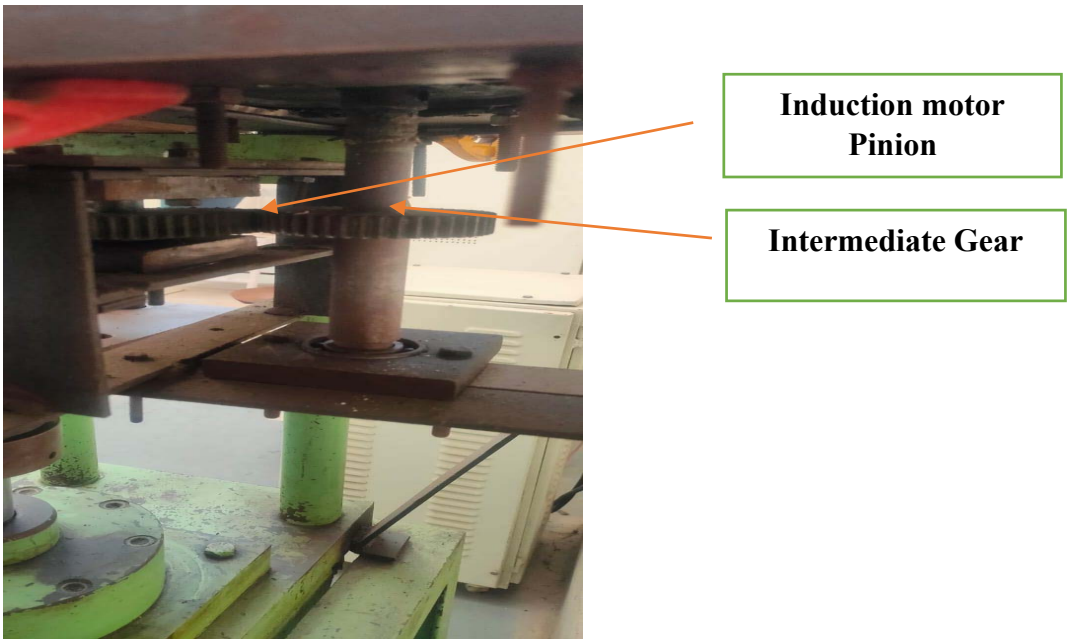

Fig.6.6 Gear set

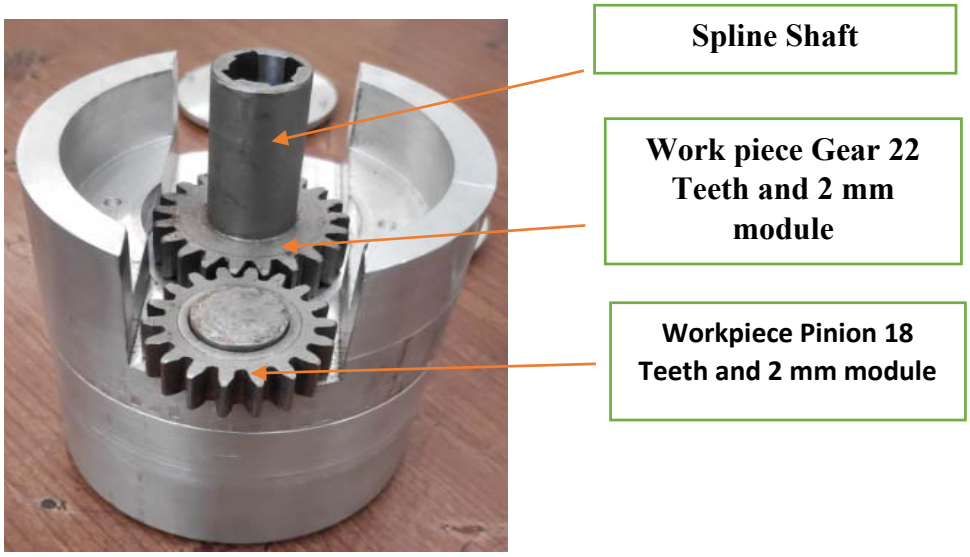

Fig.6.7. Workpiece pinion and gear

The output speed of the workpiece for one revolution of the Induction motor is given by

$\frac{44}{58} x \frac{58}{18} x \frac{18}{22} = 2$, which means one revolution of the Induction motor gives two revolutions for the workpiece.

6.2.3 Aluminium Fixture: An aluminum fixture specially designed for the Surface finishing of the Internal Spline shaft comprises four important blocks, which will accommodate other components. They are

a. Top Cover

b. Bottom Cover

c. Middle Housing

d. Internal Spline shaft

e. Magnet Housing

The assembly drawing of the fixture is shown in Fig.6.8 and 6.9 below is made from Al 6061 grade comprising up to 98% of Aluminium by weight. Other elements are chromium, Ferrous, Copper, and Manganese which contribute 2% by weight.

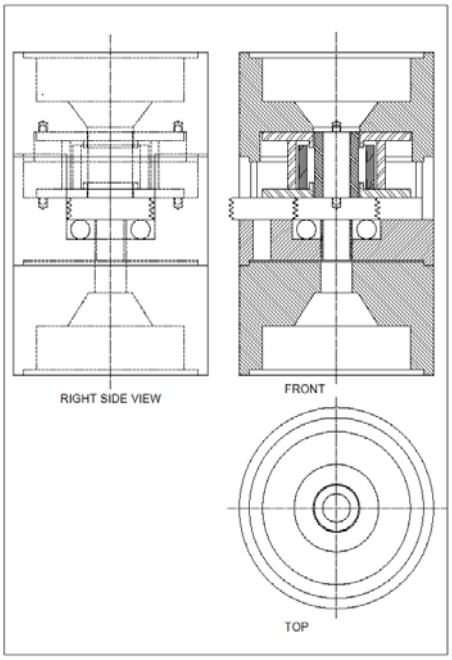

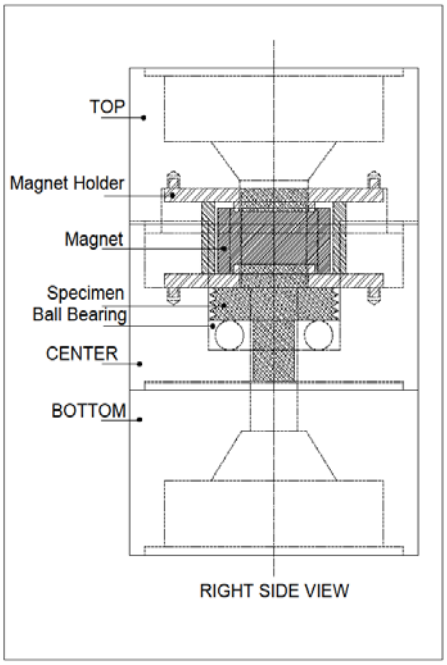

Fig. 6.8 Assembly Drawing **Fig. 6.9 Assembly drawing – Right side view**

6.2.3.1 Top Cover: Part drawings of Top cover and the fabricated piece of Aluminium top cover are shown respectively in Fig.6.10 and 6.11 below. The bottom Tapered portion is in contact with the upper portion of the Internal Spline shaft.

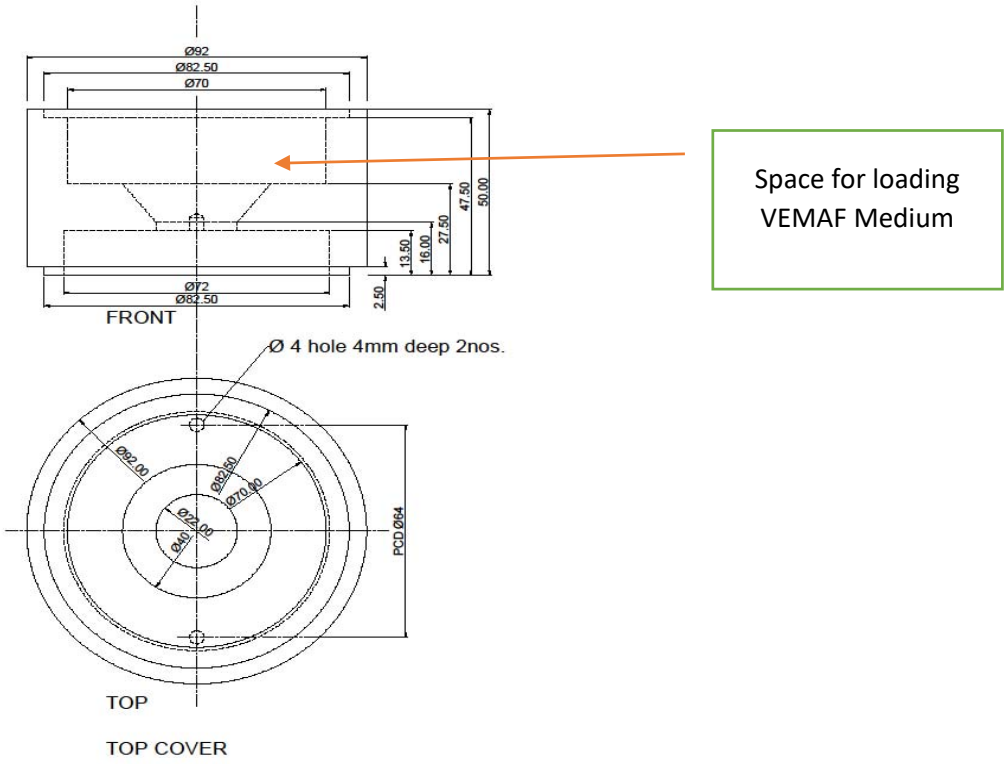

Fig. 6. 10 Part Drawing of Top Cover

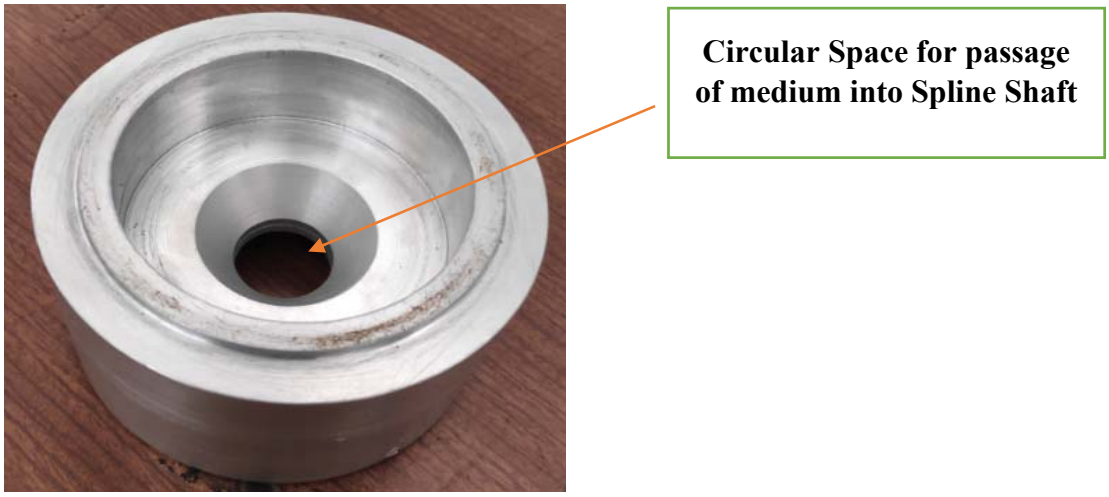

Fig.6.11 Aluminium Top Cover

6.2.3.2 Bottom Cover: Fig. 6.12 is the Part drawing of the Bottom cover and 6.13 is the fabricated piece of Aluminium Bottom cover, which sits over the bottom cylinder through which the VEMAF medium enters into the bottom cover and passes to the top through the internal spline shaft. Middle housing, which accommodates the Magnetic housing sits on the bottom cover

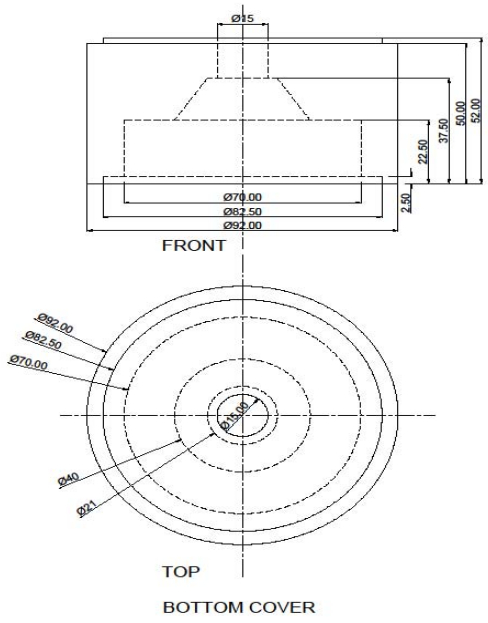

Fig. 6.12.Part drawing of the Bottom cover

Fig.6.13. Aluminum Bottom Cover

6.2.3.3 Middle Housing: Assembly drawing of the Middle Housing and Fabricated Aluminium Middle housing are shown in Fig.6.14 and 6.15 respectively. Central portion

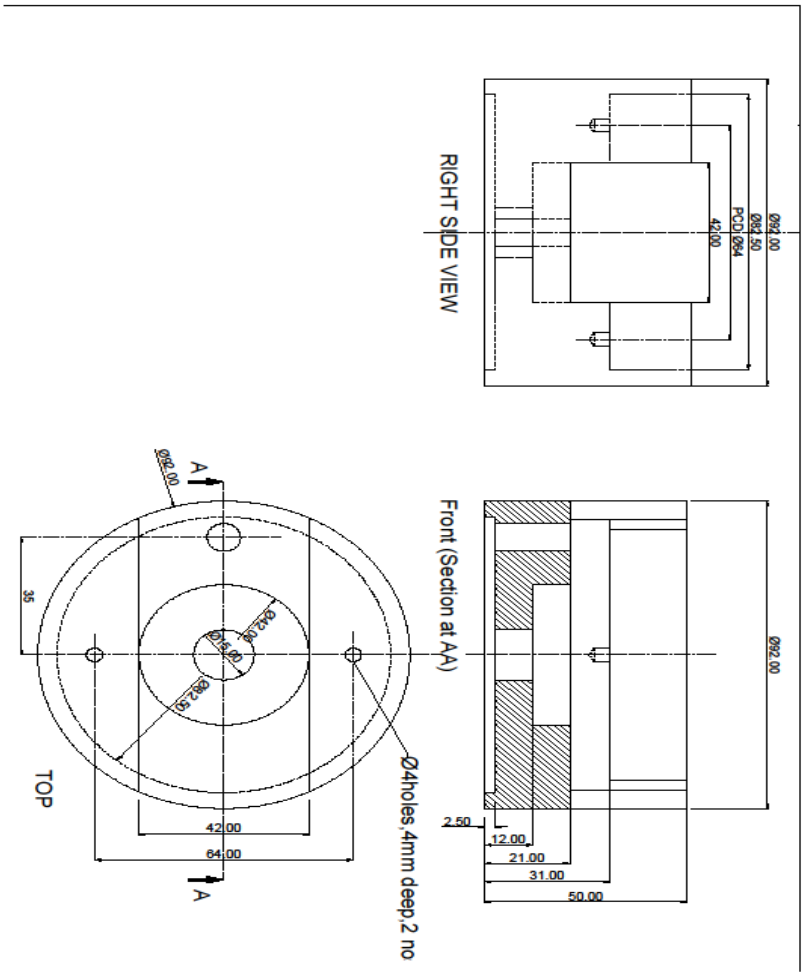

Fig.6.14 Part Drawing of Middle housing

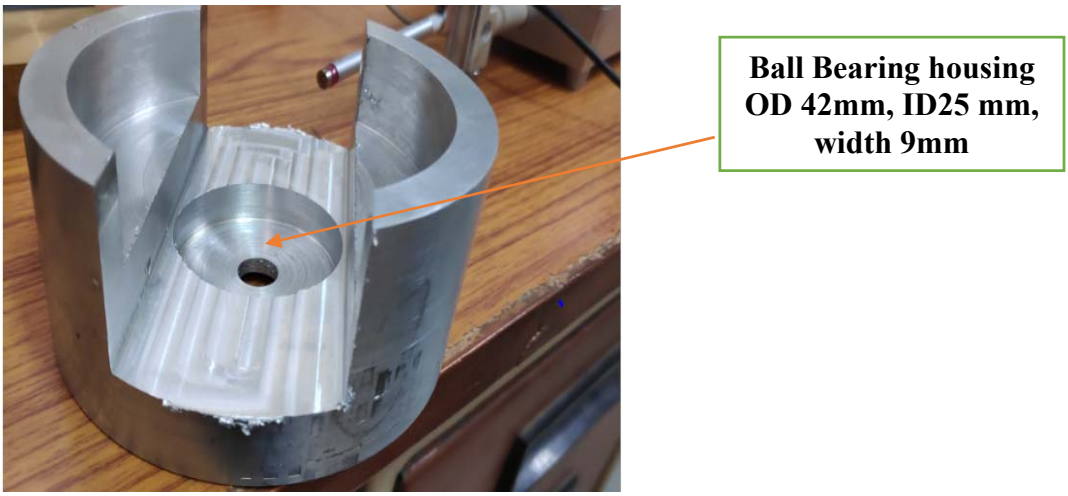

Fig.6.15. Aluminum Middle Housing

The Middle housing has got a circular recess as shown in Fig.6.15 which accommodates Roller bearing of Outer diameter 42 mm and Inner diameter of 25 mm and 9mm thickness and Dynamic

load rating of 8.71kN with HSN code 84821010 accommodates the bottom portion of the Spline shaft. The outermost diameter of the Aluminium Middle housing is 92 mm. Fig.6.16 shows the Middle housing that accommodates the spline shaft, Gear and Pinion set under meshing. The pinion meshes with the bigger gear on the AFM frame having 58 teeth and 2 mm module and this gear meshes with the gear on the Induction motor shaft having 44 teeth and 2mm module. This configuration as discussed in 6.2.2.1 gives two rotations for every single rotation of the Induction motor spindle. Relative motion between the gear and the spline shaft is arrested with a small sunk key having 20 mmx5 mm x5 mm dimensions.

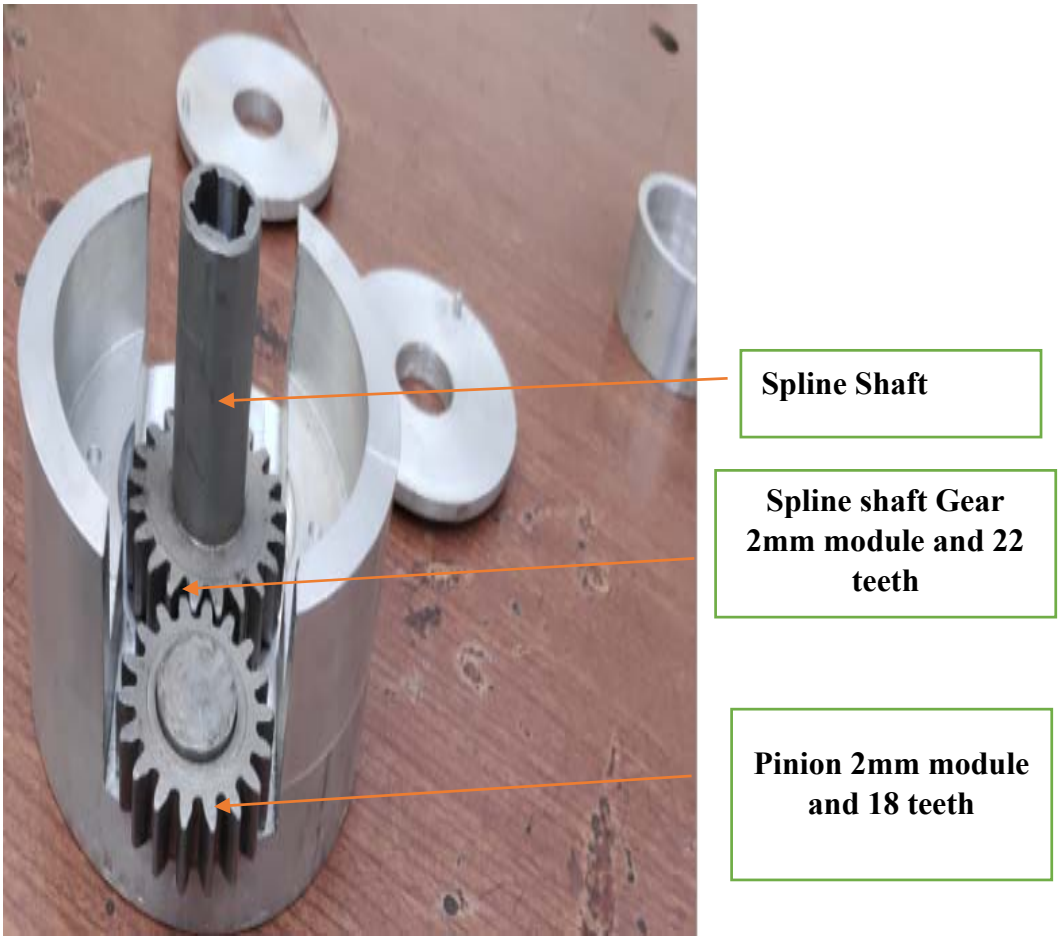

6.16 Middle housing with Gear and Pinion

6.2.3.4 Internal Spline Shaft: Internal Spline shafts, which have been finished in the present research work with Viscoelastic Magnetic abrasive medium are made of Low Carbon Steel of AISI Grade 1020. Some of the important properties of the Internal Spline shaft material have been mentioned below.

Table.6.1 Properties of AISI 1020 Steel

S.no	Property	Magnitude
1	Density	7.87 g/cc
2	Hardness (BHN)	121
3	Shear Modulus	80 GPa
4	Tensile Strength (Ultimate)	420 MPa
5	Yield Strength	350 MPa

During the present research work, nine splined shafts have been chosen for finishing operation and each spline shaft is subjected to three finishing operations under different conditions of flux density, Extrusion pressure, etc. Spline shaft has been manufactured by broaching, followed by reaming and fine finishing such that the surface roughness is of the order of 0.4 μm. The dimensions of the Spline shafts are shown in Table 6.2 below.Fig.617, Fig.6.18, and Fig.6.19 are the images of the spline shaft used for internal finishing.

Table 6.2 Dimensions of Spline shaft

Sample No.	**A** Dimension-1 LENGTH end to end	**B** Dimension-2 Head Width	**C** Dimension-3 Internal Hole Dia.	**D** Dimension-4 Head Dia	**E** Dimension-5 Lower Part Slot Width 1	**F** Dimension-6 Slot width 2	**G** Dimension-7 Dia
	mm	mm	mm	mm	mm	mm	mm
1	**62.598**	**9.7155**	**12.6365**	**25.0320**	**15.45590**	**12.68730**	**20.0914**
2	**61.951**	**9.2075**	**12.6365**	**24.990**	**15.34160**	**12.53490**	**19.8374**
3	**62.065**	**8.7630**	**12.5984**	**25.0470**	**15.26540**	**12.72540**	**19.8501**
4	**62.306**	**10.1219**	**12.6365**	**25.0380**	**15.36700**	**12.72540**	**19.9898**
5	**62.217**	**9.3218**	**12.6238**	**25.0240**	**15.15110**	**12.67460**	**20.3835**
6	**61.836**	**9.0551**	**12.6111**	**25.0220**	**15.27810**	**12.57300**	**20.2136**
7	**61.900**	**8.9154**	**12.5222**	**25.0300**	**15.29080**	**12.59840**	**20.0.820**
8	**62.027**	**9.2202**	**12.6365**	**25.0150**	**15.45590**	**12.68730**	**19.8247**
9	**62.028**	**8.968**	**12.6245**	**25.0750**	**15.4880**	**12.56725**	**20.0245**

Average values	**62.103**	**9.254**	**12.614**	**25.0303**	**15.3437**	**12.6415**	**19.97**

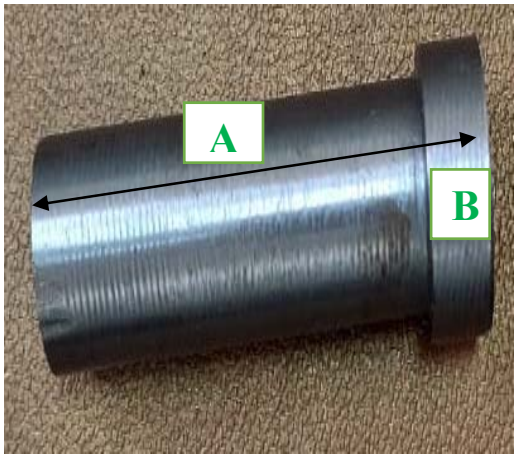

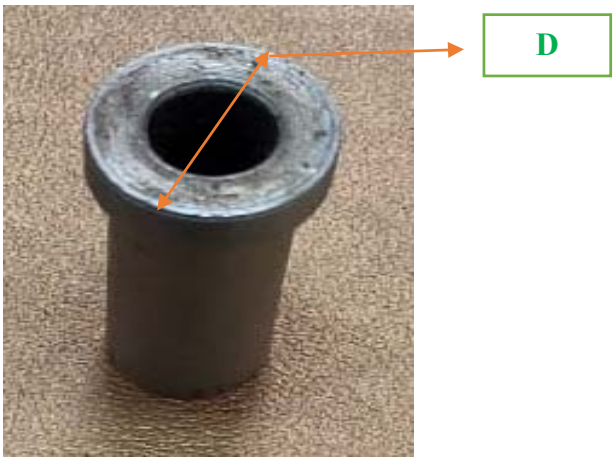

Fig.6.17 Spline shaft Length & Width **6.18 Spline shaft Head diameter**

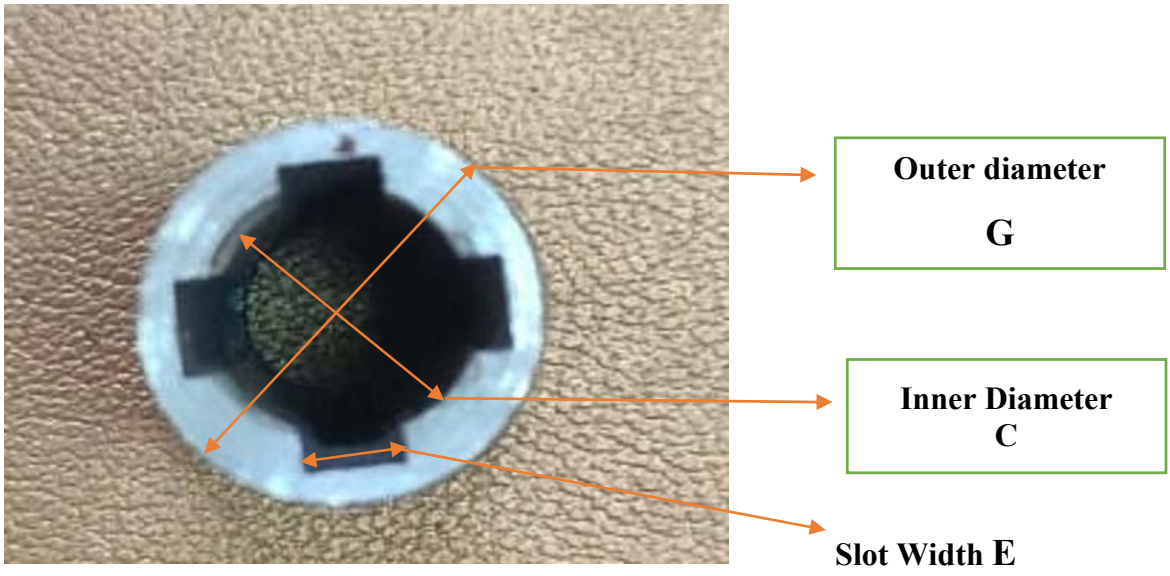

Fig.6.19 Spline shaft Outer and Inner diameter

6.2.3.5 Magnet Housing: Magnet housing accommodates segmental Permanent magnet, Top and bottom cover plates, Aluminium hollow cylindrical ring (body) to accommodate Permanent magnets. Part drawing of the Magnet Housing, which would be placed on the Middle housing is shown in Fig.6.20 below.

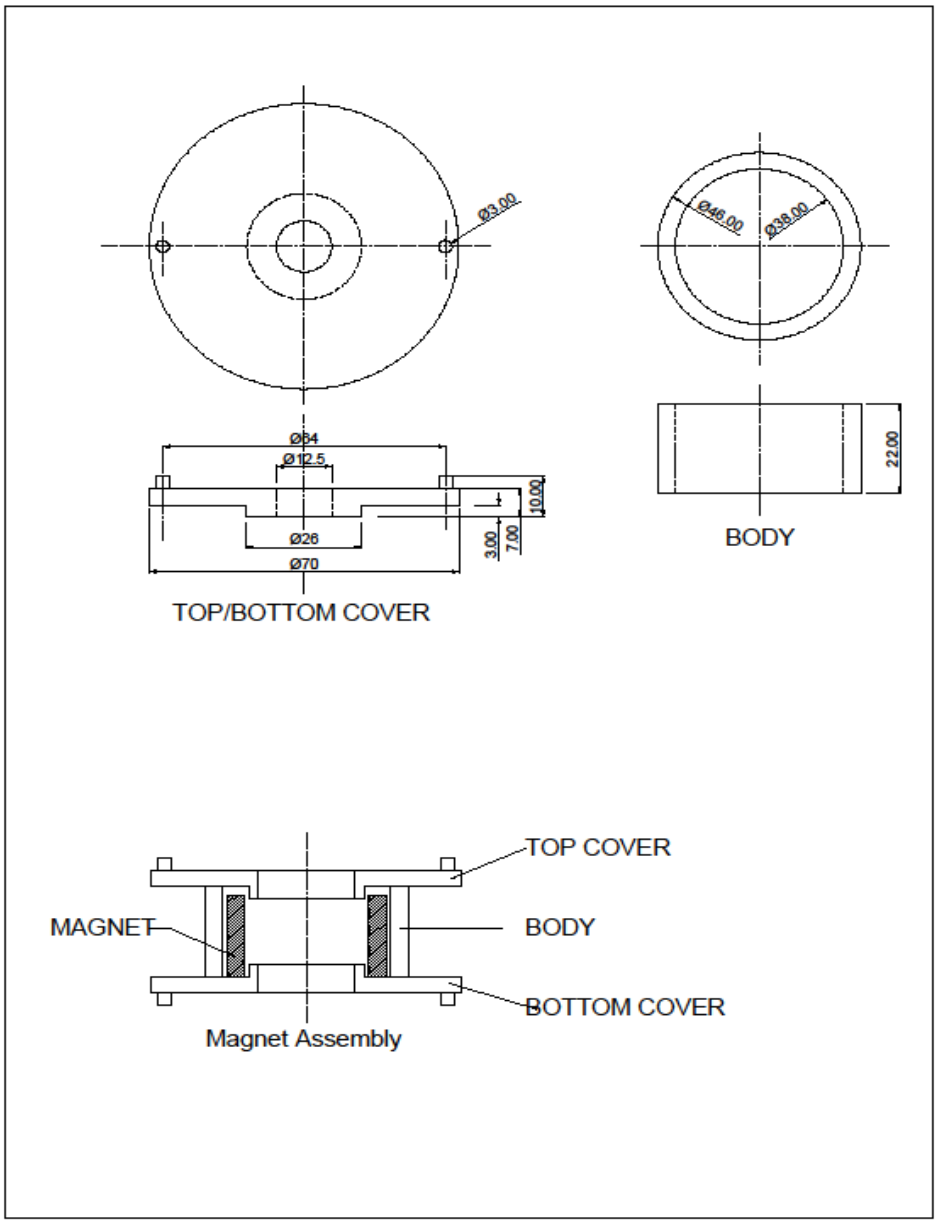

Fig.6.20 Part drawing of Magnet Housing

6.2.3.5.1 Permanent Magnet: Fig. 6.21 shows the Permanent magnet used for the present research. The permanent magnet used in the present research work is having Eight Segmental magnets with a height of 20 mm, Arc angle of 45^{o}, an Inner diameter of 28 mm, and an outer diameter of 36 mm. These magnets are made of NdFeb material having a designation of N42 and used in Wind Turbines for generating Electricity. During the experiment, three levels of flux density have been considered.

In the first level, two permanent magnets have been kept at 180^{o} and the remaining space is occupied by the aluminum segmental pieces having the same specification as

that of the segmental magnets. In the second level, four segmental magnets have been considered, kept at 90^{o} angle, and in the third level, all the Eight Magnets have been considered.

Fig.6.21 N42 Permanent Magnet

6.2.3.5.2 Hollow Cylindrical ring: This accommodates the segmental permanent magnet has a height of 22 mm, an outer diameter of 46 mm, an inner diameter of 38mm. So there will be a 1mm gap between the outer diameter of the Permanent magnet and the inner surface of the Hollow cylindrical ring. Fig.6.22 shows the Hollow cylindrical ring.

Fig.6.22 Hollow Cylindrical ring

6.2.3.5.3 top and bottom cover plates: Top and Bottom cover plates are used for holding the Segmental Magnet such that the Magnet will not get displaced from their assembled position when the Spline shaft is inserted through them. Assembly drawing shown in Fig.6.20 describes how the Magnets are being held between the top and bottom cover plates. Fig.6.23 & Fig.6.24 are bottom and Top cover plates and Fig.6.25 shows the Magnet assembly comprising a bottom plate, cylindrical ring and

Fig 6.23 Bottom Cover plate Fig. 6.24 Top Cover plate Fig.6.25 Magnet Assembly

Magnet. Fig.6.26 below shows the Complete Magnet assembly placed on the Middle housing.

Fig.6.26 Magnet Assembly

Fig.6.27 and Fig.6.28 below show the Complete Assembly of Aluminium fixture, which will be placed between the Upper and Lower Cylinder of the Abrasive Flow Machine. Fig.6.27 shows the Spline shaft from the top and Fig. 6.28 shows the pinion that mates with the Intermediate gear with 58 teeth located on the frame of the machine shaft. Packing material has been used as a protection against the lateral leakage of the VEMAF medium at very high Extrusion pressure.

6.27 Aluminium Fixture view I **6.28 Aluminium Fixture View II**

6.2.4 Viscoelastic Magnetic Abrasive Medium: In chapter 3 from section 3.6.3 to 3.6.7 a detailed discussion has been made about the preparation of the Viscoelastic Magnetic abrasive medium. Initially, the Silicone oil, Red Transformer oil, White Transformer oil AP3 grease samples have been tested for their viscosity. Polymer medium and Gel have been prepared and their viscosity has been found. The polymer has a viscosity of 231.43 mPa-s and the Gel has got a Viscosity of 13589 mPa-s. Polymer and Gel have been thoroughly mixed in a weight proportion of 8:1. CIP and SiC abrasives have been mixed thoroughly in a weight ratio of 3:1. The polymer and Gel have been mixed with the CIP and SiC mixture in the weight ratio of 2:1. The viscosity obtained is 0.954 mPa-s and the density is 1781 kg/m^3.

6.3 Simulated results of Flux densities: In chapter 5 detailed Simulation and the Modelling of Segmental Permanent magnets used in the present research work have been discussed for three levels from sections 5.2.2.1 to 5.2.2.3. It is observed from the simulation shown in Fig.6.29, Fig.6.30, and 6.31 that the maximum Flux densities are 1.035 T, 1.513 T, and 1.599 T, which are on the external surface of the spline shaft just below the magnets. However, Maximum flux density obtained through simulation is confined to a particular zone only. So, the median value

of the Magnetic flux densities has been considered for optimization. Which are respectively 0.5175T, 0.7014T, and 0.8015T for Two magnets, Four Magnets, and Eight magnets considered. Also, the flux density produced by N42 magnets is 20% higher than the Simulated values as ANOSOFT 16 supports only N35 magnets. Accordingly, the flux densities considered for the present experimental work are 0.6210 T, 0.8417T, and 0.9618T.

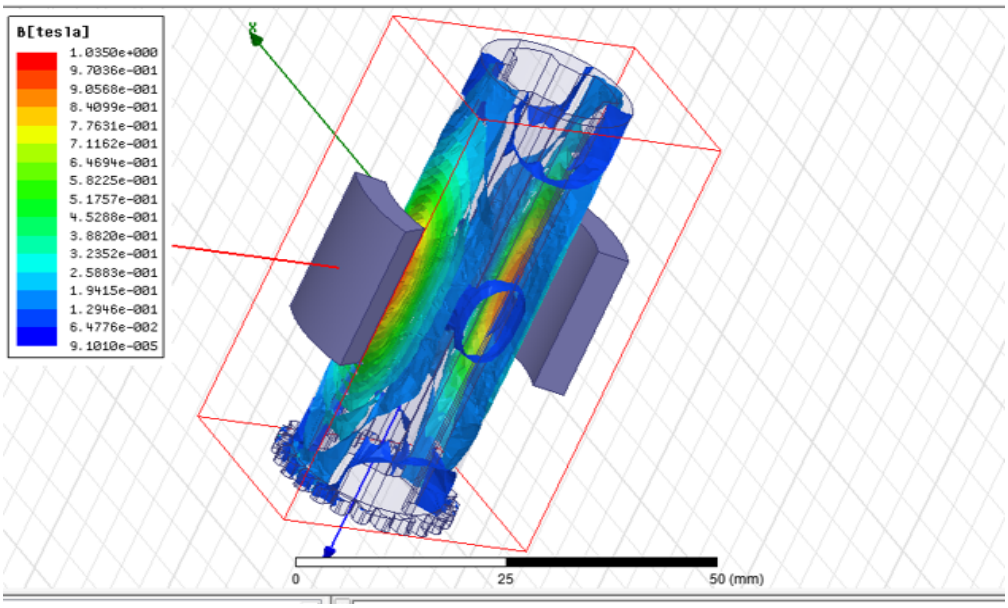

Fig. 6.29 Two Segmental magnets with 180^{o} angle

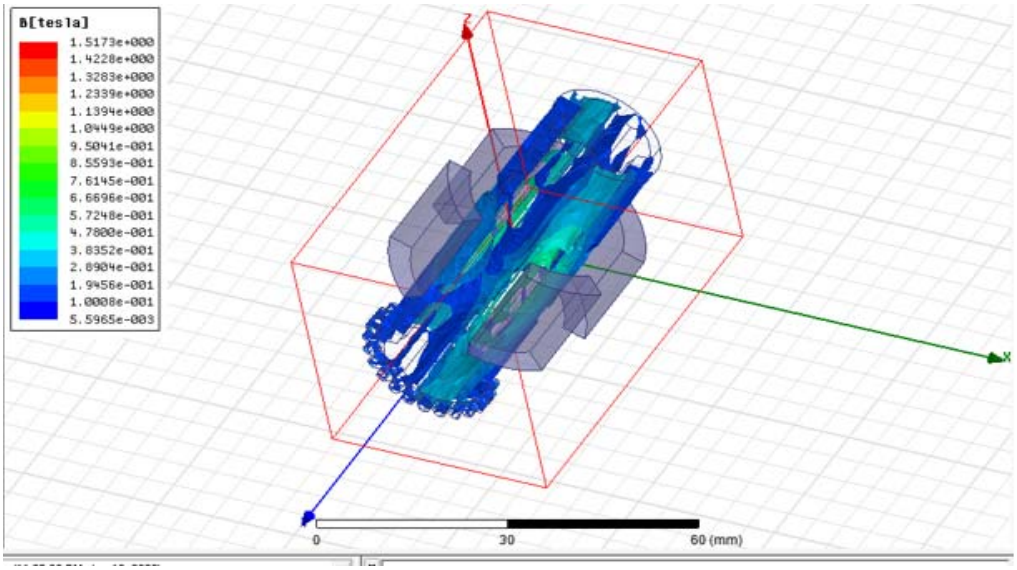

Fig.6.30 Four Segmental Magnet with 90^{o} Angle

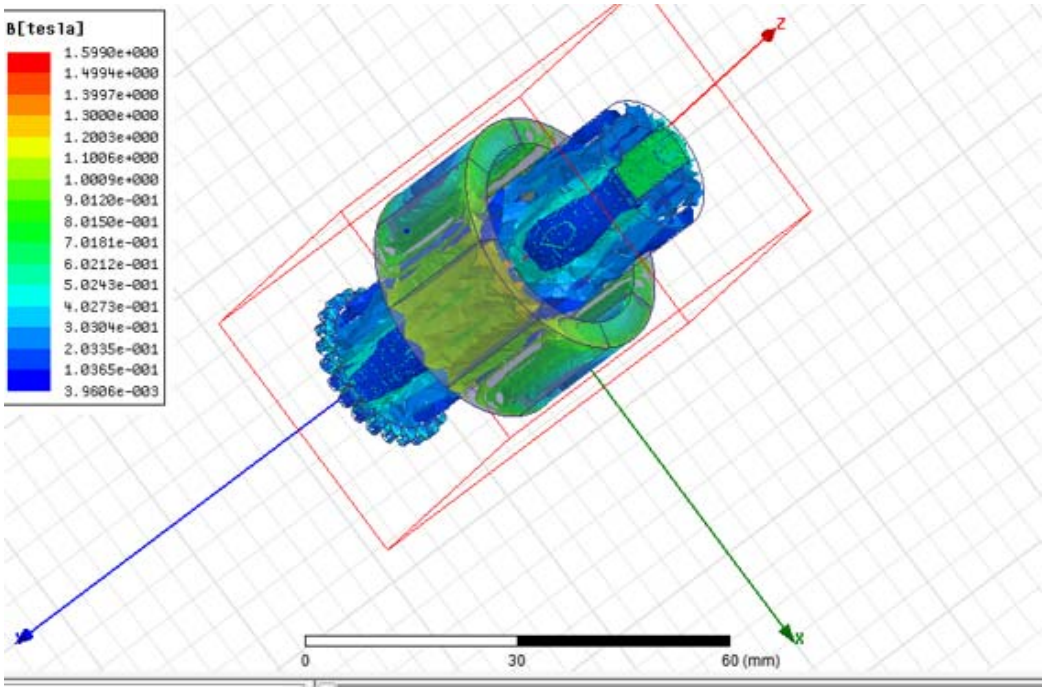

Fig.6.31 Eight Segmental magnets with 45^{o} Angle

6.3.1 Flux densities measured by Gaussmeter: Six of the Eight N42 Arc Magnets have been shown in Fig.6.32**.**Gaussmeter is used for measuring the Flux densities of the N42 Segment magnets. Some of the results obtained have been shown below. From Fig.6.33 to Fig.6.37Measurements shown are taken from the top surface of one of the segmental magnets. Flux measured are in Tesla(T). Values are between 1.56T to 2.96T

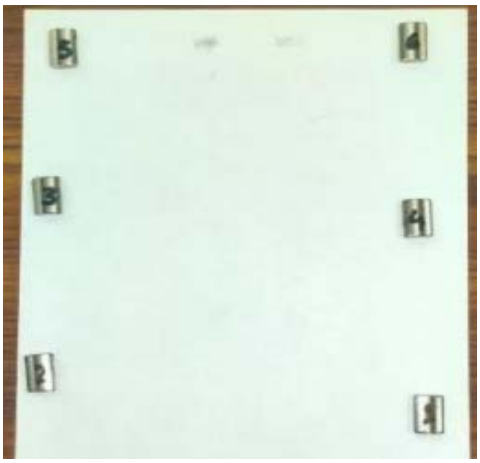

Fig. 6.32 Segmental Magnets **Fig.6.33 Flux density on Outer surface**

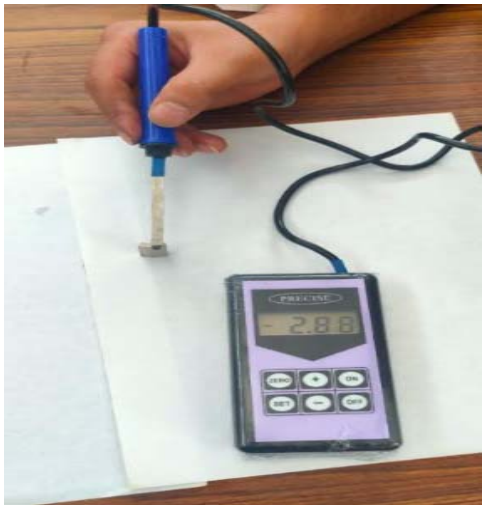

Fig.6.34. Flux density on Top Surface

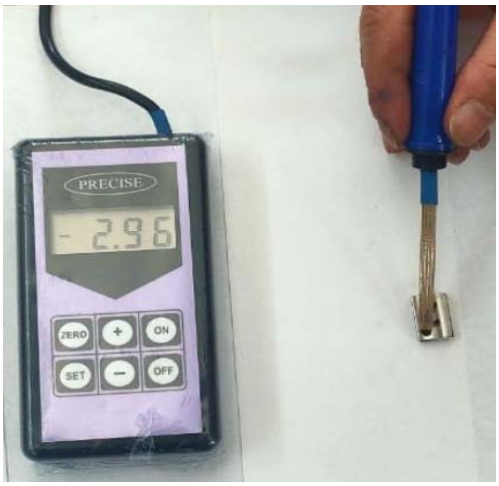

Fig.6.35 Flux density on Inner surface

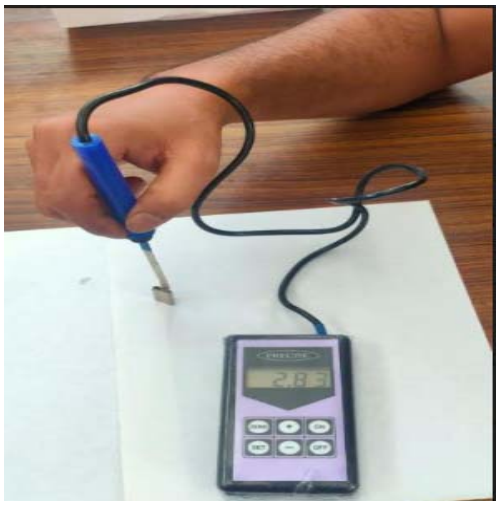

Fig. 6.36 Flux density on top surface

Fig. 6.37 Flux density on the corner

6.4 Modelling and Simulation of Flow parameters in finishing Internal Splines:

Finishing of Internal splines comprises of rotation of the Spline shaft through the gear and Pinion Mechanism. The gear is arranged on the spline shaft which is in contact with the pinion and this pinion gets the rotary motion through the gear mounted on Three Phase Induction Motor.

Fig 6.38 shows the solid model create on CREO 3.0, where the Arc Magnet surrounds the Spline shaft. The outer diameter of the arc magnet is 36 mm and the inner diameter of the arc magnet is 28 mm with Eight arc magnets having a Centre angle of 45^{o} and height of 20 mm. Viscoelastic Abrasive medium moves through the Internal spline shaft due to pressure difference, meanwhile, the gear attached to the spline shaft gets rotary motion through an intermediate gear, which in turn meshes with Motor gear.

Fig.6.38 Solid model of Spline shaft and the Arc magnet

6.4.1 Spline shaft Mesh in ANSYS FLUENT 15: Figure 6.39 below shows the mesh of the SPLINE SHAFT obtained on the ANSYS FLUENT 15. The total number of Nodes is 300000 and the total number of elements was 1060000. It may be noted that this is the configuration for a coarse Mesh. The result has been checked for the finer and medium mesh also and it has been found that the result is independent of the mesh size. it is important to note that the use of CFD simulation leads to better and faster design, lesser the cycle time, free from external environment and gives full-scale simulations. So the selection of ANSYS FLUENT is based on the above important inference.

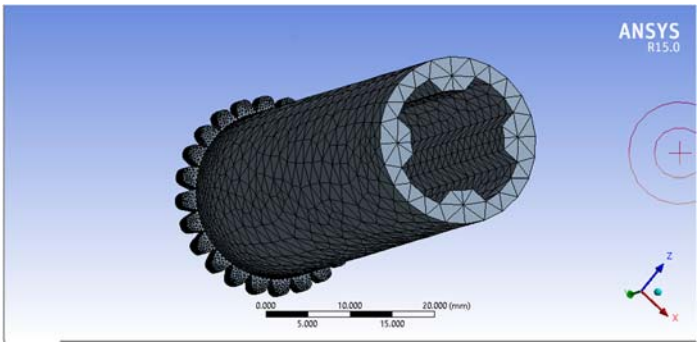

Fig. 6.39 Spline Shaft Mesh

6.4.2 Simulation and Modelling of Spline shaft Assembly Mesh: Figure 6.40 below shows the mesh of the SPLINE SHAFT ASSEMBLY obtained on the ANSYS FLUENT 15. The total number of Nodes is 368549 and the total number of elements was 1069268. It contains the spline shaft along with the magnet which is circumscribing the fluid domain that is representing the viscous fluid whose viscosity and density are 0.954 Kg m/sec and the density of the medium is 1781 Kg/m3. The boundary condition taken for the simulation is the pressure inlet and outlet. Note that this is the configuration for a coarse mesh. The result has been checked for the finer and medium mesh and it has been found that the result is independent of the mesh size. The important point to be noted here is that the solution given by the CFD is Discreet as the data

available is only at the grid or mesh nodes, we do not have the solution in between the mesh size, to overcome that the mesh size must be taken small or very close to each other.

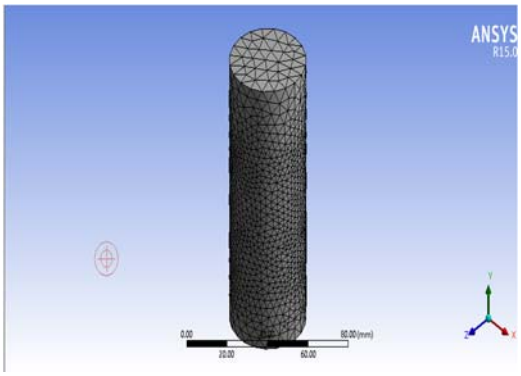

Fig. 6.40 Spline Shaft Assembly Mesh

The file was further analyzed for 3 different extrusion pressure where the extrusion pressure is the difference between the upper and the lower values of pressures considered. Extrusion pressures taken considered during the simulation are10, 15, and 20 MPa, and a graph is plotted between the total number of iterations and the X, Y, and Z velocity and energy Vs iterations for each case.

6.4.3 Modelling and Simulation for 10 Mpa Extrusion Pressure:

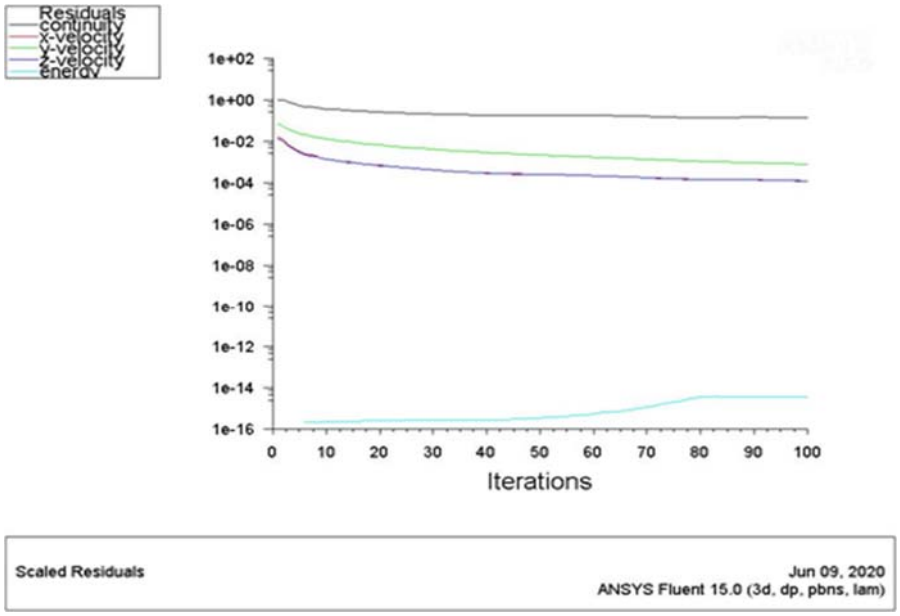

Graph.6.1 Velocity vs Iteration Graph for 10 MPa Extrusion Pressure

Graph.6.1. above shows the variations of velocities with the iterations. It may be noted here that that the total energy curve varies from the 60th iteration when the extrusion pressure is 10 MPa. Also, another important thing to be noted here is that the total energy curve must be below the velocity curves to make a stable and smooth flow. The simulation of the Spline shaft on ANSYS

FLUENT 15 software under the extrusion pressure of 10 MPa which means the difference of the upper and lower pressure is 10 MPa. The upper pressure applied is 20 MPa which is inlet pressure for simulations and the lower pressure applied is 10 MPa which is the outlet pressure.

Fig.6.41 below shows the pressure distribution for the spline shaft. The simulation results show that the maximum value of pressure is at the entry of the spline shaft which is about 18.91 MPa and the minimum pressure is 4.41 MPa. It is evident and satisfies the phenomenon of the bell effect.

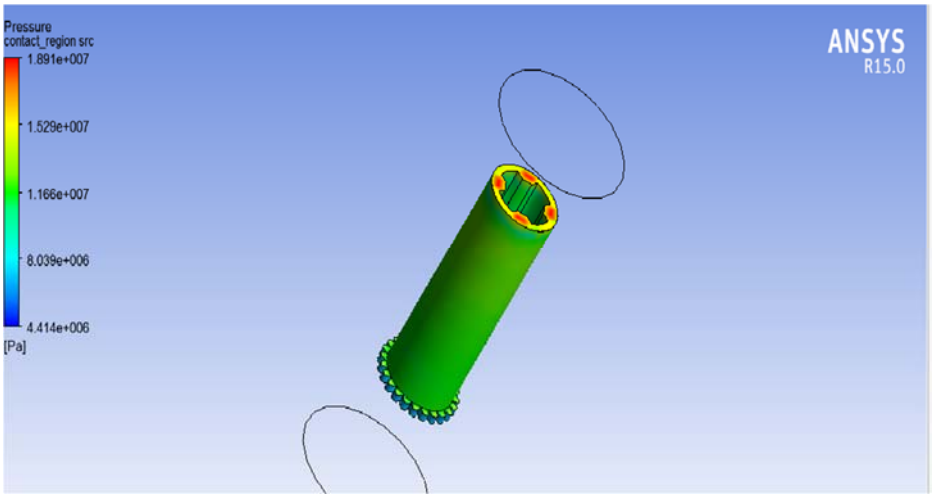

Fig.6.41 Pressure distribution for 10 MPa Extrusion Pressure

Fig.6.42 below shows the force distribution due to an extrusion pressure of 10 MPa. The simulation results show that the maximum value of the force applied by the fluid on the surface of the splined shaft is 121.9 N under the 10 MPa Extrusion pressure, while the minimum force is about 0.1493 N.

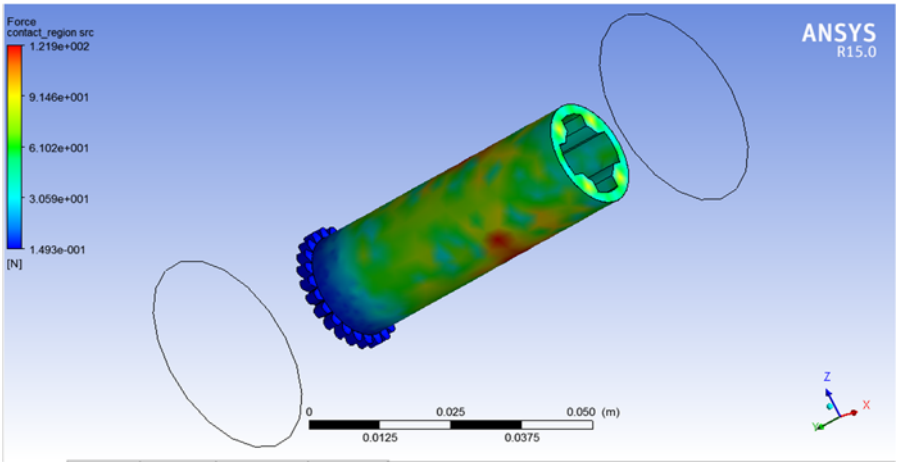

Fig.6.42 Force distribution for 10 MPa Extrusion Pressure

Fig. 6.43 below shows the Velocity distribution for an extrusion pressure of 10 Mpa. The simulation results show that the maximum value of the velocity is 94.14 m/s and the minimum value is 0.3122 m/s.

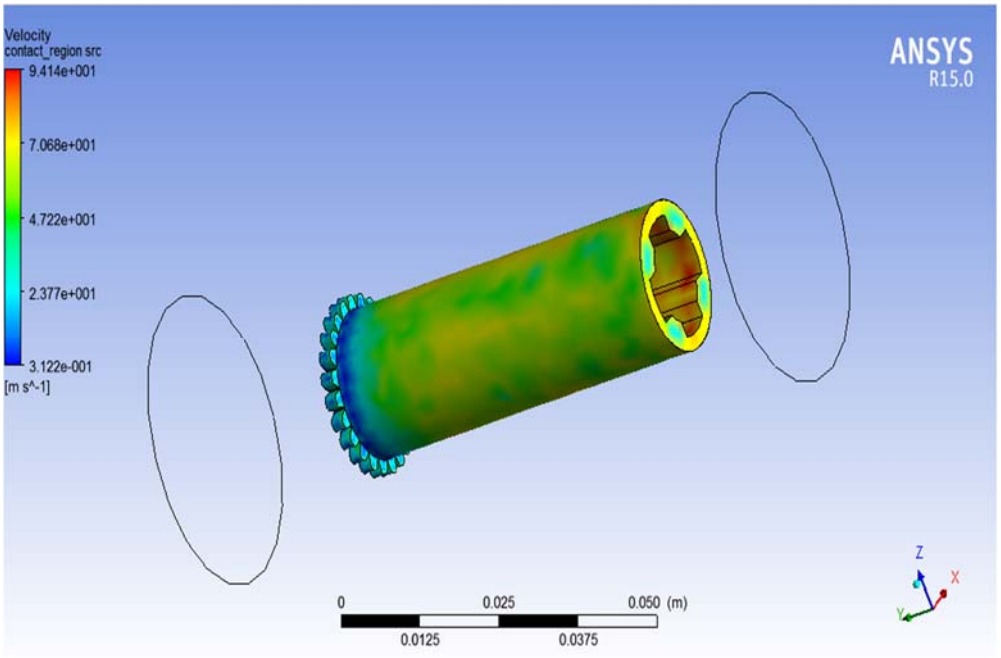

Fig.6.43 Velocity distribution for 10 MPa Extrusion Pressure

6.4.4 Modelling and simulation for 15 MPa Extrusion Pressure:

Graph.6.2 below shows the variation of velocities with the iterations. It may be noted here that that the total energy curve varies with the 65th iteration when the extrusion pressure is 15 MPa. Also, another important thing to be noted here is that the total energy curve must be below the velocity curves (Velocity in, X, Y, and Z directions) to make a stable and smooth flow. The simulation of the Spline shaft on ANSYS FLUENT 15 software under the extrusion pressure of 15 MPa which means that the difference between the upper and lower pressure is 15 MPa. The upper pressure applied is 20 MPa which is inlet pressure for simulations and the lower pressure applied is 5 MPa which is the outlet pressure.

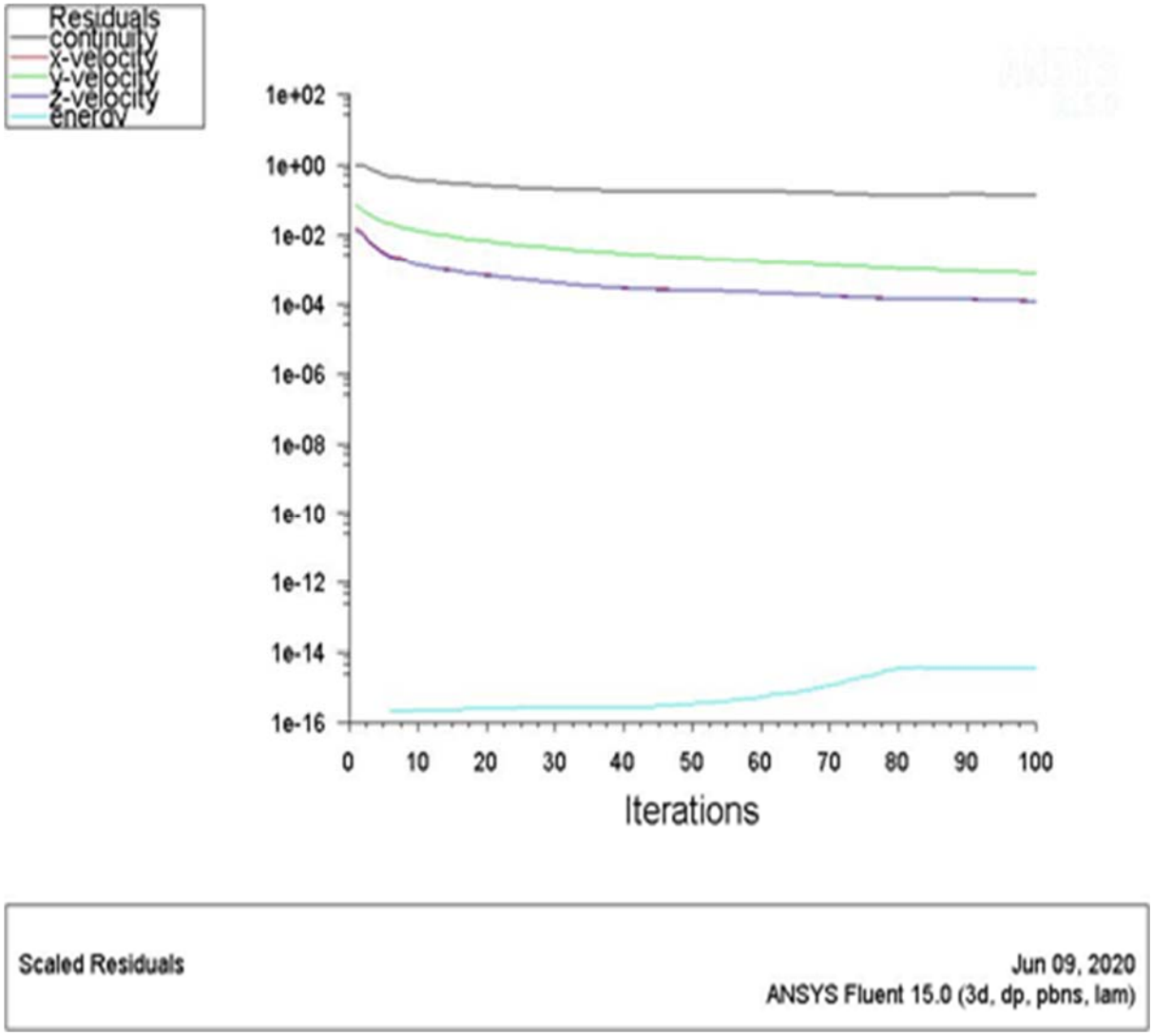

Graph.6.2. Velocity vs Iteration Graph for 15 MPa Extrusion Pressure

Fig.6.44 below shows the pressure distribution for the spline shaft. The simulation results show that the maximum value of pressure is at the entry of the spline shaft which is about 22.18 MPa and the minimum pressure is – 13.8 MPa, it is evident and satisfies the phenomenon of the bell effect.

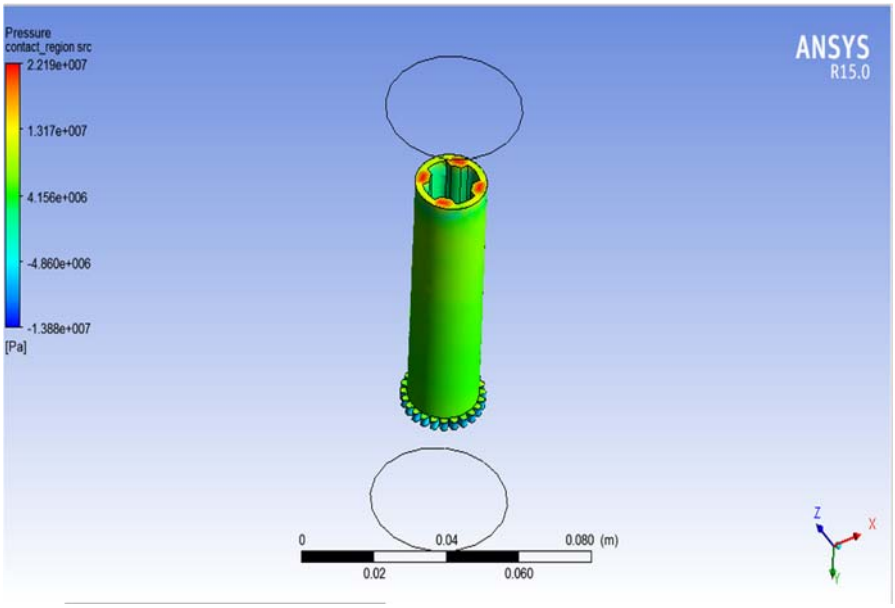

Fig. 6.44 Pressure distribution for 15 MPa Extrusion Pressure

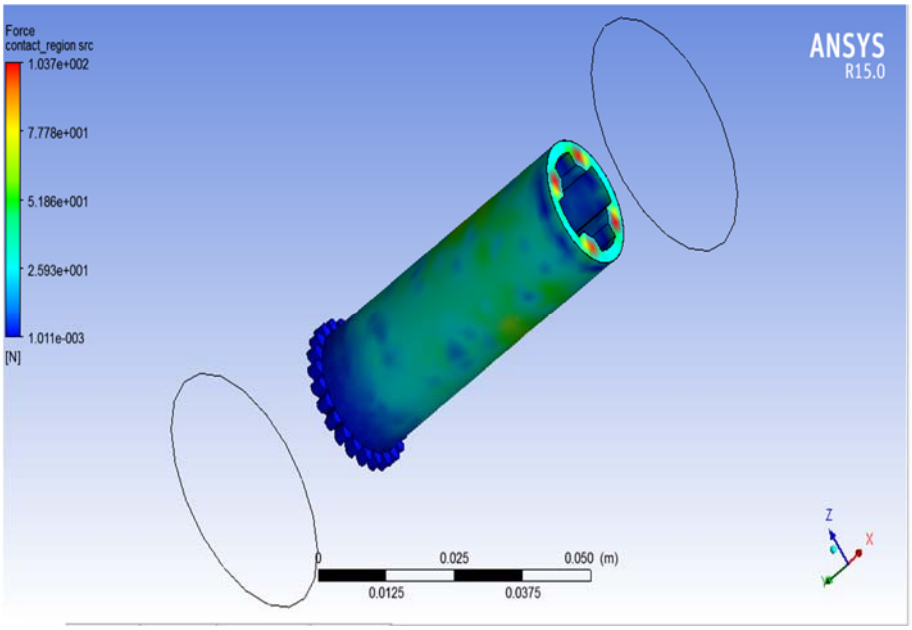

Fig. 6.45 Force distribution for 15 MPa Extrusion Pressure

Fig.6.45 above shows the force distribution for an Extrusion pressure of 15 MPa. The simulation results show that the maximum value of the force applied by the fluid on the surface of the splined shaft is 103.7 N, while the minimum force is about 0.01 N.

Fig.6.46 below shows the velocity distribution for an Extrusion pressure of 15 MPa. The simulation results show that the maximum value of Velocity is 153.9 m/s and the minimum value of velocity is 0.2963 m/s.

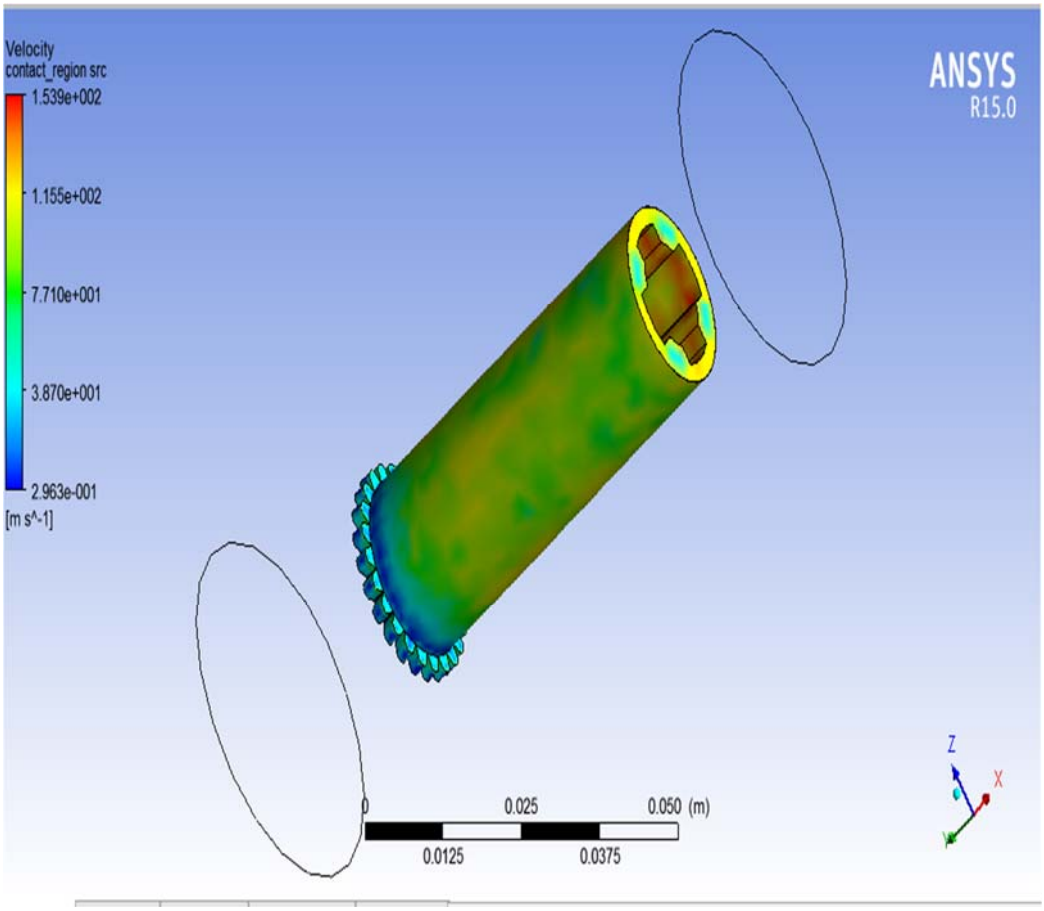

Fig.6.46 Velocity distribution for 15 MPa Extrusion Pressure

6.4.5 Modelling and Simulation for 20 MPa Extrusion Pressure:

Graph.6.3 below shows the variation of velocities with the iterations. It may be noted here that that the total energy curve varies with the 75th iteration when the extrusion pressure is 20 MPa. Also, another important thing to be noted here is that the total energy curve must be below the velocity curves (Velocity in, X, Y, and Z directions) to make a stable and smooth flow. The simulation of the Spline shaft on ANSYS FLUENT 15 software under the extrusion pressure of 20 MPa which means that the difference between the upper and lower pressure is 20 MPa. The upper pressure applied is 21.5MPa which is inlet pressure for simulations and the lower pressure applied is 1.5 MPa which is the outlet pressure.

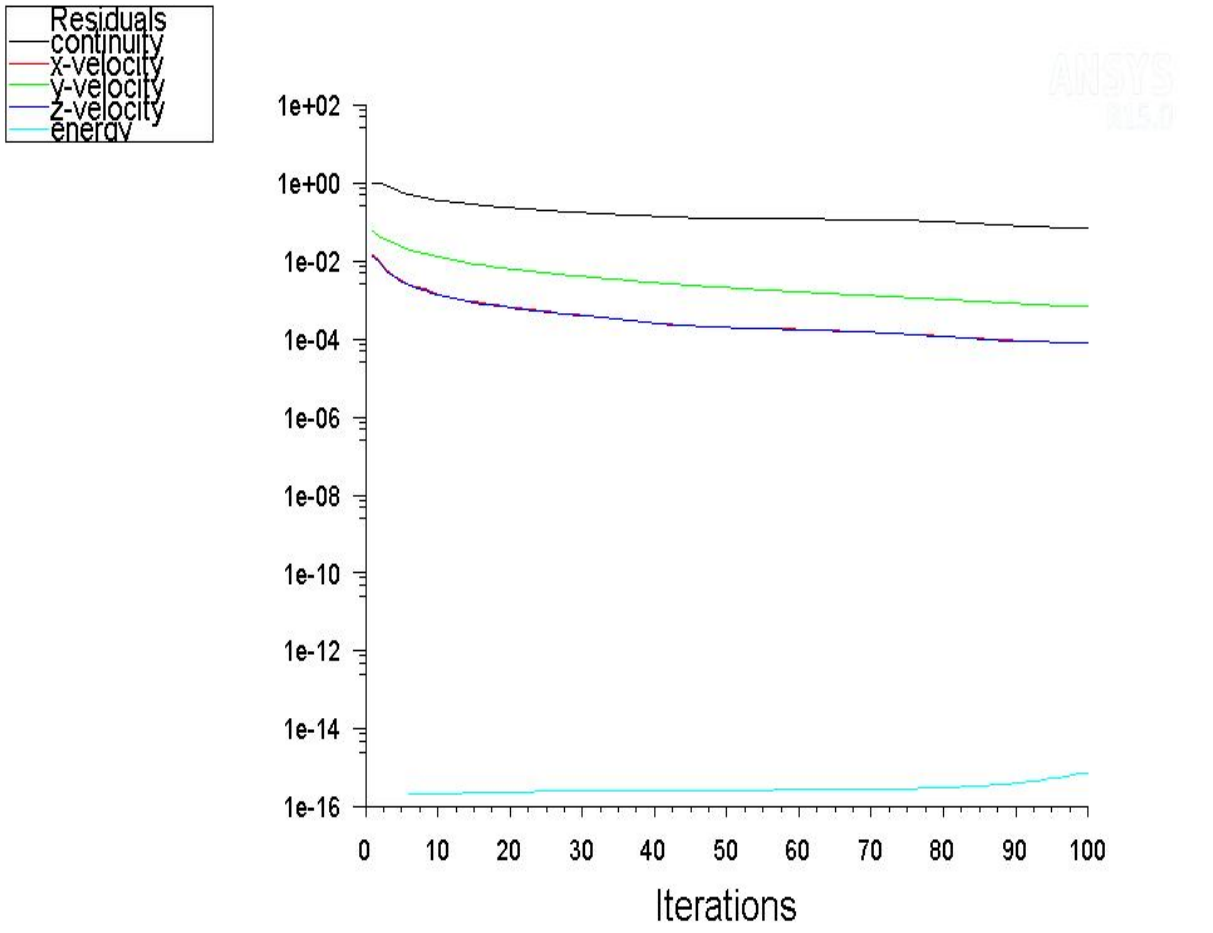

Graph.6.3. Velocity vs Iteration Graph for 20 MPa Extrusion Pressure

Fig.6.47 below shows the pressure distribution for the spline shaft. The simulation results show that the maximum value of pressure is at the entry of the spline shaft which is about 38.27 MPa and the minimum pressure is 12.23 MPa, it is evident and satisfies the phenomenon of the bell effect.

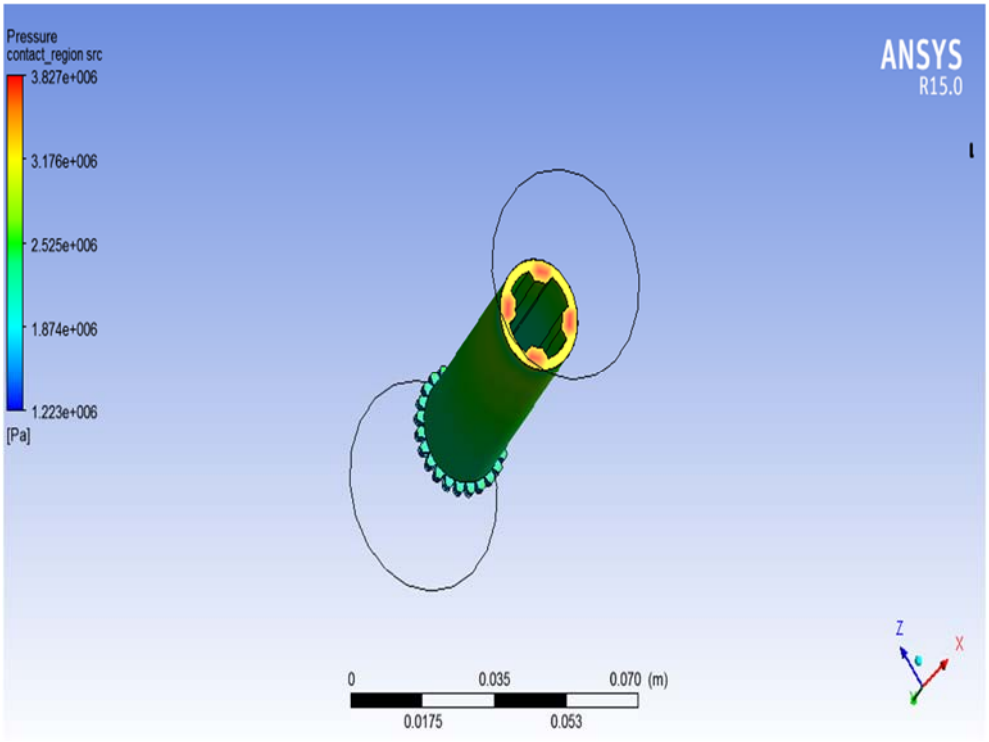

Fig.6.47 Pressure distribution for 20 MPa Extrusion Pressure

Fig.6.48 below shows the force distribution for an Extrusion pressure of 20 Mpa. The simulation results show that the maximum value of the force applied by the fluid on the surface of the splined shaft is 25.60 N, while the minimum force is about 0.003785 N.

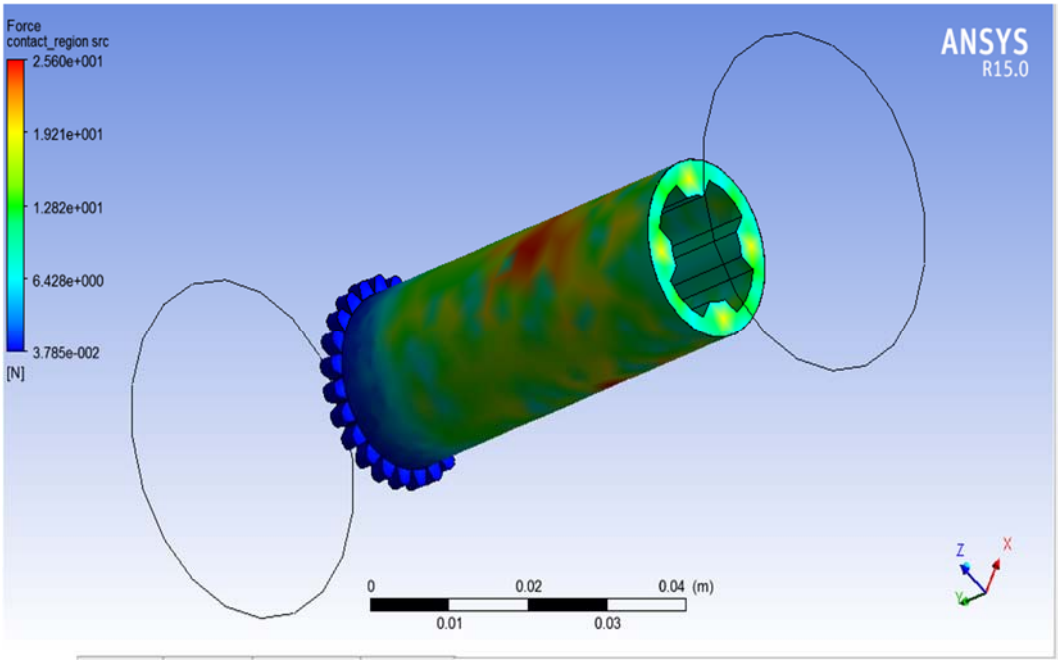

Fig.6.48.Force distribution for 20 MPa Extrusion Pressure

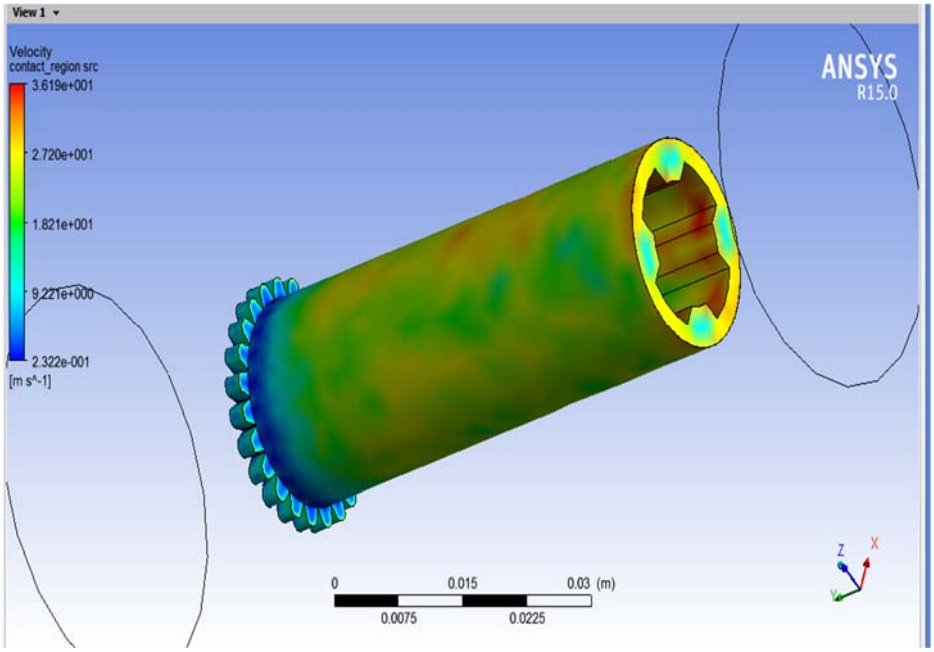

Fig.6.49 Velocity distribution for 20 MPa Extrusion Pressure

Fig.6.49 above shows the velocity distribution for an Extrusion pressure of 20 Mpa.The simulation results show that the maximum value of Velocity is 36.19 m/s and the minimum value of velocity is 0.2322 m/s.

6.4.6 Analysis of flow parameters Simulated from 6.4.3 to 6.4.5: In Viscoelastic Magnetic abrasive flow finishing of Internal spline shafts, the flow parameters have been Simulated and their result has been tabulated below. In total three Extrusion pressures; 10 MPa, 15 MPa, and 20 MPa have been considered and the numerical values of the flow parameters have been tabulated for all the three extrusion pressures as mentioned in Table 6.3 below.

Table 6.3 Analysis of Flow parameters for 10 MPa, 15MPa & 20MPa extrusion pressure.

Extrusion Pressure 10 MPa			**Extrusion Pressure 15MPa**			**Extrusion Pressure 20 MPa**		
Pressure	**Force**	**Velocity**	**Pressure**	**Force**	**Velocity**	**Pressure**	**Force**	**Velocity**
$1.881x10^{7}$	121.9	94.14	$2.21x10^{7}$	103.7	153.9	$3.827x10^{6}$	25.6	36.19
$1.529x10^{7}$	91.4	70.61	$1.317x10^{7}$	77.7	115.5	$3.176x10^{6}$	19.21	27.2
$4.156x10^{6}$	***51.86***	***47.22***	***$4.146x10^{6}$***	***51.86***	***77.10***	***$2.525x10^{6}$***	***12.82***	***18.21***
$8.039x10^{6}$	30.59	23.77	$4.08x10^{6}$	25.83	38.7	$1.87x10^{6}$	6.428	9.221
$4.41x10^{6}$	14.93	0.312	$-1.31x10^{7}$	$1.01x10^{-3}$	0.293	$1.22x10^{6}$	0.03875	0.2322

6.5. Description of Taylor Hobson's Tally surf: Fig 6.50 below shows the surface measurement instrument known as TalySurf. Works with DC battery power source, with a rated voltage of 3Volts. It can be used for finding Surface Roughness(Ra), Rz, It can be used for measuring the surface roughness of Gears, Crankshafts, etc. For every surface, 5 values have been recorded and the median value has been considered for analysis. The maximum linear length that could be measured is 60 mm.

Fig. 6.50 Surface roughness measurement of Internal Spline by TalySurf

6.6. Precision Balance: Fig 6.51 Shows the Precision balance used for measuring the

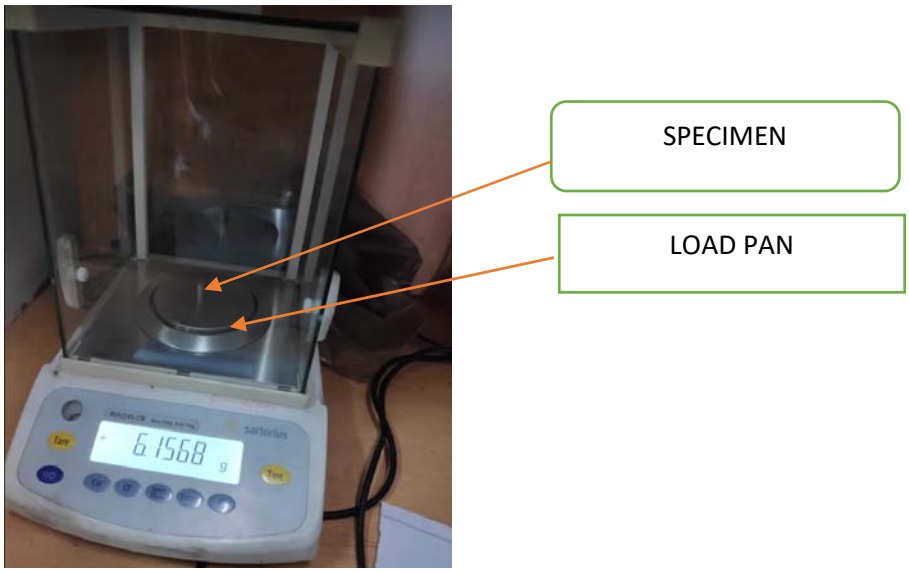

Fig.6.51. Precision balance

Specimen. The static weight is measured based on the load cell principle. Sartorius company makes Precision balance with a capacity of 200 grams with a resolution of 0.10 mg is used during present research work.

6.7 Process Parameters considered for internal finishing of the Spline shaft:

Six parameters with each having three levels have been considered The parameters considered are mentioned below.

The following process parameters have been considered for experimenting.

I. Magnetic Flux density[MFD]
II. Extrusion pressure [EP]
III. Abrasive mesh number [AMN]
IV. Rotational Speed of the Workpiece [RSOW]
V. Number of Cycles[NOC]
VI. Finishing Time [FT]

The magnitude of three process parameters has been shown in Table.6.4

Table 6.4 Three Levels of Process Parameters

	PROCESS PARAMETERS					
LEVEL	MFD[T]	EP [MPa]	AMN	RSOW Rpm	No of Cycles[NOC]	FINISHING TIME
1	0.6201	10	320	120	12	180
2	0.8471	15	400	180	15	240
3	0.9618	20	600	240	18	300

6.8. Effect of Process parameters on Internal Finishing: A brief discussion will be made about the effect of process parameters based on the literature survey for the internal finishing of the surfaces based on Magnetic Abrasive flow finishing, which is the basis for internal finishing of the present research work.

i. **Magnetic Flux density:** As per Takeo Shinmura et al [35] Magnetic Flux density does not depend on the size of the Carbonyl Particle. So, the flux density variation due to the CIP size variation, if any in the Viscoelastic Magnetic Abrasive medium is negligible. Hitomi Y.Wang et al. [38] in their investigation found that the Magnetic field strength decides the finishing conditions of the internal finishing process. As per Sehijpal Singh et al [41], the higher the flux density, the better would be the surface finish obtained. As per Yan Wang et al.[44,46] the utility of two permanent magnets, would jumble the abrasive and the carbonyl mixture as the flux distribution is not uniform and improper finishing takes place. Sunil Jha Et al. [47] in their

research finding found that the finishing increases with the increase in flux density, however not in proportion.

ii. **Extrusion pressure:** Extrusion pressure is the pressure difference between the inlet and outlet pressures. As per V K Jain et al. [48], Higher extrusion pressures transfer more amount of energy to the abrasive particles for removing the material. However, after an optimum value of extrusion pressure, the finishing becomes difficult. The velocity of the medium flow depends on the Extrusion pressure, for better finishing the medium flow should not be very high as at higher velocities abrasive particles do not contact the surface[36].

iii. **Abrasive Mesh Number:** Abrasive Mesh number has an important role in the finishing process. As per Yan Wang et al.[46] A smaller grain size would give a better surface finish. For material removal (Δm) to be higher abrasive size must be bigger.

iv. **The rotational speed of the Workpiece:** In an experimental investigation at 20000 rpm of the workpiece by Junmokang et al.[54] it has been found that at high speeds due to centrifugal forces the indentation takes place on the surface and this increases the metal removal, however, it reduces the surface finish. Yan Wang et al. [2005] in their research work observed that Considerable improvement in metal removal is observed with the increase in rotational speed, however, very high speeds increase the frictional forces dominate the magnetic force.

v. **No of cycles:** Material removal depends upon the no of cycles, however an increase in no of strokes or cycles will not increase the metal removal proportionally, after reaching an optimal value further finishing becomes difficult.

vi. **Finishing Time:** Material removal is proportional to the Finishing time. However, after reaching an optimum value, no material removal takes place as the no of peaks to be sheared would considerably reduce.

6.9. Assumptions made for Finishing of Internal Splines using VEMAF process:

1. Flow-through the internal spline shaft is considered to be axisymmetric.
2. Viscoelastic Magnetic Abrasive medium flows through the Magnetic field obeys the Linear Viscosity principle.
3. VEMAF medium is homogeneous and properties are isotropic.
4. VEMAF medium does not leak laterally.
5. Flow for a particular extrusion pressure is assumed to be Steady flow.
6. Abrasive geometry has been assumed to be Spherical.

6.10. Mechanism of Material removal in Internal finishing of Spline Shafts:

The mechanism of material removal applicable to Abrasive Flow Machining can be applied to the Finishing of the Internal Spline shafts using Viscoelastic Magnetic abrasive medium. Rajender K. Jain et al. (39) in their research work on modeling of the Abrasive Jet machining have proposed Certain points which would be considered in present research work also. In the present research work, the specimen used is made of Mild Steel, which is considered to be ductile. The Mechanism of material removal for the ductile material are as mentioned below:

i. The Viscoelastic Magnetic Abrasive Finishing (VEMAF) Medium prepared is considered to behave as Self deformable abrasive stone.
ii. The pressure generated inside the specimen, in the present case, internal spline shaft would start indenting once the local pressure reaches the yield stress value of the specimen. Mild steel is having a yield stress value of 250 MPa and as per the simulation work carried for all the three extrusion pressures considered for the present research work, the magnitude of pressures produce is higher than the Yield stress of the specimen material.
iii. Due to the magnetic field around the specimen, the CIP particles in the VEMAF medium reorient themselves and form a chain-like structure spreading in the radial direction and these chains entrap the Silicon Carbide (SiC) abrasive and project them to the internal surface of the spline shaft.
iv. As the medium inside the specimen flows with steady velocity and the specimen rotates with uniform angular velocity, the abrasive particles entrapped by the Carbonyl Iron Particles, strike the surface of the specimen at a small angle.
v. Material removal comprises two stages. In stage 1, when the abrasive strikes the internal surface, makes a micro indent and a ridge. The material displaced from the indent forms these ridges. In stage 2 the removal of the material in the form of chips takes place. Owing to the reciprocal motion of the medium inside the Spline shaft material removal takes place due to micro plowing and micro-cutting
vi. More number of abrasive particles contribute to Micro indentation and material removal in the form of Micro-chips and due to the reciprocal motion of the medium, the chip removal can be considered to be due to Low Cycle Fatigue Fracture.

6.11. The objective of the present Experimentation: The objective of the present experimental work is to obtain the minimum Surface roughness $\mathbf{R_a}$, the maximum metal removal $\Delta\mathbf{m_{ax}}$, and Maximum reduction in the surface roughness ΔRa.

It is assumed in the present work that the variation in a process parameter is significant for the value of the p-value is less than 010. ***So optimization has been done by using Taguchi's Orthogonal array of the experiment for Maximum material removal [∆m] only.***

6.12. Experiment Procedure: The following procedure has been adopted for performing the Experiment.

1. Experiments have been performed based on Taguchi's Orthogonal Array of Design principle. For finding the set of process parameters to be chosen, Minitab 17 software is used, and accordingly, the L27 table has been prepared.
2. In total Nine specimens have been used and the first nine experiments have been performed based on the Magnetic flux density Level I, accordingly the Fixture is loaded with two magnets.
3. Three different Viscoelastic Magnetic Abrasive media has been prepared and loaded in the medium cylinder based on the experimental parametric values.
4. Extrusion pressure, No of cycles, Finishing time, and rotational speed of the Workpiece is selected.
5. Initial surface roughness and weight has been measured and recorded in the table.
6. After completing each experiment final value of the mass and surface roughness is measured.
7. The same nine pieces have been used for the second level of experiments, accordingly, four magnets for the second level have been placed in the Aluminium fixture.
8. Fresh Viscoelastic Magnetic Abrasive medium has been used for each experiment.
9. Measuring the weight and surface roughness has been carried out after completing the experiment and the data has been recorded.
10. The same procedure has been followed for the third level of the flux density also.
11. After completion of each experiment, the specimen is thoroughly cleaned with Acetone such that there are no loose particles are not left inside the spline shaft.

Table.6.5 L27 Orthogonal Array of Design of experiments.

MFD T	EP MPa	AMN	RSOW Rpm	NOC	FT Sec	Initial mass m_i (g)	Final mass m_f (g)	Metal removal Δm(g)	**Ra Initial µm**	***Ra Final µm***	**Δ Ra *µm***
0.6210	10	320	120	12	180	91.0369	91.0337	0.0032	0.444	***0.441***	0.003
0.6210	10	320	120	15	240	88.6743	88.6691	0.0052	0.201	***0.193***	0.008
0.6210	10	320	120	18	300	90.5962	90.5853	0.0109	0.248	***0.243***	0.005
0.6210	15	400	180	12	180	92.3642	92.3559	0.0083	*0.383*	***0.359***	0.024
0.6210	15	400	180	15	240	91.4411	91.4225	0.0186	*0.322*	***0.305***	0.017
0.6210	15	400	180	18	300	89.8562	89.8271	0.0291	0.331	***0.306***	0.025
0.6210	20	600	240	12	180	89.3149	89.3107	0.0042	0.429	***0.42***	0.009
0.6210	20	600	240	15	240	89.4643	89.4607	0.0036	0.305	***0.273***	0.032
0.6210	20	600	240	18	300	90.7643	90.7578	0.0065	0.42	***0.375***	0.045
0.8417	10	400	240	12	240	90.7578	90.7377	0.0201	*0.375*	***0.299***	0.076
0.8417	10	400	240	15	300	91.0337	90.9962	0.0375	0.441	***0.345***	0.096
0.8417	10	400	240	18	180	88.6691	88.6549	0.0142	0.193	***0.163***	0.03
0.8417	15	600	120	12	240	91.4225	91.4169	0.0056	0.305	***0.245***	0.06
0.8417	15	600	120	15	300	90.5853	90.5781	0.0072	*0.243*	***0.153***	0.09
0.8417	15	600	120	18	180	89.4607	89.4555	0.0052	0.273	***0.165***	0.108
0.8417	20	320	180	12	240	92.3559	92.3483	0.0076	*0.359*	***0.273***	0.079
0.8417	20	320	180	15	300	89.8271	89.8024	0.0186	*0.306*	***0.207***	0.099
0.8417	20	320	180	18	180	89.3107	89.3041	0.0066	0.42	***0.322***	0.098
0.9618	10	600	180	12	300	90.9962	90.9826	0.0136	*0.345*	***0.223***	0.122
0.9618	10	600	180	15	180	89.3041	89.2885	0.0156	*0.322*	***0.22***	0.102
0.9618	10	600	180	18	240	92.3483	92.32	0.0283	*0.273*	***0.164***	0.109
0.9618	15	320	240	12	300	90.5781	90.5677	0.0104	*0.153*	***0.101***	0.052
0.9618	15	320	240	15	180	89.8024	89.7731	0.0293	0.207	***0.104***	0.103
0.9618	15	320	240	18	240	91.4169	91.3888	0.0281	0.245	***0.152***	0.093
0.9618	20	400	120	12	300	89.4555	89.4507	0.0048	*0.165*	***0.111***	0.054
0.9618	20	400	120	15	180	88.6691	88.6649	0.0042	*0.163*	***0.103***	0.06
0.9618	20	400	120	18	240	90.7377	90.7133	0.0064	*0.299*	***0.201***	0.098

6.13. **Surface roughness Measurement after completion of experiments L19 to L27:**

Average surface roughness (Ra) has been measured using TalySurf after completing each experiment. However, the surface roughness after completing the last nine experiments has been given furnished in the thesis. L19 to L27 in the last nine rows of L27 of Orthogonal Array of Design of experiments

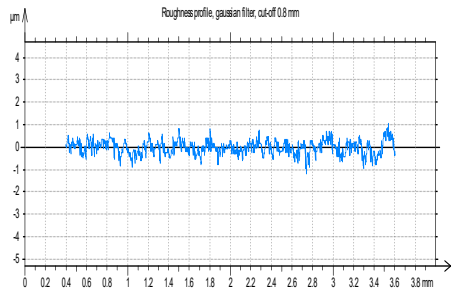

Parameters calculated on the profile Profile

* Parameters calculated by mean of all the sampling lengthes.
* A microroughness filtering is used, with a ratio of 2.5 µm.

Roughness Parameters, Gaussian filter, 0.8 mm

Ra = 0.223 µm

Graph.6.4. The surface roughness of specimen after L19

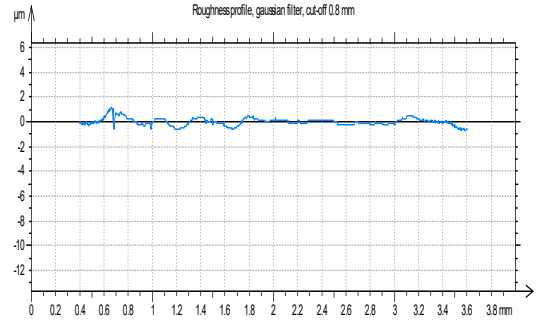

Parameters calculated on the profile Profile

* Parameters calculated by mean of all the sampling lengthes.
* A microroughness filtering is used, with a ratio of 2.5 µm.

Roughness Parameters, Gaussian filter, 0.8 mm

Ra = 0.22 µm

Graph.6.5. The surface roughness of specimen after L20

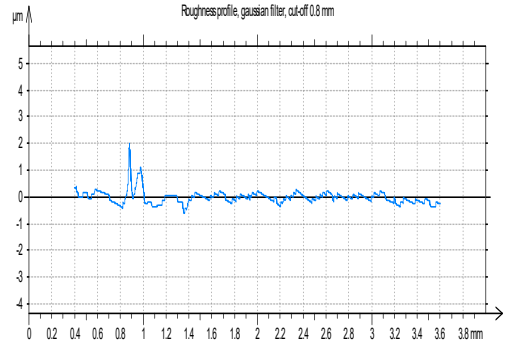

Parameters calculated on the profile Profile

* Parameters calculated by mean of all the sampling lengthes.
* A microroughness filtering is used, with a ratio of 2.5 µm.

Roughness Parameters, Gaussian filter, 0.8 mm

Ra = 0.164 µm

Graph.6.6. The surface roughness of specimen after L21

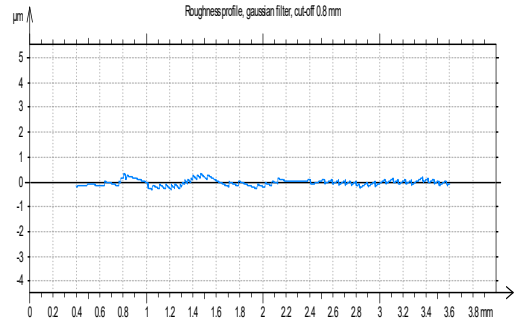

Parameters calculated on the profile Profile

* Parameters calculated by mean of all the sampling lengthes.
* A microroughness filtering is used, with a ratio of 2.5 µm.

Roughness Parameters, Gaussian filter, 0.8 mm

Ra = 0.101 µm

Graph.6.7. The surface roughness of specimen after L22

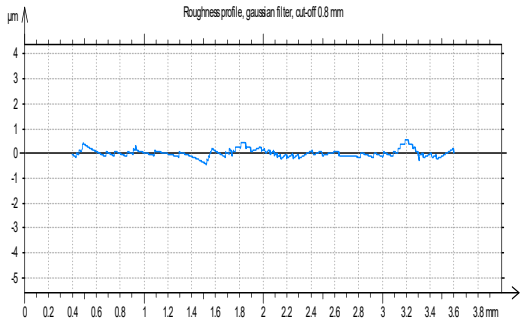

Parameters calculated on the profile Profile

* Parameters calculated by mean of all the sampling lengthes.
* A microroughness filtering is used, with a ratio of 2.5 µm.

Roughness Parameters, Gaussian filter, 0.8 mm

Ra = 0.104 µm

Graph.6.8. The surface roughness of specimen after L23

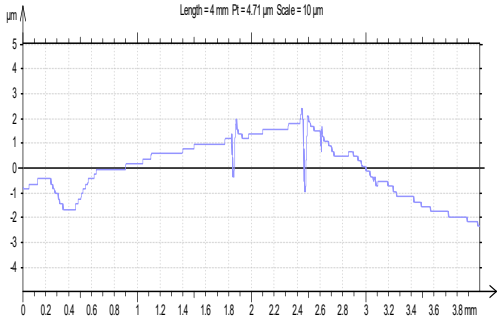

Parameters calculated on the profile Profile

* Parameters calculated by mean of all the sampling lengthes.
* A microroughness filtering is used, with a ratio of 2.5 µm.

Roughness Parameters, Gaussian filter, 0.8 mm

Ra = 0.152 µm

Graph.6.9. The surface roughness of specimen after L24

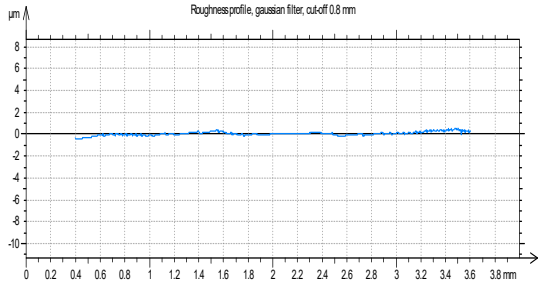

Parameters calculated on the profile Profile

* Parameters calculated by mean of all the sampling lengthes.
* A microroughness filtering is used, with a ratio of 2.5 µm.

Roughness Parameters, Gaussian filter, 0.8 mm

Ra = 0.111 µm

Graph.6.10. The surface roughness of specimen after L25

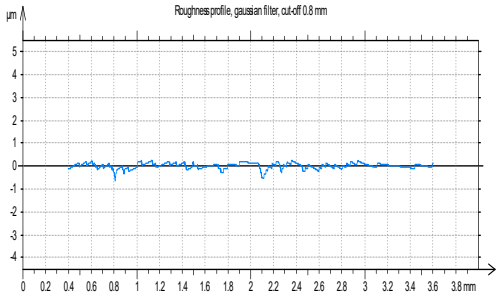

Parameters calculated on the profile Profile

* Parameters calculated by mean of all the sampling lengthes.
* A microroughness filtering is used, with a ratio of 2.5 µm.

Roughness Parameters, Gaussian filter, 0.8 mm

Ra = 0.103 µm

Graph.6.11. The surface roughness of specimen after L26

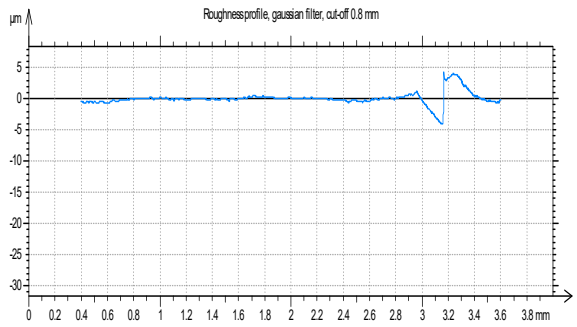

Parameters calculated on the profile Profile

```
* Parameters calculated by mean of all the sampling
lengthes.
* A microroughness filtering is used, with a ratio of
2.5 µm.

Roughness Parameters, Gaussian filter, 0.8 mm

   Ra    = 0.201 µm
```

Graph.6.12. The surface roughness of specimen after L27

6.14. Optimization Based on Taguchi's Optimisation Model:

Minitab 17 is used for finding the Optimization values for the experiments performed based on Taguchi's Orthogonal Array of Design. The objective is to find the ranking of the process parameters for obtaining the maximum material removal [Δm].

Taguchi Analysis: Δm versus MFD, EP, AMN, RSOW, NOC, FT

Linear Model Analysis: SN ratios versus MFD, EP, AMN, RSOW, NOC, FT

Estimated Model Coefficients for SN ratios

Term	Coef	SE Coef	T	P
Constant	-39.9658	0.5853	-68.284	0.000
MFD 0.6210	-2.4708	0.8277	-2.985	0.010
MFD 0.8417	0.6789	0.8277	0.820	0.426
EP 10	2.3359	0.8277	2.822	0.014
EP 15	1.9805	0.8277	2.393	0.031
AMN 320	0.3237	0.8277	0.391	0.702
AMN 400	1.7273	0.8277	2.087	0.056
RSOW 120	-5.1658	0.8277	-6.241	0.000
RSOW 180	3.0787	0.8277	3.720	0.002
NOC 12	-2.6753	0.8277	-3.232	0.006
NOC 15	1.1346	0.8277	1.371	0.192
FT 180	-2.2152	0.8277	-2.676	0.018
FT 240	0.3673	0.8277	0.444	0.664

S = 3.041 R-Sq = 87.9% R-Sq(adj) = 77.6%

Analysis of Variance for SN ratios

Source	DF	Seq SS	Adj SS	Adj MS	F	P
MFD	2	87.99	87.99	43.995	4.76	0.027
EP	2	252.09	252.09	126.046	13.63	0.001
AMN	2	65.65	65.65	32.827	3.55	0.057
RSOW	2	364.68	364.68	182.340	19.71	0.000
NOC	2	97.37	97.37	48.684	5.26	0.020
FT	2	76.11	76.11	38.054	4.11	0.039
Residual Error	14	129.49	129.49	9.249		
Total	26	1073.38				

Linear Model Analysis: Means versus MFD, EP, AMN, RSOW, NOC, FT

Estimated Model Coefficients for Means

Term	Coef	SE Coef	T	P
Constant	0.013070	0.001252	10.437	0.000
MFD 0.6210	-0.003115	0.001771	-1.759	0.100
MFD 0.8417	0.000552	0.001771	0.312	0.760
EP 10	0.003441	0.001771	1.943	0.072
EP 15	0.002685	0.001771	1.516	0.152
AMN 320	0.000252	0.001771	0.142	0.889
AMN 400	0.002841	0.001771	1.604	0.131
RSOW 120	-0.007215	0.001771	-4.074	0.001
RSOW 180	0.003185	0.001771	1.799	0.094
NOC 12	-0.004426	0.001771	-2.499	0.026
NOC 15	0.002463	0.001771	1.391	0.186
FT 180	-0.002981	0.001771	-1.684	0.114
FT 240	0.000652	0.001771	0.368	0.718

S = 0.006507   R-Sq = 76.4%   R-Sq(adj) = 56.2%

Analysis of Variance for Means

Source	DF	Seq SS	Adj SS	Adj MS	F	P
MFD	2	0.000149	0.000149	0.000075	1.76	0.208
EP	2	0.000509	0.000509	0.000255	6.01	0.013
AMN	2	0.000159	0.000159	0.000080	1.88	0.189
RSOW	2	0.000706	0.000706	0.000353	8.34	0.004
NOC	2	0.000266	0.000266	0.000133	3.14	0.075
FT	2	0.000133	0.000133	0.000066	1.57	0.243
Residual Error	14	0.000593	0.000593	0.000042		
Total	26	0.002515				

Response Table for Signal to Noise Ratios
Larger is better

Level	MFD	EP	AMN	RSOW	NOC	FT
1	-42.44	-37.63	-39.64	-45.13	-42.64	-42.18
2	-39.29	-37.99	-38.24	-36.89	-38.83	-39.60
3	-38.17	-44.28	-42.02	-37.88	-38.43	-38.12
Delta	4.26	6.65	3.78	8.24	4.22	4.06
Rank	3	2	6	1	4	5

Response Table for Means

Level	MFD	EP	AMN	RSOW	NOC	FT
1	0.009956	0.016511	0.013322	0.005856	0.008644	0.010089
2	0.013622	0.015756	0.015911	0.016256	0.015533	0.013722
3	0.015633	0.006944	0.009978	0.017100	0.015033	0.015400
Delta	0.005678	0.009567	0.005933	0.011244	0.006889	0.005311
Rank	5	2	4	1	3	6

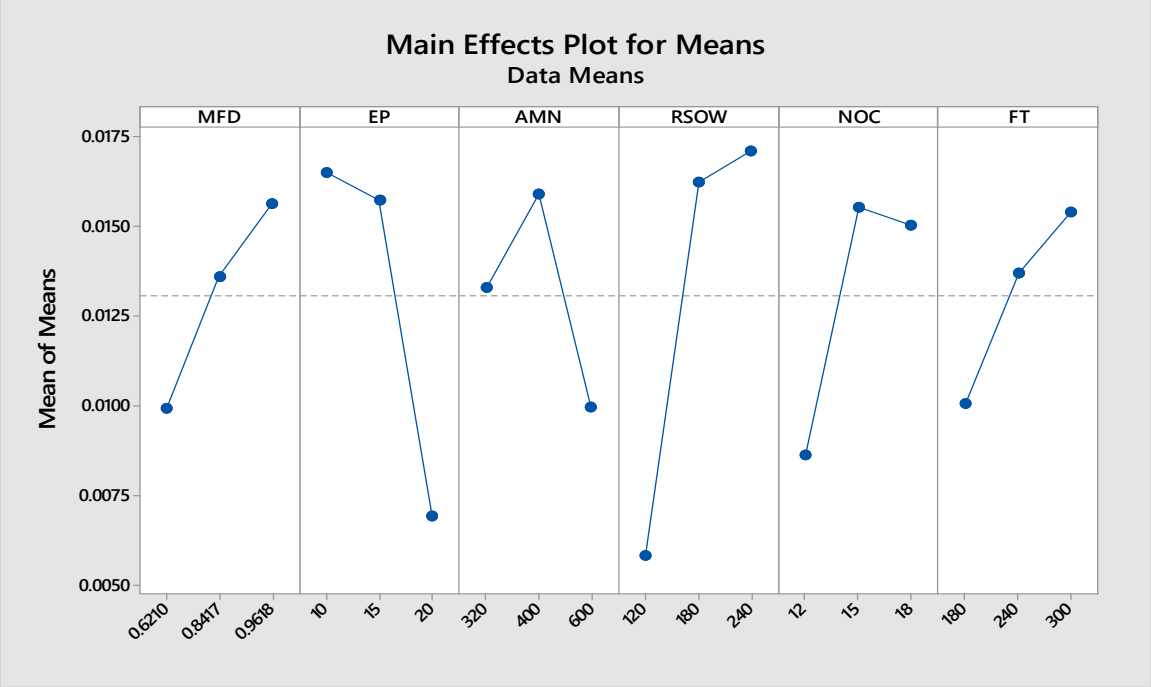

Graph.6.13 Main Plot for Means

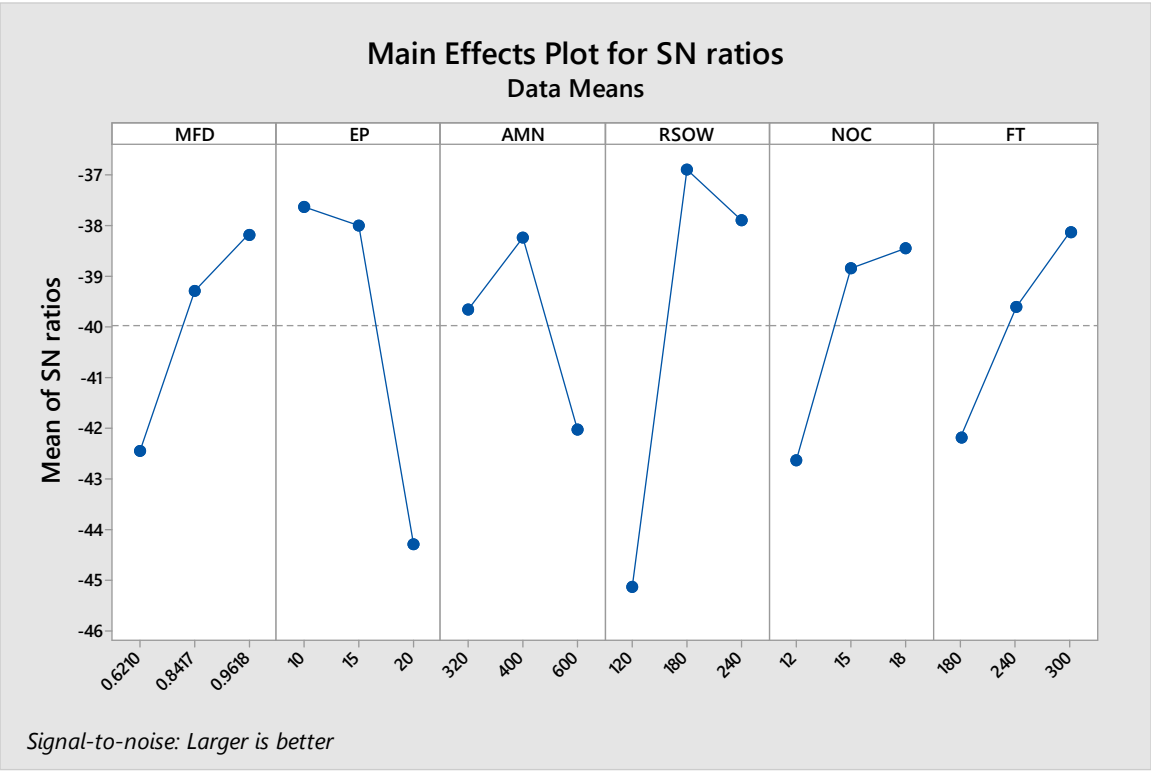

Graph.6.14 Main Plot for SN Ratio

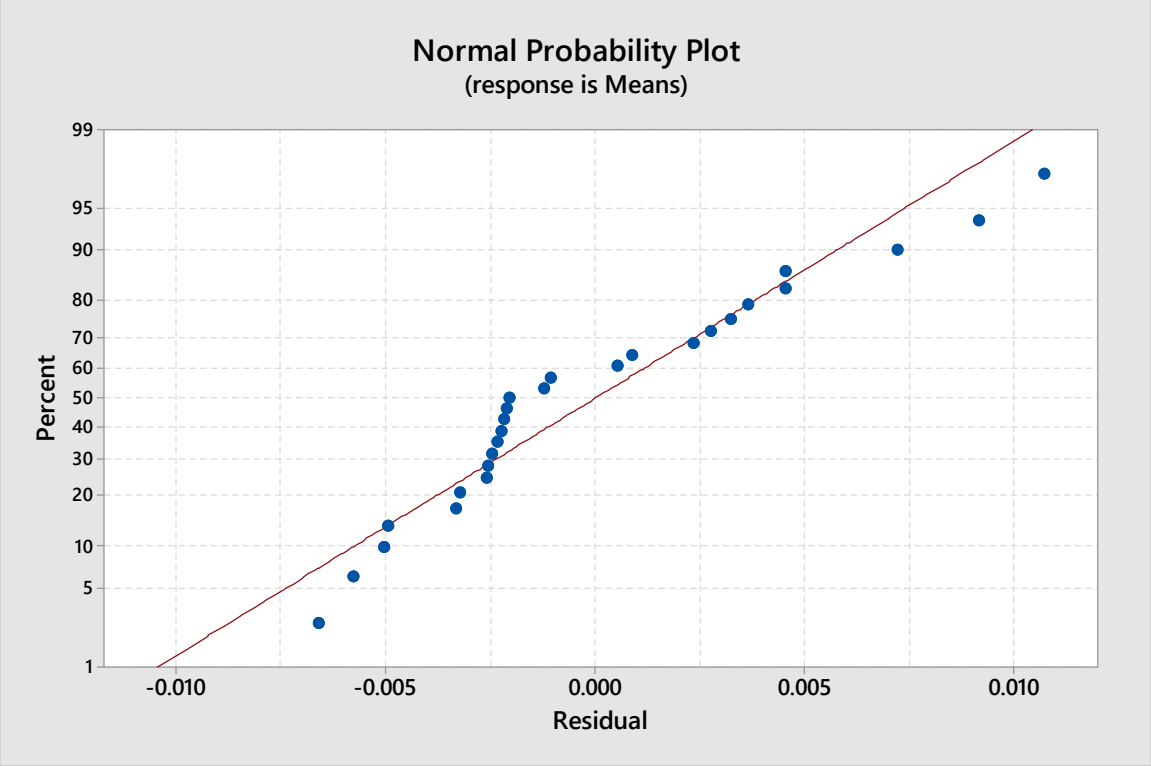

Graph.6.15 Normal Probability plot (Means)

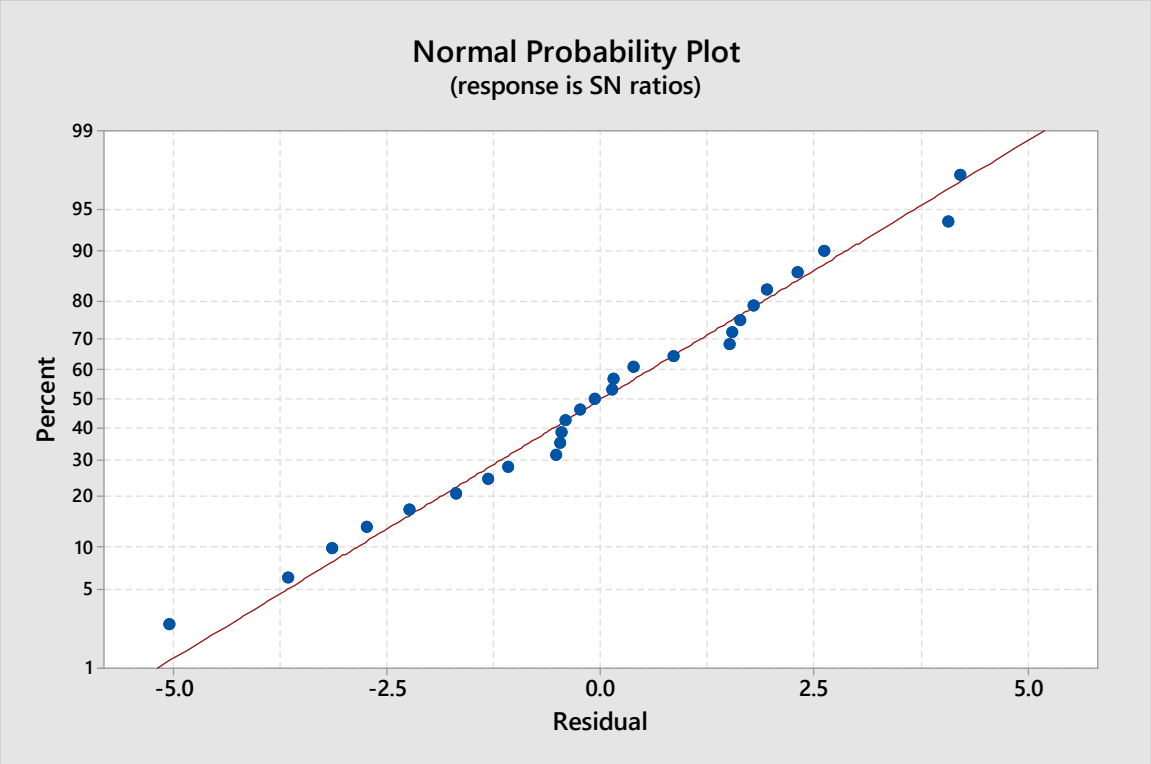

Graph. 6.16.Normal Probability Plot (SN ratio)

Fig.6.52.Finished Internal Spline Shafts

6.15. Result and Discussion:

The following observation has been made based on the Experiments conducted on the Internal Spline shaft.

1. In the present research work, the values of the flux densities considered are the median values as the maximum flux densities obtained for all the levels are confined to a specified area on the outer Cylindrical Surface of the Internal spline shaft. Whereas most of the research done earlier on internal finishing considered the maximum flux density only.
2. The minimum surface finish obtained is 0.101 μm and the initial value of the specimen decides the obtainable surface roughness, in the present case the internal spline shaft is subjected to three cycles, and the surface roughness is reduced to 0.101 μm from an initial value of surface roughness of 0.248 μm. This is in confirmation of Sunil Jha et al.[2006] research on Magnetic abrasive flow finishing.
3. Maximum reduction in the surface roughness ΔRa obtained is 0.122 μm; corresponding process parameters are :
   i. **Magnetic Flux density 0.9618T[Level 3]:** This indicates that for getting a maximum reduction in surface roughness higher amount of flux density maintains the CIP chain efficiently and hence projects the SiC abrasives to the surface to be finished. Also, the Magnetic flux density of Level 3 comprises Eight arc magnets that encompass the external surface of the Spline shaft.
   ii. Extrusion pressure 10 MPa [Level 1]: It is evident that a higher value of the
   iii. Abrasive Mesh number 600 [level 3]

iv. The rotational speed of the workpiece 180 rpm [level 2]
v. No of cycles 12 [Level1]
vi. Finishing time 300 seconds [Level 3]

4. Surface roughness (Ra) shown in Graphs 6.4, 6.6, 6.6,6.8,6.9, and 6.12 clearly show that the waviness is more prominent, especially for abrasive Meh number 320, which is coarser compared to the remaining two Abrasive Mesh numbers.
5. Reduction in surface roughness is lesser for row one of L27, where all the process parameters are at level '1'
6. Based on Taguchi's Optimisation model done for maximum material removal[Δm] with Minitab 17, the following points may be observed:
   a. Graphs 6.15 and 6.16 clearly show that all the response points are nearer to the Normal distribution line and hence the model is accepted.
   b. Values of R-Sq and R-Sq[adj] are having higher percentages respectively 87.9% and 77.6%. So the assumption of the Normal distribution is valid for Normal distribution and all the process parameters are significant.
   c. Relative ranking of the process parameters, their level and significance have been given in table 6.8 below:

Table.6.6. Status of the process parameters based on Optimisation

Process Parameter	Magnetic Flux Density[T]	Extrusion Pressure EP[MPa}	Abrasive Mesh Number	The rotational speed of the workpiece	No of Cycles	Finishing time
Ranking	3	2	6	1	4	5
Level	3	1	2	2	3	3
'p' value	0.027	0.001	0.057	0.000	0.020	0.039
Delta value	4.26	6.65	3.78	8.24	4.22	4.06

   a. The value of 'p' for five of the process parameters is having values lesser than 0.05, which signifies that these parameters are significant. However, the Abrasive Mesh number is having a value of 0. 057. Since, this value is not much higher than 0.05, we can't conclude that the variation in Abrasive mesh numbers is non-significant as the 'p' value between 0.05 to 0.10 signifies "suggestive against H_o and in most of the

cases, when ‘p’ is between 0.05 to 0.10 the variation in process parameter is significant and accepted.

SUMMARY

1.Internal finishing of the spline shaft has been done with a newly prepared medium known as Viscoelastic Magnetic abrasive Medium.

2. An Aluminium fixture has been designed and fabricated for performing the internal surface finish of the splined shaft.

3. A powerful Segmental Arc Magnet that is used for producing the Electricity by Wind turbines is used for providing sufficient Magnetic flux density for the

3. Surface roughness got reduced considerably and the minimum surface roughness obtained with this new process called Viscoelastic magnetic abrasive flow finishing is 0.101µm.

4. Only nine specimens are used for finishing and each specimen is subjected to finishing under a different set of Process parameters as designed by L27 Orthogonal Array of Design of experiments.

5. Material removal [∆m] as the response parameter Optimisation has been done Using Taguchi’s Optimisation Model and found that all the process parameters are significant under the value of p< 0.10.

CHAPTER 7. FINISHING OF EXTERNAL FLAT SURFACES BY VISCOELASTIC MAGNETIC ABRASIVE MEDIUM

In this chapter External surface finishing of the specimen made of Steel, Brass and Aluminium have been done under the same levels of process parameters. Specially prepared Viscoelastic Magnetic Abrasive Medium is used for finishing the surface of the Steel, Brass and Aluminium specimen. A CNC Vertical Drilling and Tapping Machine center are used for this purpose. The objective is to find the metal removal and Change in surface finish. Optimization for metal removal is done for all the three materials by using Taguchi's Optimisation model using Minitab 17. Comparison of change in surface roughness of all the three materials under Ultrasonic vibration is done. Results have been critically examined.

7.1. Introduction to finishing of External surfaces with VEMAF Process:

Surface finishing of the eternal surfaces is one of the challenging tasks for any researcher. Magnetic abrasive finishing is one of the promising methods used for the finishing of the external surfaces. Though finishing the external surfaces is in practice for many centuries, proper documentation in the form of research publications is active from the 1960s onwards only. During the present research, the first research paper considered in the present work is from Kuppuswamy [61], who discussed the finishing of the eternal surfaces by diamond paste. Researchers' experimental validation of theoretical concepts started in the early 1980s. Initially finishing of the surfaces using Magnetic Abrasive Finishing (MAF) was done(62,63,77). The mechanism of finishing was the next step and some of the researchers (66,96,74) did their work in this area. Parameters affecting the MAF process have been discussed by Dhirendra K Singh et al. (2004) and S.O.Kim et al. (2008). A study of polishing of the Non-Magnetic material had been done by some of the researchers (86,92,98,102,103, 112). The next change in the direction of the MAF process is Vibration Assisted finishing process (67,68,75,86,126). The concept of Viscoelastic Magnetic abrasive finishing, which is an Offspring of the MAF process is brought into focus by W.Li et al. (2013). Present research work is based on the concept introduced by W.Li. In this chapter material removal of the external surface has been done with a specially prepared medium. For experimenting, the test rig is prepared. The CNC Drilling and Tapping Machine in the Machine shop of DTU is used for this purpose.

7.2. Description of the Test Rig: The test rig used for the present experiment comprises of the following components.

i. Vertical Drilling and Tapping Machining Center

ii. VEMAF Polishing Tool.

iii. Ultrasonic generator

iv. Viscoelastic Magnetic Abrasive Polishing medium.

7.2.1. Vertical Drilling and Tapping Machining Center: Basic description of the CNC machine is shown in Table 7.1 below.

Table 7.1 Basic Information of Vertical Drilling and Tapping Machining Center

Index	Unit	TD-500A
Worktable size (L*W)	mm	650*400 (TD500 is 620*420)
Max weight capacity of worktable	kg	200
X travel	mm	500
Y travel	mm	400
Z travel	mm	300
Distance from spindle center line to stand rear face	mm	341
Distance from spindle end face to worktable face	mm	200 to 500
X,Y,Z cutting speed	mm/min	0-20000
X,Y,Z quick feed speed	m/min	48/48/48
Spindle turn speed range	r/min	50-12000
Spindle taper		No.30(7:24)
Spindle power	k w	5.5/3.7 (35/23.5Nm) Mitsubishi M70VA SJ-V5.5-01T
Tool storage		tool arm type 14
Time of changing tool	s	3
Location accuracy	mm	X, Y,Z : 0.010
Repeat location accuracy	mm	X, Y,Z : 0.006
CNC system		Mitsubishi M70VA
Machine size(L*W*H)	mm	1540*1480*2100
Machine weight	kg	2100

7.2.1.1 Main Features: TD-500A Vertical Drilling and Tapping Machining Center is produced with international advanced technology and developed by its research, which is widely used in 3C industry, war industry, spaceflight, auto parts, small mold processing, medical and other industries of small and medium-sized plate parts, disc parts, and shell processing.

After one-time clamping, which can complete milling operation, boring operation, drilling operation, and tapping process, with high precision, better automation, highest reliability, the higher degree of Mechanical and Electrical integration, simple operation, overall modeling beautiful generous, etc. Especially suitable for medium and small batch or single processing;

The machine is equipped with a flying saucer type automatic tool change system (ATC), automatic centrally controlled lubricating system, cooling system, automatic chip removal system, manual operation device (MPG), and fully enclosed protection cover. Table 7.2 gives the complete Specifications of the CNC machining Centre.

Table 7.2. Specifications of the CNC machine

ITEMS	SPECIFICATIONS	NOTES
Worktable size	650×400 mm	OP:700×420 mm
Worktable capacity	300kg	
X/Y/Z coordinate travel	500/400/330 mm	
Distance between spindle centerline and vertical front side	400 mm	
Distance between spindle end face and worktable upper side	150~480 mm	
X/Y/Z cutting speed	0~20000 mm/min	
X/Y/Z rapid movement speed	48/48/48 mm/min	(OP:60/60/60)
Spindle speed range	50~20000rpm	
Spindle taper	No.30 (7:24)	
Tool changer	16pcs swing flying saucer	(OP: 21pcs)
Tool shank/rivet type	BT30-45°	
Max tool weight	2 kg	
Max tool diameter	φ80/φ150 (Adjacent)mm	

Max tool length			200mm	
Tool changing time (16T/21T)			1.5/1.8 S	
T-slot (N0.* W* Pitch)			3×14 mm×125 mm	
Positioning accuracy			X/Y/Z: 0.010 mm	
Repeatability accuracy			X/Y/Z: 0.006 mm	
Air pressure			0.5~0.7 MPa	
Air Ventilation			200 L/min	
Machine dimensions (L×W×H)			2146×1600×2280 mm	Standard Accessory
Machine weight			2750 kg	
Controller & Drive motor	Mitsubishi M70VB (A)	20000r/min Spindle motor	SJ-DL5.5/200-01 (3.7/5.5kW) (14.1/17.5/21 Nm)	Optional Accessory
		12000r/min Spindle motor	SJ-D5.5/120-01 (3.7/5.5kW) (23.5/35 Nm)	Optional Accessory
		24000r/min Spindle motor	SJ-VL15-25FZT(F) (2.2/3.7kW) (7/10.5/17.7Nm)	Optional Accessory
		X/Y/Z Drive motor	X/Y: HF154S-A48/4000 Z: HF224BS-A48/4000 (1.5/1.5/2.2) (9/9/12 Nm)	Optional Accessory
	FANUC 0i MF(1)/(5)	20000r/min Spindle motor	ai2/20000 (3.7/5.5/9kW) (11.7/17.5/28.7 Nm)	Standard Accessory
		12000r/min Spindle motor	ai3/12000 (3.7/5.5kW) (23.5/35 Nm)	Optional Accessory
		X/Y/Z Drive motor	X/Y:αis8/4000 Z:αis 12/4000	Standard Accessory

			(2.5/2.5/2.7) (8/8/12 Nm)	
	SIEMENS 828D	20000r/min Spindle motor	1PH8083-1SN02-0MA1 (4.8/5.8kW) (10/12.3 Nm)	Optional Accessory
		X/Y/Z Drive Motor	X/Y: 1FK7063-2AF71-1RG1 Z: 1FK7083-2AF71-1RH1 (2.3/2.3/3.3) (11/11/16 Nm)	Optional Accessory
	Huazhong 818AM	24000r/min Spindle motor	SVM-75L-30-24 (3.7/5.5kW) (12/20.8 Nm)	Optional Accessory
		X/Y/Z Drive Motor	X/Y: 130ST-M0961530LMDD Z: 180ST-MM18020HMBB-Z (1.5/1.5/3.1) (9.6/9.6/18 Nm)	Optional Accessory
	DMTG .α	24000r/min Spindle motor	SVM-75L-30-24 (3.7/5.5kW) (12/20.8 Nm)	Optional Accessory
		X/Y/Z Drive Motor	X/Y: 130ST-M0961530LMDD Z: 180ST-MM18020HMBB-Z (1.5/1.5/3.1) (9.6/9.6/18 Nm)	Optional Accessory

7.2.1.2 Standard accessory: Details of the standard accessories used have been mentioned in table 7.3 below.

Table.7.3 Details of Standard Accessory

NO	NAME	NO	NAME
1	Automatic tool change system (ATC)	8	Spindle gas seal
2	Workpiece cooling system	9	big flow stamping
3	Full closed protection cover	10	Portable chips air gun
4	Working lights	11	spindle taper hole blower
5	Auto lubrication system	12	Warning lights
6	Rigid tapping	13	Tool kit
7	Foundation bolts and pads		

7.2.1.3 Optional Accessory: The following table describes the Optional Accessories of the CNC Test rig.

Table 7.4 Details of Optional Accessory:

NO	NAME	NO	NAME
1	4th rotation table	6	Heightening column(100/200)
2	Cooling water and high-pressure cooling unit	7	workpiece measurement system
3	Stampings nozzle	8	Cutter blower
4	Cutting tools measurement system	9	Protection door interlock switch
5	Electric cabinet temperature control device (air conditioning)	10	M30 auto power outage system

7.2.1.4 Main Components List: Main Components list is shown in table 7.5 below

Table 7.5 Main Components List

NO	ITEMS	QTY	MANUFACTURER
1	CNC Controller	1 set	FANUC
2	Spindle servo motor	1 set	FANUC
3	X/Y/Z servo motor	1 set	FANUC
4	Spindle front bearing	1 group	NSK
5	Spindle rear bearing	1 group	NSK
6	X/Y/Z screw bearing	1 group	NSK
7	X/Y/Z ball screw	1 group	HPS
8	X/Y/Z linear roller guide	1 group	HPS
9	Spindle unit	1 set	DMTG
10	16pcs swing flying saucer	1 group	DMTG
11	X/Y axis protection cover	1 group	Pinrick Heiniger
12	Z-axis protection cover	1 group	Taiwan brand
13	Cutting liquid water pump	1 set	Taiwan brand
14	Auto lubrication system	1 set	Chinese brand
15	Main electric components	1 group	Chinese brand
16	Main pneumatic components	1 group	SMC

7.2.1. 5 Tools List: The List of the tools is mentioned in Table 7.6

Table 7.6 Tools List

NO.	NAME	SPECIFICATION OR MARK		QTY	REMARKS
1		1	TD500A-69101	6	

	Foundation bolts assembly		2	M24X1.5; GB/T6173	6	For machine installation
			3	TD500A-69702A	6	
2	Bracket assembly for fixing headstock		1	M10×25; GB/ T70	1	For fixing spindle box
			2	10; GB/T 97.1	3	
			3	10; GB93	3	
			4	TD500A-69701	1	
			5	M10; GB/T 6170	2	
			6	M10X45;GB37	2	
			7	TD500A-69501	1	
3	Tools supplied with the machine	Fork wrench	1	12×13; S91-1A	1	Packed in the tool kit
		Fork wrench	2	16×17; S91-1A	1	
		Allen Key	3	6; GB5356	1	
		Allen Key	4	8; GB5356	1	
		Allen Key	5	10; GB5356	1	
		Allen Key	6	12; GB5356	1	
		Allen Key	7	14; GB5356	1	
		Toolkit	8	CH555	1	

7.2.1. 6 Working Environment:

i. Three-phase alternating-current supply: 380V±10%, -15%; 50Hz±1Hz; Power capacity 16KVA

ii. Environment temperature: 8~40C^{o}

iii. Relative humidity: ≤80%

iv. Air pressure: 0.5~0.7 MPa

Figure 7.1 shows the CNC Test rig comprising the CNC machining center and Ultrasonic generator and the Magnetic Polishing tool and the Viscoelastic Magnetic abrasive Medium.

Fig.7.2 below shows the Magnetic polishing tool, workpiece and the Vice for holding the workpiece.

Fig. 7.1. CNC Test Rig

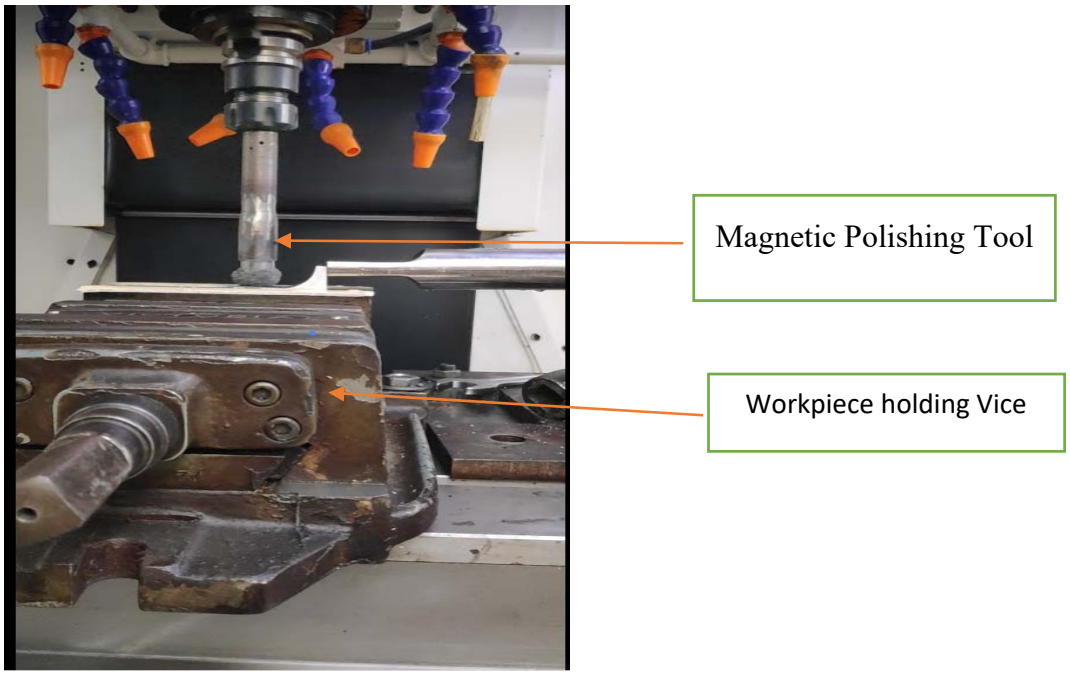

Fig .7.2 Vice for holding the workpiece

7.2.2 VEMAF Polishing Tool: Comprises of a Tool holder and Permanent Magnet.

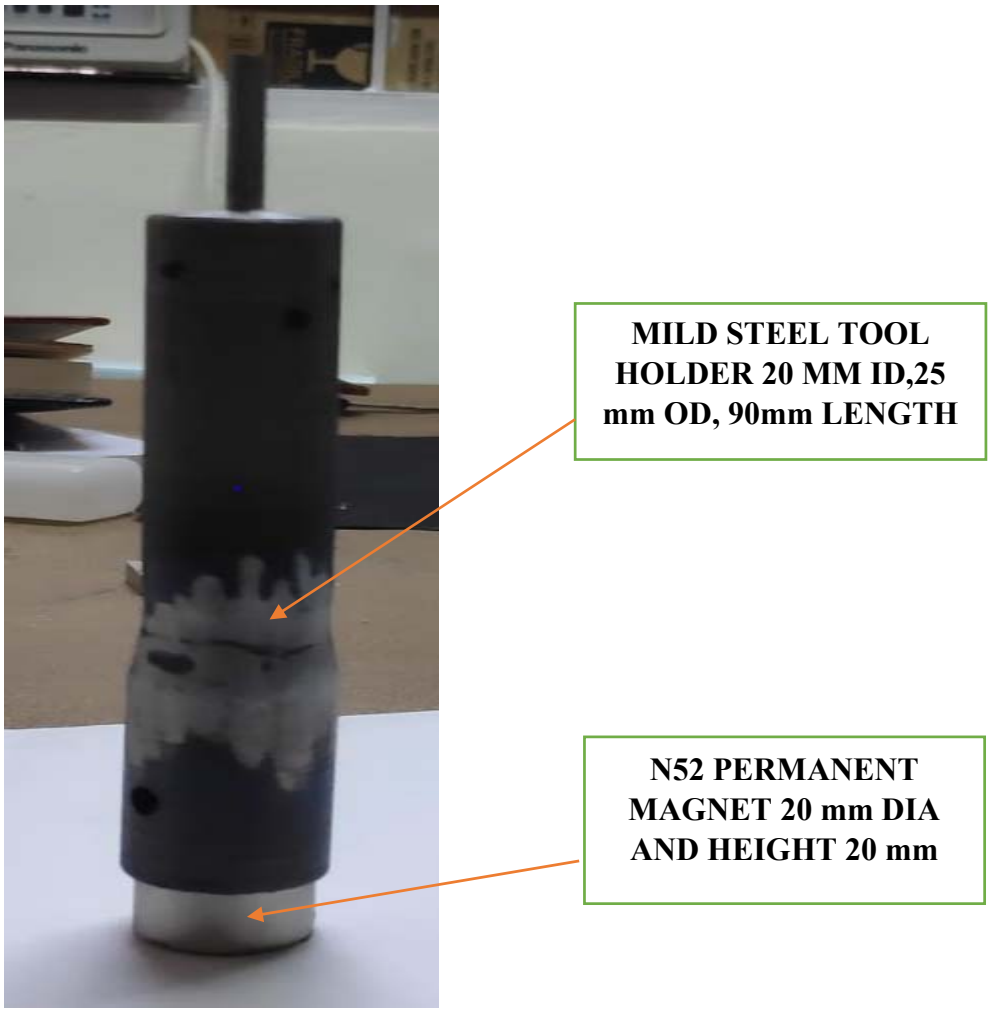

Fig.7.3 VEMAF Polishing Tool

7.2.2.1 Mild Steel Tool Holder: VEMAF tool shown in Fig 7.3 comprises of Mild steel Tool holder having an overall length of 90 mm, 25 mm Outer diameter, and an internal diameter of 20 mm. The tool holder has a bore of 20 mm for a depth of 10 mm. The top 15 mm of the tool holder having 4 mm diameter will be used for fixing the polishing tool to the spindle of the CNC Machine Center. Two threads of 2.5 mm diameter have been tapped on the bottom portion of the tool holder, and Low carbon steel Screws have been inserted through the thread, which will not permit the Magnet to move during the actual finishing operation.

7.2.2.2 Permanent Magnet: Permanent Magnet with grade N52 having 20 mm diameter and height 20 mm is used for the finishing of the external surfaces. The flux densities measured Using Gauss Meter is shown in Fig.7.4 below. The readings shown are in Tesla (T). The flux densities

recorded for the N52 Magnet are 3.11 T, 2.99 T, 2.8T, and 2.59 respectively have been shown below.

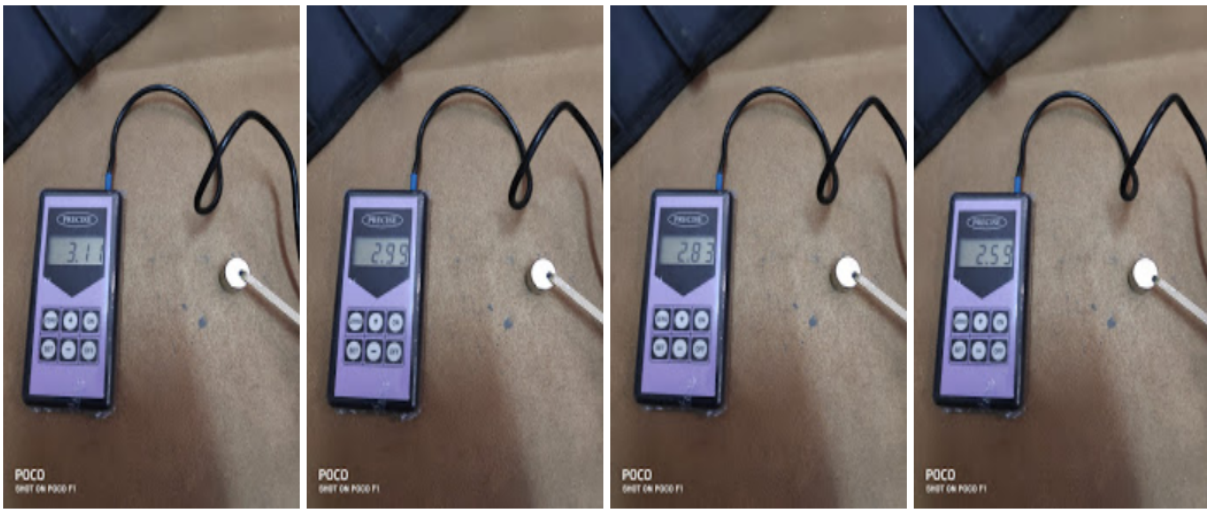

Fig.7.4 Flux Density Measurement

7.2.3 Ultrasonic Generator: Ultrasonic generator used for the present research work produces fixed frequency Ultrasonic waves of 25kHz and can produce Ultrasonic waves having a range of 11µm to 99 µm. Ultrasonic generator is Manufactured by Kamsonic company, basically used for Friction Stir Welding process of the advanced manufacturing lab of DTU.

Fig.7.5. Ultrasonic Generator (Fixed Frequency)

7.2.4 Viscoelastic Magnetic Abrasive Polishing Medium: The Viscoelastic Magnetic abrasive medium used for external finishing is made of Red color Transformer oil. The procedure of preparation and the experimental results has been discussed in section 3.6.8.1 The medium comprises a mixture of Polymer –Gel(Polymer plus Gel) and CIP- Sic powder. The results show that the Viscosity is of the order of 2926.2 Pa-s. During experimentation, it has been observed that the Magnetic abrasive brush behaves as a sem solid body. Fig.7.6 shows the Magnetic abrasive brush.

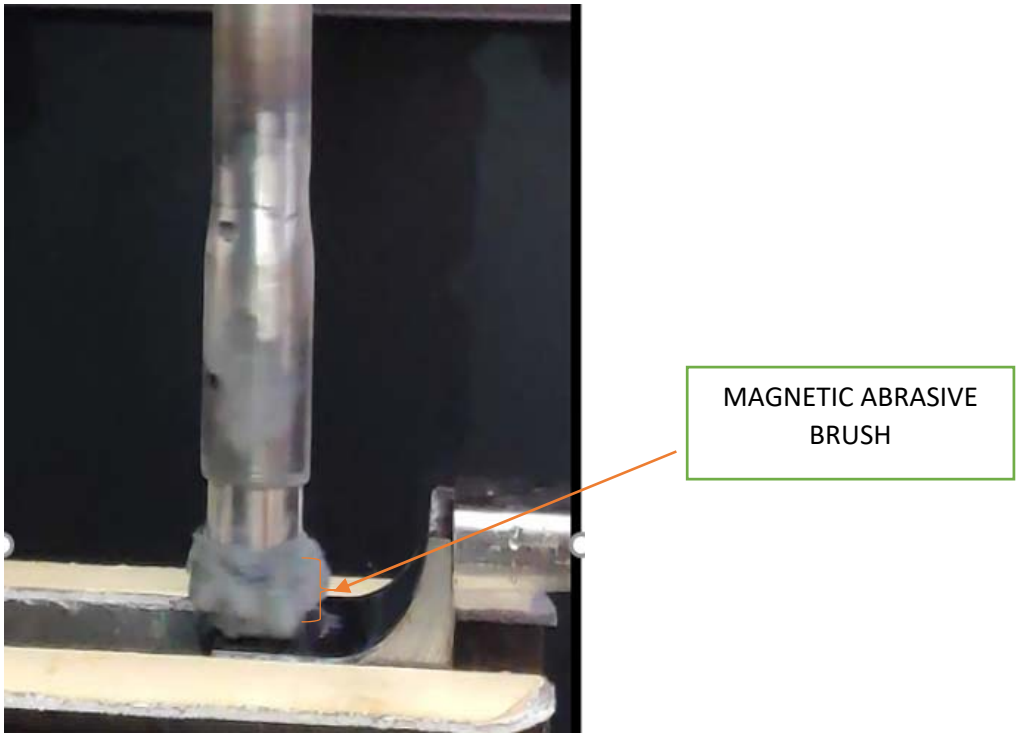

Fig.7.6 Magnetic Abrasive Brush

7.2.5. Residual Stress Analyser:

Fig.7.7.Residual Stress analyzer and Monitor

Change in the magnitude of the residual stresses takes place during the finishing of the external surfaces. In the present research work, the residual stresses of the Specimen before and after finishing has been measured. The residual stress analyzer situated in the Advanced Manufacturing process laboratory has been used for this purpose. Some of the details of the Residual analyzer used in the present work are as mentioned below.

Type of medium used: X-Rays

Measurement method: single incident angle method also known as Cosα method.

The light source used: X-Ray

Type of Sensor: Gyro sensor

Diffraction angle: 2Θ

7.3. Description of the Workpiece: The Workpiece finished with Viscoelastic Magnetic Abrasive medium is shown in Fg. 7.7 Below. It has an L shape and the top surface is having a Flat surface for 25 mm on the longer leg followed by the curved surface. The thickness is 5 mm and the width is 40 mm. The Front view of the specimen is shown in Fig. 7.8. A shorter Leg will be used for contacting the Ultrasonic horn.

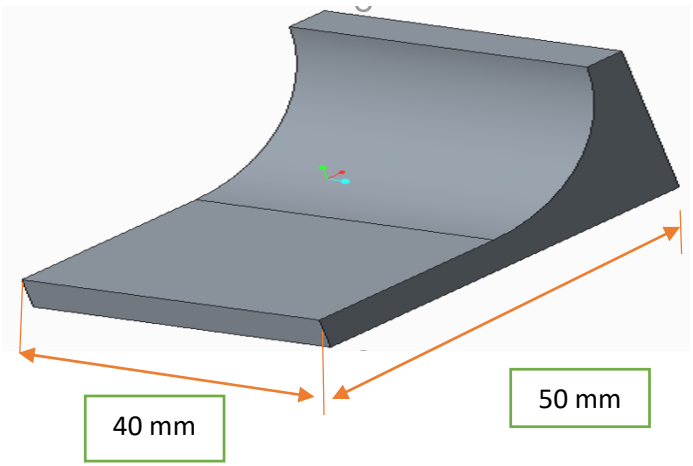

Fig.7.8 3D Model of the Specimen in External Finishing

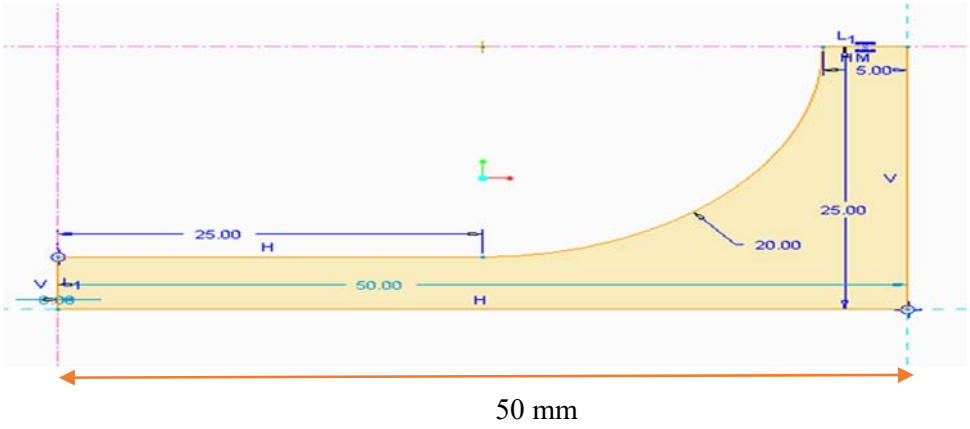

Fig.7.9 Front View of the External Finishing Specimen

7.3.1. **Material and Fabrication of the Specimen**: Steel, Brass, and Aluminium have been used as the material for the Fabrication of the Specimen. Nine Specimen each have been prepared from all these materials. Steel and Aluminium have been prepared by CNC milling available in Delhi Technological University. The brass specimen is prepared by wire cut EDM from an external source.

7.3.1.1. **Properties of the Mild Steel**: Some of the important mechanical properties of the Low carbon Steel specimen with AISI Grade 1020 has been mentioned in the table below.

Table.7.7 Properties of AISI 1020 Steel

S.no	Property	Value
1	Density	7.87 g/cc
2	Tensile Strength (Ultimate)	420 MPa
3	Yield Strength	350 MPa
4	Hardness (BHN)	121

7.3.1.2. **Properties of Brass:** For the present research work, the brass material used has the following chemical composition by weight:

Copper: 55-60%

Zinc : 43% (Max)

Aluminium : 0.10 to 0.6%

Table 7.8. Properties of Brass

PROPERTY	VALUE
Density	8.7 g/cc
Yield Strength	280 MPa
Tensile Strength	338 to 469 MPa
Hardness (BHN)	110

7.3.1.3. **Properties of Al 6351 T6:** Aluminium Alloy used for the present research work is having the following chemical composition:

Table 7.9 Chemical Properties of Al 6351 T6

Al	Si	Mg	Fe	Zn	Ti	Cu	Others
96 to 98.5%	0.7 to 1.3%	0.4 to 0.8%	0 to 0.5%	0 to 0.2%	0 to 0.2%	0 to 0.15%	0 to 0.15%

Table.7.10. Mechanical Properties Al 6351T6

Property	Value
Yield Strength	285 Mpa
Tensile Strength	310 Mpa
Hardness [BHN]	90- 100
Density	2.7 g/cc

7.4. Assumptions made in Finishing of External Surfaces Viscoelastic Abrasive Medium:

i. Viscoelastic Magnetic abrasive medium has been thoroughly mixed and there is no segregation of the material.

ii. Viscoelastic Magnetic Abrasive Medium behaves as a Composite material and the abrasive particles contribute as reinforcement particles in particulate composites.

iii. Viscoelastic Magnetic Abrasive polishing brush behaves as a Semi-Solid tool during the Finishing operation and is assumed to be a flexible brush.

iv. Throughout the finishing operation, there will not be an appreciable change in the Viscosity of the medium.

v. Stress-induced on the surface to be machined under the Magnetic finishing tool due to the magnetic lines of force is uniform throughout the area under the N52 permanent magnet.

vi. Based on the Simulation work done the flux density on the flat Specimen surface just below the N52 permanent magnet is almost constant, which is the maximum value obtained in the Simulation done for Brass, Aluminium, and Steel for all three gaps considered.

vii. Magnetic flux densities considered for external finishing with N52 magnets during experimentation would give flux densities *1.49 times higher* values as compared to the simulated values obtained, as the simulation software ANOSOFT 16(student version) simulates N35 magnets only. N52 magnets 1.49 times higher flux densities compared to N35 magnets. Accordingly, the flux densities for the present experimental work are given in Table.7.11

Table 7.11. Magnetic Flux density for Steel, Brass, and Aluminium

	MATERIAL		
WORKING GAP	The magnetic Flux density of Steel [T]	The magnetic Flux density of Brass [T]	The magnetic Flux density of Aluminium [T]
2 mm	1.071	0.3577	0.3577
1.5 mm	1.208	0.4226	0.4226
1 mm	1.319	0.4814	0.4814

7.5. Mechanism of Viscoelastic Magnetic Abrasive Finishing of external surfaces: The Mechanism of the Viscoelastic Magnetic abrasive finishing process is similar to that of Magnetic Abrasive Polishing. The advantage of Viscoelastic Magnetic Abrasive Medium is that it would considerably reduce the Segregation of the Carbonyl Particles in the absence of a Magnetic field. The basic mechanism comprises the following steps.

i. Formation of the Flexible Magnetic brush in presence of the magnetic field, which generates Magnetic force that acts perpendicular to the surface to be finished. The Magnitude of the Normal force generated as per T.Mori et al. (2003) is given by equation 1 mentioned below

$$F_N = \frac{\beta^2}{2\mu_o}\left[1 - 1/\mu_m\right]A_v \quad \text{---------- 1}$$

Where, β is the Flux density, μ_o and μ_m are the permeability in the Vacuum and Specific permeability of the Magnetic brush. A_v is the virtual area of contact. The value of permeability of the medium could be found by the relation given by T.Mori et al.[2003] , which is given by equation 2 mentioned below

$$\frac{\mathbf{2} + \mu_f - \mathbf{2}(\mathbf{1}-\mu_f)\,\mathbf{Vf}}{\mathbf{2} + \mu_f + (\mathbf{1}-\mu_f)\mathbf{Vf}} \quad \text{---------- 2}$$

Where $\boldsymbol{\mu_f}$ is the relative permeability of the iron and $\mathbf{V_f}$ is the volume fraction of the iron, which would be calculated based on the ingredients mixed for making the Viscoelastic Magnetic abrasive medium. Keeping other parameters as constant, $F_N \alpha \beta^2$. So higher Flux

density gives higher Magnetic force, which indents the surface at a microscale level. The indent formed makes micro ridges.

ii. Due to rotation of the Viscoelastic Magnetic abrasive tool centrifugal force that develops acts tangentially on the abrasive particles. These abrasive particles sit in the valleys formed due to micro indentation, during the rotary motion will remove the peaks, and hence finishing would be done.

So, Micro indentation and microchipping are the Mechanisms in the external Finishing of the surfaces with Viscoelastic Magnetic Abrasive Medium.

7.6. Process Parameters for the External VEMAF process: Six process parameters of each 3 levels have been selected for experimenting. Taguchi's Orthogonal Array of experiments L27 has been selected for deciding the Level of each process parameter during the experiment. Process parameters considered here are

i. Magnetic Flux Density [MFD]
ii. Abrasive Mesh Number [AMN]
iii. Magnetic Tool Rotational Speed [MTRS}
iv. Finishing Time[FT]
v. Feed [mm/min]
vi. Ultrasonic Amplitude [USAMP]

The levels of each process parameter are mentioned in the table below.

Table.7.12. Levels of Process Parameters

	PROCESS PARAMETER							
LEVEL	**MFD in Tesls[T]**			**AMN**	**MTRS Rpm**	**FT Minutes**	**FEED Mm/min**	**USAMP µm**
	Steel	Aluminum	Brass					
1	1.071	0.3577	0.3577	400	480	6	12	15
2	1.208	0.4226	0.4226	600	600	9	18	30
3	1.319	0.4814	0.4814	800	720	12	24	45

7.7. Effect of Process parameters as per literature review: A brief discussion about the effect of each process parameter on the Magnetic field-assisted abrasive finishing process has been discussed below.

7.7.1. Flux Density: Most of the researchers found that Magnetic Flux density and the flux density increases with a reduction in the working gap and higher the has proposed that the Material removal increases with an increase in Magnetic field strength[[61, 85, Dhirendra K Singh et al[69] proposed that the magnetic field strength is maximum at the outer surfaces of the magnet and reduces as we approach the center of the Magnet. H. Yamaguchi et al.[85] in their experimental investigation found that the higher flux density increases surface finish. Increased flux density makes the CIP particles stick to the surface of the workpiece and metal removal reduces considerably[86]. Jae-Seob KWAK [92] in their investigation found that in permanent magnets the flux density is minimum at the center and increases towards the edges. Anant Kumar Singh et al.[96] in their Ball end, the Magnetorheological process proposed that the higher Magnetic Field Strength increases both metal removal and surface finish.

7.7.2: Abrasive Mesh Number: Increased abrasive mesh number would reduce the percentage improvement in surface finish and also material removal reduces [71,103]

7.7.3: Magnetic Tool Rotational Speed: Berhanu Girma et al. [77] in their experimental investigation found that Lower spindle speeds effectively reduce the peaks and valleys, so a better surface finish is obtained and with increased rotational speed scratches will develop and hence surface finish would be spoiled. Bongsu Jung et al.[82] in their experimental investigation found that the continuous increase in rotational speed would increase the Centrifugal force, which would become more than the Magnetic force that reduces the metal removal. Significance of for better surface finish, the effect of rotational speed is non-significant [71]. Increased surface finish with increased rotational speed is prominent at lower speeds of rotation only and no significance for change of speeds at higher speeds [72]. Ajay Sidpara et al. [89] observed that increased rotational speed of the tool increases the normal force and reduces the Tangential Force. Patrick Munyensanga et al.[120] in their investigation found that the increased rotational speed would reduce the surface finish.

7.7.4. Feed: Feed is the lateral movement of the polishing tool in the lateral direction (40 mm width)in mm/min. Yuewu Gao et al. (130) found that the feed of 10mm/min has given a better surface finish in copper alloy compared to SS316.

7.7.5. Finishing Time. G.Y. Liu et al. (2014) in their experimental investigation on Al 6061, for hybrid MAF, found that the increase in finishing time up to 10 minutes. Lida Heng et al. (2017)

found that finishing time is the most important process parameter and surface finish increases with increase in the finishing time.

7.7.6. Ultrasonic Amplitude: Vibration Assisted MAF process reduces the finishing time[67,68]. Rahul S. Mulik et al.[87,88] observed that Ultrasonic assisted magnetic abrasive finishing(MAF) gives a better surface finish than the MAF process. Prateek Kala et al.[98] found that finer abrasives under Ultrasonic Assisted MAF percentage change in surface finish got reduced. However, Ultrasonic vibration increases surface finish due to increased collision of abrasive particles. Nitesh Sihag et al. (2017) in their experimental investigation on Tungsten coated steel material found that the ultrasonic Assisted MAF would increase the surface finish by 21.9% compared to the MAF process [108].

Fig.7. 10. Surface roughness Measurement of Unfinished Brass Specimen

7.8. Experimental Design for Finishing of External surfaces of Steel Specimen:

Experiments have been performed based on Taguchi's Design of Experiments called Orthogonal Array of Experiments. The first Nine specimens have been subjected to finishing operation for Flux density of Level 1, other process parameters are chosen as per the L27 table. The first Nine experiments are conducted based on L1 to L9 on the nine specimens, followed by the next nine experiments; L10 to L18 and finally L19 to L27. From L10 onwards the specimen are machined in a randomised fashion.

Table7.13. L27 Orthogonal Array of Experiments for Steel

MFD [T]	AMN	MTRS RPM	FT Minutes	FEED mm/Min	USAMP µm	Ra Initial µm	Ra Final µm	ΔRa µm	Initial MASS[g]	Final MASS[g]	Metal removal Δm[g]
1.071	400	480	6	12	15	0.546	0.545	0.001	137.4325	137.4290	0.0035
1.071	400	480	6	18	30	0.330	0.326	0.004	139.3402	139.3321	0.0081
1.071	400	480	6	24	45	0.311	0.303	0.008	138.4831	138.4721	0.0110
1.071	600	600	9	12	15	0.411	0.393	0.018	140.3644	140.3595	0.0045
1.071	600	600	9	18	30	0.318	0.303	0.015	136.8132	136.7978	0.0154
1.071	600	600	9	24	45	0.311	0.293	0.018	139.2030	139.1925	0.0105
1.071	800	720	12	12	15	0.305	0.298	0.007	139.7089	139.7053	0.0036
1.071	800	720	12	18	30	0.322	0.298	0.024	141.7624	141.7391	0.0233
1.071	800	720	12	24	45	0.288	0.248	0.040	142.6408	142.5819	0.0589
1.208	400	600	12	12	30	0.393	0.264	0.129	140.3595	140.2739	0.0856
1.208	400	600	12	18	45	0.303	0.199	0.104	138.4721	138.3811	0.0910
1.208	400	600	12	24	15	0.293	0.225	0.068	139.1925	139.0709	0.1216
1.208	600	720	6	12	30	0.303	0.239	0.064	136.7978	136.7790	0.0188
1.208	600	720	6	18	45	0.298	0.222	0.076	141.7391	141.6370	0.1021
1.208	600	720	6	24	15	0.298	0.192	0.106	139.7053	139.6788	0.0265
1.208	800	480	9	12	30	0.545	0.436	0.109	137.4290	137.3456	0.0834
1.208	800	480	9	18	45	0.326	0.223	0.103	139.3321	139.2154	0.1167
1.208	800	480	9	24	15	0.248	0.142	0.106	142.5819	142.5398	0.0421
1.319	400	720	9	12	45	0.192	0.104	0.088	139.6788	139.5657	0.1131
1.319	400	720	9	18	15	0.199	0.0913	0.1077	138.3811	138.2601	0.1210
1.319	400	720	9	24	30	0.436	0.382	0.054	137.3456	137.1993	0.1463
1.319	600	480	12	12	45	0.142	0.0855	0.0565	142.5398	142.4788	0.0610
1.319	600	480	12	18	15	0.223	0.113	0.11	137.3456	137.2931	0.0525
1.319	600	480	12	24	30	0.222	0.103	0.119	141.6370	141.5730	0.0640
1.319	800	600	6	12	45	0.264	0.132	0.132	140.2739	140.2746	0.0263
1.319	800	600	6	18	15	0.239	0.059	0.18	136.7790	136.7665	0.0125
1.319	800	600	6	24	30	0.225	0.083	0.142	139.0709	139.0504	0.0205

7.8.1. Surface roughness of the Steel Specimen: Surface roughness of the specimen has been measured after completing each experiment. In the present experimental set up Nine specimens have been chosen, which are subjected to finishing operation based on L27 Orthogonal Array of Taguchi. The surface roughness obtained after completing the final 9 experiments has been shown below. Here L1, L2, L3, L4, etc. are referred to as the process parameters and output from row 1, row 2, row 3, row 4, etc. in the L27 Orthogonal array of experiments table.

7.8.1.1. Surface roughness (Ra) measurement data for L19 to L27:

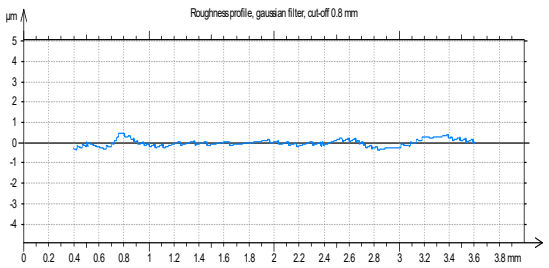

Parameters calculated on the profile Profile

* Parameters calculated by mean of all the sampling lengthes.
* A microroughness filtering is used, with a ratio of 2.5 µm.

Roughness Parameters, Gaussian filter, 0.8 mm

Ra = 0.104 µm

Graph7.1. The surface roughness of the finished piece of Steel L19

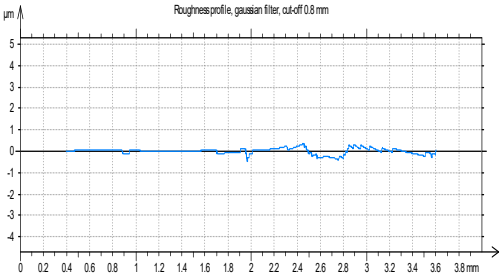

Parameters calculated on the profile Profile

* Parameters calculated by mean of all the sampling lengthes.
* A microroughness filtering is used, with a ratio of 2.5 µm.

Roughness Parameters, Gaussian filter, 0.8 mm

Ra = 0.0913 µm

Graph7.2. The surface roughness of the finished piece of Steel L20

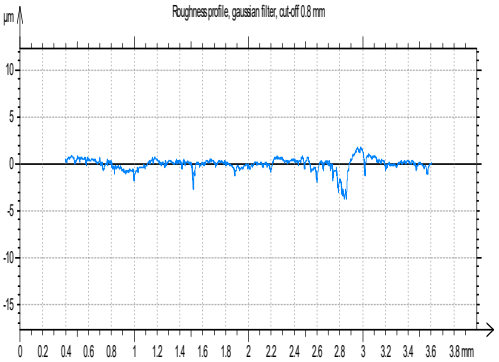

Parameters calculated on the profile Profile

* Parameters calculated by mean of all the sampling lengthes.
* A microroughness filtering is used, with a ratio of 2.5 µm.

Roughness Parameters, Gaussian filter, 0.8 mm

Ra = 0.382 µm

Graph7.3. The surface roughness of the finished piece of Steel L21

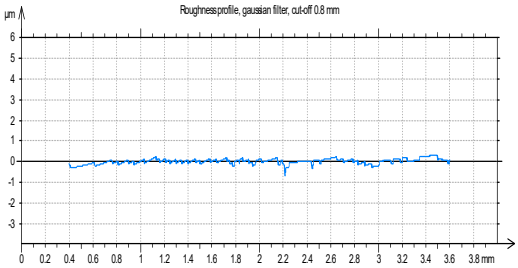

Parameters calculated on the profile Profile

* Parameters calculated by mean of all the sampling lengthes.
* A microroughness filtering is used, with a ratio of 2.5 µm.

Roughness Parameters, Gaussian filter, 0.8 mm

Ra = 0.0855 µm

Graph7.4. The surface roughness of the finished piece of Steel L22

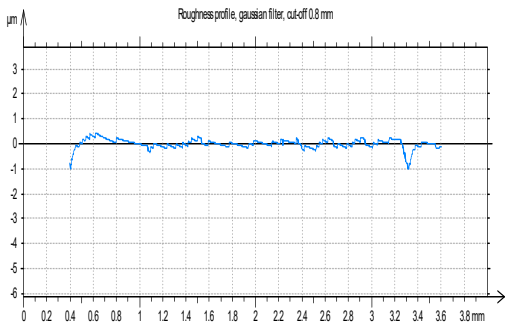

Parameters calculated on the profile Profile

* Parameters calculated by mean of all the sampling lengthes.
* A microroughness filtering is used, with a ratio of 2.5 µm.

Roughness Parameters, Gaussian filter, 0.8 mm

Ra = 0.113 µm

Graph7.5. The surface roughness of the finished piece of Steel L23

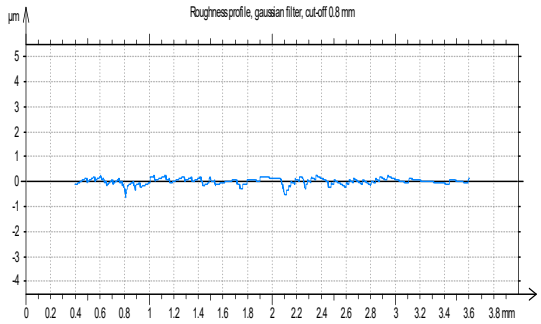

Parameters calculated on the profile Profile

* Parameters calculated by mean of all the sampling lengthes.
* A microroughness filtering is used, with a ratio of 2.5 µm.

Roughness Parameters, Gaussian filter, 0.8 mm

Ra = 0.103 µm

Graph7.6. The surface roughness of the finished piece of Steel L24

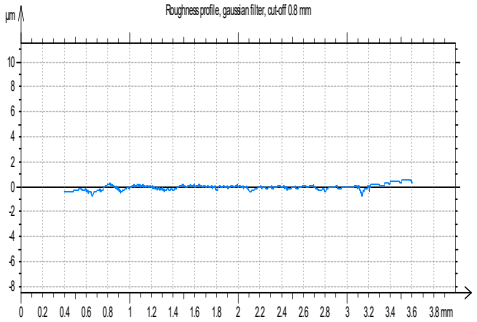

Parameters calculated on the profile Profile

* Parameters calculated by mean of all the sampling lengthes.
* A microroughness filtering is used, with a ratio of 2.5 µm.

Roughness Parameters, Gaussian filter, 0.8 mm

Ra = 0.132 µm

Graph7.7. The surface roughness of finished piece of Steel L25

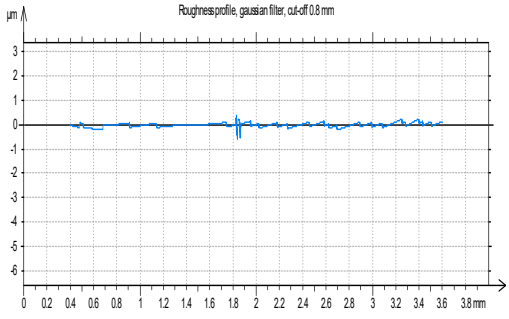

Parameters calculated on the profile Profile

* Parameters calculated by mean of all the sampling lengthes.
* A microroughness filtering is used, with a ratio of 2.5 µm.

Roughness Parameters, Gaussian filter, 0.8 mm

Ra = 0.059 µm

Graph7.8. The surface roughness of the finished piece of Steel L26

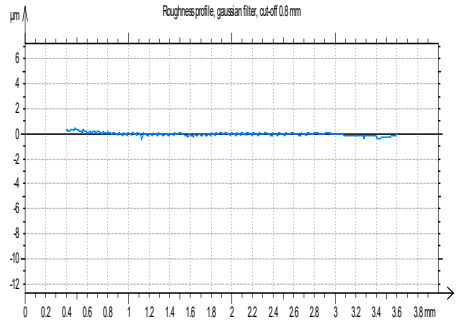

Parameters calculated on the profile Profile

```
* Parameters calculated by mean of all the sampling
lengthes.
* A microroughness filtering is used, with a ratio of
2.5 µm.

Roughness Parameters, Gaussian filter, 0.8 mm

   Ra    = 0.083 µm
```

Graph7.9. The surface roughness of the finished piece of Steel L27

7.8.2. Residual Stresses of Steel Specimens: Residual Stresses of the specimen before finishing and after finishing has been shown below from Graph.7.10 to Graph.7.18 The specimens taken are in order from the L27 table. The first specimen is from L1, the Second specimen is from L2, the Third Specimen is from L3, and so on. After completion of the first cycle of finishing, these specimens are subjected to the second cycle from L10 to L18 and finally the last cycle from L19 to L27, from the second cycle onwards the specimen have been chosen randomly and finished. The residual stresses after completing the Last cycle (third cycle) for each specimen has been recorded and shown in the graphs below. The left side graph shows the residual stress before finishing and the right-side graph shows after finishing. Results show that the compressive residual stresses have been induced due to finishing operation

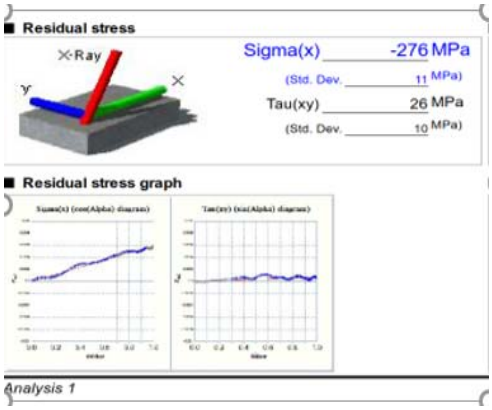

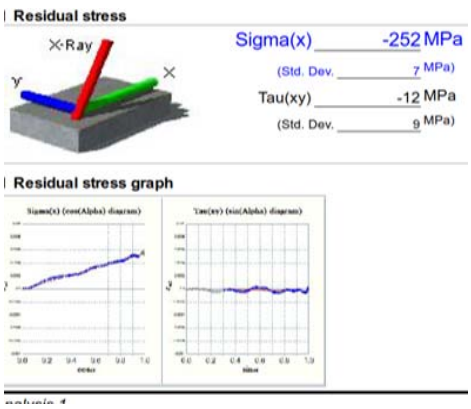

Graph.7.10 Residual stresses of Steel specimen 1 Before and After finishing

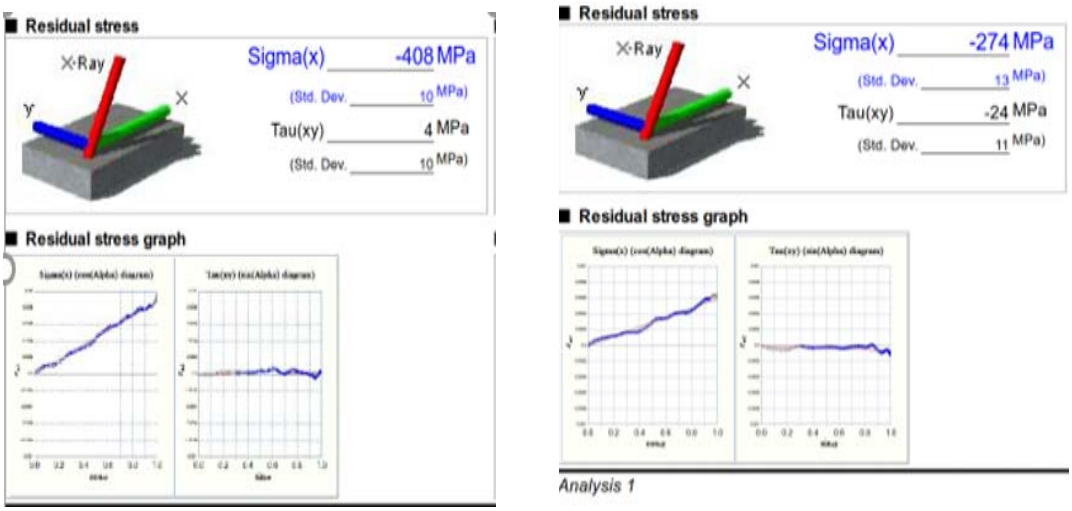

Graph.7.11 Residual stresses of Steel specimen 2 Before and After finishing

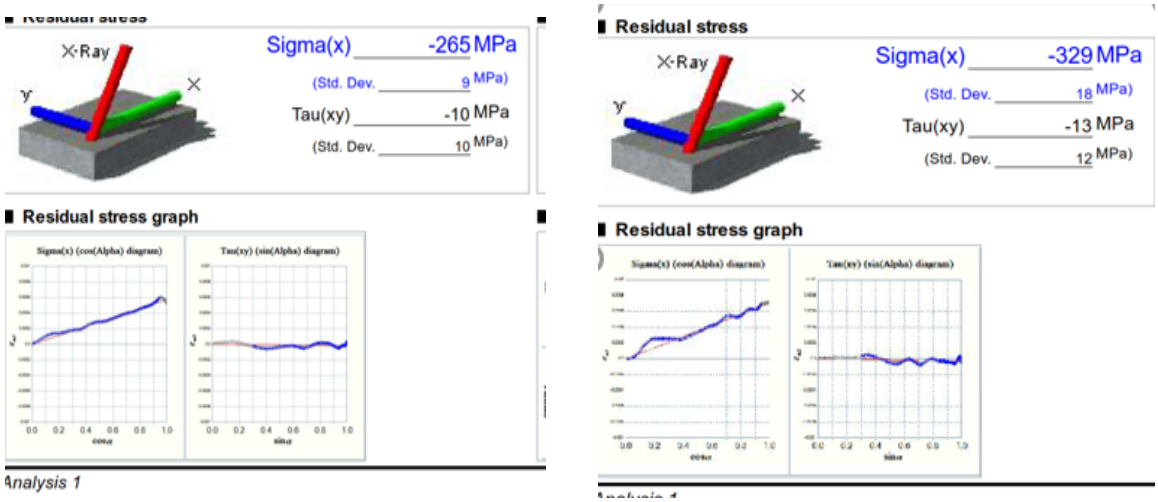

Graph.7.12 Residual stresses of Steel specimen 3 Before and After finishing

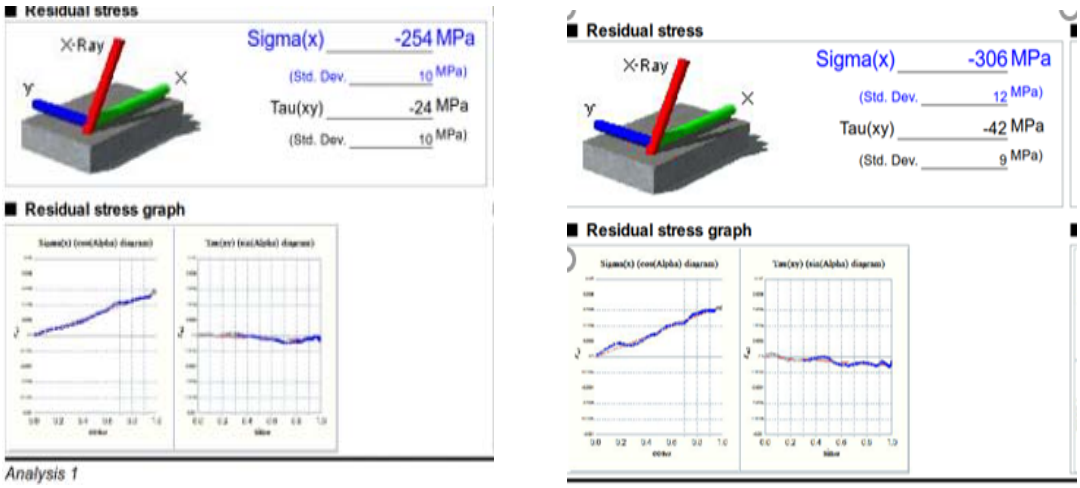

Graph.7.13 Residual stresses of Steel specimen 4 Before and After finishing

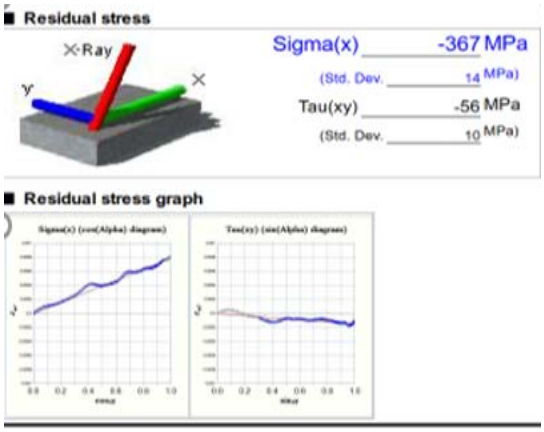

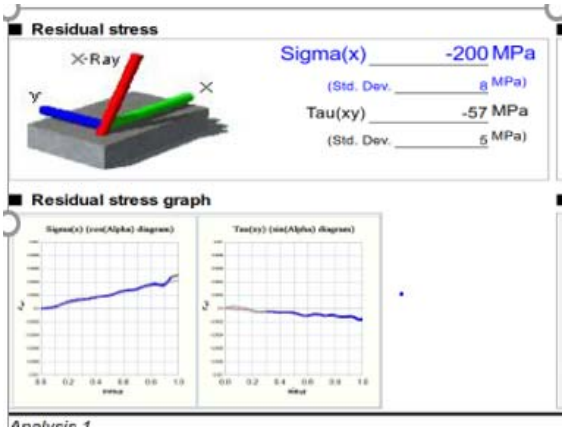

Graph.7.14. Residual stresses of Steel specimen 5 Before and After finishing

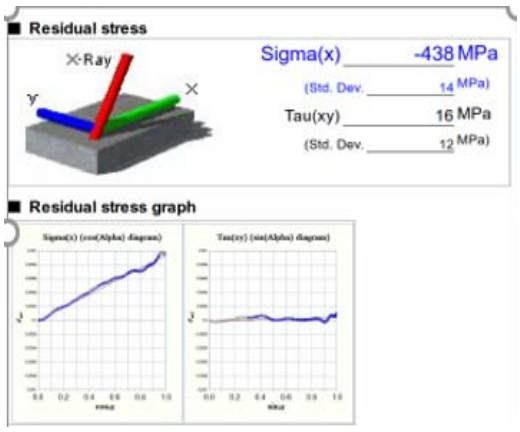

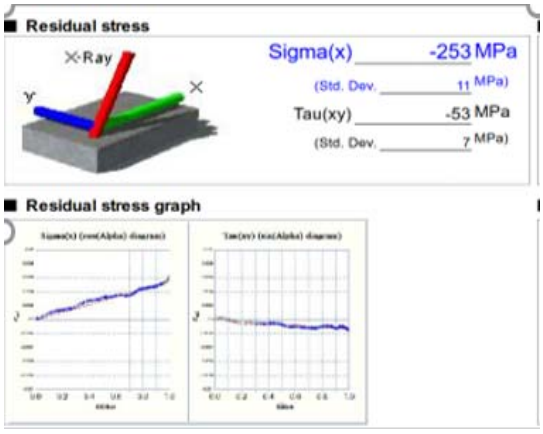

Graph.7.15. Residual stresses of Steel specimen 6 Before and After finishing

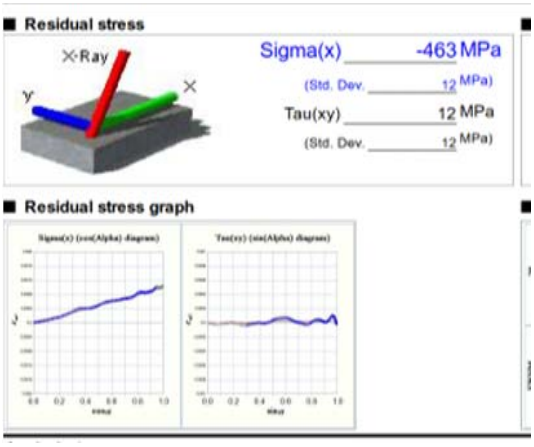

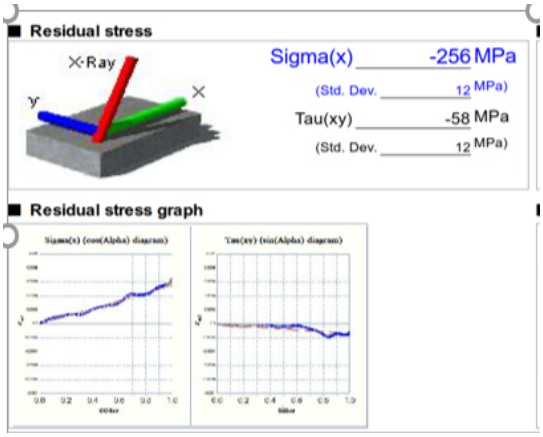

Graph.7.16. Residual stresses of Steel specimen 7 Before and After finishing

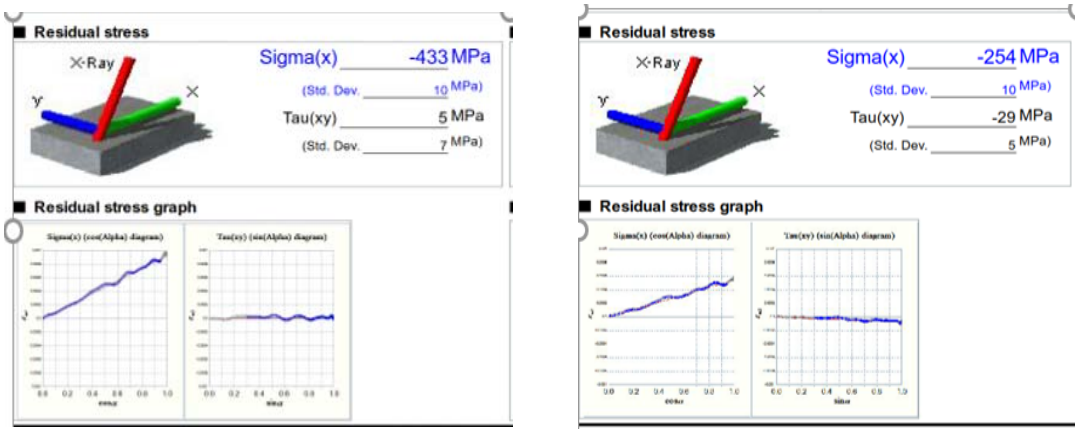

Graph.7.17. Residual stresses of Steel specimen 8 Before and After finishing

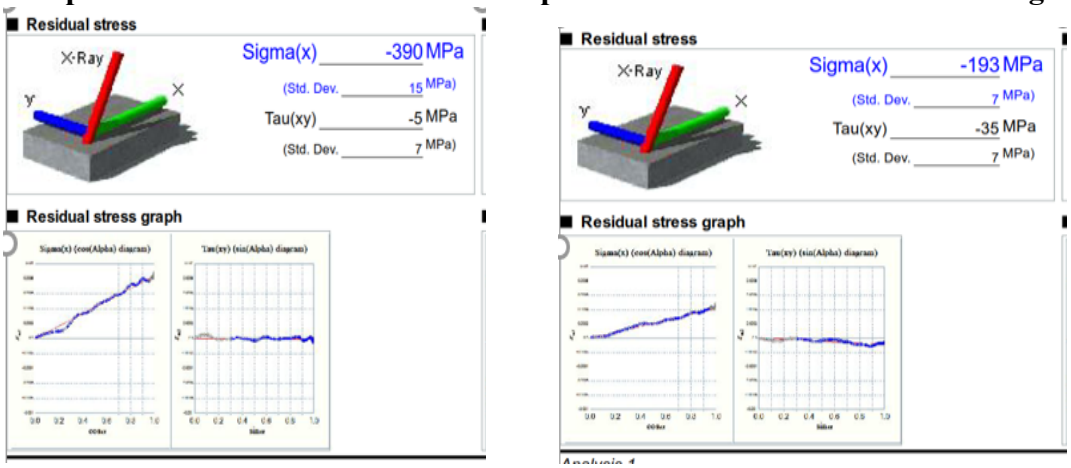

Graph.7.18. Residual stresses of Steel specimen 9 Before and After finishing

7.8.3. Results of Optimisation of Steel Specimens: Results obtained based on the experiments performed as per L27 Orthogonal Array of experiments has been shown below. MiniTab 17 software is used for the Optimisation of the process parameters based on Taguchi's Optimisation Model.

```
Taguchi Orthogonal Array Design

L27(3^6)

Factors:  6
Runs:    27


Columns of L27(3^13) Array

1 2 3 4 5 6
```

Taguchi Analysis: Δm versus MFD, AMN, MTRS, FT, FEED, USAMP

Linear Model Analysis: SN ratios versus MFD, AMN, MTRS, FT, FEED, USAMP

```
Estimated Model Coefficients for SN ratios
```

Term	Coef	SE Coef	T	P
Constant	-29.7875	0.7566	-39.368	0.000
MFD 1.071	-10.1021	1.0700	-9.441	0.000
MFD 1.208	5.9995	1.0700	5.607	0.000
AMN 400	2.6140	1.0700	2.443	0.028
AMN 600	-1.5902	1.0700	-1.486	0.159
MTRS 480	-0.3944	1.0700	-0.369	0.718
MTRS 600	-2.0636	1.0700	-1.929	0.074
FT 6	-5.7036	1.0700	-5.330	0.000
FT 9	2.6229	1.0700	2.451	0.028
FEED 12	-3.2344	1.0700	-3.023	0.009
FEED 18	1.7839	1.0700	1.667	0.118
USAMP 15	-4.0216	1.0700	-3.758	0.002
USAMP 30	0.6194	1.0700	0.579	0.572

S = 3.932 R-Sq = 91.8% R-Sq(adj) = 84.7%

Analysis of Variance for SN ratios

Source	DF	Seq SS	Adj SS	Adj MS	F	P
MFD	2	1393.91	1393.91	696.96	45.09	0.000
AMN	2	93.69	93.69	46.84	3.03	0.081
MTRS	2	94.10	94.10	47.05	3.04	0.080
FT	2	440.11	440.11	220.05	14.24	0.000
FEED	2	141.73	141.73	70.86	4.58	0.029
USAMP	2	253.18	253.18	126.59	8.19	0.004
Residual Error	14	216.40	216.40	15.46		
Total	26	2633.12				

Linear Model Analysis: Means versus MFD, AMN, MTRS, FT, FEED, USAMP

Estimated Model Coefficients for Means

Term	Coef	SE Coef	T	P
Constant	0.053474	0.004206	12.715	0.000
MFD 1.071	-0.038052	0.005948	-6.398	0.000
MFD 1.208	0.022948	0.005948	3.858	0.002
AMN 400	0.024437	0.005948	4.109	0.001
AMN 600	-0.013996	0.005948	-2.353	0.034
MTRS 480	-0.004330	0.005948	-0.728	0.479
MTRS 600	-0.010374	0.005948	-1.744	0.103
FT 6	-0.027996	0.005948	-4.707	0.000
FT 9	0.019081	0.005948	3.208	0.006
FEED 12	-0.009052	0.005948	-1.522	0.150
FEED 18	0.006815	0.005948	1.146	0.271
USAMP 15	-0.010385	0.005948	-1.746	0.103
USAMP 30	-0.001763	0.005948	-0.296	0.771

S = 0.02185 R-Sq = 87.2% R-Sq(adj) = 76.3%

Analysis of Variance for Means

Source	DF	Seq SS	Adj SS	Adj MS	F	P
MFD	2	0.019824	0.019824	0.009912	20.76	0.000
AMN	2	0.008119	0.008119	0.004059	8.50	0.004
MTRS	2	0.003083	0.003083	0.001542	3.23	0.070
FT	2	0.011046	0.011046	0.005523	11.57	0.001
FEED	2	0.001200	0.001200	0.000600	1.26	0.315
USAMP	2	0.002327	0.002327	0.001163	2.44	0.124
Residual Error	14	0.006686	0.006686	0.000478		
Total	26	0.052285				

Response Table for Signal to Noise Ratios
Larger is better

Level	MFD	AMN	MTRS	FT	FEED	USAMP
1	-39.89	-27.17	-30.18	-35.49	-33.02	-33.81
2	-23.79	-31.38	-31.85	-27.16	-28.00	-29.17
3	-25.68	-30.81	-27.33	-26.71	-28.34	-26.39
Delta	16.10	4.20	4.52	8.78	5.02	7.42
Rank	1	6	5	2	4	3

Response Table for Means

Level	MFD	AMN	MTRS	FT	FEED	USAMP
1	0.01542	0.07791	0.04914	0.02548	0.04442	0.04309
2	0.07642	0.03948	0.04310	0.07256	0.06029	0.05171
3	0.06858	0.04303	0.06818	0.06239	0.05571	0.06562
Delta	0.06100	0.03843	0.02508	0.04708	0.01587	0.02253
Rank	1	3	4	2	6	5

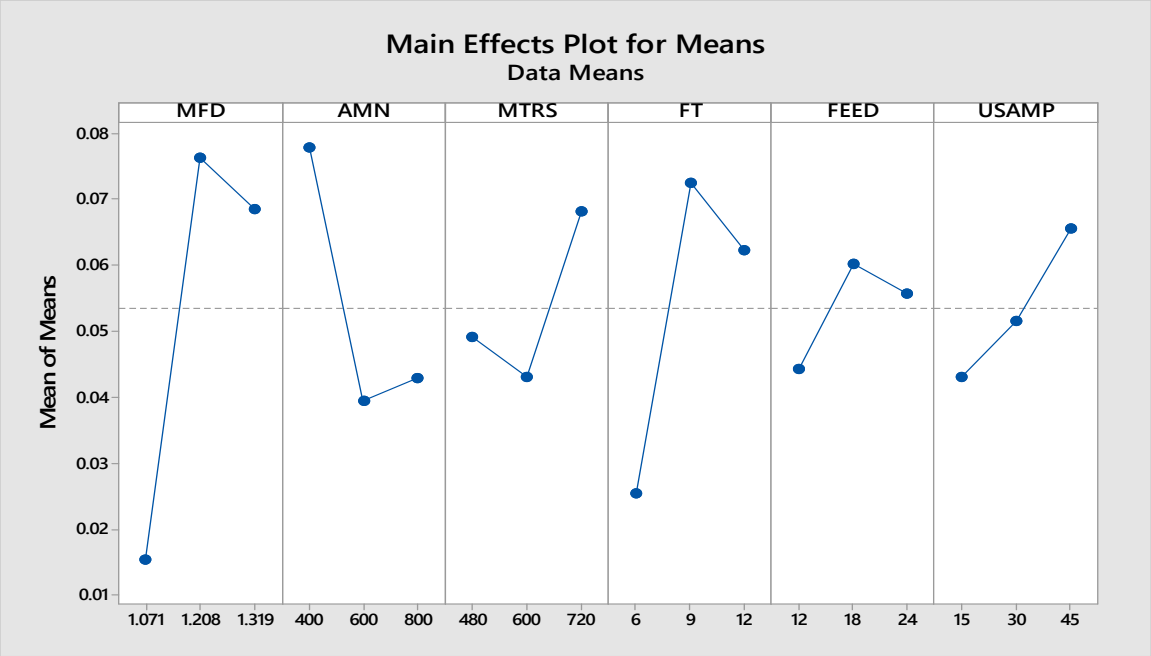

Graph.7.19. Main effect plot for means

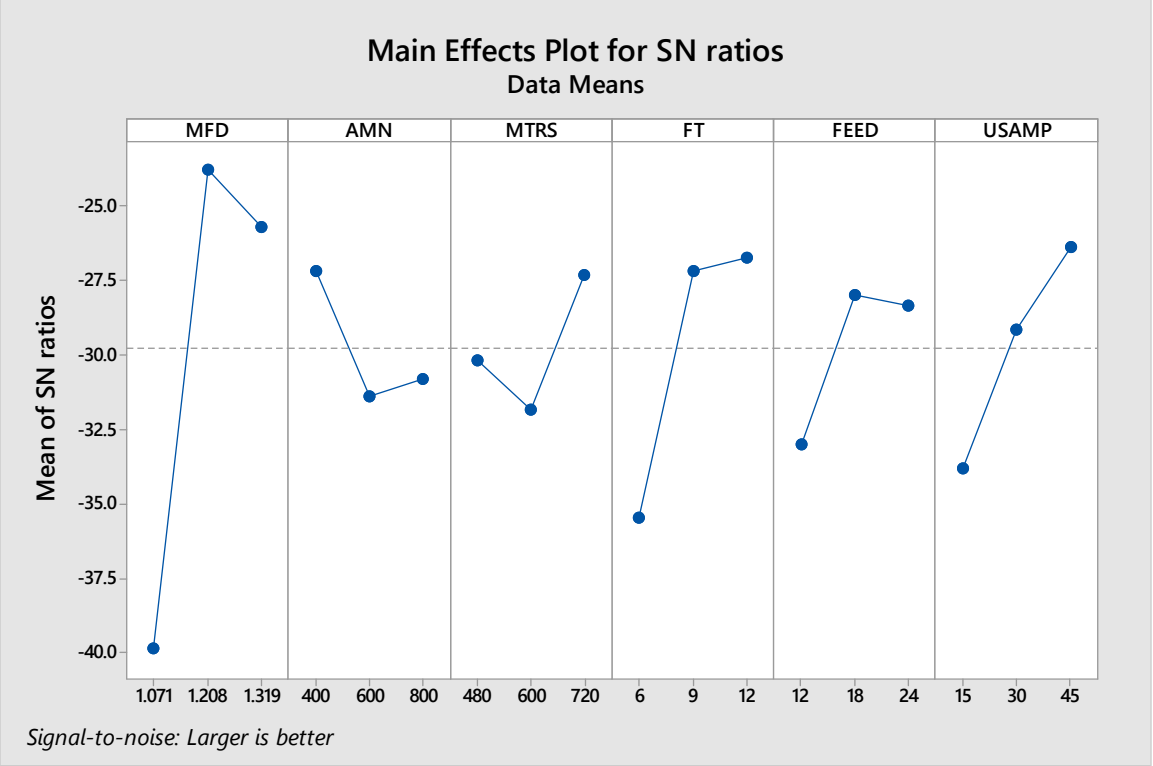

Graph.7.20. Main effect Plot for SN Ratio

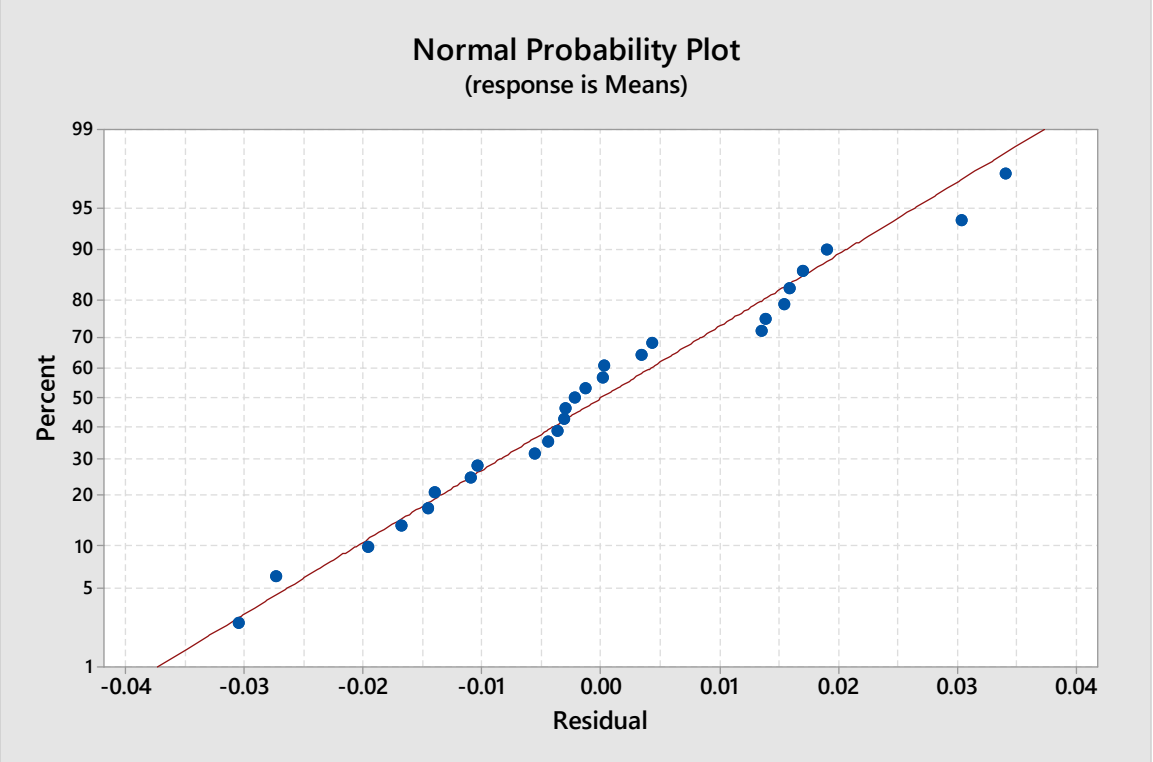

Graph.7.21. Normal Probability Plot for means

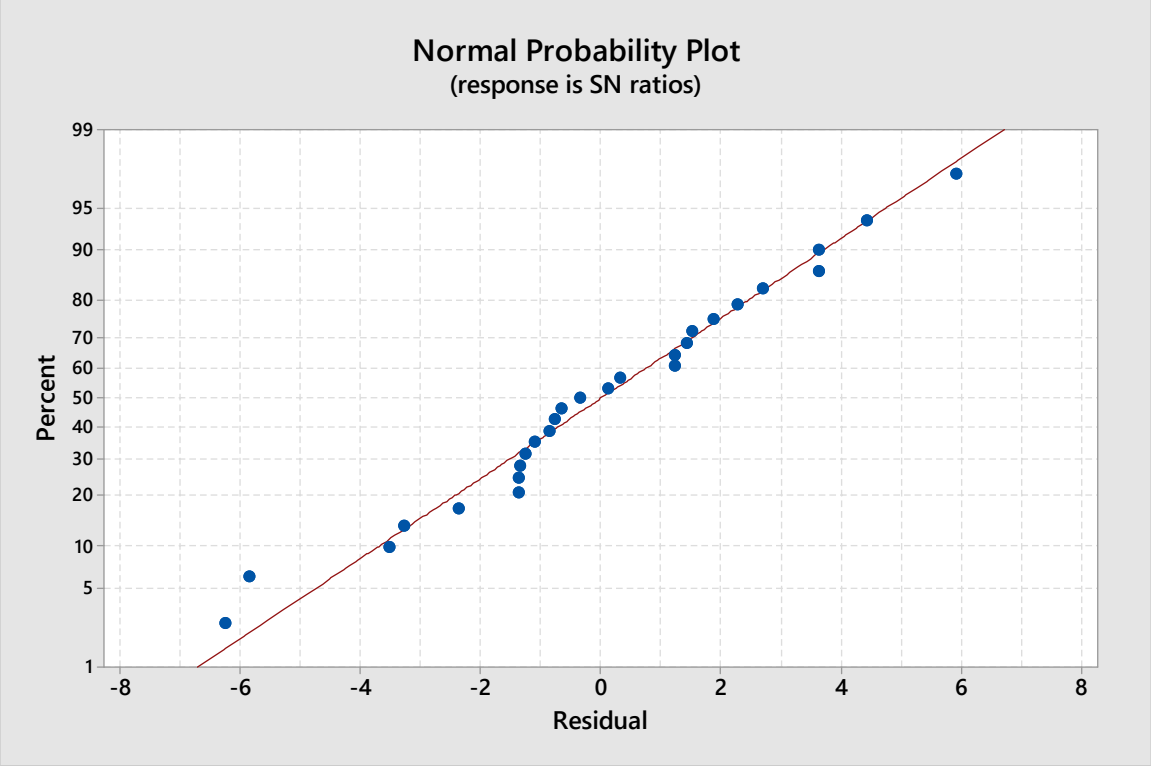

Graph. 7.22 Normal Probability Plot (SN ratio)

Fig. 7.11. Steel Specimen Finished with Viscoelastic Magnetic Abrasive Medium

Fig. 7.12. Etched Steel Specimen finished with VEMAF Process 500X

7.8.3.1. Result and Discussion of External surface finishing of Steel Specimens:

1. Both the Change in the surface finish(ΔRa) and Metal removal (Δm) are low at L1, where all the process parameters are having the least value.
2. Maximum material removal (Δm) occurred for Abrasive Mesh Number 400, which is the coarsest abrasive at a feed of 24 mm/min (level 3), at 720 rpm (level 3), with Ultrasonic amplitude of 30 μm. Most of the researchers found that maximum removal of the material is possible with relatively coarser size only.
3. Change in material removal is in increasing trend from level 1 to Level 3 Magnetic flux densities. The higher the Magnetic flux density, the better would be the ability to make a deeper micro indent, which forms the ridges around and these ridges will be sheared by the abrasives.
4. The maximum change in the surface finish (ΔRa) is obtainable for the Maximum flux density (Level 3), with the finest abrasive (Level 3), least time (Level 1) at the highest feed 24 mm/min(Level 3), and Ultrasonic Vibration of 30 μm (Level 2).
5. The parameters (L27) that contributed to the highest change in surface roughness ΔRa, would not produce the finest surface finish as the surface finish always depends on the initial surface roughness of the Specimen.
6. The finest surface finish obtained from this process is 0.059 μm obtained in three cycles of finishing from an initial value of 0.318 μm.
7. The observations made from the Optimisation of TSGUCHI's optimization model are as mentioned below.

i. The assumption of Normal distribution is valid as all the response points (Δm) are nearer to the Normal distribution line. Ranking of the process parameters, ranking, and significance is tabulated below.

Table 7. 14 Comparison of Ranking and their levels and Significance values.

Process Parameter	MFD T	AMN	MTRS Rpm	FT Minutes	FEED Mm/Min	USAMP μm
Ranking	1	6	5	2	4	3
Level	2	1	3	2	2	3
'p' Value	0.00	0.081	0.080	0.000	0.029	0.004
Delta	16.10	4.20	4.52	8.78	5.02	7.42

ii. All the process parameters are having ‘p’ values less than 0.10, which signifies that the variable values in each parameter are significant. Since ‘p’ is a statistical tool that signifies the significance of variations in process parameters and the variation varies from discipline to discipline in Engineering values below 0.10 are significant if R-Sq and R-Sq [adj] is showing a higher percentage. Here these values are 91.8% and 84.7%, which are higher only.

iii. Abrasive Mesh number is ranked least. The reason being at lower abrasive sizes; the difference in abrasive diameters between the successive sizes is less compared to coarse abrasives.

iv. Higher flux density gives better holding power, however, the level preferred as per Taguchi’s Optimisation model is level 2, the obvious reason is that increasing the flux density would make the CIP stick to the specimen as the specimen, which is a magnetic material gets the polarity due to induction.

v. Similarly, finishing time has got Level 2 in optimization as after finishing for 9 minutes under the prevailing experimental conditions, saturation will be reached and no advantage would be derived by increasing the finishing time to the next higher value, which is 12 minutes.

vi. Magnetic tool rotational speed as per the optimization is 480 rpm as at this speed the abrasives will rotate with the tool without slip and hence remove the material efficiently.

vii. The feed is the motion of the tool in the lateral direction along the width. The width of the specimen is 40 mm and the preferred feed as per the Optimisation is 24 mm/minute.

viii. Ultrasonic Amplitude as per Optimisation is 30 µm. Due to Ultrasonic vibration, the abrasives sitting in the valleys will be made to rotate along with the Magnetic Tool.

ix. Observation of the Surface roughness Graphs shown from 7.1 to 7.9 revealed that there is no waviness on the surfaces finished by VEMAF process.

7.9. Experimental Design for Finishing of External surfaces of Brass Specimens:

Experiments have been performed on Brass specimens based on Taguchi’s Design of Experiments called Orthogonal Array of Experiments. The first Nine specimens have been

subjected to finishing operation for Flux density of Level 1, other process parameters are chosen as per the L27 table. The first Nine experiments are conducted based on L1 to L9 on the nine specimens, followed by the next nine experiments; L10 to L18 and finally L19 to L27. From L10 onwards the specimens are machined in a randomized fashion.

Table. 7.15. Orthogonal Array of Experiments for Brass.

MFD [T]	AMN	MTRS RPM	FT Minutes	FEED mm/Min	USAMP µm	Ra Initial µm	Ra Final µm	ΔRa µm	Initial MASS[g]	Final MASS[g]	Metal removal Δm[g]
0.3577	400	480	6	12	15	0.421	0.413	0.008	148.2735	148.2690	0.0045
0.3577	400	480	6	18	30	0.367	0.345	0.022	146.4392	146.4287	0.0105
0.3577	400	480	6	24	45	0.400	0.371	0.029	147.0463	147.0330	0.0133
0.3577	600	600	9	12	15	0.280	0.271	0.009	146.5102	146.5102	0.0054
0.3577	600	600	9	18	30	0.331	0.305	0.026	147.0524	147.0337	0.0187
0.3577	600	600	9	24	45	0.445	0.417	0.028	146.3246	146.3120	0.0126
0.3577	800	720	12	12	15	0.365	0.340	0.025	146.0216	146.0171	0.0045
0.3577	800	720	12	18	30	0.298	0.271	0.027	148.1432	148.1367	0.0065
0.3577	800	720	12	24	45	0.359	0.322	0.037	148.9317	148.9245	0.0072
0.4246	400	600	12	12	30	0.271	0.181	0.09	148.1367	148.0330	0.1037
0.4246	400	600	12	18	45	0.322	0.220	0.102	148.9245	148.1430	0.1102
0.4246	400	600	12	24	15	0.340	0.215	0.125	146.0171	145.8675	0.1496
0.4246	600	720	6	12	30	0.345	0.245	0.1	146.4287	146.4059	0.0228
0.4246	600	720	6	18	45	0.371	0.264	0.107	147.0330	146.9684	0.0646
0.4246	600	720	6	24	15	0.413	0.290	0.123	148.2690	148.2371	0.0319
0.4246	800	480	9	12	30	0.305	0.214	0.091	147.0337	146.9310	0.1027
0.4246	800	480	9	18	45	0.417	0.290	0.127	146.3120	146.1692	0.1428
0.4246	800	480	9	24	15	0.271	0.193	0.078	146.5102	146.4592	0.0510
0.4814	400	720	9	12	45	0.290	0.199	0.091	146.1692	145.9924	0.1768
0.4814	400	720	9	18	15	0.193	0.079	0.114	146.4592	146.3232	0.1360
0.4814	400	720	9	24	30	0.214	0.103	0.111	146.9310	146.8290	0.1020
0.4814	600	480	12	12	45	0.215	0.143	0.072	145.8675	145.7655	0.1020
0.4814	600	480	12	18	15	0.181	0.114	0.067	148.0330	147.9220	0.1110
0.4814	600	480	12	24	30	0.220	0.0776	0.1424	148.1430	148.0342	0.1088
0.4814	800	600	6	12	45	0.264	0.149	0.115	146.9684	146.8868	0.0816
0.4814	800	600	6	18	15	0.290	0.152	0.138	148.2371	148.1657	0.0714
0.4814	800	600	6	24	30	0.245	0.082	0.163	146.4059	146.3379	0.0680

7.9.1. Surface roughness of the Brass Specimens: Surface roughness of the specimen has been measured after completing each experiment. In the present experimental set up Nine specimens have been chosen, which are subjected to finishing operation based on L27

Orthogonal Array of Taguchi. The surface roughness obtained after completing the final 9 experiments has been shown below. Here L1, L2, L3, L4, etc. are referred to as the process parameters and output from row 1, row 2, row 3, row 4, etc. in the L27 Orthogonal array of experiments table.

7.9.1.1: Surface roughness (Ra) measured data for Brass Specimens L19 to L27:

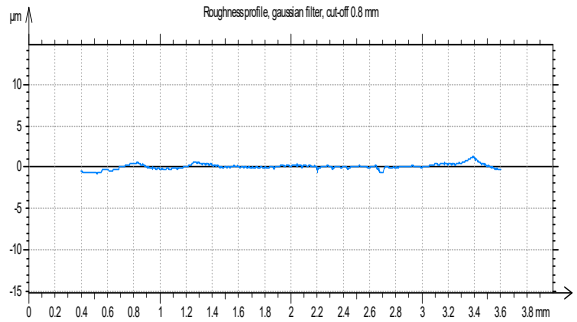

Parameters calculated on the profile Profile

* Parameters calculated by mean of all the sampling lengthes.
* A microroughness filtering is used, with a ratio of 2.5 µm.

Roughness Parameters, Gaussian filter, 0.8 mm

Ra = 0.199 µm

Graph7.23. Surface roughness of finished Brass Specimen L19

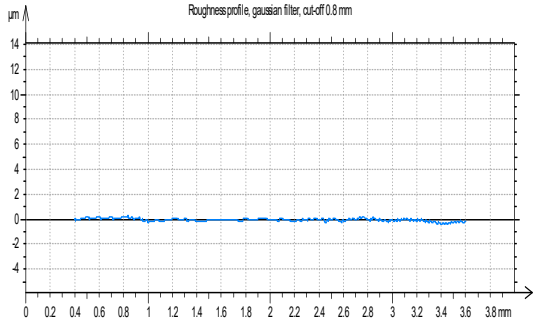

Parameters calculated on the profile Profile

* Parameters calculated by mean of all the sampling lengthes.
* A microroughness filtering is used, with a ratio of 2.5 µm.

Roughness Parameters, Gaussian filter, 0.8 mm

Ra = 0.079 µm

Graph7.24. Surface roughness of finished Brass Specimen L20

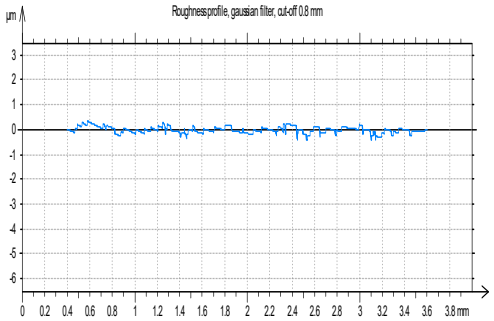

Parameters calculated on the profile Profile

* Parameters calculated by mean of all the sampling lengthes.
* A microroughness filtering is used, with a ratio of 2.5 µm.

Roughness Parameters, Gaussian filter, 0.8 mm

Ra = 0.103 µm

Graph7.25. Surface roughness of finished Brass specimen L21

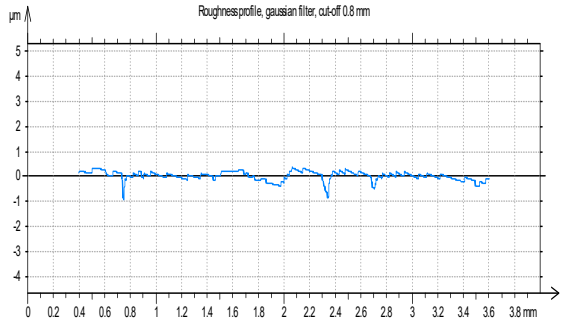

Parameters calculated on the profile Profile

* Parameters calculated by mean of all the sampling lengthes.
* A microroughness filtering is used, with a ratio of 2.5 µm.

Roughness Parameters, Gaussian filter, 0.8 mm

Ra = 0.143 µm

Graph7.26. Surface roughness of finished Brass Specimen L22

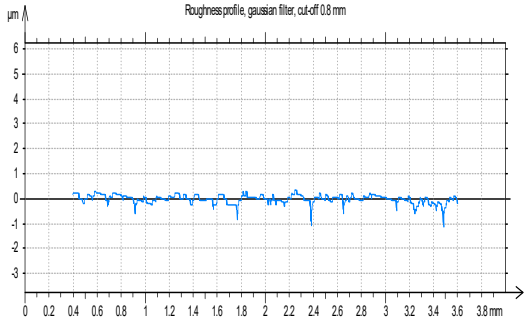

Parameters calculated on the profile Profile

* Parameters calculated by mean of all the sampling lengthes.
* A microroughness filtering is used, with a ratio of 2.5 µm.

Roughness Parameters, Gaussian filter, 0.8 mm

Ra = 0.114 µm

Graph7.27. Surface roughness of finished Brass Specimen L23

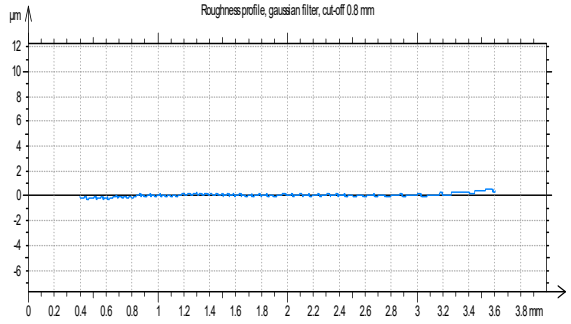

Parameters calculated on the profile Profile

* Parameters calculated by mean of all the sampling lengthes.
* A microroughness filtering is used, with a ratio of 2.5 µm.

Roughness Parameters, Gaussian filter, 0.8 mm

Ra = 0.0776 µm

Graph7.28. Surface roughness of finished Brass Specimen L24

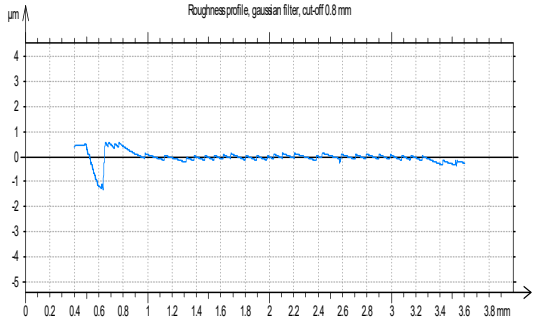

Parameters calculated on the profile Profile

* Parameters calculated by mean of all the sampling lengthes.
* A microroughness filtering is used, with a ratio of 2.5 µm.

Roughness Parameters, Gaussian filter, 0.8 mm

Ra = 0.149 µm

Graph7.29. Surface roughness of finished Brass SpecimenL25

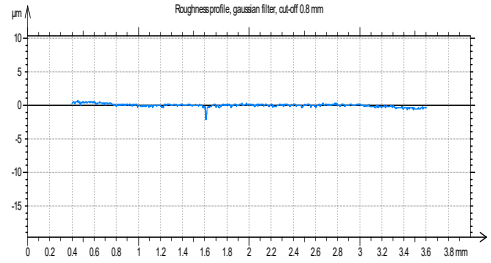

Parameters calculated on the profile Profile

* Parameters calculated by mean of all the sampling lengthes.
* A microroughness filtering is used, with a ratio of 2.5 µm.

Roughness Parameters, Gaussian filter, 0.8 mm

Ra = 0.152 µm

Graph7.30. Surface roughness of finished Brass SpecimenL26

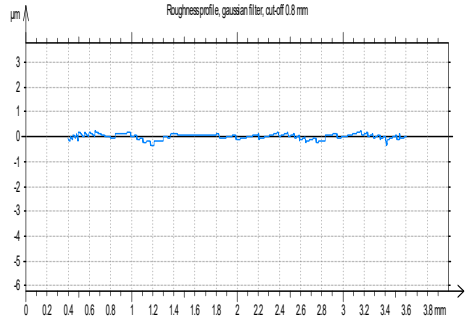

Parameters calculated on the profile Profile

* Parameters calculated by mean of all the sampling lengthes.
* A microroughness filtering is used, with a ratio of 2.5 µm.

Roughness Parameters, Gaussian filter, 0.8 mm

Ra = 0.082 µm

Graph7.31. Surface roughness of finished piece Brass Specimen L27

7.9.2. Residual Stresses of Brass Specimens: Residual Stresses of the specimens before finishing and after finishing has been shown below from Graph. 7.32 to Graph.7.40 The specimens taken are in order from the L27 table. The first specimen is from L1, the second specimen is from L2, the Third Specimen is from L3, and so on. After completion of the first cycle of finishing, these specimens are subjected to the second cycle from L10 to L18 and finally the last cycle from L19 to L27, from the second cycle onwards the specimens have been chosen randomly and finished. The residual stresses after completing the Last cycle (third cycle) for each specimen has been recorded and shown in the graphs below. The left side graph shows the residual stress before finishing and the right-side graph shows after finishing. Results show that the compressive residual stresses have been induced due to finishing operation

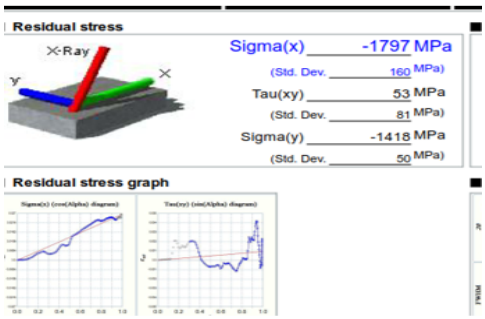

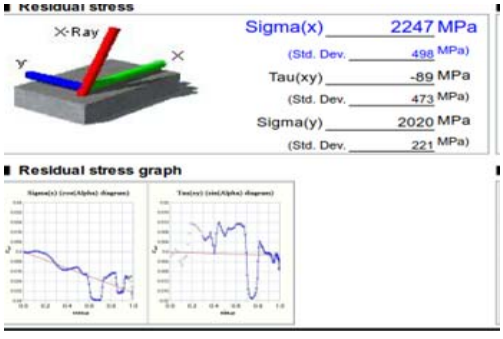

Graph.7.32 Residual stresses of Brass specimen 1 Before and After finishing

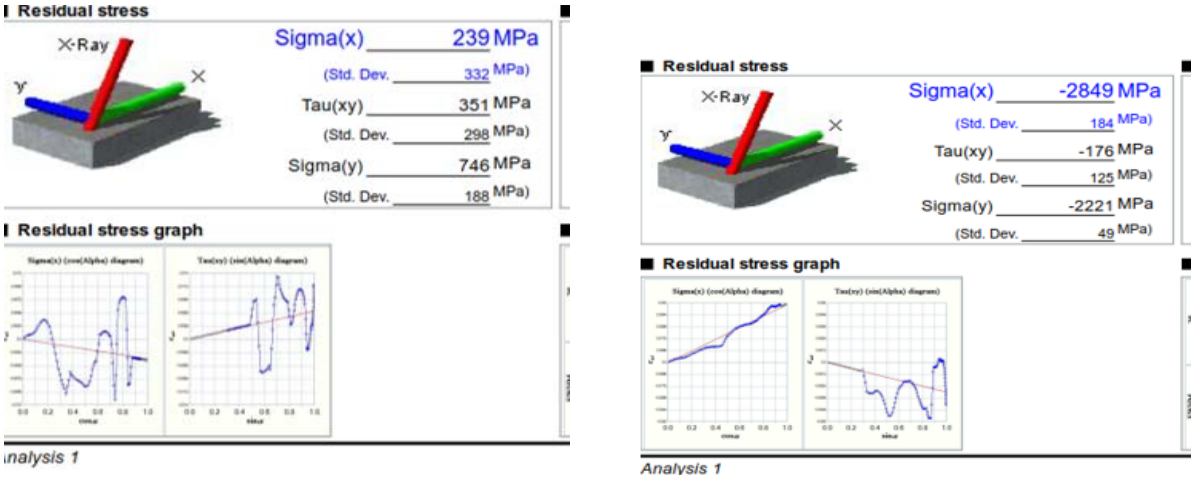

Graph.7.33 Residual stresses of Brass specimen 2 Before and After finishing

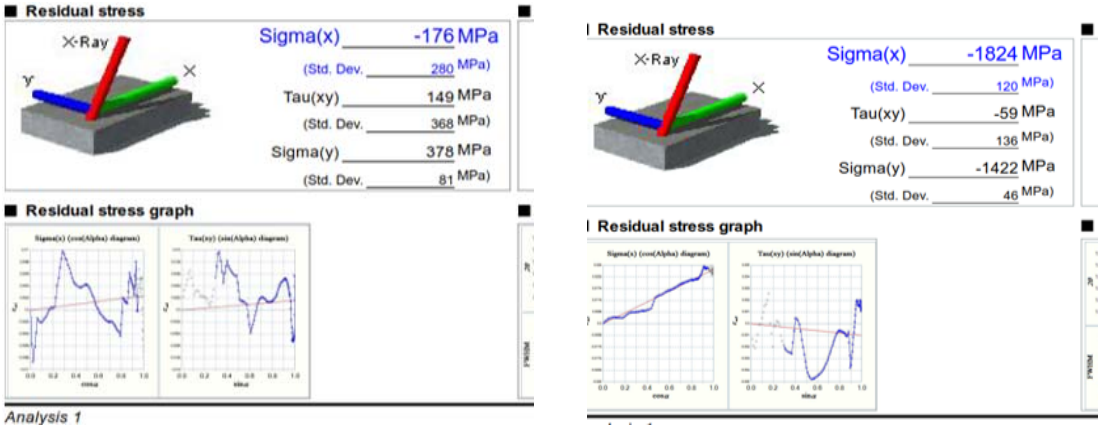

Graph.7.34 Residual stresses of Brass specimen 3 Before and After finishing

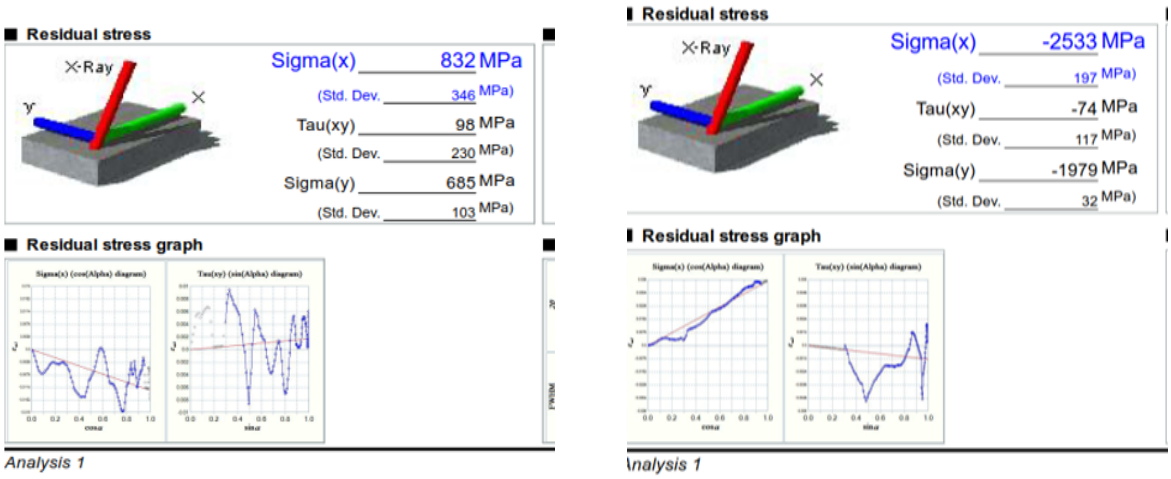

Graph.7.35 Residual stresses of Brass specimen 4 Before and After finishing

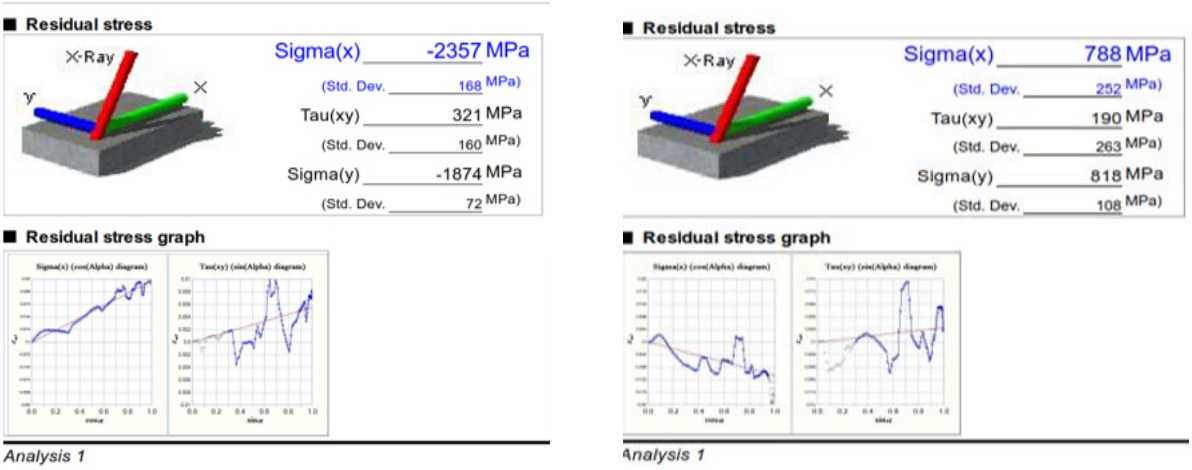

Graph.7.36 Residual stresses of Brass specimen 5 Before and After finishing

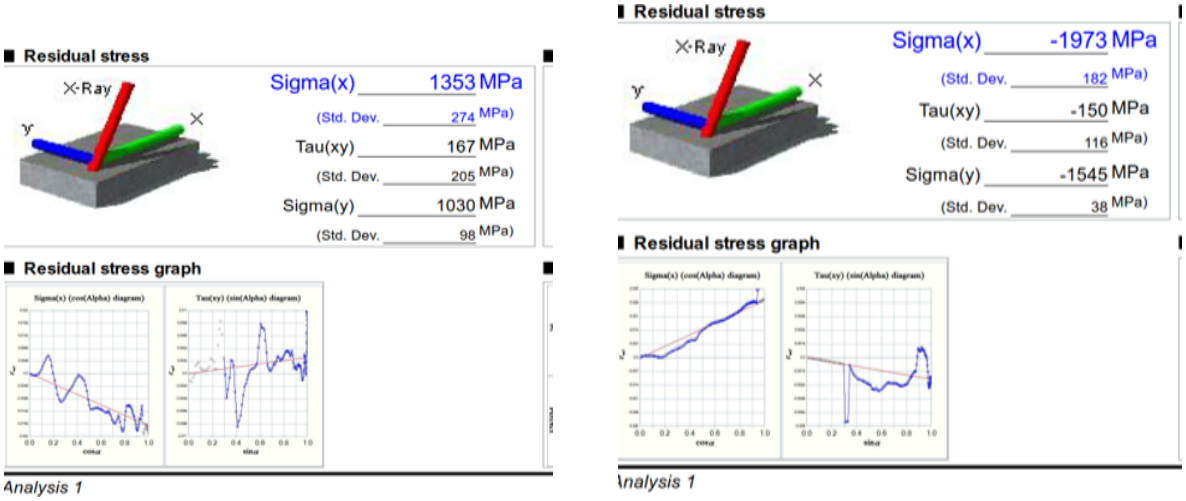

Graph.7.37 Residual stresses of Brass specimen 6 Before and After finishing

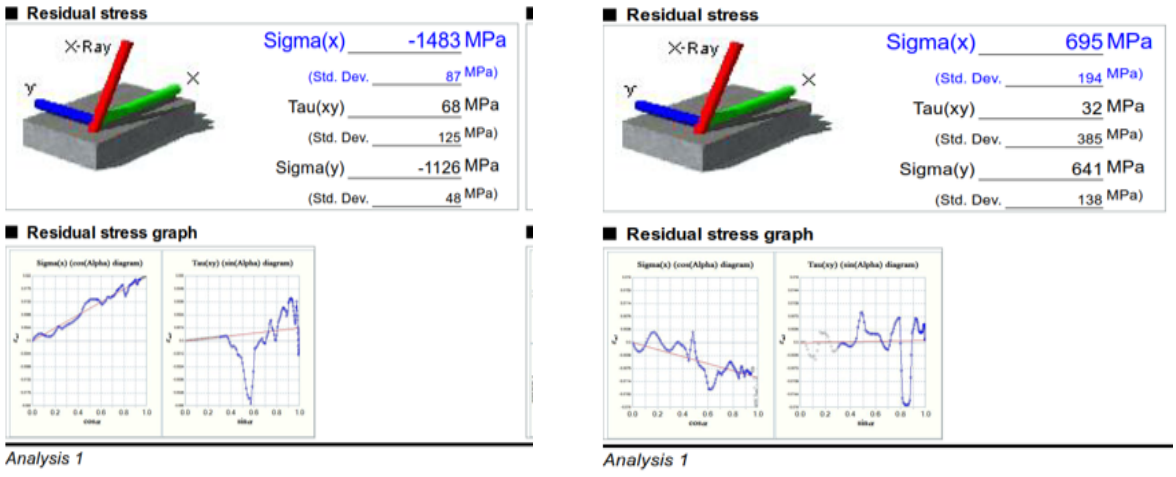

Graph.7.38 Residual stresses of Brass specimen 7 Before and After finishing

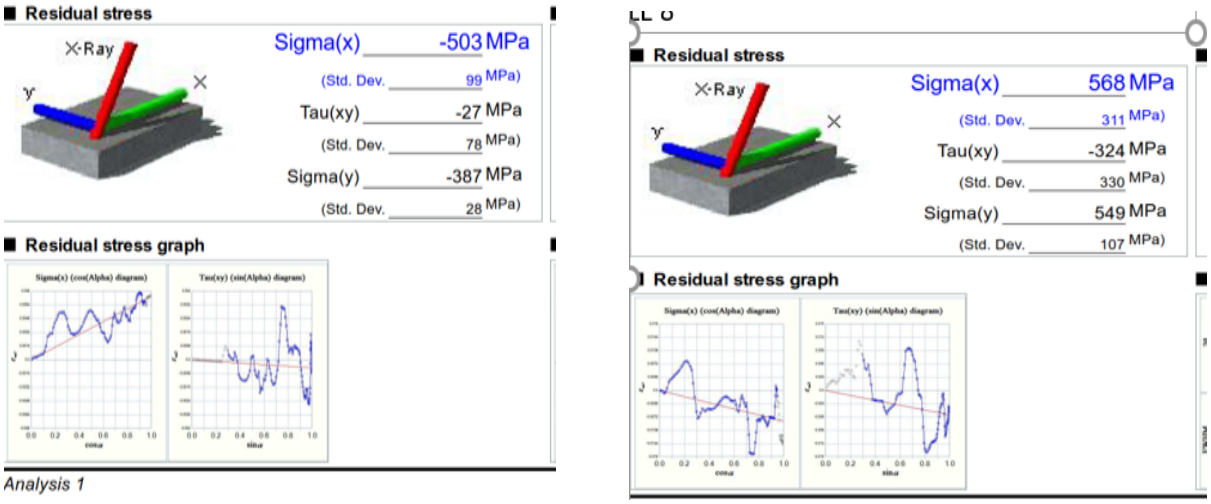

Graph.7.39 Residual stresses of Brass specimen 8 Before and After finishing

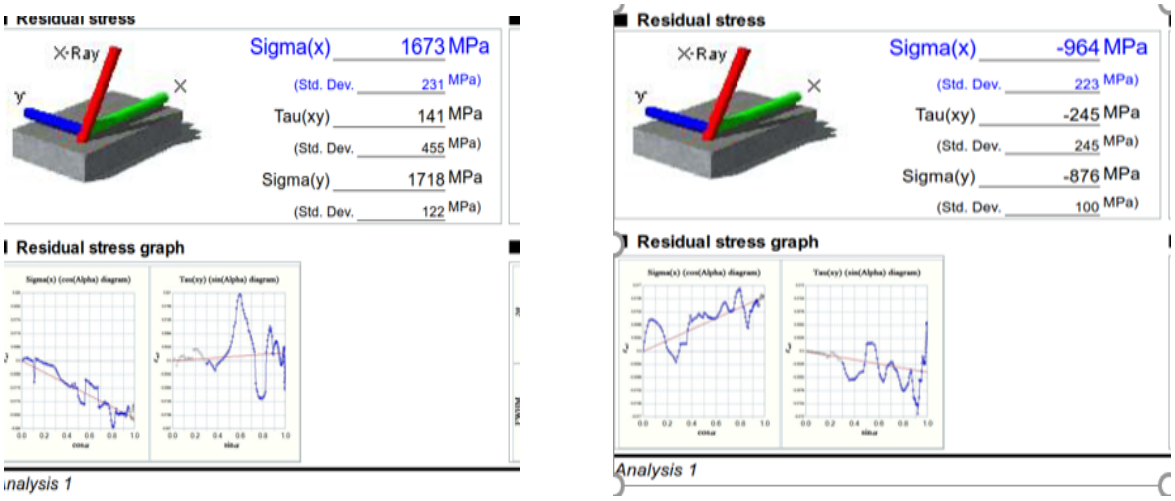

Graph.7.40 Residual stresses of Brass specimen 9 Before and After finishing

7.9.3. Results of Optimisation of Brass Specimen: Results obtained based on the experiments performed as per L27 Orthogonal Array of experiments has been shown below. MiniTab 17 software is used for the Optimisation of the process parameters based on Taguchi's Optimisation Model.

Optimization results based on Taguchi's Model for Brass.

Results for: Worksheet 2

Taguchi Design

```
Taguchi Orthogonal Array Design
```

L27(3^6)

Factors: 6
Runs: 27

Columns of L27(3^13) Array

1 2 3 4 5 6

Taguchi Analysis: Δm versus MFD, AMN, MTRS, FT, FEED, USAMP

Linear Model Analysis: SN ratios versus MFD, AMN, MTRS, FT, FEED, USAMP

Estimated Model Coefficients for SN ratios

Term	Coef	SE Coef	T	P
Constant	-28.0866	0.5056	-55.547	0.000
MFD 0.3577	-13.6327	0.7151	-19.065	0.000
MFD 0.4246	5.3726	0.7151	7.513	0.000
AMN 400	2.3550	0.7151	3.293	0.005
AMN 600	-1.0976	0.7151	-1.535	0.147
MTRS 480	0.8925	0.7151	1.248	0.232
MTRS 600	1.2764	0.7151	1.785	0.096
FT 6	-2.8732	0.7151	-4.018	0.001
FT 9	2.2379	0.7151	3.130	0.007
FEED 12	-1.7092	0.7151	-2.390	0.031
FEED 18	1.7436	0.7151	2.438	0.029
USAMP 15	-2.0075	0.7151	-2.807	0.014
USAMP 30	0.0176	0.7151	0.025	0.981

S = 2.627   R-Sq = 96.8%   R-Sq(adj) = 94.1%

Analysis of Variance for SN ratios

Source	DF	Seq SS	Adj SS	Adj MS	F	P
MFD	2	2546.50	2546.50	1273.25	184.45	0.000
AMN	2	74.98	74.98	37.49	5.43	0.018
MTRS	2	64.17	64.17	32.08	4.65	0.028
FT	2	123.00	123.00	61.50	8.91	0.003
FEED	2	53.66	53.66	26.83	3.89	0.045
USAMP	2	71.91	71.91	35.95	5.21	0.020
Residual Error	14	96.64	96.64	6.90		
Total	26	3030.87				

Linear Model Analysis: Means versus MFD, AMN, MTRS, FT, FEED, USAMP

Estimated Model Coefficients for Means

Term	Coef	SE Coef	T	P
Constant	0.067411	0.004234	15.923	0.000
MFD 0.3577	-0.058167	0.005987	-9.715	0.000
MFD 0.4246	0.019178	0.005987	3.203	0.006
AMN 400	0.022211	0.005987	3.710	0.002
AMN 600	-0.014322	0.005987	-2.392	0.031
MTRS 480	0.004433	0.005987	0.740	0.471
MTRS 600	0.001611	0.005987	0.269	0.792
FT 6	-0.026456	0.005987	-4.419	0.001
FT 9	0.015700	0.005987	2.622	0.020
FEED 12	-0.000300	0.005987	-0.050	0.961
FEED 18	0.007222	0.005987	1.206	0.248
USAMP 15	-0.004600	0.005987	-0.768	0.455

```
USAMP 30    -0.007000  0.005987  -1.169  0.262

S = 0.02200   R-Sq = 90.8%   R-Sq(adj) = 83.0%


Analysis of Variance for Means

Source          DF    Seq SS    Adj SS    Adj MS      F      P
MFD              2  0.047442  0.047442  0.023721  49.02  0.000
AMN              2  0.006846  0.006846  0.003423   7.07  0.008
MTRS             2  0.000529  0.000529  0.000265   0.55  0.591
FT               2  0.009559  0.009559  0.004779   9.88  0.002
FEED             2  0.000902  0.000902  0.000451   0.93  0.417
USAMP            2  0.001842  0.001842  0.000921   1.90  0.186
Residual Error  14  0.006775  0.006775  0.000484
Total           26  0.073894


Response Table for Signal to Noise Ratios
Larger is better

Level     MFD     AMN     MTRS      FT    FEED   USAMP
1      -41.72  -25.73  -27.19  -30.96  -29.80  -30.09
2      -22.71  -29.18  -26.81  -25.85  -26.34  -28.07
3      -19.83  -29.34  -30.26  -27.45  -28.12  -26.10
Delta   21.89    3.61    3.45    5.11    3.45    4.00
Rank        1       4       6       2       5       3


Response Table for Means

Level       MFD       AMN       MTRS         FT       FEED      USAMP
1      0.009244  0.089622  0.071844  0.040956  0.067111  0.062811
2      0.086589  0.053089  0.069022  0.083111  0.074633  0.060411
3      0.106400  0.059522  0.061367  0.078167  0.060489  0.079011
Delta  0.097156  0.036533  0.010478  0.042156  0.014144  0.018600
Rank          1         3         6         2         5         4
```

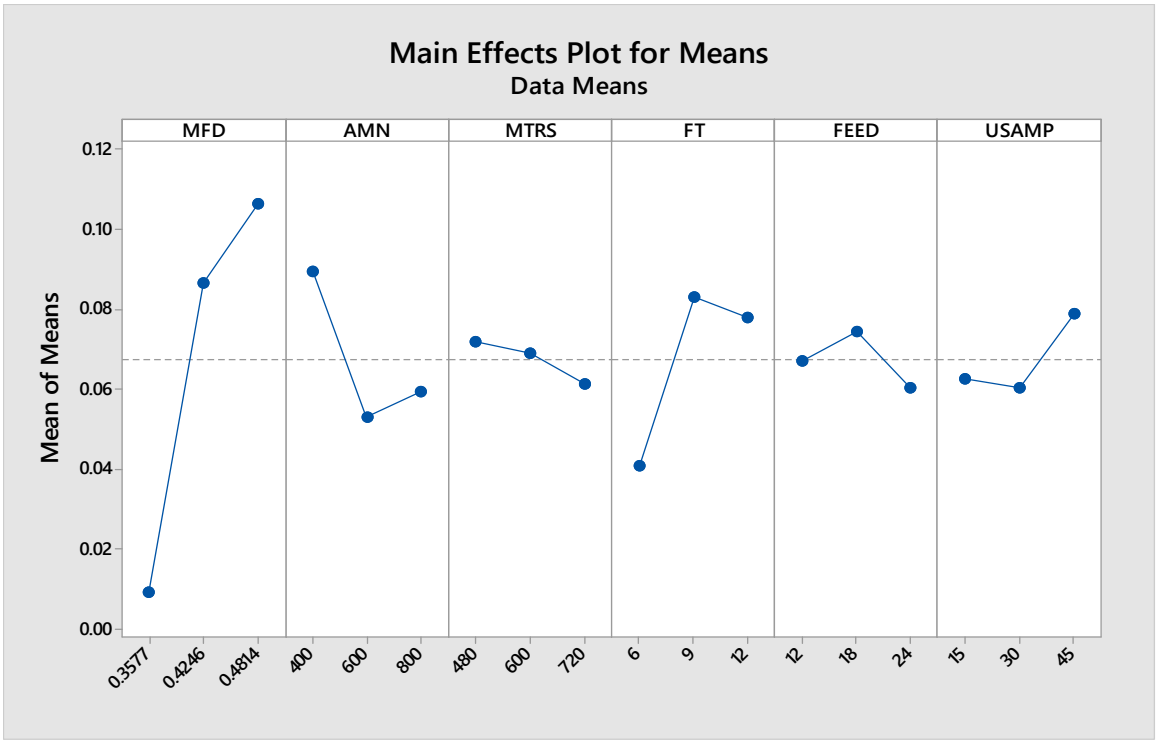

Graph.7.41. Main effect plot for means

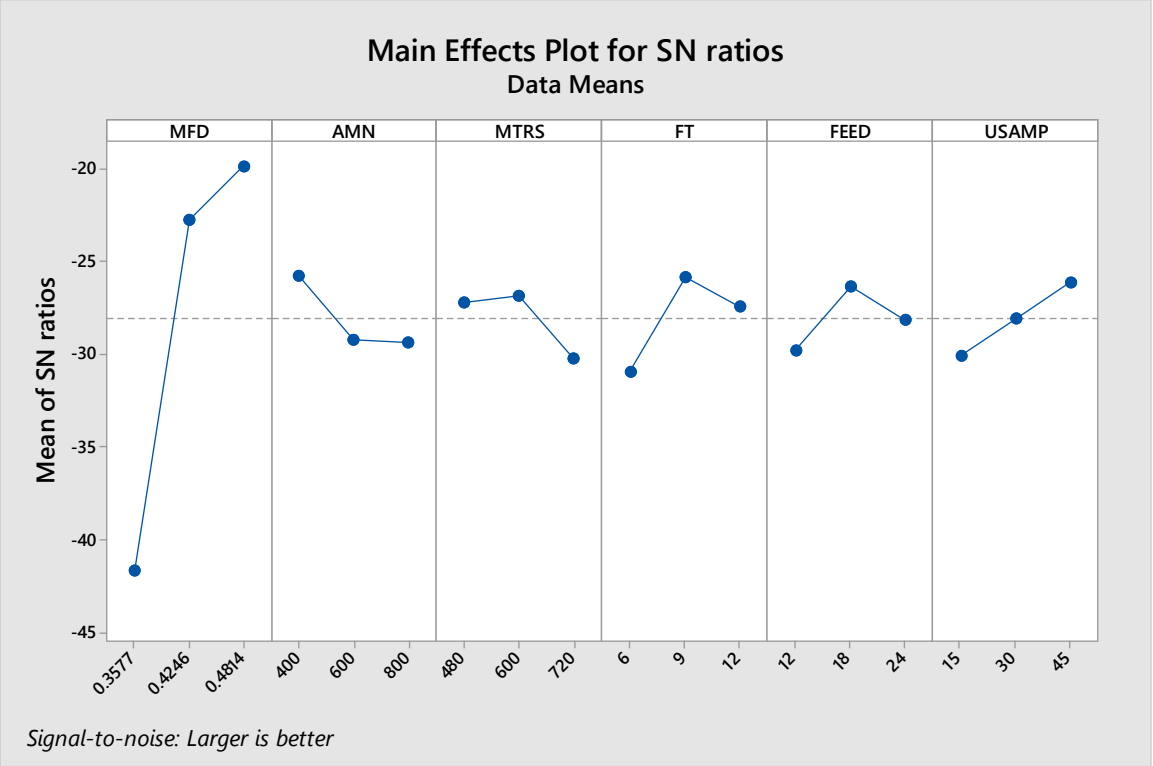

Graph.7.42. Main effect plot for means

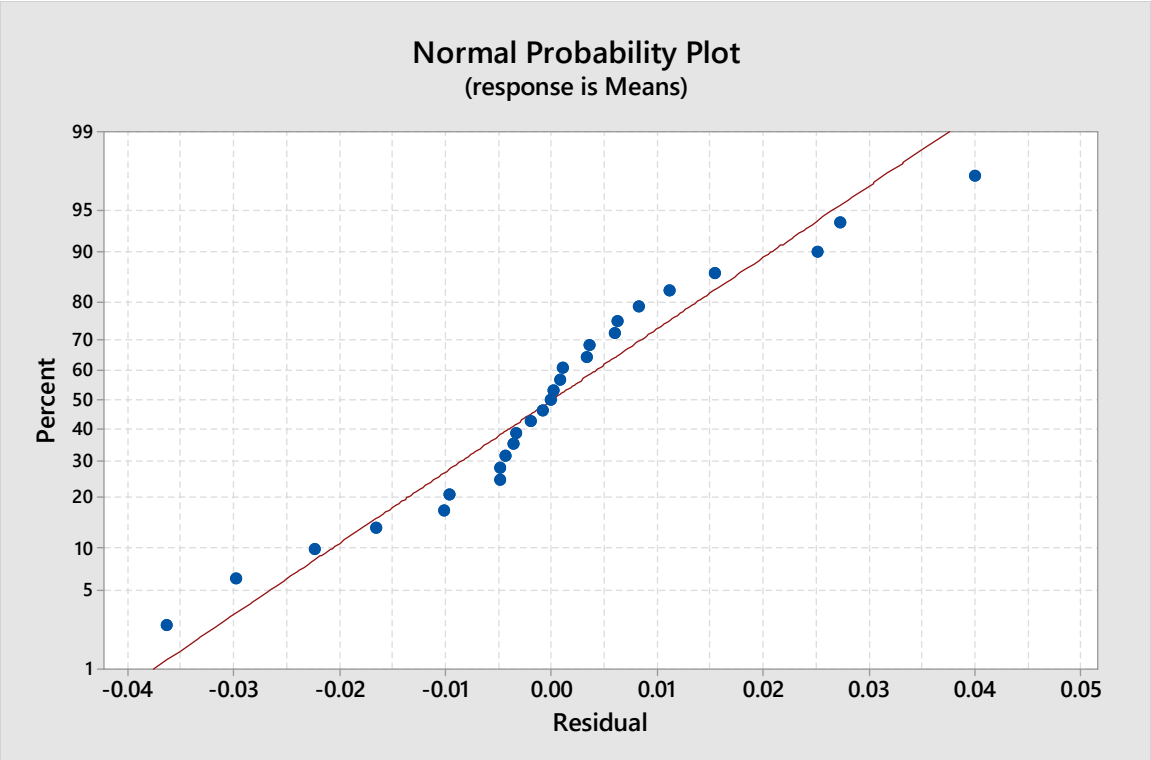

Graph. 7.43.Normal Probability plot (Means)

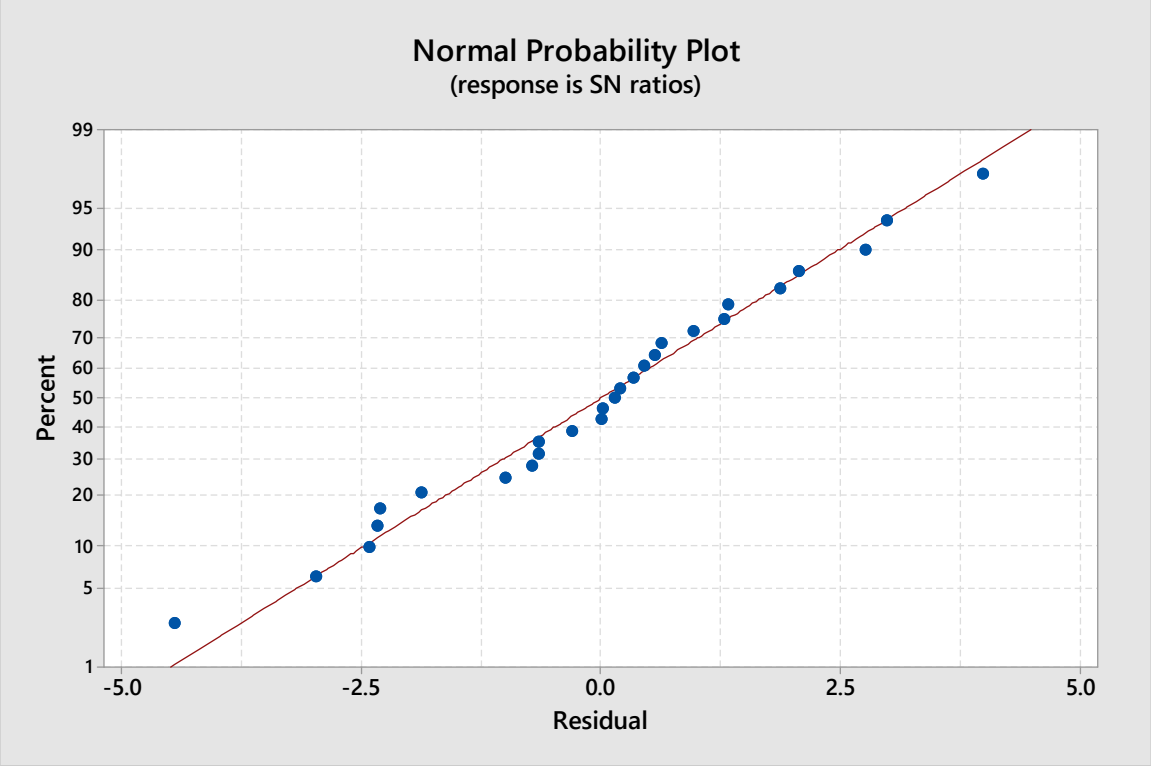

Graph.7.44.Normal Probability Plot (SN ratio)

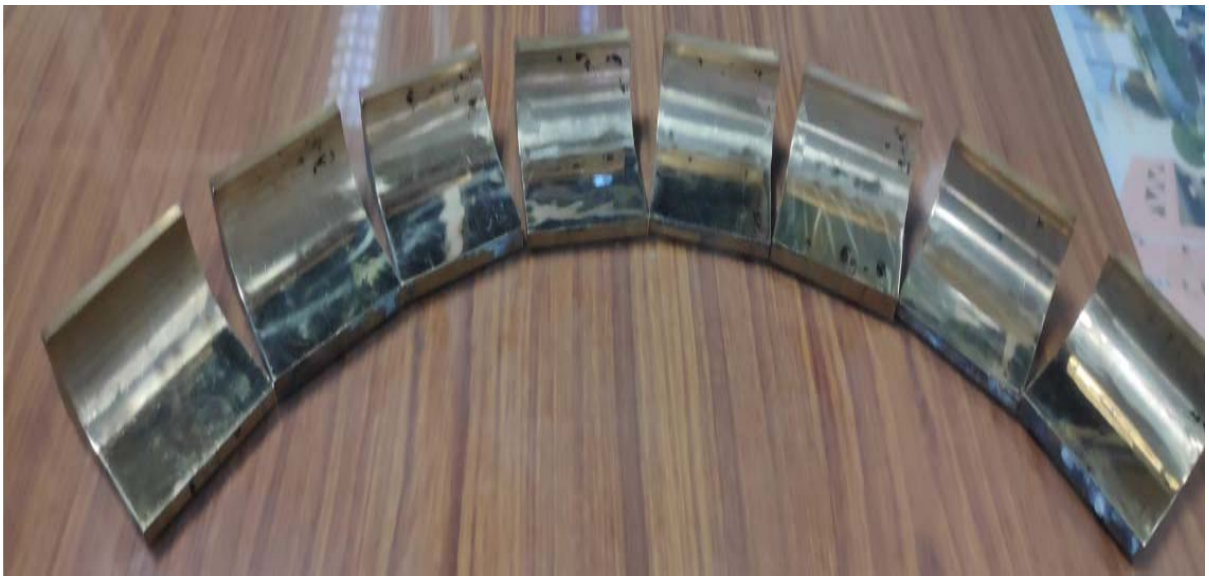

Fig. 7.13. Brass Specimen Finished with Viscoelastic Magnetic Abrasive Medium

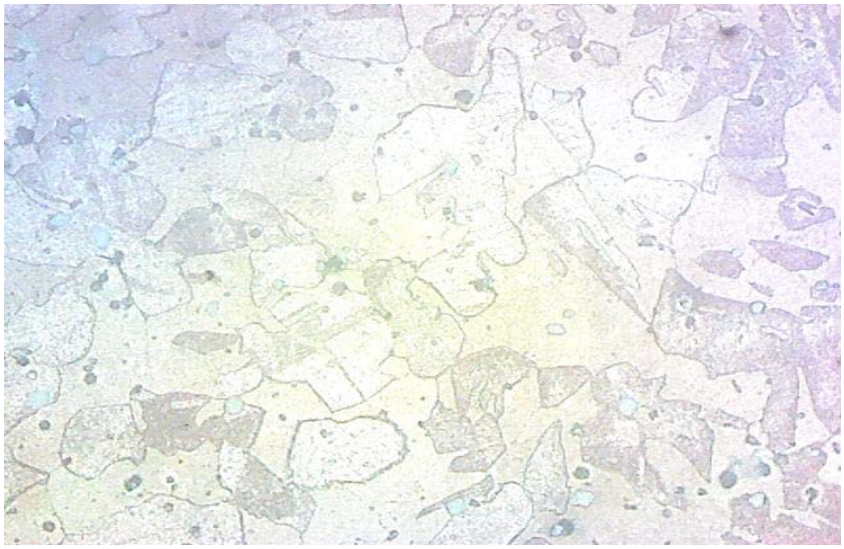

Fig.7.14. Etched Brass Specimen finished with VEMAF Process 500X

7.9.3.1. Result and Discussion of External surface finishing of Brass Specimens:

1. Both changes in the surface finish(ΔRa) and Metal removal (Δm) are low at L1, where all the process parameters are having the least value.
2. Maximum material removal (Δm) is 0.1768 grams that occurred for L19 having Magnetic Flux density value of 0.4814 T, Abrasive Mesh Number 400, Rotational speed of 720 Rpm, Finishing time of 9 minutes(Level 2), Feed of 12 mm/min, and Ultrasonic amplitude of 45 μm.
3. Change in material removal is in increasing trend from level 1 to Level 3 of Magnetic flux densities. The higher the Magnetic flux density, the better would be the ability to make a deeper micro indent, which forms the ridges around and these ridges will be sheared by the abrasives.
4. The maximum change in the surface finish(ΔRa) is obtainable for the Maximum flux density (Level 3), Abrasive Mesh number 800(Level 3), Rotational speed of 600 Rpm(Level 2), Finishing time of 6 minutes(Level 1) and Ultrasonic Amplitude of 45 (μm).
5. The parameters [l27] contributed to the highest reduction in surface roughness ΔRa, however, it did not produce the finest surface finish as the surface finish always depends on the initial surface roughness of the Specimen. Here every specimen is finished in three cycles with a different set of process parameters.
6. The finest surface finish obtained from this process is 0.0776 μm obtained in three cycles of finishing from an initial value of 0.359 μm.

7. The observations made from the Optimisation of TAGUCHI's optimization model are as mentioned below.
   i. The assumption of Normal distribution is valid as all the response points (Δm) are nearer to the Normal distribution line. Ranking of the process parameters, ranking, and significance is tabulated below.

Table 7. 16. Comparison of Ranking, Levels, and Significance values for Brass.

Process Parameter	MFD T	AMN	MTRS Rpm	FT Minutes	FEED Mm/Min	USAMP µm
Ranking	1	4	6	2	5	3
Level	3	1	2	2	2	3
p	0.00	0.018	0.028	0.003	0.045	0.020
Delta	21.89	3.61	3,45	5.11	3.45	4.00

   ii. All the process parameters are having 'p' values less than 0.05, which signifies that the variable values in each parameter are significant. Since 'p' is a statistical tool that signifies the significance of variations in the process. R-Sq and R-Sq [adj] are showing higher percentages. Here these values are 96.8% and 94.1%, which are higher only. So experiment parameters are highly significant.
   iii. For Non- Magnetic material the Magnetic Flux density is the highest, as the indentation force is higher at the Maximum Flux density.
   iv. Abrasive Mesh number is ranked 4th and the abrasive size is 400, which removes more material. This is in confirmation with most of the researchers' work which prefers coarser abrasive for more amount of material removal.
   v. The rotational speed is 600 Rpm, and it gives the necessary Tangential force to remove the peaks. However, increased Rotational Speed of the Magnetic tool would through the VEMAF medium in a tangential direction and further finishing and material removal would reduce.
   vi. Similarly, finishing time has got Level 2 in optimization as after finishing for 9 minutes under the prevailing experimental conditions, saturation will be reached and no advantage would be derived by increasing the finishing time to the next higher value, which is 12 minutes.
   vii. The feed is the motion of the tool in the lateral direction along the width. The width of the specimen is 40 mm and the preferred feed as per the Optimisation is 18 mm/minute, which is the optimum value as the increase in speed would leave the

medium behind and finishing can't be performed efficiently.

viii. Ultrasonic Amplitude as per Optimisation is 45 μm. Due to Ultrasonic vibration, the abrasives sitting in the valleys will be made to rotate along with the Magnetic Tool.

ix. Observation of the Surface roughness Graphs shown from 7.1 to 7.9 revealed that there is no waviness on the surfaces finished by VEMAF process.

7.10. Experimental Design for Finishing of External surfaces of Aluminium Specimens: Experiments have been performed based on Taguchi's Design of Experiments called Orthogonal Array of Experiments. The first Nine specimens have been subjected to finishing operation for Flux density of Level 1, other process parameters are chosen as per the L27 table. The first Nine experiments are conducted based on L1 to L9 on the nine specimens, followed by the next nine experiments; L10 to L18 and finally L19 to L27. From L10 onwards the specimens are machined in a randomized fashion

Table. 7.17. Orthogonal Array of Experiments for Aluminium

MFD [T]	AMN	MTRS RPM	FT Minutes	FEED mm/Min	USAMP μm	Ra Initial μm	Ra Final μm	ΔRa μm	Initial MASS[g]	Final MASS[g]	Metal removal Δm[g]
0.3577	400	480	6	12	15	0.568	0.562	0.006	46.4332	46.4319	0.0013
0.3577	400	480	6	18	30	0.454	0.443	0.011	45.3043	45.3012	0.0031
0.3577	400	480	6	24	45	0.584	0.561	0.027	47.0124	47.0085	0.0039
0.3577	600	600	9	12	15	0.39	0.375	0.015	45.9325	45.9309	0.0016
0.3577	600	600	9	18	30	0.544	0.512	0.032	46.0428	46.0373	0.0055
0.3577	600	600	9	24	45	0.415	0.379	0.036	46.7829	46.7792	0.0037
0.3577	800	720	12	12	15	0.343	0.321	0.023	47.3242	47.3229	0.0013
0.3577	800	720	12	18	30	0.326	0.292	0.034	46.1287	46.1268	0.0019
0.3577	800	720	12	24	45	0.34	0.281	0.059	45.3214	45.3193	0.0021
0.4246	400	600	12	12	30	0.561	0.467	0.094	47.0085	46.9780	0.0305
0.4246	400	600	12	18	45	0.512	0.411	0.101	46.0373	46.0049	0.0324
0.4246	400	600	12	24	15	0.443	0.343	0.100	47.0085	46.9645	0.0440
0.4246	600	720	6	12	30	0.562	0.447	0.115	46.4319	46.4252	0.0067
0.4246	600	720	6	18	45	0.281	0.155	0.126	45.3193	45.3003	0.0190
0.4246	600	720	6	24	15	0.375	0.264	0.111	45.9309	45.9215	0.0094
0.4246	800	480	9	12	30	0.379	0.311	0.088	46.7792	46.7492	0.0300
0.4246	800	480	9	18	45	0.292	0.172	0.120	46.1268	46.0848	0.0420
0.4246	800	480	9	24	15	0.321	0.237	0.084	47.3229	47.3079	0.0150
0.4814	400	720	9	12	45	0.447	0.341	0.106	46.4252	46.3732	0.0520
0.4814	400	720	9	18	15	0.343	0.219	0.124	46.9645	46.9145	0.0400

0.4814	400	720	9	24	30	0.467	0.359	0.108	46.9780	46.9350	0.0430
0.4814	600	480	12	12	45	0.264	0.182	0.082	45.9215	45.8915	0.0300
0.4814	600	480	12	18	15	0.411	0.318	0.093	46.0049	45.9679	0.0370
0.4814	600	480	12	24	30	0.172	0.0804	0.0916	46.0848	46.0528	0.0320
0.4814	800	600	6	12	45	0.155	0.0783	0.0767	45.3003	45.2673	0.0240
0.4814	800	600	6	18	15	0.311	0.142	0.169	46.7492	46.7282	0.0210
0.4814	800	600	6	24	30	0.237	0.097	0.14	47.3079	47.2829	0.0250

7.10.1. Surface roughness of the Aluminium Specimen: Measured values of Surface roughness of Brass has been shown below. Values of the surface roughness are the surface roughness of the final nine experiments based on the L27 Orthogonal Array of experiments of Taguchi.

7.10.1.1. Surface roughness (Ra) measured data for Aluminium:

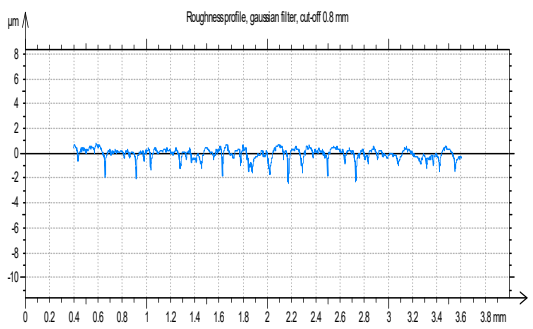

Parameters calculated on the profile Profile

* Parameters calculated by mean of all the sampling lengthes.
* A microroughness filtering is used, with a ratio of 2.5 µm.

Roughness Parameters, Gaussian filter, 0.8 mm

Ra = 0.341 µm

Graph7.45. Surface roughness of finished Aluminium specimen L19

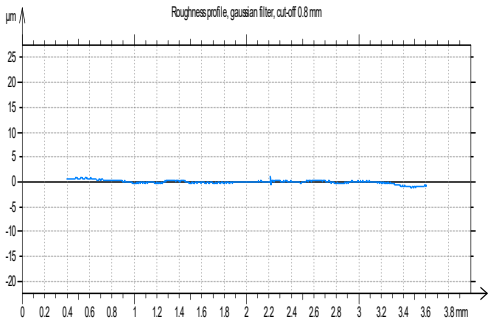

Parameters calculated on the profile Profile

* Parameters calculated by mean of all the sampling lengthes.
* A microroughness filtering is used, with a ratio of 2.5 µm.

Roughness Parameters, Gaussian filter, 0.8 mm

Ra = 0.219 µm

Graph7.46. Surface roughness of finished Aluminium specimen L20

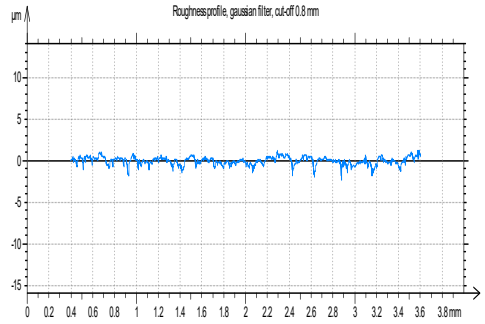

Parameters calculated on the profile Profile

* Parameters calculated by mean of all the sampling lengthes.
* A microroughness filtering is used, with a ratio of 2.5 µm.

Roughness Parameters, Gaussian filter, 0.8 mm

Ra = 0.359 µm

Graph7.47. Surface roughness of finished Aluminium specimen L21

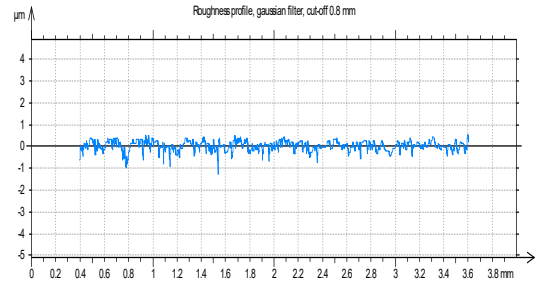

Parameters calculated on the profile Profile

* Parameters calculated by mean of all the sampling lengthes.
* A microroughness filtering is used, with a ratio of 2.5 µm.

Roughness Parameters, Gaussian filter, 0.8 mm

Ra = 0.182 µm

Graph7.48. Surface roughness of finished Aluminium specimen L22

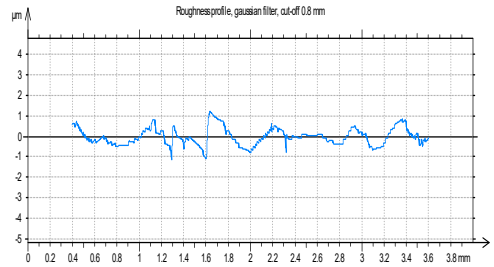

Parameters calculated on the profile Profile

* Parameters calculated by mean of all the sampling lengthes.
* A microroughness filtering is used, with a ratio of 2.5 µm.

Roughness Parameters, Gaussian filter, 0.8 mm

Ra = 0.318 µm

Graph7.49. Surface roughness of finished Aluminium specimen L23

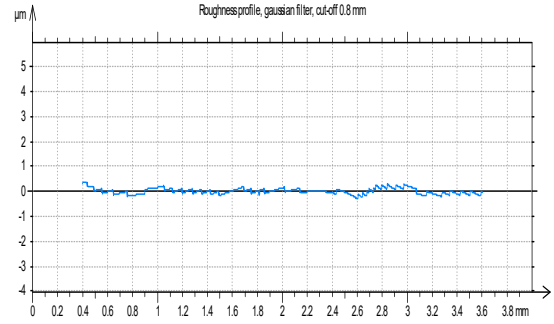

Parameters calculated on the profile Profile

* Parameters calculated by mean of all the sampling lengthes.
* A microroughness filtering is used, with a ratio of 2.5 µm.

Roughness Parameters, Gaussian filter, 0.8 mm

Ra = 0.0804 µm

Graph7.50. Surface roughness of finished Aluminium specimen L24

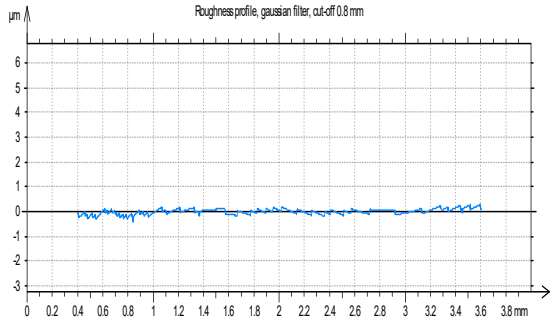

Parameters calculated on the profile Profile

* Parameters calculated by mean of all the sampling lengthes.
* A microroughness filtering is used, with a ratio of 2.5 µm.

Roughness Parameters, Gaussian filter, 0.8 mm

Ra = 0.0783 µm

Graph7.51. Surface roughness of finished Aluminium specimen L25

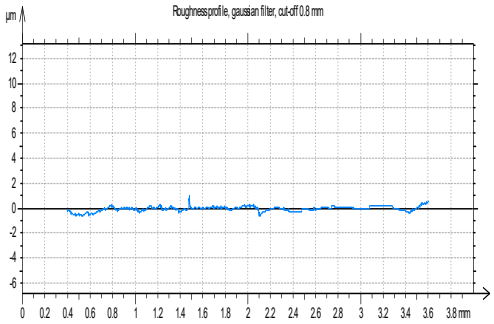

Parameters calculated on the profile Profile

* Parameters calculated by mean of all the sampling lengthes.
* A microroughness filtering is used, with a ratio of 2.5 µm.

Roughness Parameters, Gaussian filter, 0.8 mm

Ra = 0.142 µm

Graph7.52. Surface roughness of finished Aluminium specimen L26

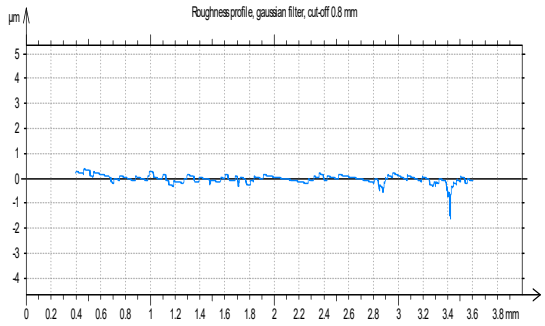

Parameters calculated on the profile Profile

* Parameters calculated by mean of all the sampling lengthes.
* A microroughness filtering is used, with a ratio of 2.5 µm.

Roughness Parameters, Gaussian filter, 0.8 mm

Ra = 0.097 µm

Graph7.53. Surface roughness of finished Aluminium specimen L27

7.10.2. Residual Stresses of Aluminium Specimens: Residual Stresses of the specimen before finishing and after finishing has been shown below from Graph.7.54 to Graph.7.62. The Specimen taken are in order from the L27 table. The first specimen is from L1, the Second specimen is from L2, the Third Specimen is from L3, and so on. After completion of the first cycle of finishing, these specimens are subjected to the second cycle from L10 to L18 and finally the last cycle from L19 to L27, from the second cycle onwards the specimen have been chosen

randomly and finished. The residual stresses after completing the Last cycle (third cycle) for each specimen has been recorded and shown in the graphs below. The observation of the residual stresses shows that due to the finishing operation Compressive Residual stresses got induced in the specimens.

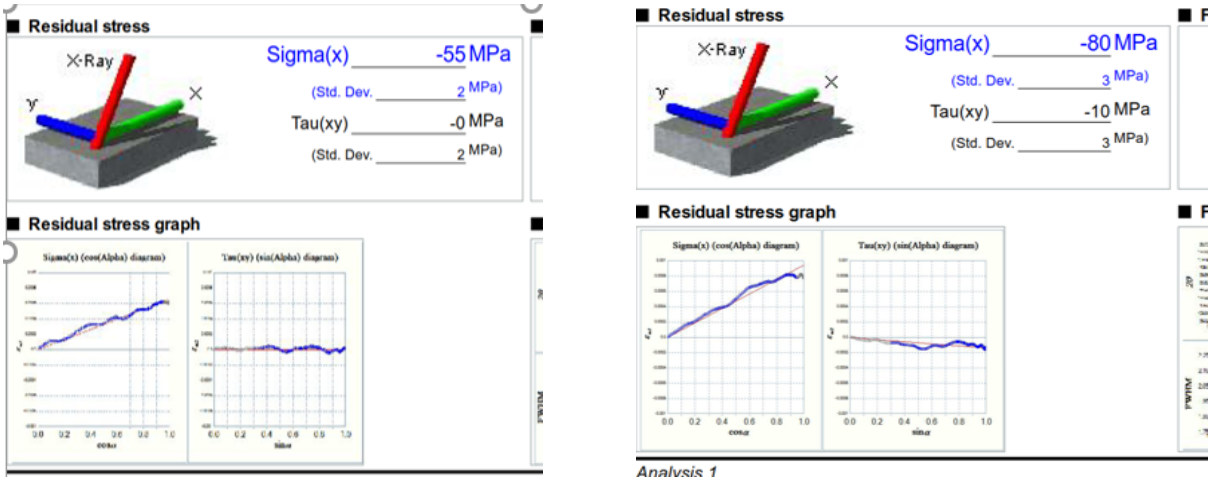

Graph.7.54 Residual stresses of Aluminium specimen 1 Before and After finishing

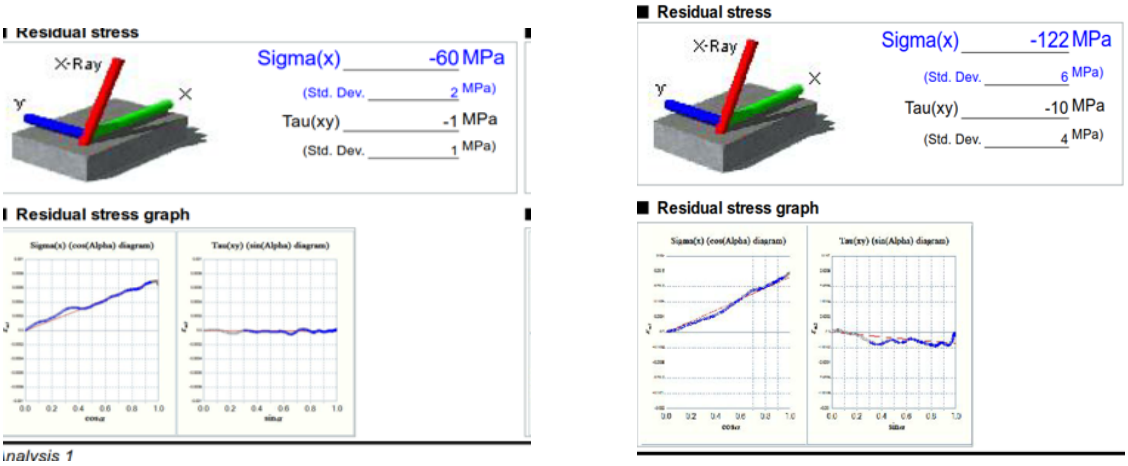

Graph.7.55 Residual stresses of Aluminium specimen 2 Before and After finishing

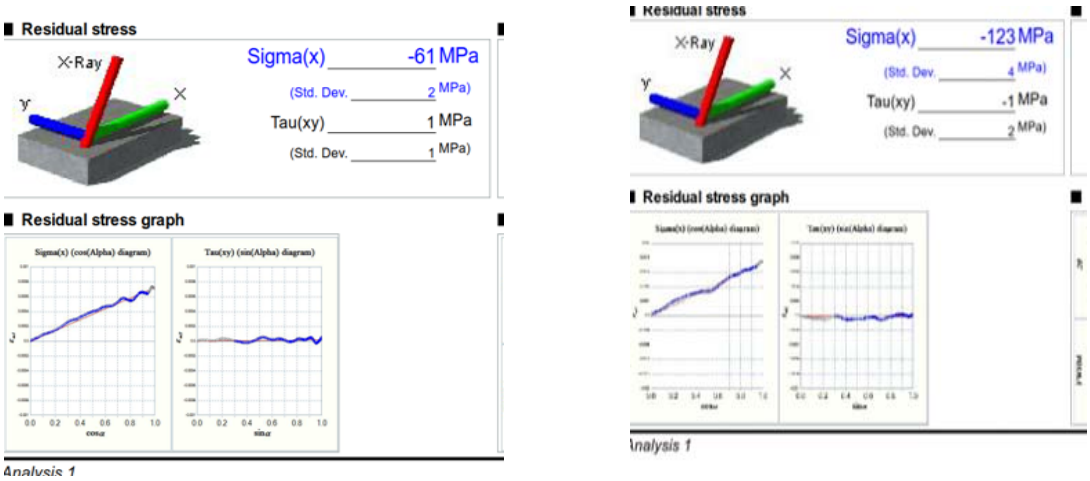

Graph.7.56 Residual stresses of Aluminium specimen 3 Before and After finishing

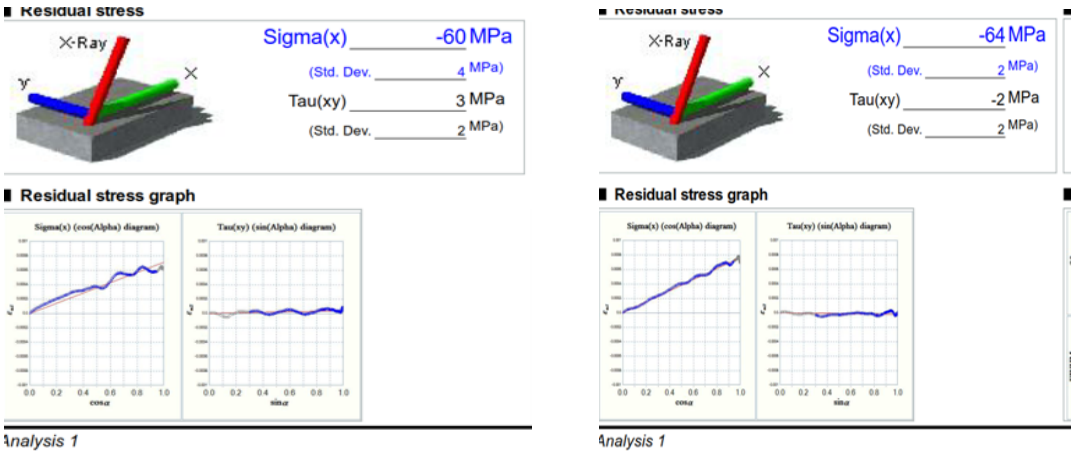

Graph.7.57 Residual stresses of Aluminium specimen 4 Before and After finishing

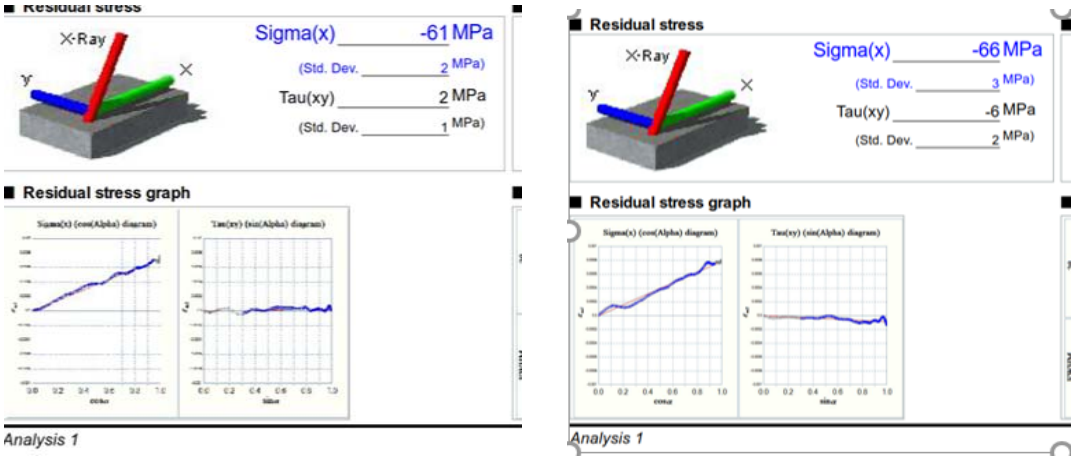

Graph.7.58 Residual stresses of Aluminium specimen 5 Before and After finishing

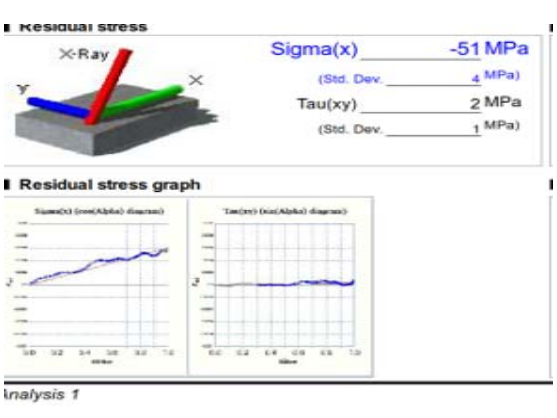

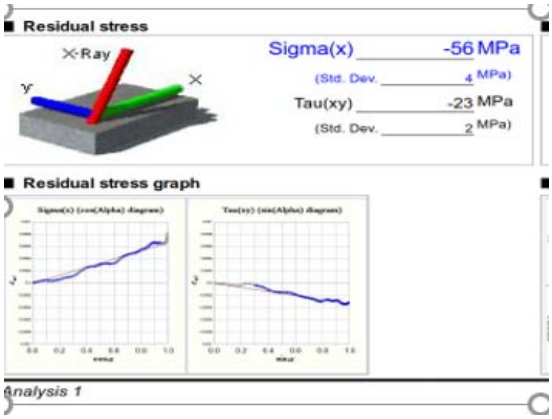

Graph.7.59 Residual stresses of Aluminium specimen 6 Before and After finishing

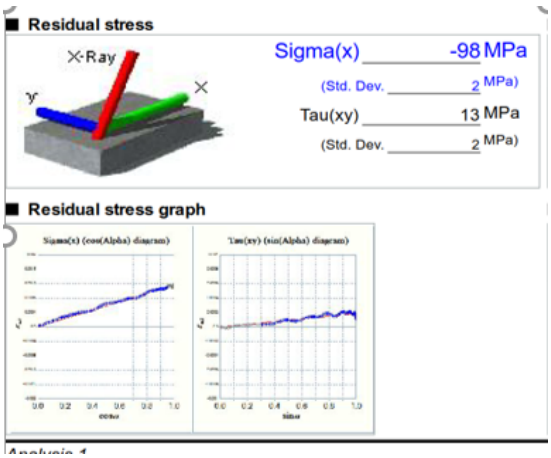

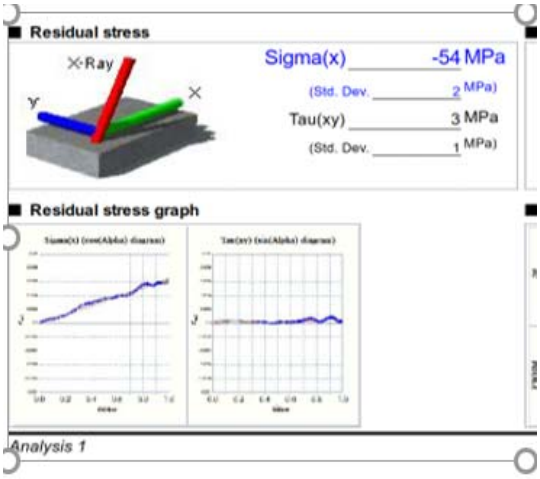

Graph.7.60 Residual stresses of Aluminium specimen 7 Before and After finishing

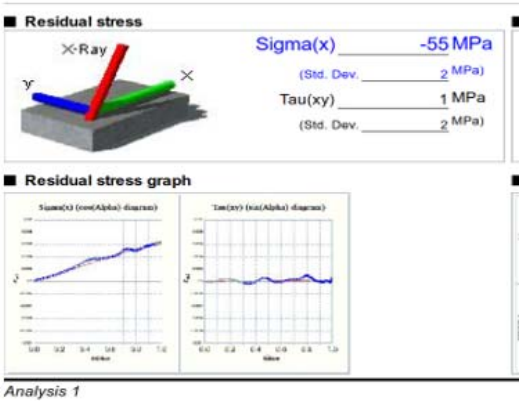

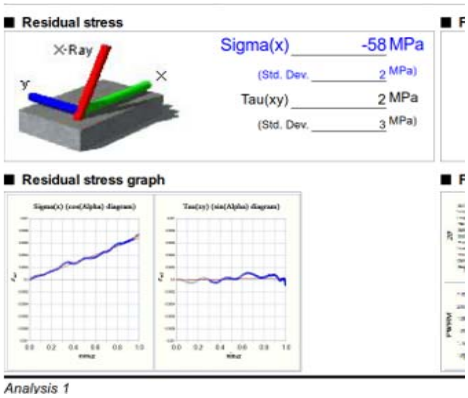

Graph.7.61 Residual stresses of Aluminium specimen 8 Before and After finishing

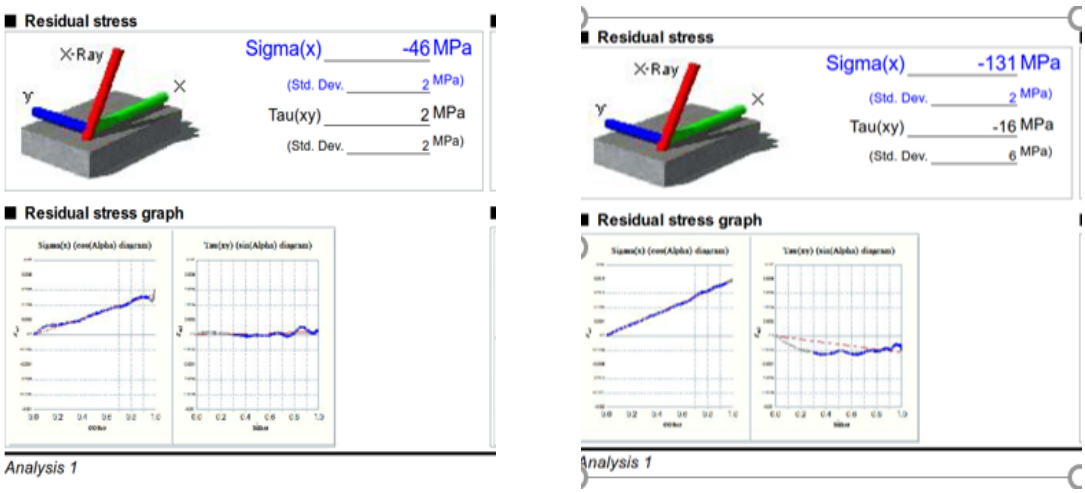

Graph.7.62 Residual stresses of Aluminium specimen 9 Before and After finishing

7.10.3. Results of Optimisation of Aluminium Specimens: Results obtained based on the experiments performed as per L27 Orthogonal Array of experiments has been shown below. MiniTab 17 software is used for the Optimisation of the process parameters based on Taguchi's Optimisation Model.

Taguchi Analysis: Δm versus MFD, AMN, MTRS, FT, FEED, USAMP

Linear Model Analysis: SN ratios versus MFD, AMN, MTRS, FT, FEED, USAMP

Estimated Model Coefficients for SN ratios

Term	Coef	SE Coef	T	P
Constant	-38.5044	0.4785	-80.469	0.000
MFD 0.3577	-13.8868	0.6767	-20.521	0.000
MFD 0.4246	5.1549	0.6767	7.618	0.000
AMN 400	2.4737	0.6767	3.656	0.003
AMN 600	-1.1820	0.6767	-1.747	0.103
MTRS 480	0.7784	0.6767	1.150	0.269
MTRS 600	1.2852	0.6767	1.899	0.078
FT 6	-2.8852	0.6767	-4.264	0.001
FT 9	2.3726	0.6767	3.506	0.003
FEED 12	-1.9560	0.6767	-2.890	0.012
FEED 18	1.6500	0.6767	2.438	0.029
USAMP 15	-2.1241	0.6767	-3.139	0.007
USAMP 30	0.3589	0.6767	0.530	0.604

S = 2.486 R-Sq = 97.2% R-Sq(adj) = 94.9%

Analysis of Variance for SN ratios

Source	DF	Seq SS	Adj SS	Adj MS	F	P
MFD	2	2660.95	2660.95	1330.48	215.22	0.000
AMN	2	82.67	82.67	41.33	6.69	0.009
MTRS	2	58.64	58.64	29.32	4.74	0.027
FT	2	127.94	127.94	63.97	10.35	0.002
FEED	2	59.78	59.78	29.89	4.83	0.025
USAMP	2	69.81	69.81	34.91	5.65	0.016
Residual Error	14	86.55	86.55	6.18		

```
Total           26  3146.34
```

Linear Model Analysis: Means versus MFD, AMN, MTRS, FT, FEED, USAMP

```
Estimated Model Coefficients for Means

Term             Coef   SE Coef        T      P
Constant     0.020644  0.001200   17.208  0.000
MFD 0.3577  -0.017933  0.001697  -10.570  0.000
MFD 0.4246   0.004800  0.001697    2.829  0.013
AMN 400      0.007156  0.001697    4.217  0.001
AMN 600     -0.004544  0.001697   -2.678  0.018
MTRS 480     0.000944  0.001697    0.557  0.587
MTRS 600     0.000211  0.001697    0.124  0.903
FT 6        -0.008044  0.001697   -4.741  0.000
FT 9         0.005222  0.001697    3.078  0.008
FEED 12     -0.000933  0.001697   -0.550  0.591
FEED 18      0.001789  0.001697    1.054  0.310
USAMP 15    -0.001689  0.001697   -0.995  0.336
USAMP 30    -0.000900  0.001697   -0.530  0.604

S = 0.006234   R-Sq = 92.2%   R-Sq(adj) = 85.5%


Analysis of Variance for Means

Source          DF    Seq SS    Adj SS    Adj MS      F      P
MFD              2  0.004654  0.004654  0.002327  59.88  0.000
AMN              2  0.000708  0.000708  0.000354   9.11  0.003
MTRS             2  0.000020  0.000020  0.000010   0.26  0.772
FT               2  0.000900  0.000900  0.000450  11.57  0.001
FEED             2  0.000043  0.000043  0.000022   0.56  0.586
USAMP            2  0.000093  0.000093  0.000047   1.20  0.330
Residual Error  14  0.000544  0.000544  0.000039
Total           26  0.006963



Response Table for Signal to Noise Ratios
Larger is better

Level     MFD     AMN    MTRS      FT    FEED   USAMP
1      -52.39  -36.03  -37.73  -41.39  -40.46  -40.63
2      -33.35  -39.69  -37.22  -36.13  -36.85  -38.15
3      -29.77  -39.80  -40.57  -37.99  -38.20  -36.74
Delta   22.62    3.77    3.35    5.26    3.61    3.89
Rank        1       4       6       2       5       3


Response Table for Means

Level       MFD       AMN      MTRS        FT      FEED     USAMP
1      0.002711  0.027800  0.021589  0.012600  0.019711  0.018956
2      0.025444  0.016100  0.020856  0.025867  0.022433  0.019744
3      0.033778  0.018033  0.019489  0.023467  0.019789  0.023233
Delta  0.031067  0.011700  0.002100  0.013267  0.002722  0.004278
Rank          1         3         6         2         5         4
```

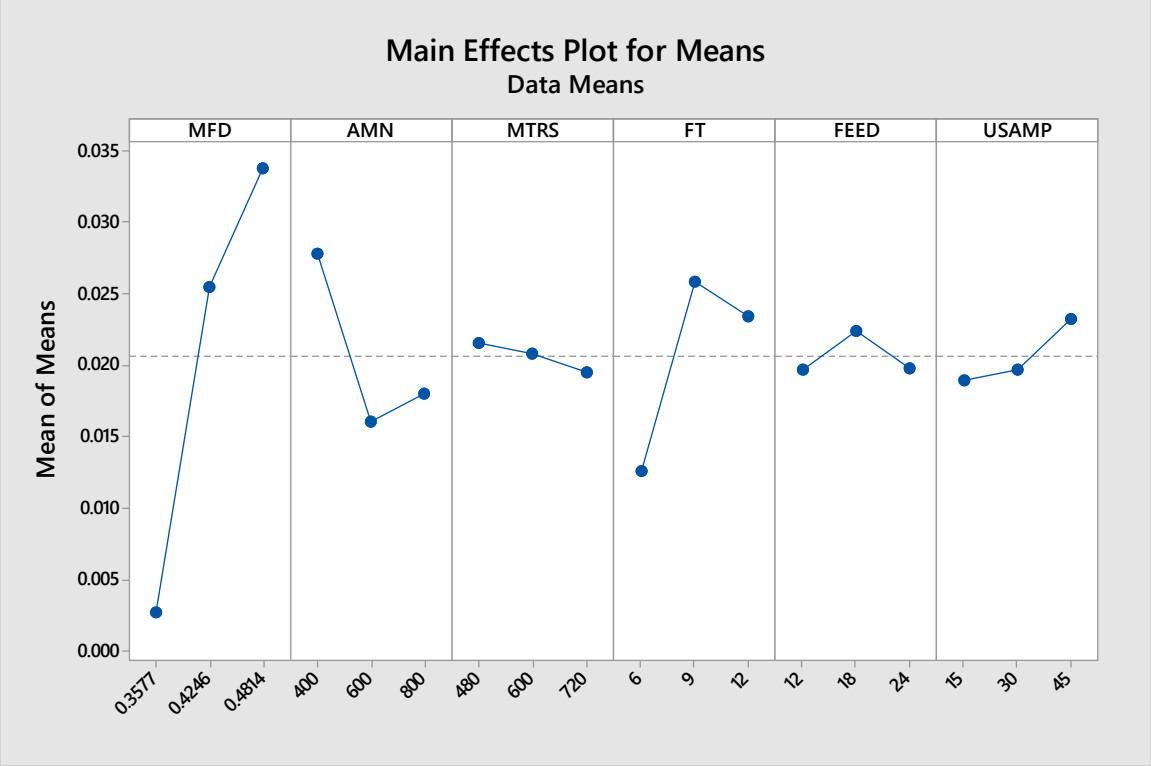

Graph.7.63. Main Plot for Means

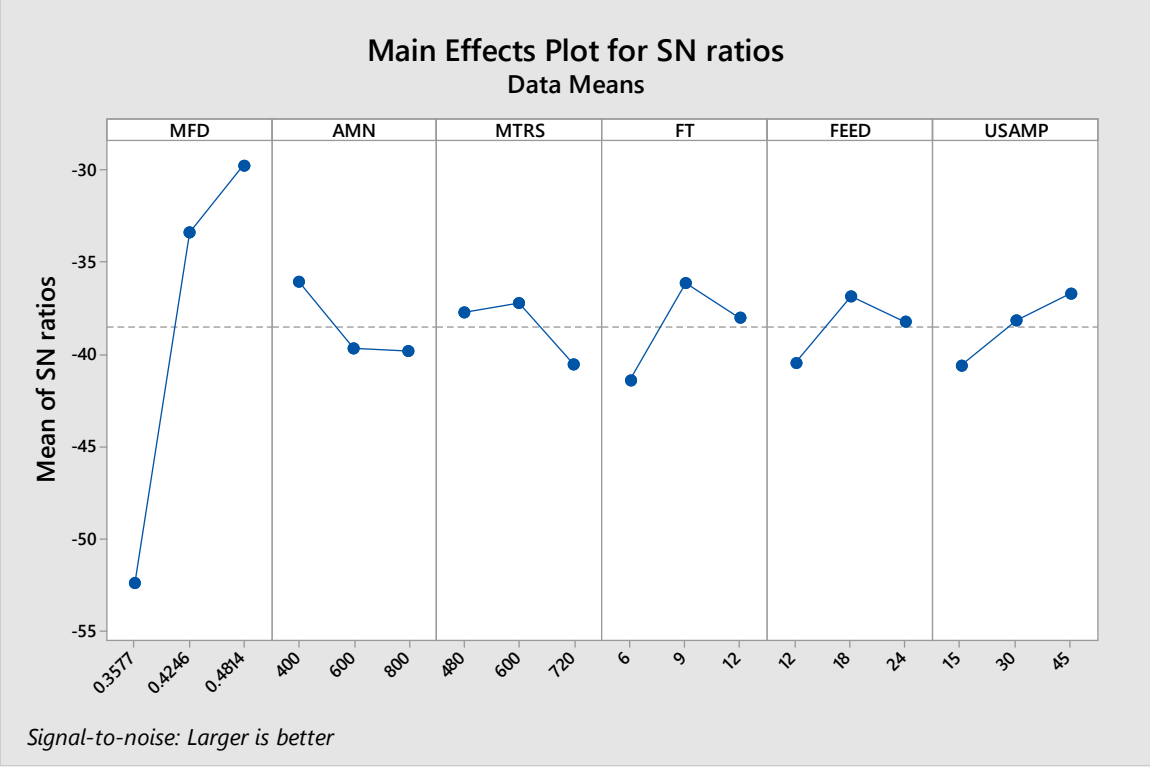

Graph.7.64. Main Plot for SN Ratio

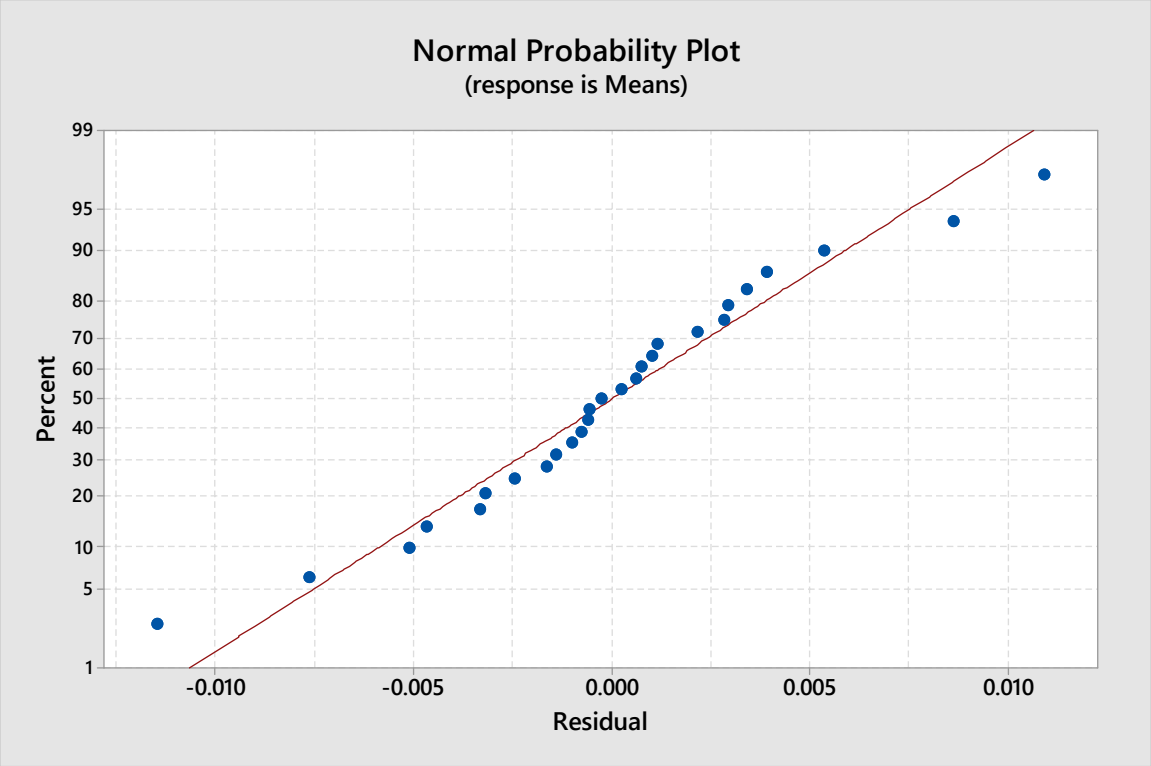

Graph.7.65.Normal Probability plot (Means)

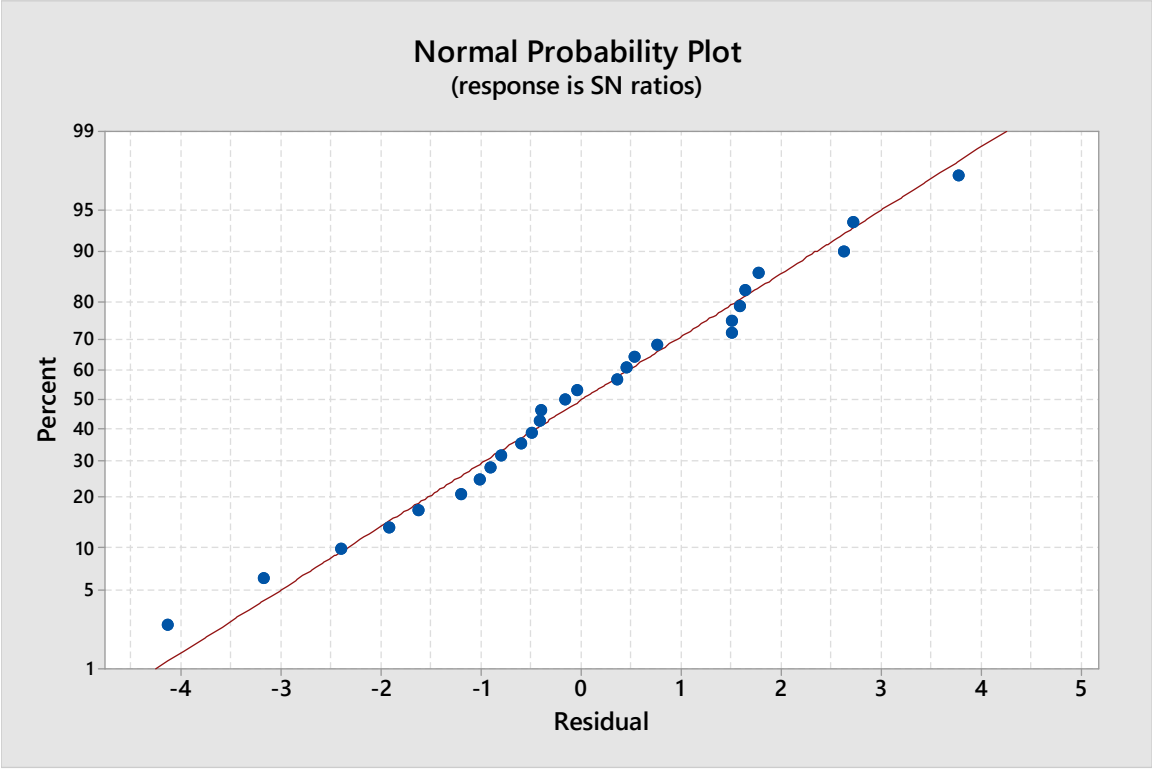

Gaph.7.66. Normal Probability Plot (SN ratio)

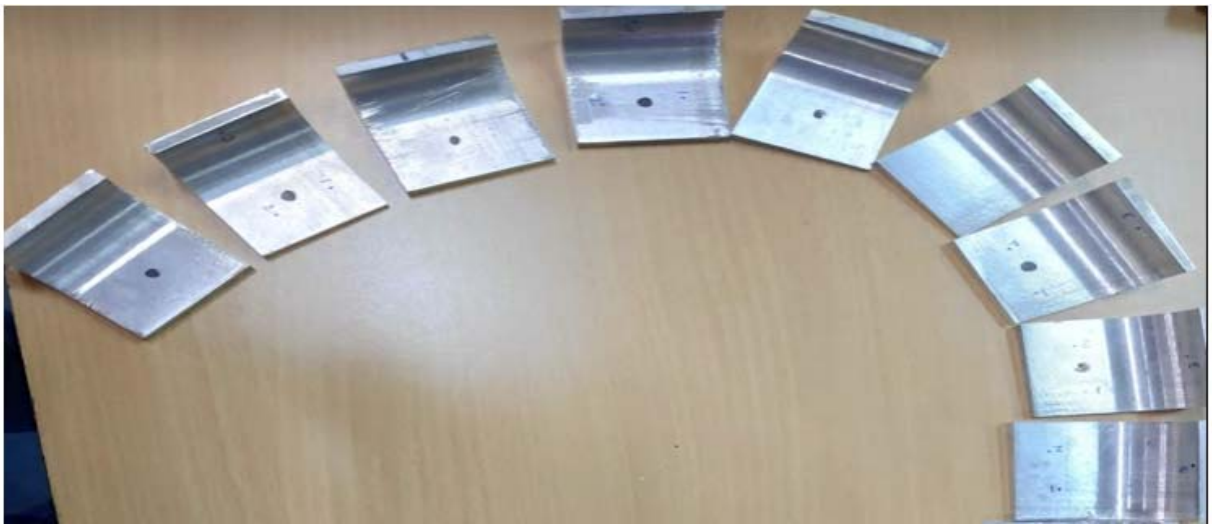

Fig.7.15. Aluminum Specimen finished with Viscoelastic Magnetic Abrasive Medium

Fig.7.16 Etched Aluminium piece finished with VEMAF Process 500X

7.10.3.1. Result and Discussion of External surface finishing of Aluminium Specimens:

1. Both changes in the surface finish(ΔRa) and Metal removal (Δm) are low at L1, where all the process parameters are having the least value.
2. Maximum material removal (Δm) is 0.0520 grams that occurred for L19 having Magnetic Flux density value of 0.4814 T, Abrasive Mesh Number 400, Rotational speed of 720 Rpm, Finishing time of 9 minutes (Level 2), Feed of 12 mm/min, and Ultrasonic amplitude of 45 μm.
3. Change in material removal is in increasing trend from level 1[0.3577T] to Level 3 [0.4814T] of Magnetic flux densities. The higher the Magnetic flux density, the better would be the ability to make a deeper micro indent, which forms the ridges around and these ridges will be sheared by the abrasives.
4. The maximum change in the surface roughness (ΔRa) is 0.169 μm, obtainable for the

Maximum flux density 0.4814 T(Level 3), Abrasive Mesh number 800(Level 3), Rotational speed of 600 Rpm(Level 2), Finishing time of 6 minutes(Level 1), Feed 18 mm per minute (Level 1) and Ultrasonic Amplitude of 15 μm (Level 1).

5. The parameters [L26] contributed to the highest reduction in surface roughness ΔRa which has a magnitude of 0.169 μm, however, it did not produce the finest surface finish as the surface finish always depends on the initial surface roughness of the Specimen. Here every specimen is finished in three cycles with a different set of process parameters.
6. The finest surface finish obtained from this process is 0.0783 μm obtained in three cycles of finishing from an initial value of 0.340 μm.
7. The observations made from the Optimisation of TAGUCHI's optimization model are as mentioned below.
   x. The assumption of Normal distribution is valid as all the response points (Δm) are nearer to the Normal distribution line. Ranking of the process parameters, ranking, and significance is tabulated below.

Table 7. 18 Comparison of Ranking, Levels, and Significance values for Aluminium.

Process Parameter	MFD T	AMN	MTRS Rpm	FT Minutes	FEED Mm/Min	USAMP μm
Ranking	1	4	6	2	5	3
Level	3	1	1	2	2	3
p	0.00	0.009	0.027	0.002	0.005	0.016
Delta	22.62	3.77	3.35	5.26	3.61	3.89

   xi. All the process parameters are having 'p' values less than 0.05, which signifies that the variable values in each parameter are significant. Since 'p' is a statistical tool that signifies the significance of variations in the process. R-Sq and R-Sq [adj] are showing higher percentages. Here these values are 97.2% and 94.9%, which are higher only. So experiment parameters are highly significant.
   xii. For Non- Magnetic material the Magnetic Flux density is the highest, as the indentation force is higher at the Maximum Flux density.
   xiii. Abrasive Mesh number is ranked 4th and the abrasive size is 400, which removes more material. This is in confirmation with most of the researchers' work which prefers coarser abrasive for more amount of material removal.
   xiv. The rotational speed is 480 Rpm, and it gives the necessary Tangential force to remove the peaks. However, increased Rotational Speed of the Magnetic tool

would through the VEMAF medium in a tangential direction and hence further finishing and material removal would reduce.

xv. Similarly, finishing time has got Level 2 in optimization as after finishing for 9 minutes under the prevailing experimental conditions, saturation will be reached and no advantage would be derived by increasing the finishing time to the next higher value, which is 12 minutes.

xvi. The feed is the motion of the tool in the lateral direction along the width. The width of the specimen is 40 mm and the preferred feed as per the Optimisation is 18 mm/minute, which is the optimum value as the increase in speed would leave the medium behind and finishing can't be performed efficiently.

xvii. Ultrasonic Amplitude as per Optimisation is 15 μm. Due to Ultrasonic vibration, the abrasives sitting in the valleys will be made to rotate along with the Magnetic Tool.

xviii. Observation of the Surface roughness Graphs shown from 7.1 to 7.9 revealed that there is no waviness on the surfaces finished by VEMAF process.

xix. A Test experiment has been conducted based on the optimization parameters yielded a better result.

SUMMARY

1. **Specimen with similar geometry made of three different materials; Steel, Brass, and Aluminium have been finished with a Viscoelastic Magnetic Abrasive finishing process.**
2. **Maximum flux densities of all the three levels of each material are based on the maximum flux densities obtained during the simulation as the maximum flux density is mostly Uniform for all these cases.**
3. **Maximum flux density is the most important process parameter.**
4. **Some of the surfaces finished for Steel and Aluminium produced waviness.**
5. **The initial surface finish of the specimen always important for getting the desired surface finish under the process parameters selected in this Thesis work.**

CHAPTER 8. WEAR BEHAVIOUR OF THE SPECIMEN FINISHED UNDER VEMAF PROCESS

In this chapter, an experimental investigation has been made about the wear behavior of Nine specimens each for Aluminium, Steel, and Brass using a Reciprocating wear test rig. These specimens have been prepared from the workpieces finished with VEMAF process. The wear mechanism under consideration is dry sliding wear. The experiment has been designed based on the Design of experiments of Taguchi, Optimisation has been done using Minitab Software and the results have been analyzed.

8.1 Introduction to Wear: Wear is the separation of the material from the outer surfaces due to their contact. In the year 1987 Ashby and Lim proposed the concept of Wear Mapping. Wear mapping considers the rate of wear, Mechanisms of wear, and modes of wear. During wear, the material gets separated due to any of the following three factors [162], they are:

1. Microfracture
2. Chemical Dissolution
3. Melting at the contact surfaces.

As per Burwell, there are four fundamental or basic modes due to which wear occurs, they are:

a. Abrasive
b. Adhesive
c. Fatigue
d. Corrosive wear

When wear takes place, it cannot be attributed to a single Basic wear mechanism or wear Mode. Always complex situation exists during the wear. Friction between the surfaces under contact has got a dominant role in the wear of the surfaces.

8.1.1 Wear Volume curves: Fig.8.1 below shows the wear volume curves. Type I shows the constant wear rate, Type II represents an initial high wear rate followed by the decrement in wear rate, Metallic wear is a good example for this type of wear, whereas Type III represents slow initial wear rate followed by Catastrophic wear, Fatigue wear belongs to this type of wear and mostly Ceramic materials fall under this category of wear. The hardness of the surface under

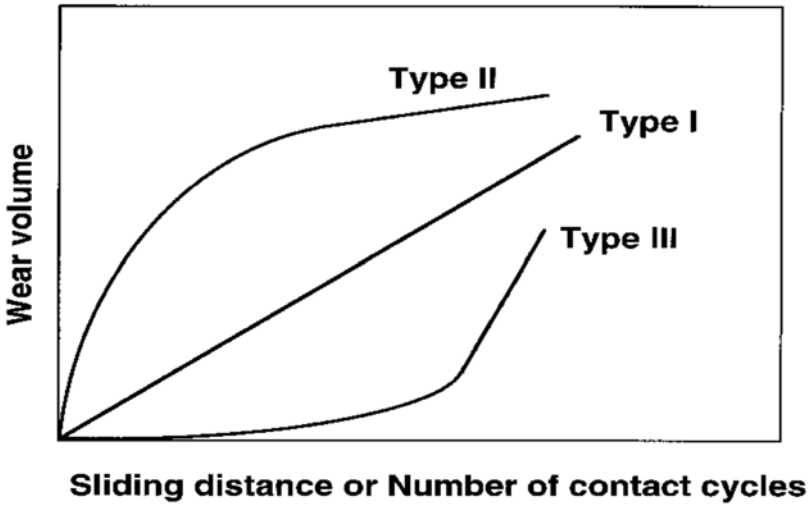

Fig.8.1 Wear volume Curves[162]

the study, Surface finish, and Frictional conditions are dominant factors for the wear of the surfaces.

8.1.2 Effect of No of Contact cycles on Surface roughness of worn surfaces: Fig 8.2 below shows the variation of surface roughness of the with no of cycles. It may be observed that in Type I wear, the constant surface roughness is maintained throughout the number of cycles of operation. In type II wear, the surface roughness raises but with a decrement rate and remains constant after attaining the maximum value. In type III wear, surface roughness decreases from the initial value, and from there it maintains the constant value. This happens normally in running in the process.

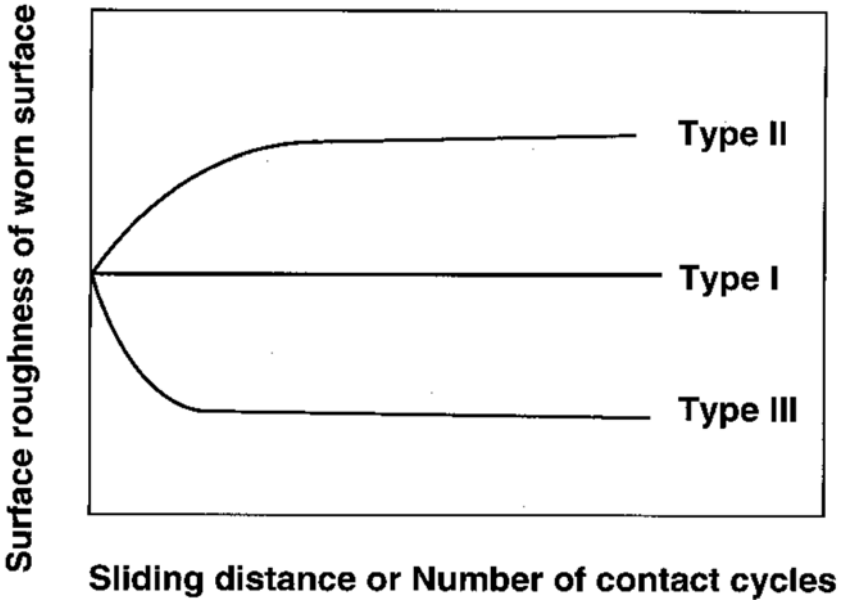

Fig.8.2 Surface roughness Changes in repeated contacts [162]

8.2 Sliding Wear in Metals: Archard, who did pioneering work in metallic sliding wear had observed that for one Joule of energy expended the wear is expected to have a wear range of $10^{-15}mm^3$ to $10^{-1}mm^3$. Fig. 8.3 below shows the wear that could be expected under different

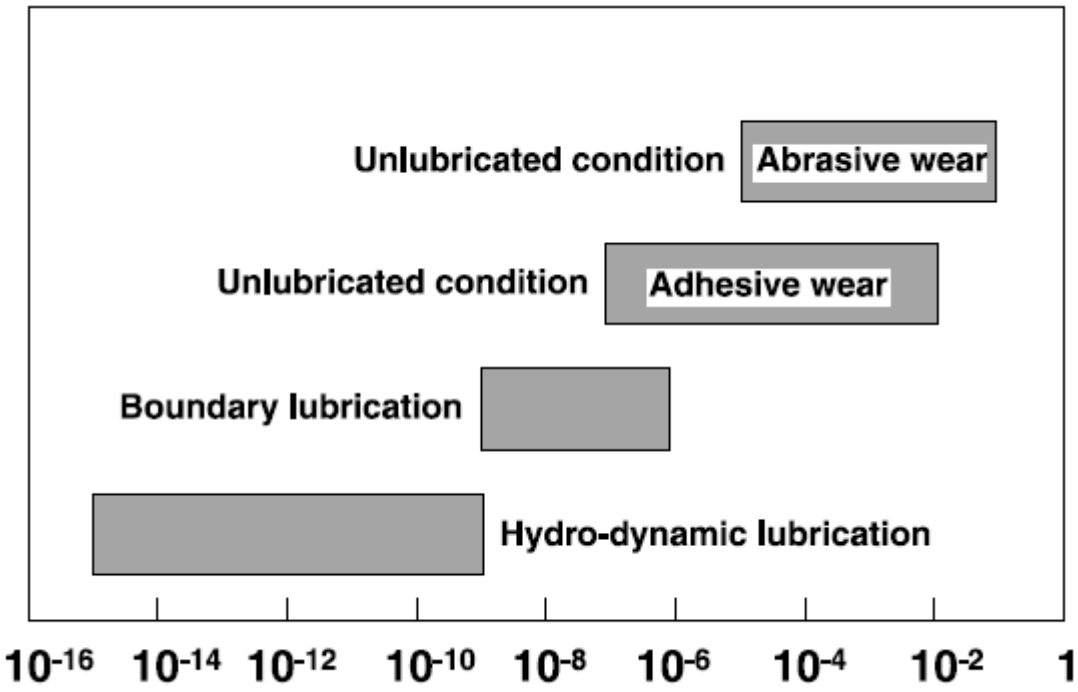

Fig.8.3 Specific Wear rate W_S in mm^3/J [162]

lubricating conditions. The Specific wear rate has a maximum value for Abrasive wear, where the wear is about 0.10 mm^3/J. The Mechanisms that fall under the Unlubricated condition are Abrasive wear and Adhesive wear. Though, both fall under Unlubricated wear modes both is having different mechanisms of wear, which has been discussed briefly below.

8.2.1 Abrasive Wear: Abrasive wear is due to the interlocking of peaks and valleys of contacting surfaces and subsequent shearing of these peaks due to sliding. During the Abrasive wear plowing by the sharp asperity of the hard material into the contacting surface of the soft material takes place. If one of the surfaces is Ductile, the size of the worn-out material looks like a long ribbon. This is known to be Micro-cutting. On the other hand, if the contacting surfaces are brittle, wear is due to the propagation of the crack. Fig. 8.4 below shows the Abrasive wear between the surfaces [162]

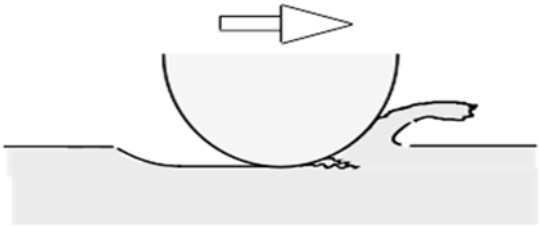

Fig.8.4 Abrasive wear [162]

8.2.2. Adhesive Wear: During unlubricated sliding between the components, Adhesive wear takes place. Adhesion is due to plastic deformation of the surfaces followed by the creation of localized bonding at certain points. The shearing of these localized bonding due to compressive forces makes the removal of the material from the surfaces. The crack that creates during the adhesive wear is having both tensile and Shear fracture modes as well as Compressive and shear fracture mode. The fractographic analysis shows that Flake like wear particles indicate Compressive and Shear stresses are involved, on the other hand, if wedge-like particles are observed, the wear is due to Tensile and Shear stresses. Fig.8.5 shows the Adhesive wear (161) between the surfaces.

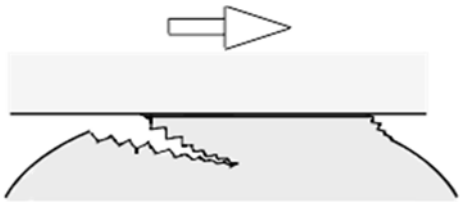

Fig. 8.5 Adhesive Wear[162]

In the present research work Test specimen having 20 mm x 20mm square cross-section and 5mm thickness, made of Aluminium, Brass and Steel are subjected to Dry sliding. All the Specimen have been prepared from the components finished by Viscoelastic Magnetic abrasive finishing process. Cylindrical specimens having a diameter of 8 mm have been prepared from the same material as the test specimen have been prepared. The wear takes place due and the sliding between the Square cross-section specimen and the Cylindrical specimen.

Details of the Test rig, Mechanism of wear applicable to Dry Sliding wear, Experiment procedure, Optimisation by using Taguchi experiment has been discussed in the following sections.

8.3. Description of Wear Test Rig: Linear reciprocating Tribometer, a floor-standing model located in Tribology lab of Delhi Technological University has been used for finding the

magnitude of wear of specimen made of Aluminium, Brass and Steel. Coefficient of friction, Frictional force would be recorded during the experimentation and due to which the wear Characteristics could be estimated. The Bottom specimen is fixed in the Bottom specimen holder and the load (Deadweight) would be transferred to the top specimen holder through a shaft, which in turn presses the bottom specimen. A servo motor is used for giving necessary reciprocating motion to the top specimen through a predefined mechanism.

Fig.8.6 below shows the experimental test rig comprises of three zones, First one is the Specimen loading chamber, where the specimen is fixed on the horizontal table and Top Specimen holder and the load transferring mechanism. The second one is the Deadweight loading chamber where loads of 5 N to 50 N could be placed. The third one is the Monitor and the Desktop system for recording and analyzing the experimental results.

Fig. 8.6 Linear Reciprocating Tribometer

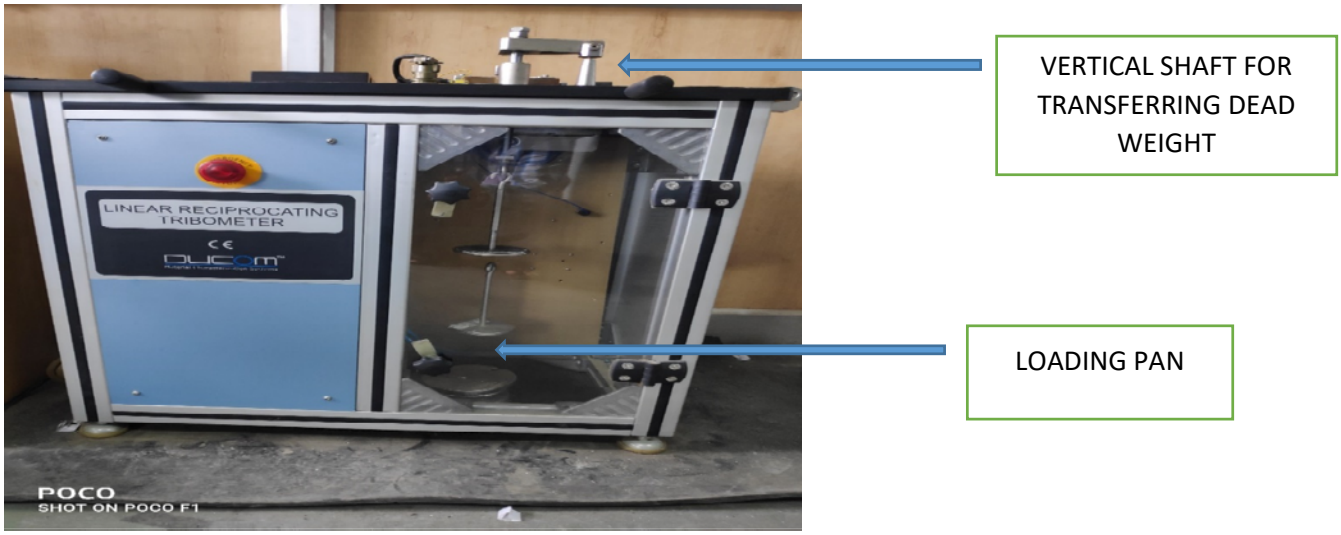

Fig.8.7. Dead Weight Loading Chamber

The weight from the dead weight Loading Chamber would be transferred to the Horizontal specimen through the vertical specimen. The vertical specimen gets the loading from the vertical shaft. Vertical Specimen presses the horizontal specimen. Reciprocating motion is imparted to the Vertical specimen, which starts rubbing against the horizontal specimen. The environmental chamber is shown in Fig. 8.9 shields the Specimen from the Toxic environment and Corrosive environment. Fig.8.10 shows the top and bottom, specimen holders. The top specimen holder would

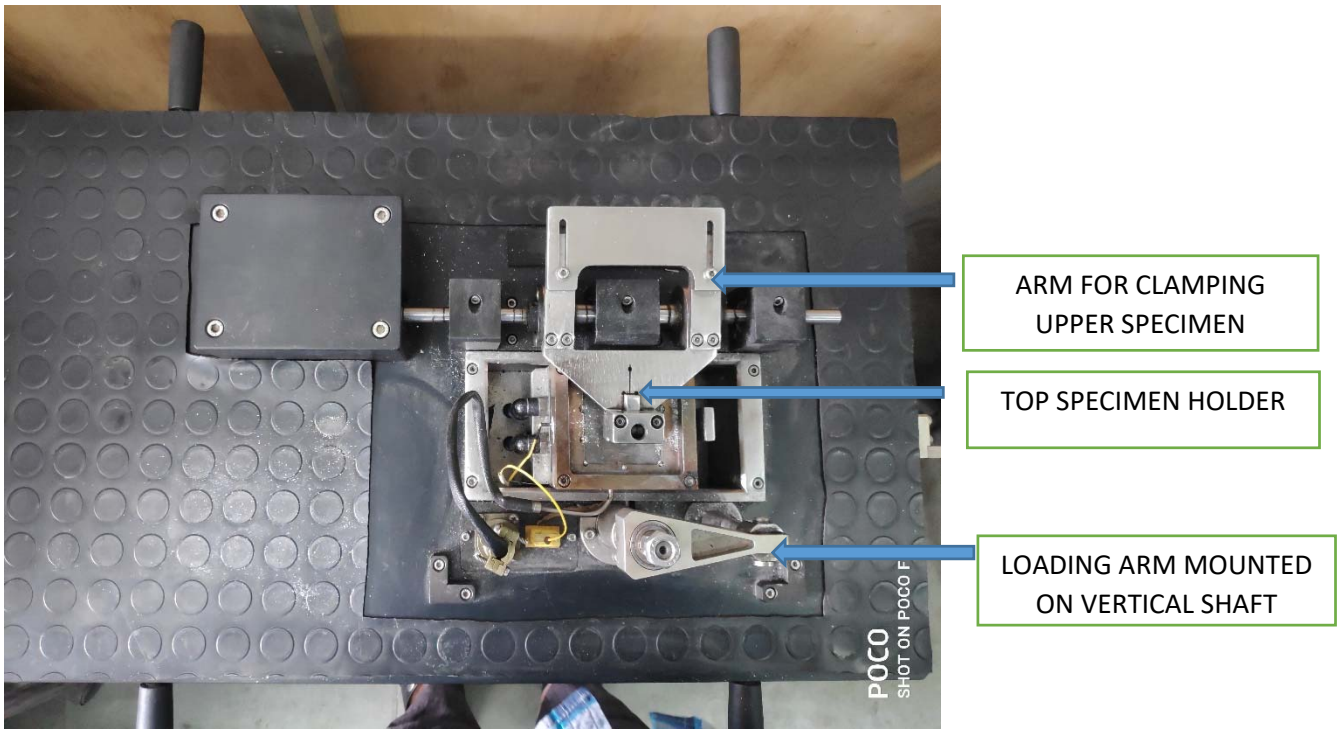

Fig.8.8 Top Portion of Linear Reciprocating Tribometer

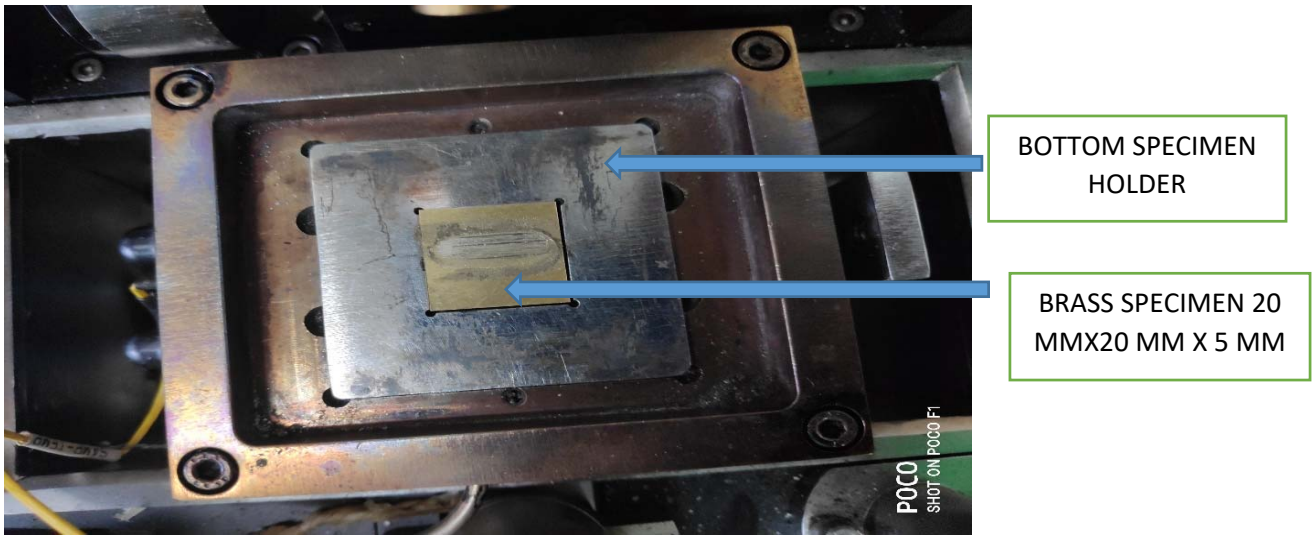

Fig.8.9 Bottom Specimen Loading Plate

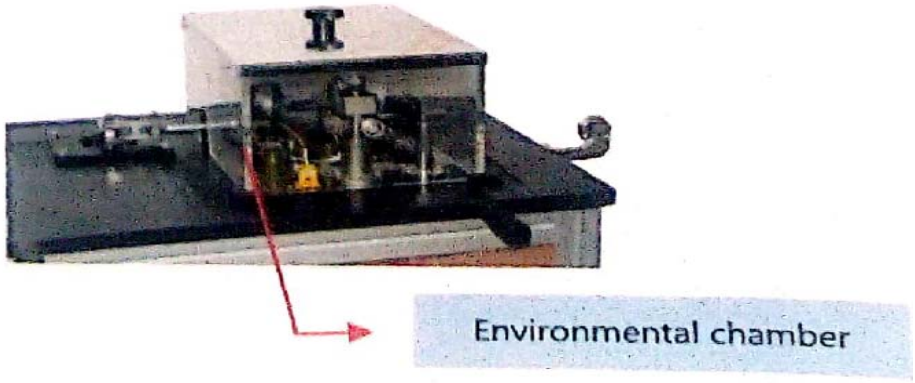

Figure.8.10. Environmental Chamber

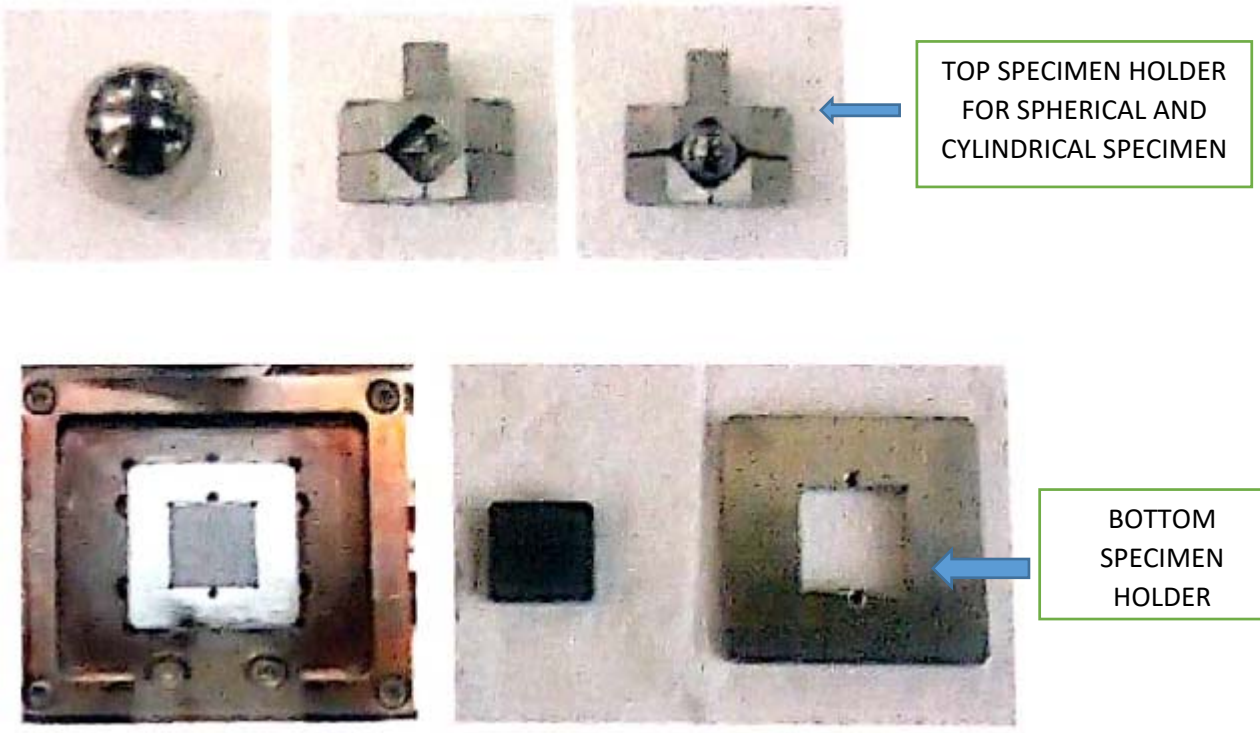

Fig.8.11 Top and Bottom Specimen Holders

accommodate specimen with Cylindrical and Spherical shape. Load, frequency, stroke length, temperature, and test duration are the input parameters of the experiment, which would be fed as input parameters for the Software. The software used is WINDUCOM 2010. The frictional force would be measured through the sensor and would be displayed on the monitor. Kinetic Coefficient of friction as a function of time also would be displayed on one of the screens of the

monitor. Dimensions before and after the test for the top specimen and the bottom specimen would give the wear volume. However, the usual practice is to note the weight of the specimen (both bottom and top) and then the difference would be the wear in grams. The volume would be calculated by the density, mass, and volume relation.

The Technical Data and Specifications have been mentioned below

8.3. 1. Technical DATA:

The detailed specifications of the Linear Tribometer have been mentioned below.

1. Size of the equipment lxbxh in mm : 600x520x920
2. Normal load : 5 N to 50 N in steps of 5 N
3. Frequency : Up to 50 Hz.
4. Stroke length : 1 mm- 20 mm.
5. Permitted frequency and Stroke length:

Table.8.1. Frequency vs Stroke length

FREQUENCY (Hz)	STROKE LENGTH (mm)
1-8	20
8-10	16
10-20	15
20-30	05
30-40	02
40-50	01

6. Specifications of the Top specimen:
   i. Spherical specimen: Diameters 4 mm, 6 mm, 8 mm, 10 mm, and 12 mm
   ii. Cylindrical pin: Diameters 4 mm, 6 mm, 8 mm, 10 mm, and 12 mm and length 15 mm.

7. **Sensor Specifications:**
   i. Frictional force measurement:

Sensor : Piezo sensor

Range : 44 N

Least count : 0.01 N

Accuracy : (0.01± 1% of measured value) in N

ii. Specimen Temperature:

Sensor : K- Type Thermo couple

Range : 550°C

Least count : 1°C

Accuracy : (0.01± 1% of measured value) in °C

iii. Heater Temperature :

Sensor : K- Type Thermo couple

Range : 550°C

Least count : 1°C

Accuracy : (0.01± 1% of measured value) in °C

iv. Frequency :

Sensor : End coder output

Range : 50 Hz

Least count : 0.01 Hz

Accuracy : (0.01± 1% of measured value) in Hz.

8.4. Process parameters and their effect on the Wear as per Literature review: Three process parameters, each having three levels have been considered for the sliding Wear test. The impact of these parameters has been discussed below. Following table 8.1 gives the Levels of Three process parameters.

Table 8.2 Process Parameters

PROCESS PARAMETER	LEVEL I	LEVEL II	LEVEL III
LOAD (N)	25	35	45
FREQUENCY (Hz)	10	15	20
TIME (Minutes)	3	4.5	6.0

8.4.1. Load: Lim et al. [144] in their investigation on the dry sliding wear found that higher wear is obtained when the load is more. Terchesi et al. [146] in their experimental investigation on

cylindrical liner wear concluded that the load is very sensitive to wear and friction. At higher loads with higher speeds a molten layer forms on the surface and hence the coefficient of friction decreases [144]. As per Wang et al. [156], the higher amount of load will cause melting wear especially in metals with lower melting temperature. The load is the most important factor; however, the wear does not increase proportionally to the load [157,158,159]

8.4.2. Time: One of the important parameters of Dry Sliding wear is Time. It has been observed from the literature review[145,147,148,152,154, 162] that the amount of wear is not in proportion to the time.

8.4.3. Frequency: Frequency is the measure of the velocity of the sliding, higher initial velocity reduces wear initially and then the wear starts again [141]. As per Kojikato et al. [149], wear rate depends on the sliding speed, which is proportional to Frequency. At higher frequencies, the melting of the material starts [162].

8.5. Assumptions made during Wear study:

i. Material is homogeneous and the properties are uniform in all directions.

ii. Wear is due to Dry sliding conditions.

iii. Material of the pin and the square block is the same.

iv. The pins used for the experiment are having average surface roughness values of ±5%.

v. A constant stroke length of 15 mm is adopted for all the experiments.

vi. A value of $p < 0.10$ is considered to be significant.

8.6. Specimen preparation: In total 9 Wear Test specimens, each 20 mm X 20 mm X 5 mm has been prepared. For this, Brass, Aluminium, and Steel specimen already finished with Viscoelastic Magnetic Abrasive Finishing [VEMAF] Process, having least surface roughness have been selected and they have been cut to the required size of 20 mm X 20 mm x 5mm. Nine specimens have been used for experimenting based on the L9 Orthogonal array of Experiments of Taguchi. Table 8.2 below shows the surface roughness of the Square specimen rough and Finished and cylindrical reciprocating Specimen.

Table.8.3. Roughness details of Square and Cylindrical specimen

Specimen Type	The roughness of Square Specimen 20 mmX20 mmX5 mm Ra [μm]	The roughness of Cylindrical Specimen dia 8 mm and length 15 mm. Ra [μm]
Brass Rough	*0.4 μm ±10%	**0.09 μm ±10%
Brass Finished	0.0776 μm to 0.082 μm	**0.09 μm ±10%
Steel Rough	*0.4 μm ±10%	**0.09 μm ±10%
Steel Finished	0.085 μm to 0.093 μm	**0.09 μm ±10%
Aluminium Rough	*0.4 μm ±10%	**0.09 μm ±10%
Aluminium finished	00804 μm to 0.093 μm	**0.09 μm ±10%

* Square specimen cut from the Specimen finished by Viscoelastic Magnetic abrasive medium. The rear side of the Brass, Steel, and Aluminium specimen have been finished up to Ra value of 0.4 μm ±10% and the top portion has been finished with VEMAF Tool.

**Cylindrical specimen made of the same material as that of the Brass, Steel, and Aluminium square specimen and carefully finished with lapping to get the desired surface finish.

8.7. Mechanism of Dry Sliding wear: As per the Karl -Heinz Zum Heigr [165] the dry sliding wear involves the following for most of the Dry Sliding Wear between metals. One or more than one Mechanism applies to all the metals subjected to Dry Sliding Wear.

i. Formation of Adhesive Junctions, breaking of these junctions, transfer of material and hence making micro groves.

ii. In Ductile material fatigue on the surfaces in contact due to repeated plastic deformation.

iii. Surface Fatigue is the dominant factor in Brittle material that develops surface cracks.

iv. The tribo-chemical reaction that takes place during Dry Sliding forms a reactive surface layer and breaking of this film contributes to wear.

8.8. Experiment Procedure: Block diagram shown in Fig.8.11 below describes the sequential steps to be followed during the Wear Test on the Linear Tribometer. The process includes the procurement of the specimen from the best specimen obtained from VEMAF process, cutting to the required size, cleaning for removing greasiness of the square specimen. Recording the initial

weight, performing the experiment based on Orthogonal Array of experiments of Taguchi, recording the final weight, calculating the wear, which is the difference between of initial weight and the final weight. Recording for the values of Coefficient of friction between the contacting surfaces has been done for each experiment with the help of Software. Analysis has been made in two steps first by using the Taguchi analysis main effects in qualitative terms has been evaluated. The Second Step Analysis of Variance (ANOVA) is used for identifying the relative influence of the factors on the variation of the results in the discrete system.

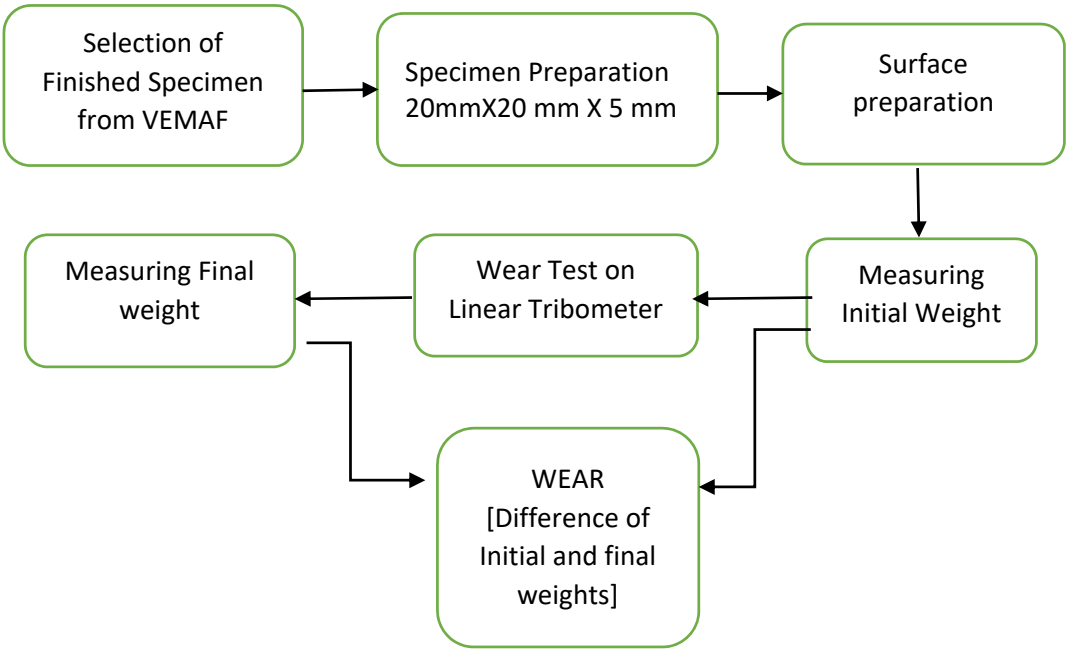

Fig.8.12 Block diagram for Wear Test.

In the present experiment, three process parameters, each having three levels are considered and the experiment has been conducted based on L9 the initial mass of the specimen and the final mass of the specimen has been noted, from which the magnitude of wear would be obtained.

8.9. Wear Test on Brass Specimens: The following table gives the L9 Design for Orthogonal Array of Experiments for ***Brass Rough*** and **Finished specimens**. Rough specimens tested are the rear side of the finished specimen. All the Brass Specimen are having a surface roughness of the order of 0.4 µm ± 10% as these specimens have been polished uniformly to get this value. The finished specimen has been cut from the Brass specimen finished by VEMAF process and having surface roughness values from 0.0776 to 0.079 µm. Experiments have been conducted as per Taguchi's L9 Orthogonal array of experiments. The parameters considered for each level, Initial mass, final mass, and wear have been tabulated in Table 8.5 below.

Table 8.5. Orthogonal Array of Experiments [Brass Rough and Finished Specimen]

			BRASS ROUGH SPECIMEN			BRASS FINISHED SPECIMEN		
LOAD (N)	**TIME (Minutes)**	**Frequency (Hz)**	**Initial Mass (grams)**	**Initial Mass (grams)**	**Wear Mass (grams)**	**Initial Mass (grams)**	**Initial Mass (grams)**	**Wear Mass (grams)**
25	3.0	10	20.7641	20.7406	0.0235	20.7406	20.721	0.0196
25	4.5	15	20.6930	20.6244	0.0686	20.6244	20.5663	0.0581
25	6.0	20	20.6882	20.6181	0.0701	20.6181	20.5606	0.0575
35	3.0	15	20.7359	20.6955	0.0364	20.6955	20.6652	0.0303
35	4.5	20	20.5720	20.4722	0.0998	20.4722	20.3930	0.0792
35	6.0	10	20.7354	20.7025	0.0329	20.7025	20.676	0.0265
45	3.0	20	20.7307	20.6397	0.0910	20.6397	20.5570	0.0827
45	4.5	10	20.5540	20.4660	0.088	20.4660	20.3933	0.0667
45	6.0	15	20.7713	20.6361	0.1352	20.7611	20.6389	0.1222

8.10. Experimental Results for Brass Rough Specimens: Minitab 17 is used for the analysis and Optimisation of the experimental data. The objective is to achieve minimum wear for Rough Brass Specimens.

Taguchi Design

```
Taguchi Orthogonal Array Design

L9(3^3)
Factors:  3
Runs:     9

Columns of L9(3^4) Array

1 2 3
```

Taguchi Analysis: Δm versus LOAD, TIME, FREQUENCY

Linear Model Analysis: SN ratios versus LOAD, TIME, FREQUENCY

```
Estimated Model Coefficients for SN ratios

Term            Coef  SE Coef       T      P
Constant     24.0777   0.3834  62.798  0.000
LOAD 25       2.2349   0.5422   4.122  0.054
LOAD 35       2.0728   0.5422   3.823  0.062
TIME 3.0      3.3142   0.5422   6.112  0.026
TIME 4.5     -2.6106   0.5422  -4.815  0.041
```

```
FREQUENC 10   3.7040   0.5422   6.831  0.021
FREQUENC 15  -0.9337   0.5422  -1.722  0.227

S = 1.150   R-Sq = 98.7%   R-Sq(adj) = 94.9%

Analysis of Variance for SN ratios

Source          DF   Seq SS  Adj SS  Adj MS      F      P
LOAD             2   83.543  83.543  41.771  31.57  0.031
TIME             2   54.884  54.884  27.442  20.74  0.046
FREQUENCY        2   66.798  66.798  33.399  25.24  0.038
Residual Error   2    2.646   2.646   1.323
Total            8  207.870
```

Linear Model Analysis: Means versus LOAD, TIME, FREQUENCY

```
Estimated Model Coefficients for Means
Term              Coef   SE Coef       T      P
Constant      0.071722  0.007225   9.927  0.010
LOAD 25      -0.017656  0.010217  -1.728  0.226
LOAD 35      -0.015356  0.010217  -1.503  0.272
TIME 3.0     -0.021422  0.010217  -2.097  0.171
TIME 4.5      0.013744  0.010217   1.345  0.311
FREQUENC 10  -0.023589  0.010217  -2.309  0.147
FREQUENC 15   0.008344  0.010217   0.817  0.500

S = 0.02167   R-Sq = 91.1%   R-Sq(adj) = 64.4%

Analysis of Variance for Means

Source          DF    Seq SS    Adj SS    Adj MS     F      P
LOAD             2  0.004912  0.004912  0.002456  5.23  0.161
TIME             2  0.002120  0.002120  0.001060  2.26  0.307
FREQUENCY        2  0.002575  0.002575  0.001288  2.74  0.267
Residual Error   2  0.000940  0.000940  0.000470
Total            8  0.010547

Response Table for Signal to Noise Ratios
Smaller is better

Level   LOAD   TIME  FREQUENCY
1      26.31  27.39      27.78
2      26.15  21.47      23.14
3      19.77  23.37      21.31
Delta   6.54   5.92       6.47
Rank       1      3          2
```

Response Table for Means

Level	LOAD	TIME	FREQUENCY
1	0.05407	0.05030	0.04813
2	0.05637	0.08547	0.08007
3	0.10473	0.07940	0.08697
Delta	0.05067	0.03517	0.03883
Rank	1	3	2

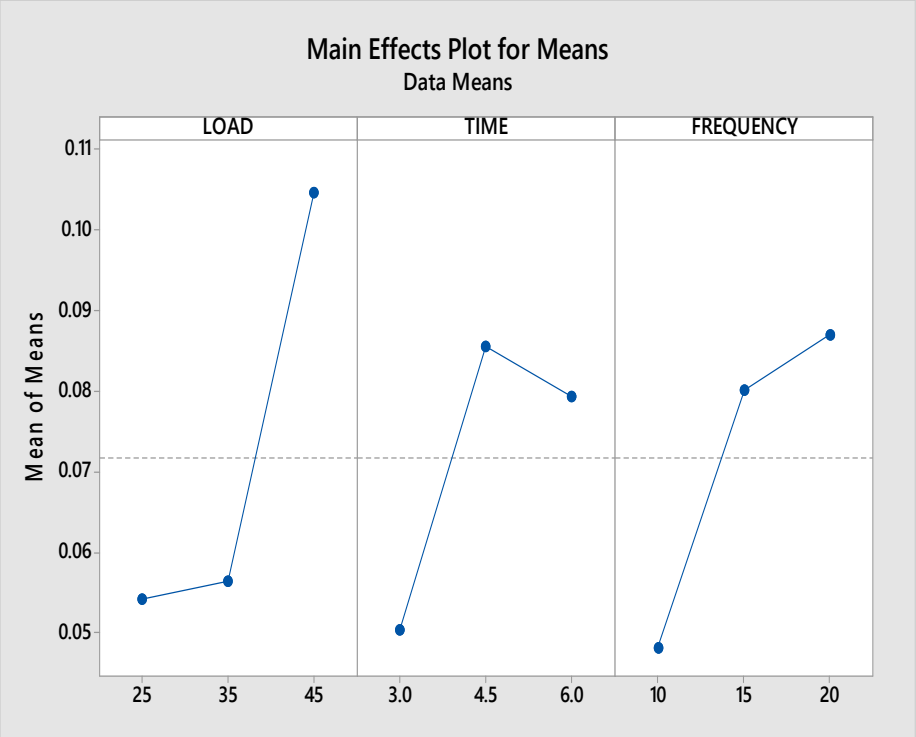

Graph. 8.1 Main Effects Plot for Means[Brass Rough Specimens]

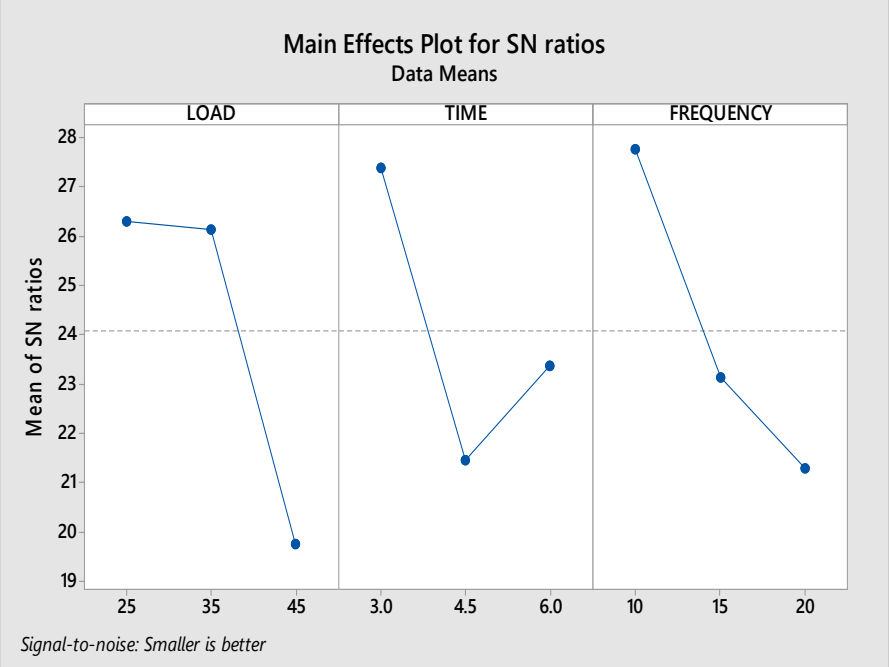

Graph. 8.2.Main Effects Plot for S/N ratios [Brass Rough Specimens]

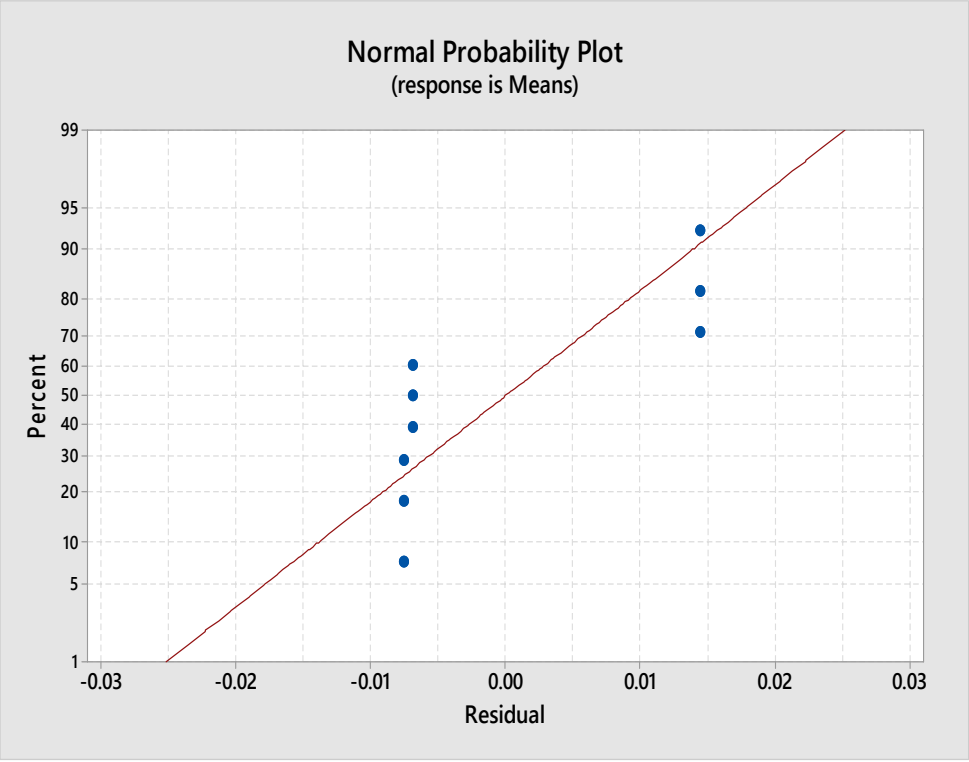

Graph.8.3. Normplot of Residuals for Means[Brass Rough Specimens]

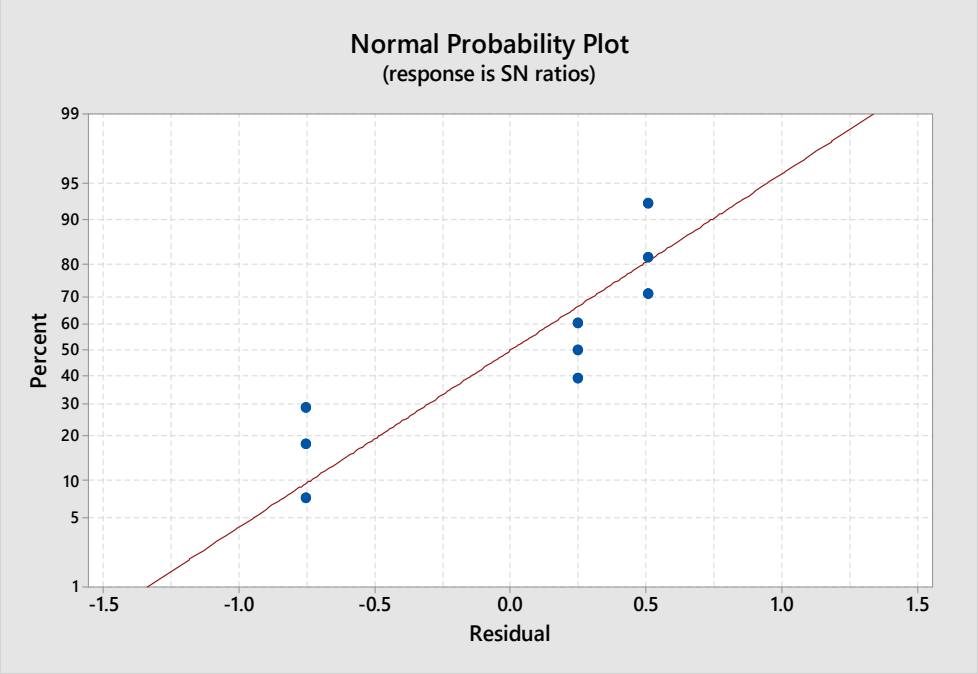

Graph. 8.4.Normplot of Residuals for SN ratios [Brass Rough Specimens]

8.11. Experimental Results for Brass Finished Specimen: Minitab 17 is used for the analysis and Optimisation of the experimental data. The objective is to achieve minimum wear for Rough Brass Specimen.

Taguchi Analysis: Δm versus LOAD, TIME, FREQUENCY

Linear Model Analysis: SN ratios versus LOAD, TIME, FREQUENCY

Estimated Model Coefficients for SN ratios

Term	Coef	SE Coef	T	P
Constant	25.671	0.4356	58.935	0.000
LOAD 25	2.222	0.6160	3.607	0.069
LOAD 35	2.307	0.6160	3.745	0.064
TIME 3.0	3.055	0.6160	4.959	0.038
TIME 4.5	-2.251	0.6160	-3.654	0.067
FREQUENC 10	4.065	0.6160	6.599	0.022
FREQUENC 15	-1.222	0.6160	-1.984	0.186

S = 1.307 R-Sq = 98.4% R-Sq(adj) = 93.8%

Analysis of Variance for SN ratios

Source	DF	Seq SS	Adj SS	Adj MS	F	P
LOAD	2	92.300	92.300	46.150	27.03	0.036
TIME	2	45.130	45.130	22.565	13.22	0.070
FREQUENCY	2	78.309	78.309	39.155	22.93	0.042

Residual Error	2	3.415	3.415	1.708
Total	8	219.154		

Linear Model Analysis: Means versus LOAD, TIME, FREQUENCY

Estimated Model Coefficients for Means

Term	Coef	SE Coef	T	P
Constant	0.060311	0.006790	8.882	0.012
LOAD 25	-0.015244	0.009603	-1.587	0.253
LOAD 35	-0.014978	0.009603	-1.560	0.259
TIME 3.0	-0.016111	0.009603	-1.678	0.235
TIME 4.5	0.007689	0.009603	0.801	0.507
FREQUENC 10	-0.022711	0.009603	-2.365	0.142
FREQUENC 15	0.009889	0.009603	1.030	0.411

S = 0.02037 R-Sq = 90.2% R-Sq(adj) = 60.7%

Analysis of Variance for Means

Source	DF	Seq SS	Adj SS	Adj MS	F	P
LOAD	2	0.004110	0.004110	0.002055	4.95	0.168
TIME	2	0.001169	0.001169	0.000584	1.41	0.415
FREQUENCY	2	0.002334	0.002334	0.001167	2.81	0.262
Residual Error	2	0.000830	0.000830	0.000415		
Total	8	0.008443				

Response Table for Signal to Noise Ratios
Smaller is better

Level	LOAD	TIME	FREQUENCY
1	27.89	28.73	29.74
2	27.98	23.42	24.45
3	21.14	24.87	22.83
Delta	6.84	5.31	6.91
Rank	2	3	1

Response Table for Means

Level	LOAD	TIME	FREQUENCY
1	0.04507	0.04420	0.03760
2	0.04533	0.06800	0.07020
3	0.09053	0.06873	0.07313
Delta	0.04547	0.02453	0.03553
Rank	1	3	2

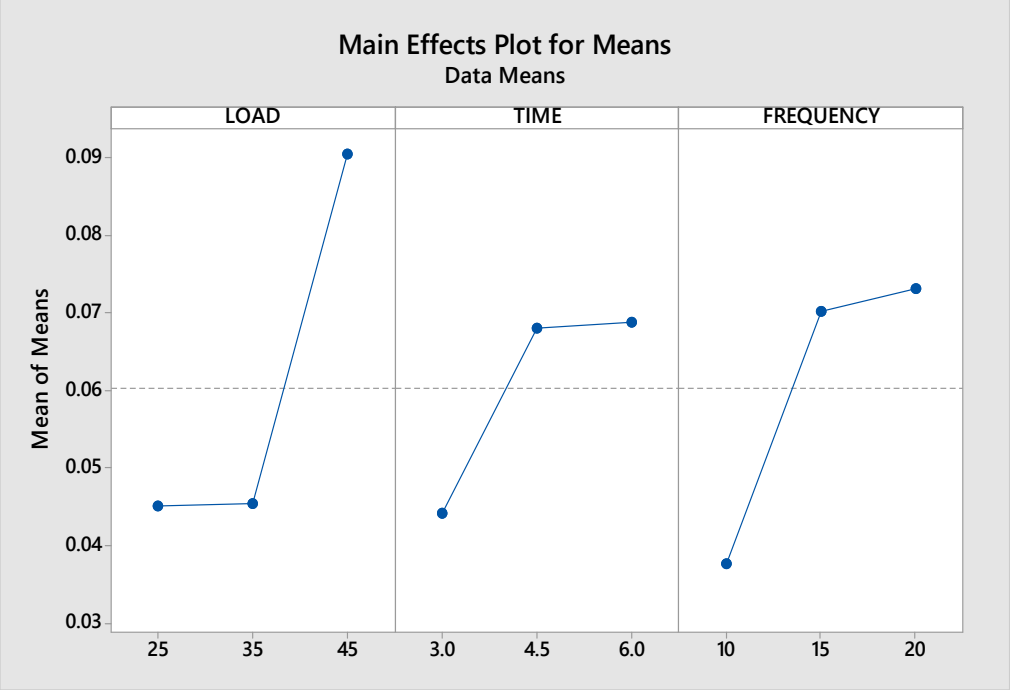

Graph.8.5.Main Effects Plot for Means [Brass Finished specimens]

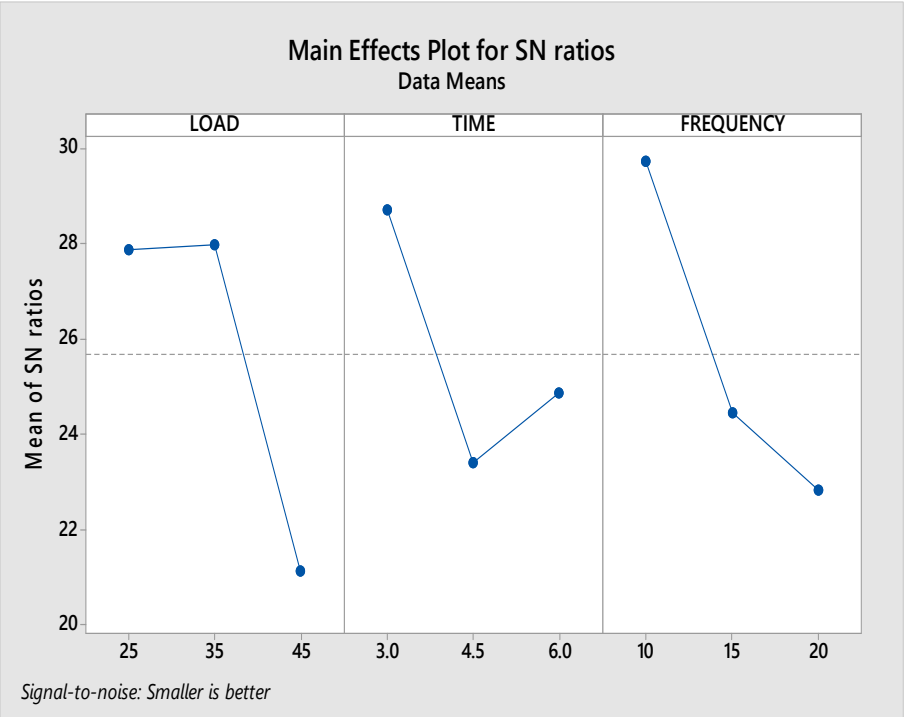

Graph.8.6. Main Effects Plot for SN Ratio [Brass finished specimens]

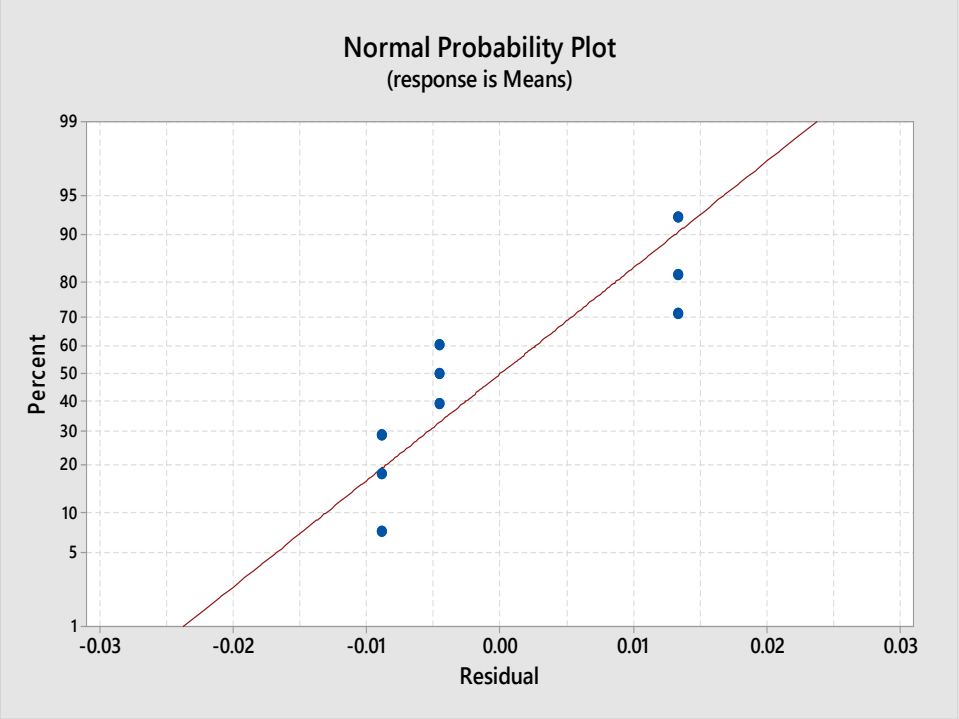

Graph.8.7Normal plot for Means [Brass Finished Specimens]

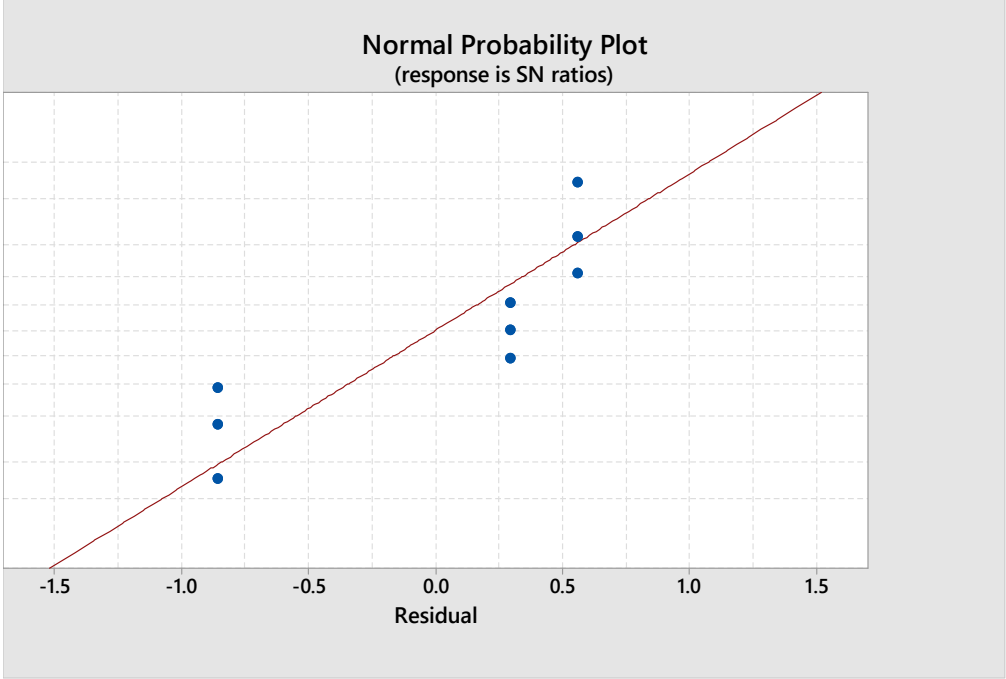

Graph. 8. 8.Normal plot of for SN ratios [Brass finished specimens]

8.12. Comparison of Coefficients of friction of Rough and Finished Brass Specimens: During the Wear test the coefficients of friction between the square block having 20mm x 20 mm x 5mm size and 8 mm diameter pin is recorded for all the nine experiments conducted. A comparative graph for L1 of the L9 table for the Coefficient of friction of the Brass specimen and the coefficient of friction of the finished

brass specimen have been compared from graphs 8.9 to 8.17. Except at graphs 8.12 and 8.16 all other graphs show almost coincidence of coefficients of friction(μ) after initial 1minute of wear. Mostly the coefficient of friction for all the rough and finished specimens is ranging between 0.20 to 0.30.

Graph.8.9. Comparison of Coefficient of friction of Brass Rough and finished specimen L1

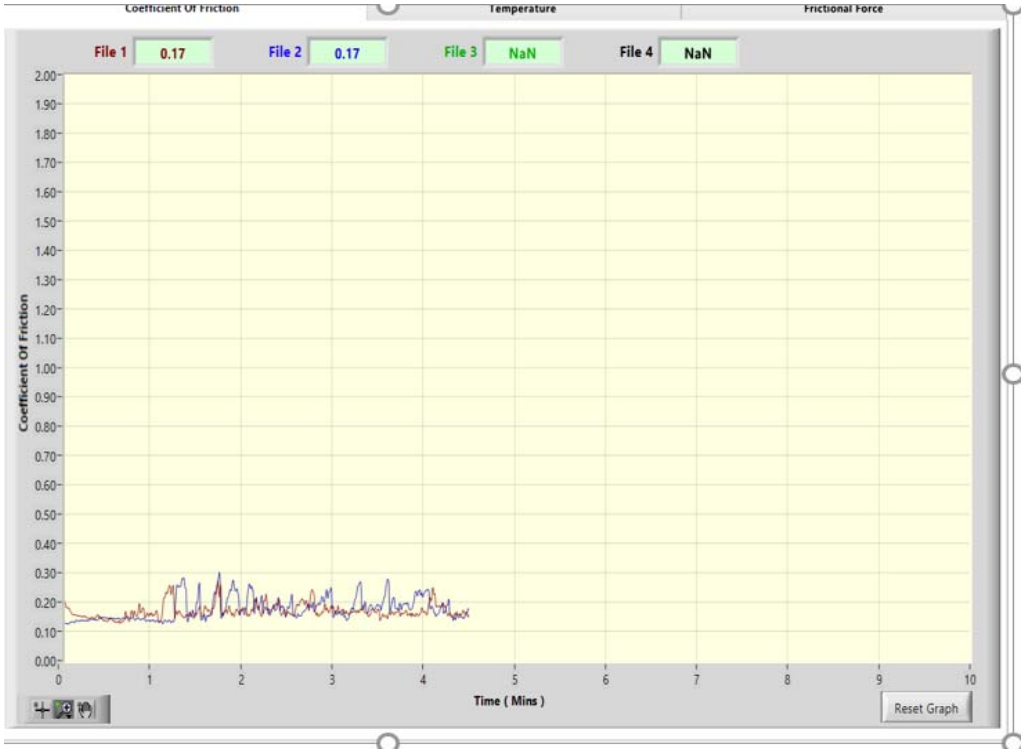

Graph.8.10. Comparison of Coefficient of friction of Brass Rough and finished specimen L2

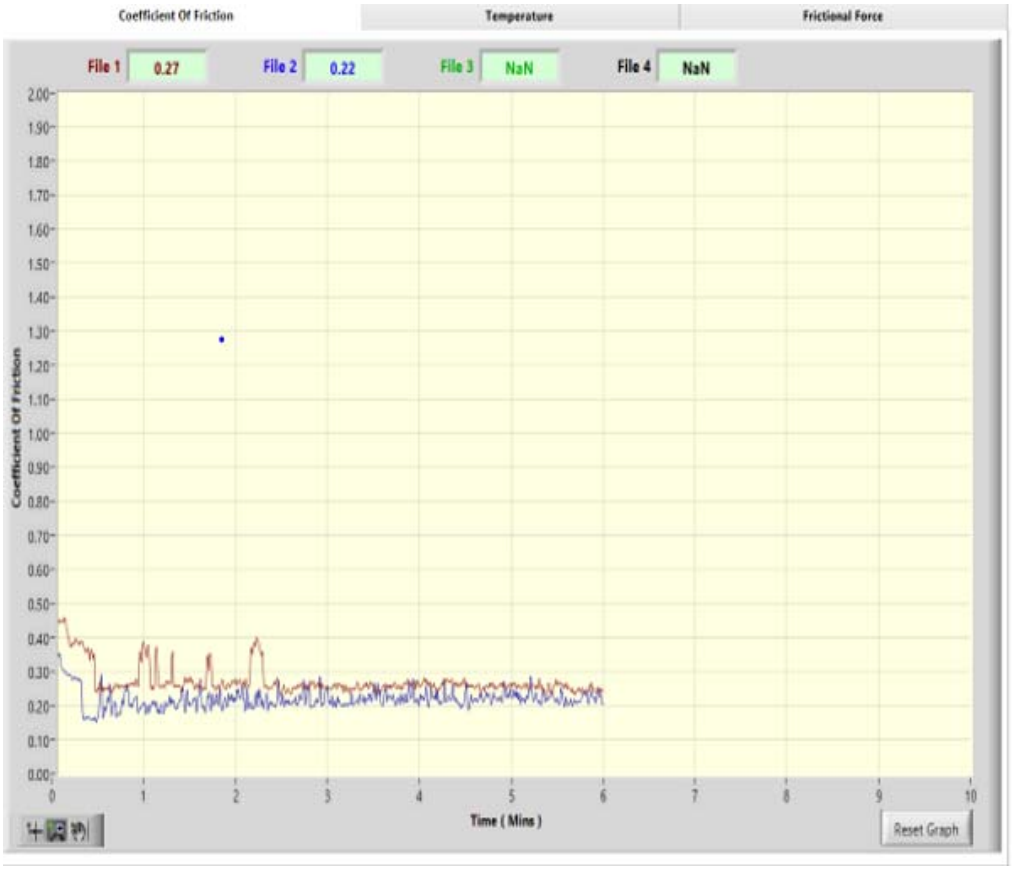

Graph.8.11. Comparison of Coefficient of friction of Brass Rough and finished specimen L3

Graph.8.12. Comparison of Coefficient of friction of Brass Rough and finished specimen L4

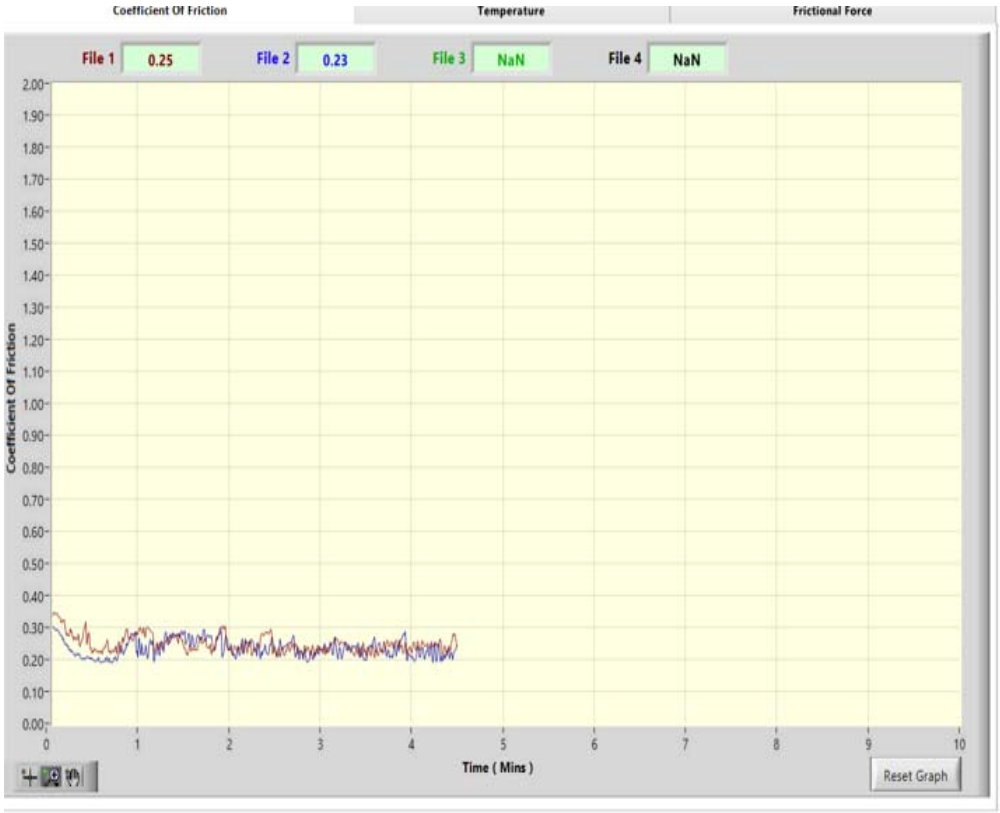

Graph.8.13 Comparison of Coefficient of friction of Brass Rough and finished specimen L5

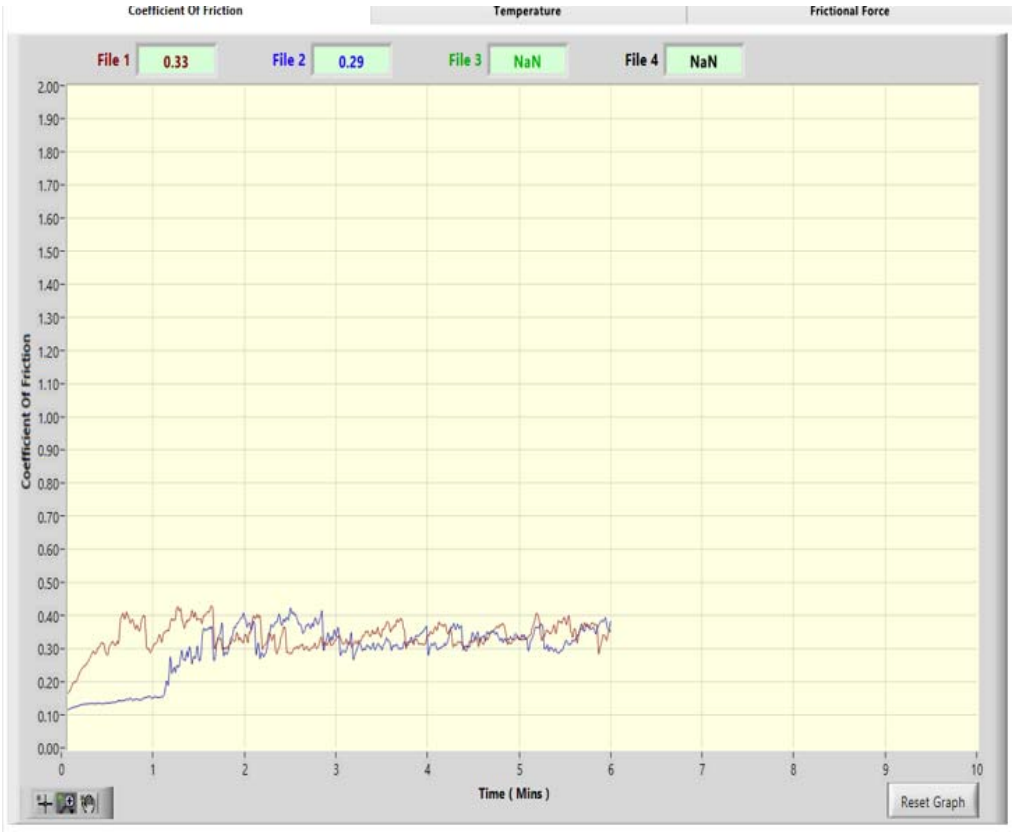

Graph.8.14. Comparison of Coefficient of friction of Brass Rough and finished specimen L6

Graph.8.15. Comparison of Coefficient of friction of Brass Rough and finished specimen L7

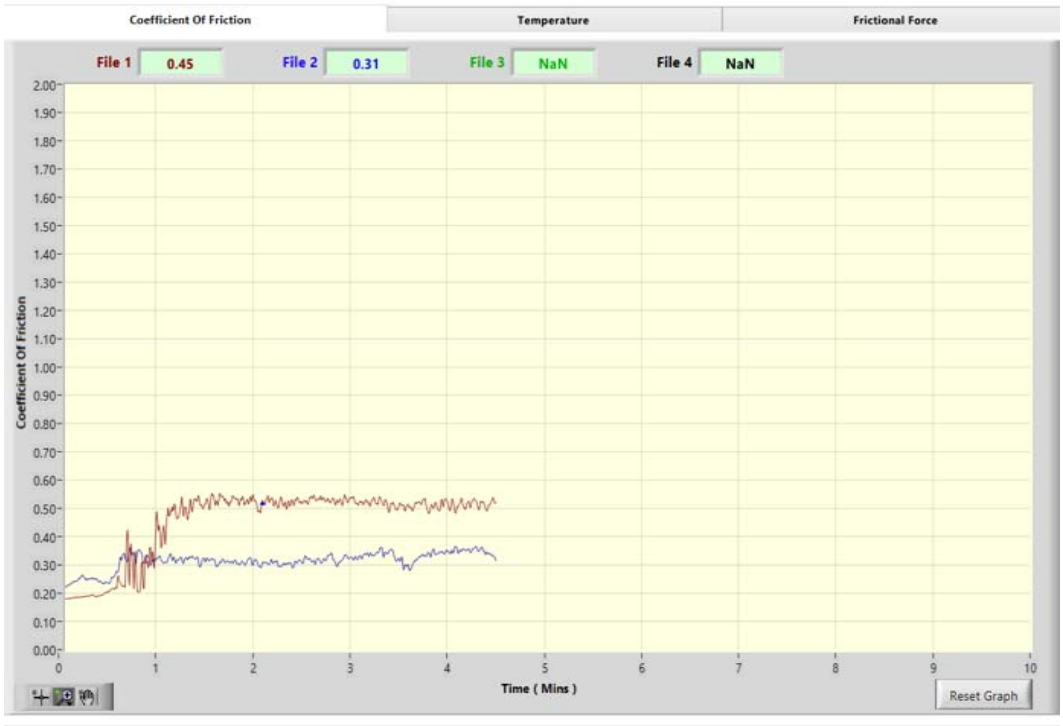

Graph.8.16. Comparison of Coefficient of friction of Brass Rough and finished specimen L8

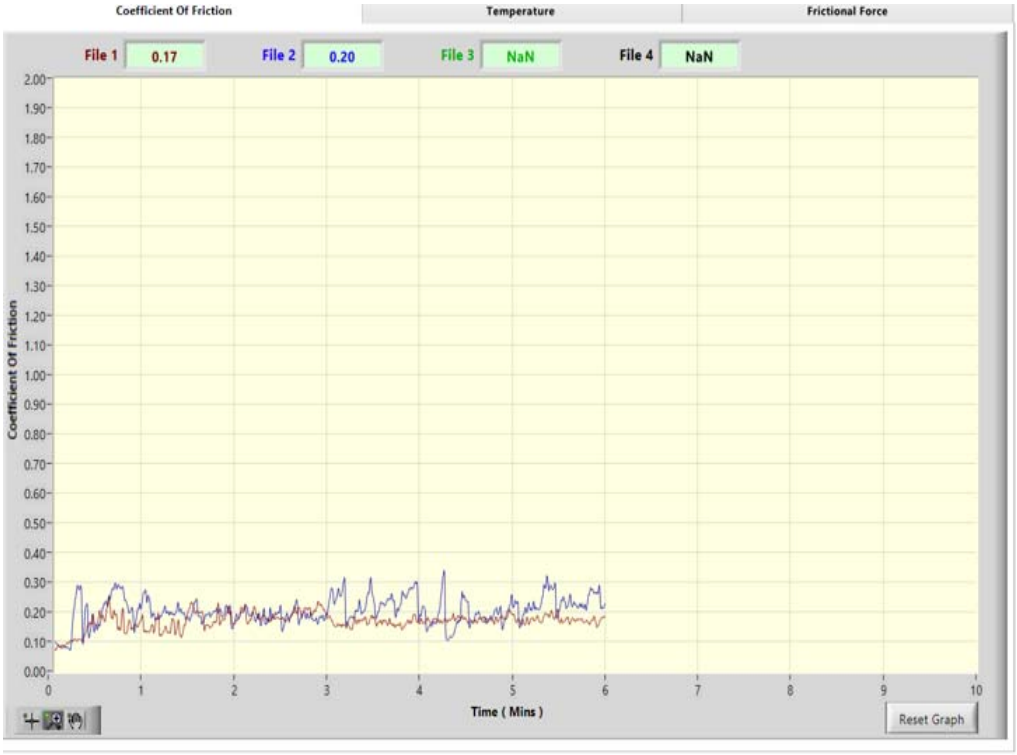

Graph.8.17. Comparison of Coefficient of friction of Brass Rough and finished specimen L9

Fig. 8.13 Brass Rough Specimen after wear

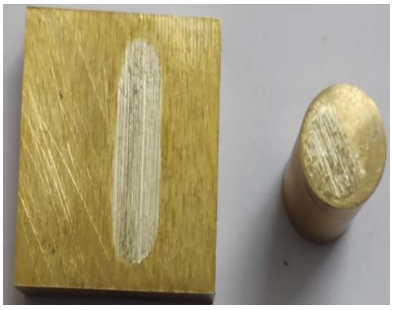

Fig. 8.14 Brass Finished specimen after Wear

8.13. Result Analysis and Discussion for Wear Test on Brass rough and Finished Specimens:

Results obtained based on Taguchi's Regression analysis with Minitab 17 are as mentioned below.

1. For the tests performed on both the Rough specimen and the finished specimen, the points of wear are nearer to the Normal distribution line, which indicates that the Normal Distribution Model is significant.
2. Logically, for getting minimum wear the process parameters have to be minimum, however, the significance of the process parameter is not the same and hence the ranking obtained has to

be considered, which has been tabulated below.

Table. 8.6 Comparison of ranking for Brass Rough and Finished Specimen

	Load	Time	Frequency
Brass Rough	**1**	**3**	**2**
Brass Finished	**2**	**3**	**1**

3. The above table describes that the load is the most significant parameter, followed by the frequency and Time for the rough specimen. For the Finished specimen, the frequency(Velocity) is ranked 1 followed by load and time. Subbaryan Sivasankaran [2019] in his experiment of Brass under similar test conditions found that the Velocity is the most important parameter for the Dry wear condition. The frequency which is proportional to the velocity has an impact on minimum wear. The obvious reason is at higher speeds the surface layer on the finished specimen, which has a lesser amount of surface roughness would be removed quickly. So the lesser frequency means lesser velocity would not remove the surface layer quickly, so the abrading action is slower.

4. The significance level has been tabulated below.

Table. 8.7. Comparison of significance for Brass Rough and Finished Specimen

	Load	Time	Frequency
Brass Rough	**0.031**	**0.046**	**0.038**
Brass Finished	**0.036**	**0.070**	**0.042**

For most of the experiments p-value < 0.05 has been considered, however in practical terms p< 0.10 also considered to be significant. For finding the significance of the experiment R-Sq and R-Sq[adj] must be higher here both are above 90%, so the results are considered to be significant.

5. Graphs 8.9 to 8.17 clearly show that the Coefficient of friction of the rough specimen shown in blue color is higher than the coefficient of friction of the finished specimen shown in Red color.

6. Material removal for the rough specimen is higher than the coefficient of friction for the rough specimen. This is primarily due to the fact that the no of peaks to be removed for the rough specimen is higher than that of the Finished specimen.

7. Fig. 8.13 and 8.14 show that the type of Wear at the selected process parameters is Abrasive wear.

8.14. Wear Test on Steel Specimens: The following table gives the L9 Design for Orthogonal Array of Experiments for ***Steel Rough*** and **Finished specimens**. Rough specimens tested are the rear side of the finished specimen. All the Steel Specimen are having a surface roughness of the order of 0.4 μm ± 10% as these specimens have been polished uniformly to get this value. The finished specimen has been cut from the Steel specimen finished by VEMAF process and having surface roughness values of 0.059μm to 0.083 μm. Experiments have been conducted as per Taguchi's L9 Orthogonal array of experiments. The parameters considered for each level, Initial mass, final mass, and wear have been tabulated in Table 8.8 below.

Table 8.8. L9 Orthogonal Array of Experiments [Steel Rough and finished Specimen]

			STEEL ROUGH SPECIMEN			STEEL FINISHED SPECIMEN		
LOAD (N)	TIME (Minutes)	Frequency (Hz)	Initial Mass (grams)	Initial Mass (grams)	Wear Mass (grams)	Initial Mass (grams)	Initial Mass (grams)	Wear Mass (grams)
25	3.0	10	17.0200	16.9588	0.0612	16.9588	15.8547	0.0489
25	4.5	15	17.3140	17.1352	0.1788	17.1352	14.9920	0.1453
25	6.0	20	17.4978	17.3350	0.1628	17.3350	15.1385	0.1368
35	3.0	15	17.0730	16.9788	0.0942	16.9788	15.8331	0.0753
35	4.5	20	17.1700	16.9284	0.2416	16.9284	15.8384	0.1980
35	6.0	10	16.9488	16.8715	0.0773	16.8715	15.6104	0.0655
45	3.0	20	17.3842	17.1258	0.2584	17.1258	15.9985	0.2067
45	4.5	10	16.9804	16.776	0.2038	16.776	15.5959	0.1657
45	6.0	15	17.0288	16.6855	0.3433	16.6855	16.0250	0.2910

8.15. Experimental Results for Steel Rough Specimen: Minitab 17 is used for the analysis and Optimisation of the experimental data. The objective is to achieve minimum wear for Steel Rough Specimen.

Taguchi Design

Taguchi Orthogonal Array Design

L9(3^3)

Factors: 3

Runs: 9

1 2 3

Taguchi Analysis: Δm versus LOAD, TIME, FREQUENCY

Linear Model Analysis: SN ratios versus LOAD, TIME, FREQUENCY

Estimated Model Coefficients for SN ratios

Term	Coef	SE Coef	T	P
Constant	16.104	0.4188	38.455	0.001
LOAD 25	2.224	0.5922	3.756	0.064
LOAD 35	2.261	0.5922	3.817	0.062
TIME 3.0	2.742	0.5922	4.630	0.044
TIME 4.5	-2.402	0.5922	-4.055	0.056
FREQUENC 10	4.002	0.5922	6.757	0.021
FREQUENC 15	-1.184	0.5922	-2.000	0.184

S = 1.256 R-Sq = 98.5% R-Sq(adj) = 94.0%

Analysis of Variance for SN ratios

Source	DF	Seq SS	Adj SS	Adj MS	F	P
LOAD	2	90.520	90.520	45.260	28.68	0.034
TIME	2	40.210	40.210	20.105	12.74	0.073
FREQUENCY	2	76.069	76.069	38.035	24.10	0.040
Residual Error	2	3.157	3.157	1.578		
Total	8	209.956				

Linear Model Analysis: Means versus LOAD, TIME, FREQUENCY

Estimated Model Coefficients for Means

Term	Coef	SE Coef	T	P
Constant	0.18016	0.01835	9.819	0.010
LOAD 25	-0.04589	0.02595	-1.768	0.219
LOAD 35	-0.04246	0.02595	-1.636	0.243
TIME 3.0	-0.04222	0.02595	-1.627	0.245
TIME 4.5	0.02791	0.02595	1.076	0.395
FREQUENC 10	-0.06606	0.02595	-2.546	0.126
FREQUENC 15	0.02528	0.02595	0.974	0.433

S = 0.05504 R-Sq = 91.3% R-Sq(adj) = 65.1%

Analysis of Variance for Means

Source	DF	Seq SS	Adj SS	Adj MS	F	P
LOAD	2	0.035139	0.035139	0.017570	5.80	0.147
TIME	2	0.008300	0.008300	0.004150	1.37	0.422

FREQUENCY	2	0.019995	0.019995	0.009998	3.30	0.233
Residual Error	2	0.006060	0.006060	0.003030		
Total	8	0.069494				

Response Table for Signal to Noise Ratios
Smaller is better

Level	LOAD	TIME	FREQUENCY
1	18.33	18.85	20.11
2	18.36	13.70	14.92
3	11.62	15.76	13.29
Delta	6.75	5.14	6.82
Rank	2	3	1

Response Table for Means

Level	LOAD	TIME	FREQUENCY
1	0.1343	0.1379	0.1141
2	0.1377	0.2081	0.2054
3	0.2685	0.1945	0.2209
Delta	0.1342	0.0701	0.1068
Rank	1	3	2

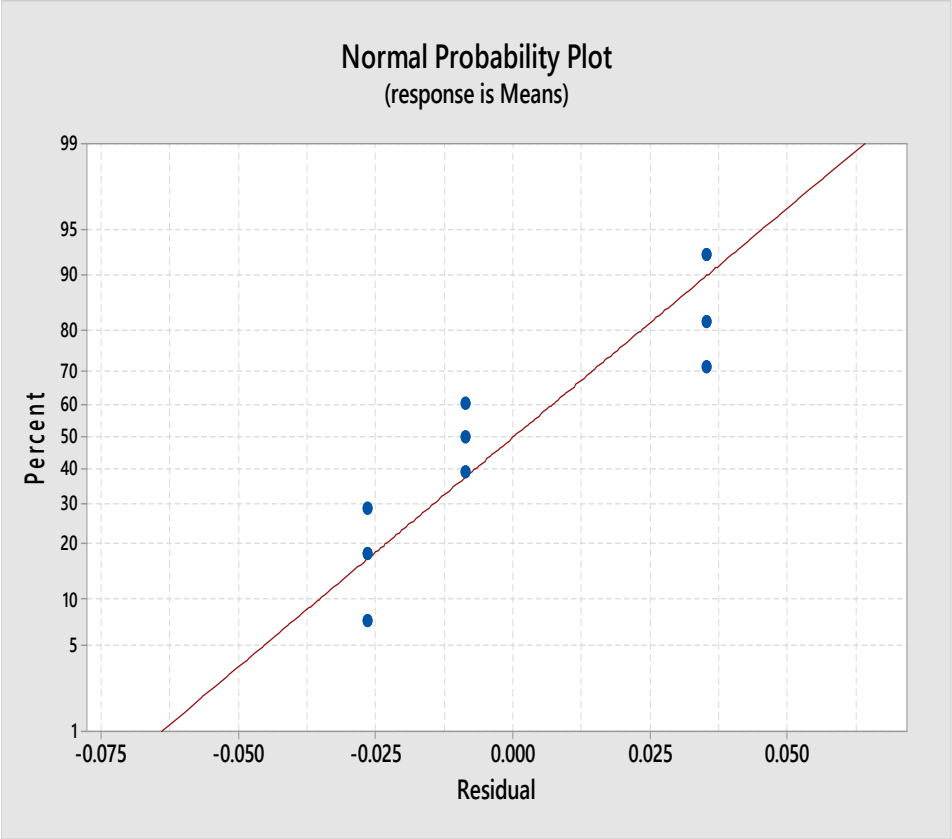

Graph. 8.18 Normal plot of Means [Steel Rough specimens]

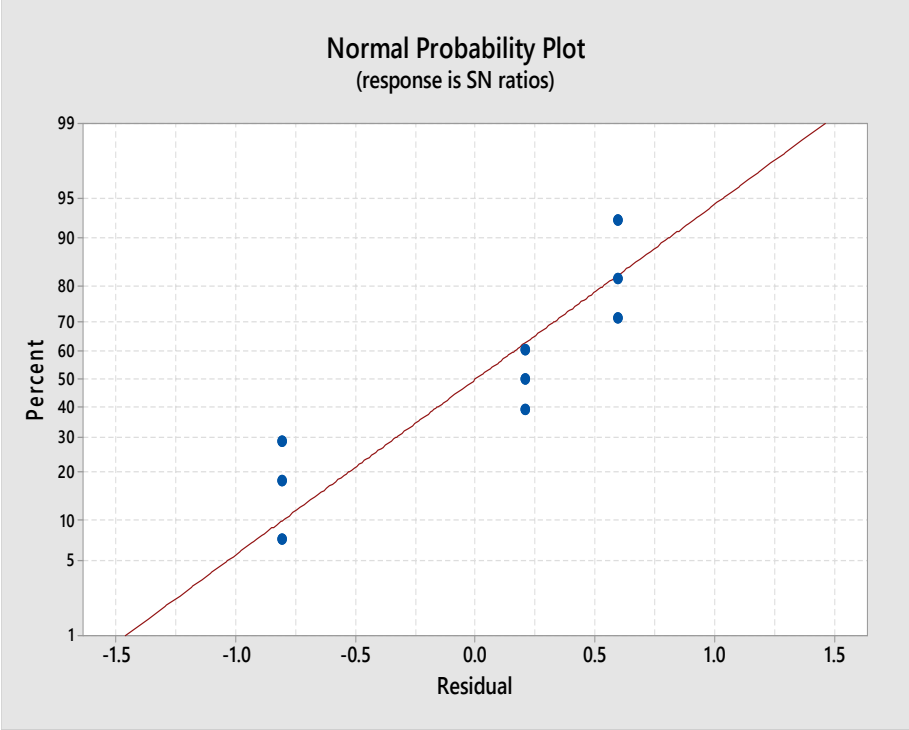

Graph. 8.19 Normal plot of SN ratios[Steel Rough Specimens]

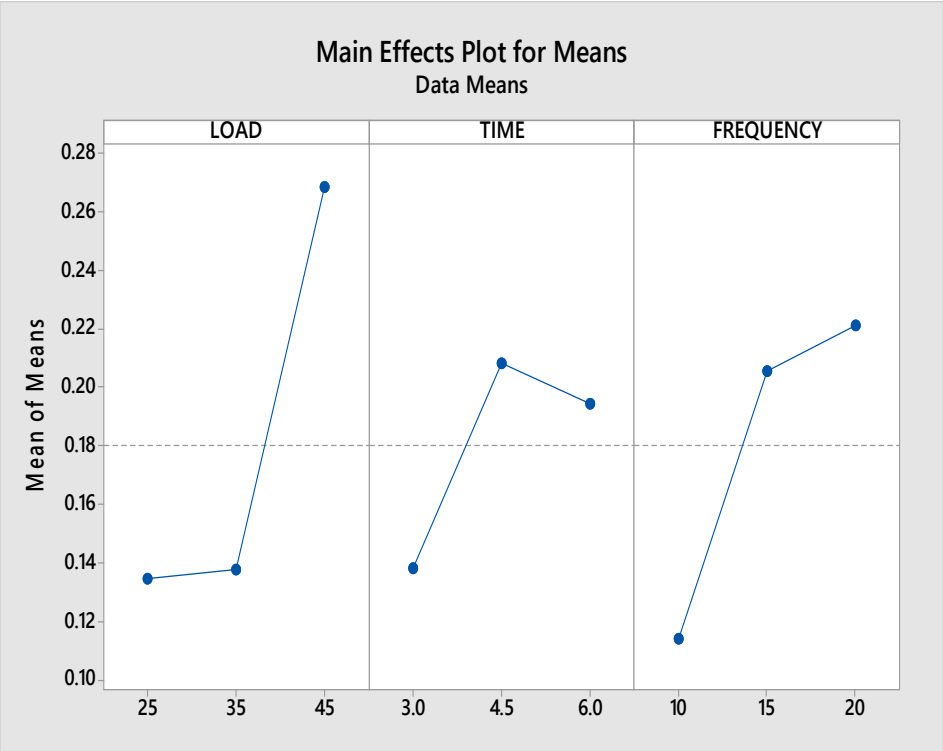

Graph. 8.20.Main Effects Plot for Means [Steel Rough Specimens]

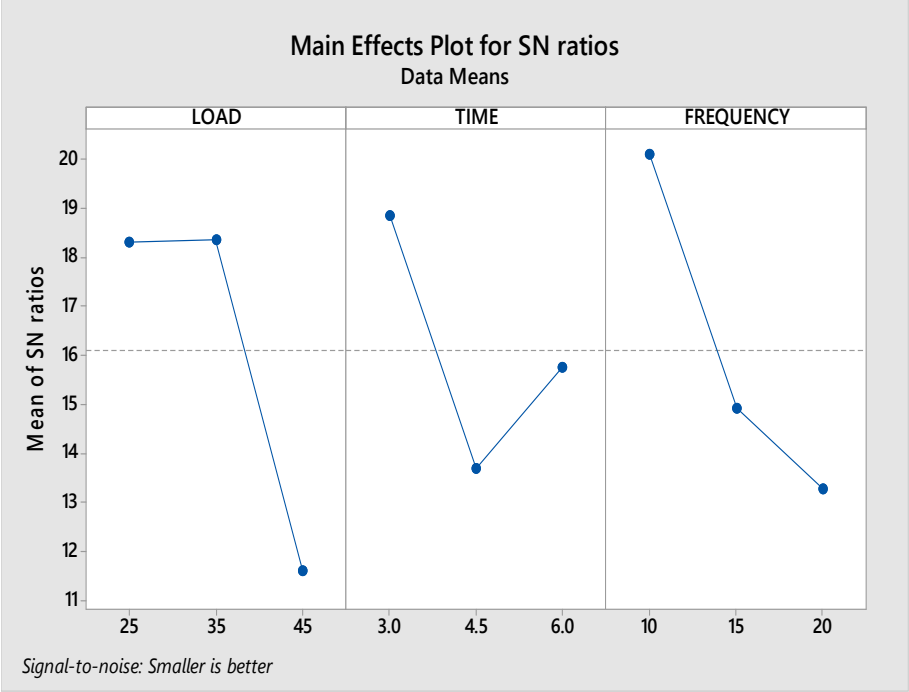

Graph.8.21.Main Effects Plot for SN ratios[Steel Finished Specimens]

8.16. Experimental Results for Steel Finished Specimens: Minitab 17 is used for the analysis and Optimisation of the experimental data. The objective is to achieve minimum wear for Steel Rough Specimens.

Taguchi Analysis: Δm versus LOAD, TIME, FREQUENCY

Linear Model Analysis: SN ratios versus LOAD, TIME, FREQUENCY

Estimated Model Coefficients for SN ratios

Term	Coef	SE Coef	T	P
Constant	17.831	0.4318	41.293	0.001
LOAD 25	2.251	0.6107	3.686	0.066
LOAD 35	2.237	0.6107	3.664	0.067
TIME 3.0	2.959	0.6107	4.846	0.040
TIME 4.5	-2.353	0.6107	-3.853	0.061
FREQUENC 10	4.003	0.6107	6.555	0.022
FREQUENC 15	-1.184	0.6107	-1.939	0.192

S = 1.295 R-Sq = 98.4% R-Sq(adj) = 93.7%

Analysis of Variance for SN ratios

Source	DF	Seq SS	Adj SS	Adj MS	F	P
LOAD	2	90.653	90.653	45.327	27.01	0.036

TIME	2	43.980	43.980	21.990	13.10	0.071
FREQUENCY	2	76.110	76.110	38.055	22.68	0.042
Residual Error	2	3.356	3.356	1.678		
Total	8	214.100				

Linear Model Analysis: Means versus LOAD, TIME, FREQUENCY

Estimated Model Coefficients for Means

Term	Coef	SE Coef	T	P
Constant	0.14813	0.01604	9.233	0.012
LOAD 25	-0.03780	0.02269	-1.666	0.238
LOAD 35	-0.03520	0.02269	-1.551	0.261
TIME 3.0	-0.03783	0.02269	-1.667	0.237
TIME 4.5	0.02153	0.02269	0.949	0.443
FREQUENC 10	-0.05477	0.02269	-2.414	0.137
FREQUENC 15	0.02240	0.02269	0.987	0.428

S = 0.04813 R-Sq = 90.5% R-Sq(adj) = 62.0

Analysis of Variance for Means

Source	DF	Seq SS	Adj SS	Adj MS	F	P
LOAD	2	0.023991	0.023991	0.011995	5.18	0.162
TIME	2	0.006482	0.006482	0.003241	1.40	0.417
FREQUENCY	2	0.013646	0.013646	0.006823	2.94	0.253
Residual Error	2	0.004634	0.004634	0.002317		
Total	8	0.048753				

Response Table for Signal to Noise Ratios
Smaller is better

Level	LOAD	TIME	FREQUENCY
1	20.08	20.79	21.83
2	20.07	15.48	16.65
3	13.34	17.23	15.01
Delta	6.74	5.31	6.82
Rank	2	3	1

Response Table for Means

Level	LOAD	TIME	FREQUENCY
1	0.11033	0.11030	0.09337
2	0.11293	0.16967	0.17053
3	0.22113	0.16443	0.18050
Delta	0.11080	0.05937	0.08713

Rank 1 3 2

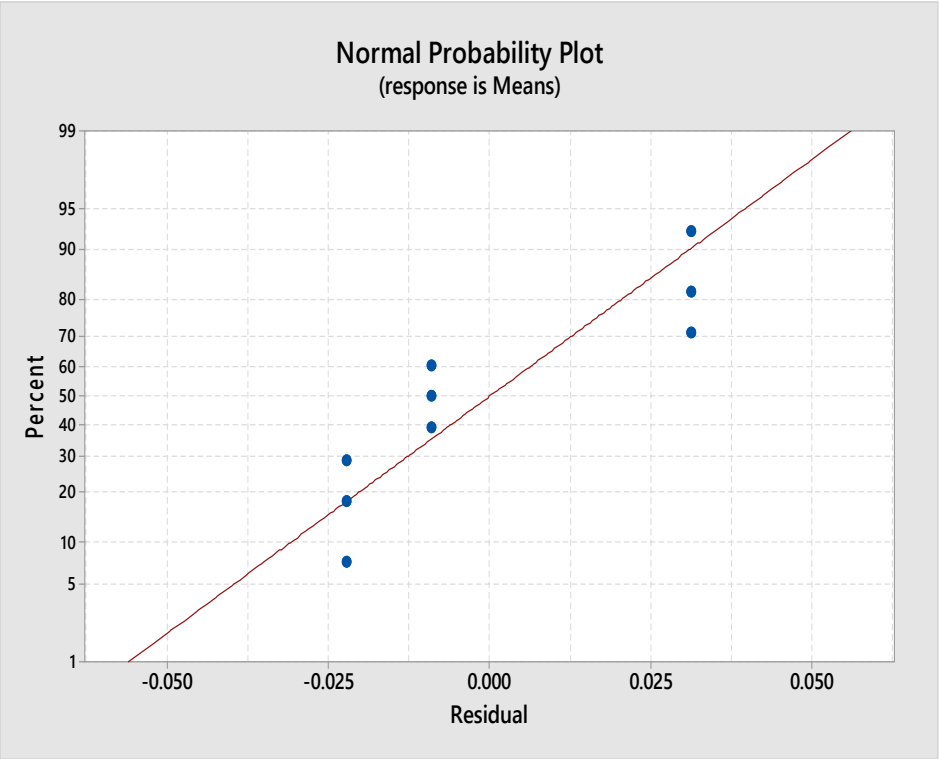

Graph. 8.22. Normal plot for Means [Steel finished specimens]

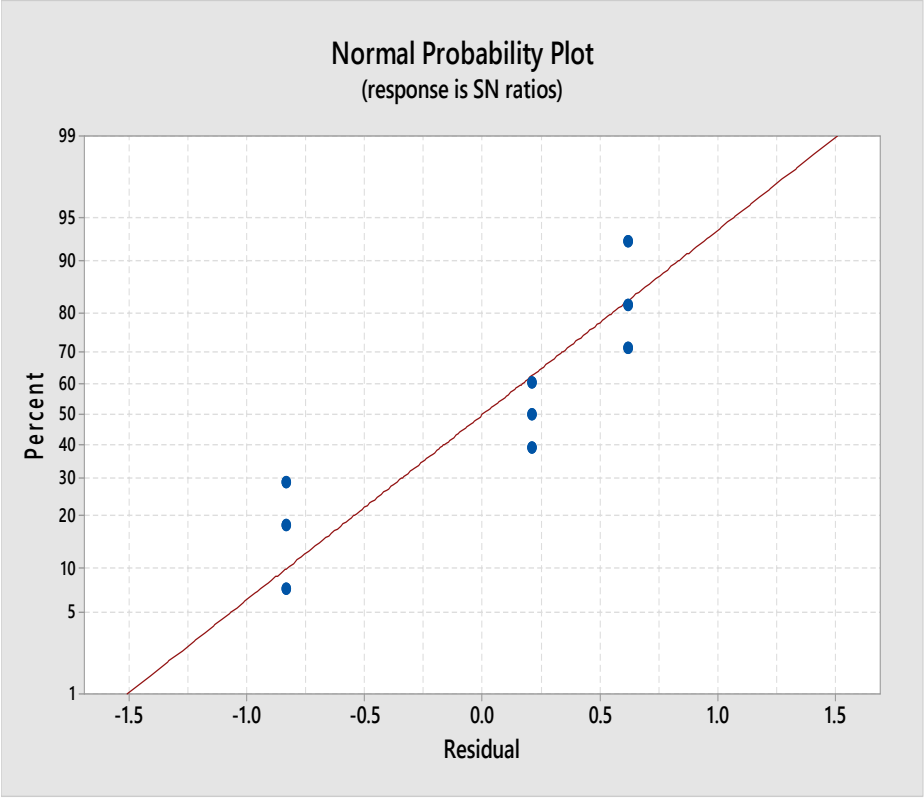

Graph.8.23.Normal plot for SN ratios Steel Finished Specimens]

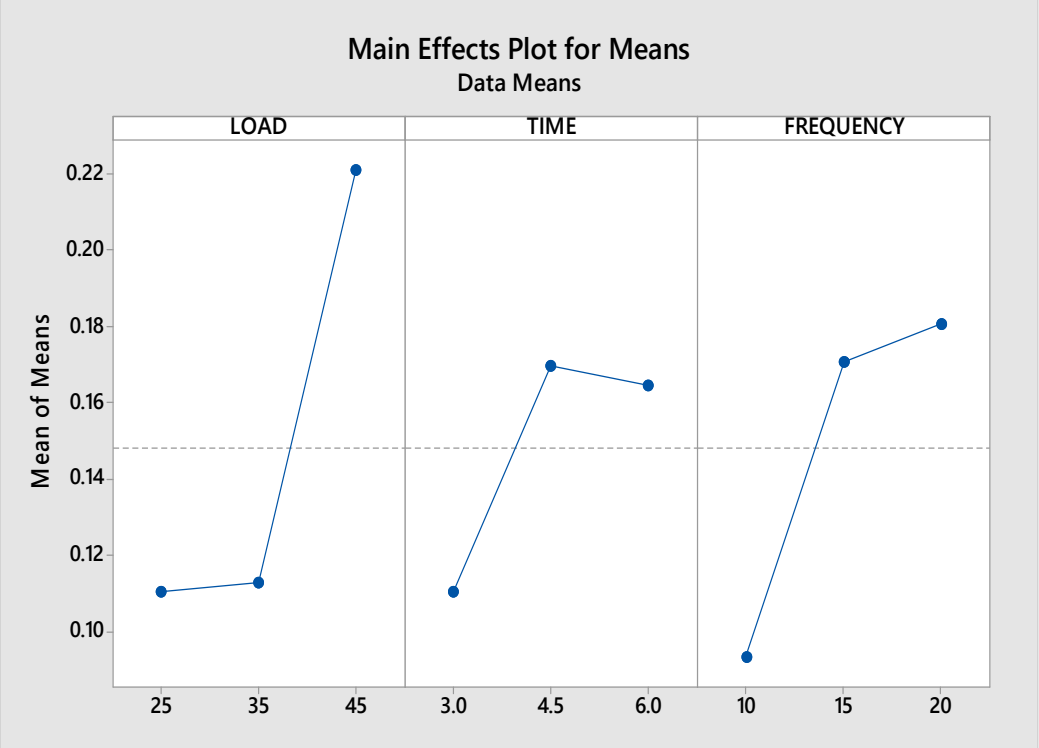

Graph 8.24 Main Effects Plot for Means [Steel Finished specimens]

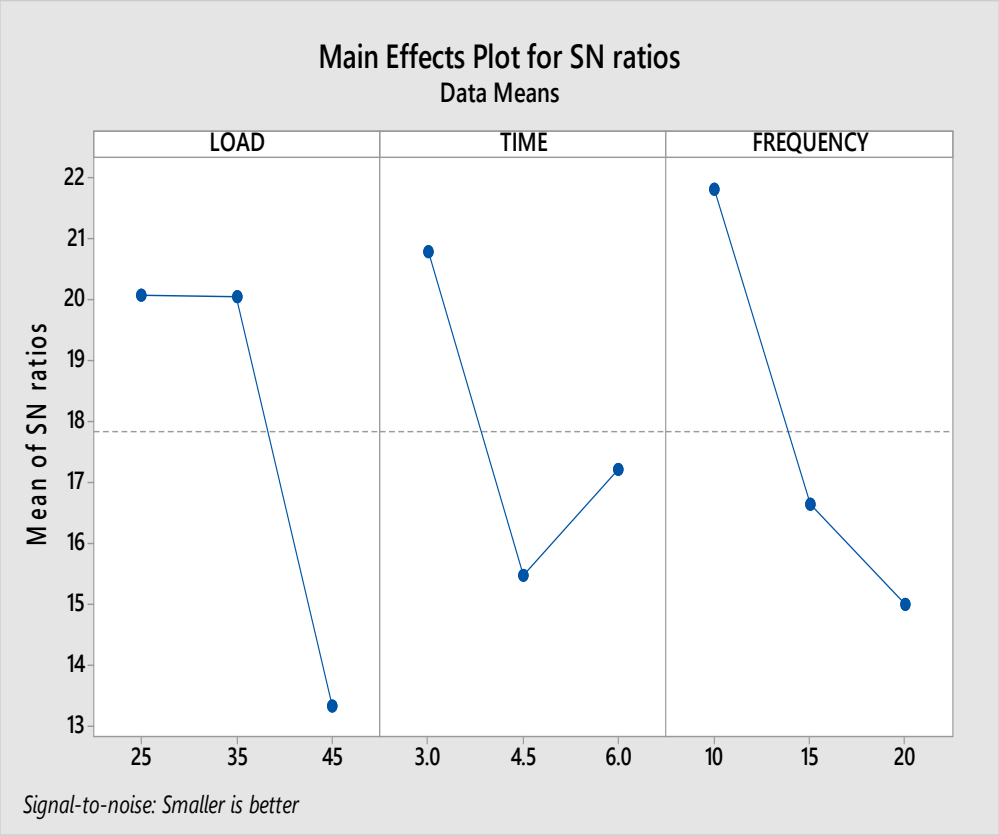

Graph.8.25. Main Effects Plot for SN ratios [Steel finished specimens]

8.17. Comparison of Coefficient of Friction[μ] of Steel Rough and Finished specimens: During the Wear test the coefficients of friction between the square block having 20mm x 20 mm x 5mm size and 8 mm diameter pin is recorded for all the nine experiments conducted. A comparative graph for L1 of the L9 table for the Coefficient of friction of the Steel rough specimens and the coefficient of friction of the finished Steel specimens have been compared from graphs 8.25 to 8.34. Except for graphs 8.30,8.31 and 8.32, all other graphs show that there is a considerable difference in the initial friction between the Rough Steel specimen and the finished specimen. The coefficient of friction[μ] has a range of 0.20 to 1.0 the average values of friction are lying between 0.5 to 0.6.

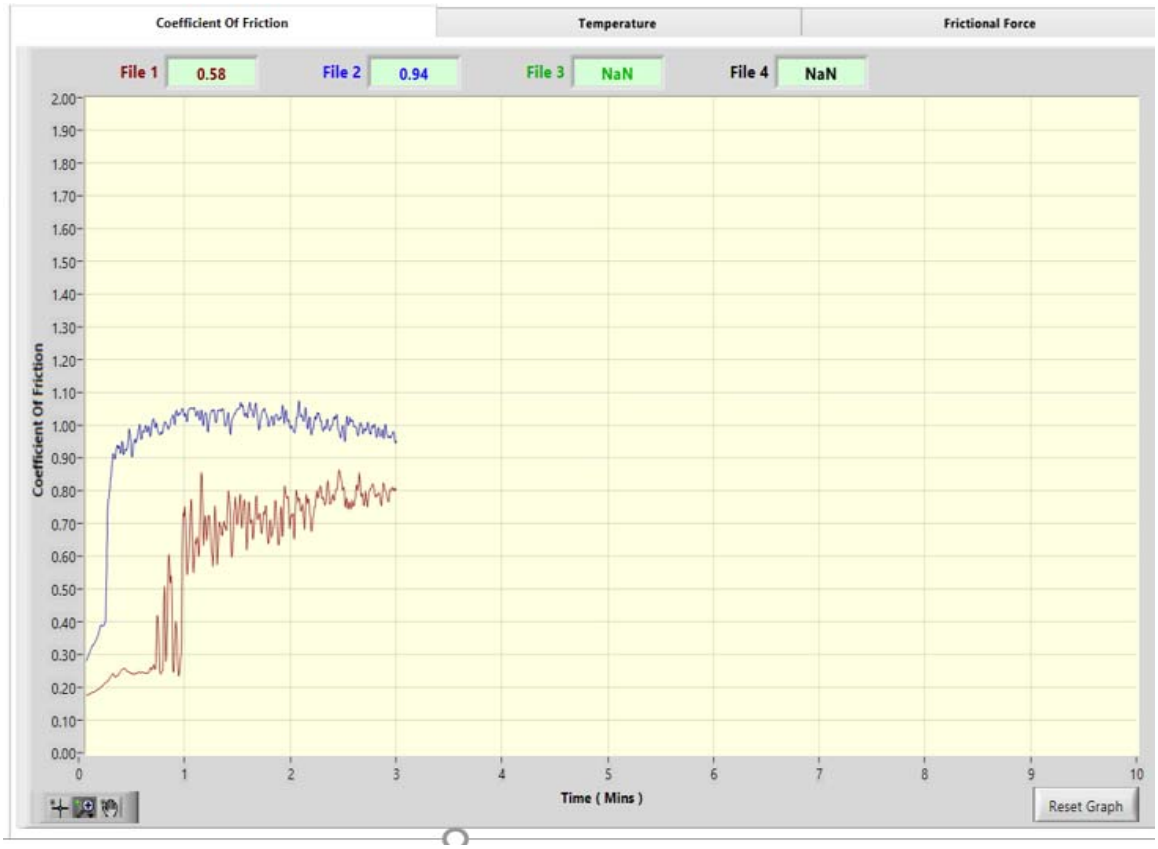

Graph.8.26. Comparison of Coefficient of friction of Steel Rough and finished specimens L1

Graph.8.27 Comparison of Coefficient of friction of Steel Rough and finished specimens L2

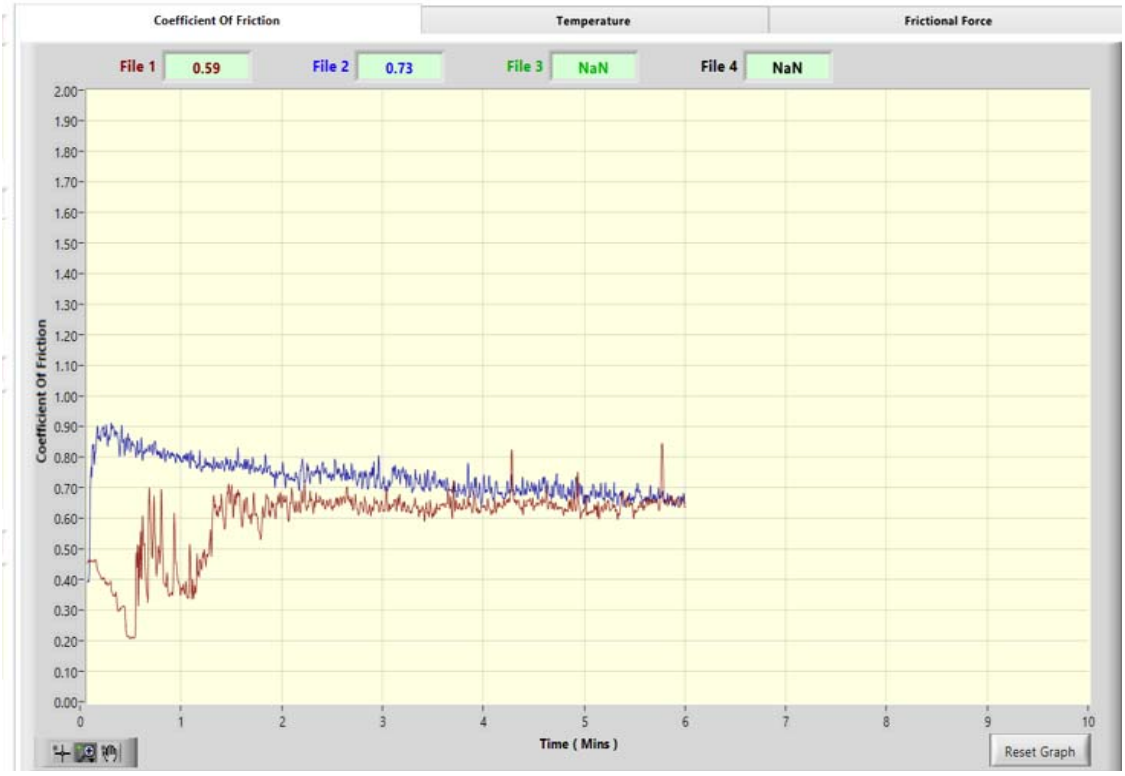

Graph.8.28. Comparison of Coefficient of friction of Steel Rough and finished specimens L3

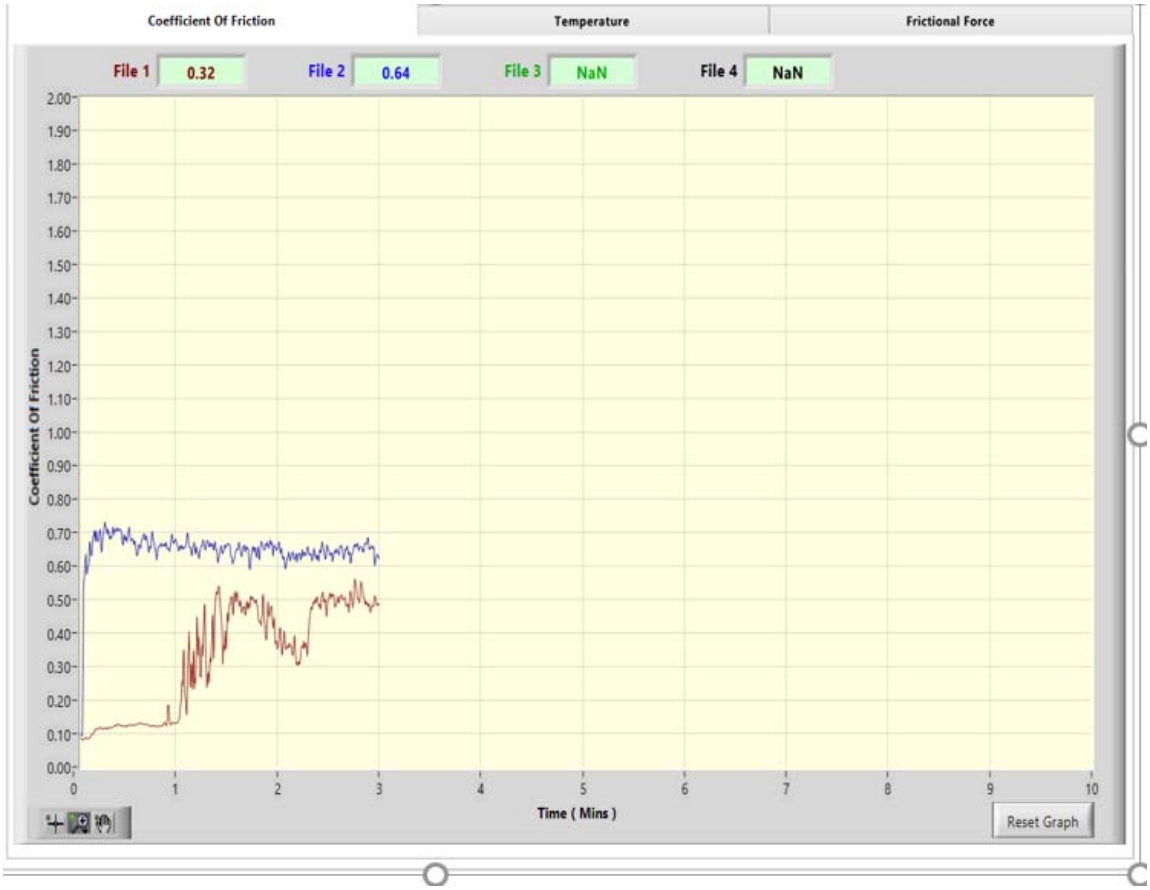

Graph.8.29. Comparison of Coefficient of friction of Steel Rough and finished specimens L4

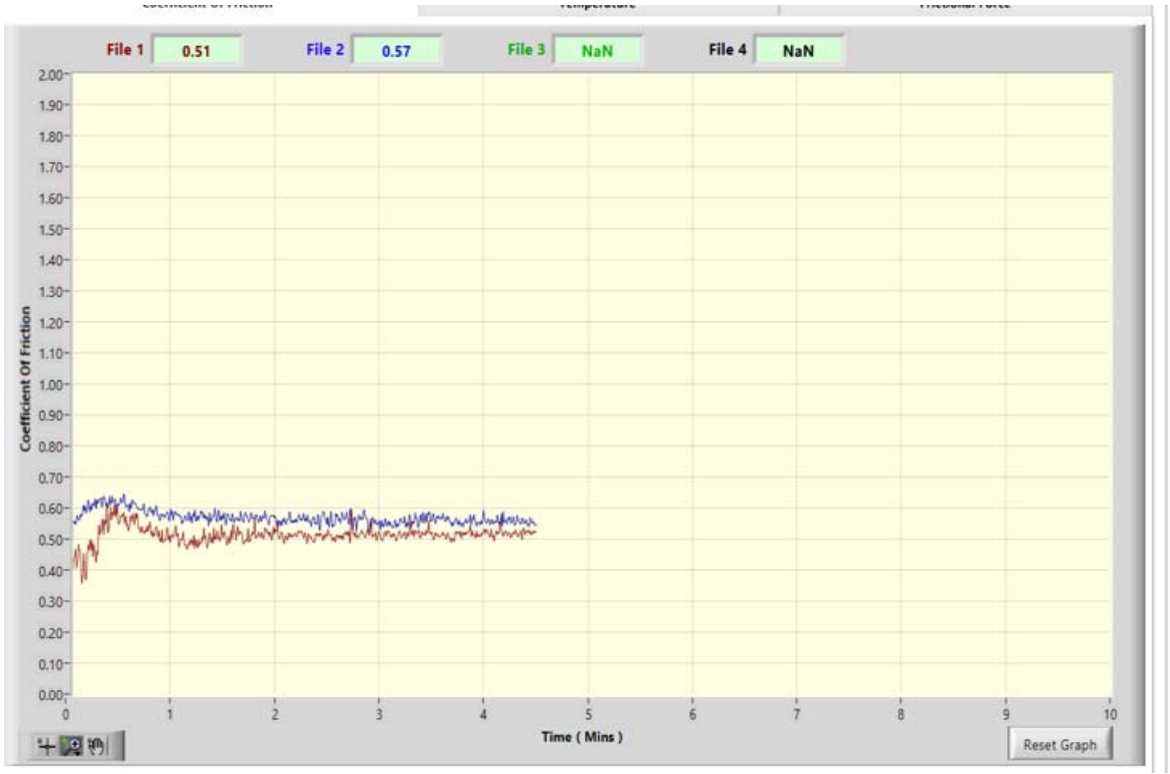

Graph.8. 30. Comparison of Coefficient of friction of Steel Rough and finished specimens L5

Graph.8.31. Comparison of Coefficient of friction of Steel Rough and finished specimens Steel L6

Graph.8. 32. Comparison of Coefficient of friction of Steel Rough and finished specimen L7

Graph.8.33 Comparison of Coefficient of friction of Steel Rough and finished specimen L8

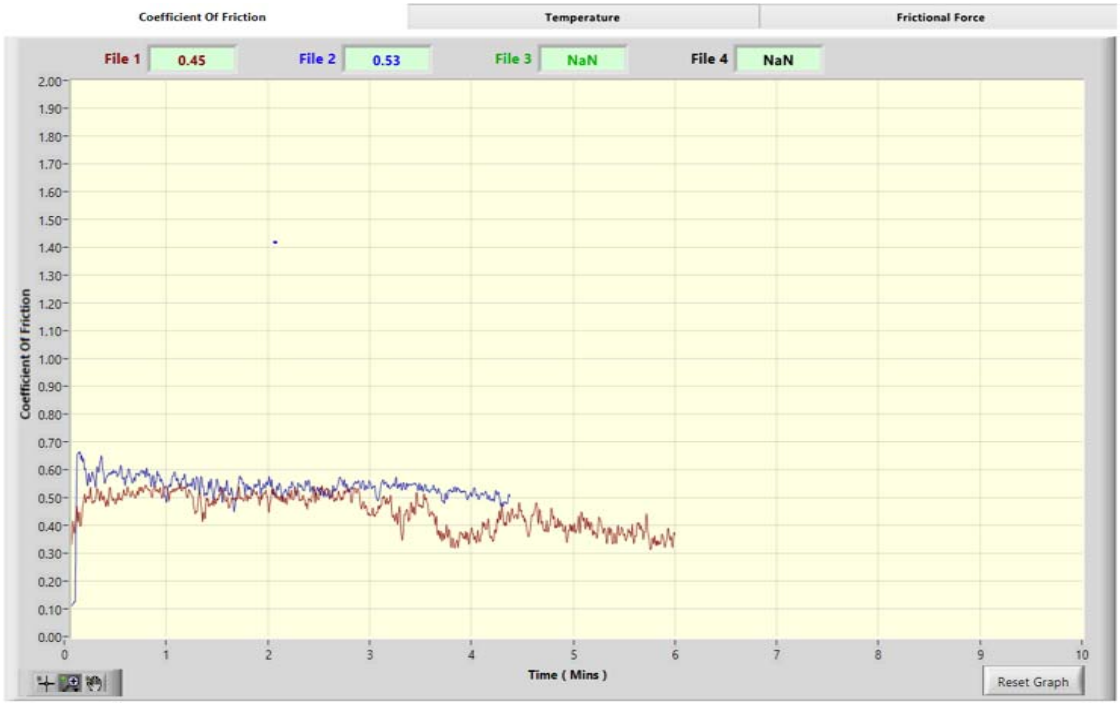

Graph.8.34. Comparison of Coefficient of friction of Steel Rough and finished specimen L9

Fig. 8.15. M S Rough Specimen after wear **Fig. 8.16 M S Finished Specimen after wear**

8.18. Result Analysis and Discussion for Wear Test performed on Steel rough and Finished Specimen:

Results obtained based on Taguchi's Regression analysis with Minitab 17 are as mentioned below.

1. For the tests performed on both the Rough specimen and the finished specimen the points of wear are nearer to Normal distribution line, which indicates that the Normal distribution Model is significant.

2. For getting minimum wear the process parameters have to be minimum, however the significance of the process parameter is not same and hence the ranking obtained has to be considered, which have been tabulated below.

Table. 8.9 Comparison of ranking for Brass[Rough and Finished Specimen]

	Load	Time	Frequency
Steel Rough	**2**	**3**	**1**
Steel Finished	**2**	**3**	**1**

3. Above table describes that Frequency is the most significant parameter, followed by the load and Time for both rough and finished Steel specimen.

4. Significance level has been tabulated below.

Table. 8.10 Comparison of significance for Steel Rough and Finished Specimen

	Load	Time	Frequency
Steel Rough	**0.034**	**0.073**	**0.040**

Steel Finished	**0.036**	**0.071**	**0.042**

For most of the experiments p-value < 0.05 has been considered, however in practical terms p< 0.10 also considered to be significant. For finding the significance of the experiment R-Sq and R-Sq[adj] must be higher here both are above 90%, so the results are considered to be significant.

5. Graphs 8.26 to 8.34 clearly show that the Coefficient of friction of the rough specimen shown in blue color is higher than the coefficient of friction of the finished specimen shown in Red color.

6. Material removal for the rough specimen is higher than the coefficient of friction for the rough specimen.

7. Coefficient of friction is of the order 0.5 or above for almost all the cases and sharp rise in coefficient of friction is observed, so more frictional forces and hence more amount of Wear

8. Fig. 8.13 and 8.14 shown above are the specimens subjected to Dry sliding wear. The images are corresponding to the maximum worn out pieces. A deep grove may be observed on the surface of the steel [AISI1020] specimen. In this case, the wear is due to both Abrasion and adhesion.

8.19. Wear Test on Aluminium Specimens: The following table gives the L9 Design for Orthogonal Array of Experiments for ***Aluminium Rough*** and **Finished specimen**. Rough specimens tested are the rear side of the finished specimen. All the Aluminium Specimens are having a surface roughness of the order of 0.4 μm ± 10% as these specimens have been polished uniformly to get this value. The finished specimen has been cut from the Steel specimen finished by VEMAF process and having surface roughness values of 0.0776μm to 0.079μm. Experiments have been conducted as per Taguchi's L9 Orthogonal array of experiments. The parameters considered for each level, Initial mass, final mass, and wear have been tabulated in Table 8.11 below.

Table 8.11 L9 Orthogonal Array of Experiments Aluminium [Rough and Finished Specimen]

			ALUMINIUM ROUGH SPECIMEN	ALUMINIUM FINISHED SPECIMEN

LOAD (N)	TIME (Minutes)	Frequency (Hz)	Initial Mass (grams)	Initial Mass (grams)	Wear Mass (grams)	Initial Mass (grams)	Initial Mass (grams)	Wear Mass (grams)
25	3.0	10	**6.1836**	**6.1704**	**0.0132**	**6.1704**	**5.1559**	**0.0110**
25	4.5	15	**6.2035**	**6.1870**	**0.0165**	**6.1870**	**5.1720**	**0.0140**
25	6.0	20	**6.1946**	**6.1758**	**0.0188**	**6.1758**	**5.1558**	**0.0162**
35	3.0	15	**6.1796**	**6.1673**	**0.0123**	**6.1673**	**5.1596**	**0.0102**
35	4.5	20	**6.2046**	**6.1859**	**0.0187**	**6.1859**	**5.1685**	**0.0158**
35	6.0	10	**6.1874**	**6.1726**	**0.0148**	**6.1726**	**5.162**	**0.0122**
45	3.0	20	**6.1928**	**6.1817**	**0.0111**	**6.1817**	**5.1649**	**0.0092**
45	4.5	10	**6.1832**	**6.1718**	**0.0114**	**6.1718**	**5.1655**	**0.0096**
45	6.0	15	**6.1906**	**6.1780**	**0.0126**	**6.1780**	**5.1679**	**0.0108**

8.20. Experimental results of a Wear test on Aluminium Rough Specimens:

Optimization for the process parameters has been done for minimum wear(Δm) using Minitab 17, result includes optimization of process parameters, their ranking, and significance. The results have been shown below.

Taguchi Analysis: Δm versus LOAD, TIME, FREQUENCY

Linear Model Analysis: SN ratios versus LOAD, TIME, FREQUENCY

```
Estimated Model Coefficients for SN ratios

Term            Coef  SE Coef        T      P
Constant     38.5108   0.1672  230.368  0.000
LOAD 25      -1.1577   0.2364   -4.897  0.039
LOAD 35      -0.4683   0.2364   -1.981  0.186
TIME 3.0      1.3973   0.2364    5.910  0.027
TIME 4.5     -0.6912   0.2364   -2.924  0.100
FREQUENC 10   0.7557   0.2364    3.196  0.086
FREQUENC 15   0.2348   0.2364    0.993  0.425

S = 0.5015   R-Sq = 98.1%   R-Sq(adj) = 92.5%

Analysis of Variance for SN ratios

Source          DF   Seq SS   Adj SS  Adj MS      F      P
LOAD             2  12.6101  12.6101  6.3050  25.07  0.038
TIME             2   8.7866   8.7866  4.3933  17.47  0.054
FREQUENCY        2   4.8222   4.8222  2.4111   9.59  0.094
```

Residual Error	2	0.5030	0.5030	0.2515
Total	8	26.7219		

Linear Model Analysis: Means versus LOAD, TIME, FREQUENCY

Estimated Model Coefficients for Means

Term	Coef	SE Coef	T	P
Constant	0.012111	0.000219	55.336	0.000
LOAD 25	0.001622	0.000310	5.241	0.035
LOAD 35	0.000622	0.000310	2.010	0.182
TIME 3.0	-0.001978	0.000310	-6.390	0.024
TIME 4.5	0.001022	0.000310	3.303	0.081
FREQUENC 10	-0.001178	0.000310	-3.805	0.063
FREQUENC 15	-0.000444	0.000310	-1.436	0.288

S = 0.0006566 R-Sq = 98.4% R-Sq(adj) = 93.8%

Analysis of Variance for Means

Source	DF	Seq SS	Adj SS	Adj MS	F	P
LOAD	2	0.000024	0.000024	0.000012	28.03	0.034
TIME	2	0.000018	0.000018	0.000009	20.42	0.047
FREQUENCY	2	0.000013	0.000013	0.000006	14.67	0.064
Residual Error	2	0.000001	0.000001	0.000000		
Total	8	0.000055				

Response Table for Signal to Noise Ratios
Smaller is better

Level	LOAD	TIME	FREQUENCY
1	37.35	39.91	39.27
2	38.04	37.82	38.75
3	40.14	37.80	37.52
Delta	2.78	2.10	1.75
Rank	1	2	3

Response Table for Means

Level	LOAD	TIME	FREQUENCY
1	0.013733	0.010133	0.010933
2	0.012733	0.013133	0.011667
3	0.009867	0.013067	0.013733
Delta	0.003867	0.003000	0.002800
Rank	1	2	3

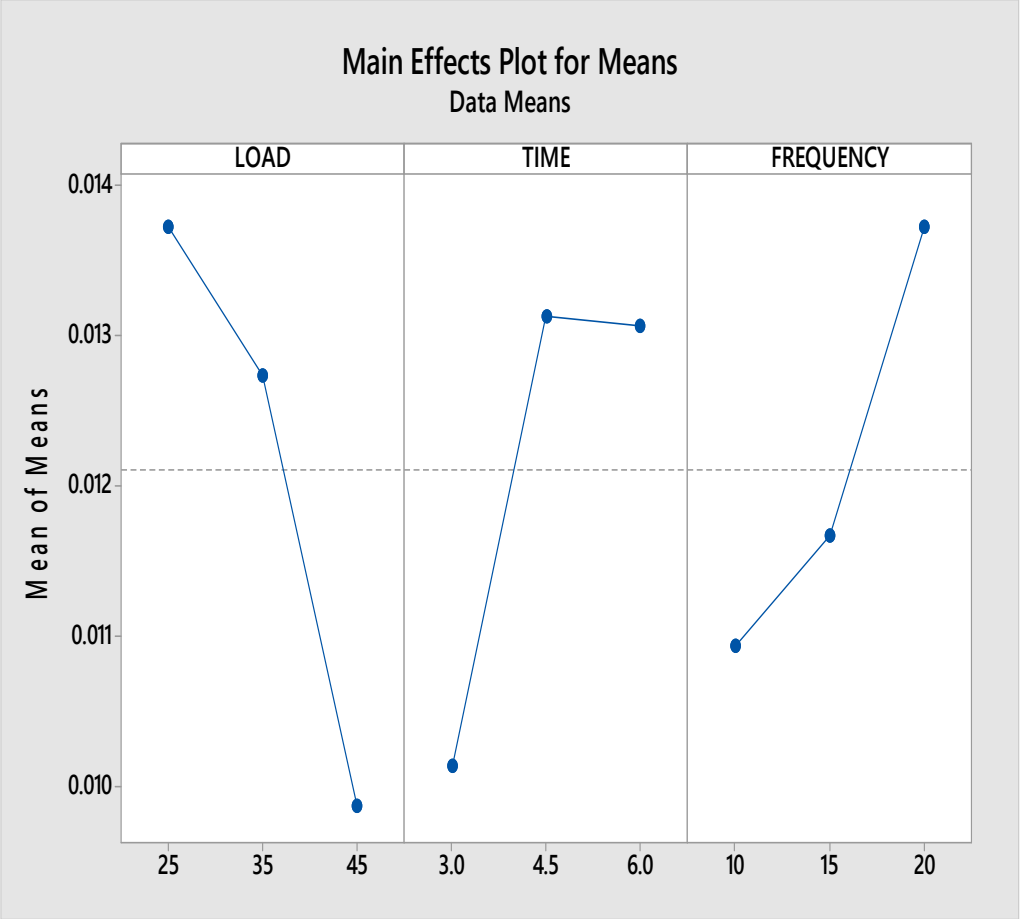

Graph. 8.35. Main Effects Plot for Means [Aluminium Rough Specimens]

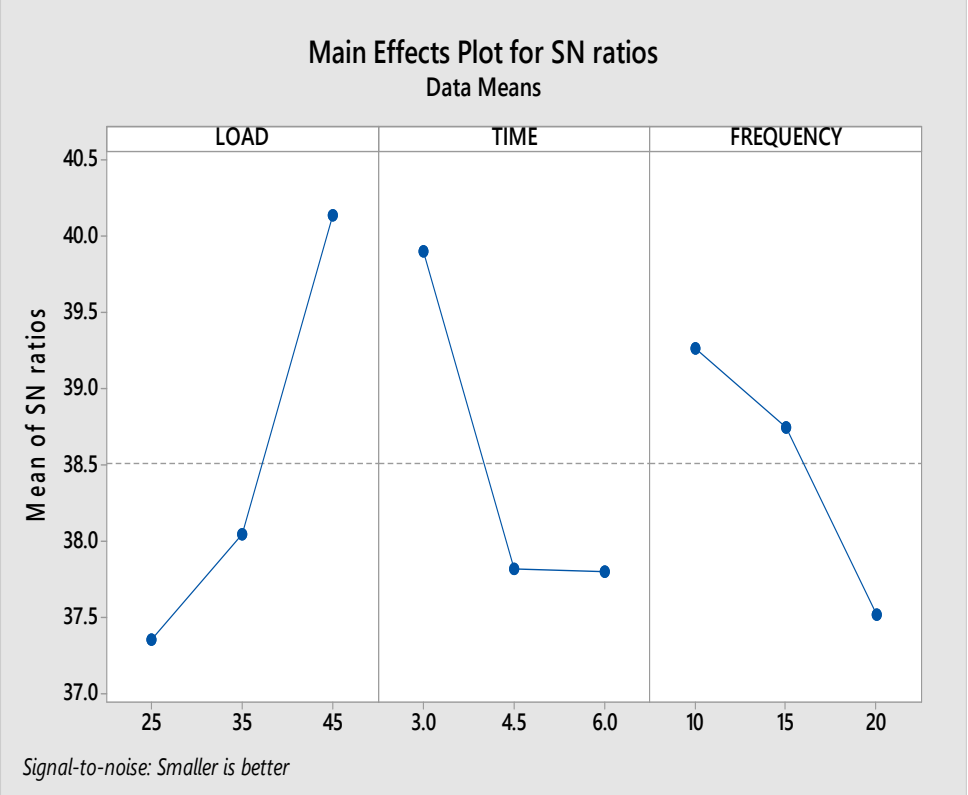

Graph.8.36. Main Effects Plot for SN ratios [Aluminium Rough Specimens]

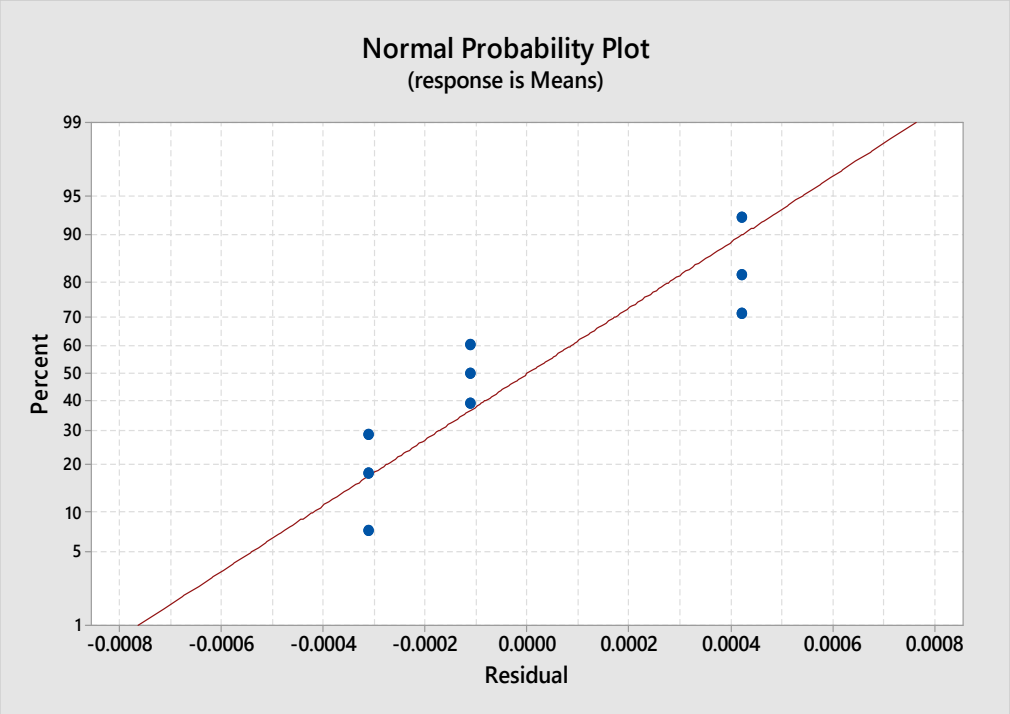

Graph.8.37. Normal plot for means [Aluminium Rough specimens]

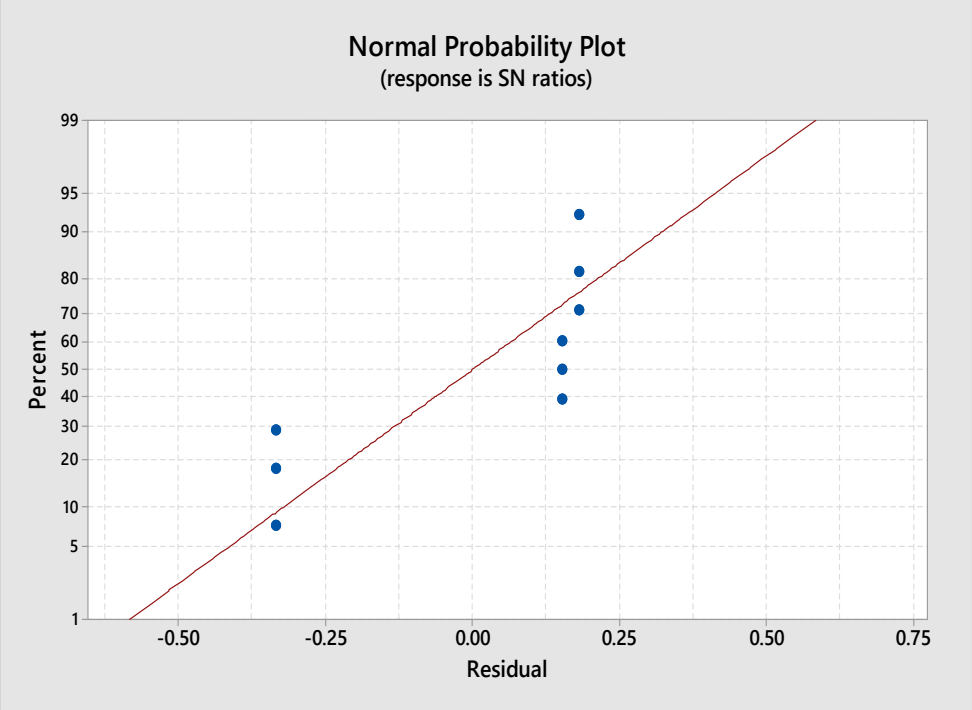

Graph.8.38. Normal plot of for SN ratios [Aluminium Rough specimens]

8.21. Experimental results of the Wear test on Aluminium finished Specimens:

Optimization for the process parameters has been done for minimum wear(Δm) using Minitab 17, result includes optimization of process parameters, their ranking, and significance. The results have been shown below

Taguchi Analysis: Δm versus LOAD, TIME, FREQUENCY

Linear Model Analysis: SN ratios versus LOAD, TIME, FREQUENCY

Taguchi Design

```
Taguchi Orthogonal Array Design

L9(3^3)

Factors:  3
Runs:     9


Columns of L9(3^4) Array

1 2 3
```

Taguchi Analysis: WEAR versus LOAD, TIME, FREQUENCY

Linear Model Analysis: SN ratios versus LOAD, TIME, FREQUENCY

Estimated Model Coefficients for SN ratios

Term	Coef	SE Coef	T	P
Constant	38.5108	0.1672	230.368	0.000
LOAD 25	-1.1577	0.2364	-4.897	0.039
LOAD 35	-0.4683	0.2364	-1.981	0.186
TIME 3.0	1.3973	0.2364	5.910	0.027
TIME 4.5	-0.6912	0.2364	-2.924	0.100
FREQUENC 10	0.7557	0.2364	3.196	0.086
FREQUENC 15	0.2348	0.2364	0.993	0.425

S = 0.5015 R-Sq = 98.1% R-Sq(adj) = 92.5%

Analysis of Variance for SN ratios

Source	DF	Seq SS	Adj SS	Adj MS	F	P
LOAD	2	12.6101	12.6101	6.3050	25.07	0.038
TIME	2	8.7866	8.7866	4.3933	17.47	0.051
FREQUENCY	2	4.8222	4.8222	2.4111	9.59	0.092
Residual Error	2	0.5030	0.5030	0.2515		
Total	8	26.7219				

Linear Model Analysis: Means versus LOAD, TIME, FREQUENCY

Estimated Model Coefficients for Means

Term	Coef	SE Coef	T	P
Constant	0.012111	0.000219	55.336	0.000
LOAD 25	0.001622	0.000310	5.241	0.035
LOAD 35	0.000622	0.000310	2.010	0.182
TIME 3.0	-0.001978	0.000310	-6.390	0.024
TIME 4.5	0.001022	0.000310	3.303	0.081
FREQUENC 10	-0.001178	0.000310	-3.805	0.063
FREQUENC 15	-0.000444	0.000310	-1.436	0.288

S = 0.0006566 R-Sq = 98.4% R-Sq(adj) = 93.8%

Analysis of Variance for Means

Source	DF	Seq SS	Adj SS	Adj MS	F	P
LOAD	2	0.000024	0.000024	0.000012	28.03	0.034
TIME	2	0.000018	0.000018	0.000009	20.42	0.047
FREQUENCY	2	0.000013	0.000013	0.000006	14.67	0.064
Residual Error	2	0.000001	0.000001	0.000000		
Total	8	0.000055				

Response Table for Signal to Noise Ratios
Smaller is better

Level	LOAD	TIME	FREQUENCY
1	37.35	39.91	39.27
2	38.04	37.82	38.75
3	40.14	37.80	37.52
Delta	2.78	2.10	1.75
Rank	1	2	3

Response Table for Means

Level	LOAD	TIME	FREQUENCY
1	0.013733	0.010133	0.010933
2	0.012733	0.013133	0.011667
3	0.009867	0.013067	0.013733
Delta	0.003867	0.003000	0.002800
Rank	1	2	3

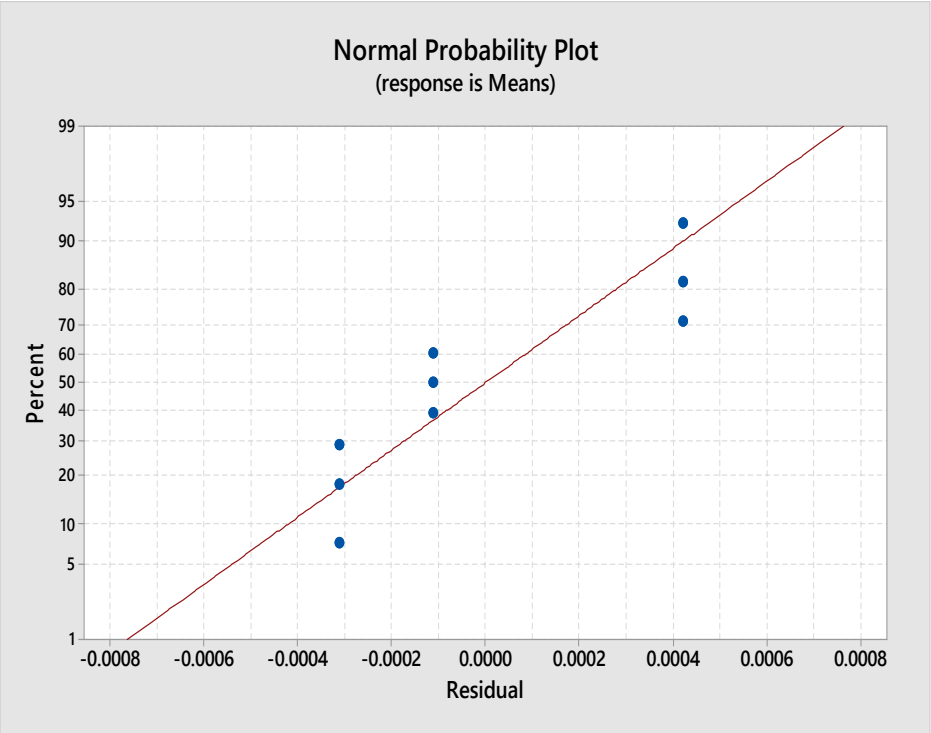

Graph. 8.39. Normal plot of for Means [Aluminium finished specimens]

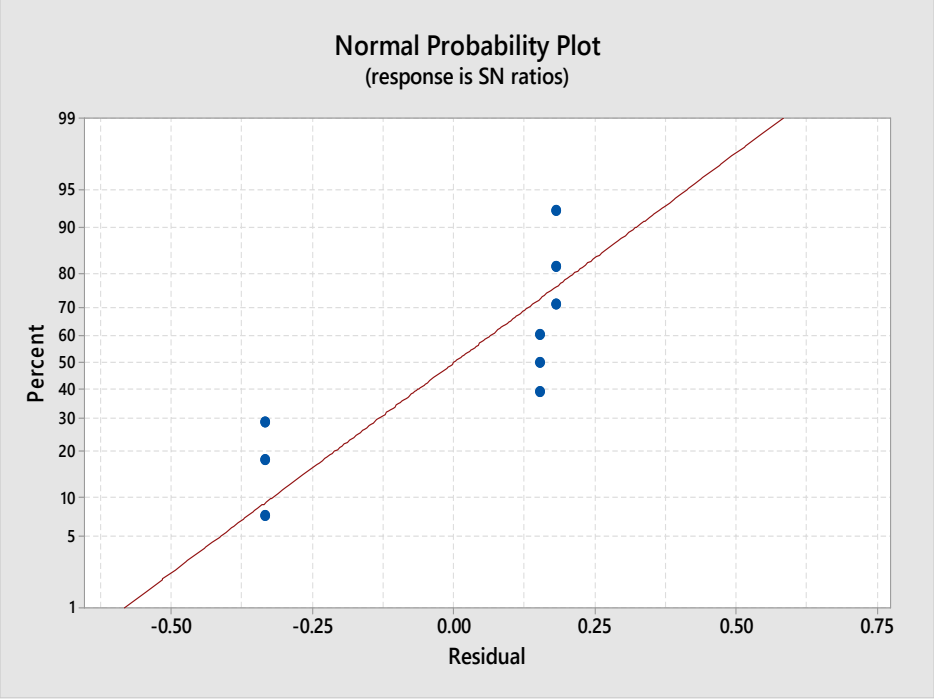

Graph.8.40 Normal plot of Residuals for SN ratios [Aluminium finished specimen]

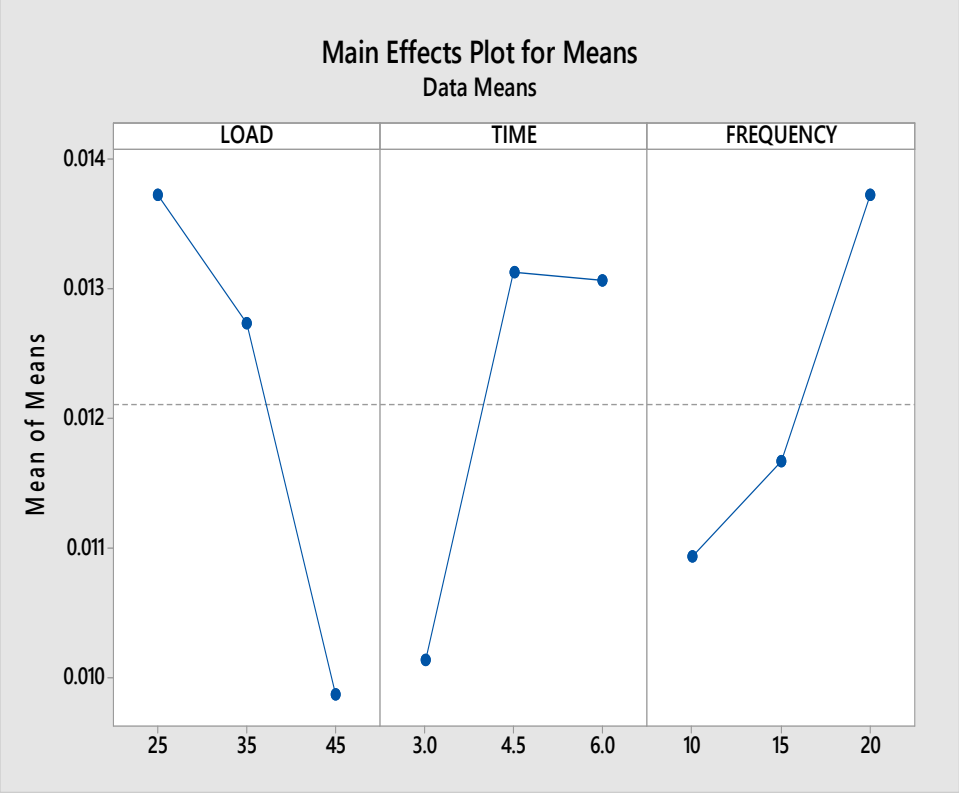

Graph.8.41.Main Effects Plot for Means [Aluminium finished Specimens]

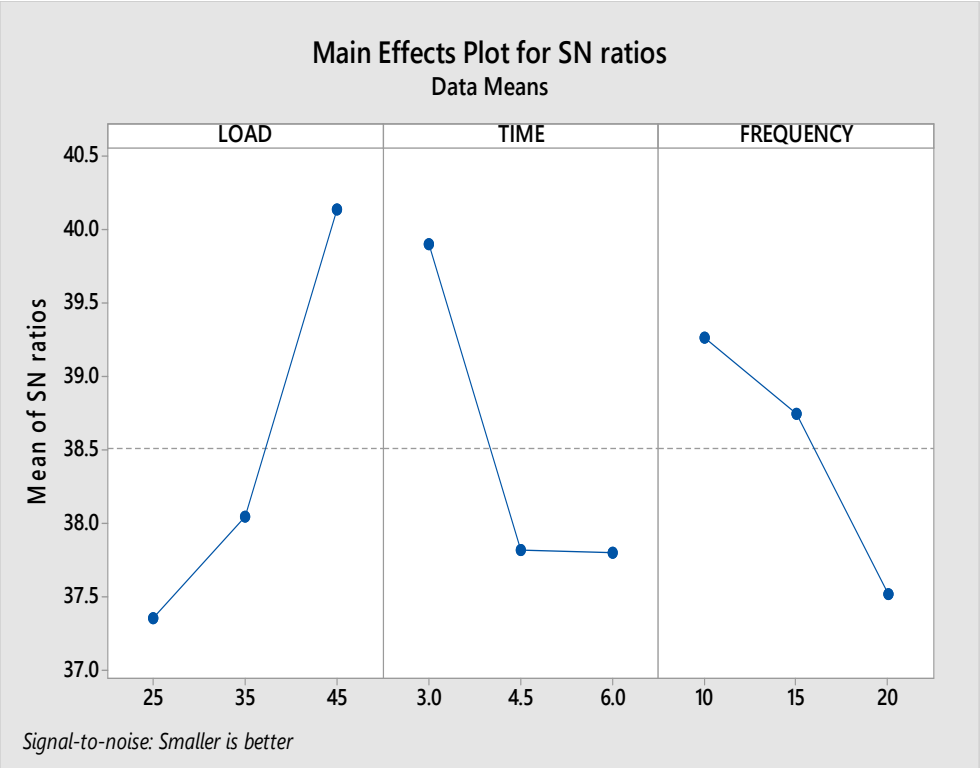

Graph.8.42.Main Effects Plot for SN ratio [Aluminium finished Specimens]

8.22. Comparison of Coefficient of Friction[μ] of Aluminium Rough and Finished specimens: During the Wear test the coefficients of friction between the square block having 20mm x 20 mm x 5mm size and 8 mm diameter pin is recorded for all the nine experiments conducted. A comparative graph for L1 of the L9 table for Coefficient of friction of the Rough Aluminium specimens and the coefficient of friction of the finished Steel specimens have been compared from graphs 8.25 to 8.34. Except for graphs 8.30,8.31 and 8.32 all other graphs show that there is considerable difference in the initial friction between the Rough Steel specimen and the finished specimen. Coefficient of friction[μ] has a range of 0.20 to 1.0 the average values of friction are lying between 0.5 to 0.6.

Graph.8.43. Comparison of Coefficient of friction of Steel Rough and finished specimen L1

Graph.8.44. Comparison of Coefficient of friction of Steel Rough and finished specimen L2

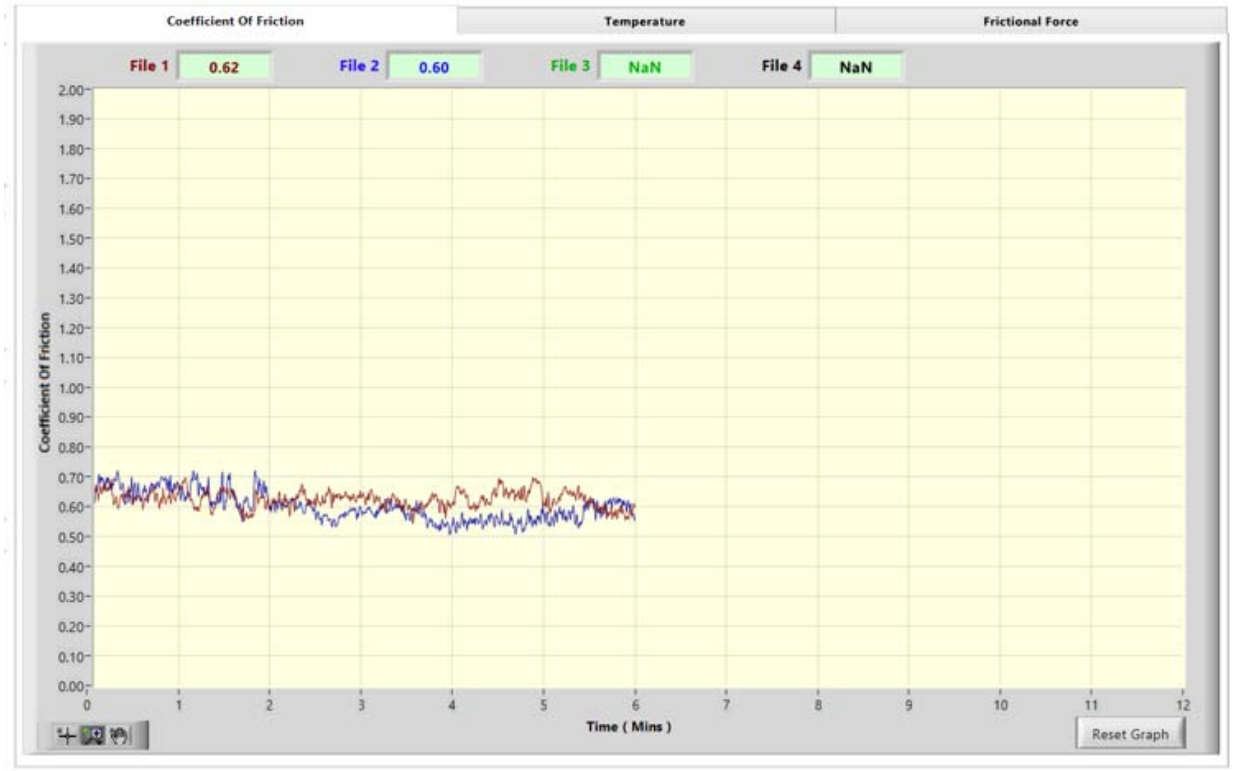

Graph.8.45. Comparison of Coefficient of friction of Steel Rough and finished specimen L3

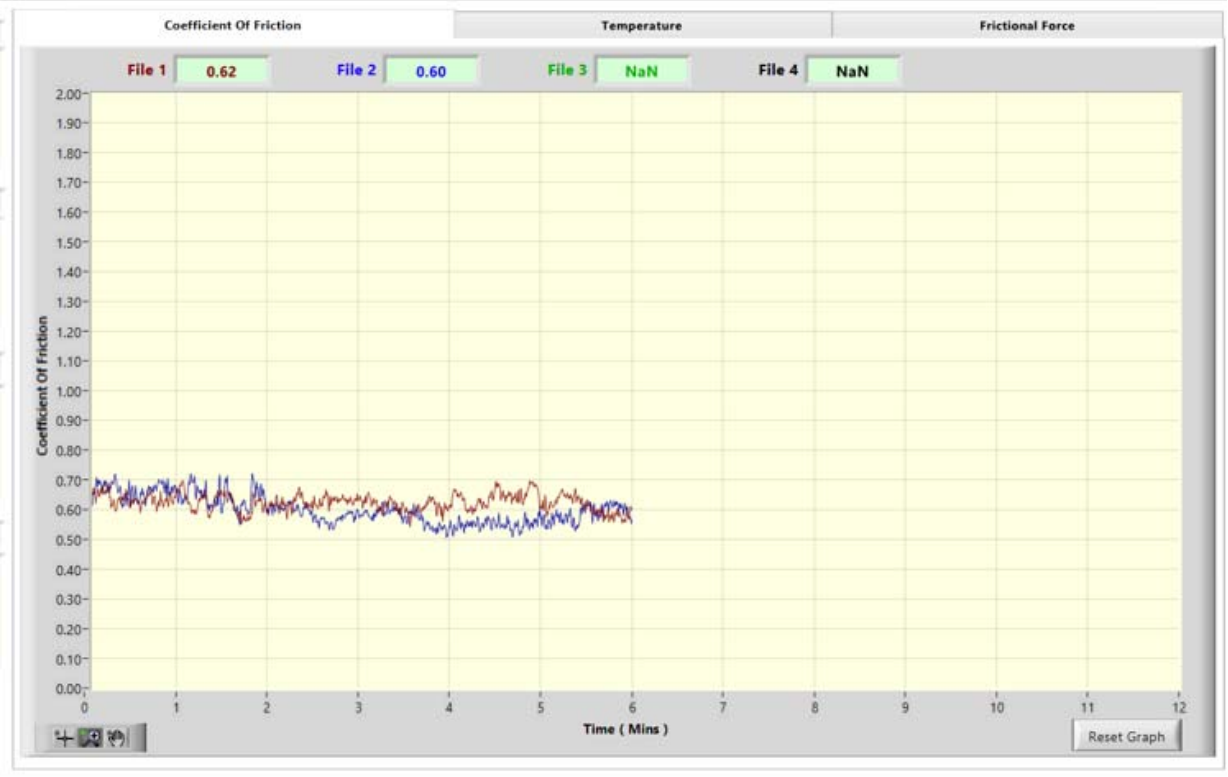

Graph.8.46. Comparison of Coefficient of friction of Steel Rough and finished specimen L4

Graph.8.47. Comparison of Coefficient of friction of Steel Rough and finished specimen L5

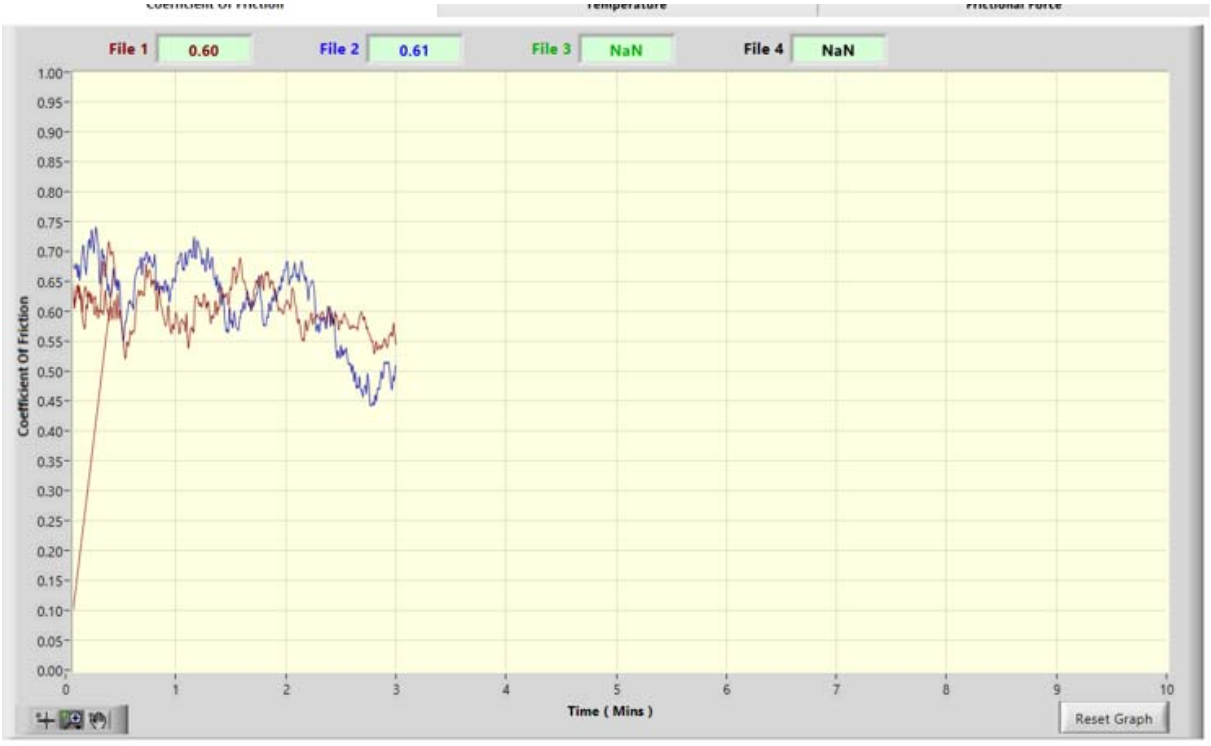

Graph.8.48. Comparison of Coefficient of friction of Steel Rough and finished specimen L6

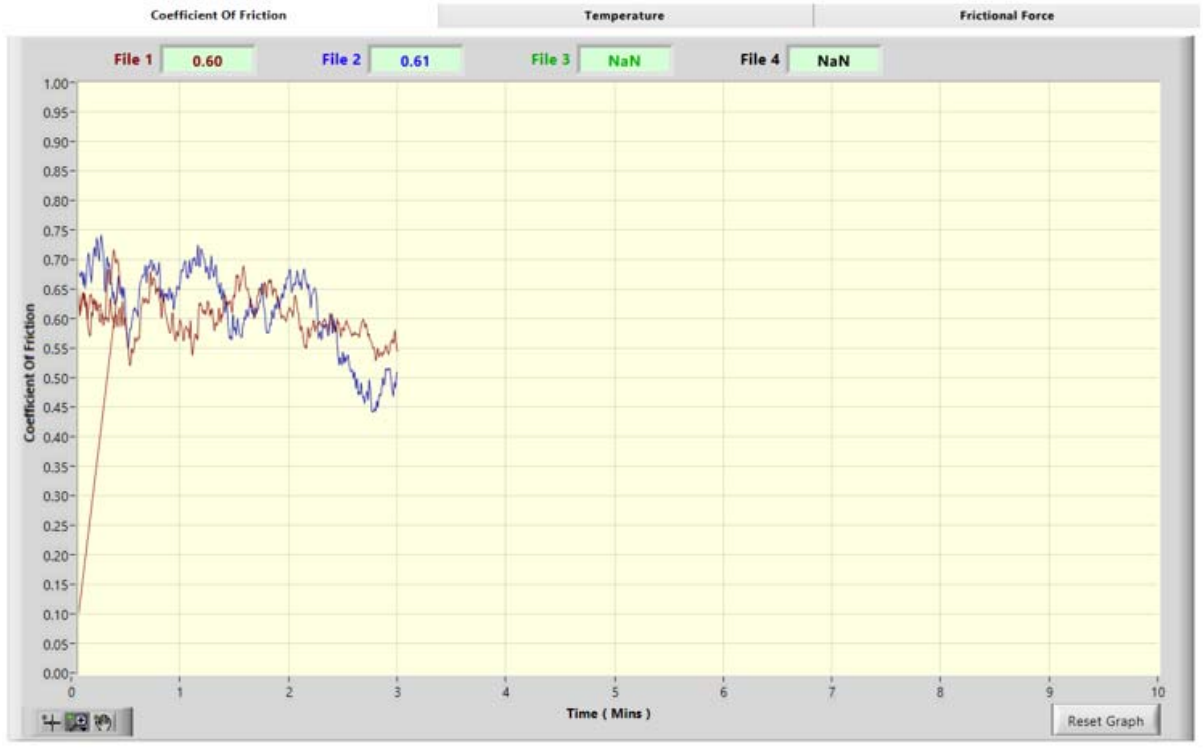

Graph.8.49. Comparison of Coefficient of friction of Steel Rough and finished specimen L7

Graph.8.50. Comparison of Coefficient of friction of Steel Rough and finished specimen L8

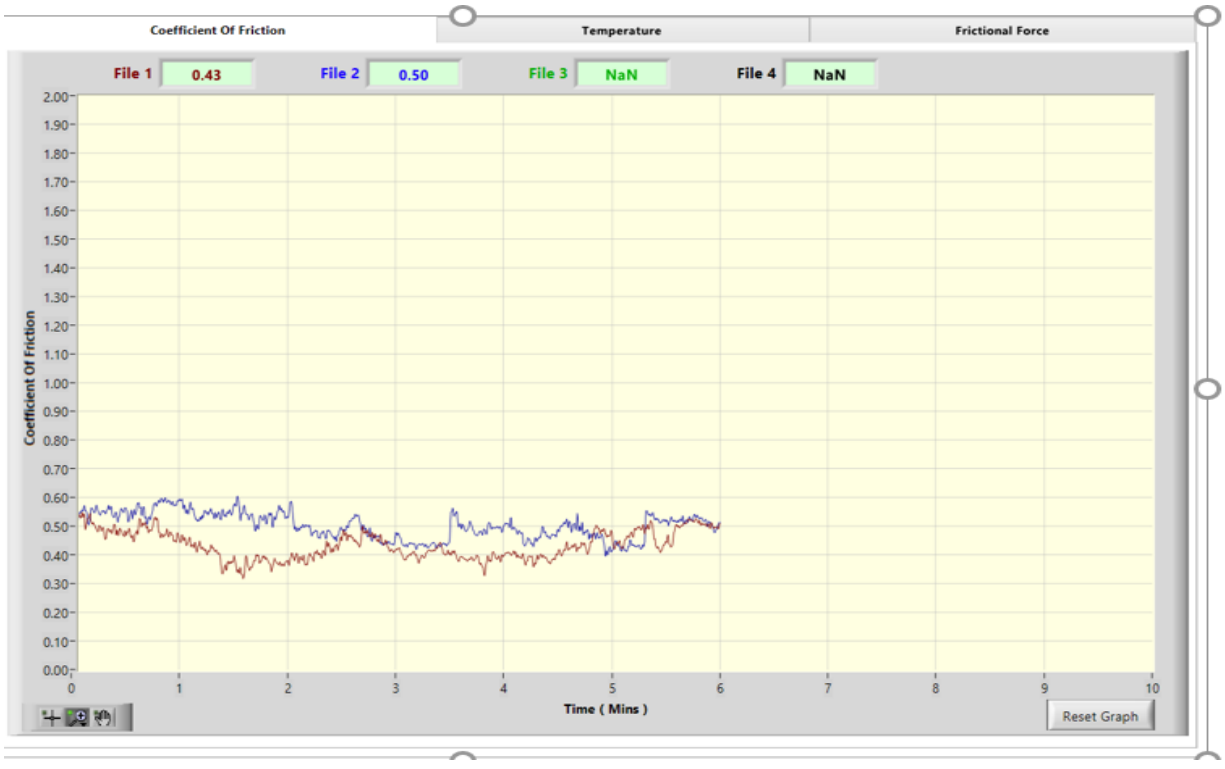

Graph.8.51. Comparison of Coefficient of friction of Steel Rough and finished specimen L9

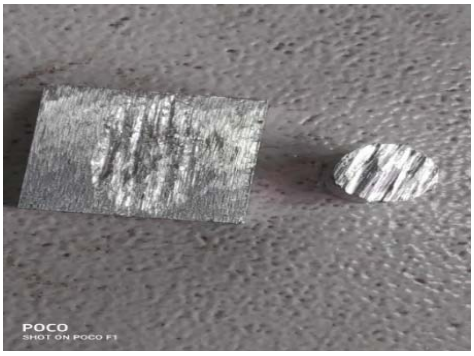

Fig.8.17. Aluminum Rough Specimen after wear **Fig.8.18. Aluminum finished Specimen after wear**

8.23. Result Analysis and Discussion for Wear Test on Aluminium rough and Finished Specimen:

Results obtained based on Taguchi's Regression analysis with Minitab 17 are as mentioned below.

1. For the tests performed on both the Rough specimen and the finished specimen, the points of wear are nearer to the Normal distribution line, which indicates that the Normal distribution Model is significant.
2. For getting minimum wear the process parameters have to be minimum, however, the significance of the process parameter is not the same and hence the ranking obtained based on the response to the given set of process parameters. Process parameters are as enlisted below.

Table. 8.12 Comparison of ranking for Aluminium Rough and Finished Specimen

	Load	Time	Frequency
Aluminium Rough	**1**	**2**	**3**
Aluminium Finished	**1**	**2**	**3**

3. The above table describes that Load is the most significant parameter, followed by the Time and frequency for both rough and finished Steel specimen.

4. The significance level has been tabulated below.

Table. 8.13 Comparison of significance for Aluminium Rough and Finished Specimen

	Load	Time	Frequency
Steel Rough	**0.038**	**0.054**	**0.094**
Steel Finished	**0.038**	**0.051**	**0.092**

For most of the experiments 'p' value < 0.05 has been considered to be significant, however, in practical terms p< 0.10 is also considered to be significant. For finding the significance of the experiment R-Sq and R-Sq[adj] must be higher here both are above 90%, so the results are considered to be significant.

5. Graphs 8.35 to 8.43 clearly show that the Coefficient of friction of the rough specimen shown in blue color is higher than the coefficient of friction of the finished specimen shown in Red color.

6. Material removal for the rough specimen is higher than the coefficient of friction for the rough specimen.

7. Coefficient of friction is of the order 0.6 or above for almost all the cases and for L1 Coefficient of friction is even more than1,

8. Fig. 8.15 and 8.16 shown above are the specimens subjected to Dry sliding wear. The images are corresponding to the maximum worn out pieces. Deep groves may be observed on the surface of the Aluminium specimen. In this case, the wear is dominantly due to Adhesion, followed by abrasion. Clearly welded zones on the worn-out surface have been observed during experimentation.

9. From Graphs 8.38 and 8.42, the **Main Effects Plot for SN ratios,** it may be observed that

The minimum wear occurs at 45N, which is the highest load in the present case. This is due to the fact that Aluminium, which is a ductile material, crushing of the peaks takes place and Wear reduces at higher loads.

8.24. Comparison of the Wear based on the time of contact:

The magnitude of Wear obtained for three different times viz, 3 minutes, 4.5 minutes and 6 minutes based on the experiments performed [L9 orthogonal Array of design] for Brass, Steel, Aluminium has been measured and represented Graphically from Graphs.8.44 to 8.49. These graphs compare the wear behavior under a constant time with the other two parameters being variable has been shown below.

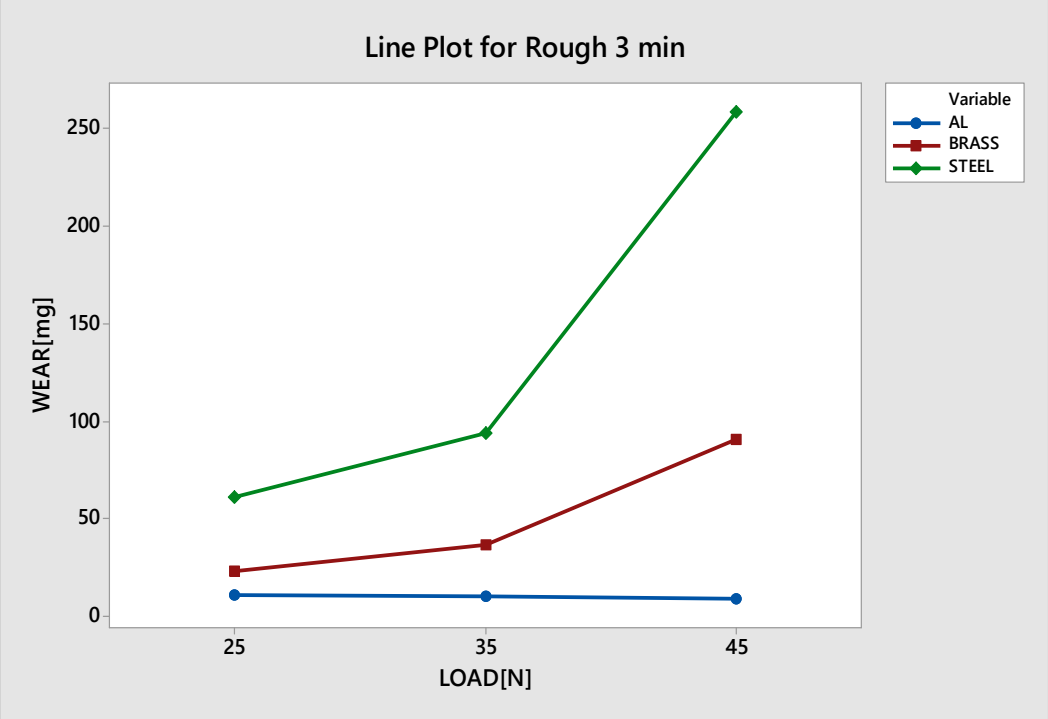

Graph.8.52. Wear comparison for 3 minutes [Rough]

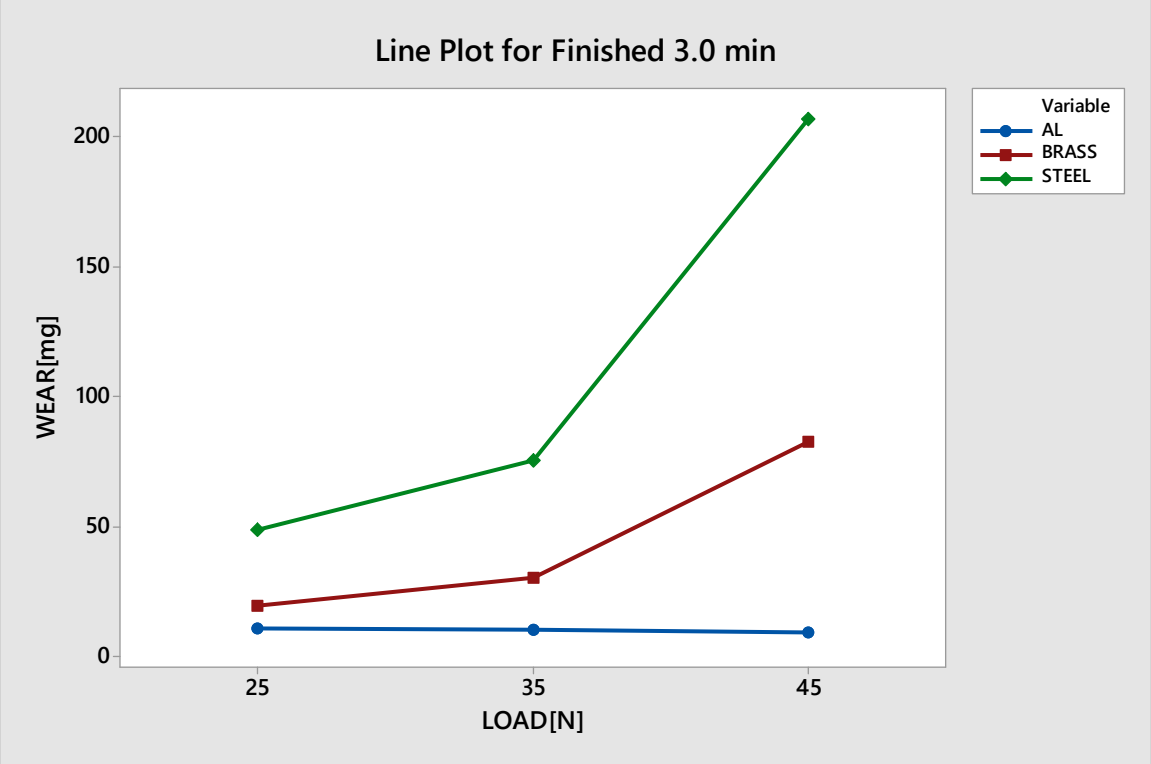

Graph.8.53. Wear comparison for 3 minutes [Finished]

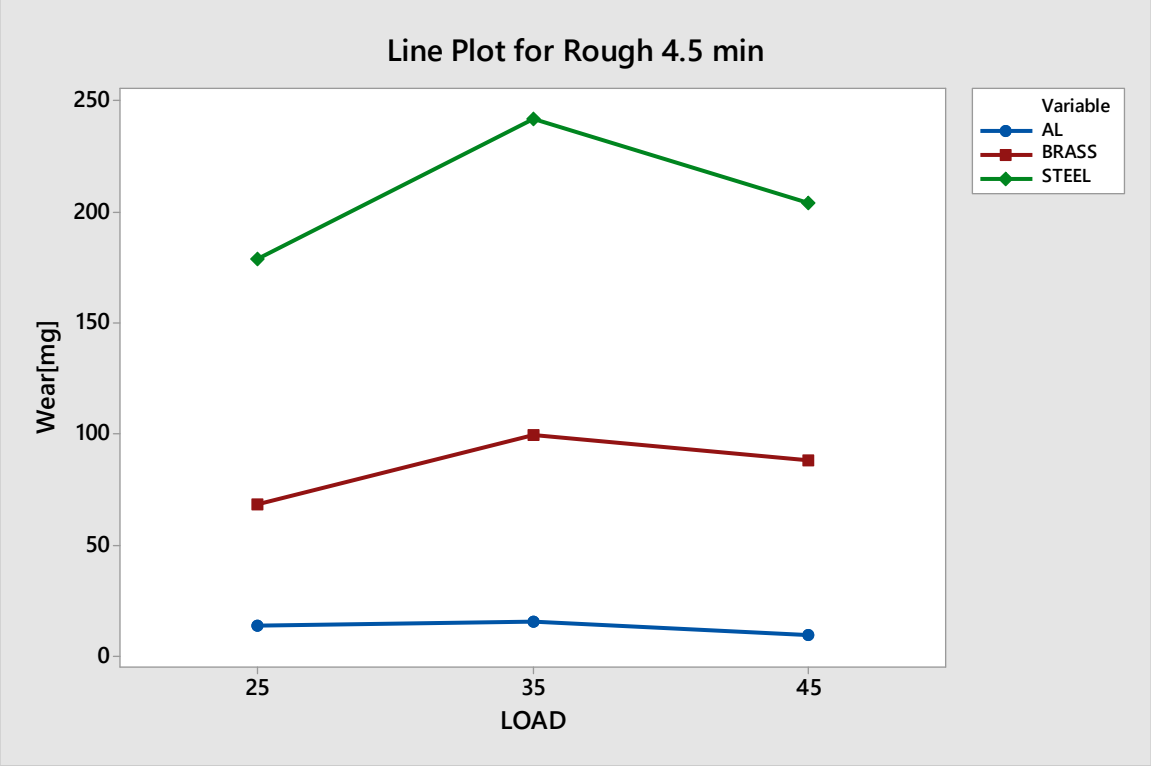

Graph.8.54. Wear comparison for 4.5 min [Rough]

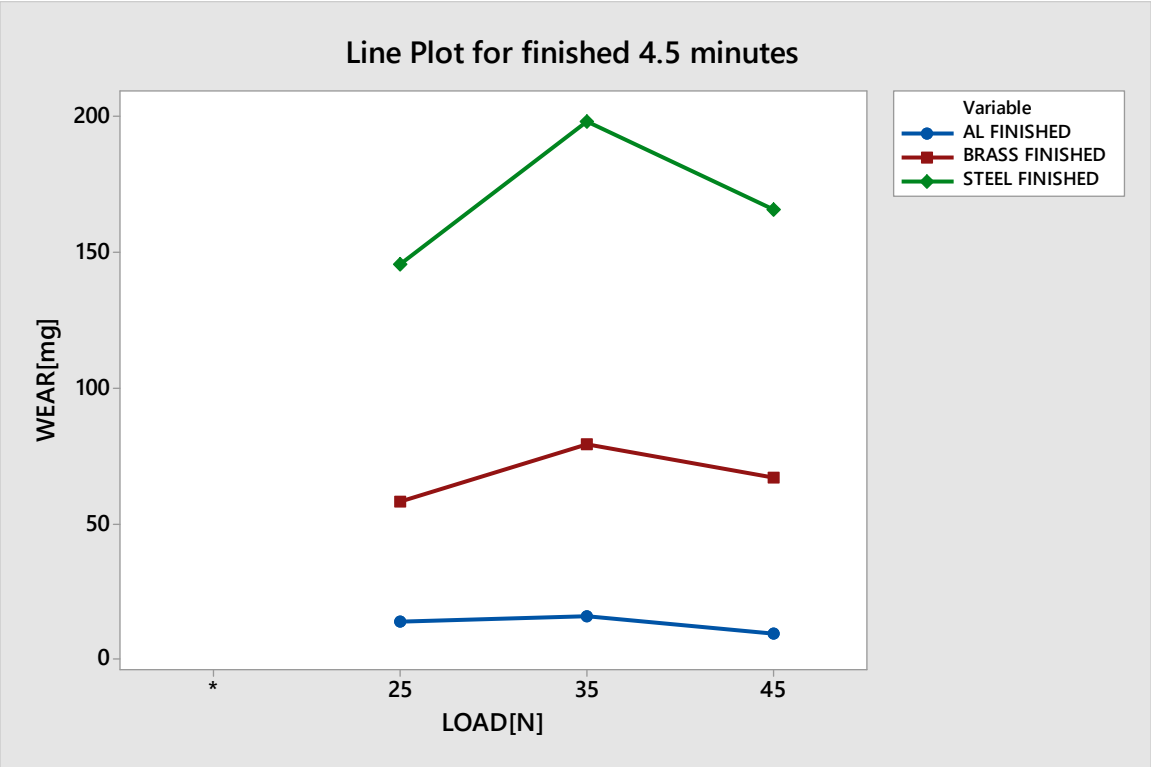

Gaph.8.55. Wear comparison for 4.5 min [Finished]

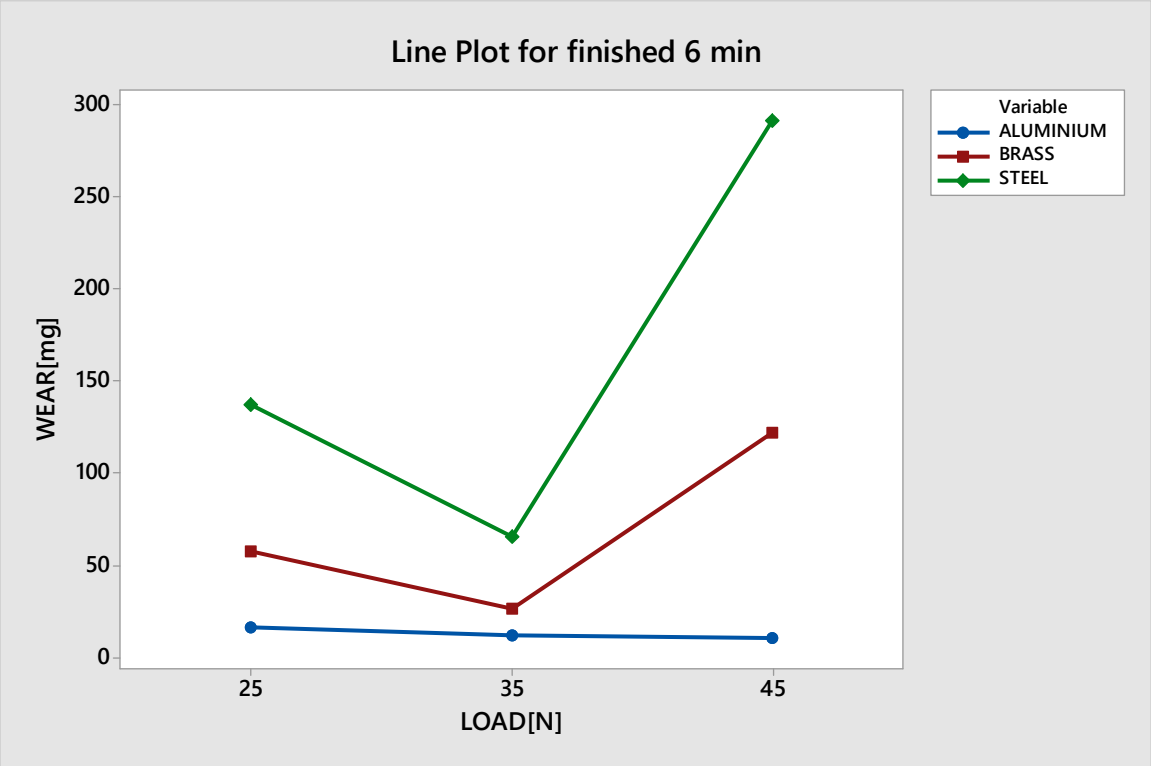

Graph.8.56. Wear comparison for 6 min [Rough]

Graph.8.57. Wear comparison for 6 min [Finished]

The following observations have been made from Graphs.8.51 to 8.56.

1. Graphs 8.51 and 8.52 are for 3 minutes' test under different loads and frequency as per L9 orthogonal Array of Experiments of Taguchi. The graph clearly indicates that there is a sharp rise in the magnitude of Wear[Δm] from 35N to 45N for Steel, to a lesser extent to Brass. However, variation based on the loads for 3 minutes is not appreciable for Aluminium. For both Rough and finished specimen the same wear behavior is observed.
2. Graphs 8.53 and 8.54 are for 4.5 minutes' test under different loads and frequency as per L9 orthogonal Array of Experiments of Taguchi. Graphs show that there is an increase in Wear from 25N to 35N and the maximum value of wear is obtained at 35N and from there, the magnitude of Wear [Δm] falls for a load of 45N. This wear behavior is observed for both rough and finished specimens.
3. Graphs 8.55 and 8.56 are for 6 minutes' test under different loads and frequency as per L9 orthogonal Array of Taguchi. Graphs show that there is a decrease in the magnitude of Wear [Δm] from 25N to 35N and then increases from 35N to 45 N loads. This is observed prominently for Steel and Brass only. This wear behavior is observed for both rough and finished specimens.

SUMMARY

1. ***Process parameters considered for dry sliding wear; Load, Time, and Frequency are found to be significant for a 'p' value of lesser than 0.10.***
2. ***For the Brass mechanism of wear is pure Abrasive wear, for Steel, it is the combination of Abrasive wear and Adhesive wear, Whereas for Aluminium [Al6351T6], it is adhesive mass transfer and plowing mechanism.***
3. ***At 35 N the wear becomes lesser as the surfaces attain maximum smoothness and only upon increasing the load new valleys form and hence the wear will take place further.***
4. ***The coefficient of friction during sliding wear is Maximum for Aluminium, followed by Steel and Brass in this order.***
5. ***The initial difference of Coefficient of Friction between the rough and finished specimen gets reduced considerably after 30 seconds of operation for all three materials under all experimental conditions.***

CHAPTER.9 CONCLUSIONS AND FUTURE SCOPE OF RESEARCH

In this chapter, conclusions have been made based on the Modelling and Simulation work done, Experimental work done at different stages of the research work, and the Optimisation done for the process parameters.

9.1.Conclusions:

- **During the experimentation on Rheometer for the Viscosity, it has been observed that the Viscoelastic Magnetic abrasive medium prepared with Silicone oil and the Transformer oil (Red color) are well suited for experimentation for finishing off both the internal surfaces and external surfaces.**
- **Grease though gives required Viscosity at the laboratory level, could not be used for performing the internal and external surface finishing processes as the viscosity drastically decreases due to a rise in temperature during actual internal and external finishing operation.**
- **The Viscoelastic magnetic abrasive medium has addressed the problem of sedimentation of Carbonyl Iron particles, in the absence of a Magnetic field. Since the Viscoelastic medium does not permit the CIP to settle down, the problem of sedimentation got reduced considerably.**
- **The Viscoelastic Magnetic abrasive medium has started increasing its viscosity as time passes and has been observed that the viscosity got increased from 954.06 mPa-s to 5688 Pa-s in 30 days from the date of preparation.**
- **The size of the abrasive particles does not affect the viscosity significantly for the abrasive sizes selected i.e AMN 320, 400, 600, 800, for preparing the Viscoelastic Magnetic abrasive medium.**
- **The viscosity of the medium prepared for external finishing is *2926.2 Pa-s* and at this viscosity magnitude the medium behaved like a flexible semisolid and hence, it was able to perform better finishing operation**.
- **Based on the simulation work done for finding the Magnetic flux density of the commercially available magnets, for a given volume, Fan-shaped Magnets will produce the highest Magnetic flux density followed by Arc magnets.**
- **For internal finishing, the flux densities considered for optimization are based on the Median value of the Magnetic flux density obtained from simulation done with ANOSOFT 16, whereas most of the researchers, considered the Maximum flux**

density value as the process parameter.

- **Magnets used for internal finishing of the spline shafts in this thesis work are N42 permanent magnets which are normally used for generating electricity for Wind turbine plants and the flux density generated by these magnets is adequate for internal finishing operation.**
- **An Aluminium fixture prepared for Internal finishing is a unique fixture designed for the internal finishing of the Spline shafts.**
- **For material removal most important factor is the rotational speed, however best result is obtained at 180 rpm as at the higher speed the abrasive gel along with Carbonyl Iron Particles will be thrown on to the surface of the internal spline and the finishing operation can't be performed efficiently beyond 180 Rpm. This is in concurrence with the observation made by V K Jain[2006] in his internal finishing of circular shafts.**
- **Magnetic flux densities for external finishing have been considered to be the maximum value as the simulation results show that the Magnetic flux density variation from the center of the Magnet towards the radius is almost constant and having a Maximum value.**
- **For external finishing done under similar testing conditions of the working gap, abrasive size, Magnetic tool rotational speed Feed, Finishing time and Ultrasonic amplitude; for Brass, Aluminium and Steel, it has been found that Magnetic flux density is ranked at 1.**
- **The Level of the Magnetic flux density is level 2[1.5 mm gap] as the increase in the magnetic field further did not increase in producing better result towards surface finish or metal removal.**
- **Magnetic flux density for both Brass and Aluminium as per the Optimisation is Level 3[1 mm gap]. At this level, both the change in surface finish and the metal removal is higher.**
- **Ultrasonic Amplitude is having significance for all three metals.**
- **For steel and Aluminium waviness of the surface is observed during the surface roughness measurement.**
- **The dry wear test conducted on the Rough and Finished specimen reveals that the Wear is marginally higher for rough specimens compared to the finished specimen.**
- **The pattern of wear is similar for both the finished and the rough surfaces. The reason might be the surface layer formed due to VEMAF could not increase the**

hardness appreciably.

9.2.Future scope of research work:

- **Complex internal surfaces like internal cams, Internal gears may be finished with VEMAF medium.**
- **External surfaces having the curved geometry may be finished with VEMAF process.**
- **Force analysis for both Ferrous and Non Ferrous metals under different magnetic field strengths has not yet been done satisfactorily.**

REFERENCES

The research papers referred to during the present research work have been mentioned in the order. References 1 to 34 are the research papers referred for Viscoelastic Magnetic Abrasive Medium preparation. References 35 to 60 are the research papers referred for Internal finishing by Magnetic abrasive flow finishing. References 61 to 140 are the Research papers referred for External Finishing by Magnetic Abrasive finishing process. References 141 to 170 are the Research papers referred for Dry Sliding wear

1. A. B. Metzner, "The Significant Rheological Characteristics of Lubricants", Journal of lubrication Technology, Transactions of ASME, July 1968.
2. H Schiessel, R Metzelr, A Blumen, T F Nonnemacher, "Generalized Viscoelastic models: Their Fractional Equations with solutions"; J Phys.A: Math.Gen.28(1995), 6567-6584.
3. Mark R Jolly, J David Carlson, and Beth C Munoz, "A model of the behavior of magnetorheological materials", Smart Mater. Struct. **5** (1996) 607–614.
4. B. J. de Gans, C. Blom, A. P. Philipse and J. Mellema, "Linear viscoelasticity of an inverse Ferrofluid ", PHYSICAL REVIEW, VOLUME 60, NO.4, October 1999.
5. Byung Doo Chin, Jong Hyeok Park, Moo Hyun Kwan, O.Ok Park; " Rheological properties and dispersion stability of Magnetorheological (MR) suspensions", Rheol Acta (2001) 40: 211-219, Springer- Verlag 2001.
6. Pardeep Kumar, Hari Mohan, and Gursharn Jit Singh, "Rayleigh–Taylor Instability of Rotating Oldroydian Viscoelastic Fluids in Porous Medium in Presence of a Variable Magnetic Field", Transport in Porous Media **56:** 199–208, 2004.
7. Jerome Claracq, Jerome Sarrazin, Jean- Pierre Montfrort, "Viscoelastic properties of Magnetorheological fluids; Rheol Acta(2004) : 43: 38-49.
8. Haobo Cheng, Yam Yeung, Hang Tong, "Viscosity behavior of magnetic suspensions in fluid-assisted finishing", Progress in Natural Science 18 (2008) 91–96.
9. Haining A, Stephen J. Picken and Eduardo Mendes, "Enhanced hardening of soft self-assembled copolymer gels under homogeneous magnetic fields", Royal Society of Chemistry, Soft matter, 2010, 6, 4497- 4503.
10. D. N. Chirikov, S. P. Fedotov, L. Yu. Iskakova and A. Yu. Zubarev, "Viscoelastic properties of Ferrofluids", PHYSICAL REVIEW E 82, 051405 2010.

11. Bong Jun Park, Fei Fei Fang, and Hyoung Jin Choi, “Magneto rheology: materials and application”, Soft Matter, 2010, 6, 5246–5253.
12. Ji Eun Kim and Hyoung Jin Choi, “Magnetic Carbonyl Iron Particle Dispersed in Viscoelastic Fluid and Its Magnetorheological Property”, IEEE Transactions on Magnetics, Vol. 47, No. 10, October 2011.
13. Min Su Kim , Ying Dan Liu , Bong Jun Park , Chun-Yeol You, Hyoung Jin Choi, “Carbonyl iron particles dispersed in a polymer solution and their rheological characteristics under the applied magnetic field”, Journal of Industrial and Engineering Chemistry 18 (2012) 664–667.
14. J. P. Segovia-Gutiérrez, C. L. A. Berli, and J. de Vicen, “Nonlinear viscoelasticity and two-step yielding in magnetorheology: A colloidal gel approach to understand the effect of particle concentration.
15. Song Li , H. Guotian2 ,Zengzhi, Ma Yan,Li Ming, Zhang De-sheng,Wang Song,Ran Yingchun, “The Model and Simulation of Magnetorheological Grease Characteristics”, Applied Mechanics and Materials Vols. 246-247 (2013) pp 1214-1219.
16. Miao Yu, Benxiang Ju,Jie Fu, Shuzhi Liu, and Seung-Bok Choi, “ Magnetoresistance Characteristics of Magnetorheological Gel under a Magnetic Field”, Industrial & Engineering Chemistry research, pubs.acs.org/IECR 2014.
17. Bablu Mordina, Rajesh Kumar Tiwari, Deepak Kumar Setua and Ashutosh Sharma, “Magnetorheology of Polydimethylsiloxane Elastomer/$FeCo_3$ Nanocomposite, J. Phys. Chem. C 2014, 118, 25684−25703.
18. Vyacheslav S. Molchanov, Gennady V. Stepanov, Viktor G. Vasiliev, Elena Yu. Kramarenko, Alexei R. Khokhlov, Zhao-Dong Xu, Ying-Qing Guo, “Viscoelastic Properties of Magnetorheological Elastomers for Damping Applications; Macromol. Mater. Eng. 2014, 299, 1116–1125.
19. Shreedhar Kolekar, Rajashekar V. Kurahatti, Prashanth P.K, Vikram Kamble, Nitin Reddy, “Preparation of a Silicon oil-based Magneto Rheological Fluid and an Experimental Study of its Rheological Properties using a Plate and Cone Type Rheometer”, J. ISSS 2014 Vol. 3 No. 2, pp. 23-26.
20. Seung Hyuk Kwon, Cheng Hai Hong, Phu Xuan Do, Seung-Bok Choi, and Hyoung Jin Choi, “Magneto rheology of a Carbonyl Iron Microsphere Suspension with a Halloysite Additive and Its Damping Force Characteristics”, Ind. Eng. Chem. Res. 2015, 54, 4655−4663.

21. Dongdong Wang, Xinhua Liu, Lifeng Wang, Yankun Ren, and Qiuxiang Zhang, “Study on the Saturation Properties of Silicone Oil-Based Magnetorheological Fluids in Mechanical Engineering”, The Open Mechanical Engineering Journal, 2015, 9, 682-686.
22. Vikram G. Kamble, Shreedhar Kolekar, and Chetan Madivalar, “Preparation of Magnetorheological Fluids Using Different Carriers and Detailed Study on Their Properties”, American Journal of Nanotechnology 2015, 6 (1): 7.15.
23. ya-Hsien Chou, A Cheng Wang, Yan- Cherng Lin, “Elucidating the rheological effect of gel abrasives in Magnetic abrasive finishing”, Procedia CIRP 42 (2016) 866 – 871.
24. Wei Gao, Xingzhe Wang, Wenhan Xu, “Magneto-Mechanical properties of Polydimethylsiloxane Composites with a Binary Magnetic filler system”, Published online in Wiley Online Library (wileyonlinelibrary.com).VC 2017, Society of Plastics Engineers.
25. Kashif Ali Abroa, Mirza Mahmood Baig, Mukarrum Hussain, “Inuences of magnetic field in viscoelastic fluid”, Int. J. Nonlinear Anal. Appl. 9 (2018) No. 1, 99-109.
26. N. Mohamad, Ubaidillah, S. A. Mazlan1, F. Imaduddin, Seung-Bok Choi, M. Yazid, “A comparative work on the magnetic field dependent properties of plate-like and spherical iron particle-based magnetorheological grease”, Journal.pone.0191795 April 9, 2018.
27. Shuhei Sasaki, Mayuko Watanabe, Mika Kawai and Tetsu mitsumata “Chain formation for uncross-linked and cross-linked polyurethane magnetic elastomers”, Research and Reviews in Materials Science and Chemistry, Vol. 8, Issue 1, 2018, Pages 1-20.
28. Siti Aishah Abdul Aziz, Saiful Amri Mazlan, U Ubaidillah , Muhammad Kashfi Shabdin , Nurul Azhani Yunus, Nur Azmah Nordin, Seung-Bok Choi ,and Rizuan Mohd Rosnan, “ Enhancement of Viscoelastic and Electrical Properties of Magnetorheological Elastomers with Nanosized Ni-Mg Cobalt-Ferrites as Fillers”, Materials 2019, 12, 3531.
29. Huixing Wang, Guang Zhang, Ziong Wang, “Normal force of lithium-based magnetorheological grease under quasi-static shear with large deformation”, RSC Adv., 2019, 9, 27167–2717.
30. Irfan Bahiuddin, Nurul AAWahab, Mohd I Shapiai, Saiful A Mazlan, Norzilawati Mohamad, Fitrian Imaduddin and Ubaidillah, “Prediction of field-dependent rheological properties of magnetorheological grease using extreme learning machine method”, Journal of Intelligent Material Systems and Structures 2019, Vol. 30 (11) 1727–1742.
31. Tiger Hu Sun, Junyu Ge, Zhihang Jia, Nan Huang; “Preparation of Magnetorheological Greases and Study Their Rheological Characteristics Considering the Variety of Factors”, International Journal of Materials Engineering 2019, 9(2): 34-38.

32. Huixing Wang , Guang Zhang and Jiong Wang, “Quasi-Static Rheological Properties of Lithium-Based Magnetorheological Grease under Large Deformation”, Materials 2019, 12, 2431.
33. Norzilawati Mohamad, Ubaidillah , Saiful Amri Mazlan , Seung-bok Choi, Siti Aishah Abdul Aziz and Masataka Sugimoto, “The Effect of Particle Shapes on the Field-Dependent Rheological Properties of Magnetorheological Greases”, Int. J. Mol. Sci. 2019, 20, 1525.
34. Kejie Wang , Xiaomin Dong, Junli Li, Kaiyuan Shi and Keju Li, “Effects of Silicone Oil Viscosity and Carbonyl Iron Particle Weight Fraction and Size on Yield Stress for Magnetorheological Grease Based on a New Preparation Technique”, Materials 2019, 12, 1778.
35. Takeo Shinmura, Hitomi Yamaguchi, “Study on a new internal Finishing process by application of Magnetic abrasive finishing (Internal finishing of stainless tube and clean gas bomb)”, series C, Vol 38, No.4,1995, JSME International Journal.[one]
36. Jeong Du-Kim,Min Seog Choi, “Development and Finite Element Analysis of the finishing system Using rotating magnetic field, International Journal of Machine Tools, Vol 36, no 2, PP 245-253, 1996.
37. Jeong Du-Kim,Youn-Hee Kang, Young-Han Bae, Su- Won Lee, “ Development of Magnetic abrasive jet machining for Precision internal polishing of circular tubes, Journal of Material processing technology 71 (1997) 384-393.
38. Hitomi Yamaguchi , Takeo Shinmura, “Study of the surface modification resulting from an internal magnetic abrasive finishing process”, Wear 225–229 _1999. 246–255.
39. Rajender K.Jain, Vijay K. Jain, P.M.Dixit, “Modeling of material removal and surface roughness in abrasive flow machining process, International Journal Machine Tools & Manufacture 39 (1999) 1902-23.
40. Hitomi Yamaguchi, Takeo Shinmura, “Study of an internal magnetic abrasive finishing using a pole rotation system Discussion of the characteristic abrasive behaviour”, Journal of the International Societies for Precision Engineering and Nanotechnology,24 (2000) 237–244
41. Sehijpal Singh, H.S. Shan, “Development of magneto abrasive flow machining process”, International Journal of Machine Tools & Manufacture 42 (2002) 953–959.
42. Hitomi Yamaguchi, Takeo Shinmura, “Internal finishing process for alumina ceramic components by a magnetic field-assisted finishing process”, Precision Engineering 28 (2004) 135–142.

43. Sunil Jha, V.K. Jain, " Design and development of the magnetorheological abrasive flow finishing (MRAFF) process", International Journal of Machine Tools & Manufacture 44 (2004) 1019–1029.
44. Y. Wang, D.J. Hu and Q.L. Deng, "Study on Internal Magnetic Abrasive Finishing of Thin and Long Austenitic Stainless Steel Tube", Key Engineering Materials Vols. 259-260, 2004; Advances in Grinding and Abrasive Processes
45. Debin Wang, Takeo Shinmura, Hitomi Yamaguchi, "Study of magnetic field assisted mechanochemical polishing process for inner surface of Si3N4 ceramic components Finishing characteristics under wet finishing using distilled water", International Journal of Machine Tools & Manufacture 44 (2004) 1547–1553.
46. Yan Wang, Dejin Hu, "Study on the inner surface finishing of tubing by magnetic abrasive finishing", International Journal of Machine Tools & Manufacture 45 (2005) 43–49.
47. Sunil Jha, V.K. Jain, "Modeling and simulation of surface roughness in magnetorheological abrasive flow finishing (MRAFF) process", Wear 261 (2006) 856–866.
48. Manas Das, V.K. Jain_, P.S. Ghoshdastidar, "Fluid flow analysis of magnetorheological abrasive flow finishing (MRAFF) process", International Journal of Machine Tools & Manufacture 48 (2008) 415–426.
49. K. Hanada , H. Yamaguchi b, H. Zhou, "New spherical magnetic abrasives with carried diamond particles for internal finishing of capillary tubes", Diamond & Related Materials 17 (2008) 1434–1437.
50. M. RaviSankar,V.K.Jain , J.Ramkumar, "Rotational abrasive flow finishing (R-AFF) process and its effects on finished surface topography", International Journal of Machine Tools & Manufacture 50 (2010) 637–650.
51. Sehijpal Singh, H.S. Shan*, P. Kumar, "Wear behavior of materials in magnetically assisted abrasive flow machining", Journal of Materials Processing Technology 128 (2002) 155–161.
52. Amit M. Wani, Vinod Yadava , Atul Khatri, "Simulation for the prediction of surface roughness in magnetic abrasive flow finishing (MAFF)", Journal of Materials Processing Technology 190 (2007) 282–290.

53. Hitomi Yamaguchi, Takeo Shinmura, and Atsushi Kobayashi, “Development of an internal Magnetic Abrasive Finishing Process for Nonferromagnetic complex shape tubes”, JSME International Journal, series C, Vol 44 no1, 2010.
54. Junmo Kang, Hitomi Yamaguchi, “Internal finishing of capillary tubes by magnetic abrasive finishing using a multiple pole-tip system”, Precision Engineering 36 (2012) 510– 516.
55. Junmo Kang, Andrew George, Hitomi Yamaguchi, “High-speed Internal Finishing of Capillary Tubes by Magnetic Abrasive Finishing”, 5th CIRP Conference on High Performance Cutting 2012, Procedia CIRP 1 (2012) 414 – 418.
56. ZhengHao Yu, Bing Han & Song Chen & Yan Chen & Zheng Wei Yan “Study on the inner surface finishing of irregular spatial elbow pipe by the centreline reconstruction”, International Journal Advanced Manufacturing Technology, published online 13 July 2017.
57. Valens Nteziyaremye, Yancheng Wang, Weisi Li , Albert Shih, Hitomi Yamaguchi, “Surface Finishing of Needles for High-Performance Biopsy”, 6th CIRP International Conference on High Performance Cutting, HPC2014. Procedia CIRP 14 (2014) 48 – 53.
58. Hitomi Yamaguchi,Takeo Shinmura, Ryota Ikeda, “Study of Internal Finishing of Austenitic Stainless Steel Capillary Tubes by Magnetic Abrasive Finishing”, Journal of Manufacturing Science and Engineering OCTOBER 2007, Vol. 129 / 885.
59. Talwinder Singh Bedi & Anant Kumar Singh, “Development of magnetorheological fluid-based process for finishing of ferromagnetic cylindrical workpiece”, Machining Science and Technology, An International Journal, ISSN: 1091-0344 (Print) 1532-2483 (Online), 2018.
60. Sahil Kajal, V. K. Jain, J. Ramkumar, Leeladhar Nagdeve1 , “Experimental and theoretical investigations into internal magnetic abrasive finishing of a revolver barrel”, Int J Adv Manuf Technol (2019) 100:1105–1122[105g]
61. Kuppuswamy, “An Investigation of the effect of a Magnetic field on electrolytic diamond polishing”, Wear, 54 (1979) 257 – 272.

62. T. Shinmura, K. Takazawa, E. Hatano, M. Matsunaga, Toyo-Kenmazai Co./Japan, "Study on Magnetic Abrasive Finishing", CIRP Annals Volume 39, Issue 1, 1990, Pages 325-328.
63. Jeong-Du Kim, Min Seog-Chi, "Simulation for the prediction of surface accuracy in Magnetic abrasive finishing", Journal of Material Processing Technology, 53 (1995) 630-642.
64. Jeong-Du Kim, Min Seng-Choi, "Development of the magneto- Electrolytic Abrasive polishing system and finishing characteristics of a CR-coated roller", International Journal of Machine Tool Manufacture, Vol 37, No.3, No.7, PP 99701006,1997.
65. Jeong-Du Kim, Yan-Meng Xu, Youn-Hee Kang, "Study on the characteristics of Magneto-Electrolytic-Abrasive Polishing by using the newly developed nonwoven-abrasive pads", International Journal of Machine Tools & Manufacture 38 (1998) 1031–1043.
66. T. Mori, K. Hirota, Y. Kawasthima, "Clarification of Magnetic Abrasive Finishing Mechanism", Journal of Materials Processing Technology 143–144 (2003) 682–686.
67. Shaohui Yin, Takeo Shinmura, "Vertical vibration-assisted magnetic abrasive finishing and deburring for magnesium alloy", International Journal of Machine Tools & Manufacture 44 (2004) 1297–1303.
68. Shaohui Yin , Takeo Shinmura, "A comparative study: polishing characteristics and its mechanisms of three vibration modes in vibration-assisted magnetic abrasive polishing", International Journal of Machine Tools & Manufacture 44 (2004) 383–390.
69. Dhirendra K Singh, V K Jain, V Raghuram," Parametric Study of magnetic abrasive finishing process", Journal of Material Processing Technology 149 (2004) 22-29.
70. S.C. Jayswal · V.K. Jain · P.M. Dixit, "Modeling and simulation of magnetic abrasive finishing process", Int J Adv Manuf Technol (2005) 26: 477–490.
71. Dhirendra K. Singh, V.K. Jain, V. Raghurama, R. Komanduri, "Analysis of surface texture generated by a flexible magnetic abrasive brush", Wear 259 (2005) 1254–1261.
72. N. Umehara, T. Kirtane, R. Gerlick, V.K. Jain, R. Komanduri, "A new apparatus for finishing large size/large batch silicon nitride (Si3N4) balls for hybrid bearing applications by magnetic float polishing (MFP)", International Journal of Machine Tools & Manufacture 46 (2006) 151–169.
73. Xiaozuoyi, "Researching for the unbounded magnetic abrasive application in magnetic abrasive finishing", international technology and innovation conference 2006.

74. S.L.Ko, Yu M.Baron, J.I.Pak, “Micro deburring for precision using magnetic abrasive finishing method”, Journal of Materials Processing Technology 187-188 (2007) 19-25.
75. S. Yin and T. Shinmura, “Vibration-Assisted Magnetic Abrasive Polishing”, Key Engineering Materials Vol 329 (2007) pp 207-212.
76. Ching-Tien Lin. Lieh-Dai Yang. Han-Ming Chow, “Study of magnetic abrasive finishing in free-form surface operations using the Taguchi method”, Int J Adv Manuf Technol (2007) 34: 122-130.
77. Berhanu Girma , Suhas S. Joshi , M. V. G. S. Raghuram & R. Balasubramaniam, “An experimental analysis of magnetic abrasives finishing of plane surfaces”, Machining Science and Technology, (2007)10:323–340.
78. Yan-Cherng Lin, Ho-Shiun Lee, “Machining characteristics of magnetic force-assisted EDM”, International Journal of Machine Tools & Manufacture 48 (2008) 1179– 1186.
79. S. O. Kim, J. S. Kwak,, “Magnetic force improvement and parameter optimization for magnetic abrasive polishing of AZ31 magnesium alloy”, Transactions of Non Ferrous metals Society of China 18(2008) s369-s273.
80. A. Sadiq, M.S. Shunmugam, “Investigation into magnetorheological abrasive honing (MRAH)”, International Journal of Machine Tools & Manufacture 49 (2009) 554–560.
81. A.C.Wang, S.J.Lee, “Study the characteristics of magnetic finishing with gel abrasive”, International Journal of Machine Tools & Manufacture 49 (2009) 1063–1069.
82. Bongsu Jung , Kyung-In Jang , Byung-Kwon Min , Sang Jo Lee , Jong won Seok, “Magnetorheological finishing process for hard materials using sintered iron-CNT compound abrasives”, International Journal of Machine Tools & Manufacture 49 (2009) 407–418.
83. Yan-Cherng Lin, Yuan-Feng Chen, Der-An Wang, Ho-Shiun Lee, “Optimization of machining parameters in magnetic force assisted EDM based on Taguchi method”, journal of materials processing technology 2 0 9 (2 0 0 9) 3374–3383.
84. V.K. Jain, P. Ranjan, V.K. Suri, R. Komanduri “Chemo-mechanical magneto-rheological finishing (CMMRF) of silicon for microelectronics applications”, CIRP Annals - Manufacturing Technology 59 (2010) 323–328.
85. H. Yamaguchi, R.E. Riveros , I. Mitsuishi , U. Takagi , Y. Ezoe , N. Yamasaki, K. Mitsuda , F. Hashimoto “Magnetic field-assisted finishing for micropore X-ray focusing mirrors fabricated by deep reactive ion etching”, CIRP Annals - Manufacturing Technology 59 (2010) 351–354.

86. A. Sadiq , M.S.Shunmugam, “A novel method to improve finish on non-magnetic surfaces in magneto- rheological abrasive honing process”, Tribology International 43 (2010) 1122–1126.
87. Rahul S. Mulik & Pulak M. Pandey, “Mechanism of Surface Finishing in Ultrasonic-Assisted Magnetic Abrasive Finishing Process”, *Materials and Manufacturing Processes*, 25: 1418–1427, 2010.
88. Rahul S. Mulik, Pulak M. Pandey, “Ultrasonic assisted magnetic abrasive finishing of hardened AISI 52100 steel using unbonded SiC abrasives”, Int. Journal of Refractory Metals and Hard Materials 29 (2011) 68–77.
89. Ajay Sidpara, V.K. Jain, “Experimental investigations into forces during magnetorheological fluid based finishing process”, International Journal of Machine Tools & Manufacture 51 (2011) 358–362.
90. H. Yamaguchi, J. Kang, F. Hashimoto, “Metastable austenitic stainless steel tool for magnetic abrasive finishing”, CIRP Annals - Manufacturing Technology 60 (2011) 339–342.
91. Ajay Sidpara, V.K. Jain, “Theoretical analysis of forces in magnetorheological fluid based finishing process”, International Journal of Mechanical Sciences 56 (2012) 50–59.
92. Jae-Seob KWAK, “Mathematical model determination for improvement of surface roughness in magnetic-assisted abrasive polishing of nonferrous AISI316 material”, Trans. Nonferrous Met. Soc. China 22(2012) s845−s850
93. Ajay Sidpara, V.K. Jain, “Nano–level finishing of single crystal silicon blank using magnetorheological finishing process”, Tribology International 47 (2012) 159–166.
94. Hitomi Yamaguchi, Anil K. Srivastava, Michael A. Tan, Raul E. Riveros, Fukuo Hashimoto, “Magnetic abrasive finishing of cutting tools for machining of titanium alloys”, CIRP Annals - Manufacturing Technology 61 (2012) 311–314.
95. Jisheng Pana, Qiusheng Yana, Xipeng Xu , Jiangting Zhua, Zhancheng Wua and Zhenwei Baia, “Abrasive Particles Trajectory Analysis and Simulation of Cluster Magnetorheological Effect Plane Polishing”, Physics Procedia 25 (2012) 176 – 184.
96. Anant Kumar Singh,SunilJha, Pulak M.Pandey, “Mechanism of material removal in ball end magnetorheological finishing process”, Wear 302 (2013) 1180–1191.
97. K.B. Judal, Vinod Yadava, Modeling and simulation of cylindrical electro-chemical magnetic abrasive machining of AISI-420 magnetic steel, Journal of Materials Processing Technology 213 (2013), 2089-2100.

98. Prateek Kala, Sumit Kumar & Pulak M. Pandey, "Polishing of Copper Alloy Using Double Disk Ultrasonic Assisted Magnetic Abrasive Polishing", Materials and Manufacturing Processes, Published online: 05 Feb 2013.
99. Ajay Sidpara, V.K. Jain, "Analysis of forces on the freeform surface in magnetorheological fluid based finishing process", International Journal of Machine Tools & Manufacture 69 (2013) 1–10.
100. Wenhui Li, Xiuhong Li, "New Viscoelastic Abrasive and its Surface Finishing Process", Advanced Materials research, 1662- 8985, Vol. 314-316, pp 300-303.
101. H. Suzuki , M. Okada , W. Lin , S. Morita , Y. Yamagata , H. Hanada , H. Araki , S. Kashima , " Fine finishing of ground DOE lens of synthetic silica by magnetic field-assisted polishing", CIRP Annals, Manufacturing Technology 63 (2014) 313-316.
102. G.Y. Liu, Z.N. Guo, S.Z. Jiang, N.S. Qu, Y.B. Li,, "A study of processing Al 6061 with electrochemical magnetic abrasive finishing", Procedia CIRP 14 (2014) 234 – 238.
103. Prateek Kala and Pulak M. Pandey, "Experimental Study On Finishing Forces In Double Disk Magnetic Abrasive Finishing Process While Finishing Paramagnetic Workpiece". Procedia Materials Science 5 (2014) 1677 – 1684.
104. T.C. Kanis , P. Kuppan, S. Narayanan, S. Denis Ashok, "Fuzzy Logic based Model to predict the improvement in surface roughness in Magnetic Field Assisted Abrasive Finishing", Procedia Engineering 97 (2014) 1948 – 1956.
105. Hitomi Yamaguchi , Anil K. Srivastava, Michael Tan, Fukuo Hashimoto, "Magnetic Abrasive Finishing of cutting tools for high-speed machining of titanium alloys", CIRP Journal of Manufacturing Science and Technology 7 (2014) 299-304.
106. Prateek Kala, Pulak M. Pandey, "Comparison of finishing characteristics of two paramagnetic materials using double disc magnetic abrasive finishing", Journal of Manufacturing Process 17 (2015) 63-77.
107. K. Saraswathamma, Sunil Jha, P.V. Rao, "Experimental investigation into Ball End Magnetorheological Finishing of silicon", Precision Engineering 42 (2015) 218-223.
108. Nitesh Sihag, Prateek Kala, Pulak M. Pandey, "Chemo Assisted Magnetic Abrasive Finishing: Experimental Investigations", Procedia CIRP 26 (2015) 539 – 543.
109. Satish Kumar, V.K. Jain, Ajay Sidpara, "Nano-finishing of freeform surfaces (Knee joint implant) by rotational-magnetorheological abrasive flow finishing (R-MRAFF) process", Precision Engineering 42 (2015) 165-178.
110. Zsolt Kovacs, "The investigation of tribological characteristics of surface improved by magnetic polishing and roller burnishing", Procedia Engineering 149 (2016) 183 – 189.

111. Junji Murata , YoshihitoUeno , KoushiYodogawa , TakahitoSugiura, “Polymer/CeO2–Fe3O4 multicomponent core–shell particles for high-efficiency magnetic-field-assisted polishing processes”, International Journal of Machine Tools & Manufacture 101 (2016) 28-34.
112. Yuyue Wang,Yun Zhang, Zhijing Feng, “ Analyzing and improving surface texture by dual-rotation magnetorheological finishing “, Applied Surface Science 360 (2016) 224-233.
113. Mehrdad Vahdati and Seyed Alireza Rasouli, “Evaluation of Parameters Affecting Magnetic Abrasive Finishing on Concave Freeform Surface of Al Alloy via RSM Method, Hindawi Publishing Corporation Advances in Materials Science and Engineering Volume 2016, Article ID 5256347, 14 pages.
114. Nitesh Sihag, Prateek Kala and Pulak M Pandey, “Analysis of Surface Finish Improvement during Ultrasonic Assisted Magnetic Abrasive Finishing on chemically treated Tungsten substrate”, Procedia Manufacturing 10 (2017) 136 – 146.
115. Rui Wang, Pyo Lim, Lida Heng and Sang Don Mun, “Magnetic Abrasive Machining of Difficult-to-Cut Materials for Ultra-High-Speed Machining of AISI304 Bars”, Materials **2017**, 10, 1029; doi:10.3390/ma10091029.
116. Prateek Kala, Varun Sharma, Pulak M. Pandey, “Surface roughness modelling for Double Disk Magnetic Abrasive Finishing process”, Journal of Manufacturing Processes 25 (2017) 37-48.
117. Vipin C. Shukla, Pulak M. Pandey, Uday S. Dixit, Anish Roy, Vadim Silber Schmidt, “Modeling of normal force and finishing torque considering shearing and ploughing effects in ultrasonic assisted magnetic abrasive finishing process with sintered magnetic abrasive powder”, Wear 390-391(2017) 11-22.
118. Saraswathamma. K, Sunil Jha and Venkateswara Rao, “Rheological behaviour of Magnetorheological polishing fluid for Si polishing”, Materials Today: Proceedings 4 (2017) 1478–1491.
119. Hitomi Yamaguchi, Omar Fergani, Pei-Ying Wu, “Modification using magnetic field-assisted finishing of the surface roughness and residual stress of additively manufactured components”, CIRP Annals - Manufacturing Technology 66 (2017) 305-308.
120. Patrick Munyensanga, P. Paryanto, Moh Nor Ali Aziz, “Application of Polishing AISI 316L Stainless Steel Ball Bearing with A Magnetic Abrasive Finishing Process: A Review”, Munyensanga, dkk. / ROTASI, Vol. 20 No. 4 (October 2018) Hal. 249-257.

121. Jiang Guo, Kui Liu, Zhenfeng Wang, Guan Leong Tnay, "Magnetic field-assisted finishing of a mold insert with curved microstructures for injection molding of microfluidic chips", Tribology International 114 (2017) 306-314.
122. Anwesa Barman, Manas Das, "Design and fabrication of a novel polishing tool for finishing free form surfaces in magnetic field assisted finishing (MFAF) process", Precision Engineering 49 (2017) 61-68.
123. Prateek Kala, Pulak M. Pandey, Girish C. Verma, Varun Sharma, "Understanding flexible abrasive brush behavior for double disk magnetic abrasive finishing based on force signature", Journal of Manufacturing Processes 28 (2017) 442-448.
124. Zafar Alam, Sunil Jha, " Modeling of surface roughness in ball end magnetorheological finishing (BEMRF) process", Wear 374-375 (2017) 54-62.
125. Kanish T C, Narayanan S, Kuppan P, Denis Ashok S, "Investigations on the finishing forces in Magnetic Field Assisted Abrasive Finishing of SS316L", Procedia Engineering 174 (2017) 611 – 620.
126. Aviral Misra , Pulak M. Pandey, U.S. Dixit, " Modeling and simulation of surface roughness in ultrasonic assisted magnetic abrasive finishing process", International Journal of Mechanical Sciences 133 (2017) 344-356.
127. Lida Heng, Yon Jig Kim, and Sang Don Mun, "Review of Superfinishing by the MagneticAbrasive Finishing Process", High Speed Mach. 2017; 3:42–55 DE GRUYTER OPEN.
128. Pei-Yeing Wu, Hitomi Yamaguchi, "Material removal mechanism of Additively Manufactured Components Finished Using Magnetic Abrasive Finishing", Precedia Manufacturing 26 (2018) 394-402.
129. Sachindra J. Doshi & Ketan S Vaghosi, "Some investigations on Magnetic Abrasive Finishing of Aluminium Alloy", IJRAR- International Journal of Research and Analytical Reviews [VOLUME 5 I ISSUE 4 I OCT. – DEC. 2018].
130. Yuewu Gao, Yugang Zhao, Guixiang Zhang, Guiguan Zhang & Fengshi Yin, "Polishing of paramagnetic materials using atomized magnetic abrasive powder", Materials and Manufacturing Processes ISSN: 1042-6914 (Print) 1532-2475 (Online).
131. Rajneesh Kumar Singha, D.K. Singh and Swati Gangwar," Advances in Magnetic Abrasive Finishing for Futuristic Requirements - A Review", Materials Today: Proceedings 5 (2018) 20455–20463.

132. D. Sai Chaitanya Kishore, S.M. Jameel Basha," Optimization of Process Parameters in Surface Finishing of Al6061 by using Magnetic Abrasive Finishing Process", Materials Today: Proceedings 18 (2019) 3365–3370.

133. Huijun Xie, Yanhua Zou, Chaowen Dong, Jinzhong Wu, "Study on the magnetic abrasive finishing process using alternating magnetic field: investigation of mechanism and applied to aluminium alloy plate", The International Journal of Advanced Manufacturing Technology (2019) 102:1509–1520.
134. Henan Liu, Jian Cheng, TingzhangWang, Mingjun Chen, "Magnetorheological finishing of an irregular-shaped small-bore complex component using a small ball-end permanent-magnet polishing head", Nanotechnology and Precision Engineering 2 (2019) 125-129.
135. Jiong Zhang, Akshay Chaudhari, Hao Wang, "Surface quality and material removal in magnetic abrasive finishing of selective laser melted 316L stainless steel", Journal of Manufacturing Processes 45 (2019) 710-719.
136. Meng Nie , Jianguo Cao, Jianyong Li, Maohui Fu, "Magnet arrangements in a magnetic field generator for magnetorheological finishing", International Journal of Mechanical Sciences 161-162 (2019) 105018.
137. Mohammad Mosavat, Abdolreza Rahimi, "Numerical-experimental study on polishing of silicon wafer using magnetic abrasive finishing process", Wear 424-425 (2019), 143-150.
138. Ravi Datt Yadav, Anant Kumar Singh, "A novel magnetorheological gear profile finishing with high shape accuracy", International Journal of Machine Tools and Manufacture, 139 (2019) 75-92.
139. Jiang Guo, Wenhe Feng, Henry Jia Hua Jong, Hirofumi Suzukic, Renke Kang, "Finishing of rectangular micro features by localized vibration-assisted magnetic abrasive polishing method", Journal of Manufacturing Processes 49 (2020) 204-213.
140. Jiabao Liu, Xiaoyuan Li, Yunfei Zhang, Dong Tian, Minheng Ye, Chao Wang, "Predicting the Material Removal Rate (MRR) in surface Magnetorheological Finishing (MRF) based on the synergistic effect of pressure and shear stress", Applied Surface Science 504 (2020) 1444492.

141. A Rac.:" Influence of load and speed on wear characteristic of grey cast iron, in dry sliding-selection for minimum wear", Tribology international, 0301 679X/85/010029-05 © 1985 Butterworth & Co (Publishers) Ltd.

142. Komvopoulos, K., Saka, N., Suh, N.P.:" Plowing Friction in Dry and Lubricated Metal Sliding", Journal of Tribology, JULY 1986, Vol. 108/301.
143. Hokirikawa, K., KATO, K.:" The effect of hardness on the transition of the abrasive wear mechanism of steels", Wear, 123 (1988) 241 - 251, TX, U.S.A., April 5 - 9, 1987.
144. Lim, S.C., ASHBY, M. F., BRUNTON, J. H.:" THE Effects of Sliding Conditions on the Dry Friction of Metals.", Vol. 37, No. 3, pp. 161-112,1 1989 OOOI-6160.
145. Dwyer-Joyce, R.S., Sayles, R.S., Ioannides, E.:" An investigation wear into the mechanisms of closed three-body abrasive", Wear, 175 (1994) 133-142, Received August 12, 1993; accepted December 2, 1993.
146. Terheci, M., Manory, R.R., Herder, J.H.:" The friction and wear of automotive grey cast iron under dry sliding conditions Part 1 -relationships between wear loss and testing parameters", Wear 180 (1995) 73-78, Received 13 June 1994; accepted 15 September 1994.
147. Wang, You., Lei , Tingquan., "Wear behavior of steel 1080 with different microstructures during dry sliding", Wear 194 (1996) 4L53, Received 11 April 1995; accepted 2 June 1995.
148. Kato, K., Hokkirigawa, K., Kayaba, T., Endo, Y.," Three Dimensional Shape Effect on Abrasive Wear", AS ME, 346/Vol. 108, JULY 1996.
149. Kato, Koji."Abrasive wear of Metals", Tribology International Vol. 30, No. 5, pp. 333-338. 1997, PII: SO301-679X(96)00063-1.
150. Gahr, K.H. Zum." Wear by hard particles", Tribology International Vol. 31, No. 10, pp. 587–596, 1998, PII: S0301–679X(98)00079–6.
151. Wang, You., Lei, Tingquan., Liu, Jiajun.:" Tribo-metallographic behavior of high carbon steels in dry sliding I. Wear mechanisms and their transition", Wear 231 _1999. 1–11, Received 3 March 1999; accepted 3 March 1999.
152. Sudhakar, K.V., Sampathkumaran, P., Dwarakadasa, E.S.:" Dry sliding wear in high density Fe–2%Ni based PM alloys", Wear 242 _2000. 207–212.
153. Straffelini, G., Molinari, A.:" Dry sliding wear of ferrous PM materials", Powder Metallurgy 2001 Vol. 44 No. 3, ISSN 0032–5899.
154. Singh, Sehijpal ., Shan, H.S., Kumar, P." Wear behaviour of materials in magnetically assisted abrasive flow machining", Journal of Materials Processing Technology 128 (2002) 155–161.

155. Guan, Xingsheng., Iwasaki, Kunihiko., Kishi, Katsuhiro., Yamamoto, Masafumi., Tanaka, Ryohei.:" Dry sliding wear behaviour of Fe–28Al and Fe–28Al–10Ti alloys", Materials Science and Engineering A366 (2004) 127–134.
156. Straffelini, G., Maines, L., Pellizzari, M., Scardi, P.:" Dry sliding wear of Cu–Be alloys", Wear 259 (2005) 506–511.
157. Wan, Y.Z., Chen, G.C., Raman, S., Xin, J.Y., Li, Q.Y., Huang, Y., Wang, Y.L., Luo, H.L.:" Friction and wear behavior of three-dimensional braided carbon fiber/epoxy composites under dry sliding conditions", Wear 260 (2006) 933–941.
158. Singh, J.B., Cai, W., Bellon, P.:" Dry sliding of Cu–15 wt%Ni–8 wt%Sn bronze Wear behaviour and microstructures", Wear 263 (2007) 830–841.
159. Basavarajappa, S., Chandramohan, G., Davim, J. Paulo.:" Application of Taguchi techniques to study dry sliding wear behaviour of metal matrix composites", Materials and Design 28 (2007) 1393–1398.
160. An, J., Li, R.G., Lu, Y., Chen, C.M., Xu, Y., Chen, X., Wang. L.M.:" Dry sliding wear behaviour of magnesium alloys", Wear 265 (2008) 97–104.
161. Gåård, A., Krakhmalev, P., Bergström, J.:" Influence of tool steel microstructure on origin of galling initiation and wear mechanisms under dry sliding against a carbon steel sheet", Wear 267 (2009) 387–393, doi: 10.1016/j.wear.2008.11.013
162. Koji Kato,Koshi adachi,"Modern Tribology Hand Book", Tohuku University, Japan.
163. Ajith Arul Daniela, Sakthivel Murugesana, Manojkumara, Sudhagar Sukkasamya, "Dry Sliding Wear Behaviour of Aluminium 5059/SiC/MoS2 Hybrid Metal Matrix Composites", Materials Research. 2017; 20(6): 1697-1706.
164. Subbarayan Sivasankaran, "Optimization on dry sliding wear behavior of yellow brass using face centered composite design", AIMS Materials Science, 6(1): 80–96, 02 Feb 2019.
165. Karl -Heinz Zum Heigr - Chapter. 6. Trbology series, Microstructure and Wear of Materials, Volume 10, 1987, Pages 351- 495.
166. Todor Sheiretov , Hyung Yoon & Cris Cusano ,"Scuffing Under Dry Sliding Conditions—-Part II:Theoretical Studies", Tribology Transactions by Taylor and Francis, ISSN: 1040-2004 (Print) .
167. A. Gaard*, P. Krakhmalev, J. Bergström , "Influence of tool steel microstructure on origin of galling initiation and wear mechanisms under dry sliding against a carbon steel sheet", Wear 267 (2009) 387–393

168. G.B. Veeresh Kumar, C.S.P. Rao, N. Selvaraj, “Studies on mechanical and dry sliding wear of Al6061–SiC composites”, Composites: Part B 43 (2012) 1185–1191.

169. S Sivakumar1, KP Padmanaban2 and M Uthayakumar, “Wear behavior of the Al (LM24)–garnet particulate composites under dry sliding conditions”, Proc IMechE Part J: Engineering Tribology 2014, Vol. 228(12) 1410–1420, IMechE 2014

170. Pushkar JHA, Rakesh Kumar GAUTAM, Rajnesh TYAGI, “Friction and wear behavior of Cu–4 wt.%Ni–TiC composites under dry sliding conditions”, Friction **5**(4): 437–446 (2017).

RESEARCH PUBLICATIONS

JOURNALS:

1. **Krovvidi Srinivas, Q. Murtaza, A K Agrawal, "Modeling of Viscoelastic fluid in finishing Process, International Journal of Scientific & Technology Research, Volume 8, issue 9, September 2019, ISSN:2277-8616, UGC CARE and Scopus Indexed Journal [Source ID: 21100894501]**
2. **K.Srinivas, Q. Murtaza, A K Agrawal, "Effect of shape of Magnet on the Machining of workpiece", International Journal of Recent Technology and Engineering, Volume 8, Issue-2S11, September 2019, ISSN:2278-0181, UGC CARE, and Scopus indexed [Source ID: 21100814505].**
3. **Krovvidi Srinivas, Q. Murtaza, A K Agrawal, "Effect of permanent Magnetic pole orientation on Field strength in Viscoelastic Magnetic abrasive finishing Process", International Journal of Mechanical & Production Engineering Research and Development, ISSN(P): 2249-6890; ISSN€: 2249-8001, Vol 9, Issue 5 Oct 2019, 43-52 [Source ID: 21100814505]**

CONFERENCES:

1. **K.Srinivas, Q. Murtaza, A K Agrawal, " Effect of Magnetic pole orientation on Viscoelastic Magnetic Viscoelastic Magnetic abrasive finishing process", International Conference on Emerging Trends in Electro-Mechanical Technologies and Management (TEMT- 2019), HMR INSTITUTE OF Technology and Management, Hamidpur, Delhi (Publication partner Springer).**
2. **K.Srinivas, Q. Murtaza, A K Agrawal, Simulation of flow parameters and Magnetic forces in Machining of Internal Cam through Viscoelastic Magnetic Abrasive flow finishing process, International Conference on Advances in Research in Engineering (ICARI).**